buildings

Special Issue Reprint

Innovative Approaches to Climate-Responsive Building Design

Advancing Resilience and Sustainability in the Built Environment

Edited by
Lidia Badarnah and Francesco Sommese

mdpi.com/journal/buildings

MDPI

Innovative Approaches to Climate-Responsive Building Design: Advancing Resilience and Sustainability in the Built Environment

Innovative Approaches to Climate-Responsive Building Design: Advancing Resilience and Sustainability in the Built Environment

Guest Editors

Lidia Badarnah
Francesco Sommese

MDPI

Basel • Beijing • Wuhan • Barcelona • Belgrade • Novi Sad • Cluj • Manchester

Guest Editors

Lidia Badarnah
School of Architecture
and Environment
University of the West
of England
Bristol
UK

Francesco Sommese
Department of Civil, Building
and Environmental Engineering
University of Naples Federico II
Naples
Italy

Editorial Office
MDPI AG
Grosspeteranlage 5
4052 Basel, Switzerland

This is a reprint of the Special Issue, published open access by the journal *Buildings* (ISSN 2075-5309), freely accessible at: https://www.mdpi.com/journal/buildings/special_issues/Q2L71DO8IV.

For citation purposes, cite each article independently as indicated on the article page online and as indicated below:

Lastname, A.A.; Lastname, B.B. Article Title. *Journal Name* **Year**, *Volume Number*, Page Range.

ISBN 978-3-7258-7208-4 (Hbk)
ISBN 978-3-7258-7209-1 (PDF)
https://doi.org/10.3390/books978-3-7258-7209-1

© 2026 by the authors. Articles in this reprint are Open Access and distributed under the Creative Commons Attribution (CC BY) license. The reprint as a whole is distributed by MDPI under the terms and conditions of the Creative Commons Attribution-NonCommercial-NoDerivs (CC BY-NC-ND) license (https://creativecommons.org/licenses/by-nc-nd/4.0/).

Contents

About the Editors . . . . . **vii**

Preface . . . . . **ix**

Grazia Massimino and Gaetano Sciuto
Is Sustainability Really Sustainable? A Critical Review
Reprinted from: *Buildings* **2025**, *15*, 2304, https://doi.org/10.3390/buildings15132304 . . . . . **1**

Francesco Sommese, Lorenzo Diana, Simona Colajanni, Marco Bellomo, Gaetano Sciuto and Grazia Lombardo
Towards a Regenerative and Climate-Resilient Built Environment: Greening Lessons from European Cities
Reprinted from: *Buildings* **2025**, *15*, 1878, https://doi.org/10.3390/buildings15111878 . . . . . **20**

Amir Dehghan Lotfabad, Seyed Morteza Hosseini, Paolo Dabove, Milad Heiranipour and Francesco Sommese
Impacts of Vertical Greenery on Outdoor Thermal Comfort and Carbon Emission Reduction at the Urban Scale in Turin, Italy
Reprinted from: *Buildings* **2025**, *15*, 450, https://doi.org/10.3390/buildings15030450 . . . . . **46**

Yeheng Zhou, Jiang Zhu, Eryu Ni and Yanzhe Hu
Evaluation and Optimization of Outdoor Thermal Comfort of Block-Style Commercial Complex in Hot Summer and Cold Winter Regions of China
Reprinted from: *Buildings* **2025**, *15*, 929, https://doi.org/10.3390/buildings15060929 . . . . . **77**

Waseem Iqbal, Irfan Ullah, Asif Hussain, Meeryoung Cho, Jongbin Park, Keonwoo Lee and Seoyong Shin
Optimizing Energy Efficiency: Louver Systems for Sustainable Building Design
Reprinted from: *Buildings* **2025**, *15*, 1183, https://doi.org/10.3390/buildings15071183 . . . . . **105**

Mohammed M. Gomaa, Amr Sayed Hassan Abdallah, Mohammed A. Aloshan and Ayman Ragab
A Comparative Analysis of Advanced Glazing Technologies for Energy-Efficient Buildings in Jeddah City, Saudi Arabia
Reprinted from: *Buildings* **2025**, *15*, 1477, https://doi.org/10.3390/buildings15091477 . . . . . **141**

Fataneh Farmani, Seyed Morteza Hosseini, Morteza Khalaji Assadi and Soroush Hassanzadeh
Computational Evaluation of a Biomimetic Kinetic Façade Inspired by the Venus Flytrap for Daylight and Glare Performance
Reprinted from: *Buildings* **2025**, *15*, 1853, https://doi.org/10.3390/buildings15111853 . . . . . **164**

Amr Sayed Hassan Abdallah, Uthman Abdullah Alamri, Randa Mohamed Ahmed Mahmoud and Mohamed Hssan Hassan Abdelhafez
Improvement of Vernacular Building Spaces for Human Thermal Comfort in Hot Arid Climate of Egypt
Reprinted from: *Buildings* **2025**, *15*, 4450, https://doi.org/10.3390/buildings15244450 . . . . . **193**

Alex G. Nwosu, Bello Mahmud Zailani and James G. Hunter
Housing-Performance Atlas of Baltimore Row Homes: Archetype-Based Multi-Hazard Baseline of Energy, Heat, Survivability, and Durability
Reprinted from: *Buildings* **2025**, *15*, 4405, https://doi.org/10.3390/buildings15244405 . . . . . **217**

Hamish Pope, Mark Carver and Jeff Armstrong
Low-Carbon Climate-Resilient Retrofit Pilot: Construction Report
Reprinted from: *Buildings* **2025**, *15*, 3666, https://doi.org/10.3390/buildings15203666 . . . . . **242**

Ahmed Hagras, Talpe Pandithawattage Anuradha Lasantha Piyasena, Amalka Nawarathna, Marianthi Leon, Ana Karina Silverio and Abhinesh Prabhakaran
Developing a BIM-Integrated Framework for Embodied Carbon Assessment in Developing Countries: A Systematic Review and Expert Validation Study for Sri Lanka
Reprinted from: *Buildings* **2026**, *16*, 814, https://doi.org/10.3390/buildings16040814 . . . . . **269**

About the Editors

Lidia Badarnah

Lidia Badarnah is a designer, educator, and researcher in architecture at the University of the West of England (UWE), specializing in biomimetics and environmental adaptation. Her work contributes to an emerging body of research that seeks to redefine environmental design in architecture through mimicking natural systems (i.e., biomimetics), changing approaches from conventional separated building systems to adaptive and integrated solutions and methods for enhanced sustainability and resilience in architecture. She has received prestigious fellowships and awards and has been invited to deliver talks and workshops worldwide on biomimetic approaches in architecture. Her research, widely published in leading journals, exploring behavioral and morphological patterns in organisms to develop innovative, adaptive solutions for buildings. She has led and co-led a portfolio of funded projects and served as a scientific committee member for international conferences. Additionally, she acts as an expert advisor and consultant on global initiatives, leveraging insights from nature to optimize technical solutions and energy management in building design

Francesco Sommese

Building engineer and PhD in Civil Systems Engineering, cum laude. Post-doctoral researcher in Building Engineering at the University of Naples Federico II. His research focuses on biomimetic and climate-adaptive strategies for building envelopes, greening strategies for the built environment as nature-based solutions, as well as regenerative design and advanced building technologies. He is a speaker at national and international conferences and co-supervisor of undergraduate theses. He has received awards for his research activity. He is the author of numerous articles published in international scientific journals, as well as author and editor of books, and reviewer for international journals. He is an adjunct lecturer in Architectural Technology at the Polytechnic and Basic Sciences School of the University of Naples Federico II.

Preface

Our planet is undergoing constant change, with increasingly frequent and severe climate events reshaping the conditions under which the built environment must operate. In response, the construction sector faces a profound and urgent transformation: traditional building methods, developed for a relatively stable climate, are now reaching their limits, and it has become imperative to rethink how we design, construct, and retrofit buildings—seeking innovative solutions capable of adapting to environmental fluctuations while reducing their impact on our ecosystem.

This Special Issue, 'Innovative Approaches to Climate-Responsive Building Design: Advancing Resilience and Sustainability in the Built Environment', was conceived precisely around these questions: How can we create buildings that effectively address the challenges of climate change? How can we enhance the resilience of the built environment against extreme events? What role can the construction industry play in combating climate change and reducing its carbon footprint? What are the latest innovations and future directions shaping the sector? Through the analysis of state-of-the-art practices, case studies, and innovative methodologies, the collected contributions aim to equip professionals and researchers with insights into solutions that address both present and future challenges, ultimately contributing to the development of sustainable cities and communities.

The Issue opens with a necessary critical reflection on the very concept of sustainability, questioning whether current practices truly live up to their promises, and contextualizing this debate within the broader ambition of transitioning towards regenerative built environments. Drawing on lessons from European cities, the contributions advocate for a paradigm shift that goes beyond mere mitigation, embracing climate resilience as a foundational design principle.

At the urban scale, the role of vegetation and green infrastructure emerges as a key lever for improving outdoor thermal comfort and reducing carbon emissions, as demonstrated by studies conducted in Turin and in climatic contexts as different as China's hot summer and cold winter regions. These contributions highlight how urban morphology and landscape design are inseparable from questions of human wellbeing and environmental performance.

Zooming into the building scale, a series of contributions investigates the performance of innovative envelope technologies—from louver systems and advanced glazing solutions to biomimetic kinetic façades inspired by natural organisms—demonstrating how computational design and simulation tools are increasingly central to optimizing energy efficiency, daylighting, and glare control. The exploration of vernacular architecture in hot arid climates further enriches this perspective, showing how traditional spatial strategies can still offer valuable lessons for contemporary climate-responsive design.

The final section of the Issue turns to the challenges of assessment, retrofit, and decarbonization. A multi-hazard performance atlas of Baltimore row homes provides a replicable archetype-based methodology for evaluating existing building stock, while a low-carbon retrofit pilot offers concrete construction-scale evidence of climate-resilient intervention strategies. Closing the collection, a BIM-integrated framework for embodied carbon assessment in developing countries underscores the importance of adapting digital tools to local contexts, ensuring that the transition to low-carbon construction is both globally relevant and locally applicable.

Taken together, these contributions reflect the richness and urgency of current research in climate-responsive design, spanning multiple scales, climates, and disciplines. They share a common conviction—one that aligns with the founding ambition of this Special Issue—that advancing resilience and sustainability in the built environment requires not only technological innovation, but also a deeper integration of environmental, social, and cultural dimensions. It is only through this broader, more holistic understanding that the construction sector can rise to meet the defining challenge of our time.

Lidia Badarnah and Francesco Sommese
Guest Editors

buildings

MDPI

Review

Is Sustainability Really Sustainable? A Critical Review

Grazia Massimino * and Gaetano Sciuto

Department of Civil Engineering and Architecture (DICAR), University of Catania, 95125 Catania, Italy; gsciuto@dau.unict.it

* Correspondence: grazia.massimino@phd.unict.it

Abstract: In recent years, the research and development of sustainable materials have seen a growing interest. The driving force behind this is environmental policies that aim towards a transition to a circular economy. There are numerous investigations into the potential use of waste and/or by-products in building materials and components. Using such materials, called "secondary raw materials", is to be favored due to their low environmental impact. Although research is numerous, most studies are limited to a purely performance assessment. There are still a few studies that also address environmental (or sometimes economic) aspects. Lacking such considerations, is it possible to say that the industrial product of research is truly sustainable? Is it enough to use secondary raw materials to define a product with a low environmental impact? By critically reviewing publications on this topic, this paper aims to highlight possible new developments for future research. Including environmental assessments among the criteria for evaluating the impact of research would provide a vision that is not limited only to the performance profile but can capture aspects that are currently underestimated. Overcoming this limitation would make it possible to obtain products capable of responding to the demands of sustainability regulations, avoiding the strategy of greenwashing.

Keywords: sustainable materials; environmental impact; by-product; secondary raw materials

1. Introduction

It is now widely recognized that the current production system is decidedly unsustainable. In particular, the construction sector is one of the most polluting industries. A report compiled by the Global Alliance for Building and Construction, presented at COP25 in Madrid [1], revealed that the construction sector is responsible for

- 38% of the amount of global carbon dioxide dispersed into the air;
- 35% of global energy consumption;
- 50% of raw materials extracted;
- 1/3 of global consumption of drinking water.

In addition, it produces a huge amount of waste of various kinds every year, the treatment and disposal of which generates, among other effects, a considerable waste of energy that is expected to increase by 70% by 2050 [2].

It is possible to mitigate the effects and risks of global warming by improving the energy efficiency of existing buildings and promoting and incentivizing the use of low-environmental-impact, natural, and recyclable materials.

Numerous studies [3,4] state that the operational phase of buildings is responsible for a significant percentage of life cycle environmental impacts, such as the use of energy

for maintaining indoor comfort or water consumption, which in traditional buildings can account for 60% to 90% of the Cumulative Energy Demand. The remaining consumption or emissions, excluding the end-of-life scenario of the building, are linked to indirect energy use, i.e., the energy associated with the production of the materials used in construction [5].

Alongside energy-saving regulations [6–8], there is a growing number of directives promoting a change in current production systems, with an aim toward sustainable development. In order to implement this change, economic, social, and environmental aspects must be taken into account [9,10].

One of the strategies followed in recent years has been the use of low environmental impact materials and the promotion of waste recycling. The use of processing waste is preferred, as it requires low energy input during the production and processing phases, with a consequent reduction in consumption and related polluting emissions. The use of by-products from other production chains can also be useful in achieving sustainability goals. Furthermore, exploiting these materials would have two advantages: transforming waste material into a resource, with a consequent reduction in the amount of waste to be disposed of, and reducing the quantity of raw materials extracted [11].

This paper analyses the state of the art regarding the use of by-products in the construction sector. A review of the scientific literature shows that most research on by-products and their possible use focuses only on performance assessments. Mechanical and physical characteristics are studied, but aspects related to environmental assessments of the entire life cycle of these products are rarely explored in depth, even though they are crucial for demonstrating the real sustainability of the material under consideration. Evaluating only physical or mechanical performance, even if it leads to improvements, is not sufficient to define the sustainability of a product. To do so, it is necessary to assess the environmental impact of the product, focusing on each stage of its production. Including environmental assessments among the criteria for evaluating the impact of research would provide a vision that is not limited only to the performance profile but can capture aspects that are currently underestimated. Overcoming this limitation would make it possible to obtain products capable of responding to the demands of sustainability regulations, avoiding the strategy of greenwashing.

2. Materials and Methods

This research is based on a critical review [12] of scientific literature on the use of by-products from various production chains in the construction industry.

After identifying the relevant legislation, we analyzed publications and research evaluating the benefits of using different types of by-products in the manufacture of construction products (Figure 1).

This scientometric analysis was conducted for subsequent refinements, modifying the keywords for the selection of results in order to obtain meaningful results. We started with a generic search using the keyword “by-product”. This was then combined with the keyword “Sustainability” and with the keyword “Life Cycle Assessment”. Finally, the string “by-product AND Sustainability AND Life Cycle Assessment” was used. From the databases obtained, a further survey of the results was carried out, selecting only articles dealing with topics related to the construction sector. The aim was to assess how many studies also focused on environmental issues, in addition to performance, and how many carried out an environmental assessment of the product.

Subsequently, the critical issues that emerged from the analysis were identified. These served as a starting point for suggesting implementations in the search for new products with low environmental impact.

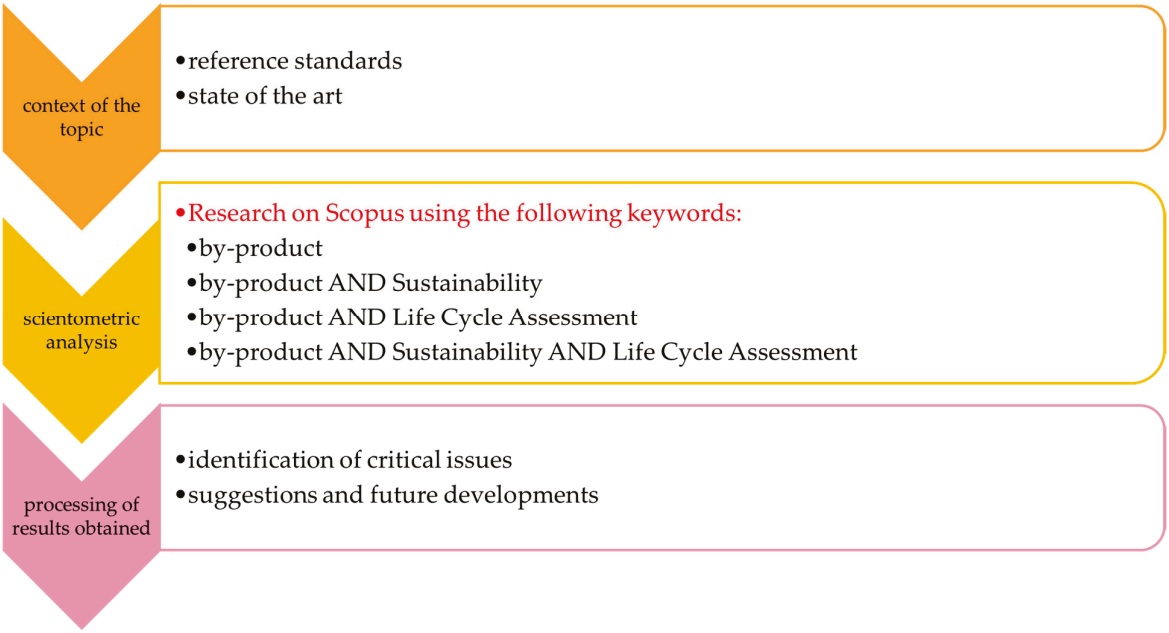


Figure 1. Methodology.

3. State of the Art

To mitigate the effects of climate change, research and development must be implemented in green materials and processes capable of combining innovation with the concepts promoted by the circular economy [13,14] and environmental policies [15]. The economic system, subject to innovative pressures, is evolving towards a circular approach that is not limited to energy efficiency alone but intervenes in a more systemic manner right from the design stage in order to reduce the use of resources and minimize waste production. It is therefore highly necessary to develop materials that are more environmentally friendly but, at the same time, capable of improving building performance.

The green economy, whose initial impetus came from the spread of renewable energy sources and energy efficiency, has also grown in recent years in the sectors of eco-friendly technologies and recycled materials. The reasons for this lie in the spread of stricter sustainability rules but also in greater awareness on the part of both users and producers.

In this transformation process, companies that produce materials and components for the building industry play a decisive role by innovating their range of construction products. The demand for these products, which combine low environmental impact and high performance, also comes from the building products market. This is an important sign of a paradigm shift: Companies are promoting change rather than just passively accepting it.

Giorgi [16] identifies three levels of circular economy applied to the construction sector: the macro level, concerning the scale of cities and urban agglomerations; the meso level, concerning the scale of buildings; and the micro level, focusing on the size of materials.

The micro level is mainly related to the scale of products and, in particular, to the management of resources and waste during production processes. Currently, research in this area is focusing on the composition of certain construction products, with an aim to replace virgin components, consisting of raw materials, with recycled components, such as secondary raw materials, scrap, or waste, including from other sectors.

By-products can be defined as "a substance or object resulting from a production process whose primary purpose is not the production of that article" [17].

Any substance generated by a production process that is not considered waste and could have a second life because it is not harmful to health or the environment is therefore classified as a by-product.

Italian legislation includes several decrees on this subject. Among the most important are the following:

- Decree No. 264 of 13 October 2016: regulation laying down indicative criteria to facilitate the demonstration of the requirements for the classification of production residues as by-products and not as waste, in which Article 2 provides definitions of product, production residue, and by-product [18]. In particular, a product is any material or substance that is deliberately obtained as part of a production process or as a result of a technical choice; production residue is any material or substance that is not deliberately produced in a production process and may or may not be waste; a by-product is a production residue that is not waste.
- Legislative Decree No. 152 of 2006, Article 184-bis, paragraph 1, specifies the requirements that a production process residue must meet in order to be considered a by-product rather than waste: "(a) 'the substance or object originates from a production process, of which it is an integral part and whose primary purpose is not the production of that substance or object'; (b) 'it is certain that the substance or object will be used in the same or a subsequent production or utilization process by the producer or a third party'; (c) 'the substance or object can be used directly without any further processing beyond normal industrial practice'; (d) 'the further use is legal, i.e., the substance or object meets, for the specific use, all relevant requirements relating to products and the protection of health and the environment and will not lead to overall adverse effects on the environment or human health' [19]".

The Decree does not contain either a list of materials that can undoubtedly be classified as by-products or a list of treatments permitted on them, as the assessment of compliance with the criteria indicated must in any case be left to a case-by-case analysis, as also specified in Article 1, paragraph 2, of Decree No. 264 of 13 October 2016.

There is extensive research into the potential use of carbon-neutral waste and/or by-products in construction materials and components. The use of secondary raw materials is to be preferred due to their low environmental impact. One possible use for by-products of various kinds and from various production chains is in the formulation of premixes.

A search in the Scopus database using the keyword "by-product" yields 5566 results, limiting the search to the field of engineering. Of these, only the first 250 results were analyzed in order of relevance. The number 250 was chosen in order to have a sample comparable to the results obtained from subsequent searches using the keywords sustainability and life cycle analysis. These 250 were further refined by reading, selecting only those relevant to the construction sector. Specifically, only 31 refer to the construction sector (Figure 2).

They were then classified and summarized in Figure 3 based on the origin of the by-products used in the categories "Agriculture," "Industry," and "Waste."

It is worth noting that most of the results focus on the use of industrial waste. The reason for this phenomenon could lie in the large volumes of waste produced by companies and their consistency due to production that is not affected by seasonality, as is the case with agriculture. Table 1 provides a summary of the studies reported in this section, which will be discussed in detail in the following sub-sections.

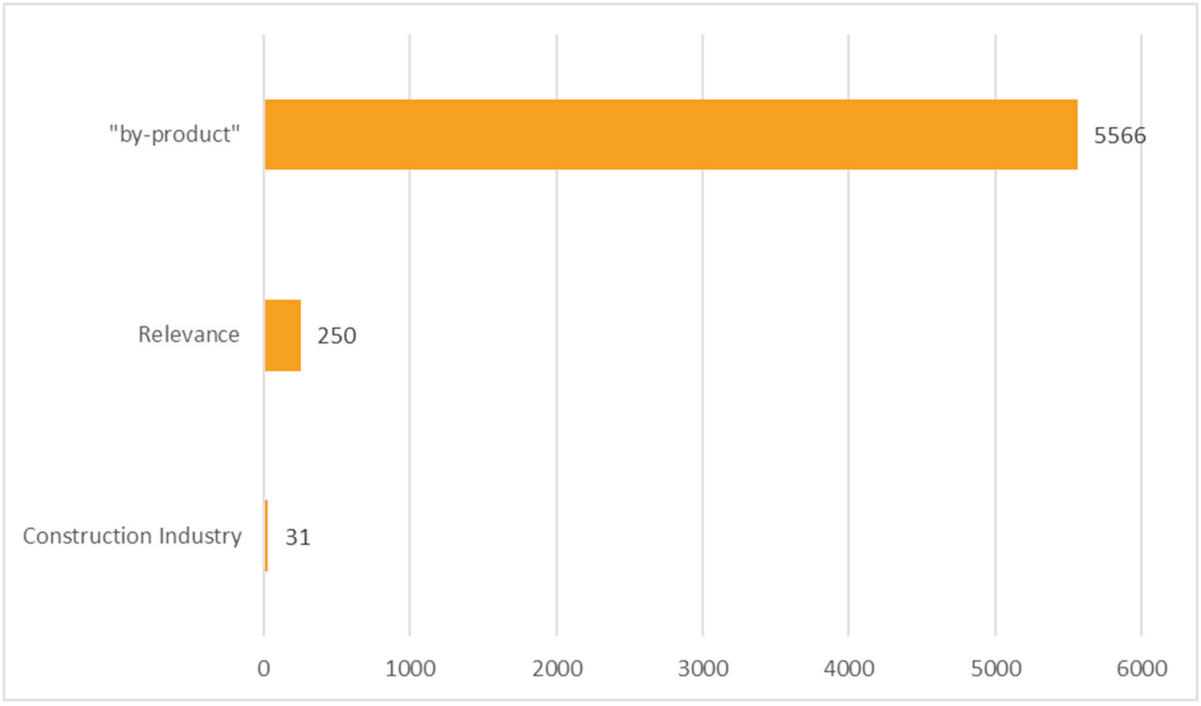


Figure 2. Schematic representation of the results obtained.

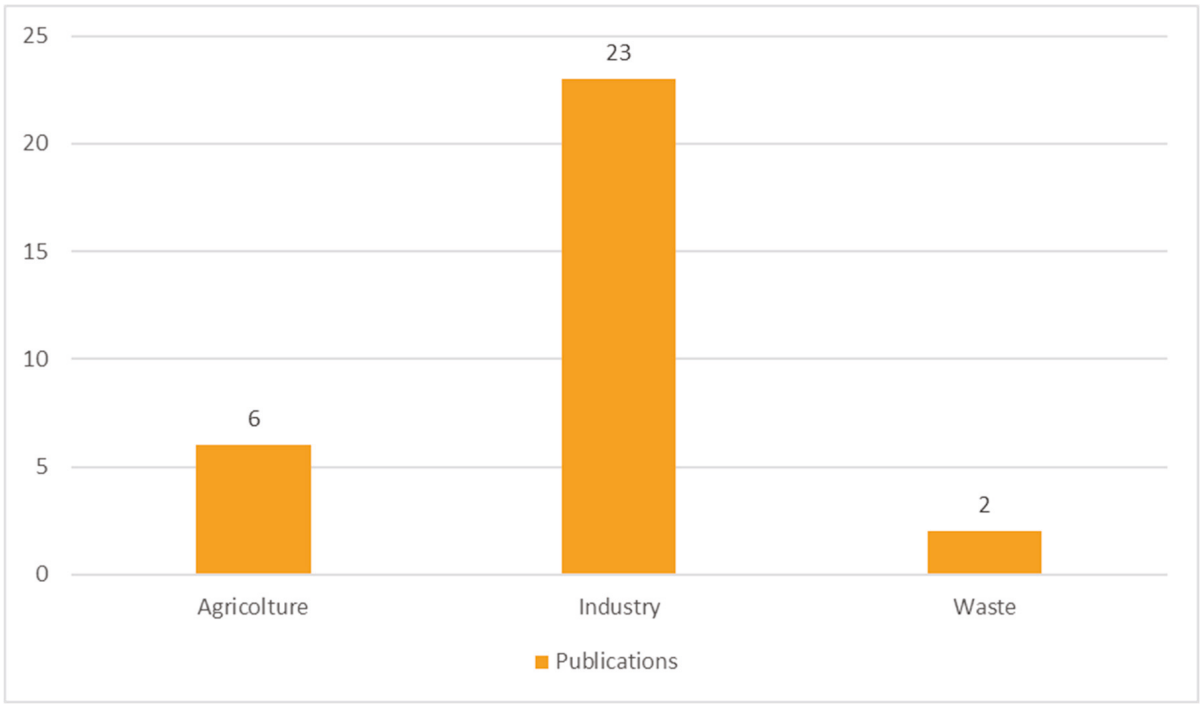


Figure 3. Classification of publications.

Table 1. Summary sheet of the studies reported in the "state of the art" session.

Authors	By-Product	Objective	Product	Results
Saeli et al. [20]	Spent coffee grounds	Demonstrate a possible alternative reuse of ground coffee waste in new eco-friendly building materials for thermal plaster applications in construction	Biocomposite mortars	Decrease in apparent density, decrease in mechanical properties, and decrease in thermal conductivity
Pintea et al. [21]	Casein, eggs, and rice gelatin	Evaluate the influence of organic polymers on the workability of fresh mortars	Mortar	Increased workability
Vitale et al. [22,23]	Citrus fruit paste	Evaluate the use of agricultural by-products for the production of thermal insulation products for building envelopes	Insulating panels	Good thermal insulation
Liuzzi et al. [24]	Leaves and twigs from pruning olive trees	Using agricultural waste materials in a mixture of clay and sand to obtain a bio-based plaster to study its hygrothermal behavior	Clay plasters	Linear reduction in density and an increase in porosity, reduction in thermal conductivity, and good capacity to exchange moisture with the surrounding environment
Schackow et al. [25]	Fired clay brick waste	Study of the effect on the durability of mortars with partial replacement (10, 25, and 40% by weight) of Portland cement with CBW	Mortar	Improved strength and density
Kumar et al. [26]	Marble processing waste	Examine the experimental results of self-compacting concrete (SCC) with marble waste as a partial replacement for fine aggregates and polypropylene fibers as an additive material	Self-compacting concrete	Increased resistance to bending and compression
Vaclavik et al. [27]	Ladle slag	Determine the optimal proportion of treated ladle slag additive and evaluate the environmental properties of the resulting cement composites	Concrete	Better workability of fresh cement paste, extended setting times, and increased water absorption of cement composites

Table 1. *Cont.*

Authors	By-Product	Objective	Product	Results
Bayat et al. [28]	Blast furnace slag and natural zeolite	Verify the possibility of using industrial and natural supplementary cementitious materials (SCM) in self-compacting concrete	Self-compacting concrete	Better water impermeability, electrical resistivity, and resistance to chloride migration
Vembu et al. [29]	Magnesite mine waste	Evaluate the suitability of using magnesite mining waste in self-compacting concrete (SCC) as a substitute for binders and aggregates, assessing fresh and hardened properties	Self-compacting concrete	Increased compressive strength
Da Silva et al. [30]	Two types of PET aggregates, PP and PF aggregates (which stand for plastic pellets and plastic flakes)	Study the effects of incorporating plastic waste into mortars	Mortar	Decrease in elasticity modulus, increase in impact resistance, and gain in water vapor permeability, preventing moisture condensation
Pedreño-Rojas et al. [31]	Biomass waste ash	Exploring the potential of using biomass ash waste as a secondary raw material for building composites	Gypsum-based composites (slabs)	Improvement of the building's energy efficiency

3.1. Agricultural Sector

When analyzing the agri-food supply chain, one of the most studied wastes is coffee powder, with applications ranging from its use in premixes to the construction of entire buildings. The study conducted by Saeli et al. [20] focused on the use of coffee waste, with percentages of up to 17.5%, to evaluate the engineering performance of the biocomposite mortars produced. The results show that a small amount of coffee waste can determine

- A decrease of up to 15.4% in apparent density (making the products comparable to a lightweight structural aggregate or lightweight plaster mortar);
- A sharp drop in mechanical performance (while still maintaining acceptable values for the plastering application considered) and in thermal conductivity (up to 47%).

The study was not limited to investigating physical performance alone but was implemented with a multi-criteria analysis, also considering aspects related to environmental and economic impact, with the result that the mix with the best results is that containing 10% waste.

Moving up the building ladder, the start-up Woodpecker, based in Bogota, Colombia, uses coffee husks to produce lightweight prefabricated buildings for residential and educational use. By combining coffee husks with recycled plastic, it is possible to create a more durable and environmentally friendly material [32]. This special composite wood-plastic material has some very interesting performance characteristics: It is self-extinguishing, pest-resistant, and moisture-resistant, making it a safe alternative for low-income hous-

ing. The system consists of standardized plastic parts that snap into a steel frame for easy installation.

The use of waste from coffee plantations not only reduces landfill but also allows for rapid construction that can be carried out by non-professional laborers.

Numerous studies have investigated the use of casein in premix formulations. Among these, an interesting study was conducted by Pintea et al. [21] on the influence of natural organic polymers on the workability of fresh mortar. In this study, the natural organic polymers used were casein, eggs, and rice, used in the form of gelatin. The addition of the three polymers resulted in an increase in workability of at least 30–45 min. Specifically, the addition of casein to plaster mortar increases workability by up to over an hour.

The use of casein has not been limited to experimental applications but has also entered the commercial market. Notable examples include the Harobau company, based in Laghetti, near Bolzano, Italy, which produces a 100% natural plaster with high dehumidifying, breathable, and waterproofing properties [33,34]. It is not the only company that has invested in the use of casein in its products. The start-up Milk Brick recovers waste milk from the dairy industry and large-scale distribution, transforming it into a new secondary raw material for use in the production of zero water impact concrete products for the construction industry [35].

Continuing the investigation, we find applications centered on citrus processing waste. Its use ranges from interior design [36] to paper [37], cosmetics [38], and leather [39]. The project developed by Vitale et al. [22,23] involved the creation of self-supporting panels obtained from the processing of orange processing waste, known as pastazzo. This mixture, composed of the outer part of the peel, the white inner part, and the seeds and pulp residues left over after the citrus fruit has been squeezed, has excellent properties that are necessary for the panel. Due to its intrinsic characteristics, the product is able to "self-bond" without the addition of chemical additives, which are often polluting or hazardous to health. In addition, the panel has excellent thermal insulation properties, in line with building products currently on the market and, in some cases, being even better. Its good properties allow it to be used in construction as a thermal and acoustic insulation panel for the external walls of buildings. Aesthetically, the panel is similar to cork, making it suitable for use as wall cladding or ceiling panels, as well as in the furniture and design sectors. The project is a concrete example of the circular economy, using a resource that is widely available in Sicily (Italy).

Remaining on the subject of waste from the agri-food chain, the study by Liuzzi et al. [24] analyzes the properties of clay plasters in which leaves and twigs from olive tree pruning have been incorporated. Soil samples with different percentages of olive fibers were prepared and tested to investigate their hygrothermal behavior. The results show that the addition of olive fibers to the soil matrix led to a linear reduction in density and an increase in porosity. This leads to a reduction in thermal conductivity and therefore a more insulating behavior of the material. The experimental tests also made it possible to characterize the hygrometric properties of the materials, which are in agreement with those of other bio-based plasters of similar density. The addition of olive fibers does not produce significant differences in the absorption curves up to 80% relative humidity. Increasing this value beyond 80%, the absorbed moisture content increased, especially for samples with a higher fiber content (C08, C012). The results in terms of ideal moisture absorption value show that all mixtures allow for a plaster with good moisture exchange capacity with the surrounding environment, ensuring good indoor air quality and greater comfort for occupants.

3.2. Industrial Sector

Moving on to the industrial sector, there are even more examples. The study conducted by Schackow et al. [25] analyzes the influence of adding fired clay brick waste to mortars on their durability. The idea came from the similarity between the characteristics of metakaolin, whose properties are already well known, and powdered fired clay brick waste (CBW). The powder was added as a partial replacement for Portland cement at percentages of 10, 25, and 40%. Hardened mortars containing CBW showed improved strength and density as a result of pore filling. Mortar without CBW, which was more porous, showed greater diffusion and greater resistance to sulfates and chloride absorption capacity. The optimal performance was found for mortar with 40% by weight CBW, whose compressive strength can be up to 130% higher than that of mortar without CBW. The properties studied suggest that a moderate addition of CBW (up to 10% by weight) is desirable to achieve comparable workability. Higher percentages require additional measures to control the workability of fresh mortars, achieving a level comparable to that of CBW-free mortar.

Other studies focus on the use of marble processing waste as a partial replacement for fine aggregates. This is the case of Kumar et al. [26], who examine its use, together with polypropylene fibers as an additive, in self-compacting concrete. Upon analyzing three mixtures, with a replacement of 20%, 30%, and 40% in natural fine aggregates and polypropylene fiber with a constant ratio of 0.4%, an increase in flexural and tensile strength was observed compared to the conventional mixture. Furthermore,

- Compressive strength increased with the replacement of 20% of marble waste and then decreased after several mixtures. Furthermore, compared to the control mixture, the compressive strength values of other portions of the mixture increased and became acceptable.
- Generally, fiber content increases the flexural and tensile strength of concrete. Compared to the control mixture, the test values of all other mixtures increased.
- Marble waste replaced up to 40% showed acceptable results for fresh concrete and also showed an increase in flexural and tensile strength. Therefore, replacing the fine aggregate with 40% marble waste together with the fiber additive is considered an optimal percentage.

A particular type of by-product that has been the subject of numerous studies is ladle slag [40–42]. Research conducted by Vaclavik et al. [27] investigated its use as a substitute for cement in the manufacture of cement products. The aim of the research was to determine the optimum proportion of additive based on the treated ladle slag and to evaluate the environmental properties of the resulting cement composites. Treated ladle slag, as a mixture, was examined together with four types of cement (CEM I, CEM II, CEM III, and CEM V). The results of the research revealed that the incorporation of coarse slag improved the workability of fresh cement paste in all the formulations tested. Furthermore, the use of treated ladle slag as a mixture in the cement paste (replacing cement) extends the setting times of all the designed recipes and slightly increases the water absorption of the cement composites, especially in the case of fine slag.

Bayat et al. [28] investigated the use of blast furnace slag and natural zeolite for the production of self-compacting concrete. The aim was to verify the possibility of using industrial and natural supplementary cementitious materials in self-compacting concrete with low embedded carbon content. Binary and ternary mixtures of ground granulated blast furnace slag (GGBFS) and natural zeolite (NZ) were used at higher replacement intervals up to 50% by weight of Portland cement (PC). The use of GGBFS and NZ has a positive synergistic effect, resulting in improved water impermeability, electrical resistivity,

and chloride migration resistance compared to binary mixtures of GGBFS + PC or NZ + PC.

3.3. Waste

A "green" self-compacting concrete was also the subject of attention by Vembu et al. [29], who focused on analyzing the effects of using magnesite mine waste instead of cement (binary and ternary mixtures) and also as aggregates (fine and coarse) in self-compacting concrete (SCC). By evaluating the fresh properties and compressive strength, an increase in compressive strength was observed due to the irregular angular shape of the coarse mine waste aggregates, which creates internal friction and bonding between the aggregates. The density of SCC with binary and ternary mixed cement decreased slightly when mining waste was added. Conversely, the density increased slightly when mining waste was replaced with aggregates.

Plastics are used in the study by Da Silva et al. [30], which considers plastic waste to study the effects of its incorporation into mortars. The results of tests conducted on three mixtures with three replacement ratios, by volume, of natural aggregate (5%, 10%, and 15%) with plastic are reported. The waste examined was two types of PET aggregates, PP and PF aggregates (which stand for plastic pellets and plastic flakes). The results show that, although the incorporation of plastic aggregates led to poorer performance in some properties, such as bulk density and compressive and flexural strength, in others, the modified mortars showed significantly better performance than the control mortar (without plastic).

The improved performance highlighted concerns about the decrease in the elastic modulus and the increase in impact resistance, leading to a more deformable mortar with a greater capacity to absorb impact energy. In addition, the impact resistance test also showed a reduction in crack width as the replacement ratio increased.

The results obtained from the dimensional stability test show a decrease in shrinkage as the plastic ratio increases. Lower shrinkage results may allow for a reduction in cracks associated with dimensional variations.

In terms of water absorption, modified mortars perform worse than conventional mortars. The difference in the shape of PET aggregates causes variations in porosity and therefore an increase in capillary absorption, resulting in improved water vapor permeability and preventing moisture condensation inside buildings.

The results of the current study have been quite encouraging and have paved the way for the recycling of PET waste aggregates in mortars.

Finally, among the studies that use production waste, we can mention Pedreño-Rojas et al. [31], who explored the potential use of biomass ash waste generated by a thermoelectric power plant as a secondary raw material for building composites. The study examines the physical and mechanical properties of gypsum-based composites containing different proportions of biomass ash waste, comparing them with reference and regulatory documents. Based on preliminary test results, the best composite was the sample containing 25% waste. Gypsum boards were made from this sample, leading to an improvement in the building's energy efficiency (up to 5%).

4. Environmental Assessment

In recent years, the use of waste from production chains other than construction has been a recurring theme in scientific studies and research. This interest is driven by various regulations [43–45] which, in order to reduce the environmental impact of the construction sector, increasingly promote the use of circular production systems. Companies are increas-

ingly interested in conducting environmental analyses of their products in order to qualify as "green" companies. The market for high environmental quality products and services is certainly a rapidly expanding market, especially in the last decade.

In order to inform users about the environmental characteristics of products, communication tools known as environmental certifications have been standardized. These are voluntary attestations that highlight compliance with certain environmental and ethical parameters. They can refer to both the product and the process, depending on whether the object of the verification is a management system rather than a product or service. Compliance with certain regulations is assessed by an accredited external body that verifies the application of the standard.

These labels stem from companies' desire to improve their image or optimize their processes. They are established by ISO 14020 [46], which sets out the guiding principles for the development and use of environmental labels and declarations. They are divided into

- Type I environmental labels—ISO 14024: voluntary certifications based on a multicriteria system that considers the entire product life cycle, subject to external authentication by an independent body. These include, for example, the European ECOLABEL ecological quality mark. They are regulated by UNI EN ISO 14024:2018 [47], which establishes the principles and procedures for the development of labeling programs.
- Type II environmental self-declarations—ISO 14021: labels bearing environmental self-declarations by manufacturers, importers, or distributors of products, without the involvement of an independent certification body (including: "Recyclable," "Compostable," etc.). The UNI EN ISO 14021:2016 standard [48] specifies the requirements, including declarations, symbols, and graphics relating to products. It also describes specific assessment, specific evaluation, and verification methods for the claims selected in this international standard.
- ISO Type III Environmental Product Declarations—ISO 14025: These contain statements based on established parameters and quantify the environmental impacts associated with the product's life cycle, calculated through an LCA assessment. They are independently verified and presented in a clear and comparable format. These include, for example, "Environmental Product Declarations." The UNI EN ISO 14025:2010 [49] standard establishes the principles and specifies the procedures for the development of Type III environmental declarations and corresponding programs. It also establishes the principles relating to the use of environmental information in addition to those provided by UNI EN ISO 14020.

Life cycle assessment (LCA) is a structured and internationally standardized method, defined by ISO 14040:2021 and ISO 14044:2021 [50,51], which allows the quantification of the potential impacts on the environment and human health associated with a good or service, starting from its resource consumption and emissions. In its traditional conception, it considers the entire life cycle of the system under analysis, from the acquisition of raw materials to end-of-life management, including the manufacturing, distribution, and use phases (an approach known as "cradle to grave"). It is often used as a decision-making tool to provide an effective and efficient contribution to the greater sustainability of goods and services.

Life cycle assessment is an iterative process comprising four main stages [52]:

- Definition of the objective and scope;
- Inventory analysis (LCI, Life Cycle Inventory);
- Impact assessment (LCIA, Life Cycle Impact Assessment);
- Interpretation.

The European Commission introduced the concept of LCA into sustainability policies a long time ago, with COM 302 (2003) [53], specifying that it is the best available methodology for assessing the potential environmental impacts of products. The calculation method, described in technical standards EN 15804 (construction products) [54] and EN 15978 (buildings) [55], is the specific LCA methodology for the construction sector and is referred to in the document in the award criteria relating to "Methodologies for optimizing design solutions for sustainability."

5. Discussion

Several studies support the use of by-products in the formulation of premixes as a positive contribution to the environmental footprint of the finished product, reducing the environmental impact associated with the extraction phase. They reiterate the importance of using raw materials with low environmental impact, a characteristic that can be broken down into several factors: origin, location, and subsequent transport and processing.

To further refine this review and also take environmental parameters into account, the search of the Scopus database using the keyword "by-product," which had yielded 5566 results, was repeated and refined, limiting the search to the field of engineering, using the following strings in succession:

- "By-product AND Sustainability";
- "By-product AND Life Cycle Assessment".

The string "By-product AND Sustainability" yielded 208 studies, while the string "By-product AND Life Cycle Assessment" yielded just under 78. Further research was carried out, combining all three keywords ("By-product AND Sustainability AND Life Cycle Assessment"). This led to a significantly lower number of results, 37 in total (Figure 4).

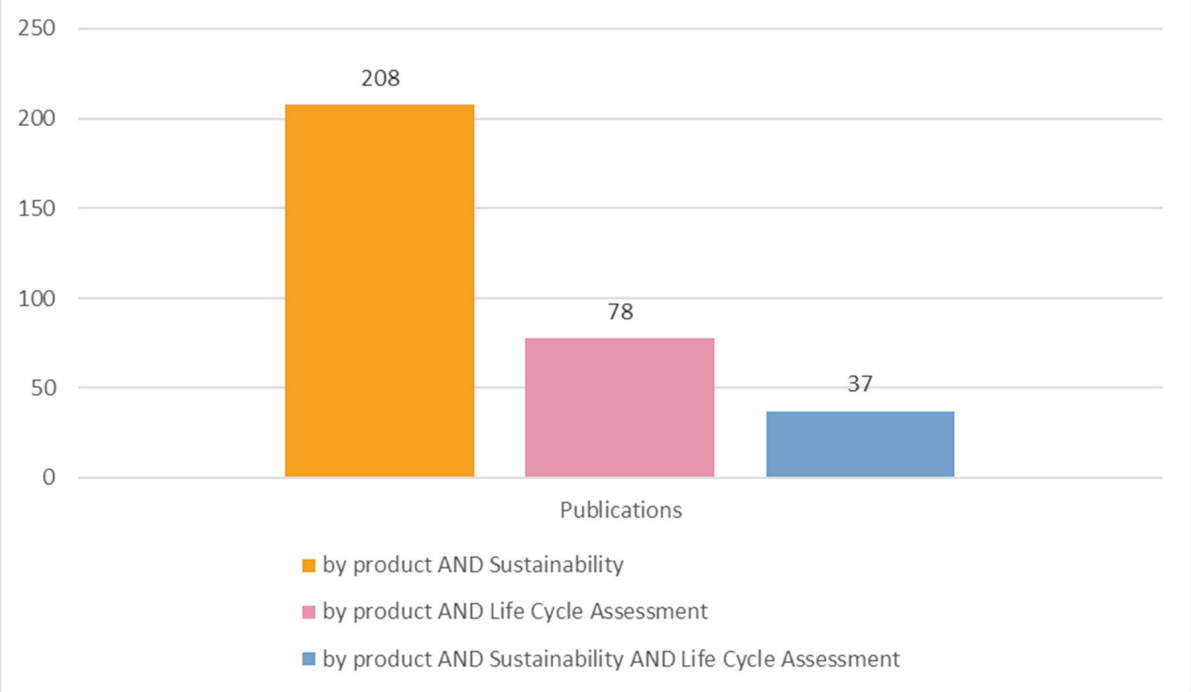


Figure 4. Classification of publications sorted by different strings.

All the results were refined by reading, selecting only studies relevant to the construction sector, arriving at 72 for the first search, 26 for the second, and only 6 for the third.

They were then categorized and summarized in Figure 5 according to the origin of the by-products used in the categories "Agriculture," "Industry," and "Waste."

Analysis of the data obtained from the research carried out shows that studies on the use of by-products in the construction sector that focus on environmental performance assessment are very limited.

In particular, analysis of the database obtained shows that LCA is used in other engineering sectors but less so in the construction sector. According to Löfgren et al. [56], LCA is an important method in modern environmental management in industry. Understanding which stages have the greatest impact is the starting point for improving the product and its production process.

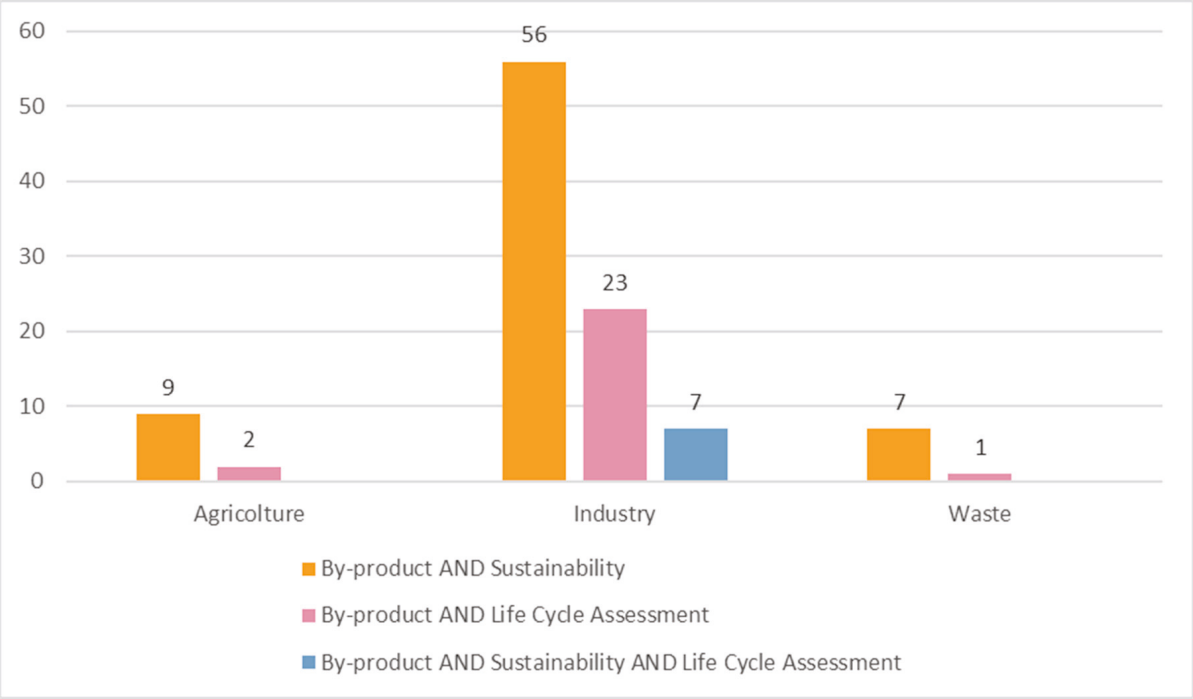


Figure 5. Histogram of refined results by keywords.

As can be seen, not all studies on building product formulations incorporating by-products are accompanied by a study on sustainability and environmental impact. In the absence of such assessments and related considerations, it is not possible to state with certainty that the environmental footprint of the product is reduced through the use of natural by-products. This is confirmed by the results of a study carried out by Carbonaro et al. [57,58], which, thanks to an LCA assessment, showed that a premixed plaster containing EPS had a lower environmental impact than other mixtures based on natural materials. This study analyzed the environmental effects of thermal plasters obtained using waste materials from local industrial and agricultural processes. The materials used were corn cobs, granular cork obtained from recycled bottle caps, and straw fiber. The mixtures analyzed were

- Cork_001: natural hydraulic lime (NHL), granular corn cobs, expanded perlite, zeolite, and additives;
- Bioart Cork: natural hydraulic lime (NHL), wheat straw granules, cork granules from bottle caps, and cellulose flakes;

- VGT_001: natural hydraulic lime (NHL), zeolite, expanded vermiculite, expanded perlite, and corn cob granules;
- VGT_014: natural hydraulic lime (NHL), Portland cement, sulfoaluminate cement, expanded perlite, corn cob granules, and wheat straw granules.

These were compared with two commercial plasters:

- Thermal plaster: natural hydraulic lime (NHL), Portland cement, EPS, and additives;
- Thermolime: natural hydraulic lime (NHL), Portland cement, expanded perlite, and additives;

used as benchmarks. At the same time, an experimental characterization of the thermal properties was carried out.

The LCA study is divided into three progressive phases: analysis of raw materials to support the formulation phase, comparison between prototypes and benchmarks, and assessment of embodied energy, also considering the effect of the installation phase. The system boundary, covering cradle-to-gate, includes all processes, from raw material extraction to transport, to production and packaging plant processes.

From the comparative study of raw materials, VGT_001 has a much higher impact than VGT_014 due to the presence of zeolite. The LCA analysis shows that the emissions related to thermal plaster with EPS, Thermolime, Bioart cork, and VGT_014 are almost comparable. The technological characteristics during application were also evaluated, comparing the quantities of each plaster required for the same surface area (1 m^2) and thickness (4 cm). This gives the "best" score to thermal plaster with a required quantity of 8.6 kg, about half that of the other plasters. An analysis of the raw material alone would have led to the exclusion of EPS from the mixture, as its optimal thermal properties and low density were not taken into account. Thanks to these characteristics, in relation to the energy incorporated, it is precisely the thermal plaster that has the lowest impact. It can be deduced that a product which, taken individually, does not have a good ecological footprint, can still achieve good environmental performance when combined with other products.

When using by-products from other supply chains, it is important to understand whether they need to be processed before they can be used in another sector. The study conducted by Pedreño-Rojas et al. [59] addressed the influence of the heating process on the reuse of gypsum waste in plasters. Gypsum, thanks to its chemical composition, which maintains its characteristics even after treatment, can be considered a completely and eternally recyclable material. Until now, most plants using gypsum waste have subjected the material to a preventive heating process, resulting in significant energy consumption and a reduction in the environmental benefits of recycling. In the first phase of the study, two different types of gypsum waste were analyzed: gypsum waste from industrial plasterboard production (GPW, gypsum waste from industrial plasterboard production) and gypsum obtained from flue gas desulfurization (FGD, Flue Gas Desulfurization Gypsum) in a central heating plant. Tests were carried out on samples containing both types of gypsum waste, heated and unheated. Since the mechanical performance of FGD-based plasters was not satisfactory, it was decided to conduct the environmental analysis only on plasters containing plasterboard waste. The categories evaluated were embodied energy and global warming potential, following the methodology described by García Martinez [60]. The data used were obtained from the Ecoinvent 3 and ITEC databases for the year 2018. The functional unit considered was the amount of raw material needed to produce 1 cubic meter of each plaster. The system boundaries included three phases: the production phase, the transport phase, and finally, the disposal phase. On the other hand, the demolition and disposal phases were neglected. The data analysis showed that the highest energy

consumption corresponds to the production phase, but the transport phase also had a significant influence on the analysis. The lowest impacts were obtained for GPW100WH plaster (wt. 100% GPW Without Heating), where a 77% reduction was found compared to the reference material. In general, the energy consumption related to the production phase decreases as the content of GPW added to the mixture increases. Finally, when comparing the different heating processes, the greatest environmental impact was attributed to plaster heated for 24 h at 100 °C. Regarding global warming potential, the results show the same trend: The lowest impacts were recorded for GPW100WH plaster, with a reduction of 83% compared to the reference material. Consumption during production decreases as the amount of GPW added to the mixture increases. Again, the greatest environmental impact is that of plaster heated for 24 h at 100 °C. The LCA analysis therefore shows that adding GPW to the mixtures reduced the environmental impact of the product, with the best results obtained for plasters containing 100% GPW without any heating process.

Finally, the study conducted by Melià et al. [61] demonstrated how the location and subsequent transport of raw materials influence the final impact of the product. Two different types of earth plaster were compared: a base plaster and a finishing plaster. In particular, two different colors were analyzed from among those available, yellow and ocher. This difference was fundamental in assessing the influence of transport: The ocher clay comes from local suppliers (based in Piedmont and northern Italy), while the yellow clay is imported from Germany. The gravel, clay, and straw used to produce the base plaster come from the same province where the manufacturing company is located (approximately 60, 14, and 24 km for the three components, respectively); the sand used for the finishing plasters comes from central Italy (approximately 550 km), while the ochre clay comes from northern Italy (approximately 250 km) and the yellow clay from Germany (approximately 530 km). The study shows that transport accounts for 67% of the energy required to produce ochre-colored finishing plaster, while in the case of yellow finishing plaster, it reaches 74%.

This shows that distance is an important factor to consider, as long distances between suppliers of by-products and the companies that will use them cancel out the beneficial effect of using secondary raw materials.

6. Conclusions

This study examined the scientific literature on the use of products in line with the principles of sustainability and the circular economy. In particular, attention was focused on the use of by-products from different production chains in the construction sector and on the assessment of their environmental impact. A search of the Scopus database using the keyword “by-product” and limiting the search to the engineering sector identified more than 5000 studies. The search was then refined by adding the keyword “sustainability” to “by-product”, yielding approximately 210 results, and finally by using the string “by-product AND life cycle assessment”, which identified just under 80 publications. It is clear that the number of studies analyzing environmental aspects is very limited, despite widespread research in the field. In order to estimate the real degree of sustainability of a building product that also incorporates by-products or secondary raw materials among its components, it is therefore desirable to also focus on environmental assessments.

As shown in Figure 6, the ideal development of a new product should be based on the evaluation of the by-product to be incorporated and the characterization of the product in terms of performance. These two evaluations will converge and constitute the overall evaluation of the product. Only if both evaluations meet the necessary requirements can the research be considered complete. Otherwise, it will be necessary to repeat one of the two initial steps: change the by-product or modify the formulations adopted. The

same evaluation system should also be adopted by certification bodies, thus extending certification to the entire process.

A building product, even if developed through innovative research and with attention to environmental needs, can only be defined as truly eco-sustainable if we do not stop at quantifying the benefits that can be obtained from its use during the operational phase, which almost always concerns the evaluation of physical and/or mechanical performance. A more comprehensive assessment is needed, covering its entire life cycle. Evaluating only physical or mechanical performance, even if it leads to improvements, is not sufficient to define the sustainability of a product. To do so, it is necessary to assess the environmental impact of the product, focusing on each stage of its production. Considering the different stages, from the procurement of raw materials to the disposal of manufactured products, would lead to a methodological approach capable of providing real data on the eco-compatibility of the product. As seen from the examples given in this paper, it is not enough to replace any raw material with a by-product or secondary raw material in order to be certain of environmental benefits. It is important to consider aspects that are sometimes considered secondary, such as transport and/or any processing required before its possible use. The impact of these stages can undermine the benefits of using a by-product or secondary raw material, even if it comes from other production sectors. From this point of view, for example, promoting the use of locally available resources is certainly one of the measures that can be taken to reduce transport-related emissions.

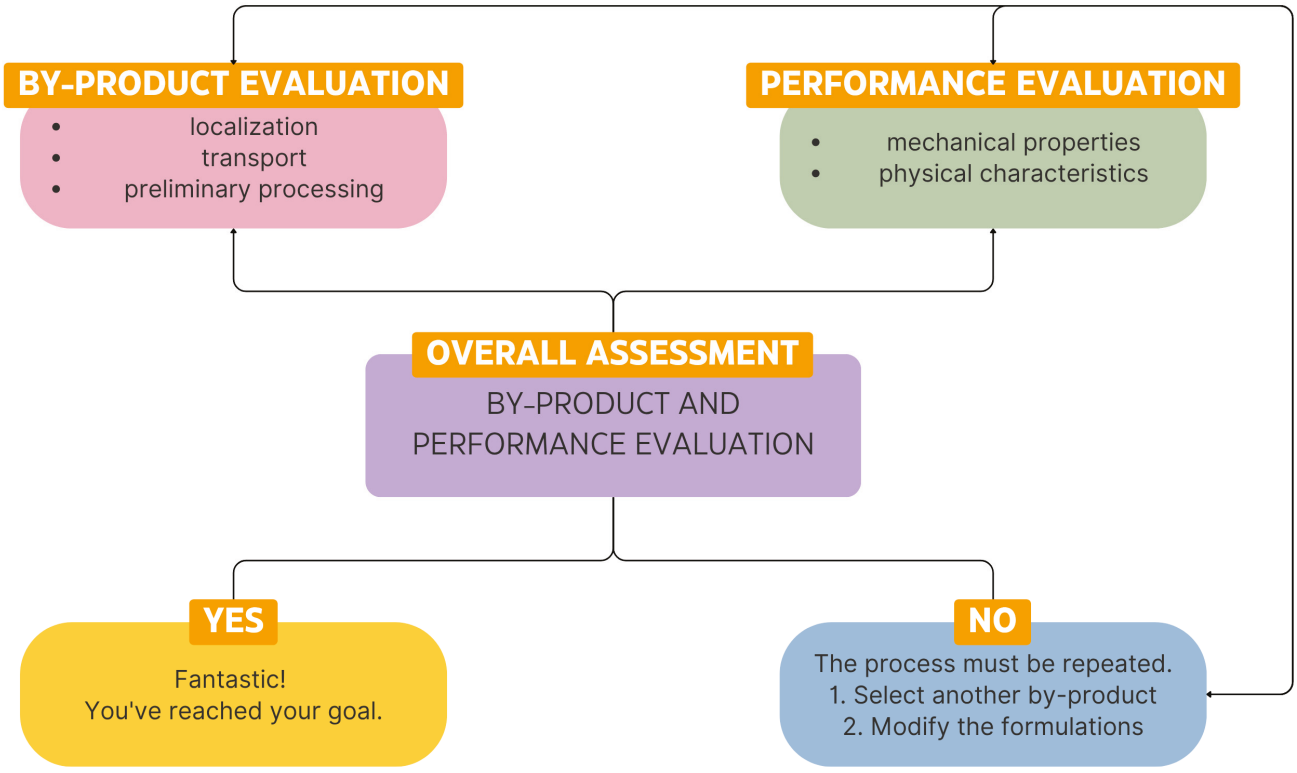


Figure 6. Diagram of the proposed methodology.

Only through an assessment covering the entire life cycle of an alternative building material to those commonly used (which, for example, incorporates by-products or secondary raw materials) will it be possible to obtain a comprehensive view of the impacts generated by the entire system, obtain an effective assessment of its sustainability, and limit the strategy of greenwashing.

Author Contributions: Conceptualization, G.M. and G.S.; methodology, G.M. and G.S.; data curation, G.M.; writing—original draft preparation, G.M.; writing—review and editing, G.M. and G.S.; visualization, G.M.; supervision, G.S.; project administration, G.M. and G.S. All authors have read and agreed to the published version of the manuscript.

Funding: This research was funded by the University of Catania under the "Nature-based materials and components to improve the energy performance of buildings" Departmental Project.

Conflicts of Interest: The authors declare no conflicts of interest.

References

1. United Nations Environment Programme. *Global Status Report for Buildings and Construction: Towards Zero Emissions, Efficient and Resilient Buildings and Construction Sector*; United Nations Environment Programme: Nairobi, Kenya, 2020.
2. Kaza, S.; Yao, L.C.; Bhada-Tata, P.; Van Woerden, F. *What a Waste 2.0: A Global Snapshot of Solid Waste Management to 2050*; World Bank: Washington, DC, USA, 2018. Available online: https://openknowledge.worldbank.org/handle/10986/30317 (accessed on 10 January 2025).
3. Karimpour, M.; Belusko, M.; Xing, K.; Bruno, F. Minimising the Life Cycle Energy of Buildings: Review and Analysis. *Build. Environ.* **2014**, *73*, 106–114. [CrossRef]
4. Ramesh, T.; Prakash, R.; Shukla, K.K. Life Cycle Energy Analysis of Buildings: An Overview. *Energy Build.* **2010**, *42*, 1592–1600. [CrossRef]
5. Lavagna, M. *LCA in Edilizia. Ambiti Applicativi e Orientamenti Futuri della Metodologia Life Cycle Assessment nel Settore delle Costruzioni*; Maggioli editore S.p.A.: Sant'Arcangelo di Romagna, Italy, 2022; p. 27.
6. European Parliament; Council of the European Union. *Directive 2002/91/EC of the European Parliament and of the Council on the Energy Performance of Buildings (16/12/2002)*; Publications Office of the European Union: Luxembourg, 2003.
7. European Parliament; Council of the European Union. *Directive 2010/31/EU of the European Parliament and of the Council on the Energy Performance of Buildings (L 153/13 of 18 June 2010)*; Publications Office of the European Union: Luxembourg, 2010.
8. European Parliament; Council of the European Union. *Directive 2012/27/EU of the European Parliament and of the Council on Energy Efficiency, (25 October 2012), Amending Directives 2009/125/EC and 2010/30/EU and Repealing Directives 2004/8/EC and 2006/32/EC*; Publications Office of the European Union: Luxembourg, 2012.
9. National Sustainable Development Strategy (NSDS). Available online: https://www.mase.gov.it/sites/default/files/archivio/allegati/sviluppo_sostenibile/SNSvS/SNSvS22_aggiornata_completa.pdf (accessed on 12 January 2025).
10. *Law No. 221 of 28 December 2015 on Provisions on Environmental Matters to Promote Green Economy Measures and to Curb Excessive Use of Natural Resources*; Istituto Poligrafico e Zecca dello Stato: Rome, Italy, 2015.
11. European Parliament. Available online: https://www.europarl.europa.eu/topics/it/article/20151201STO05603/economia-circolare-definizione-importanza-e-vantaggi (accessed on 10 February 2025).
12. Grant, M.J.; Booth, A. A typology of reviews: An analysis of 14 review types and associated methodologies. *Health Inf. Libr. J.* **2009**, *26*, 91–108. [CrossRef] [PubMed]
13. European Commission. *COM(2020) 98, Communication from the Commission to the European Parliament, the Council, the European Economic and Social Committee, and the Committee of the Regions. A New Action Plan for the Circular Economy for a Cleaner and More Competitive Europe*; European Commission: Brussels, Belgium, 2020.
14. European Commission. Changing the Way We Produce and Consume: The New Action Plan for the Circular Economy Sets out the Path to Follow to Move Towards a Climate-Neutral and Competitive Economy, in Which Consumers Are Empowered. Available online: https://ec.europa.eu/commission/presscorner/detail/it/ip_20_420 (accessed on 10 January 2025).
15. United Nations. Transforming Our World: The 2030 Agenda for Sustainable Development. Available online: https://unric.org/it/wp-content/uploads/sites/3/2019/11/Agenda-2030-Onu-italia.pdf (accessed on 10 January 2025).
16. Giorgi, S. *Progettare la Circolarità. Strategie e Strumenti per L'Economia Circolare nel Settore Edilizio*, 1st ed.; Franco Angeli s.r.l.: Milano, Italy, 2024; p. 80.
17. European Parliament; Council of the European Union. *Directive 2008/98/EC of the European Parliament and of the Council of 19 November 2008 on Waste and Repealing certain Directives (L 312/3 of 22 November 2008)*; Publications Office of the European Union: Luxembourg, 2008.
18. Decree No. 264 of 13 October 2016. Regulation Laying Down Indicative Criteria to Facilitate The Demonstration of the Requirements for the Classification of Production Residues as By-Products and Not as Waste. Available online: https://www.fao.org/faolex/results/details/en/c/LEX-FAOC168049 (accessed on 29 May 2025).

19. Legislative Decree No. 152 of 3 April 2006. Environmental Regulations. Available online: https://ampeid.org/documents/italy/legislative-decree-no-152-2006-approving-the-code-on-the-environment/ (accessed on 29 May 2025).
20. Saeli, M.; Capela, M.N.; Campisi, T.; Seabra, M.P.; Tobaldi, D.M.; La Fata, C.M. Architectural technologies for life environment: Spent coffee ground reuse in lime-based mortars. A preliminary assessment for innovative green thermo-plasters. *Constr. Build. Mater.* **2022**, *319*, 126079. [CrossRef]
21. Pintea, A.O.; Manea, D.L. Influence of natural organic polymers upon plaster mortar workability. *Procedia Manuf.* **2020**, *46*, 158–164. [CrossRef]
22. Cascone, S.M.; Vitale, M. Analisi microscopica e conducibilità termica degli scarti di agrumi per un loro utilizzo nell'edilizia sostenibile. In *Design and Construction, Tradition and Innovation in the Practice of Architecture*; Sicignano, E., Ed.; Edicom: Monfalcone, Italy, 2021; pp. 949–959.
23. Vitale, M.; Cascone, S.M. Orange peels as a potential ecological thermal insulation material for building application. *TEMA* **2022**, *8*, 76–84. [CrossRef]
24. Liuzzi, S.; Rubino, C.; Stefanizzi, P.; Petrella, A.; Boghetich, A.; Casavola, C.; Pappalettera, G. Hygrothermal properties of clayey plasters with olive fibers. *Constr. Build. Mater.* **2018**, *158*, 24–32. [CrossRef]
25. Schackow, A.; Stringa, D.; Senff, L.; Cintura, S.L.; Segãdes, A.M. Influence of fired clay brick waste additions on the durability of mortars. *Cem. Concr. Compos.* **2015**, *62*, 82–89. [CrossRef]
26. Arun Kumar, M.; Balaji, S.; Selvapraveen, S.; Kulanthaivel, P. Laboratory study on mechanical properties of self compacting concrete using marble waste and polypropylene fiber. *Clean. Mater.* **2022**, *6*, 1001156. [CrossRef]
27. Vaclavik, V.; Estokova, A.; Papesch, R.; Dvorsky, T.; Fabianova, M.; Halik, M.; Holosova, M. Investigation of the engineering and environmental properties of cement mortars incorporating ladle furnace steel slag. *Case Stud. Constr. Mater.* **2024**, *20*, e02876.
28. Bayat, H.; Banar, R.; Nikravan, M.; Farnood, P.; Ramezanianpour, A.M.; Kashani, A. Durability, mechanical, workability and environmental assessment of self-consolidating concrete containing blast furnace slag and natural zeolite. *J. Build. Eng.* **2024**, *86*, 108737. [CrossRef]
29. Vembu, P.R.S.; Ammasi, A.K. Eco-efficiency evaluation of sustainable self-compacting concrete using magnesite mine waste. *Case Stud. Constr. Mater.* **2024**, *20*, e02765. [CrossRef]
30. Da Silva, A.M.; de Brito, J.; Veiga, R. Incorporation of fine plastic aggregates in rendering mortars. *Constr. Build. Mater.* **2014**, *71*, 226–236. [CrossRef]
31. Pedreño-Rojas, M.A.; Porras-Amores, C.; Villoria-Saez, P.; Morales-Conde, M.G.; Flores-Colen, I. Characterization and performance of building composites made from gypsum and woody-biomass ash waste: A product development and application study. *Constr. Build. Mater.* **2024**, *419*, 135435. [CrossRef]
32. Eco Watch. Available online: https://www.ecowatch.com/coffee-husk-homes-2650817851.html (accessed on 3 February 2025).
33. Youtradeweb. Available online: https://www.youtradeweb.com/harobau-presenta-poromin-ip7-intonaco-base-caseina/ (accessed on 3 February 2025).
34. Poromin. Available online: http://www.poromin.it/poromin/ip7-it (accessed on 3 February 2025).
35. Milk Brick. Available online: https://www.milkbrick.com/ (accessed on 3 October 2024).
36. SANPELLEGRINO GRUPPO. Available online: https://www.sanpellegrino-corporate.it/it/news-da-scoprire/bibite-sanpellegrino-sicilys-revolution (accessed on 3 October 2024).
37. FAVINI. Available online: https://www.favini.com/news/crush-story-dagli-agrumi-alla-carta/#:~:text=Crush%20Agrumi%20%C3%A8%20la%20carta,della%20cellulosa%20proveniente%20da%20albero (accessed on 3 October 2024).
38. CEC Editore. Available online: https://www.ceceditore.com/gli-scarti-alimentari-come-fonte-di-ingredienti-cosmetici-sostenibili/ (accessed on 3 October 2024).
39. L'Espresso. Available online: https://lespresso.it/c/idee/2023/12/20/gli-scarti-di-arance-e-fichi-dindia-ora-diventano-ecopelle/47488 (accessed on 3 October 2024).
40. Thwe, K.S.; Ayawanna, J.; Mase, L.Z.; Chaiyaput, S. Utilization of ladle furnace slag and fly ash as partially replacement of cement. *Clean. Eng. Technol.* **2025**, *25*, 100910. [CrossRef]
41. Panda, S.; Pradhan, M.; Panigrahi, S.K. Sustainable self-compacting conventional concrete development with optimal content of ladle furnace slag concerning mechanical and durability characteristics. *Constr. Build. Mater.* **2025**, *471*, 140761. [CrossRef]
42. Yong, C.L.; Zhang, F.; Ma, X.; Lee, H.V.; Onn, C.C.; Koting, S.; Mo, K.M. Integrated analysis of strength, microstructure, and environmental impact of thermally activated ladle furnace slag cement mortar. *Constr. Build. Mater.* **2025**, *482*, 141712. [CrossRef]
43. European Parliament. Available online: https://www.europarl.europa.eu/topics/it/article/20210128STO96607/economia-circolare-in-che-modo-l-ue-intende-realizzarla-entro-il-2050 (accessed on 16 February 2025).

44. European Commission. *COM(2015) 614, Communication from the Commission to the European Parliament, the Council, the European Economic and Social Committee and the Committee of the Regions. Closing the Loop—An EU Action Plan for the Circular Economy*; European Commission: Brussels, Belgium, 2015.
45. European Commission. *COM(2014) 398, Communication from the Commission to the European Parliament, the Council, the European Economic and Social Committee, and the Committee of the Regions. Toward a Circular Economy: A Zero-Waste Program for Europe*; European Commission: Brussels, Belgium, 2014.
46. *UNI EN ISO 14020:2023*; Environmental Declarations and Programs for Products—General Principles and Requirements. UNI: Rome, Italy, 2023.
47. *UNI EN ISO 14024:2018*; Environmental Labels and Declarations—Type I Environmental Labeling—Principles and Procedures. UNI: Rome, Italy, 2018.
48. *UNI EN ISO 14021:2021*; Environmental Labels and Declarations—Self-Declared Environmental Claims (Type II Environmental Labeling). UNI: Rome, Italy, 2021.
49. *UNI EN ISO 14025:2010*; Environmental Labels and Declarations—Type III Environmental Declarations—Principles and Procedures. UNI: Rome, Italy, 2010.
50. *UNI EN ISO 14040:2021*; Environmental Management—Life Cycle Assessment—Principles and Framework. UNI: Rome, Italy, 2021.
51. *UNI EN ISO 14044:2021*; Environmental Management—Life Cycle Assessment—Requirements and Guidelines. UNI: Rome, Italy, 2021.
52. European Commission—Joint Research Centre—Institute for Environment and Sustainability. *International Reference Life Cycle Data System (ILCD) Handbook—General guide for Life Cycle Assessment—Detailed Guidance*, 1st ed.; Publications Office of the European Union: Luxembourg, 2010.
53. European Commission. *COM(2003) 302, Communication from the Commission to the Council and the European Parliament, Integrated Product Policy—Advancing the Environmental Life-Cycle Thinking Approach*; European Commission: Brussels, Belgium, 2003.
54. *UNI EN 15804:2021*; Sustainability of Construction—Environmental Product Declarations—Framework Rules for Product Category Development. UNI: Rome, Italy, 2021.
55. *UNI EN 15978:2011*; Sustainability of Buildings—Environmental Performance Assessment of Buildings—Calculation Method. UNI: Rome, Italy, 2011.
56. Löfgren, B.; Tillman, A.M.; Rinde, B. Manufacturing actor's LCA. *J. Clean. Prod.* **2011**, *19*, 2025–2033. [CrossRef]
57. Carbonaro, C.; Tedesco, S.; Thiebat, F.; Fantucci, S.; Serra, V.; Dutto, M. Development of vegetal based thermal plasters with low environmental impact: Optimization process through an integrated approach. *Energy Procedia* **2015**, *78*, 967–972. [CrossRef]
58. Carbonaro, C.; Tedesco, S.; Thiebat, F.; Fantucci, S.; Serra, V.; Dutto, M. An integrated design approach to the development of a vegetal-based thermal plaster for the energy retrofit of buildings. *Energy Build.* **2016**, *124*, 46–59. [CrossRef]
59. Pedreño-Rojas, M.A.; Flores-Colen, I.; De Brito, J.; Rodríguez-Liñan, C. Influence of the heating process on the use of gypsum wastes in plasters: Mechanical, thermal and environmental analysis. *J. Clean. Prod.* **2019**, *215*, 444–457. [CrossRef]
60. García-Martínez, A. Life Cycle Assessment (LCA) of Buildings. Methodological Proposal for the Development of Environmental Declarations of Dwellings in Andalusia. Doctoral Dissertation, Seville University, Seville, Spain, 2010.
61. Melià, P.; Ruggeri, G.; Sabbadini, S.; Dotelli, G. Environmental impacts of natural and conventional building materials: A case study on earth plasters. *J. Clean. Prod.* **2014**, *80*, 179–186. [CrossRef]

Disclaimer/Publisher's Note: The statements, opinions and data contained in all publications are solely those of the individual author(s) and contributor(s) and not of MDPI and/or the editor(s). MDPI and/or the editor(s) disclaim responsibility for any injury to people or property resulting from any ideas, methods, instructions or products referred to in the content.

buildings

MDPI

Article

Towards a Regenerative and Climate-Resilient Built Environment: Greening Lessons from European Cities

Francesco Sommese [1,*], Lorenzo Diana [1], Simona Colajanni [2], Marco Bellomo [2], Gaetano Sciuto [3] and Grazia Lombardo [3]

[1] Department of Civil, Building and Environmental Engineering, University of Naples Federico II, P. le Vincenzo Tecchio, 80, 80125 Naples, Italy
[2] Department of Architecture, University of Palermo, 90128 Palermo, Italy
[3] Department of Civil Engineering and Architecture, University of Catania, 95123 Catania, Italy
* Correspondence: francesco.sommese@unina.it

Abstract: Nature-Based Solutions offer a concrete opportunity to integrate nature into cities and strengthen their resilience, in response to global challenges related to climate change, biodiversity loss, and water management, which are exacerbated by urban expansion and its impacts on the built environment. This study aims to analyze various European policies and urban greening practices, considering not only some European Union member states but also other cities geographically located in Europe. The main goal is to explore how these solutions are used in various European cities to address environmental challenges and improve urban quality of life. The study highlights the growing role of greening strategies in EU urban policies as key tools to tackle global challenges. It finds that green interventions—such as green roofs, façades, and green urban spaces—offer multifunctional benefits, but their effectiveness relies on integrated planning, strong public–private cooperation, and active community involvement. Key challenges include the limited scalability of these solutions in dense or economically constrained areas and the need for long-term financial and institutional support. Overall, the study highlights that greening is not merely aesthetic but central to building regenerative and climate-resilient cities.

Keywords: urban resilience; green infrastructure; nature-based solutions; best practices; regenerative design

1. Introduction

In recent decades, urbanization has reached unprecedented levels. More than 70% of the world's population now lives in urban areas [1]. This phenomenon has determined an exponential growth in building density, accompanied by a progressive waterproofing of the soil and the reduction in natural surfaces [2]. These changes have a significant impact on the ecological balance and affect the ability of urban systems to adapt to the effects of climate change. Increasingly intense heat waves, extreme weather events, the loss of biodiversity, and an increase in hydrogeological risks are just some of the main challenges facing today's cities. This scenario highlights the need to rethink urban planning and management strategies to promote greater resilience of the built environment and support solutions that combine environmental sustainability and social well-being.

Despite the growing attention on the sustainable management of the built environment, there is still a lack of integrated approaches that consider the factors needed to make the sustainability of the built environment effective and concrete; policies and strategies

often remain only theoretical approaches with few practical applications. To effectively implement and evaluate urban sustainability, for example, it is necessary to conduct a complex and integrated analysis of its morphology, paying particular attention to the various levels that compose it, since each of them exerts a specific and interconnected influence on the sustainability parameters [3]. An innovative response to these problems is represented by Nature-Based Solutions (NbSs), a set of strategies and interventions that are based on the use of natural processes and functions to address environmental and climate challenges [4]. According to the European Commission's definition, NbSs are "nature-inspired and nature-supported, economically sustainable solutions that deliver environmental, social and economic benefits and contribute to strengthening the resilience of ecosystems and communities" [5].

The effectiveness of NbSs strongly depends on the ability to integrate them with the existing urban morphology; therefore, the design and implementation of NbSs must take into account the physical and spatial characteristics of the city to promote urban well-being and health.

Implementing greening strategies in a compact and densely built urban fabric, such as that of a historic city center, presents very different challenges compared to applying the same solutions in neighborhoods with lower building density and fewer physical constraints. Key examples of NbSs include green and blue infrastructure such as urban parks, green roofs and walls, rain gardens, artificial wetlands, and sustainable drainage systems. These measures not only improve the adaptability of cities to the effects of climate change but also provide numerous co-benefits, including improving air quality, regulating the urban microclimate, and enhancing the aesthetic and recreational value of public spaces. The European Union (EU) has recognized the crucial role of NbSs in the green transition and is promoting their uptake through several strategic initiatives, including the European Green Deal and the Horizon Europe program. However, despite the growing evidence of its benefits, large-scale implementation of NbSs still faces several obstacles, including regulatory fragmentation, difficult access to funding and the need for greater coordination between different levels of government. The lack of common standards and effective evaluation methods is another obstacle to the dissemination and replicability of NbSs together with the lack or the reduced diffusion of reliable guidelines and implementation frameworks [6].

The aim of this study is to analyze current European policies to promote greening strategies in cities in order to strengthen their resilience and promote the transition to a more sustainable urban model. Through a detailed analysis of plans, urban strategies, and specific case studies, the solutions adopted to address key environmental challenges such as hydrogeological risks, heat waves, and biodiversity loss are examined. The research, carried out in different climatic contexts, aims to identify the most effective and replicable best practices and to highlight the degree of alignment with European goals, in particular the Sustainable Development Goals (SDGs) of Agenda 2030 [7].

Finally, from a regenerative design perspective, the work aims to propose a reflection on the opportunities that NbSs offer to rethink cities and promote urban development models that not only reduce environmental impact but are also capable of creating ecological and social benefits over time.

2. Materials and Methods

This study is based on a critical review approach [8], critically analyzing the main European policies, plans, initiatives, and measures to outline the current state of greening strategies implemented across Europe to address climate change and enhance urban re-

silience. The analysis is not limited to EU member states but also includes countries that are geographically part of Europe.

The analytical research framework is structured into 3 main areas (Figure 1):

i. European policy framework that provides an overview of the European Union's strategies and programs in the field of NbSs and climate adaptation.
ii. Urban–territorial plans and strategies focusing on key European cities to identify intervention models and emerging trends.
iii. Emblematic case studies selected based on their relevance to the plans analyzed in the previous phase, to further investigate the effectiveness and replicability of the solutions adopted.

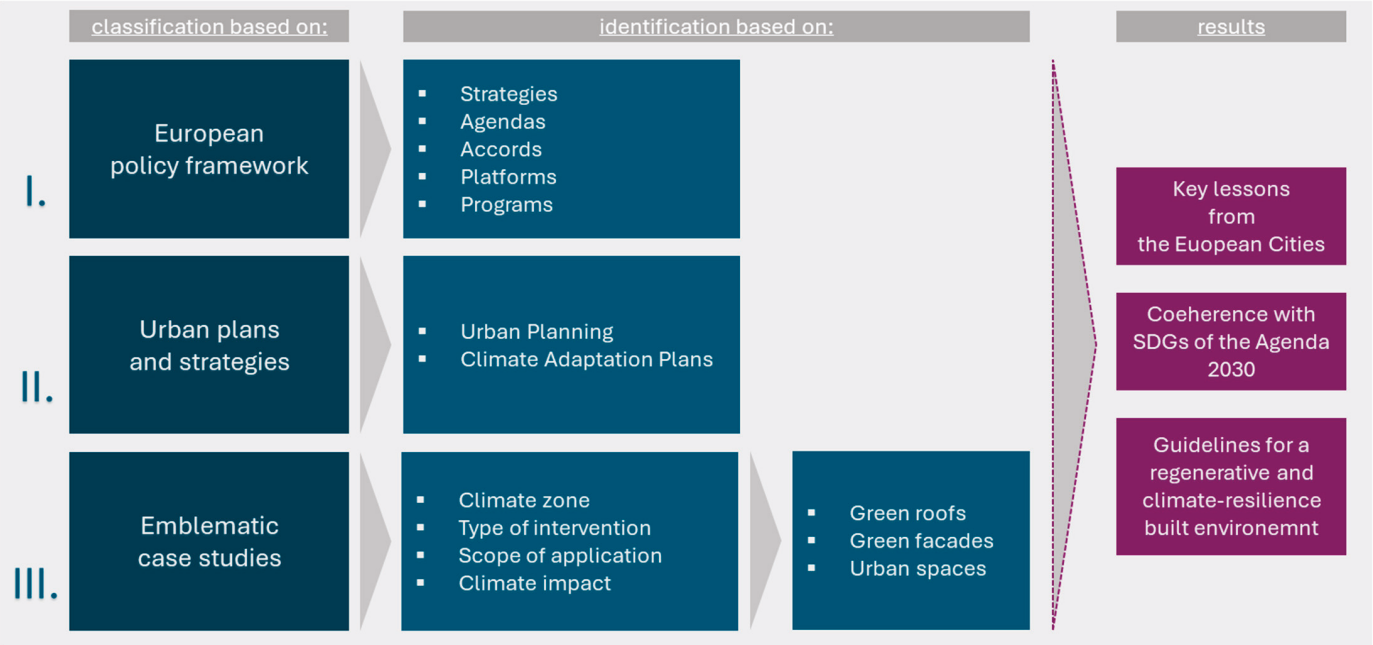


Figure 1. Research framework.

The data analyzed for each of the three research areas were gathered through an in-depth web-based investigation. Specifically, the official websites of the European Union were consulted to identify relevant policies and initiatives at the European level. Urban and territorial planning documents were examined through institutional websites of local governments. Finally, the case studies were selected through targeted online research, based on the planning frameworks discussed in the previous sections.

For the evaluation of cases from research areas II and III, a classification is proposed that takes several key factors into account:

- Climate zones, based on the official Köppen–Geiger classification [9], to determine the adaptability of solutions to different climate zones;
- Types of intervention or action, taking into account the main objective of the intervention in terms of climate impact (e.g., water management, mitigation of urban temperatures, protection of biodiversity);
- The scale of the intervention (building envelope, such as façades and green roofs, neighborhoods, parks, streets, etc.).

The classification of interventions (in terms of typology, topology and technology) and their fields of application follows the model proposed by Sommese [10] in his study on the taxonomy of Nature-Based Solutions. This methodological structure makes it possible to

obtain a complete and multidimensional picture of greening strategies at the European level, which favors the identification of replicable models in line with the European objectives of climate neutrality.

3. Green Strategies in the Policy Framework of the European Union

NbSs are at the center of many European Union (EU) policies and initiatives aimed at promoting urban greening, climate change resilience, and biodiversity protection. These solutions, which utilize natural processes to address environmental, social, and economic challenges, are integrated into various EU policy instruments [11]. The EU Strategy on Adaptation to Climate Change [12] aims to strengthen the EU's capacity to respond to the impacts of climate change, with the objective of becoming a resilient society by 2050. In this context, NbSs are part of the adaptation strategies, which are divided into three categories: "gray" measures, which include traditional infrastructure such as dams and artificial drainage systems; "green" measures, which include interventions such as planting trees, creating wetlands, and restoring ecosystems to mitigate the effects of climate change; and "soft" measures, which involve non-structural measures such as awareness raising, governance, and sustainable urban planning [12]. The EU Biodiversity Strategy for 2030 [13], which is an integral part of the European Green Deal, also recognizes NbSs as tools to restore degraded ecosystems through measures such as the creation of ecological corridors, the renaturation of rivers, and the expansion of urban green spaces that improve habitat connectivity and promote ecosystem resilience. Another important instrument is the EU Green Infrastructure Strategy adopted in 2013 [14], which promotes the creation of natural infrastructure for local climate regulation, stormwater management, and the improvement of air quality in cities through green roofs, urban parks, and sustainable drainage systems. In parallel, the EU's New Urban Agenda [15] emphasizes the importance of integrating NbSs into urban planning policies in order to reduce greenhouse gas emissions and improve the quality of life in European cities. In the context of the European Green Deal [16], the EU has strengthened the role of NbSs as key instruments for the green transition and promoted them in the fight against climate change, the protection of biodiversity, and the promotion of the circular economy. The EU Forest Strategy [17] also recognizes the role of forests as NbSs in the fight against climate change and for biodiversity conservation through reforestation and sustainable management of forest heritage. At the urban level, the EU has introduced several initiatives to encourage the adoption of NbSs. The Green City Accord [18] is an agreement that invites European cities to engage in five key areas of environmental management: air quality, nature and biodiversity, circular economy and waste management, noise and water. NbSs play a central role in achieving the objectives of the Green City Accord, in particular in the promotion of green spaces and sustainable management of water resources. Furthermore, platforms such as the Urban Nature Platform [19] promote the sharing of best practices and knowledge among European cities, providing tools and resources to integrate NbSs into urban policies. The Horizon Europe Programme [20] also fits into this scenario, funding research and innovation projects on NbSs to address issues related to climate change, biodiversity loss, and pollution. In conclusion, the European Union has developed a set of policies, strategies, and instruments to foster the adoption of NbSs and urban greening strategies, contributing to the creation of greener, more resilient and sustainable cities. The integration of NbSs into urban and territorial policies not only addresses the main environmental challenges but also offers economic and social benefits, contributing to the creation of more livable urban spaces in harmony with natural ecosystems. This approach, in line with the European Green Deal and the SDGs of Agenda 2030, represents a strategic direction for the future of urban and environmental planning in Europe.

Table 1 presents a list of the most recent EU initiatives cited above. As evident, there has been a noticeable increase in the number of initiatives in recent years, reflecting a heightened political awareness of environmental issues, particularly in the aftermath of the COVID-19 pandemic.

Table 1. The European Union's latest initiatives in the field of Nature-Based Solutions.

Year	Name	Aim
2013	**EU Green Infrastructure Strategy**	Promotes the use of green infrastructure such as green roofs, urban parks, and sustainable drainage systems to improve the environmental quality and resilience of cities.
2016	**New EU Urban Agenda**	Emphasizes the importance of NbSs for reducing greenhouse gas emissions and improving the quality of life in cities by incorporating them into urban planning policy.
2019	**European Green Deal**	Key EU initiative for the ecological transition, which considers NbSs as key for decarbonisation, biodiversity protection, and circular economy.
2020	**EU Biodiversity Strategy 2030**	Aims to restore biodiversity through NbSs such as ecological corridors, the renaturalization of rivers, and the expansion of urban green spaces.
2020	**Green City Accord**	Voluntary agreement calling on European cities to improve environmental management in five key areas: air quality, nature and biodiversity, circular economy and waste, noise pollution and water management, through the use of NbSs.
2020	**Urban Nature Platform**	Facilitates the exchange of best practices between European cities to integrate NbSs into urban policy.
2021	**EU Forest Strategy**	Promotes reforestation and sustainable forest management as NbSs to combat climate change and protect biodiversity.
2021 (2013)	**EU Strategy Adaptation to Climate Change**	Promotes actions to adapt to climate change, divided into gray, green and soft actions.
2021	**Horizon Europe Program**	Research and innovation program that funds NbS projects to address climate change, biodiversity loss, and pollution.

4. European Territorial Plans and Strategies

European cities are gradually adopting innovative strategies to contrast climate change and integrating NbSs into their adaptation plans (Table 2). From a methodological perspective, the shortlist of territorial plans and strategies selected in this section refers to case studies that are considered exemplary, well-known, and paradigmatic in terms of practical applicability and, often, linked to the political sensitivity toward environmental issues. The selected plans and, even more, the specific interventions detailed in Section 5 differ according to the climatic zone and the specific climatic challenges they are designed to address.

Barcelona, for example, has updated its "Plan Clima" and introduced the "Plan Calor", which includes targeted measures such as the air-conditioning of schools and the creation of widespread climate houses, emphasizing the urgency of responding to the rise in urban temperatures [21]. Similarly, Copenhagen has developed an advanced stormwater management system through the integration of green spaces that absorb stormwater runoff and thus reduce the risk of flooding [22]. Rotterdam is taking a similar approach with its "Rotterdam Climate Proof" plan, which promotes the use of green roofs and floating infrastructure to improve urban resilience [23].

Hamburg has also structured its "Klimaplan" around NbSs, emphasizing the creation of green corridors and the planting of trees to reduce air pollution and counteract the heat island effect [24]. With the "ForestaMi" project, Milan has set itself the ambitious goal of planting three million trees by 2030, not only to reduce carbon emissions but also to regenerate the city ecologically [25]. In parallel, Paris has included a strong greening component in its "Plan Climat Air Energie 2024–2030" and is promoting green roofs and walls to increase natural cooling capacity [26].

Other cities have developed targeted strategies for specific climate issues. Berlin has introduced the "StEP Klima KONKRET" [27], a plan that addresses the heat island effect and the sustainable use of water resources, while Vienna "has placed a special focus on reducing urban overheating through large-scale NbS measures with its "Urban Heat Island Strategy Plan" [28]. Stockholm and Oslo have developed climate action plans that include sustainable stormwater management and increased urban greening, while Helsinki and Zurich focus on reducing emissions through integrated strategies that combine tree planting with efficient natural resource management.

Finally, cities such as Brussels and Lisbon have adopted regional climate plans that incorporate green corridors and green infrastructure to improve territorial resilience and water management. In general, the European approach to NbSs is not limited to individual measures, but tends towards systemic planning that takes into account the climatic and urban specificities of each context.

Table 2. The most important adaptation plans that include greening strategies. Climate [9]: hot-summer Mediterranean (Csa); humid subtropical (Cfa); temperate oceanic (Cfb); cold semi-arid (BSk); warm-summer humid–continental (Dfb).

Year	City	Country	Climate	Plan	Aim
2011	Copenhagen	Denmark	Cfb	Climate Adaptation Plan	Green spaces to absorb and manage water runoff
2011	Hamburg	Germany	Cfb	Klimaplan	Green corridors and tree planting to improve air quality and climate resilience
2012	Stockholm	Sweden	Dfb	Stockholm Action Plan for Climate and Energy	Sustainable stormwater management and expansion of green spaces
2014	Helsinki	Finland	Dfb	Helsinki City Strategy	Integration of NbSs such as tree planting and creation of green spaces for improving climate resilience
2014	Zurich	Switzerland	Cfb	Masterplan Energie	Sustainable stormwater management and green space expansion to improve urban resilience
2015	Rotterdam	The Netherlands	Cfb	Rotterdam Climate Proof	Integrating green roofs and floating parks to manage stormwater and reduce the heat island effect
2015	Oslo	Norway	Dfb	Climate and Energy Strategy	Creation of urban parks and sustainable management of water resources
2015	Bruxelles	Belgium	Cfb	Brussels Regional Climate Plan	Use of NbSs as green corridors and water management to improve climate resilience
2016	Berlin	Germany	Cfb	StEP Klima KONKRET	Using NbSs to reduce the heat island effect and manage water resources
2017	Lisbon	Portugal	Csa	Lisbon Climate Change Adaptation Strategy	Tree planting and creation of green spaces to address climate challenges and improve the quality of urban life
2018	Paris	France	Cfb	Plan Climat Ènergie	Urban greening with green roofs and walls to improve urban resilience to climate change
2018	Vienna	Austria	Cfb	Urban Heat Island Strategy Plan	Reducing urban overheating through NbSs such as tree planting and creating green spaces
2019	Milan	Italy	Cfa	ForestaMi	Planting 3 million trees by 2030 to improve air quality and climate resilience
2020	Barcelona	Spain	Csa	Plan Clima Plan Calor	Urban heat adaptation strategies, school climate control, climate shelters, and cooling spaces

5. Green Roofs

After outlining European policies, exemplary territorial plans and urban strategies, Section 5, Section 6, and Section 7 present a selection of case studies featuring interventions recognized as best practices for green roofs, green facades, and urban spaces, respectively.

Green roofs have become a key solution for urban sustainability and offer numerous environmental, social, and economic benefits. This paragraph presents the most significant case studies from various European cities (Table 3). The case studies have been classified according to climatic zones, building use, typology, topology, technology, and climatic impact. In this regard, the city of Basel is a leader in the implementation of green roofs with numerous projects that have improved the urban environment and contributed to environmental sustainability. In 1999, the city of Basel introduced a cantonal law requiring the construction of green roofs on new and renovated buildings with a roof pitch of less than 10 degrees [29]. In this way, it became the first city in the world to make the greening of new buildings a legal requirement. Currently, around 50% of Basel's flat roofs are green, which also serve as ecological compensation areas [29]. The regulations stipulate the use of native plants in order to promote urban biodiversity.

Table 3. Identification of some green roofs in the European context. **Climate** [9]: hot-summer Mediterranean (Csa); humid subtropical (Cfa); temperate oceanic (Cfb); cold semi-arid (BSk); warm-summer humid–continental (Dfb). **Typology:** green roof (GR), blue roof (BR), blue-green roof (BGR). **Topology:** extensive (E), intensive (I), semi-intensive (SI). **Technology** [30]: no-tech (NT), high-tech (HT), low-tech (LT). **Climate impact:** extreme temperature (T); water management (W); pollutant (P); biodiversity loss (B).

Building Name	City	Country	Climate	Building Use	Typology	Topology	Technology	Climate Impact
Opus	Dublin	Ireland	Cfb	Residential	BGR	I	HT	T; W
Basecamp	Copenhagen	Denmark	Cfb	Social housing	BGR	E	HT	W; B
Vierhanstrip	Rotterdam	The Netherlands	Cfb	Social park	BGR	I	HT	W
Max Planck Institute	Hamburg	Germany	Cfb	Educational	BGR	I; E	HT	T; W; B
Escape Bievenue	Paris	France	Cfb	Educational	BGR	E	HT	T; W; B
Axel Springer Haus	Berlin	Germany	Cfb	Editorial office	BGR	E	HT	T; P
Mcer	Lods	Poland	Dfb	Multifunctional	BGR	E	LT	W; B
St. Jakobshalle	Basel	Sweden	Cfb	Sport	BGR	E	HT	T; W; P

A prime example is the St. Jakobshalle (1976), a sports facility that has transformed its roof into a habitat for urban biodiversity. This project utilized local seeds from the Reinacher Heide nature reserve, encouraging the growth of native plants and the presence of various animal species, including wild bees and butterflies. The initiative has improved the environmental quality of the area and is a good example of how green roofs can promote biodiversity in the city. The implementation of the green roof on St Jakobeshalle has led to a number of environmental benefits, including a reduction in the urban heat island effect, improved air quality, and more efficient rainwater management.

The city of Copenhagen has introduced a policy that encourages the installation of green roofs to manage rainwater and reduce urban temperatures [22]. Indeed, city policies encourage the use of green roofs on new and existing buildings to improve climate resilience. In particular, new buildings must be equipped with green roofs that can absorb at least 50–80% of precipitation, have an insulating effect on the building, contribute to lowering temperatures in the city, double the lifespan of the roof itself by protecting it from UV rays, and help to beautify Copenhagen architecturally and aesthetically to improve the quality of life of citizens. Green roofs in Copenhagen must also be installed on existing buildings with flat roofs or a slope of less than 30°.

A prime example for the city of Copenhagen is Basecamp Lyngby (Figure 2), an expression of the integration of housing and environmental sustainability. One of the characteristic features of the project is the extensive green roof, which extends over

20,000 square meters [31]. The green space not only helps to enhance the aesthetic appearance of the building but also performs significant social and ecological functions, including the management of stormwater and the enhancement of urban biodiversity. The project has received awards such as the Green Cities Europe Award 2023, underlining its focus on environmental sustainability and social cohesion [32].

Hamburg is one of the greenest cities in Europe and the first in Germany to develop a green roof strategy. The city has made the installation of green roofs mandatory and offers financial incentives that cover 30 to 60 per cent of the costs for voluntary installations. The aim is to green 70 per cent of new buildings and renovated roofs. This corresponds to a total area of 100 hectares of green roofs, 20 per cent of which are earmarked for recreational areas.



Figure 2. BaseCamp. (**a**) Front view of the complex. Credits: KraghBerglund. (**b**) Roof paths seen from above. Credits: SayskyRace -KraghBerglund. (**c**) Integrated vegetation on the roof. Credits: SofieCold-Ravnkilde—KraghBerglund. (**d**) General view of the architectural complex. Credits: KraghBerglund.

One of the most remarkable examples is the Max Planck Institute for the Structure and Dynamics of Matter, designed by Landschaftsarchitektur+. The 3870 m^2 roof is largely green, with a combination of an extensive, multi-layered roof and a roof garden on the terraces and in the dining area. It includes perennials, herbs, and trees, offers relaxation areas and paths with ramps and stairs [33]. This project was awarded the "Green Roof of the Year 2021" prize by the German Green Building Association (BUUG). The green roof of the Max Planck Institute for the Structure and Dynamics of Matter is an innovative project that combines environmental sustainability, human well-being, and social cohesion. Thanks to extensive planting with perennials, trees, and shrubs, it improves biodiversity and helps regulate the microclimate, thereby reducing the building's energy consumption [31]. Furthermore, the rainwater collection system optimizes the use of water resources and reduces disposal and irrigation costs [34]. In addition to the ecological aspects, the roof was designed as a social space for researchers and visitors, offering walking paths, relaxation areas, and an outdoor café. The design, inspired by the natural landscapes of northern Germany, makes the roof a point of reference for the campus and encourages interaction between the various scientific institutions.

Rotterdam has taken several measures to promote the introduction of green roofs, as they are recognized as effective tools for adapting to climate change. In 2014, the city installed over 185,000 m^2 of green roofs, demonstrating its strong commitment to sustainable solutions [35]. In addition, the "RoofScape" project has mapped the city's

rooftops and identified 130 potential uses, including rainwater harvesting and energy generation, to improve urban resilience.

A prime example of these initiatives is the Roofpark Vierhavenstrip in Rotterdam's Delfshaven neighborhood. Opened in summer 2013, this roof park is the largest in Europe with a length of 1 km, a width of 80 m, and a total area of 80,000 m^2. Built on the site of a former marshalling yard, the park rises above a number of commercial activities and combines green spaces with urban functions. Designed by Buro Sant en Co, the park offers an attractive and well-maintained environment that is easily accessible from the surrounding neighborhood, with themed areas, children's playgrounds, and refreshment facilities [36].

Dublin, the capital of Ireland, is a city that combines a rich cultural history with a growing commitment to environmental sustainability. In recent years, the city has seen an increasing number of initiatives to promote sustainable architecture, although there is little specific information on green roofs. Of note, however, is the OPUS building project (by MDO Architects), which includes extensive rooftop gardens and communal areas on the roof that contribute to biodiversity. The planting includes over 20 species of herbs, shrubs, and trees such as lavender and rosemary, which attract pollinators and birds [37]. This green design not only improves the quality of life for residents but also promotes a healthier environment by reducing the heat island effect and contributing to rainwater management.

The Berlin Climate Plan envisages the introduction of green roofs as a measure to improve the urban microclimate and water management, and to promote the thermal insulation of buildings. The integration of plant elements into urban architecture helps to reduce the heat island effect and improve the energy efficiency of buildings, thereby promoting the ecological sustainability of the city.

The green roof of the Axel Springer publishing house in Berlin, designed by Rem Koolhaas' OMA, is an innovative example of sustainable architecture. It combines nature and design and provides green spaces that improve thermal insulation and reduce environmental pollution. It not only serves as a recreational space but also promotes rainwater management and urban biodiversity. The roof helps reduce the heat island effect and improves air quality. The project integrates the building into the urban context and creates a symbolic and functional landmark. The selection of different plants promotes an ecological and regenerative environment.

Paris' urban planning instruments include incentives for the installation of green roofs and green walls as well as subsidies for urban greening projects to improve air quality and energy efficiency. One notable example is the undulating green roof of the Espace Bienvenüe, designed by Jean-Philippe Pargade, which combines aesthetics and sustainability. It is accessible to visitors and consists of layers of drainage, waterproofing and plant substrate that contribute to thermal insulation, reduce energy consumption and absorb rainwater. The native vegetation promotes biodiversity and counteracts the heat island effect. The design, which blends perfectly into the landscape, creates a natural terrace that is accessible to all.

In recent years, Poland has also begun to pay more attention to green roofs, although this practice is not yet as widespread as in other parts of Europe. Some municipalities are utilizing the concept of green roofs in urban redevelopment. A notable example is the MCER building (Młodsze Centrum Ekologiczne i Rewitalizacji), in Lods, which is the only environmentally friendly public building in Poland to have a green roof, which is one of the distinguishing features of this complex and was designed to improve the building's thermal and acoustic insulation and reduce energy consumption. It also contributes to rainwater management, reducing the risk of flooding in the surrounding areas. The green roof improves biodiversity by providing shelter for insects and birds.

Vienna promotes the use of green roofs to mitigate the urban heat island effect and offers financial incentives for their installation on residential and commercial buildings. The integration of plant elements into architecture helps to improve air quality and reduce pollution thanks to the absorption of carbon dioxide and the release of oxygen by plants. In addition, green roofs provide natural insulation that improves the energy efficiency and environmental comfort of buildings.

In Oslo, Norway, incentives are planned for the introduction of green roofs on public and private buildings to reduce CO_2 emissions and improve water management. The city is even considered the eco-capital of Norway.

These examples represent only a small selection within the broader European context. The collection presented here is not intended to be exhaustive and numerous additional examples can be identified.

6. Green Facades

Among various greening strategies, green facades are one possible solution and an effective approach to improving the quality of urban life. These interventions not only improve the quality of public and private spaces, but also offer numerous environmental and social benefits: improvement of air quality, due to the purifying action of plants [38–40]; thermal and acoustic insulation [41–45]; and protection of urban biodiversity. In addition, they do not require the occupation of land and make available a greater surface area of the building envelope, which goes beyond the exploitation of the roof alone. Several European cities have successfully implemented green façade projects (Table 4).

Table 4. Identification of some Vertical Greenery Systems in the European context. **Climate** [9]: hot-summer Mediterranean (Csa); humid subtropical (Cfa); temperate oceanic (Cfb); cold semi-arid (BSk); warm-summer humid–continental (Dfb). **Typology:** green façade (GF), living wall (LW), plants in pots (PP). **Function:** insulation (I), screening (S). **Technology** [30]: no-tech (NT), high-tech (HT), low-tech (LT). **Climate impact:** extreme temperature (T); water storage (W); pollutant (P); biodiversity loss (B).

Building Name	City	Country	Climate	Building Use	Typology	Function	Technology	Climate Impact
Fiordaliso shopping center	Rozzano, Milan	Italy	Cfa	Commercial	LW	I	HT	T, W
VIU Hotel	Milan	Italy	Cfa	Hotel	GF, PP	I, S	HT	T
Tower Flower	Paris	France	Cfb	Residential	PP	I	HT	T, P
Oasis d'Aboukir	Paris	France	Cfb	Residential	LW	I	HT	T, P, B
Edgware Road tube station	London	England	Cfb	Infrastructure	LW	I	HT	T, P
Regal House	London	England	Cfb	Residential	LW	I	HT	T, W, P, B
Hill House—Shoe Lane Library	London	England	Cfb	Residential, Office	PP	S	NT	T, P, B
Citicape House	London	England	Cfb	Hotel	LW	I	HT	T, W, P
Intermediate Contemporary Archive	Barcelona	Spain	Csa	Office	GW	I	HT	T, B
Sportplaza Mercator	Amsterdam	The Netherlands	Cfb	Social	LW	I	HT	T
Ravel Plaza Complex	Amsterdam	The Netherlands	Cfb	Residential, Office, Commercial	PP	S	NT	T, P, B
Ducati Business Center	Rimini	Italy	Cfa	Office	GW	S	HT	T
Ricola Company Office Building	Laufen	Swiden	Cfb	Office	GW	S	HT	T
CaixaForum	Madrid	Spain	Cfa	Museum	LW	I	HT	T, W, B

Among the best practices, we find the immense green wall covering 1250 square meters of area at the Fiordaliso shopping center in Rozzano, near Milan,

designed by Architect Francesco Bollani. To create it, 44,000 plants were used, belonging to more than 200 different species of succulents such as Sedums and many hardy, almost weedy ornamental grasses capable of withstanding difficult environmental conditions. A total of 11,000 metal boxes were used, which are lightweight, water-resistant and able to facilitate maintenance. Chilean sphagnum moss, a fiber that does not rot even when in continuous contact with water, was used as "soil" to best grow the plants in a vertical position. Plants live on this type of moss by growing roots without contact with soil. The wall has a drip system that, thanks to thin channels that reach each box, brings water directly near the roots, without wasting it. Under the building, two 800-cubic-meter cisterns have been buried for rainwater, which is filtered and also used for irrigation of the surrounding greenery.

Another interesting example is the two large green walls of about 500 square meters each at Hotel VIU in Milan, designed by AG&P greenscape [46]. The main objective was to make the intervention sustainable from a maintenance point of view to ensure quality and durable vegetation. Taking advantage of the location of the two stairs located at the ends of the building behind the blind walls, easily accessible external steel walkways were built at each stringer. Metal pots were placed on each walkway so that they could take advantage of the correct amount of soil for their growth. By connecting the walkways to each other on the outer side with steel cables every 20 cm, it was possible to create a mix of vegetation: drooping from the same metal tubs, climbing thanks to the presence of the steel cables placed between each floor, and shrubby to ensure a thicker cover, always taking into account the different sun exposures of the two walls (northeast and southwest). The green wall spaced from the wall of the building also allowed for natural insulation of the building resulting in effective energy savings, as well as protection from the weather.

The "Paris Green" project, which promotes the installation of vertical gardens on public and private buildings, has been approved in Paris. The French capital's sensitivity to ecological and naturalistic issues is evidenced by the presence of numerous emblematic examples of the creation of vegetated walls by botanist Patrick Blanc, who pioneered the integration of "vertical gardens" in buildings. Some of his works worth mentioning are as follows:

The Quai Branly Museum was built in 2004; it has an area of 800 square meters and consists of about 15,000 plants of 150 different types; in 2017, it was enriched with 350 different species from all over the world. It integrates a water collection and runoff system near the façade openings and a drip system that provides nutrients and irrigation.

The BHV Homme, in the 4th arrondissement, built in 2007, features a large living wall above the entrance to the store. The "Mur végétal" at Rue d'Alsace, in the 10th arrondissement, planted in 2008, has an area of 1400 square meters and a height of 27 m; it contains 40,000 plants of more than 110 different species. The Green Hotel 13 at 90 rue de Patay was built in 2016, in which the green wall occupies all six floors of the facade.

An example of integration between vegetation and construction is the Tower Flower, a residential building constructed between 1999 and 2004, designed by architect Edouard François, in the Porte d'Asnière urban expansion area [47]. It can be seen as a true vertical extension of the neighboring park, with its 400 large pots arranged at the ends of the terraces that surround the building along its entire perimeter, within which bamboo plants are placed. The large pots also serve the function of protection, partially replacing the parapets. The shrubs and foliage of the bamboo act as a vegetal filter, shielding the view of the city.

An interesting intervention of creating a living wall in an existing building is the redevelopment of the façade of Oasis d'Aboukir, a residential building with five floors above ground, carried out in 2013 [48]. A vertical garden consisting of about 7600 plants of 273 different species placed on a felt-based technological support applied to the existing wall was created

on the side facade. The plant layer thus created promotes urban biodiversity, improves the thermal insulation of the wall in both winter and summer, helps reduce air pollution (pollutant particles are slowly decomposed and mineralized on the felt, transforming into fertilizer for the plants), and improves the microclimate through the phenomenon of evapotranspiration.

In recent years, London has shown increasing interest in implementing green facades as part of a strategy to improve urban sustainability. The City of London has adopted the "Living Roofs and Walls" program, with guidelines and policies to encourage the development of green roofs and walls by integrating them into urban planning projects. Tax incentives and funding were provided to encourage owners and planners to invest in green solutions.

One of London's most interesting living walls is located on the side elevation of Edgware Road tube station, at the corner of Marylebone Road [49]. In 2011, the City of London commissioned the company Biotecture to design and install this green wall in an effort to combat air pollution in the city. This living wall was built by adopting a modular hydroponic system and occupies an area of about 200 square meters. It contains 14,000 plants of 15 different species with smaller leaves and a variety of textures, which were specially chosen because they are better air filters for PM10, the harmful particulate matter produced by car exhaust. The planting design of the Living Wall at Edgware Road was set on intersecting wavy vertical lines to create as natural an effect as possible, which has the effect of softening the shape of the building. In addition to reducing the building's heat load, mitigating the heat island phenomenon and limiting CO_2 emissions, this green wall also contributes to improving air quality by reducing environmental pollution. In this regard, the benefits of the aforementioned living wall on air quality have been monitored by Imperial College London, which has analyzed leaf samples at regular intervals to determine the amount of particulate matter absorbed by them.

An emblematic example of a vertical park is the living wall on the facade of Regal House, at the entrance to the Covent Garden area, created in 2017 by the company Biotecture, commissioned by Capital and Counties [50]. The living wall consists of more than 8000 plants of 21 different varieties. The main objective when designing the wall was to include as many colors as possible, taking into account the orientation of the facade and local conditions. The choice of plants had to ensure both biodiversity and improved air quality. In particular, efforts were made to encourage the presence of native birds and invertebrates and flowering plants that would provide nectar. Irrigation of the living wall is partly provided by a rainwater harvesting system, with a storage tank placed in the basement of the building. A custom solution had to be developed for the installation of the greening system on the facade of the existing building; a steel frame was attached to the brickwork of the building, adapting to the morphological characteristics of the facade and the presence of the windows.

A recent example of urban regeneration that includes a green envelope is the proposed 2024 redevelopment of the Hill House complex and Shoe Lane Library in the City of London by APT Architects [51]. The office building will feature a façade with cascading green roof terraces, with the goal of creating a sustainable and healthy workplace. Each floor will have an outdoor space designed to accommodate plants of various sizes that will envelop the building and make a major contribution to improving indoor air quality, reducing the heat island effect, and protecting biodiversity. The building-scale intervention will be part of a larger redevelopment plan to green the roadway and add new public green spaces.

Another interesting example of a green envelope in a new building is the Citicape House project, designed in 2019 by architecture firm Sheppard Robson and currently under construction [52]. It is a concrete example of the urban greening policy introduced by the New

London Plan. It is a luxury hotel on whose shell is placed a green wall of the total development of about 3700 square meters, the largest in Europe, with 400,000 plants capable of capturing 8 tons of air pollution each year, producing 6 tons of oxygen, lowering the surrounding temperature by 3 to 5 degrees and significantly improving the local air quality by trapping about 500 kg of particulate matter (PM2.5 and PM10) per year. There is also a rainwater harvesting system in the building, which is functional for irrigating the green wall.

Also in London, a negative example that underscores how green walls need constant and careful maintenance, without which the intervention can even be detrimental to the building and its surroundings, is the Paradise Park Children's Centre. The building was designed by DSDHA Studio with a green façade designed by landscape architect Marie Clarke and made with a modular steel cage inside which rock wool is placed to allow hydroponic plant cultivation. Constructed in 2006, the vegetation on the wall died completely after 3 years, probably due to the irrigation system fed by recycled water, leaving the facade bare and with the supporting substructure exposed.

In Barcelona, with both the Superilles project for the city and the Metropolitan Urban Master Plan (in Spanish, Piano Direttore Urbano—PDU) for the entire metropolitan area, the goal is pursued of creating a more livable and healthy city with a harmonious relationship with its environment by protecting the system of open spaces, defined as ecosystems that benefit humans. In particular, the PDU adopts the notion of green infrastructure referring to the planned system of natural elements that are capable of conserving and enhancing metropolitan biodiversity.

An example of the adoption of vertical greening systems for the improvement of environmental quality is the wall of the Barcelona Intermediate Contemporary Archive in the Laguna del Poblenou neighborhood. Photovoltaic panels and climbing plants of 12 different species coexist on the wall over a total area of 560 square meters. An 8000 L reservoir collects rainwater from the roof of the building, which will be used to water the plants through a drip irrigation system. The intervention was carried out by the Municipal Institute of Urban Landscape and Quality of Life, with the collaboration of the Parks and Gardens Department and the Sant Martí District.

In the city of Amsterdam, attention to environmental issues has led planners to integrate greening systems into buildings.

An early emblematic example of the integration of green walls is the Sportplaza Mercator, built in 2006 and designed by Venhoeven Architecture Studio [53]. It is a building dedicated to leisure and socialization in a multicultural and multiethnic neighborhood. It includes bars, restaurants and a swimming pool. Because it stands in a park, to integrate it more into the context and to preserve the environment and biodiversity, it was entirely covered with vegetation. On the vertical envelope, a living wall with a pocket system and grassed panels was created, which characterizes the entire building. Through its green envelope, the Sportplaza Mercator ideally marks the beginning of the Rembrandtpark.

A relatively recent project by the studio MVRDV that integrates trees and other vegetation into the building's various floors is the Ravel Plaza Complex in Amsterdam's financial district [54]. The project, which promotes sustainable development and biodiversity, involves three tower buildings of varying heights joined together. The complex will contain apartments, offices and businesses and will feature visually striking green elements. The various floors are staggered so as to allow for the creation of large balconies full of plants and vegetation, which will help improve the area's microclimate and clean the air of the entire neighborhood.

Other significant interventions do not fit into specific urban greening programs.

The Ex Ducati Business Center in Rimini, Italy, was built between 2003 and 2006, designed by Mario Cucinella Architects [55]. In this building, a double vegetal skin, made of a 60 × 60 cm stainless steel grid on which Trachelospermum Jasminoides grows, covers the curved volume to the south. The green wall functions to screen and protect the building's distribution walkways. The plants are placed inside reinforced concrete planters arranged on each floor.

The Dutch Pavillion IGA in Rostock, Germany, was designed by Atelier Kempe Thill in 2003. The plant screen that forms the closure of the Dutch Pavilion at the International Garden Exhibition (IGA 2003), consisting of Dutch ivy, is able to modulate light and limit introspection.

The Ricola Company Office Building in Laufen, Switzerland, was designed by Jacques Herzog and Pierre De Meuron and built from 1997 to 1999 [56]. Wire mesh is attached to the intrados of the projecting roof to allow the growth of evergreen creepers and deciduous essences that act as sunscreens on the facades.

The CaixaForum Museum, located in the heart of Madrid's cultural district, features a green wall designed by Patrick Blanc [57]. It includes more than 15,000 plants of nearly 300 different species, all chosen by Patrick Blanc to take into account the extreme climate that characterizes the city: very hot in summer and cold in winter. The plants are housed in special pockets of a non-biodegradable felt mat in which the plants' roots grow. The total weight of the vertical garden is estimated at 30 kg per square meter. An irrigation and fertilization system, divided into zones at different heights, ensures adequate sustenance for the plants. In addition, there is a system at the base of the green wall for the recovery and subsequent recirculation of water from runoff that occurs along the leaves and stems.

Despite the specificities related to the design and implementation of VGSs, two integrated regeneration examples, although related to small cities, testify to how it is possible to plan urban greening works that effectively combine urban-scale interventions (reforestation, increase in permeable and/or reflective surfaces, regeneration of public areas) with those at the building scale (green roofs and walls).

This is the case of social housing projects by Stefano Boeri Architetti, still under construction, in several cities such as Monza and Prato (Italy), where energy upgrading and social inclusion are the two pillars of a regeneration of social housing that implements different scales of urban forestation interventions.

In Monza, the intervention for Aler social housing covers a total area of 8270 square meters and involves the reconnection between two buildings, which are currently divided. In both buildings, a climbing green system with support in metal cables anchored to the ground has been integrated into the facades, in which vegetation is planted directly in the areas adjacent to the building, so as to promote its growth and reduce its maintenance. Both solutions aim to create green walls by increasing the outdoor spaces pertaining to the apartments, with two different approaches: the first punctual, with prefabricated aluminum structures to create balconies, and the second continuous longitudinal, creating a prefabricated aluminum balcony. In both cases, the new prefabricated structures become the support for climbing plants that modify and enliven the facade. The resulting effect is that of a vertical extension along the facades of horizontal greenery.

The Municipality of Prato has developed the Urban Jungle project, with which it aims to improve the social and environmental quality of the urban context through urban forestation interventions, increased permeable surfaces, and the implementation of innovative and sustainable Nature-Based Solutions specifically designed and applied on facades and green roofs. As part of this project, the firm Stefano Boeri Architetti developed the design for the redevelopment of an office building and public housing complex [58]. The project

brings forward a new conception of open spaces and green areas in the city, where nature is an active tool for safeguarding the health of citizens.

7. Urban Spaces

Nature embedded in urban design functions not only as a strategy for environmental adaptation, but also as a catalyst for inclusion, social regeneration and collective identity. When NbSs are integrated coherently into the urban fabric, they produce effects that exceed the mitigation of climate impacts, creating spaces for gathering, informal education, food production and participatory management. In both European and extra-European contexts, the widespread implementation of NbSs has led to the development of shared green areas that act as urban commons—spaces co-managed by communities that reinforce cohesion, activate local knowledge and renew the relationship between citizens and place [59].

These spaces work as hybrid socio-ecological infrastructures, particularly effective in neighborhoods exposed to physical or social vulnerability (Table 5). Examples such as the community gardens in Thessaloniki, the participatory reforestation experiences in Potenza, or the rain gardens in Rotterdam show how the success of these interventions often lies in the inclusion of local actors throughout the design and management phases. From this perspective, the most effective NbSs are those that emerge from a combination of ecological performance, social demand and cultural specificity. Their implementation is reinforced when embedded in collaborative governance systems that facilitate active participation by citizens, institutions, and third-sector organizations, fostering a form of environmental democracy in which shared management replaces traditional top-down planning [60].

Table 5. Identification of some green urban spaces in European cities. **Climate** [9]: hot-summer Mediterranean (Csa); humid subtropical (Cfa); temperate oceanic (Cfb); cold semi-arid (BSk); warm-summer humid–continental (Dfb). **Typology:** green corridor (GC), green infrastructure (GI), urban park (UP), edible garden (EG). **Technology** [30]: no-tech (NT), high-tech (HT), low-tech (LT).

Project Name	City	Country	Climate	Intervention Type	Typology	Technology
Green Corridors	Barcelona	Spain	Csa	Pollinators, Corridors, Meadow streets	GC	HT
Victoria BID	London	UK	Cfb	Green corridors, Rain gardens	GC	HT
Biblioteca degli alberi	Milan	Italy	Cfa	Multifunctional Urban park	UP	LT
Toyenparken	Oslo	Norway	Dfb	Community urban park	UP	LT
Stadtgarten	Leipzig	Germany	Cfb	Urban gardens	EG	NT

However, while some cities have consolidated institutional frameworks and urban living labs capable of sustaining these models over time, the replicability of such systems remains a major challenge. In contexts with lower administrative capacity or fewer financial resources, the diffusion of NbSs is often slowed by fragmented policies or limited access to evidence-based design. Initiatives such as the Urban Nature Platform or the Green City Accord play a key role in supporting the mainstreaming of NbSs, offering transferable typologies and common evaluation metrics that can guide urban decision-makers in tailoring NbSs to their specific socio-spatial context [59,60].

In recent years, there has been growing attention on equity-oriented planning strategies and the role of food systems in shaping inclusive urban spaces. Within this framework, the paradigm of the edible city has gained momentum as an approach that aligns nature-

based urbanism with social justice and food security. Urban agriculture, community gardening and edible landscaping are increasingly seen not only as climate-resilient infrastructures, but also as platforms for social innovation and cultural expression [61]. Projects such as Incredible Edible in Todmorden or the Essbare Stadt initiatives in Leipzig and Berlin show how urban food production can activate dormant spaces, support economic regeneration and foster intergenerational dialogue [60].

These edible strategies contribute to the regeneration of peri-urban and inner-city areas by reconnecting citizens with natural cycles and enhancing access to healthy food, particularly for marginalized communities. Moreover, rooftop gardens, balcony farms and other zero-acreage farming systems are proving to be effective even in high-density urban environments, providing benefits in terms of thermal regulation, biodiversity, and microclimate resilience. Their multifunctionality allows them to contribute simultaneously to ecosystem services, civic engagement and education, making them highly adaptable to diverse socio-ecological settings.

These dynamics are not limited to cities at large. Increasingly, they are being tested and refined in more controlled environments such as university campuses, which function as microcosms of urban systems. The concept of the campus as a "living lab" fosters a dynamic interplay between theoretical knowledge and applied sustainability, enabling students and staff to co-design and monitor NbSs in real time. Through the integration of lifecycle-based approaches and participatory practices, institutions like the University of Copenhagen and the University of Oxford are demonstrating how campuses can reduce their carbon footprint, enhance biodiversity, and build resilience to climate risks, while simultaneously educating future generations in environmental stewardship.

Moreover, national initiatives such as the EU Green Campus Life and locally grounded strategies—as seen in the University of Parma's commitment to shared governance and the development of climate-resilient open spaces—highlight how higher education institutions are not only contributing to the green transition but also shaping new cultural paradigms around sustainability, care, and community involvement. This positioning of campuses as both symbolic and operational actors in the ecological transition reinforces the systemic nature of NbSs, bridging urban planning, institutional responsibility, and transformative education. In parallel, the paradigm of edible cities, although still fragmented in urban strategies, offers a complementary perspective to Nature-Based Solutions by introducing productive green spaces that reinforce food resilience and social inclusion. The convergence between green campuses and edible cities suggests a systemic evolution in urban design, where the urban metabolism is reconnected with natural and food cycles through shared educational and productive environments. Several real-world implementations confirm the transformative potential of Nature-Based Solutions. Cities such as Barcelona, London, Milan, Oslo, and Leipzig are now widely referenced as exemplary cases for integrating ecological thinking with social infrastructure through both top-down and community-led interventions. In Barcelona, the city's Green Infrastructure and Biodiversity Plan promotes the renaturalization of public space by turning overbuilt streets into green corridors and introducing meadows and pollinator-friendly species in formerly impervious zones. The projects by the architecture office 08014 Arquitectura stand out for their tactical approach: through the gradual removal of asphalt and the reintroduction of native soil and vegetation, they enable spontaneous biodiversity while reclaiming street space for pedestrians and local communities (Figure 3a,b).



Figure 3. (**a**) Plaça de les Glòries, Barcelona: park view. Green urban regeneration project integrating vegetation and recreational space within a dense urban context. Photo by Marco Bellomo, 2024. (Project completion year: 2025.) (**b**) San Martí district, Barcelona: street view. Example of nature-based urban regeneration focused on pedestrian comfort, vegetation recovery and climate adaptation in a high-density residential context. Photo by Marco Bellomo, 2024.

In London, the Victoria Business Improvement District (Victoria BID) has implemented green corridors and urban rain gardens to enhance biodiversity, improve pedestrian comfort, and mitigate flooding risks in a densely urbanized area. In Milan, the Biblioteca degli Alberi offers a multifunctional urban park that integrates ecological connectivity, recreational spaces, and climate mitigation features in one of the most densely built parts of the city. In Oslo, the transformation of Tøyenparken highlights the role of community engagement in the creation and management of multifunctional green spaces that promote both social inclusion and biodiversity. Similarly, Leipzig's Stadtgärten initiative demonstrates how urban gardens and edible city strategies can revitalize vacant lots, foster community cohesion, and contribute to urban food sovereignty [62]. Together, these interventions illustrate how integrating ecological functionality with social accessibility can generate multifunctional spaces that respond to both planetary and human needs. Moreover, the geographical distribution of these case studies across different climate zones—ranging from the hot-summer Mediterranean climate of Barcelona, through the temperate oceanic climates of London and Leipzig, to the humid subtropical environment of Milan and the cold continental conditions of Oslo—demonstrates the remarkable adaptability of Nature-Based Solutions. Their success across such diverse contexts highlights that, when properly tailored, NbSs can act as effective socio-ecological infrastructures capable of enhancing urban resilience, fostering social inclusion, and supporting ecosystem services independently of climatic constraints.

8. Discussions

8.1. European Policies and Urban Management

The temporal analysis of European initiatives on urban greening, or more broadly on NbSs, reveals a significant intensification of actions starting from 2010 (Figure 4): a phenomenon attributable to various dynamics. First, the adoption of the EU Strategy on adaptation to climate change in 2013 provided a framework for action at local, regional and national levels, encouraging cities to develop their own adaptation strategies. Furthermore,

initiatives such as the Covenant of Mayors for Climate and Energy promoted the adoption of concrete measures by local governments.



Figure 4. Timeline of the key milestones in EU NbS policy development.

European cities that have adopted climate adaptation plans are distributed across different climate zones. Cities with an oceanic climate (Cfb), such as London, Paris, Brussels, Hamburg, Rotterdam and Copenhagen, characterized by moderate temperatures, year-round rainfall and non-extreme winters, have focused their strategies on stormwater management, as in the case of Rotterdam and Hamburg, on the creation of green corridors, as in Paris, and on the mitigation of the urban heat island effect, as in the policies adopted by London. Cities with a Mediterranean climate (Csa, Csb), including Barcelona, Milan and Lisbon, instead face high summer temperatures and long periods of drought, which is why their strategies focus on urban shading measures, such as the "Plan Clima" in Barcelona, reforestation, as in the "ForestaMi" project in Milan, and heat wave management. Cities with a humid continental climate (Dfb), such as Vienna, Berlin, Stockholm and Oslo, characterized by harsh winters and well-distributed precipitation, have developed plans that focus in particular on water management and thermal insulation through Nature-Based Solutions. Helsinki, which falls within the subarctic climate (Dfc), has adopted strategies aimed at balancing the need for heating with sustainability, implementing multifunctional green spaces and green roofs. Zurich, with its transitional alpine climate (Cfb/Dfb depending on the altitude), has instead focused on NbSs to mitigate hydrogeological risk and stabilize the territory. The geographical and temporal distribution of these plans highlights a greater adoption in cities with oceanic and Mediterranean climates, where the increase in summer temperatures and the risk of extreme weather events have prompted a more timely response. The post-2010 acceleration in the adoption of these plans can be traced back to the European Union's commitment to providing a reference regulatory and strategic framework, with key documents such as the 2013 European Strategy for Adaptation to Climate Change and the 2020 Biodiversity Strategy, as well as initiatives such as the 2020 Green City Accord, which has strengthened the promotion of Nature-Based Solutions. However, a critical analysis shows that cities with harsh winters, such as Oslo and Helsinki, have adopted strategies later than Mediterranean or oceanic ones, probably because the climate challenges in these contexts require different solutions. Furthermore, although most cities have developed strategies based on soft and green actions, gray infrastructures are less integrated into the plans, limiting in some cases the effectiveness of the measures adopted. In particular, cities with high vulnerabilities, such as Mediterranean ones, exposed to droughts and heat waves, or Nordic ones, where cold management is a central challenge, may require even more incisive interventions to ensure effective and long-lasting resilience over time. It should be noted, as already mentioned in the introduction, that despite the numerous benefits of NbSs, their large-scale implementation is hindered by several factors, including regulatory fragmentation, limited access to funding, weak coordination among different levels of government, and the lack of shared standards and effective evaluation tools. However, these challenges can be overcome through careful and integrated planning and design, capable of harmonizing regulations, facilitating the definition of investment

priorities, strengthening institutional coordination, and promoting the development of common guidelines and operational frameworks, thereby making NbSs more accessible, replicable, and scalable.

8.2. Green Roofs

The comparative analysis of the European case studies (Table 3) highlights the growing strategic importance of green roofs in urban planning and climate change policies. What emerges as particularly significant is not only the diversity of solutions adopted but also their adaptability to specific local conditions, signaling a shift from isolated technical installations to integrated, multifunctional systems that contribute meaningfully to urban regeneration. This design flexibility is an important factor for the large-scale adoption of green roofs; however, it is crucial to emphasize the need for a careful analysis of structural characteristics along with a set of parameters and variables, especially when working on existing buildings [6].

Among these factors, climate plays a fundamental role, exerting a direct influence on the design of green roofs, particularly in the selection of plant species and the management of rainwater. The examples analyzed in paragraph 5 focus on green roofs implemented in cities with predominantly temperate oceanic (Cfb) and humid continental (Dfb) climates. Basel and Berlin, for instance, characterized by moderate precipitation and cold winters, favor the use of native and resilient plant species, whereas Copenhagen and Rotterdam, experiencing higher levels of rainfall, primarily emphasize strategies for water retention. Particularly noteworthy is the systemic approach adopted by some cities, which have not limited themselves to promoting individual projects, but have instead embedded green roofs within broader urban strategies. These cities distinguish themselves not only through their quantitative ambitions (in terms of green surface area created) but also through the quality of their policies and implementation mechanisms. These include regulatory frameworks, financial incentives, technical guidelines, and monitoring systems. From this perspective, the models developed in Basel, Hamburg, and Copenhagen represent exemplary practices that can serve as references for other contexts, provided they are critically analyzed and adapted to local specificities.

A particularly relevant aspect is the capacity of some projects to transcend purely environmental goals, incorporating social, cultural, and even symbolic functions. In fact, green roofs become spaces for community engagement, educational tools, and identity-forming elements within the urban landscape. This holistic approach enhances the public value of such interventions and supports their stable integration into long-term urban planning policies. However, not all cities have reached solid maturity in this regard and, in some cases, the green roof is reduced to a simple technical or aesthetic intervention, not connected to a broader discussion aimed at increasing the climate resilience of the built environment. Promoting this type of broader approach, aimed at climate resilience, is not easy due to several aspects. The most advanced cases have developed within contexts equipped with strong economic resources, administrative capacities, and a mature planning culture. The gap with emerging contexts—where green roofs are still fragmented or experimental—underscores the need for coordinated political and technical support at supralocal levels to ensure equitable and structured diffusion. Furthermore, despite their proven effectiveness, many of the projects lack systematic long-term impact assessments. The evaluation of effects on microclimate, biodiversity, energy efficiency, or social well-being is often absent or limited to qualitative indicators. To consolidate green roofs as essential urban infrastructure rather than supplementary features, it is crucial to imple-

ment more rigorous monitoring and evaluation systems capable of generating objective, comparable data.

Thus, the examples analyzed provide an overview, though not yet exhaustive, of the achievements to date, but more importantly, they indicate a clear direction for the future. The most resilient cities will be those capable not only of adopting effective technical solutions and integrating them into their urban systems in an inclusive, measurable, and strategic manner. In this regard, green roofs should not be seen merely as additional features, but as fundamental components of green infrastructure essential for promoting the ecological transition.

8.3. Green Facades

Although the greening measures and plans adopted by several European cities mainly focus on urban-scale interventions in public spaces and areas adjacent to buildings, in some cities, such as Copenhagen and Berlin (Green Roof and Wall Program), planning tools for building interventions actively promote the creation of green roofs and facades. Often, these projects are specific and punctual initiatives driven by private developers.

Even the Metro Adapt project, prepared by the City of Milan, defines the implementation of VGSs as a punctual intervention at the building scale. This could be ascribable to the peculiarities specific to vertical greening interventions, for which buildings, whether new or existing, must possess certain specific characteristics in terms of orientation, morphology, geometry and the ratio of opaque to transparent surfaces.

In relation to façade orientation, the application of VGSs is very useful on east- or west-facing elevations, where they can validly contribute to both shading of opaque walls and shielding of incoming solar radiation from glazed surfaces, with significant benefits in the summer period in terms of reducing surface temperatures and improving indoor comfort. On south-facing elevations, the presence of VGSs is advisable when facades are devoid of overhangs or balconies that, in summer, may already be sufficient to provide shading and screening for vertical closures, both opaque and transparent.

The application of VGSs is strongly conditioned by the morphology of the building. The presence of projections such as cornices, stringcourses, or balconies means that VGSs must be advanced relative to the façade. The presence of porches, commercial activities, or garages on the ground floor greatly limits the construction of VGSs, not allowing the placement of plants on the ground.

In relation to the presence of glazed surfaces in the elevations, it will be necessary to carefully consider which greening system to use also depending on the required performance (shading of opaque surfaces or screening of glazed ones).

8.4. Urban Spaces

The growing integration of NbSs into the design and transformation of urban spaces marks a paradigmatic shift in how cities address environmental and social challenges. Beyond their ecological functions, these interventions generate hybrid spaces that promote inclusion, health, and cultural expression, aligning with regenerative and systemic design approaches. Recent European experiences, such as the green corridors and pollinator-friendly streets in Barcelona, demonstrate how NbSs can reconcile environmental performance with the enhancement of everyday urban life through low-tech, community-centered, and spatially inclusive interventions [63,64].

Increasingly, university campuses are emerging as strategic testing grounds for the real-world implementation of NbSs. Institutions such as the University of Copenhagen and the University of Oxford are promoting integrated approaches that combine lifecycle

assessment, biodiversity enhancement, and participatory research, transforming campuses into microcosms of urban resilience [65]. Initiatives like EU Green Campus Life and actions by universities such as Parma further demonstrate how higher education environments can foster climate adaptation strategies while embedding environmental values in daily academic practices.

These developments reinforce the broader need to reframe urban spaces—whether public streets, community gardens, or academic campuses—as multifunctional systems capable of delivering ecosystem services, social cohesion, and health co-benefits simultaneously. The Millennium Ecosystem Assessment already recognized the intertwined nature of ecological and human well-being [66], while more recent research has clarified how urban green infrastructure can address complex socio-environmental risks in dense urban contexts [67]. Conceptual frameworks such as regenerative cities [68] and planetary boundaries stress the urgency of integrating nature into built environments to avoid ecological tipping points and enhance urban resilience. In this context, Nature-Based Solutions emerge as critical policy tools for systemic transformation [69] calling for innovative governance models and cross-scalar collaborations to embed sustainable practices into everyday urban and academic life.

Nevertheless, the long-term effectiveness of NbSs within urban settings is not guaranteed by design quality alone. Their success also hinges on the governance and maintenance strategies that support them over time. As these spaces are increasingly recognized as shared commons, their durability requires a balance between institutional responsibility and civic engagement. Public entities must provide adequate resources and adaptive management frameworks, while communities are called upon to nurture a collective sense of stewardship. Without this shared care, even well-designed interventions risk degradation or disengagement. Embedding NbSs into urban life therefore means integrating not only ecological performance, but also intelligent and inclusive models of long-term maintenance. This perspective also highlights the need for greater coordination among different dimensions of Nature-Based Solutions. For instance, integrating green campus strategies with edible city initiatives could foster hybrid urban models that combine environmental education, food sovereignty, and social equity. From this viewpoint, future urban policies should explicitly consider the synergistic potential of these practices, emphasizing their environmental, cultural, and community-driven value.

9. Towards a Regenerative Design

The integration of green roofs, green façades, and the revitalization of urban spaces through greening interventions represents a concrete response to the challenges outlined in the 2030 Agenda, as shown in Figure 5. Urban greening supports SDG 11 by enhancing the livability and resilience of cities, helping to mitigate the urban heat island effect and reducing energy demand for cooling. The creation of ecological corridors promotes urban biodiversity (SDG 15) by connecting natural habitats. At the same time, the greening of the built environment acts as a "green lung", absorbing carbon dioxide and combating climate change (SDG 13), with a direct impact on reducing greenhouse gas emissions. The widespread presence of green areas improves air quality, fosters physical and mental well-being among citizens (SDG 3), and encourages healthier lifestyles. Moreover, through natural drainage solutions and the purification of stormwater, greening strategies contribute to more efficient and sustainable water resource management, aligning with SDG 6. Ultimately, urban green infrastructure emerges as an essential element for building more sustainable, resilient, and inclusive cities.

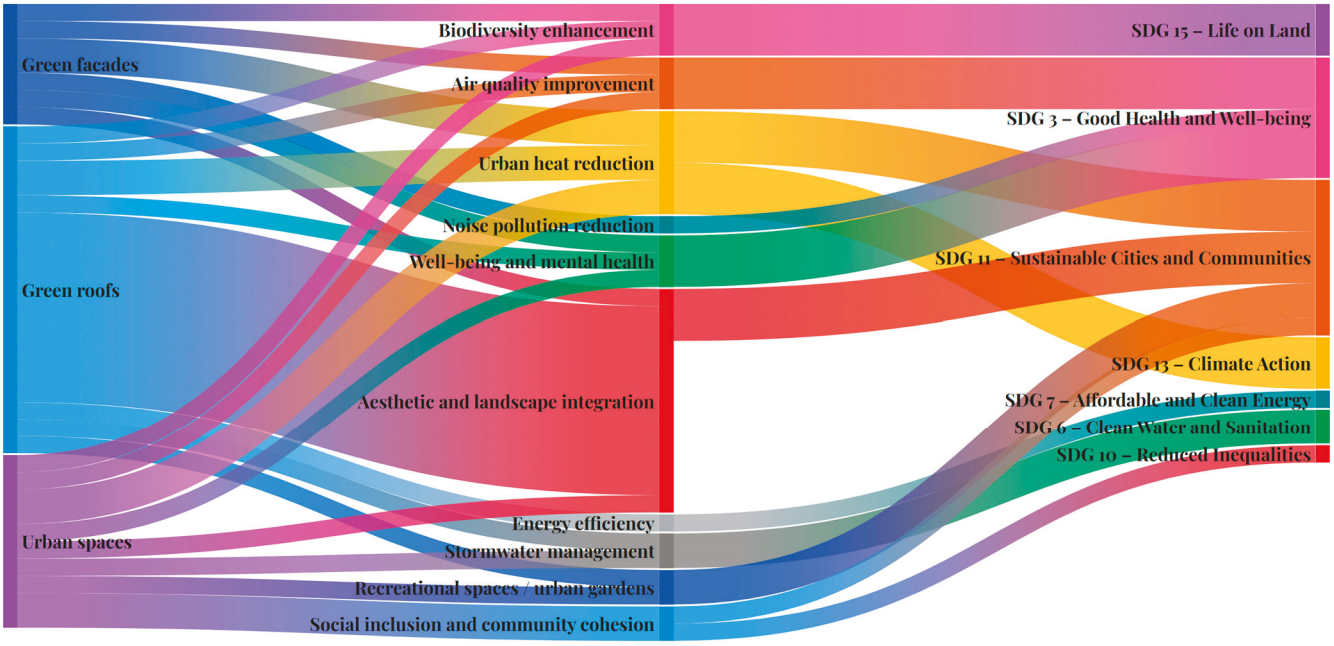


Figure 5. Connections between greening strategies, resulting benefits, and SDGs of the 2030 Agenda.

However, it is important to emphasize that greening strategies do not merely aim to preserve the existing urban environment in a sustainable way. On the contrary, they introduce transformative dynamics that enrich the quality of the built space, turning the urban environment into a more complex, interconnected, and productive ecosystem. The creation of new urban habitats, the increase in biodiversity, and the reduction in air and noise pollution, as well as urban heat island effects, are just some of the positive impacts that go beyond simple environmental compensation, generating tangible added value for both local contexts and the entire planet. In this regard, the greening of the built environment aligns perfectly with the principles of regenerative design, which, moving beyond mere sustainability, seeks to regenerate, restore, and enhance natural systems [70,71]. It can thus be considered as a progression beyond simple mitigation and adaptation strategies in response to climate change. According to this approach, indeed, the built environment is no longer considered as an external or opposing element to nature, but rather as an integral part of an evolving ecosystem, capable of producing resources, hosting life, and improving over time. Greening solutions, such as Nature-Based Solutions, undoubtedly represent a fundamental pillar of regenerative design due to their ability to restore ecosystems, enhance urban resilience, and provide environmental, social, and economic benefits. However, they are not the only tools available. To achieve a truly regenerative approach, these solutions must be complemented by other strategies and instruments, including the use of bio-based, renewable, and low-impact materials. It is also essential to assess and quantify environmental impacts through lifecycle assessment. Moreover, the support of smart technologies can be a promising avenue for evaluating the effectiveness of specific interventions in regenerative design. Therefore, to strengthen the methodological framework of regenerative design, future research should develop measurable indicators aligned with the SDGs, create simulation models to assess ecological and social performance, and analyze real-world case studies where the integration of greening, innovative materials, and intelligent technologies yields tangible results.

10. Conclusions

This study offers a comprehensive overview of the strategies and initiatives implemented at the European level, providing a valuable reference for policymakers, urban planners, and built environment practitioners committed to promoting a regenerative transition.

Since 2010, the European Union has increasingly prioritized greening policies as critical tools to address challenges such as rising temperatures, hydrogeological risks, and biodiversity loss. However, issues remain regarding the scalability and replicability of greening solutions, particularly in densely built or economically constrained urban contexts. The long-term effectiveness of these strategies will largely depend on their integration with broader urban policies and the availability of sustained financial support to ensure meaningful impacts on urban resilience.

The principal lessons derived from this study can be synthesized as follows:

- Greening the built environment must be understood not merely as an aesthetic intervention, but as a multifunctional strategy that delivers environmental, social, and economic benefits;
- The incorporation of green roofs, green façades, and the ecological regeneration of urban spaces requires a holistic approach and integrated planning across multiple governance levels;
- The success of such initiatives is strongly contingent upon public–private collaboration and active community engagement;
- Economic incentives, clear regulatory frameworks, and robust awareness-raising campaigns are essential to foster the widespread adoption of greening practices;
- Systematic monitoring and evaluation of impacts are crucial to validate the effectiveness of these strategies and to refine future policies aimed at enhancing urban climate resilience.

It strongly emerges that these strategies go beyond the pursuit of sustainability, aiming instead at the regeneration of the built environment. Their tangible impact fosters the creation of spaces that enhance biodiversity and ecosystem health, thereby contributing to the development of a climate-resilient urban fabric that harmoniously integrates with the natural environment. Finally, it is worth noting that the long-term success of nature-based strategies depends not only on their design and policy alignment, but also on how they are maintained and cared for over time. Ensuring continuity and effectiveness requires shared responsibility between public institutions and local communities, fostering a culture of co-management and stewardship of green urban assets. Despite the progress made in implementing green strategies for the built environment, several issues still require further investigation and represent promising directions for future research. Among these is the need to develop more accurate indicators and dynamic monitoring systems capable of assessing the real impacts of greening strategies over time on climate resilience, urban well-being, and biodiversity. At the same time, to keep pace with emerging challenges, it is essential to explore the potential of digital tools—such as GIS, digital twins, and artificial intelligence—in supporting the planning, management, and simulation of resilient green urban scenarios.

Author Contributions: Conceptualization, F.S.; methodology, F.S.; data curation, F.S.; writing—original draft preparation, F.S.—G.S. and G.L. (par. 6 e 8.3)—S.C. and M.B. (par. 7 e 8.2); writing—review and editing, F.S., L.D.—G.S. and G.L. (par. 6 e 8.3)—S.C. and M.B. (par. 7 e 8.2); visualization, F.S.; supervision, L.D., S.C., G.S. and G.L.; project administration, L.D., S.C. and G.S. All authors have read and agreed to the published version of the manuscript.

Funding: This research was funded by the European Union EU Next Generation Italian PRIN 2022 PNRR Programme under the "Greenwork—An interdisciplinary framework for urban health and urban resilience enhancement based on greening strategies on buildings and open spaces" project, CUP: E53D23019110001.

Data Availability Statement: No new data were created or analyzed in this study.

Conflicts of Interest: The authors declare no conflicts of interest.

References

1. Diana, L.; Sommese, F.; Ausiello, G.; Polverino, F. New Green Spaces for Urban Areas: A Resilient Opportunity for Urban Health. In *Resilience vs. Pandemics: Innovations in Public Places and Buildings*; Cheshmehzangi, A., Sedrez, M., Zhao, H., Li, T., Heath, T., Dawodu, A., Eds.; Springer Nature: Singapore, 2024; pp. 37–53, ISBN 978-981-99-8672-9.
2. Singh, M.; Sharston, R.; Murtha, T. Critical evaluation of the spatiotemporal behavior of UHI, through correlation analyses based on multi-city heterogeneous dataset. *Sustain. Cities Soc.* **2024**, *110*, 105576. [CrossRef]
3. Mobaraki, A.; Nikoofam, M.; Mobaraki, B. The Nexus of Morphology and Sustainable Urban Form Parameters as a Common Basis for Evaluating Sustainability in Urban Forms. *Sustainability* **2025**, *17*, 3967. [CrossRef]
4. Nature-Based Solutions | IUCN. Available online: https://iucn.org/our-work/nature-based-solutions (accessed on 18 February 2025).
5. Ascenso, A.; Augusto, B.; Silveira, C.; Rafael, S.; Coelho, S.; Monteiro, A.; Ferreira, J.; Menezes, I.; Roebeling, P.; Miranda, A.I. Impacts of nature-based solutions on the urban atmospheric environment: A case study for Eindhoven, The Netherlands. *Urban For. Urban Green.* **2021**, *57*, 126870. [CrossRef]
6. Sommese, F.; Diana, L. A holistic framework for the implementation of green roofs on existing buildings: A case study in the Mediterranean climate of Naples. *Build. Environ.* **2025**, *274*, 112811. [CrossRef]
7. UN—General Assembly. *Trasforming Our Worl: The 2030 Agenda for Sustainable Development*; UN—General Assembly: New York, NY, USA, 2015.
8. Grant, M.J.; Booth, A. A typology of reviews: An analysis of 14 review types and associated methodologies. *Health Inf. Libr. J.* **2009**, *26*, 91–108. [CrossRef] [PubMed]
9. Koppen Climate Classification | Definition, System, & Map | Britannica. Available online: https://www.britannica.com/science/Koppen-climate-classification (accessed on 19 July 2024).
10. Sommese, F. Nature-Based Solutions to Enhance Urban Resilience in the Climate Change and Post-Pandemic Era: A Taxonomy for the Built Environment. *Buildings* **2024**, *14*, 2190. [CrossRef]
11. Sommese, F. Nature-Based Solutions as Climate Change Adaptation Measures: Lessons and Best-Practices from European Cities; 2024. In Proceedings of the 11th International Conference of Ar.Tec. 2024, Palermo, Italy, 12–15 June 2024; pp. 678–691, ISBN 978-3-031-71862-5. [CrossRef]
12. European Commission. EU Adaptation Strategy. 2021. Available online: https://climate.ec.europa.eu/eu-action/adaptation-climate-change/eu-adaptation-strategy_en (accessed on 26 March 2025).
13. European Commission. Biodiversity Strategy for 2030. 2020. Available online: https://environment.ec.europa.eu/strategy/biodiversity-strategy-2030_en (accessed on 26 March 2025).
14. European Commission. Green Infrastructure. 2013. Available online: https://environment.ec.europa.eu/topics/nature-and-biodiversity/green-infrastructure_en (accessed on 26 March 2025).
15. European Commission. New Urban Agenda. 2016. Available online: https://ec.europa.eu/regional_policy/policy/themes/urban-development/new-urban-agenda_en (accessed on 26 March 2025).
16. European Commission. The European Green Deal. 2021. Available online: https://commission.europa.eu/strategy-and-policy/priorities-2019-2024/european-green-deal_en (accessed on 26 March 2025).
17. European Commission. New EU Forest Strategy for 2030. 2021. Available online: https://environment.ec.europa.eu/strategy/forest-strategy_en (accessed on 26 March 2025).
18. European Commission. Green City Accord. 2020. Available online: https://environment.ec.europa.eu/topics/urban-environment/green-city-accord_en (accessed on 26 March 2025).
19. European Commission. Urban Nature Platform. 2020. Available online: https://environment.ec.europa.eu/topics/urban-environment/urban-nature-platform_en (accessed on 26 March 2025).
20. European Commission. Horizon Europe. 2021. Available online: https://research-and-innovation.ec.europa.eu/funding/funding-opportunities/funding-programmes-and-open-calls/horizon-europe_en (accessed on 26 March 2025).
21. Pla Clima | Barcelona City Hall. Available online: https://www.barcelona.cat/barcelona-pel-clima/en/el-pla-clima (accessed on 26 March 2025).

22. Climate Plan 2035 | Copenhagen. Available online: https://international.kk.dk/about-copenhagen/liveable-green-city/2035-climate-plan (accessed on 26 March 2025).
23. City of Rotterdam | Rotterdam Cilmate Proof, 'Rotterdam Adaptation Strategy'. 2013. Available online: https://www.urbanisten.nl/work/rotterdam-adaptation-strategy (accessed on 26 March 2025).
24. Hamburg City, 'The Hamburg Climate Action Plan'. 2011. Available online: https://www.hamburg.de/resource/blob/169842/e7fd3227d510b68f5bfdf53445b41a30/d-booklet-2011-ksk-englisch--data.pdf (accessed on 26 March 2025).
25. Comune di Milano. Forestami | Piantiamo 3 Milioni di Alberi Entro il 2030. Available online: https://forestami.org/ (accessed on 26 March 2025).
26. Conseil de Paris. Plan Climat Air Energie de Paris 2024–2030. 2024. Available online: https://cdn.paris.fr/paris/2024/12/18/planclimatparis2024-2030_controlelegalite-DKwD.pdf (accessed on 26 March 2025).
27. Berlin City Stadtentwicklungsplan (StEP) Klima 2.0. Available online: https://www.berlin.de/sen/stadtentwicklung/planung/stadtentwicklungsplaene/step-klima-2-0/ (accessed on 26 March 2025).
28. Urban Heat Islands—Strategy Plan Vienna. Available online: https://climate-adapt.eea.europa.eu/en/metadata/publications/urban-heat-islands-2013-strategy-plan-vienna (accessed on 26 March 2025).
29. Edifici Verdi: La Vita Sboccia su Molti tetti Della Città. Available online: https://www.bafu.admin.ch/bafu/it/home/temi/paesaggio/dossier/webzine2024-2-focus/edifici-verdi-la-vita-sboccia-su-molti-tetti-della-citta.html (accessed on 26 March 2025).
30. Lars Gitz Architects Basecamp. Available online: https://www.larsgitz.com/project/basecamp/ (accessed on 26 March 2025).
31. Denmark—The Green Cities Europe Award—2024. Available online: https://award.thegreencities.eu/award-2023/denmark/ (accessed on 26 March 2025).
32. Snep, R.P.; Voeten, J.G.; Mol, G.; Van Hattum, T. Nature Based Solutions for Urban Resilience: A Distinction Between No-Tech, Low-Tech and High-Tech Solutions. *Front. Environ. Sci.* **2020**, *8*, 599060. [CrossRef]
33. The Winner "BuGG Green Roof of the Year" 2021 Is Announced!—World Green Infrastructure Network. Available online: https://worldgreeninfrastructurenetwork.org/the-winner-bugg-green-roof-of-the-year-2021-is-announced/ (accessed on 26 March 2025).
34. Germany—The Green Cities Europe Award—2024. Available online: https://award.thegreencities.eu/award-2023/germany/ (accessed on 26 March 2025).
35. C40 Guide di Buone Pratiche: Rotterdam—Strategia di Adattamento ai Cambiamenti Climatici—C40 Città. Available online: https://www.c40.org/it/case-studies/c40-good-practice-guides-rotterdam-climate-change-adaptation-strategy/ (accessed on 27 March 2025).
36. Four Harbour Roof Park by Buro Sant en Co. Available online: https://landezine.com/four-harbour-roof-park-by-buro-sant-en-co/ (accessed on 26 March 2025).
37. Ireland—The Green Cities Europe Award—2024. Available online: https://award.thegreencities.eu/award-2022/ireland/ (accessed on 26 March 2025).
38. Graham, P. Building Ecology: First Principles For A Sustainable Built Environment | Wiley. 2004. Available online: https://www.wiley.com/en-us/Building+Ecology:+First+Principles+For+A+Sustainable+Built+Environment-p-9780632064137 (accessed on 24 May 2025).
39. Ottelé, M. *The Green Building Envelope: Vertical Greening*; TU Delft: Delft, The Netherlands, 2011; ISBN 978-90-90-26217-8.
40. Sternberg, T.; Viles, H.; Cathersides, A.; Edwards, M. Dust particulate absorption by ivy (*Hedera helix* L.) on historic walls in urban environments. *Sci. Total Environ.* **2010**, *409*, 162–168. [CrossRef] [PubMed]
41. Hunter, A.M.; Williams, N.S.G.; Rayner, J.P.; Aye, L.; Hes, D.; Livesley, S.J. Quantifying the thermal performance of green façades: A critical review. *Ecol. Eng.* **2014**, *63*, 102–113. [CrossRef]
42. Papadakis, G.; Tsamis, P.; Kyritsis, S. An experimental investigation of the effect of shading with plants for solar control of buildings. *Energy Build.* **2001**, *33*, 831–836. [CrossRef]
43. Susca, T.; Zanghirella, F.; Colasuonno, L.; Del Fatto, V. Effect of green wall installation on urban heat island and building energy use: A climate-informed systematic literature review. *Renew. Sustain. Energy Rev.* **2022**, *159*, 112100. [CrossRef]
44. Wong, N.H.; Kwang Tan, A.Y.; Chen, Y.; Sekar, K.; Tan, P.Y.; Chan, D.; Chiang, K.; Wong, N.C. Thermal evaluation of vertical greenery systems for building walls. *Build. Environ.* **2010**, *45*, 663–672. [CrossRef]
45. Zhang, L.; Deng, Z.; Liang, L.; Zhang, Y.; Meng, Q.; Wang, J.; Santamouris, M. Thermal behavior of a vertical green facade and its impact on the indoor and outdoor thermal environment. *Energy Build.* **2019**, *204*, 109502. [CrossRef]
46. Hotel VIU Milan. AGP Greenscape. Available online: https://agep.it/progetti/hotel-viu/ (accessed on 26 April 2025).
47. Maison Edouard François. Available online: https://www.edouardfrancois.com (accessed on 26 March 2025).

48. Welcome to Vertical Garden Patrick Blanc | Vertical Garden Patrick Blanc. Available online: https://www.verticalgardenpatrickblanc.com/ (accessed on 26 March 2025).
49. Edgware Road Living Wall Blooms on Tube Station, Marylebone. Available online: https://www.biotecture.uk.com/portfolio/edgware-road-tube-station-marylebone/ (accessed on 26 March 2025).
50. Covent Garden Living Wall Brings Plants into Central London. Available online: https://www.biotecture.uk.com/portfolio/regal-house-covent-garden/ (accessed on 26 March 2025).
51. This Is Apt | Architects in London. Available online: https://apt.london/404 (accessed on 26 March 2025).
52. Citicape House. Available online: https://nla.london/projects/citicape-house (accessed on 26 March 2025).
53. VenhoevenCS Architecture+Urbanism. Available online: https://venhoevencs.nl/ (accessed on 26 March 2025).
54. MVRDV—Architects. Available online: https://www.mvrdv.com/ (accessed on 26 March 2025).
55. Mario Cucinella Architects. Available online: https://www.mcarchitects.it/ (accessed on 26 March 2025).
56. Herzog & de Meuron. Available online: https://www.herzogdemeuron.com/ (accessed on 26 March 2025).
57. Caixa Forum Museum Vertical Garden. Greenroofs.com. Available online: http://www.greenroofs.com/projects/caixa-forum-museum-vertical-garden/ (accessed on 26 March 2025).
58. Urban Jungle | Prato. Stefano Boeri Archit. Available online: https://www.stefanoboeriarchitetti.net/project/prato-urban-jungle/ (accessed on 26 March 2025).
59. Raymond, C.M.; Frantzeskaki, N.; Kabisch, N.; Berry, P.; Breil, M.; Nita, M.R.; Geneletti, D.; Calfapietra, C. A framework for assessing and implementing the co-benefits of nature-based solutions in urban areas. *Environ. Sci. Policy* **2017**, *77*, 15–24. [CrossRef]
60. Colding, J.; Barthel, S. The potential of 'Urban Green Commons' in the resilience building of cities. *Ecol. Econ.* **2013**, *86*, 156–166. [CrossRef]
61. Artmann, M.; Sartison, K. The Role of Urban Agriculture as a Nature-Based Solution: A Review for Developing a Systemic Assessment Framework. *Sustainability* **2018**, *10*, 1937. [CrossRef]
62. Paudel, S.; States, S.L. Urban green spaces and sustainability: Exploring the ecosystem services and disservices of grassy lawns versus floral meadows. *Urban For. Urban Green.* **2023**, *84*, 127932. [CrossRef]
63. Emilsson, T.; Ode Sang, Å. Impacts of Climate Change on Urban Areas and Nature-Based Solutions for Adaptation. In *Nature-Based Solutions to Climate Change Adaptation in Urban Areas: Linkages Between Science, Policy and Practice*; Kabisch, N., Korn, H., Stadler, J., Bonn, A., Eds.; Springer International Publishing: Cham, Switzerland, 2017; pp. 15–27, ISBN 978-3-319-56091-5.
64. Ajuntament de Barcelona. *Pla del Verd i de la Biodiversitat de Barcelona*; Ajuntament de Barcelona: Barcelona, Spain, 2020.
65. University of Copenhagen Green Campus 2020. Strategy for Resource Efficiency and Sustainability at the University of Copenhagen. 2020. Available online: https://nordicsustainablecampusnetwork.wordpress.com/wp-content/uploads/2016/11/ku_blogpostnov2016_sdstrategy.pdf (accessed on 26 March 2025).
66. Maes, J.; Fabrega, N.; Zulian, G.; Barbosa, A.; Vizcaino, P.; Ivits, E.; Polce, C.; Vandecasteele, I.; Rivero, I.M.; Guerra, C. *Mapping and Assessment of Ecosystems and their Services*; European Commission: Brussels, Belgium, 2015.
67. Green and Blue Infrastructure (GBI) and Urban Nature-Based Solutions (NbS) Contribution to Human and Ecological Well-Being and Health | Oxford Open Infrastructure and Health | Oxford Academic. Available online: https://academic.oup.com/ooih/article/doi/10.1093/ooih/ouad004/7322050 (accessed on 26 March 2025).
68. HCU—HafenCity University Hamburg Regenrative Cities. Available online: https://www.worldfuturecouncil.org/wp-content/uploads/2016/01/WFC_2010_Regenerative_Cities.pdf (accessed on 26 March 2025).
69. Turner, B.; Devisscher, T.; Chabaneix, N.; Woroniecki, S.; Messier, C.; Seddon, N. The role of nature-based solutions in supporting social-ecological resilience for climate change adaptation. *Annu. Rev. Environ. Resour.* **2022**, *47*, 123–148. [CrossRef]
70. Cole, R.J.; Oliver, A.; Robinson, J. Regenerative design, socio-ecological systems and co-evolution. *Build. Res. Inf.* **2013**, *41*, 237–247. [CrossRef]
71. Naboni, E.; Havinga, L.C. *Regenerative Design In Digital Practice. A Handbook for the Built Environment*; Eurac Research: Bolzano, Italy, 2019; ISBN 978-3-9504607-2-8.

Disclaimer/Publisher's Note: The statements, opinions and data contained in all publications are solely those of the individual author(s) and contributor(s) and not of MDPI and/or the editor(s). MDPI and/or the editor(s) disclaim responsibility for any injury to people or property resulting from any ideas, methods, instructions or products referred to in the content.

buildings

MDPI

Article

Impacts of Vertical Greenery on Outdoor Thermal Comfort and Carbon Emission Reduction at the Urban Scale in Turin, Italy

Amir Dehghan Lotfabad [1], Seyed Morteza Hosseini [2,*], Paolo Dabove [1], Milad Heiranipour [3] and Francesco Sommese [4]

[1] Department of Environment, Land and Infrastructure Engineering, Politecnico di Torino, Corso Duca degli Abruzzi, 24, 10129 Turin, Italy; amir.dehghanlotfabad@studenti.polito.it (A.D.L.); paolo.dabove@polito.it (P.D.)
[2] Department of Architecture, Design & Media Technology, Aalborg University Copenhagen, A.C. Meyers Vænge 15, 2450 Copenhagen SV, Denmark
[3] Department of Energy, Politecnico di Torino, Corso Duca degli Abruzzi, 24, 10129 Turin, Italy; milad.heiranipour@polito.it
[4] Department of Civil, Building and Environmental Engineering, University of Naples Federico II, P.le Vincenzo Tecchio, 80, 80125 Naples, Italy; francesco.sommese@unina.it
* Correspondence: smho@create.aau.dk

Abstract: Urban heat islands (UHIs) increase urban warming and reduce outdoor thermal comfort due to changing surface characteristics and climate change. This study investigates the role of green walls (GWs) in mitigating UHI, improving outdoor thermal comfort, and reducing carbon emissions under current and future (2050) scenarios. Focusing on Via della Consolata, Turin, Italy, the study combines remote sensing for UHI detection and numerical simulations for thermal analysis during seasonal extremes. The results show that GWs slightly reduce air temperatures, with a maximum decrease of 1.6 °C in winter (2050), and have cooling effects on mean radiant temperature (up to 2.27 °C) during peak summer solar radiation. GWs also improve outdoor comfort, reducing the Universal Thermal Climate Index by 0.55 °C in the summer of 2050. The energy analysis shows that summer carbon emission intensity is reduced by 31%, despite winter heating demand increasing emissions by 45%. The study highlights the potential of GWs in urban climate adaptation, particularly in dense urban environments with low sky view factors. Seasonal optimization is crucial to balance cooling and heating energy demand. As cities face rising temperatures and heat waves, the integration of GWs offers a sustainable strategy to improve microclimate, reduce carbon emissions, and mitigate the effects of UHI.

Keywords: air temperature; climate change; green wall; mean radiant temperature; urban heat island

1. Introduction

1.1. Background

In today's world, over half of the world's population (54 percent) lives in urban areas. The coming decades will bring further profound changes to the size and spatial distribution of the global population. The world's population in 2050 is projected to be 66 percent urban dwellers, with the global urban population projected to grow by 2.5 billion urban dwellers between 2014 and 2050 [1]. Urbanization can cause problems for city inhabitants. One of the more prominent problems is the UHI effect of the urban canopy layer, which can also

increase energy consumption [2]. The UHI effect is responsible for having higher air and surface temperature [3]. On a sunny day, solar irradiation will heat up the surfaces during the day, while at night, the temperature in the environment will be lower, and the surfaces will exchange the absorbed heat with their colder surroundings. The surface temperature is the main parameter affecting the mean radiant temperature (Tmrt) and consequently the universal thermal climate index (UTCI), alongside relative humidity and wind speed. Understanding the factors influencing the UHI effect is crucial for better use of urban heat reduction strategies and solutions. The most utilized research methods in this area of research were numerical model simulation, followed by mobile or stationary ground-based measurements and remote sensing. While satellite-based observations focus on surface temperature on a mesoscale, numerical simulations and field measurements provide further environmental parameters that allow for human thermal comfort analysis at the pedestrian level and consider the air temperature instead of the surface temperature, which is essential to predict the effect of heat events on human health and energy consumption [4–6]. It is also known that the diurnal profiles of surface urban heat islands (SUHIs) differ from those of canopy UHIs. Large SUHI generally occurs during the daytime, while large canopy UHI generally occurs at night, and therefore spatial assessment of canopy UHI through remote sensing techniques at a fine scale may introduce estimation error [7].

1.2. Examining the Factors Influencing UHI

The studies with statistical models such as stepwise multiple linear regression (SMLR), XGBoost, bivariate and multivariate analysis, and Pearson correlation analysis highlight the effects of urban morphology, building geometries, and surface properties on the UHI. Findings consistently demonstrate a strong correlation between urban morphology and UHI effects, particularly in densely built areas with high-rise structures. The UHI effect is influenced by several key morphological parameters, including building height, density, size, aspect ratio, sky view factor (SVF), area, and orientation [6,8]. Of these factors, orientation is unique in its effects on energy use intensity and thermal comfort [9,10].

Building height and volume would increase nighttime SUHI as they store heat during the day and release it at night, and density increases daytime SUHI by elevating heat absorption and increasing heat retention in cities. Conversely, wider urban canyons could reduce SUHI by allowing better air circulation as wind speed reduces nighttime SUHI [11]. Findings show that the three main morphological parameters affecting UHI are SVF, street length (SL), and pervious surface fraction. Two main parameters of the increase in the total length of the streets in the site and the decrease in the SVF, which has a negative correlation with the ratio of mean building height to mean street width in the sample site (H/W), would exacerbate the SUHI [7]. SVF ranges from 0 to a maximum of 1, which is completely open to the sky and is defined as the percentage of free sky at a specific location [12,13]. A moderate-to-high SVF can mitigate UHI, whereas extremely high SVF levels intensify it [14]. In a simulation study with Envi-met [15] of the effect of the built environment (H/W), urban greenery, and SVF on thermal comfort, a regression analysis showed that the effect of SVF on air temperature was smallest. In contrast, its effect on surface temperature and consequently Tmrt, as an important parameter influencing UTCI [16], is the largest. A 0.1 unit increase in SVF led to an increase of 1.6 °C and 2.4 °C in air temperature and 17.9 °C and 16.7 °C in Tmrt within N-S and E-W streets, respectively. It also proves the effect of the orientation of buildings, to be considered by designers for the future development of cities [17]. Ref. [18] concerned with the best urban morphology parameters on air temperature, solar radiation, wind speed, Tmrt, and Physiological Equivalent Temperature (PET) in three different sites in Nanjing, China, without considering anthropogenic heat emissions. They found that, in

general, by increasing SVF, the air temperature would increase, and increasing building area is not the main cause of the increase in air temperature. However, the variation in Tmrt was greater than air temperature. The correlation between Tmrt and SVF is different between day and night, with a positive correlation in daytime and a negative correlation in nighttime. The Tmrt correlates positively with the distance between buildings, gaining solar radiation in the daytime, and has a negative correlation with building heights. They also found areas with lower SVF, lower distance between buildings, lower solar radiation, and consequently lower Tmrt and better PET [11]. Also mentioned other factors influencing SUHI and indicated that, instead of urban morphology, climate background has a weak correlation with SUHI, and the relationship between different climate zones and geographical locations is varied. Conversely, surface properties, such as enhanced vegetation index, are the most critical factor for mitigating daytime heat, since urbanization causes a significant reduction in greenness in urban areas, which reduces the evapotranspiration capacity within the city and subsequently enhances SUHI intensities.

1.3. Urban Heat Island Mitigation Scenarios and State-of-the-Art

One UHI mitigation strategy for existing urban context without configuration in the urban morphology and orientation is the modification and incorporation of sustainable building materials into the built environment by changing the albedo of surfaces such as pavements and facades with high thermal effects materials and painting materials to be bright and reflective in the summer [19]. However, Ref. [20] gave suggestions that changing albedo solely would not improve thermal comfort enough in extreme events and recommended using additional strategies such as shading and evaporative cooling, especially in areas with low aspect ratios. In this case, urban areas around the world are increasingly investing in networks of urban forests, gardens, and other forms of green infrastructure (Table 1) such as trees, which (irrespective of configuration) can reduce thermal sensation from "Very Hot" conditions to "Hot", irrespective of the street canyon's aspect ratio [21], green roofs, and vertical greenery systems (VGSs) for their benefits in improving a building's thermal and acoustic insulation, reducing the urban heat island effect, increasing urban biodiversity, and improving air quality [22,23], and reducing cooling energy demand, which consequently reduces CO_2 emissions in summer months [24]. Climate change also presents opportunities to promote urban green infrastructure [25], which, as a climatic background, is considered one of the factors affecting UHI. It is important to understand how to intervene in particularly compact and dense urban structures where there is not enough space to implement nature-based solutions [26]. In densely urbanized areas, buildings' surfaces (i.e., façades and rooftops) can offer room for the installation of vegetation [27]. One of the well-known green initiatives implemented in dense urban environments is vertical greening due to its small footprint and ability to cover a large surface area as well as lower installation costs [3,28]. It has also been concluded that in a densely urbanized area characterized by high-rising buildings, green walls are more beneficial in mitigating UHI than extensive green roofs (EGRs), which have a negligible effect on urban warming. Using plants is more beneficial than other devices on facades, as the temperature of the leaves is lower than other materials. Around 60% of solar radiation absorbed by plants transforms into latent heat and sensible heat by evaporative cooling, provided by evapotranspiration from the plants and the substrate [29–31]. Consequently, it can reduce the fluctuations of surface temperature, air temperature, and relative humidity, alongside the amount of particulate matter on the walls, by reducing the risk of most common degradation mechanisms induced by salts and frost in historic building materials [3] such as the once in Italy. Furthermore, the study in Turin, Italy, shows that

these mitigation strategies are more effective in mitigating summer UHI when installed in canyons parallel to the main wind direction than in perpendicular ones. It also shows that it is necessary to increase plant watering to promote the stomatal opening for adapting to UHI during summer heat waves [27]. It must be mentioned that more than three hours of direct sunlight is necessary for the growth of vegetation [32].

Table 1. Table of state-of-the-art. cei: carbon emission intensity; *AP*: air pollutants; *EC*: energy consumption; *HBvc*: heat balance of the vegetation canopy; *ILP*: indoor lighting performance; *LW*: longwave radiation; *PET*: psychological equivalent temperature; *PMV*: predicted mean vote; *RH*: relative humidity; *SW*: shortwave radiation; *Ta*: air temperature; *Tf*: foliage temperature; *Tmrt*: mean radiant temperature; *To*: operative temperature; *Ts*: surface temperature; *Twbgt*: wet bulb globe temperature; *UTCI*: universal thermal climate index; *Wd*: wind direction; *Ws*: wind speed.

Scenario and/or Goals	Year	Climate	Insite Measured Parameters (Sensor Based)	Methodology	Results	cei	Future
Study on albedo configurations for walls and floors: [20] • Low: <0.3 • Medium: 0.3–0.7 • High: >0.7	2022	Csa	*Ta*; *RH*; *Ws*; *Tmrt*	Validated simulation	*Ta*; *Tmrt*; *PET*; *Ts*	×	×
• Green roofs • Tree planting [33]	2023	Zone C	The data that has been used is confidential	Validated simulation	*EC*; *AP*; *Ta*; *Tmrt*; *LW*	×	×
Varying greenery coverage: [31] • Green roofs • Green façade	2018	Af	*Ta*; *RH*; *Ws*	Validated simulation	*Ta* averaged	×	×
Analyzing two VGSs: [34] • With soil • With plant, soil (albedo 0.43), and high-albedo walls (0.78) positioned 0.4 m	2023	Dwa	*Ta*; *Ts*; *Tmrt*; *RH*; *Ws*	Experimental study	*SW*; *LW*; *Tmrt*; *Ts*	×	×
Vegetated green façade on reduced-scale buildings [35]	2017	Cfb	*Ts* Inside; *Ta* Inside	Experimental study	*Ta*; *Ta* Inside; *Ts* Inside; *To*	×	×
Two VGSs technologies: [36] • Green Walls (GWs) • Vertical Forest	2025	Csa	*Ta*; *RH*; *Ws*; *Wd*; *SW*; *LW*; *Ts*	Validated simulation	*Tmrt*; *PET*; *UTCI*	×	×
Configurations of: • Living walls (LWs) • Green façades • EGRs Considering wind direction, scale, and orientations [27]	2023	Cfa Csa	*Ta*; *RH*; *Wd*; *Ws*	Validated simulation	*Ta*	×	×
Thermal impact of urban green systems on UHI [37]: • Trees • Living façades • High albedo pavements	2024	Cfb	Not specified	Validated simulation	*RH*; *Ts*; *Ta*; *Tmrt*; *PET*	×	✓
Thermal performance of 4 parametric green façade systems [38]	2024	BSk	Not specified	Validated simulation	*EC*; *ILP*	✓	×
Effect of GWs on urban microclimate [39]	2019	BWh	*Ta*; *Wd*; *Ws*; *RH*	Validated simulation	*Ta*; *Ta* Inside; *PMV*; *RH*	×	×
Thermal balance of vegetation canopy [29]	2019	Cfa	*SW*; *LW*; *Tf*; *Ta*; *Ts*; *Ws*; *RH*	Experimental Study	*LW*; *SW*; *Ta*; *Ws*; *HBvc*; *Ts*; *EC*; *To*; *Twbgt*	×	×

1.4. Objectives and Contributions

From the literature, it has been concluded that urban morphology, climate background, and surface properties are the main factors amplifying the UHI effect (Figure 1), leading to increased air and surface temperatures in cities. Green facades and green roofs have been widely studied for their cooling benefits, including impacts on air temperature, Tmrt, outdoor comfort, and energy efficiency, particularly during summer and heat waves, as well as in winter conditions. They conclude that vertical greenery systems have better cooling efficiency compared to horizontal surfaces such as green roofs. However, analyses

of energy efficiency and outdoor comfort are limited to small-scale assessments, focusing on a single block. Additionally, they did not consider the effect of climate change and failed to evaluate how greenery can mitigate carbon emission intensity.



Figure 1. Drivers of urban heat islands and the scope of the study.

To fill this gap, our study aims to evaluate the effect of green walls on air temperature, Tmrt, and outdoor thermal comfort, as well as its contribution to reducing the (cei) of the Heating, Ventilation, and Air Conditioning (HVAC) systems under current and future climate projections. The study is conducted on the scale of a few blocks, considering all the outdoor walls are covered entirely by green walls.

2. Materials and Methods

The methodology of this study comprises two sections, as illustrated in Figure 2. The initial section is devoted to the analysis and detection of the urban area experiencing the intense SUHI effect. This is followed by the selection of the study area through the utilization of remote sensing techniques. The subsequent section involves the evaluation and simulation of the mitigation scenario of green walls.

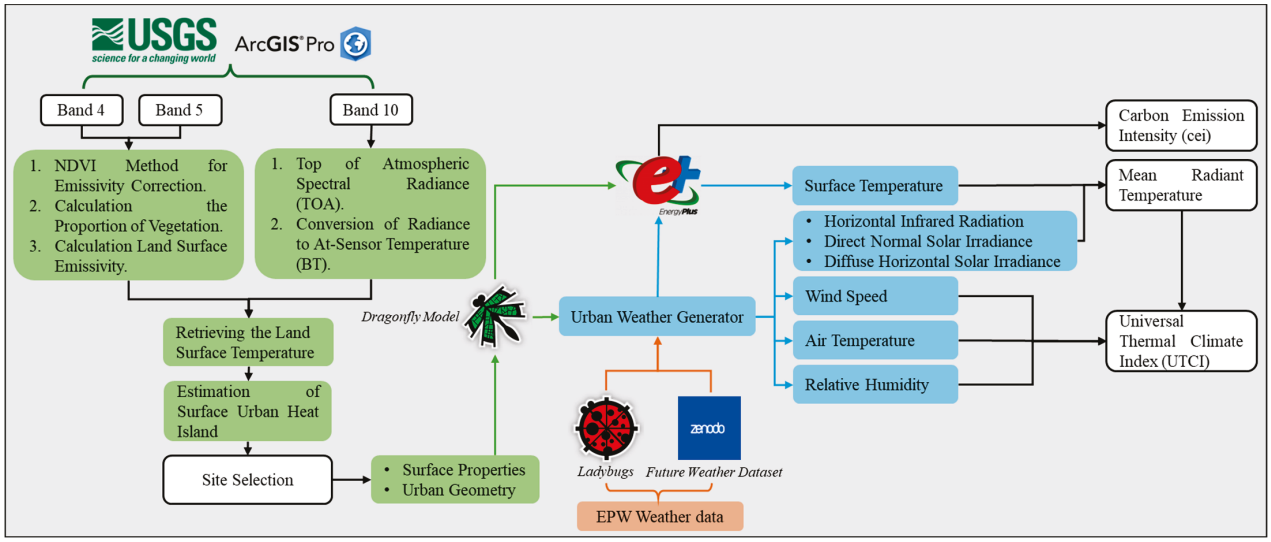


Figure 2. Flowchart of the analysis of the SHUHI and site selection along with the simulation workflow.

2.1. Data Gathering

2.1.1. Satellite Data

The surface reflectance and emittance records of the Landsat-9 satellite were utilized in this study. The three Landsat-9 bands employed in this investigation were Band 4, Band 5, and Band 10 (Table 2). It is noteworthy that Band 4, which operates within the visible spectrum, possesses extremely short wavelengths. In contrast, the remaining bands function in regions of the spectrum that are imperceptible to the human eye. Band 5, which is sensitive to near-infrared (NIR) light, was particularly insightful. This region, which is reflected at maximum by healthy plants, which are the highest natural reflectors, up to 70%, can be used for the study of ecology. Band 10 operates within the thermal infrared (TIR) spectrum, detecting emitted thermal radiation. In contrast to the measurement of air temperature by a meteorological weather station, Band 10 reports the surface temperature, which is typically significantly hotter due to the ground's greater capacity for heat absorption and retention. The Landsat-9 satellite image and associated data were retrieved on 11 July 2023 [40]. The date was selected due to its representation of both the most recent and the oldest data, which predominantly covers the Turin municipality area with minimal cloud cover.

Table 2. Landsat 9 image characteristics.

Data Type	Time	Cloud Cover	Band Number	Resolution
Landsat 9 satellite imagery "OLI_TIRS"	11 July 2023, 11:16:53.4756430Z	3.34%	Band 4—Red Band 5—Near-infrared (NIR) Band 10—Thermal infrared 1 (TIRS1)	30.00 (m) 30.00 (m) 30.00 (m)

2.1.2. Weather Data

Weather data for creating site weather conditions were retrieved from Ladybug Tools EPWmap with the hourly temporal resolution [41] and the site meteorological measurements data gathered from [42] with hourly temporal resolution. The future meteorological data of the year 2050, considering RCP 8.5, relies on dynamical downscaling, following the approach outlined by the IEA EBC Annex 80 [43]—Weather Data Task Force. The most advanced approaches and tools for producing future global projections and weather files are referenced [44].

2.2. Remote Sensing Technique to Retrieve SUHI

In recent years, due to an increasing number of extreme meteorological events potentially related to climate change, growing attention has been paid to the operational use of satellite remote sensing applied to emergency management applications. This increased focus can be attributed to the substantial and prompt availability of diverse remotely sensed data types, along with geospatial information collected in situ [45]. In this study, we employed remotely sensed data and techniques to detect the SUHI effect and select our study case.

In the initial phase of the study, the methodologies employed for the SUHI computational mapping process were delineated into seven discrete steps.

2.2.1. Top of Atmospheric Spectral Radiance

As demonstrated in Figure 2, the initial step entails the calculation of the Top of Atmospheric (TOA) L(λ) spectral radiance utilizing Equation (1) [46,47] with the Raster Calculator Tool incorporated within ArcGIS Pro 3.4.

$$\mathrm{TOA}(\mathrm{L}(\lambda)) = \mathrm{ML} \times \mathrm{Qcal} + \mathrm{AL}. \tag{1}$$

TOA (L(λ)) stands for Total Spectral Radiance (Watts/($m^2 * srad * \mu m$)), ML stands for the band-specific Multiplicative Rescaling Factor, Qcal refers to Band 10 of Landsat 9, and AL stands for the Band-Specific Additive Rescaling Factor. The MTL file is the only way to obtain the values for ML, Qcal, and AL. AL can be found in the MTL file by searching for RADIANCE ADD BAND 10 = 0.10000, and ML can be found in the MTL file by searching for RADIANCE MULT BAND 10 = 3.8×10^{-4}. Finally, Qcal is obtained by selecting Band 10 of the Landsat 9 image.

2.2.2. The Conversion of Radiance to At-Sensor Temperature

Subsequent to determining the TOA, the subsequent step entails the conversion of spectral radiance to the Top of the Atmosphere Brightness Temperature (BT), as delineated in Equation (2) [46,47]. This conversion is performed by utilizing the thermal constants K1 and K2, which are obtained from the MTL file document, and the Total Spectral Radiance (Lλ), which is the result of the preceding step.

$$\mathrm{BT} = \frac{\mathrm{K2}}{\ln\left[\left(\frac{\mathrm{K1}}{\mathrm{L}\lambda}\right) + 1\right]} - 273.15. \tag{2}$$

It can be demonstrated that K1 and K2 can be discovered by finding the values of CONSTANT BAND 10, which are 799.0284 and 1329.2405, respectively.

2.2.3. The Normalized Different Vegetation Index (NDVI) Method for Emissivity Correction

The subsequent stage in the procedure entails the employment of the NDVI method for emissivity correction, as delineated in Equation (3) [46,47]. This method holds paramount importance, as it is instrumental in determining the proportion of vegetation (P_v) through its application in calculating the Land Surface Emissivity (ε), a variable that is inextricably linked to the P_v [46,47].

$$\mathrm{NDVI} = \frac{\mathrm{NIR}(\text{ band } 5) - \text{ Red } (\text{ band } 4)}{\mathrm{NIR}(\text{ band } 5) + \text{ Red } (\text{ band } 4)}. \tag{3}$$

2.2.4. Calculation of the Proportion of Vegetation

Substituting the results of Equation (3) into Equation (4) [46,47] yields the proportion of vegetation (P_v).

$$\mathrm{P_v} = \left(\frac{\mathrm{NDVI} - \mathrm{NDVI_{min}}}{\mathrm{NDVI_{max}} - \mathrm{NDVI_{min}}}\right)^2. \quad (4)$$

2.2.5. Calculation of Land Surface Emissivity

Afterwards, the next step is to calculate the (ε) using Equation (5) [46] with the value of 0.004 and the correction value of 0.986 from the MTL file.

$$\varepsilon = 0.004 \times P_V + 0.986. \quad (5)$$

2.2.6. Retrieving the Land Surface Temperature

The final step prior to calculating the SUHI value was to compute the Land Surface Temperature (LST). Utilizing the BT value previously obtained from Equation (2), the LST in degrees Celsius (°C) can be calculated through the application of Equations (6) and (7) [46,47] and the input parameters delineated in Table 3.

$$\mathrm{LST} = \frac{\mathrm{BT}}{\left\{1 + \left[\left(\frac{\lambda \mathrm{BT}}{\rho}\right)\ln \varepsilon\right]\right\}}. \quad (6)$$

$$\rho = \mathrm{h}\frac{\mathrm{c}}{\sigma} = 1.438 \times 10^{-2}(\mathrm{mK}). \quad (7)$$

Table 3. Parameters for land surface temperature calculation.

Parameters	Values
Emitted radiance (λ)	10.800 (nm)
Stefan–Boltzmann constant (σ)	5.667×10^{-8} ($\mathrm{W/m^2k^4}$)
Light velocity (c)	2.998×10^{4} (m/s)
Planck constant (h)	6.626×10^{-34} (J)

2.2.7. Estimation of SUHI

The term SUHI has been frequently employed to denote the difference in surface temperature between urban and rural areas. This can also be defined by quantification to consider urban surfaces' local and regional climate change. The SUHI is calculated using the following Equation (8) [48], where T is LST, $\mathrm{T_m}$ is LST mean, and $\mathrm{T_{sd}}$ is the standard deviation of LST.

$$\mathrm{SUHI} = \frac{\mathrm{T} - \mathrm{T_m}}{\mathrm{T_{sd}}}. \quad (8)$$

2.3. Numerical Simulation to Retrieve Canopy Urban Heat Island Considering Urban Geometry Modeling and the Simulation Period

Accurate building footprints have significant implications for urban planning and infrastructure management [49]. The geometric model that served as the foundation for all simulations was developed using the Rhinoceros 8 modeler. The dragonfly model was created based on dragonfly buildings from footprint geometry (horizontal Rhino surfaces). The buildings were created with the extrusion from building footprints based on digital elevation models, which represent an approximation of the building massing [50]. In addition to the selection of the urban site, the decision was made to decrease the run time for the comfort analysis by employing short time periods of four days taken from typical

weeks in the (stat) file in the weather file of the weather station in Turin-Caselle Airport [41] (Table 4). The time period from 8:00 to 18:00, when the majority of activities are conducted, was selected for the simulation [12,33,51,52].

Table 4. Simulation time periods.

Typical Weeks	Selected Data
Extreme Cold Week (13 January–19 January)	12 January
Typical Spring Week (29 March–4 April)	29 March
Extreme Hot Week (27 July–2 August)	29 July
Typical Autumn Week (13 October–19 October)	15 October

2.3.1. Urban Heat Island Modeling with the Urban Weather Generator

UHI was incorporated into the present study by morphing the TMY weather data of the weather station through the integration of the validated Urban Weather Generator (UWG). The UWG approximates the thermal conditions of a city and utilizes several key geometric and material variables, as outlined in Table 5. These parameters are then entered into a generic model of the urban canyon, after which energy balance calculations are performed. Ultimately, the UWG morphed a TMY file, thereby adjusting the air temperature and relative humidity to reflect the urban conditions. Additionally, it incorporated anthropogenic heat fluxes resulting from exfiltration and waste heat from building HVAC systems [53–55].

Table 5. Ladybug urban weather generator simulation settings.

Model Parameters and Buildings Construction Set	
Climate Zone	Koppen Classification [3]/Cfa
Building Vintage	Pre–1980
Construction Type	Mass
Program	Medium Office [50], Conditioned
Terrain Properties	
Albedo (Reflectivity)	0.25 [56]
Thickness	0.5 (m)
Conductivity (Typical of Asphalt)	1 (W/mK)
Volumetric Heat Capacity (Typical of Asphalt)	1.6E6 (J/m^3K)
Traffic Parameters	
Maximum Sensible Anthropogenic Heat	20 (W/m^2)
Albedo	0.25 [57]
Fraction of the Absorbed Solar Energy by Trees	0.7
Fraction of the Absorbed Solar Energy by Grass	0.5
EPW Site Parameters	
Obstacles Height	0.01 (m)
Vegetation Coverage	0.9
Temperature Height	17
Wind Height	10
Boundary Layer Parameters	
Day Height	1000 (m)
Night Height	80 (m)
Inversion Height	150 (m)
Circulation Coefficient	1.2
Exchange Coefficient	0.2 [54]
Model Geometric Variables	
Average Height	15.7 (m)
Footprint Density	0.41
Facade to Site	1.4

Table 5. *Cont.*

Green Façade Characteristics	
Air Gap	0.05 (m) [27]
Plant Height	0.1 (m)
Leaf Area Index (LAI)	3 [27]
Substrate	0.05 (m)
Leaf Reflection	0.22
Leaf Emission	0.95
Soil Reflection	0.3
Soil Emission	0.9
Stomata Resistance	180 (s/m)
Soil Thickness	0.22 (m)
Soil Conductivity	0.35 (W/mK)
Soil Density	1100 (kg/m^3)
Soil-Specific Heat	1200 (J/kg K)

2.3.2. Mean Radiant Temperature Calculation

In this section of the research, the objective is to evaluate the impact of a canyon's geometry and surface characteristics, including ground and facade reflectivity and emissivity, on the Tmrt simulation and its spatial distribution. This analysis is conducted using the method outlined in the literature [52,53,56].

In the first step of calculating, base longwave radiation would be computed Equation (9) [53,56].

$$\mathrm{LWMRT} = \left[\sum_{i=1}^{N} F_i T_i^4\right]^{1/4} - 273.15\ ^\circ\mathrm{C}. \tag{9}$$

We consider T_i to be equivalent to the surface temperature, as derived from the EnergyPlus simulation. F_i is defined as the view factor for each surface, calculated through the ray-tracing capabilities of the Rhino 3D modeling engine. The model also incorporates the sky temperature and longwave loss to the sky in Equation (10) [53,56], utilizing the horizontal infrared radiation contained within the TMY data.

$$T_{sky} = \frac{L_a}{\left(\varepsilon_{person}\ \sigma\right)^{1/4}}. \tag{10}$$

In the context of outdoor shortwave solar radiation, which is defined as the direct incidence of solar radiation upon individuals, the SolarCal model [58] of ASHRAE-55 is defined. The SolarCal model is based on the Effective Radiant Field (ERF), a metric of the net radiant energy flux to or from the human body, as defined by Equation (11) [53,56]. ERF is employed to delineate the supplementary (positive or negative) long-wave radiation energy at the body surface when the surrounding surface temperatures deviate from the air temperature. It is in (W/m^2), where area refers to body surface area.

$$\mathrm{ERF}_{solar} = \left(0.5 \cdot f_{eff} \cdot f_{svv} \cdot (I_{diff} \cdot I_{th} \cdot R_{floor}) + A_p \cdot f_{bes} \cdot I_{dir} \cdot AD\right) \cdot (a_{sw} \cdot a_{lw}). \tag{11}$$

This ERF is converted into a Tmrt delta using the following Equation (12) [53,56]:

$$\mathrm{ERF} = f_{eff} h_r (\mathrm{MRT} - \mathrm{LWMRT}). \tag{12}$$

2.3.3. Mean Radiant Temperature Validation

In order to statistically evaluate the acceptability of the simulation and output for measuring Tmrt, a comparison will be made between them and the site-measured sensor data with the characteristics provided in Table A1. The validation was analyzed using the Mean

Bias Error (MBE) Equation (13) and the Cumulative Variation of Root Mean Squared Error (CVRMSE) Equations (14) and (15), in accordance with the ASHRAE Guideline 14 [52,59].

$$\mathrm{MBE} = \frac{\sum_{i-1}^{N_p}(M_i - S_i)}{\sum_{i=1}^{N_p} M_i}. \tag{13}$$

$$\mathrm{CVRMSE} = \frac{\sqrt{\sum_{i=1}^{N_p}(M_i - S_i)^2 / N_p}}{M_p}. \tag{14}$$

$$\left(\overline{M_p} = \frac{\sum_{i=1}^{N_p} M_i}{N_p}\right). \tag{15}$$

According to the ASHRAE Guideline 14, the acceptable limits for calibration are delineated as follows. When analyzing hourly data, the results must be within ±10% MBE and ≤30% CVRMSE. The Tmrt and validation results for the MBE and the CVRMSE, respectively, are provided in Table 6 and Figure 3.

Table 6. Mean radiant temperature validation. MBE: Mean Bias Error, CVRMSE: Cumulative Variation of Root Mean Squared Error.

Date	MBE	CVRMSE
12 January	−8.96%	22.12%
29 March	−8.35%	17.56%
15 October	−1.97%	20.15%
29 July	5.22%	14.98%

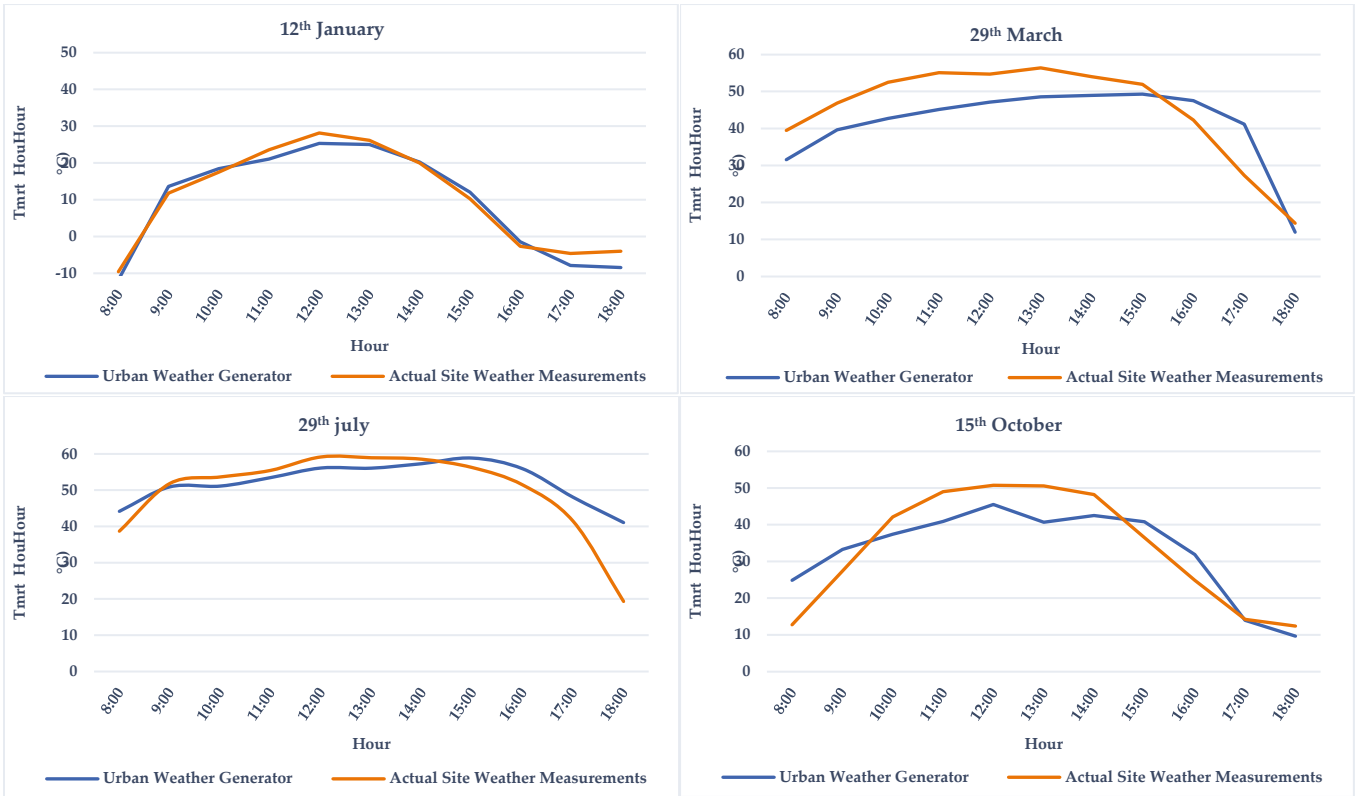


Figure 3. Mean radiant temperature validation.

2.3.4. Measuring Outdoor Thermal Comfort (UTCI)

UTCI, as an international standard for outdoor temperature sensation, is a thermal comfort model that quantifies how people perceive given weather conditions based on the range and stress category (Table 7) and is one of the most common temperatures used by meteorologists. While UTCI is designed to be valid in all climates and seasons, it operates under the assumption that human subjects are walking and that they naturally adapt their clothing to the outdoor temperature. For outdoor situations that do not fit these criteria, the Physiological Equivalent Temperature (PET) model is recommended. The calculation of the average UTCI over the specified time series, ranging from 8:00 to 18:00, necessitates the establishment of input parameters. These parameters, which are instrumental in determining the outdoor comfort levels, encompass wind speed data extracted from the designated weather file, mean air temperature measurements, relative humidity levels derived from the urban weather generator, and surface temperature values obtained from the URBANopt simulation conducted using EnergyPlus [60].

Table 7. UTCI stress categories and ranges.

Stress Category	Range °C
Extreme Cold Stress	UTCI < -40
Very Strong Cold Stress	$-40 \leq$ UTCI < -27
Strong Cold Stress	$-27 \leq$ UTCI < -13
Moderate Cold Stress	$-12 \leq$ UTCI < 0
Slight Cold Stress	$0 \leq$ UTCI < 9
No Thermal Stress	$9 \leq$ UTCI < 26
Slight Heat Stress	$26 \leq$ UTCI < 28
Moderate Heat Stress	$28 \leq$ UTCI < 32
Strong Heat Stress	$32 \leq$ UTCI < 38
Very Strong Heat Stress	$38 \leq$ UTCI < 46
Extreme Heat Stress	$46 <$ UTCI

2.3.5. Modeling of Green Wall

As stated in the article [61], which provides a categorization and comparison of various vertical greenery systems, including Green Barrier Systems, Green Coating Systems, and GWs, green walls have been found to be more effective in reducing outdoor surface temperatures and operative temperature. In this case, three categories have been proposed: the Mur Vegetal (MV), the Light Systems (LS), and the Heavy Systems (HS). The distinction between HS and LS lies in the soil thickness (less or greater than 15 cm, respectively). In the present study, LS with the material properties delineated in Table 5 was employed. The GWs systems exhibit remarkable capacity to reduce the surface temperatures, which are also lower than those of the ambient air. Among the various systems, LS and HS have emerged as the most efficient ones in reducing the maximum temperature. However, the HS has a greater reduction in operative temperature in summer, while MV's effect on operative temperature in winter is greater. The thickness of the air gap and the type of soil are almost irrelevant in influencing the external surface temperatures, while the variation in LAI influences the external surface temperatures. Green walls (GWs) are characterized by the necessity of a higher degree of greater technical specialization in comparison to the other categories. The technology package (which includes the plants and the substrate) is supported by a subsystem and forms a gap with the walls, thereby exhibiting the characteristics of a ventilated façade. The ventilated cavity has been modeled as a separate thermal zone, and it has been conceptualized as a leaky building with a flow per exchange area of 0.0006 (m^3/s per m^2 facade) and air changes per hour (ACH) of 3 [62,63].

2.4. Evaluating Carbon Emission Intensity in Energy System

The calculation can be utilized in the design of low- and net-zero-carbon buildings and districts. Carbon dioxide (CO_2) emissions per total energy supply refer to the quantity of kilograms of CO_2 released to produce a megawatt-hour (MWh) of energy. In this study, input emissions per total energy supply will be employed to calculate carbon intensity for both electricity and heating/cooling systems. The most recent carbon emissions of the Italian total energy supply for the year 2019 [64] were utilized as the reference value to compute the changes in energy consumption of our model and, consequently, the cei for the future projection 2050 emission report. In this study, the heating and cooling HVAC system was defined as a window AC with a baseboard gas boiler, and the service hot water system was defined as an electric water heater. The aggregated emission per total energy supply for the year 2019, with a value of 178.5 ($kgCO_2/MWh$), was considered in our analysis.

3. Results

3.1. SUHI Detection and Site Selection

An analysis of surface temperature distribution across the Piedmont region of Italy revealed a significant thermal gradient, with temperatures ranging from 54 °C to 91 °C (Figure 4a). Statistical analysis indicated that nearly the entirety of the city would experience SUHI. Via della Consolata exhibited a very-high-intensity heat island region, which was selected as the study area. The Santuario della Consolata (7°40.7473753′ E 45°4.6011994′ N) is located at the center of this area (Figure 4b). The meteorological sensors mounted on the building record the following parameters: dry bulb temperature (°C), wind speed (m/s) and direction, relative humidity (%), atmospheric pressure, and irradiances (W/m^2).

(**a**)

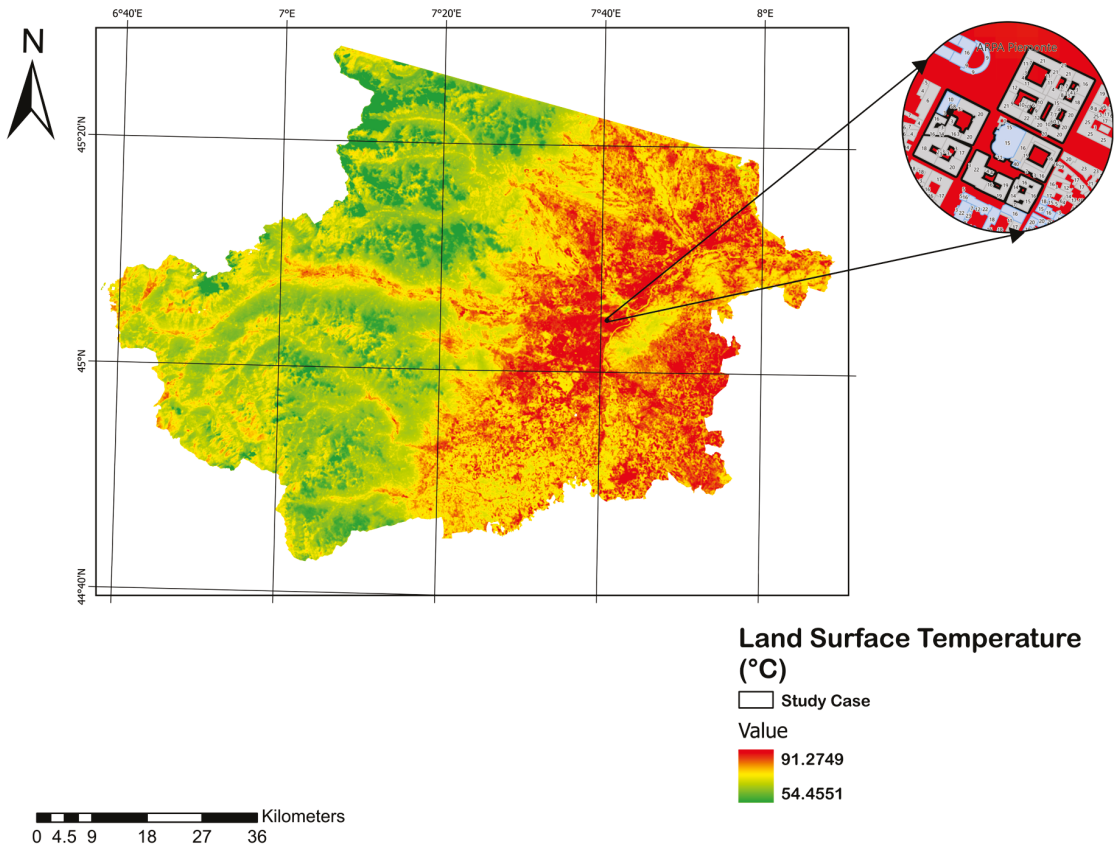


Figure 4. *Cont.*

(**b**)

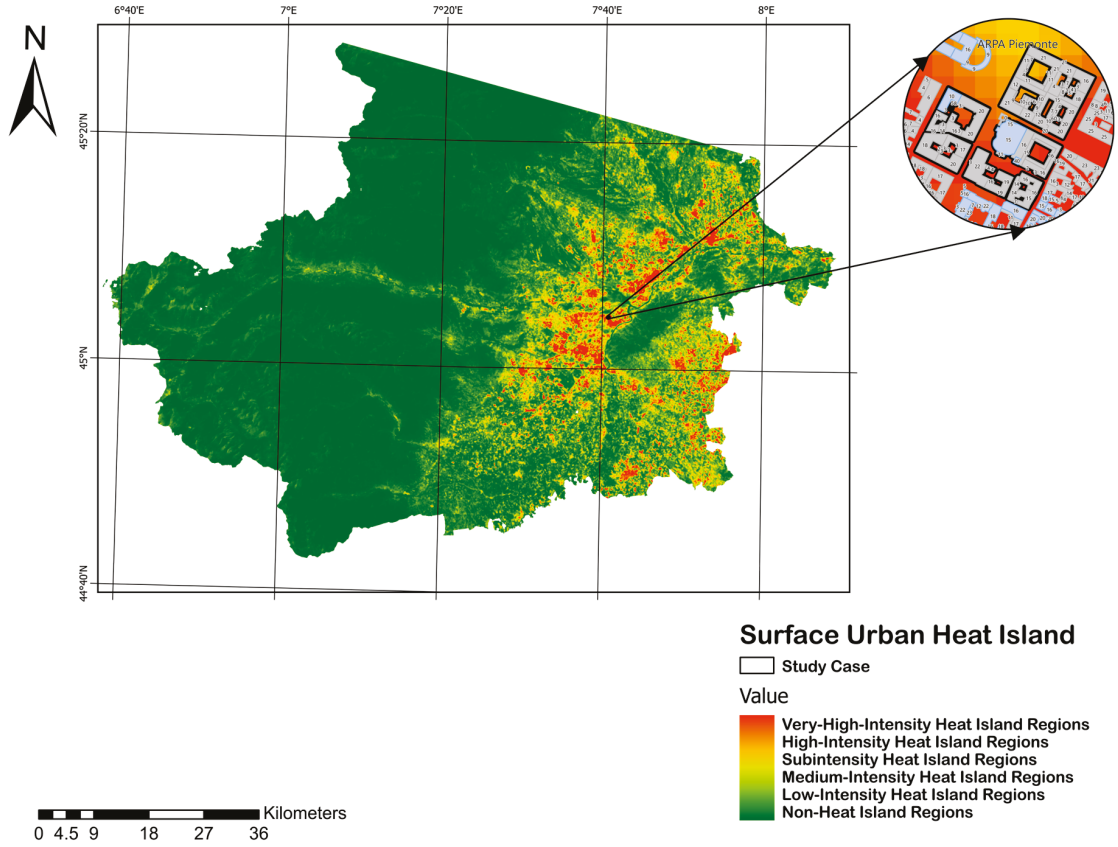


Figure 4. (**a**) Land surface temperature (°C) and study area detection; (**b**) SUHI ranges and study area detection.

3.2. Impact of Green Walls on Outdoor Air Temperature for Current Condition and Future Projection

The installation of green walls exhibited intricate temporal variations in outdoor air temperature (Table 8). Under the prevailing climate conditions, the most substantial effects were observed during winter and spring, where temperature fluctuations ranged from a decrease of 0.3 °C to an increase of 1.3 °C on 12 January and from a reduction of 1.3 °C to an increase of 1.2 °C on 29 March. These variations exhibited robust diurnal and seasonal patterns, with the most pronounced cooling effects typically occurring until mid-afternoon hours, a phenomenon that persisted until 15 October. In contrast, summer conditions, as evidenced by measurements collected on 29 July, exhibited more modest and uniform modifications, ranging from 0 °C to +0.4 °C.

In considering the broader context of urban heat island effects, future climate projections for 2050 are anticipated to exacerbate this phenomenon (Figure 5). However, the implementation of green walls could help counteract this trend by producing smaller temperature increases and more significant reductions, ranging from −1.6 °C to 0.7 °C, which highlight their potential as an effective mitigation strategy in the face of climate change. For instance, on 29 July, air temperatures under the current climate scenario exhibited some increases throughout the day. In contrast, future climate projections for 2050 demonstrated a consistent decline in temperature during the mid-afternoon hours. A similar trend was observed in winter. While early mornings—8:00 AM and 9:00 AM—under current conditions exhibited slight increases in air temperature, future projections indicated a notable decrease throughout the day, with more substantial reductions. The enhanced effectiveness

under future climate scenarios suggests that green walls may become increasingly valuable as a climate adaptation strategy.

Table 8. Air temperature variation (°C) after introducing a green wall for all the simulation periods under current and future projection climate conditions.

Current Weather Condition											
Date	Hour										
	8:00	9:00	10:00	11:00	12:00	13:00	14:00	15:00	16:00	17:00	18:00
12 January	0.6	1.3	−0.2	−0.2	−0.2	−0.2	−0.3	−0.2	−0.3	−0.2	0.6
29 March	1.1	0.1	0	0	0	−0.1	−0.1	0	1.2	0.3	−1.3
29 July	0.2	0	0	0	0	0	0	0	0	0	0.4
15 October	0	0	0	0.1	0	0	−0.1	0	−0.4	−0.6	−0.6
Future Projection 2050 (RCP8.5)											
Date	Hour										
	8:00	9:00	10:00	11:00	12:00	13:00	14:00	15:00	16:00	17:00	18:00
12 January	−0.3	−0.3	−0.3	−1.6	−0.3	−0.3	−0.2	−0.3	−0.3	−0.4	0.1
29 March	−0.2	−0.1	0	0	0	−0.1	0.3	0.2	0.3	0.7	0.5
29 July	0	0	0	0	0	0	0	−0.1	−0.1	−0.1	0.2
15 October	0	0.1	0	0	0	0	0	0	−0.1	−0.1	−0.1

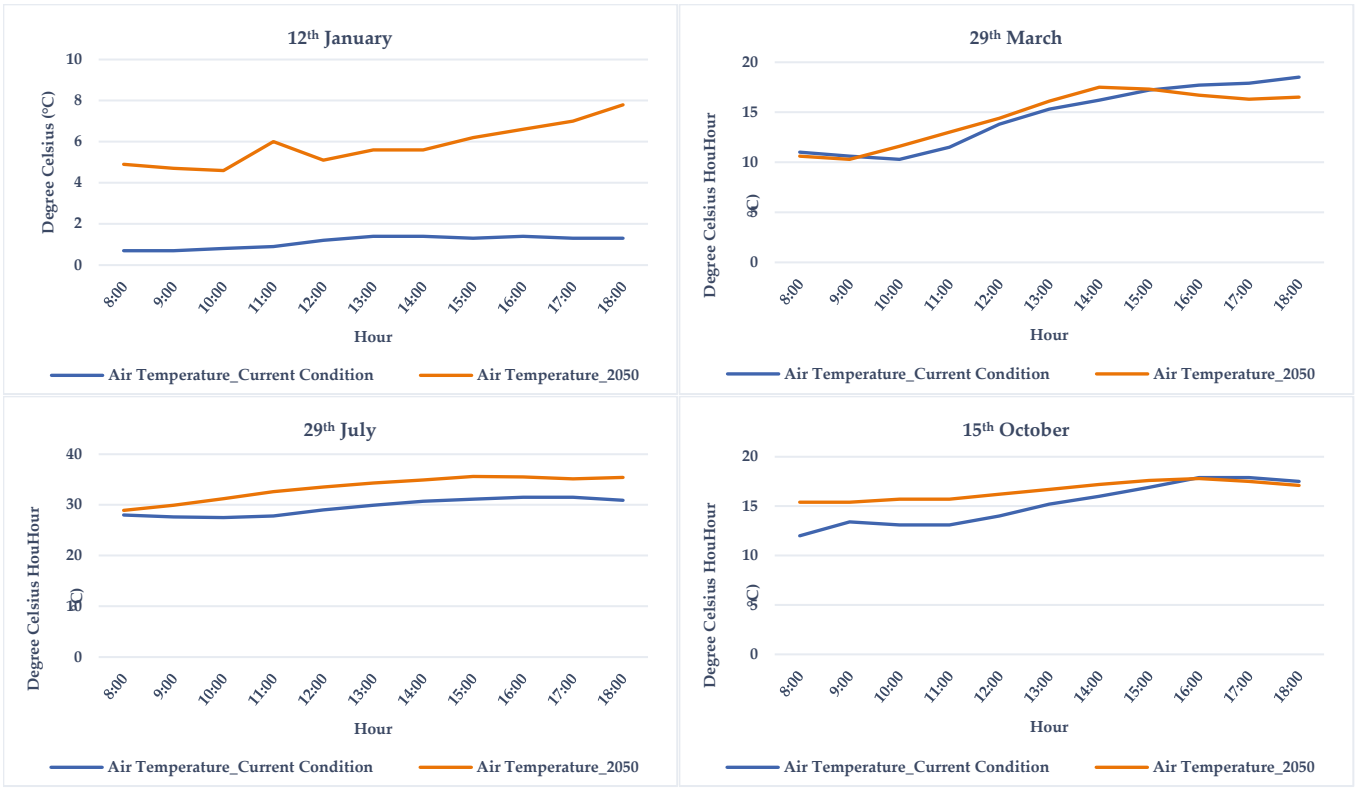


Figure 5. Comparison of air temperature (°C) during current and future projection (2050) climate conditions.

3.3. The Enhancement Effect of the Green Wall on Mean Radiant Temperature and Outdoor Comfort Under Current and Future Climate Projections (2050)

An analysis of the cooling effect of the green wall on average Tmrt under current conditions and future climate projections is presented in Figures 6 and 7. Under current climate conditions, the green wall showed varying effects across different seasons. On

12 January, the results show an insignificant reducing effect with the values from −0.41 °C to −0.22 °C, showing a relatively modest effect with colder outdoor conditions, lower sun angle, and lower evapotranspiration efficiency. On 29 March the range of reductions was relatively higher, with the range from −0.64 °C to −0.34 °C. In contrast, on 29 July, the green wall exhibited the most substantial impact with the reduction, ranging from −1.10 °C to −0.59 °C, which is the consequence of having higher outdoor temperatures typical of summer, showing the effectiveness of the green wall in mitigating the UHI effect. Finally, cooler air temperatures on 15th October showed a smaller decrease in Tmrt from −1.07 °C to −0.57 °C.

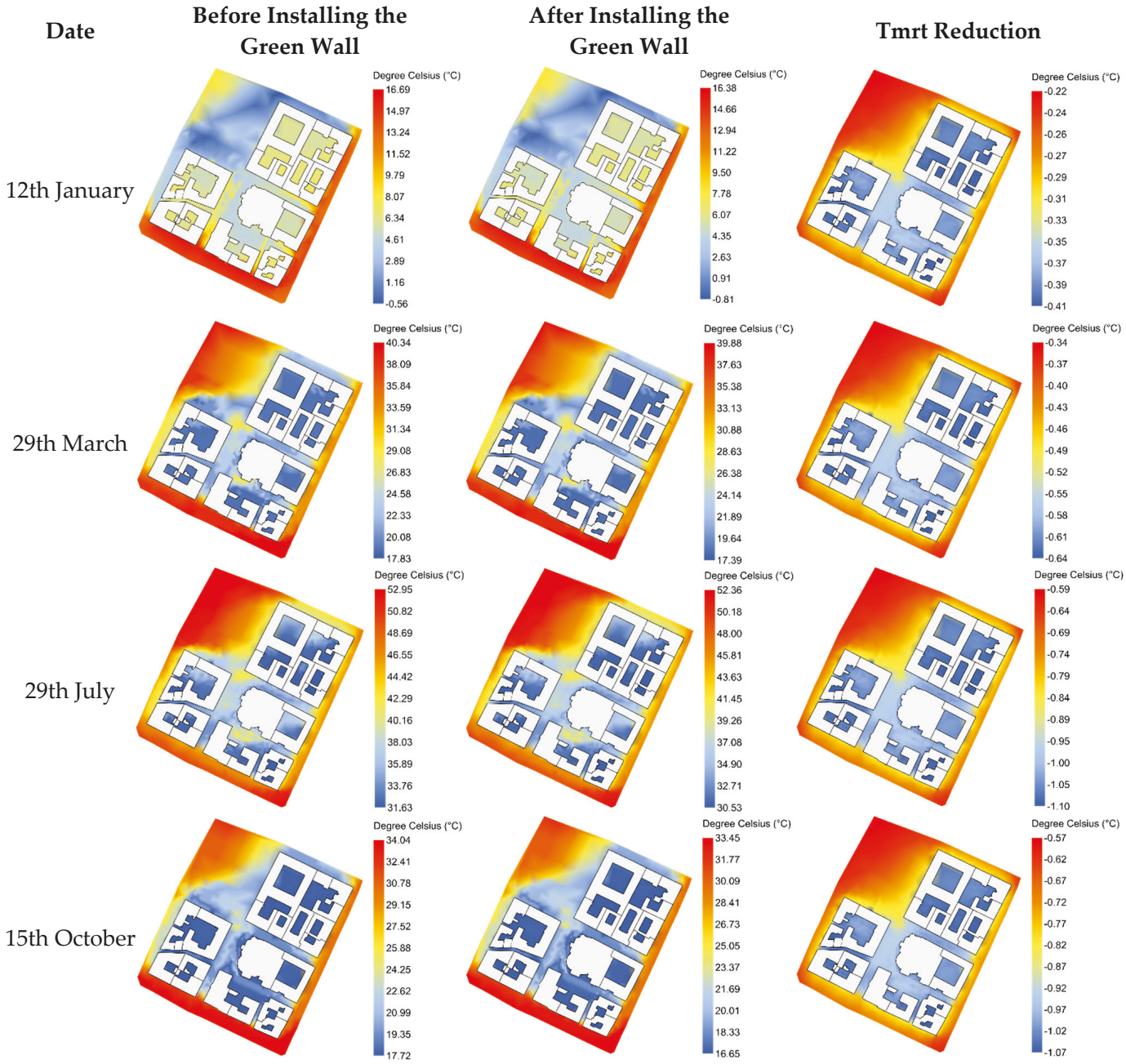


Figure 6. Mean radiant temperature (Tmrt) °C spatial heat map before and after the installation of the green walls and the enhancement effect of green walls under current weather conditions.

In the case of the future projection 2050, in all the simulation periods we will experience higher outdoor air temperatures (Figure 5). In autumn and winter, instead of having warmer outdoor temperatures, the cooling effect of green walls was less impactful, with the mitigating from −0.34 °C to −0.18 °C on 15 October and −0.13 °C to −0.07 °C on 12 January. Considering having lower spatial Tmrt in 2050 because of lower radiation (Figure A1), and since solar radiation is a key driver of evapotranspiration, this condition results in less energy available to evaporate water from the soil and transpire water through the plants, thus having less cooling potential of green walls. Similarly, on 29th March, by considering having relatively higher air temperature and lower solar radiation (Figure A1), leading to lower spatial Tmrt, and better cooling performance with the averaged reduction from −1.25 °C to −0.67 °C. This could be the result of a greater temperature difference between air and surfaces resulting in better heat transfers.

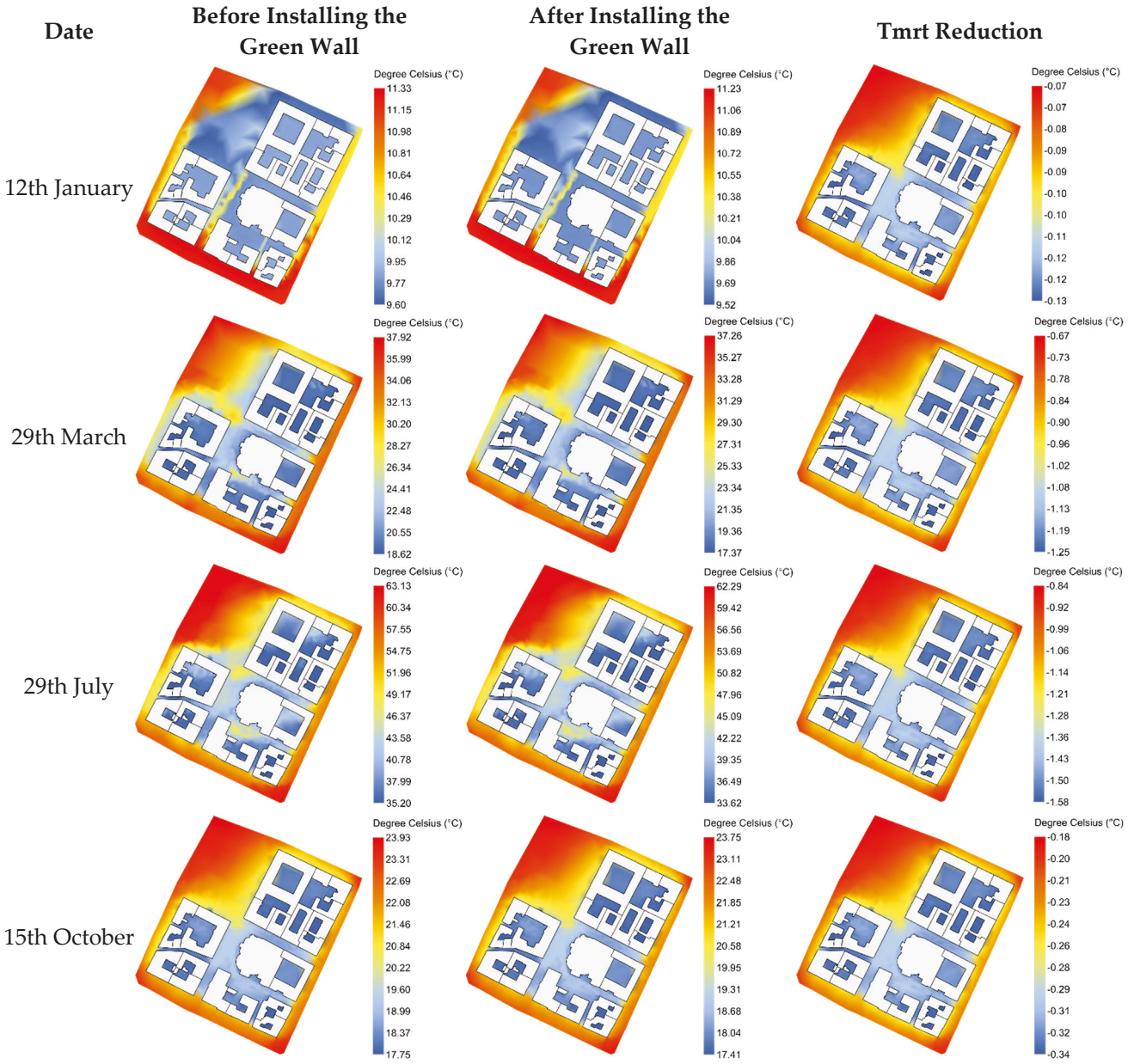


Figure 7. Mean radiant temperature (Tmrt) °C spatial heat map before and after the installation of the green walls and the enhancement effect of the green walls for future projection (2050) weather conditions.

On 29 July 2050, the relatively higher air temperature and solar radiation compared to current weather conditions cause an increase in average Tmrt and evapotranspiration by the leaves. In this case, the higher rate of evapotranspiration would result in better cooling performance of green walls with values from −1.58 °C to −0.84 °C. It is also worth noting that in all cases, the greatest reduction in Tmrt occurred in the canyons and courtyards with lower SVF and less direct sunlight exposure (Figure 8). In these areas, the main cause of higher Tmrt is longwave radiation emitted from walls and pavements as they accumulate heat during the day and re-radiate it to the surrounding area, thus the heat has restricted the scattering paths. The shading effect of green walls would reduce the surface temperatures, hence decreasing longwave radiation emissions. Compared to open areas with better heat dissipation, this leads to a more pronounced cooling effect in low-SVF areas, where longwave radiation plays a dominant role. Additionally, in open areas, the Tmrt would decrease more in areas closer to the walls.

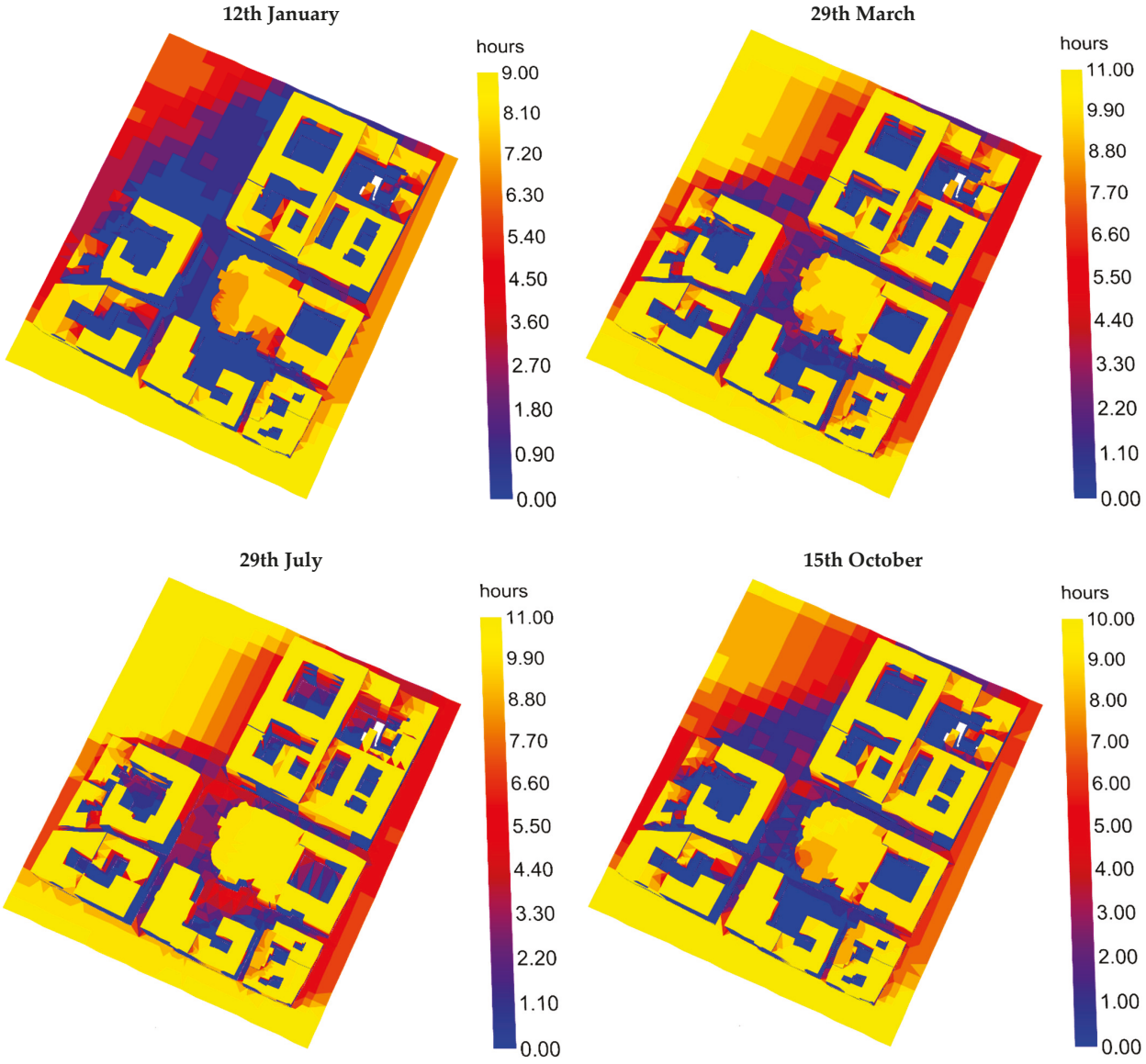


Figure 8. Number of hours of direct sunlight received in each simulation period.

As presented in the literature, the most influential parameters affecting UTCI are Tmrt [16], air temperature, and relative humidity. It can be shown in Figures 9 and 10

that the average UTCI experienced a reduction in all simulation periods after introducing the green wall to the model. The maximum reduction was recorded on 15 October by 0.44 °C and the minimum reduction on 12 January by 0.12 °C, under the current weather conditions.

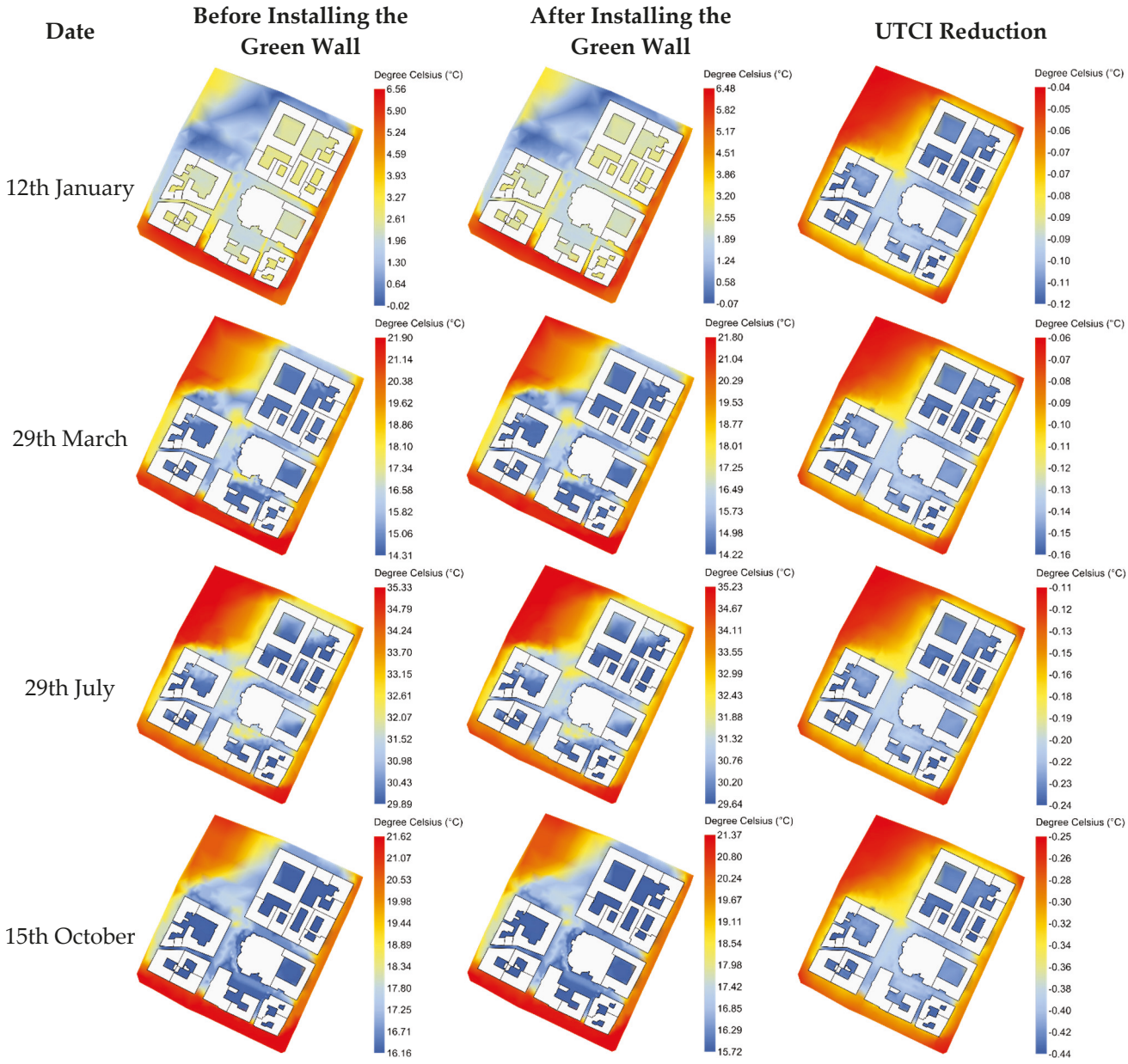


Figure 9. Outdoor comfort (UTCI) spatial heat map before and after the installation of the green walls and the enhancement effect of the green walls under current weather conditions.

Comparing the changes in outdoor comfort between future projection 2050 and current weather conditions, on 12 January and 29 July, we will experience worsening in outdoor comfort, which is the consequence of the greatest increase in air temperature (Figure 5). However, the enhancement effect of the green wall on thermal comfort would be maximum on 29 July by 0.40 °C.

In contrast, the change in air temperature was not significant on 29 March and 15 October. Furthermore, we will experience better outdoor comfort on 15 October with the

least decreasing effect of the green wall and on 29 March, which corresponds to the lower Tmrt predicted in 2050.

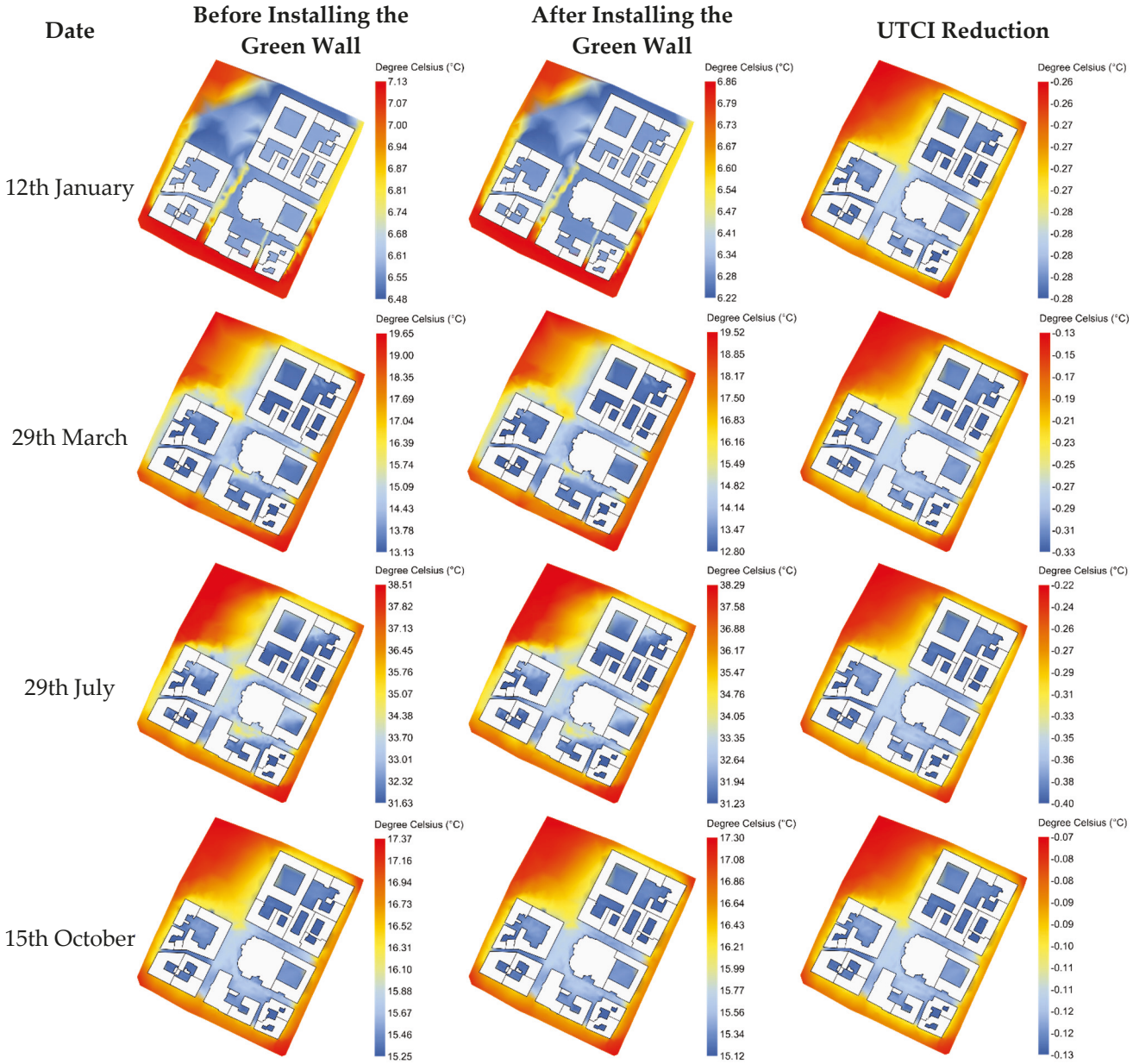


Figure 10. Outdoor comfort (UTCI) spatial heat map before and after the installation of the green walls and the enhancement effect of the green walls for future projection (2050) weather conditions.

3.4. Mitigation Effect of Green Walls in the Condition of Maximum Direct Normal Radiation

During the simulation period of the hottest week, climate change would amplify the Tmrt and UTCI. This is due to an increase in air temperature on 29th July at noon by 4.5 °C and maximum solar radiation with the values of 634 (Wh/m^2) and 749 (Wh/m^2) in current and future weather conditions, respectively. However, the cooling effect of the green wall will be more pronounced in 2050. The maximum reduction in Tmrt was recorded at 1.92 °C and 2.27 °C, and the maximum enhancement in outdoor comfort was recorded at 0.51 °C and 0.55 °C under current and future climate projections, respectively (Figure 11).

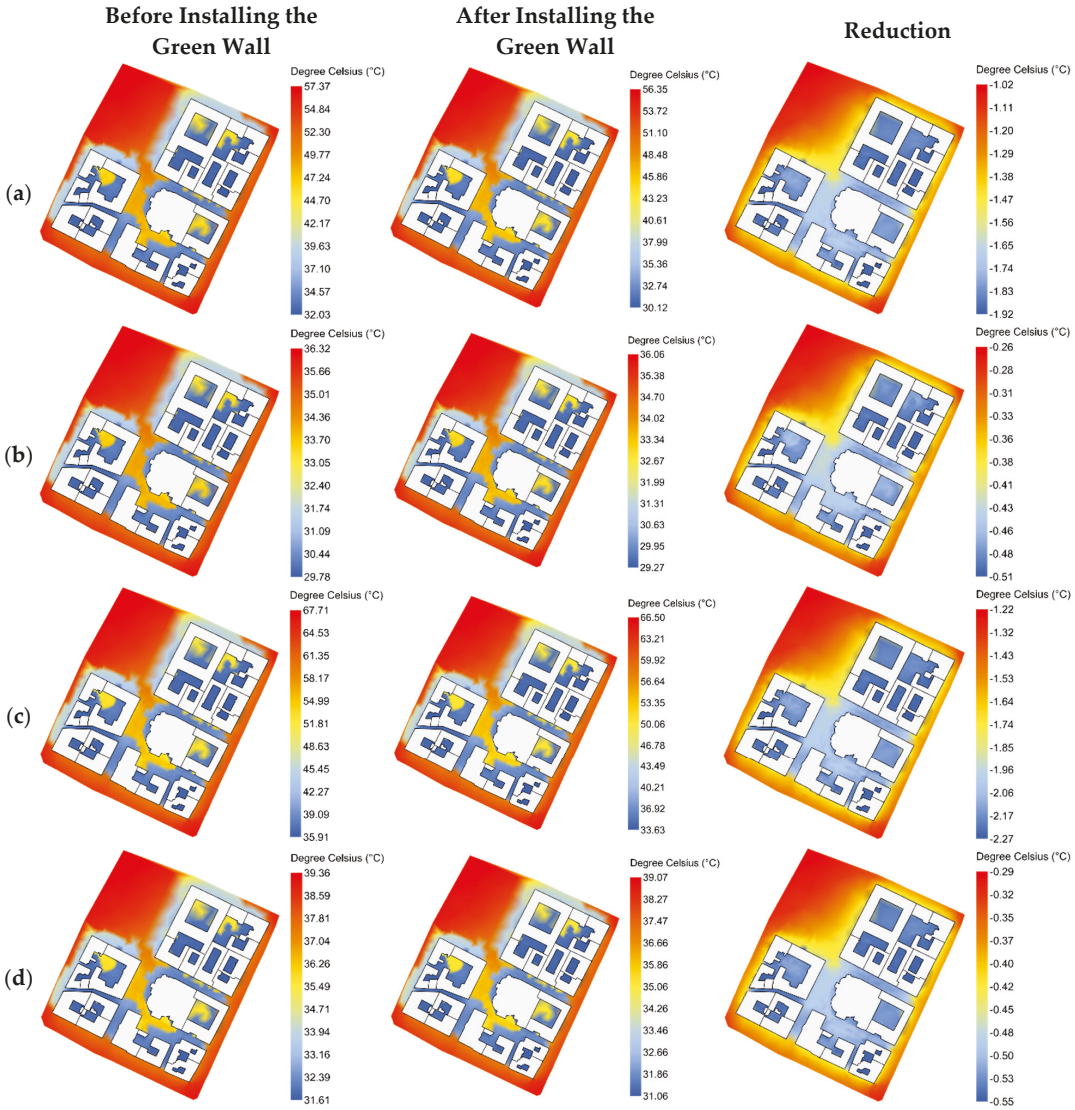


Figure 11. Enhancement of mean radiant temperature (Tmrt) °C and outdoor comfort (UTCI) at 12:00 PM on 29 July when the direct solar radiation is maximum; (**a**) mean radiant temperature changes under current climate conditions; (**b**) outdoor comfort changes under current climate conditions; (**c**) mean radiant temperature changes under future projection (2050) climate conditions; (**d**) outdoor comfort changes under future projection (2050) climate conditions.

3.5. Impact of Green Walls on Carbon Emission Intensity in 2050

On 12 January, there was an overall increase of 0.022 (kg CO_2/m^2) in the (cei), primarily due to an increase in the heating demand from 0.495 (kg CO_2/m^2) to 0.518 (kg CO_2/m^2). Conversely, on 15th October, the total increase in (cei) amounted to 0.01 (kg CO_2/m^2), with an increase in heating demand from 0.012 (kg CO_2/m^2) to 0.022 (kg CO_2/m^2). Conversely, on 29 July, a maximum reduction of 0.031 (kg CO_2/m^2) was observed. This decline is attributed to a reduction in cooling demand from 0.085 (kg CO_2/m^2) to 0.054 (kg CO_2/m^2). The implementation of the green walls on 29 March led to a decline in overall cooling demand of 0.026 (kg CO_2/m^2), reducing it from 0.028 (kg CO_2/m^2) to 0.002 (kg CO_2/m^2). Concurrently, there was an increase of 0.016 (kg CO_2/m^2) from 0.025 (kg CO_2/m^2) to 0.041 (kg CO_2/m^2) in heating demand.

As demonstrated in Table 9, the carbon emission results for each simulation day are based on the total gross floor area of 21,741 (m^2). The installation of the green walls has

been shown to result in a cooling effect, which would lead to an overall increase in energy demand during colder months and a reduction in energy demand during warmer months.

Table 9. Comparison of carbon emissions intensity (kg CO_2/m^2) between the base model without a green wall and the enhanced model after installing the green walls.

Date	End Uses		Before Installing the Green Wall	After Installing the Green Wall
12 January	Heating		0.495	0.518
	Interior Lighting		0.011	0.011
	Electric Equipment		0.018	0.017
	Pumps		0	0
	Water Systems		0.003	0.003
		cei	0.527	0.549
29 March	Heating		0.025	0.041
	Cooling		0.028	0.002
	Interior Lighting		0.019	0.019
	Electric Equipment		0.031	0.031
	Water Systems		0.005	0.005
		cei	0.108	0.098
29 July	Cooling		0.085	0.054
	Interior Lighting		0.003	0.003
	Electric Equipment		0.010	0.010
	Water Systems		0.002	0.002
		cei	0.100	0.069
15 October	Heating		0.012	0.022
	Interior Lighting		0.001	0.001
	Electric Equipment		0.008	0.008
	Water Systems		0.001	0.001
	cooling		0	0
		cei	0.022	0.032

4. Discussion

The implementation of VGSs in urban environments reveals complex and sometimes contradictory effects on microclimate parameters and building energy performance. This study's findings both challenge and confirm existing understanding of green wall performance in urban settings.

The extant literature suggests that the introduction of VGSs would result in positive cooling effects through transpiration and evaporative processes. Our results indicate minimal reductions in air temperature, and, in some cases, some similarities can be detected compared to several prominent studies in the literature. A distinguishing feature of our research is the examination of a more expansive urban area, encompassing complete facade coverage, in contrast to the smaller-scale studies and diverse typologies of vertical greenery systems and climate zones that are frequently focused on in the existing literature.

Air temperature changes, ranging from −1.6 °C to 1.3 °C, depending on the season and simulation period, show the insignificant cooling effect of green walls on outdoor air temperature and some exceptions when the heating effect occurred on several occasions [36], especially in summer. Similarly, [37] provided insignificant reduction in air temperature, ranging from −1.17 °C to −0.09 °C after the installation of LWs in different climate zones (Cfb). The cooling effect of green walls can be comprehended as well in a semi-arid climate zone (BWh) with double the thickness in the substrate. However, the range was much greater with a maximum reduction of 10 °C [39]. However, the results are partly aligned with the previous study [27] being conducted in the same study area, with the difference between the typology of the VGSs, lower substrate thickness, and coverage area. This would provide additional information that, in the same area, even with

different types of LWs, increasing the greenery coverage area would result in better cooling performance [31,55].

In addition to air temperature, the results also highlight reductions in Tmrt and outdoor thermal comfort indices [37]. Considering the effect of wall albedo configuration after introducing green walls as low-albedo surfaces with leaf and soil reflection values of 0.22 and 0.3, the findings showed better cooling effects on air temperature compared to the findings of [20]. Their study concluded that changing the albedo of the wall does not significantly improve air temperature and suggested evaporative cooling as a more effective strategy. In this context, the green walls, despite having low albedo, demonstrated enhanced cooling through the evaporative cooling effect provided by vegetation, aligning with their recommendations. Furthermore, the extant literature has explored the effect of surface albedo on localized Tmrt. Research findings indicate that modifying solely the albedo of vertical surfaces with inherently low albedo values frequently results in deterioration of the Tmrt reduction effect. The findings indicate that medium albedo walls (0.4) would have a better mean delta Tmrt reduction of -1.5 °C, which is superior to that of low albedo walls (0.1). The mean delta Tmrt reduction was found to be -0.8 °C [20], and in some cases, there was an increase in temperature, with values ranging from 1.8 °C to 3.5 °C during winter and from 2 °C to 4 °C during summer in all the climates under study [52]. However, our findings demonstrated that green walls, even with low albedo, would effectively improve Tmrt [20,52]. Our findings directly reflect the expected improvement in thermal comfort mentioned in the introduction, where green infrastructure is suggested to reduce the UTCI by mitigating heat exposure. The reduction in UTCI values indicates the effectiveness of green wall thermal properties in alleviating thermal stress as a mitigation strategy that can locally counteract the effects of climate change. The decrease in Tmrt and UTCI under current climate conditions during summer, particularly during the hours around noon, is also consistent with the literature [36], which suggests that green walls can lower Tmrt by blocking direct solar radiation and increasing local shading. UTCI values also showed similar improvement with the green walls in place.

Our findings are significantly consistent with theories about urban canyon effects on thermal performance. Studies like [14] identify SVF as a primary contributor to urban heat island intensity, suggesting that moderate-to-high SVF can mitigate UHI, whereas extremely high SVF levels intensify it, where in some studies the cooling effects of VGSs on air temperature were greater in central canyons [31]. Similarly, our results demonstrate that these areas show enhanced cooling benefits from green walls, with Tmrt reductions and outdoor comfort improvements greater than in open areas [16]. This challenges current urban design paradigms and suggests that VGSs might be particularly valuable in dense urban environments previously considered challenging for thermal management.

Results from [38] show almost a 29% reduction in annual carbon emissions can be expected [33]. Also concluded that greenery systems such as green roofs and trees would cause a reduction even in the energy performance of the buildings, which consequently results in the reduction in (cei). In our study, (cei) reduction ranges from 9% to 31% for spring and summer, although there was some increase in autumn and winter of 4% and 45%.

Our studies have shown that green walls have a significant impact on energy efficiency, especially in warm seasons. However, climate change may exacerbate or moderate these effects. Rising temperatures and the occurrence of heat waves in the future will double the importance of the cooling role of green walls, as this mitigation strategy can help reduce the urban heat island effect and increase thermal comfort. On the other hand, in cold seasons, climate change may cause changes in energy consumption patterns. A decrease in cold days or changes in the intensity of winter colds can reduce the negative impact of green

walls on energy consumption. For this reason, the design and implementation of greenery systems must be adapted to future climate conditions and possible temperature changes to increase energy efficiency and control carbon dioxide emissions.

5. Limitation

In the context of outdoor comfort analysis, there exists a paucity of modeling tools that can predict microclimatic parameters, including air temperature and Tmrt. The predominant and widely utilized methods and software for calculating Tmrt are ENVI-met and Ladybug Tools. These tools are designed to calculate radiation components, including direct, diffuse, and reflected shortwave and longwave radiation from surfaces. Notably, both tools incorporate the calculation of longwave radiation from the sky. Both tools incorporate view factors, with Ladybug Tools utilizing ray-tracing and Envi-met employing Indexed View Sphere (IVS) methods. A distinguishing feature of both tools is their capacity to model radiation exchange between buildings, vegetation, and surface temperatures, which is a critical input parameter for Tmrt calculation. The primary distinction between the two tools lies in their approach to wind profiles. Envi-met utilizes a 3D computational fluid dynamics (CFD) model, a technique that has proven to be highly effective in simulating convective cooling or warming caused by wind. In contrast, Ladybug Tools utilize weather station wind data from EPW files, similar to the approach employed in this study, or the Butterfly plug-in, which employs CFD simulations utilizing the OpenFOAM framework. Ladybug Tools effectively models vegetation by simulating evapotranspiration, radiation exchanges, and thermal properties. However, these tools have limitations, as they treat vegetation properties as static, such as plant height and leaf area index (LAI). Furthermore, the potential impact of central area pollution on solar radiation magnitude was not considered in this study, as the weather data were obtained from the Turin-Caselle Airport station, which is situated in a rural environment.

6. Conclusions

This study underscores the considerable potential of VGSs, particularly green walls, in mitigating UHI effects and enhancing urban microclimates under both current and future climate scenarios. While the reductions in outdoor air temperature were modest, with variations ranging from -1.6 °C to 1.3 °C, the impact on Tmrt was more pronounced, with reductions reaching up to -2.27 °C during peak solar radiation in summer periods. These improvements were most evident in urban canyons and areas with low SVF, thereby demonstrating the capacity of green walls to improve thermal comfort in densely populated urban environments. The UTCI also showed consistent improvements, with maximum reductions of 0.55 °C under future climate projections for 2050 at noon in summer. Green walls proved particularly effective during summer, reducing cooling demand and lowering (cei) by up to 31%. However, during winter, a slight increase in heating demand led to higher emissions, underscoring the importance of optimizing green wall designs for seasonal energy performance. The findings indicate that the effectiveness of green walls is contingent on factors such as building orientation, solar exposure, and local urban morphology. Ensuring sufficient sunlight for vegetation is imperative for sustaining growth and optimizing the cooling effects driven by evapotranspiration. In the context of projected climate change, green walls are poised to play a pivotal role in adapting urban environments to rising temperatures and increasingly frequent heat waves.

While the present study did not examine partial coverage, this is an intriguing area for future research. The optimization of the model to achieve comparable performance with reduced coverage ratios could significantly increase its practicality. Furthermore,

advancements in this field could include the incorporation of locally adapted plant species, leveraging their distinctive thermal characteristics to enhance cooling efficiency, and adapting to diverse climatic and urban conditions.

In summary, the integration of green walls emerges as a pragmatic and sustainable approach to enhance outdoor thermal comfort, curtail carbon emissions, and mitigate Urban Heat Island (UHI) effects, particularly within urban contexts characterized by densely developed environments. These findings provide a solid foundation for integrating green walls into comprehensive urban climate adaptation strategies.

Author Contributions: Conceptualization, A.D.L.; methodology, A.D.L. and S.M.H.; software, A.D.L. and S.M.H.; validation, A.D.L. and S.M.H.; formal analysis, A.D.L. and S.M.H.; investigation, A.D.L.; data curation, A.D.L. and M.H.; writing—original draft preparation, A.D.L.; writing—review and editing, S.M.H., M.H., P.D. and F.S.; visualization, A.D.L. and S.M.H.; supervision, S.M.H. and P.D. All authors have read and agreed to the published version of the manuscript.

Funding: This research received no external funding.

Data Availability Statement: The data used to support the findings of this study can be made available by the corresponding author upon request.

Acknowledgments: We would like to acknowledge that this study is part of our contribution to the project titled: "EUDP 2023-I Deltagelse i IEASHC 70 Low Carbon, High Comfort Integrated Lighting". Also, this work is part of the research activity developed by the authors within the framework of the "PNRR": SPOKE 7 "CCAM, Connected Networks, and Smart Infrastructure"-WP4.

Conflicts of Interest: The authors declare no conflict of interest.

Abbreviations

The following abbreviations are used in this manuscript:

BT	Brightness Temperature
cei	Carbon Emission Intensity
CFD	Computational Fluid Dynamics
CVRMSE	Cumulative Variation of Root Mean Squared Error
EGR	Extensive Green Roof
ERF	Effective Radiant Field
GWs	Green Wall
HS	Heavy Systems
HVAC	Heating, Ventilation, and Air Conditioning
LAI	Leaf Area Index
LS	Light Systems
LST	Last Surface Temperature
MBE	Mean Bias Error
MV	Mur Vegetal
MWh	Megawatt Hour
NDVI	Normalized Different Vegetation Index
NIR	Near-infrared
PET	Physiological Equivalent Temperature
SL	Street Length
SUHI	Surface Urban Heat Island
SVF	Sky View Factor
TIR	Thermal Infrared
Tmrt	Mean Radiant Temperature

TMY	Typical Meteorological Year
UHI	Urban Heat Island
UTCI	Universal Thermal Climate Index
UWG	Urban Weather Generator
VGSs	Vertical Greenery Systems

Nomenclature

a_{lw}	Long wave absorptivity/emissivity (clothing) default 0.95
A_p/AD	The projection factor is determined through a look-up table available at ASHRAE and is determined by solar altitude, solar azimuth, and the body's related angle.
a_{sw}	Short wave absorptivity of the person (skin and clothing) default 0.7
f_{bes}	Fraction of body exposed to direct solar radiation
f_{eff}	Fraction of the body that can radiate heat (related to posture)
f_{svv}	Sky view factor
h_r	Radiant heat transfer coefficient
I_{diff}	Diffuse radiation (W/m^2)
I_{dir}	Direct radiation (W/m^2)
I_{th}	Global horizontal radiation (W/m^2)
R_{floor}	Ground reflectance
F_i	View factors to each surface
P_v	Proportion of Vegetation
T_a	Dry bulb temperature
T_i	Surface temperature
AL	Band-Specific Additive Rescaling Factor
C	Stephan–Boltzmann constant
σ	Stefan Boltzmann constant (5.667×10^{-8})
H	Planck constant
H/W	Aspect ratio
Lλ	Total spectral radiance
ML	Band-specific multiplicative rescaling factor
Qcal	Band 10
TOA	Top of Atmospheric
ε	Land surface emissivity
λ	Emitted radiance
c	Light velocity
ε_{person}	The emissivity of the human (assumed to be 0.95)

Appendix A

High-precision meteorological data Table A1 was used to validate the simulation results, allowing for reliable comparisons between observed environmental conditions and model predictions.

Table A1. Insite measurements sensors characteristics.

Wind Vane Anemometer DV20	
Anodized aluminum weathervane/Long-life potentiometric transducer	
Measuring range	0°–360°
Resolution	0.35° for the system
Precision	±2.8°
Operating temperature	0 °C–+60 °C; −30–+60 °C with electric heater
Dimensions	561 × 406 (mm)
Weight	0.9 (kg)

Table A1. *Cont.*

Tachometer Anemometer Vv20	
Three-blade polycarbonate reel/solid-state measuring transducer with frequency output	
Safety field	0–220 (km/h), 61 (m/s)
Resolution	0.06 (m/s), 0.2 (km/h)
Sensitivity	less than 0.02 (m/s), threshold of 1.8 (km/h), 0.5 (m/s)
Precision	±0.25 (km/h), 0.07 (m/s) or 1% of reading
Operating temperature	from −30 °C to +60 °C (with heater)
Dimensions	178 (Ø) × 281 (mm)
Weight	0.9 (kg)
Support Arm BSA20	
Made entirely of stainless steel/Comes complete with cables and connectors for sensors	
Dimensions	1490 × 790 (mm)
Weight	6.5 (kg) (including sensors)
Lightning rod made of stainless steel	1700 (mm) long/10 (mm) in diameter
Pyranometer HE20K	
Measuring range	0–1500 (W/m^2)
Spherical window	305–2800 (nm)
Non-linearity	±1.5% in the range 0–1000 (W/m^2)
Operating temperature range	−40 + 60 °C
Precision	5% (daily total), 1st class WMO (ISO 9060)
Influencing factors	sensitivity dependence on temperature < 2% in the range from −10 °C to +40 °C
Dimensions	150 (Ø) × 115 (mm)
Weight	1 (kg) (with shield)
THS Thermo-Hygrometer	
Hygrometer—Measurement range	0 to 100% RH
HYGROMETER—Temperature range	−50–+100 °C
SHIELDED AIR THERMOMETER—Sensing element	PT100 1/3 Din Class A
HYGROMETER—Accuracy	±1.5% from 0 to 100% RH
SHIELDED AIR THERMOMETER—Measurement range	−50–+100 °C
SHIELDED AIR THERMOMETER—Accuracy at 23 °C	±0.2 °C
PG10 and PG10R	
Connection with Data-logger	Interface RS-485 with SDI-12 protocol
Measurement Range	up to 1000 (mm/h)
Output Resolution	0.1 (mm)
Collecting Area	1000 (cm^2)
Accuracy	Max 3% < 800 (mm/h), Max 5%, 800–1000 (mm/h)
Temperature Range	PG10: 32 °F/140 °F, 0 °C/60 °C, PG10R: −22 °F/140 °F, −30 °C/60 °C
Sensor Type	Tipping bucket rain gauge

Appendix B

Figure A1 compares the levels of direct solar radiation recorded in the EPW weather file under current conditions and future projections in 2050. It shows how the intensity and distribution of solar radiation change over time and provides valuable context for understanding future climate scenarios.

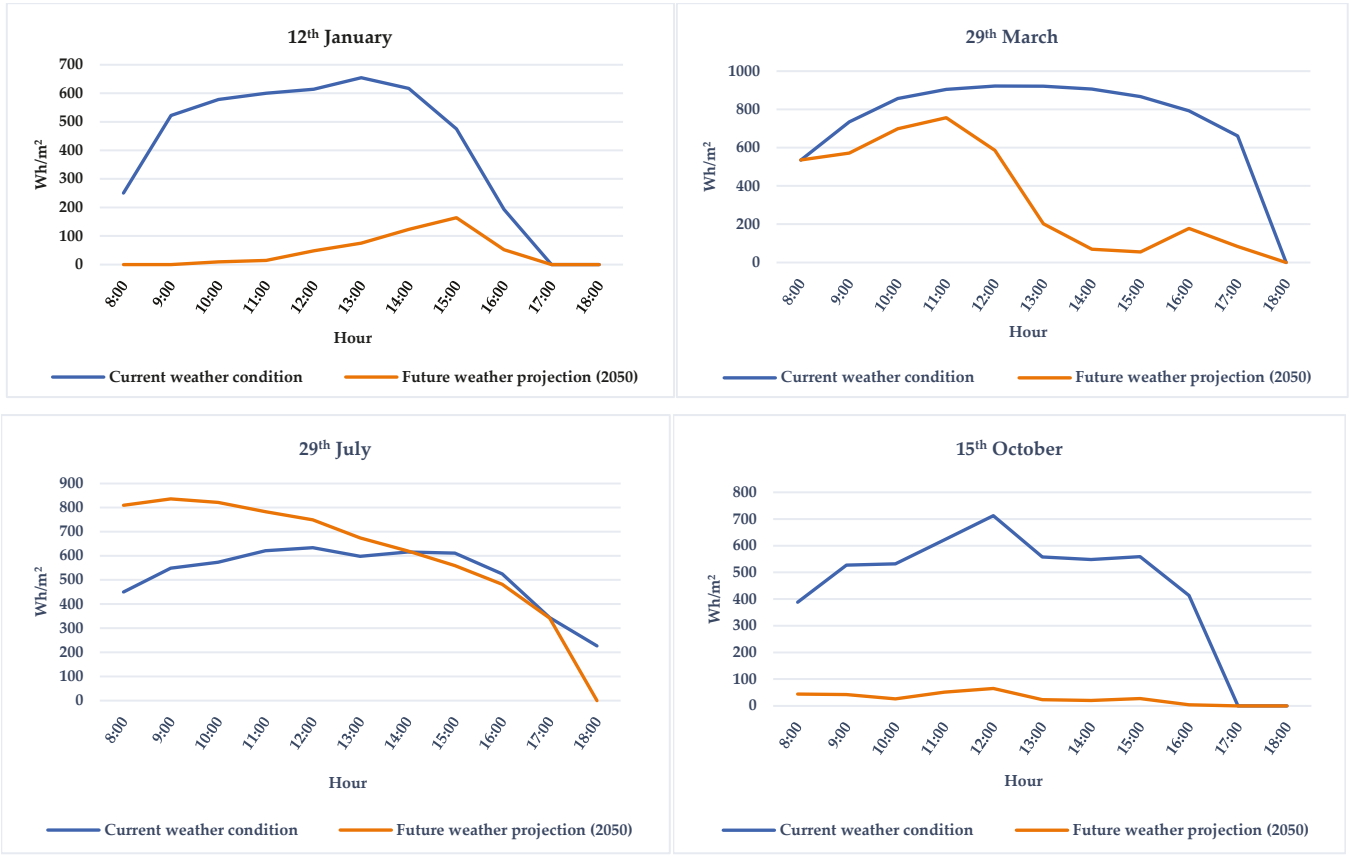


Figure A1. Direct solar radiation under current weather conditions and 2050 projection, based on data from the original EPW file.

References

1. United Nations, D. of E. and S.A.P.D. World Urbanization Prospects: The 2014 Revision; New York, 2015. 2015. Available online: https://population.un.org/wup/assets/WUP2014-Report.pdf (accessed on 20 December 2024).
2. Ng, E.; Chen, L.; Wang, Y.; Yuan, C. A Study on the Cooling Effects of Greening in a High-Density City: An Experience from Hong Kong. *Build. Environ.* **2012**, *47*, 256–271. [CrossRef]
3. De Groeve, M.; Kale, E.; Godts, S.; Orr, S.A.; De Kock, T. Impact of Vertical Greening on Urban Microclimate and Historic Building Materials: A Meta-Analysis. *Build. Environ.* **2024**, *253*, 111365. [CrossRef]
4. Boccalatte, A.; Fossa, M.; Thebault, M.; Ramousse, J.; Ménézo, C. Mapping the Urban Heat Island at the Territory Scale: An Unsupervised Learning Approach for Urban Planning Applied to the Canton of Geneva. *Sustain. Cities Soc.* **2023**, *96*, 104677. [CrossRef]
5. Cheval, S.; Amihăesei, V.-A.; Chitu, Z.; Dumitrescu, A.; Falcescu, V.; Irașoc, A.; Micu, D.M.; Mihulet, E.; Ontel, I.; Paraschiv, M.-G.; et al. A Systematic Review of Urban Heat Island and Heat Waves Research (1991–2022). *Clim. Risk Manag.* **2024**, *44*, 100603. [CrossRef]
6. Schmidt, V. Urban Morphology as a Key Parameter for Mitigating Urban Heat?–A Literature Review. *IOP Conf. Ser. Earth Environ. Sci.* **2024**, *1363*, 012074. [CrossRef]
7. Zheng, Y.; Ren, C.; Shi, Y.; Yim, S.H.L.; Lai, D.Y.F.; Xu, Y.; Fang, C.; Li, W. Mapping the Spatial Distribution of Nocturnal Urban Heat Island Based on Local Climate Zone Framework. *Build. Environ.* **2023**, *234*, 110197. [CrossRef]
8. Eslamirad, N.; Sepúlveda, A.; De Luca, F.; Sakari Lylykangas, K.; Ben Yahia, S. Outdoor Thermal Comfort Optimization in a Cold Climate to Mitigate the Level of Urban Heat Island in an Urban Area. *Energies* **2023**, *16*, 4546. [CrossRef]
9. Gholami, H.; Kamelnia, H.; Mahdavinejad, M.J.; Sangin, H. Optimizing Building Configuration and Orientation for Social Housing Projects in Iran. *Iran. J. Energy Environ.* **2025**, *16*, 289–308. [CrossRef]
10. Rabie, S.; Sangin, H.; Zandieh, M. The Orientation of Village, the Most Important Factor in Rural Sustainability in Cold Climate (Case Study: Masuleh and Uramantakht). *J. Sol. Energy Res.* **2021**, *6*, 761–776. [CrossRef]

11. Shao, L.; Liao, W.; Li, P.; Luo, M.; Xiong, X.; Liu, X. Drivers of Global Surface Urban Heat Islands: Surface Property, Climate Background, and 2D/3D Urban Morphologies. *Build. Environ.* **2023**, *242*, 110581. [CrossRef]
12. Lin, T.-P.; Matzarakis, A.; Hwang, R.-L. Shading Effect on Long-Term Outdoor Thermal Comfort. *Build. Environ.* **2010**, *45*, 213–221. [CrossRef]
13. Oke, T.R. *Boundary Layer Climates*; Routledge: London, UK, 2002; ISBN 0-203-71545-4.
14. Güller, C.; Toy, S. The Impacts of Urban Morphology on Urban Heat Islands in Housing Areas: The Case of Erzurum, Turkey. *Sustainability* **2024**, *16*, 791. [CrossRef]
15. Ahmadi Venhari, A.; Tenpierik, M.; Taleghani, M. The Role of Sky View Factor and Urban Street Greenery in Human Thermal Comfort and Heat Stress in a Desert Climate. *J. Arid Environ.* **2019**, *166*, 68–76. [CrossRef]
16. Fang, Z.; He, H.; Mao, Y.; Feng, X.; Zheng, Z.; Guo, Z. Investigating an Accurate Method for Measuring the Outdoor Mean Radiation Temperature. *Int. J. Therm. Sci.* **2023**, *188*, 108219. [CrossRef]
17. Azimi, Z.; Shafaat, A. Proposing Design Strategies for Contemporary Courtyards Based on Thermal Comfort in Cold and Semi-Arid Climate Zones. *Build. Environ.* **2024**, *266*, 112150. [CrossRef]
18. Li, J.; Wang, J.; Wong, N.H. Urban Micro-Climate Research in High Density Cities: Case Study in Nanjing. *Procedia Eng.* **2016**, *169*, 88–99. [CrossRef]
19. Irfeey, A.M.M.; Chau, H.-W.; Sumaiya, M.M.F.; Wai, C.Y.; Muttil, N.; Jamei, E. Sustainable Mitigation Strategies for Urban Heat Island Effects in Urban Areas. *Sustainability* **2023**, *15*, 10767. [CrossRef]
20. Lopez-Cabeza, V.P.; Alzate-Gaviria, S.; Diz-Mellado, E.; Rivera-Gomez, C.; Galan-Marin, C. Albedo Influence on the Microclimate and Thermal Comfort of Courtyards under Mediterranean Hot Summer Climate Conditions. *Sustain. Cities Soc.* **2022**, *81*, 103872. [CrossRef]
21. Morakinyo, T.E.; Lam, Y.F. Simulation Study on the Impact of Tree-Configuration, Planting Pattern and Wind Condition on Street-Canyon's Micro-Climate and Thermal Comfort. *Build. Environ.* **2016**, *103*, 262–275. [CrossRef]
22. Cortês, A.S.B.; Almeida, J.A.S.; Kanoun-Boulé, M.; Tadeu, A. Green Facades and Living Walls: The Portuguese Experience. In *INCREaSE*; Springer International Publishing: Cham, Switzerland, 2018; pp. 562–570; ISBN 978-3-319-70271-1.
23. Zaina, S.M.; Fadli, F.; Hosseini, S.M. Evaluation of Smart Irrigation Systems in Hot-Arid Climates for Green Roofs and Walls: Case of Doha, Qatar. *Smart Sustain. Built Environ.* **2022**, *11*, 346–367. [CrossRef]
24. Ramadhan, A.M.; Mahmoud, A.H. Evaluating the Efficiency of a Living Wall Facade as a Sustainable Energy-Saving Alternative in Hot Arid Regions. *J. Eng. Appl. Sci.* **2023**, *70*, 96. [CrossRef]
25. Reynolds, H.L.; Brandt, L.; Fischer, B.C.; Hardiman, B.S.; Moxley, D.J.; Sandweiss, E.; Speer, J.H.; Fei, S. Implications of Climate Change for Managing Urban Green Infrastructure: An Indiana, US Case Study. *Clim. Change* **2020**, *163*, 1967–1984. [CrossRef]
26. Sommese, F. Nature-Based Solutions to Enhance Urban Resilience in the Climate Change and Post-Pandemic Era: A Taxonomy for the Built Environment. *Buildings* **2024**, *14*, 2190. [CrossRef]
27. Susca, T.; Zanghirella, F.; Del Fatto, V. Building Integrated Vegetation Effect on Micro-Climate Conditions for Urban Heat Island Adaptation. Lesson Learned from Turin and Rome Case Studies. *Energy Build.* **2023**, *295*, 113233. [CrossRef]
28. Wang, P.; Wong, Y.H.; Tan, C.Y.; Li, S.; Chong, W.T. Vertical Greening Systems: Technological Benefits, Progresses and Prospects. *Sustainability* **2022**, *14*, 12997. [CrossRef]
29. Zhang, L.; Deng, Z.; Liang, L.; Zhang, Y.; Meng, Q.; Wang, J.; Santamouris, M. Thermal Behavior of a Vertical Green Facade and Its Impact on the Indoor and Outdoor Thermal Environment. *Energy Build.* **2019**, *204*, 109502. [CrossRef]
30. Larsen, S.F.; Filippín, C.; Lesino, G. Thermal Simulation of a Double Skin Façade with Plants. *Energy Procedia* **2014**, *57*, 1763–1772. [CrossRef]
31. Herath, H.M.P.I.K.; Halwatura, R.U.; Jayasinghe, G.Y. Modeling a Tropical Urban Context with Green Walls and Green Roofs as an Urban Heat Island Adaptation Strategy. *Procedia Eng.* **2018**, *212*, 691–698. [CrossRef]
32. Mutani, G.; Todeschi, V. The Effects of Green Roofs on Outdoor Thermal Comfort, Urban Heat Island Mitigation and Energy Savings. *Atmosphere* **2020**, *11*, 123. [CrossRef]
33. Ciacci, C.; Banti, N.; Di Naso, V.; Bazzocchi, F. Green Strategies for Improving Urban Microclimate and Air Quality: A Case Study of an Italian Industrial District and Facility. *Build. Environ.* **2023**, *244*, 110762. [CrossRef]
34. Kim, E.S.; Yun, S.H.; Lee, D.K.; Kim, N.Y.; Piao, Z.G.; Kim, S.H.; Park, S. Quantifying Outdoor Cooling Effects of Vertical Greening System on Mean Radiant Temperature. *Dev. Built Environ.* **2023**, *15*, 100211. [CrossRef]
35. Djedjig, R.; Belarbi, R.; Bozonnet, E. Green Wall Impacts inside and Outside Buildings: Experimental Study. *Energy Procedia* **2017**, *139*, 578–583. [CrossRef]
36. Zuckerman, N.; Shiloah, N.; Lensky, I.M. Quantifying the Impact of Vertical Greenery Systems (VGS) on Mediterranean Urban Microclimate during Heat Wave Events. *Build. Environ.* **2025**, *267*, 112151. [CrossRef]

37. Taher, H.; Elsharkawy, H.; Rashed, H.F. Urban Green Systems for Improving Pedestrian Thermal Comfort and Walkability in Future Climate Scenarios in London. *Buildings* **2024**, *14*, 651. [CrossRef]
38. Nashaat, B. Optimizing Parametric Green Facades for Daylighting and Thermal Comfort in Egypt's Hot Climates. *Port Said Eng. Res. J.* **2024**, *28*, 72–83. [CrossRef]
39. Wahba, S.; Kamil, B.; Nassar, K.; Abdelsalam, A. Green Envelop Impact on Reducing Air Temperature and Enhancing Outdoor Thermal Comfort in Arid Climates. *Civil Eng. J.* **2019**, *5*, 1124–1135. [CrossRef]
40. U.S.G. Survey. Available online: https://earthexplorer.usgs.gov/ (accessed on 12 July 2024).
41. Ladybug Tools EPW Map. Available online: https://www.ladybug.tools/epwmap/ (accessed on 8 March 2024).
42. Agenzia Regionale per la Protezione Ambientale (ARPA) Piemonte di Torino Hourly Meteorological and Hydrological Data. Available online: https://www.arpa.piemonte.it/ (accessed on 2 May 2024).
43. Machard, A.; Salvati, A.; Tootkaboni, P.M.; Gaur, A.; Zou, J.; Wang, L.L.; Baba, F.; Ge, H.; Bre, F.; Bozonnet, E.; et al. Typical and Extreme Weather Datasets for Studying the Resilience of Buildings to Climate Change and Heatwaves. *Sci. Data* **2024**, *11*, 531. [CrossRef]
44. Heiranipour, M.; Favoino, F.; Juaristi Gutierrez, M.; Avesani, S. *Typical and Extreme (Heatwave) Future Weather for Building Energy Simulations: Case for Turin and Bolzano, Italy, and De Bilt, Netherlands*; Zenodo: Genève, Switzerland, 2024.
45. Boccardo, P.; Giulio Tonolo, F. Remote Sensing Role in Emergency Mapping for Disaster Response. In *Engineering Geology for Society and Territory*; Springer International Publishing: Cham, Switzerland, 2015; Volume 5, pp. 17–24.
46. Avdan, U.; Jovanovska, G. Algorithm for Automated Mapping of Land Surface Temperature Using LANDSAT 8 Satellite Data. *J. Sens.* **2016**, *2016*, 1–8. [CrossRef]
47. Kasniza Jumari, N.A.S.; Ahmed, A.N.; Huang, Y.F.; Ng, J.L.; Koo, C.H.; Chong, K.L.; Sherif, M.; Elshafie, A. Analysis of Urban Heat Islands with Landsat Satellite Images and GIS in Kuala Lumpur Metropolitan City. *Heliyon* **2023**, *9*, e18424. [CrossRef]
48. Rahman, M.N.; Rony, M.R.H.; Jannat, F.A.; Chandra Pal, S.; Islam, M.S.; Alam, E.; Islam, A.R.M.T. Impact of Urbanization on Urban Heat Island Intensity in Major Districts of Bangladesh Using Remote Sensing and Geo-Spatial Tools. *Climate* **2022**, *10*, 3. [CrossRef]
49. Dabove, P.; Daud, M.; Olivotto, L. Revolutionizing Urban Mapping: Deep Learning and Data Fusion Strategies for Accurate Building Footprint Segmentation. *Sci. Rep.* **2024**, *14*, 13510. [CrossRef] [PubMed]
50. Regione Piemonte Geo Piemonte. Available online: https://geoportale.igr.piemonte.it/cms/ (accessed on 31 March 2024).
51. Rezaei, F.; Sangin, H.; Heiranipour, M.; Attia, S. A Multi-Objective Optimization of Window and Light Shelf Design in Office Buildings to Improve Occupants' Thermal and Visual Comfort. *J. Daylighting* **2024**, *11*, 55–68. [CrossRef]
52. Naboni, E.; Milella, A.; Vadalà, R.; Fiorito, F. On the Localised Climate Change Mitigation Potential of Building Facades. *Energy Build.* **2020**, *224*, 110284. [CrossRef]
53. Mackey, C.; Galanos, T.; Norford, L.; Sadeghipour Roudsari, M. Wind, Sun, Surface Temperature, and Heat Island: Critical Variables for High-Resolution Outdoor Thermal Comfort. In Proceedings of the Building Simulation 2017: 15th Conference of IBPSA, 7 August 2017; IBPSA: San Francisco, CA, USA; pp. 985–993.
54. Salvati, A.; Kolokotroni, M. Urban Microclimate and Climate Change Impact on the Thermal Performance and Ventilation of Multi-Family Residential Buildings. *Energy Build.* **2023**, *294*, 113224. [CrossRef]
55. Dardir, M.; Berardi, U. Development of Microclimate Modeling for Enhancing Neighborhood Thermal Performance through Urban Greenery Cover. *Energy Build.* **2021**, *252*, 111428. [CrossRef]
56. Naboni, E.; Meloni, M.; Mackey, C.; Kaempf, J. The Simulation of Mean Radiant Temperature in Outdoor Conditions: A Review of Software Tools Capabilities. In Proceedings of Building Simulation 2019: 16th Conference of IBPSA, Rome, Italy, 2–4 September 2019; pp. 3234–3241.
57. Bueno, B.; Norford, L.; Hidalgo, J.; Pigeon, G. Prediction of the Urban Heat Island Effect to Be Used in Building Energy Analyses. In Proceedings of the SimBuild Conference 2012: 5th Conference of IBPSA USA, Madison, WI, USA, 1–3 August 2012; Volume 5, pp. 236–245.
58. Arens, E.; Hoyt, T.; Zhou, X.; Huang, L.; Zhang, H.; Schiavon, S. Modeling the Comfort Effects of Short-Wave Solar Radiation Indoors. *Build. Environ.* **2015**, *88*, 3–9. [CrossRef]
59. American Society of Heating, Refrigerating, and Air-Conditioning Engineers. Measurement of Energy, Demand, and Water Savings. In *Ashrae Guideline 14-2014: Measurement of Energy, Demand and Water Savings*; American Society of Heating, Refrigerating, and Air-Conditioning Engineers: Peachtree Corners, GA, USA, 2014.
60. (NREL), N.R.E.L. EnergyPlus^{TM} 2017.
61. Arenghi, A.; Perra, C.; Caffi, M. Simulating and Comparing Different Vertical Greenery Systems Grouped into Categories Using EnergyPlus. *Appl. Sci.* **2021**, *11*, 4802. [CrossRef]

62. Hosseini, S.M.; Heiranipour, M.; Wang, J.; Hinkle, L.E.; Triantafyllidis, G.; Attia, S. Enhancing Visual Comfort and Energy Efficiency in Office Lighting Using Parametric-Generative Design Approach for Interactive Kinetic Louvers. *J. Daylighting* **2024**, *11*, 69–96. [CrossRef]
63. Stec, W.J.; Paassen, A.H.C. van Symbiosis of the Double Skin Façade with the HVAC System. *Energy Build.* **2005**, *37*, 461–469. [CrossRef]
64. The International Energy Agency (IEA) Greenhouse Gas Emissions from Energy Data Explorer. Available online: https://www.iea.org (accessed on 16 December 2024).

Disclaimer/Publisher's Note: The statements, opinions and data contained in all publications are solely those of the individual author(s) and contributor(s) and not of MDPI and/or the editor(s). MDPI and/or the editor(s) disclaim responsibility for any injury to people or property resulting from any ideas, methods, instructions or products referred to in the content.

buildings

MDPI

Article

Evaluation and Optimization of Outdoor Thermal Comfort of Block-Style Commercial Complex in Hot Summer and Cold Winter Regions of China

Yeheng Zhou [1,*], Jiang Zhu [2], Eryu Ni [3] and Yanzhe Hu [1]

[1] College of Architecture and Urban Planning, Tongji University, Shanghai 200092, China; santsteven@126.com
[2] Zhengzhou Zhengdong High Tech Industrial Development Co., Ltd., No. 136 Zhengkai Avenue, Zhengzhou 450016, China; zhujiang241005@163.com
[3] Department of Architecture, School of Architecture, South China University of Technology, Guangzhou 510641, China; erunina@outlook.com
* Correspondence: 2280001@tongji.edu.cn; Tel.:+86-13774221079

Abstract: In recent years, block-style commercial complexes have become a prominent form of commercial architecture in many Chinese cities. The thermal comfort of their outdoor spaces significantly influences people's activities and the overall quality of these areas. This study explores the relationship between the morphological elements of outdoor spaces in such complexes and thermal comfort, using quantifiable methods to identify key control indicators. Enhancing thermal comfort is crucial for improving spatial quality, increasing dwell time, and boosting commercial vibrancy. Focusing on the hot summer and cold winter climate of Shanghai, this research analyzed two representative block-style commercial complexes. It employed computer simulations and sensory comfort surveys to demonstrate that block morphology significantly impacts outdoor thermal comfort. Three control variables—street density, number of street intersections, and street orientation—were selected to study their effects. Spatial prototypes were categorized, and their thermal comfort performance was evaluated using numerical simulations. Based on these findings, spatial morphology was iteratively optimized. This study concluded by proposing evaluation indicators for spatial morphology control elements to enhance outdoor thermal comfort. It also provided external spatial layout strategies for block-style commercial complexes in similar climates, offering architects and urban designers decision-making criteria to improve thermal comfort in outdoor spaces. This research contributes to creating more comfortable and vibrant urban environments.

Keywords: block-type commercial complex; external space; human thermal comfort; spatial form control elements; evaluation index

1. Introduction

1.1. Problems Existing in the External Space of Block-Style Commercial Complexes in High-Density Urban Environments

The expansion of urban areas, rapid population growth, increased urban traffic, and industrial production contribute to the "heat island effect", where urban temperatures are notably higher than those in surrounding suburban areas during the same season. This effect is particularly severe in cities with populations exceeding 5 million, or even 10 million. Meteorological data from the past 50 years indicate a steady intensification of

the urban heat island effect in Shanghai over the last three decades: from 0.09/10 in the period of 1961 to 1970, to 0.12/10 from 1971 to 1980, and further to 0.22/10 from 1991 to 2006 [1]. The exacerbation of the urban heat island effect diminishes the overall outdoor thermal comfort of the city. Moreover, buildings and numerous artificially constructed environments disrupt wind and gas circulation, resulting in either stagnant air or localized extreme wind conditions within the city. This exacerbates air pollution and other issues, indirectly impacting solar radiation, heat dissipation, and exacerbating already compromised outdoor thermal comfort.

In fact, ensuring good thermal comfort is crucial for creating an excellent external space. It directly impacts people's willingness to stay and engage in activities within it, thereby influencing the overall quality of the external space. During the author's visits and investigations, it was observed that in winter, the outer space of a block-style commercial complex in Beijing experiences extremely high wind speeds, leading to considerable discomfort (Figure 1). Conversely, the outer space of another nearby block-style commercial complex offers noticeably more comfort, attracting more guests for shopping, leisure, and sightseeing compared to the former. Similarly, in Shanghai during the summer, even on days with equally high temperatures, the number and behavior of users in the external spaces of different block-style commercial complexes vary significantly.



Figure 1. Few pedestrians can be seen in the external space of Beijing's Galaxy SOHO, while Xin Tian Di is bustling with crowds. The author took photographs.

The external space of a block-style commercial complex serves a crucial role in fostering the vibrancy of commercial areas and is an integral component of urban public spaces, facilitating communication and leisure activities among urban residents. Poor thermal comfort in these spaces not only diminishes the commercial vitality of the complex but also reduces it to a mere thoroughfare.

1.2. Necessity of Research on Human Thermal Comfort in Outer Space

The severe urban heat island effect diminishes the overall thermal comfort of the city, impacting the microclimate of the outer spaces within block-style commercial complexes. This poor thermal environment directly influences the local microclimate, leaving the external spaces of these complexes vulnerable. Typically, these spaces feature hard pavement surfaces, which possess high heat absorption capabilities and readily heat up under solar radiation. Additionally, factors such as building enclosure design, street density, direction, and accessibility indirectly affect the solar radiation levels experienced within the external

spaces of block-style commercial complexes. Furthermore, the wind environment plays a significant role in determining their thermal comfort.

At present, many scholars have conducted research on the microclimate of public space, and it is generally believed that the physical environment of external space has a significant impact on the use of public space and people's stay [2,3]. In high-density urban environments, the thermal comfort of external spaces affects the physiological and psychological well-being of users, influencing their decision to stay and engage. Research on the thermal comfort of outer spaces within block-style commercial complexes can enhance their spatial quality and user experience, leading to increased foot traffic and heightened commercial vitality.

2. Preview the Literature on the Topic

2.1. Research on Human Thermal Comfort

Research on human thermal comfort began in the 1920s. With the widespread adoption of air conditioning, the American Society of Heating, Refrigerating, and Air-Conditioning Engineers (ASHRAE) introduced the effective temperature index after conducting numerous investigations and experiments. Subsequently, in the 1960s, a wealth of fundamental data related to thermal comfort were collected through extensive experimentation, laying the groundwork for Professor Fanger of the Technical University of Denmark to develop the thermal comfort equation for the human body. Professor Fanger integrated these data with considerations such as metabolic heat production, heat dissipation processes of the human body, and clothing insulation, employing physical equations to formulate the human thermal comfort equation. The Predicted Mean Vote (PMV) and the Predicted Percentage of Dissatisfied (PPD) were proposed as evaluation indices for human thermal comfort. Following extensive experimental validation, these indices have become essential tools for assessing human thermal comfort today [4]. To study human thermal comfort, four main parameters must be considered: air temperature, relative humidity, wind speed, and mean radiant temperature [4]. Additionally, factors such as clothing insulation and physical activity level in outdoor environments should also be considered [4]. Recent advancements have focused on integrating artificial intelligence with real-time environmental sensing to dynamically optimize thermal comfort models under climate change scenarios [5].

2.2. Relevant Research on Numerical Simulation of Microclimate

With the advancement of computer science and technology, research utilizing computer-based numerical simulation has been ongoing for a considerable period and has yielded fruitful results. Particularly noteworthy is the ENVI-met software (ENVI-met 4.4, ENVI-met, Düsseldorf, Germany), developed by Professor Bruce M. and his team at the University of Bochum in Germany, which enables comprehensive microclimate simulations of entire outdoor environments. Utilizing principles from basic fluid mechanics and thermodynamics, this software can accurately calculate microclimate variations over one or two diurnal cycles [6].

In addition, Dr. Wang Zhen from Huazhong University of Science and Technology analyzed the wind and thermal environment of Wuhan city, characterized by hot summers and cold winters, by combining field measurements with numerical computer simulations. The study investigated the factors influencing thermal comfort within urban streets and gorges [7]. Shi Yuan, Ren Chao, and Wu Enrong from the Chinese University of Hong Kong selected Xidan Commercial Street in Beijing as their research subject. They conducted numerical computer simulations to analyze the wind and thermal environment of the pedestrian street district, evaluated its wind and thermal comfort, and proposed

corresponding urban design strategies for improvement. Subsequently, through numerical computer simulation verification post-transformation, they put forward a universal urban design strategy to enhance the wind and thermal environment of urban commercial pedestrian streets [8]. Recent advancements emphasize the integration of machine learning with multi-scale microclimate modeling to improve prediction accuracy and optimize urban design interventions in real-time scenarios [9].

2.3. Research on Urban Climatology

Classification and Characteristics of the Urban Climate

In *Man, Climate, Architecture*, Barry categorizes climate into global wind zone climate, regional atmospheric climate, local topographic climate, and microclimate based on the scale of climate characteristics, considering both horizontal and vertical ranges (Table 1).

Table 1. Climatic zoning classification.

Climatic System	Approximate Scale of Climate Characteristics		Duration
	Horizontal Range (km)	Vertical Range (km)	
Global Wind Zone Climate	2000	3–10	1–6 months
Regional Macroclimate	500–1000	1–10	1–6 months
Local Topographic Climate	1–10	0.1–1	1–24 h
Microclimate	0.1–1	0.1	24 h

Microclimate is defined as the near-surface climate that occurs within a horizontal range of 1 km and is limited to a height of less than 100 m. It is determined by the structural characteristics of the underlying surface and is most significantly influenced by human activities [10].

By summarizing urban design cases from 1996 to 2006, scholar Matthias Roth explored the common problems in large and medium-sized cities in tropical and subtropical regions:

(1) The higher temperature in the city decreases the thermal comfort of the human body and brings the problem of increased mortality.
(2) Due to the decrease in wind speed caused by the man-made environment, the pollutants cannot be effectively discharged in time, which brings up the problem of air pollution retention.
(3) The energy exchange brought about by human production and life intensifies the change in urban microclimate [11].

Emerging studies now prioritize nature-based solutions, such as integrating permeable pavements and vertical greenery systems, to simultaneously mitigate urban heat islands and enhance pollutant dispersion in dense urban areas [12].

The study area of this paper is Shanghai. As a city in a hot summer and cold winter area, outdoor high temperatures and high humidity in summer reduce the thermal comfort of outdoor activities, which has an impact on people's outdoor space activities [13].

The external space of a block-style commercial complex is also a component of the city's external public space. Similar to urban outdoor spaces, its thermal comfort is closely related to factors such as its shape, spatial distribution, and enclosing interface. Additionally, the block-style commercial complex building exhibits characteristics typical of urban blocks, with specific form index factors for control [14]. Consequently, the microclimate

environment of the external space of a block-style commercial complex can be influenced by human activities.

3. Study Area and Methods

3.1. Selection of Numerical Simulation Software

In this study, the author selected Envi-met, developed by German scientist Professor Michael Bruse and his team, to simulate the physical environment of outdoor spaces and directly derive relevant thermal comfort evaluation index data. The following section will describe the software selection process in more detail.

Envi-met (ENVI-met 4.4, ENVI-met, Düsseldorf, Germany), is a 3D non-static microclimate modeling software that can calculate and simulate the microclimate environment of urban areas. In this software, the urban environment can be represented through grid modeling, with each grid's accuracy adjustable from 0.5 m to 10 m. The simulation interval is set at 10 s. Utilizing the fundamental principles of fluid mechanics and thermodynamics, the software computes the microclimate dynamics over a complete daily cycle. The key variables affecting the software's calculations include wind speed and direction, air temperature and humidity, fluctuations, radiation coefficient, bioclimatology, and gas and particle diffusion. The basic working principle is illustrated in the figure below (Figure 2):

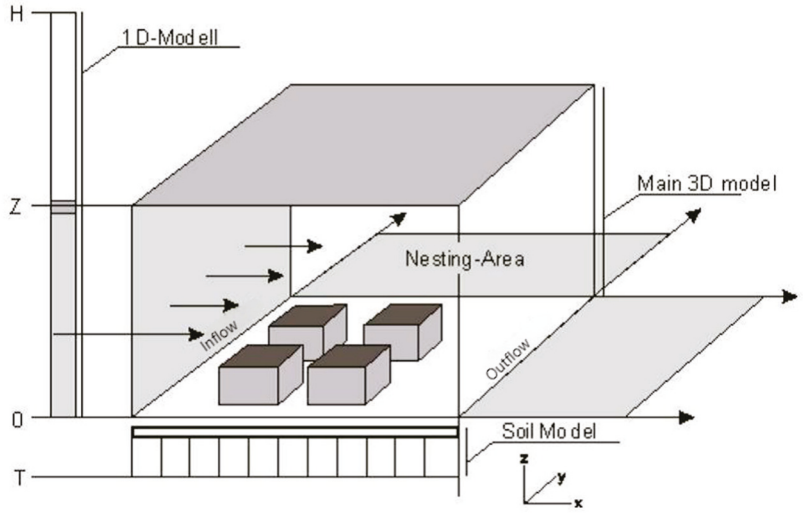


Figure 2. Envi-met software overall structure diagram; image from the Envi-met description.

The Envi-met model comprises a three-dimensional core model encompassing the atmosphere, vegetation, soil, and buildings, alongside a one-dimensional boundary layer model (Figure 2). The three-dimensional core model simulates all microclimate processes in the relevant urban environment, while the one-dimensional model converts the initial values into the boundary values of the three-dimensional core model. The one-dimensional model extends to 2500 m in the vertical direction and can simulate microclimate changes in the actual environment more accurately.

The numerical calculation of the Envi-met software involves many physical formulas related to thermodynamics, fluid mechanics, and other aspects. These have been discussed in the paper by the software development team, and relevant research and expressions can be referred to in the associated papers.

3.2. Thermal Comfort Data Index

In terms of evaluating human thermal comfort, this paper adopts a rational index developed based on the energy balance equation, combined with existing empirical data and formulas. This approach enables the calculation of a large amount of data in an unsteady thermal environment and fulfills the evaluation requirements for outdoor human thermal comfort more effectively.

Physiological Equivalent Temperature (PET) and Mean Radiant Temperature (MRT)

Physiological equivalent temperature (PET) is defined as the environmental conditions indoors (with an air temperature of 20 °C, wind speed of 0.1 m/s, humidity of 50%, air pressure of 12 hPa, and average radiation temperature equal to the air temperature), which maintain the core temperature and skin layer temperature of a typical human object at the same level as the air temperature in the indoor or outdoor environment being evaluated. PET is calculated based on the Munich Energy Model (MEMI) and is specifically used for the thermal comfort evaluation of outdoor environments [15] (Table 2).

Table 2. The relationship between PET values and the corresponding thermal sensation and physiological response levels is examined.

PET (°C)	Thermal Sensation	Physiological Response Level
4	Freezing	Extreme Cold Stress
8	Cold	Severe Cold Stress
13	Cool	Moderate Cold Stress
18	Chilly	Mild Cold Stress
23	Comfort	No Heat Stress
29	Warm	Moderate Heat Stress
35	Hot	Severe Heat Stress
41	Scorching	Extreme Heat Stress

Since the evaluation software used by the author cannot directly obtain PET data at present, the author will substitute it with another parameter that reflects outdoor thermal comfort: mean radiant temperature (MRT). By leveraging computer simulation software, the MRT value of the external space can be directly measured, enabling the evaluation of outdoor thermal comfort.

Dr. Wang Zhen from Huazhong University of Science and Technology, China, investigated the measurement of thermal comfort and conducted numerical computer simulations of urban street gap spaces. Dr. Wang found a linear relationship between physiological equivalent temperature and MRT by statistically analyzing a large dataset. This finding serves as the theoretical basis for the author's decision to use MRT as a substitute for the PET index. The equation is expressed as follows:

$$y = 0.7133\,x - 2.2744$$

where R^2 (coefficient of determination) = 0.998.

R^2 is a coefficient used to measure linear correlation and reflects the relationship between two variables. The closer R^2 is to 1, the stronger the correlation between the variables, while R^2 closer to 0 indicates a weaker linear relationship.

In Dr. Wang Zhen's simulation study, a high correlation was observed between physiological equivalent temperature and average radiation temperature. This is attributed to the significant influence of direct sunlight on both external and internal heat radiation

in the human body. Therefore, average radiation temperature holds greater practical significance than air temperature in comfort evaluation.

3.3. Research Site Selection and Examples (Data Collection of Two Commercial Complexes in Shanghai)

3.3.1. Climate Overview of Shanghai and Selection of Simulation Time

Shanghai, situated on the west coast of the Pacific Ocean, experiences high solar radiation, elevated air temperatures, and increased humidity during the summer months. These climatic conditions have a more pronounced impact on outdoor thermal comfort compared to winter, posing the primary challenge in the study of outdoor thermal comfort in Shanghai. Consequently, this paper concentrates on evaluating the thermal comfort of outdoor spaces during the summer season. August was selected as the simulation month, aligning with recent meteorological data from Shanghai.

3.3.2. Selection of Numerical Simulation Cases

The author initially selected two cases of block-style commercial complexes with similar development intensity but differing external space density to conduct a comparative study. This was done to explore potential factors influencing thermal comfort and to prepare for the establishment of an analysis model. The following outlines the basic characteristics of the two block-style commercial complexes (Table 3):

Table 3. The basic characteristics of the two block-type commercial complexes.

	Wujiaochang Wanda Plaza	**Daning International Commercial Plaza**
Construction time	2006.12	2006.10
Site area (m^2)	63,500	55,000
Gross floor area (m^2)	333,000	250,000
Floor area (m^2)	251,000	200,000
Plot ratio	3.95	3.63
Podium height (m)	24	24
Street density (km/km^2)	10	20
Street area ratio (%)	20	20
Number of street crossings	3	15
Block orientation	NWbN 26°	NWbN 32°

In Figure 3, the left side depicts Wujiaochang Wanda Plaza, while the right side shows Daning International Commercial Plaza. Both are block-style commercial complexes situated in the core urban area of Shanghai. (Figure 3) They share a similar land size, development intensity, and thermal environment. However, significant differences exist in street density and the number of street intersections between them. Additionally, the outer spaces of both complexes are predominantly hard-paved, with relatively similar underlying surfaces.



Figure 3. *Cont.*

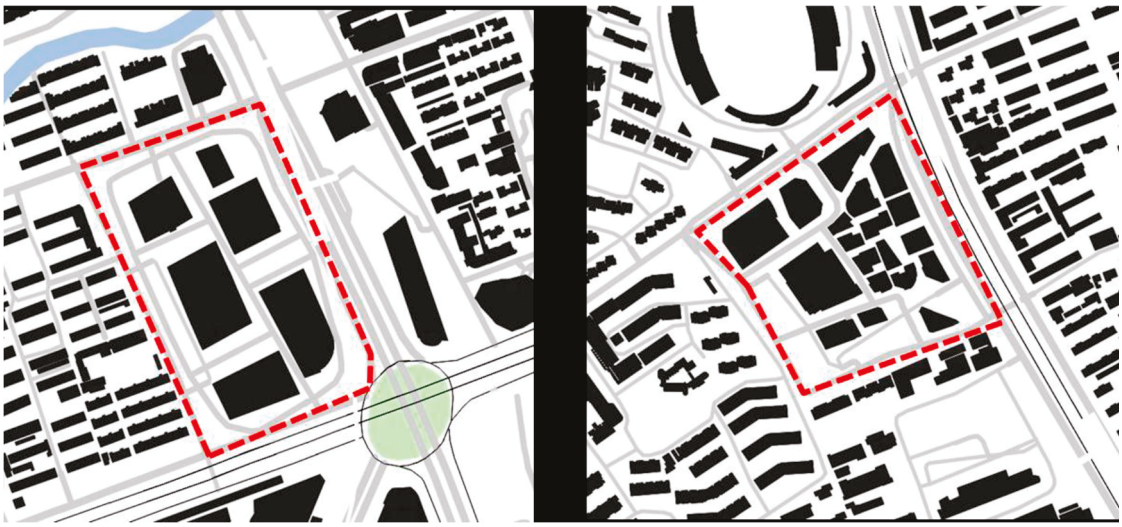


Figure 3. Texture comparison of Wujiaochang Wanda Plaza and Daning International Commercial Plaza—drawn by the author.

3.3.3. Setting of Initial Conditions for Numerical Simulation

Setting of Instance Modeling Conditions

Firstly, spaces were used to adjust the model parameters, which were obtained according to the on-site investigation of the building and its surrounding environment. The established model is shown in the figure below (Table 4):

Table 4. The established model conditions.

Location	Shanghai Urban Area (31.12° N, 121.30° E)
Simulation time	5 August 2022
Simulation period	9:00–23:00
Model grid	Wujiaochang Wanda Plaza:75/82/20 (ΔX = ΔY = 4 m, ΔZ = 8 m)
(Grid number and grid scale)	Daning International Commercial Plaza:70/70/30 (ΔX = ΔY = 4 m, ΔZ = 6 m)
Number of nested grids	5

Setting the Initial Climate Condition of the Instance

For ConfigWizard, you can obtain related parameters by referring to the meteorological data and the software's built-in database. Related parameters are set as follows (Table 5):

Table 5. Show related parameters.

Location	Shanghai Urban Area (31.12° N, 121.30° E)
Simulation time	5 August 2022
Simulation period	9:00–23:00
Atmospheric boundary condition	Initial wind speed (10 m): 3 m/s
	Wind direction: 120° (Southeast)
	Initial temperature: 300.15 K
	Initial humidity (2500 m): 2 g/kg
	Relative humidity (2 m): 50%
	Ground roughness: 0.01

Table 5. *Cont.*

Substrate temperature, humidity	Initial temperature: 293.3 K
	Relative humidity: 60%
Human physiology	Clothing thermal resistance: 0.3 clo
	Activity: 53.6 W

In this study, using measured meteorological data as computer simulation data is deemed appropriate. Due to technological and equipment limitations, relevant parameters provided by the Shanghai Meteorological Bureau were selected as the initial conditions.

3.3.4. Numerical Simulation Analysis of Examples

In fact, there are many factors that influence the thermal comfort of the exterior space of block-style commercial complexes. This paper primarily focuses on the block form, with the simulation study limited to the examination of buildings.

Overall Comparative Analysis of Two Examples

The utilization of external space in block-style commercial complexes is subject to certain temporal constraints. During an investigation of block-style commercial complexes in Shanghai, the author observed that on working days, most shops or restaurants adjacent to the outdoor spaces of these complexes open at 10:00 and remain open until 22:00 Some stores typically open at 10:00 on non-working days, with the possibility of extending their hours until 22:30 or 23:00 Based on actual investigation and observation, combined with an urban heat map derived from mobile signaling data, the author found that pedestrian flow within block-style commercial complexes peaks during noon (12–13), afternoon (14–17), and evening (19–21).

Based on the meteorological data of a sunny and high-temperature day on 5 August 2015, in Shanghai, this study conducted a microclimate simulation for the block commercial complex. It selected 16:00 as the simulation period for air temperature, wind speed, humidity, mean radiation temperature (MRT), and PMV spatial layout in the outside space of the block commercial complex. Through a comparative study, relevant data were obtained. Finally, the MRT index was taken as the evaluation result. We used two completed commercial buildings in Shanghai as model prototypes (Figure 4).

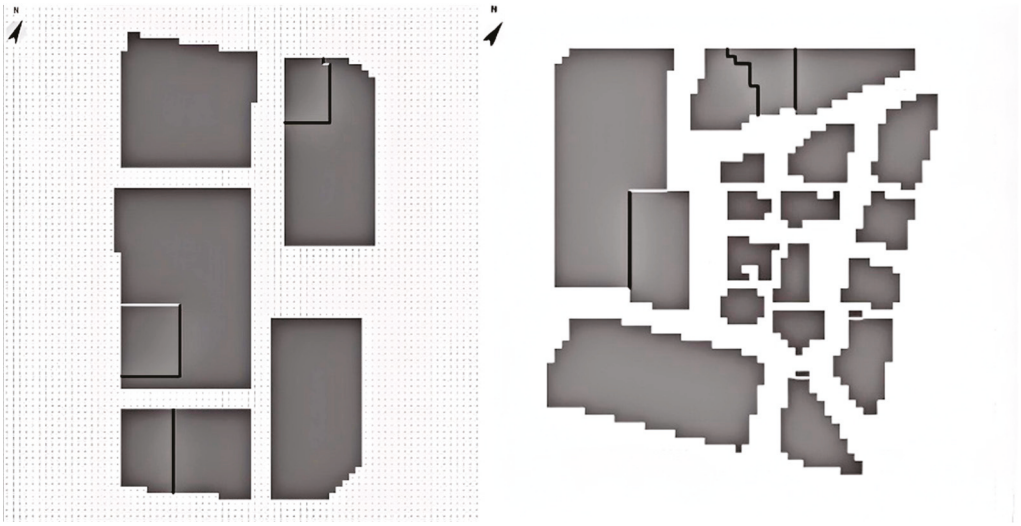


Figure 4. Wujiaochang Wanda Commercial Plaza and Daning International Envi-met model (building only)—drawn by the author.

Mean radiation temperature MRT analysis (Figures 5 and 6)

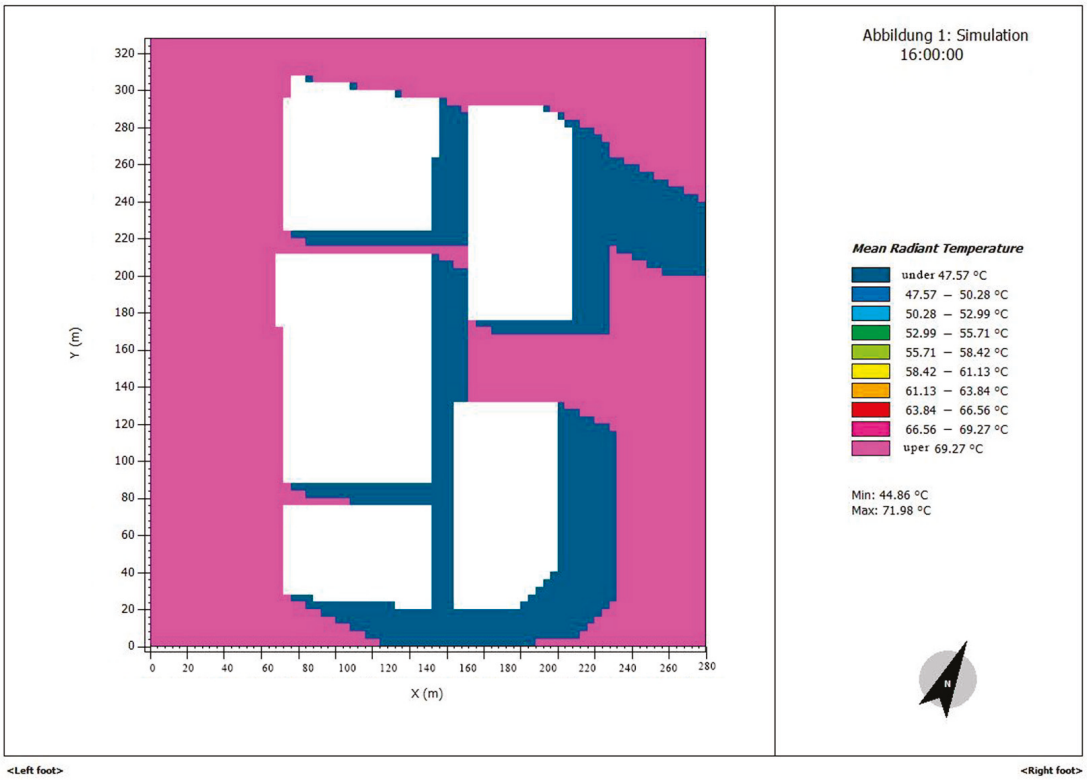


Figure 5. MRT distribution map of Wujiaochang Wanda Plaza external space (16:00, 1.2 m above ground)—drawn by the author.

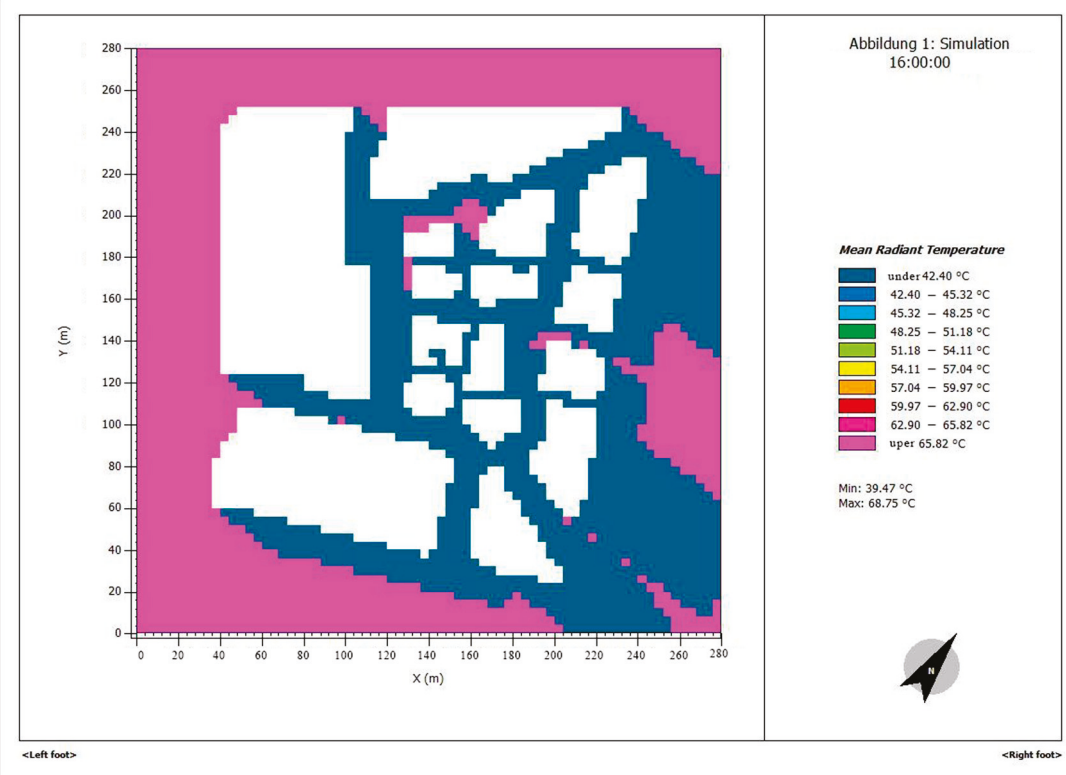


Figure 6. MRT layout of Daning International Commercial Plaza (16:00, 1.2 m above ground)—drawn by the author.

By comparison, we can find that the mean radiant temperature (MRT) value of the external space of Daning International Commercial Plaza is lower than that of Wujiaochang Wanda Plaza, with the maximum difference occurring between 14:00 and 15:00 (Figure 7).

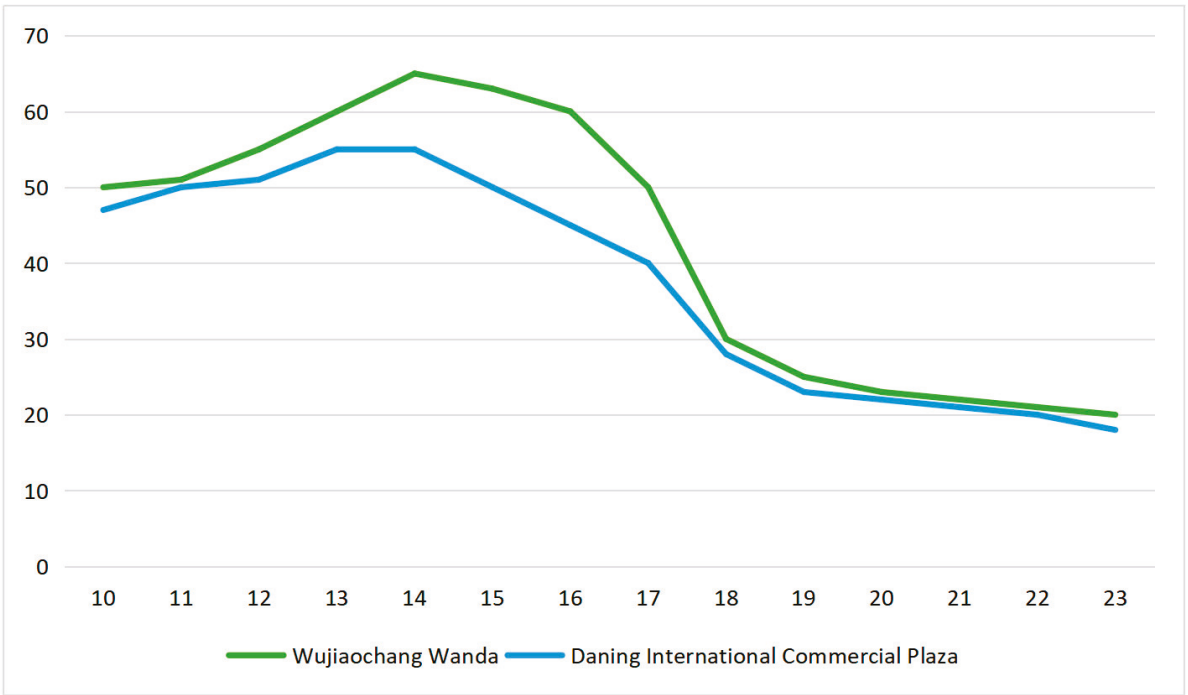


Figure 7. Comparison of MRT (°C) values of Wujiaochang Wanda and Daning International Commercial Plaza (10:00–23:00, 1.2 m above ground)—drawn by the author.

From the above practical cases, it can be seen that commercial blocks with varying street densities, intersection numbers, and street directions have different impacts on the thermal comfort of the external space. Therefore, it is necessary to analyze the effects of different factors on thermal comfort through spatial prototype simulation.

3.3.5. Questionnaire Survey on Physical Comfort of Examples

To verify the authenticity of the simulation examples mentioned above, the author conducted a random questionnaire survey on 30 groups of customers at two project sites. The survey was conducted from 14:00 to 17:00 on 20 August at Daning International Business Plaza and on 23 August at Wujiaochang Wanda Plaza during the same time frame.

The questionnaire consisted of a hierarchical survey on three general perceived comfort indexes of customers outside the commercial street, namely, temperature, humidity, wind speed, and comprehensive physical comfort. The results are as follows:

After calculating the weighted average, the comfort index of Daning Commercial Plaza is 3.33, while that of Wujiaochang Wanda Plaza is 3.02 (Table 6). According to the questionnaire survey, the physical comfort of outdoor blocks in Daning International Commercial Plaza is better than that of Wujiaochang Wanda Plaza to some extent, verifying the effectiveness of the computational model.

Table 6. Results of questionnaire survey on comfort index.

Daning International Commercial Plaza					
		Temperature	Humidity	Wind Speed	Physical Comfort
Very comfortable	5	0	3	2	3
Comfortable	4	10	15	8	13
General	3	16	10	14	9
Uncomfortable	2	2	2	4	4
Very uncomfortable	1	2	0	2	1
	Total	30	30	30	30
Wujiaochang Wanda Plaza					
		Temperature	Humidity	Wind Speed	Physical Comfort
Very comfortable	5	0	0	4	0
Comfortable	4	5	10	12	9
General	3	14	12	9	12
Uncomfortable	2	7	6	5	7
Very uncomfortable	1	4	2	0	2
	Total	30	30	30	30

3.4. Space Prototype Design

3.4.1. Design Consideration

The outer space of a block-style commercial complex is similar to the street space, but it differs in scale and spatial attributes. This research establishes a relatively perfect and representative spatial prototype and mainly uses the following indicators as the basis for the design of spatial prototypes:

(1) Block-Scale Size

At present, as an important type of commercial building in urban areas, block-style commercial complexes are mostly located in the central areas of cities due to their higher

development intensity and human flow attraction. They are often combined with urban public transportation hub nodes or laid out along urban trunk roads and secondary trunk roads. Therefore, their land size should typically range between 100 and 300 m. According to the author's actual investigation of block-style commercial complexes in Shanghai, the size of most commercial complex building plots is concentrated between 180 and 280 m (Figure 8).

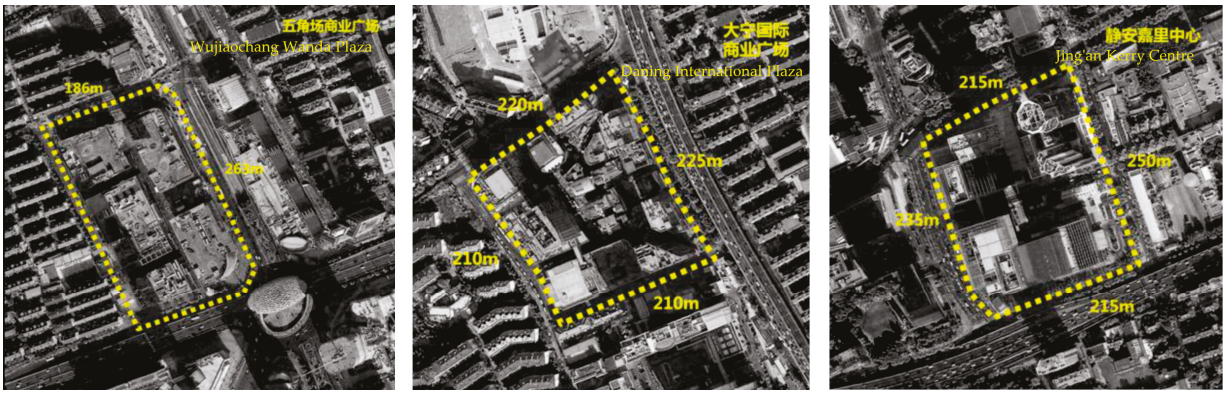


Figure 8. Schematic of typical block size for Shanghai block-style commercial complexes—drawn by the author.

In this study, the author combined traffic planning and design norms with the historical conditions of Shanghai and selected a 250 × 250 m plot as the size of the space prototype.

(2) Street Density (Line Density)

In the study of block-style commercial complexes, their external spaces are taken as the research object. Therefore, this concept is used to represent the "street" (linear external space) density of the external spaces of block-style commercial complexes.

Street density refers to the length of streets per unit area, measured in km/km^2.

According to the actual investigation, the author found significant differences in street density among block-style commercial complexes. The block-style commercial complex represented by Shanghai Wujiaochang Wanda Shopping Center features a large external space scale, with fewer interruptions caused by buildings throughout the plot. Conversely, the block-style commercial complex represented by Shanghai Daning International Plaza has a smaller external space scale, with more interruptions caused by buildings throughout the plot. The street density of the outer space of the two block-style commercial complexes is 10 km/km^2 and 20 km/km^2, respectively, indicating a considerable difference. However, the development intensity of the two complexes is similar.

During the actual visit, the author observed that these two spatial layout patterns are related to commercial formats. Wujiaochang Wanda Plaza primarily features department stores, entertainment venues, cinemas, and other major stores, requiring a sizable construction area. Conversely, Daning International Plaza is predominantly composed of small shops, such as retail and dining establishments. A higher street density is advantageous for creating a longer street interface and accommodating more shops. It also fosters stronger movement along the external commercial dynamic line space, which contributes to the emergence of additional commercial interfaces and value (Figure 9).

This study primarily examines the thermal comfort of the commercial exterior space layout density in these two typical blocks. It combines a block size setting of 250 × 250 m and modifies the exterior space by cutting it 1–4 times. Four street densities of 4 km/km^2, 8 km/km^2, 12 km/km^2, and 16 km/km^2 were chosen as variables (corresponding to street

spaces with lengths of 250 m, 500 m, 750 m, and 1000 m, respectively) to represent the street density of the spatial prototype.

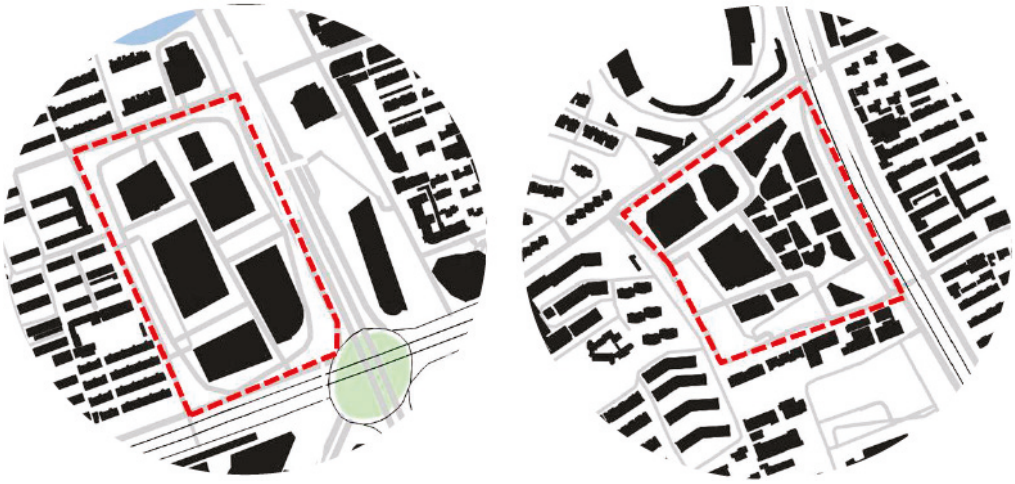


Figure 9. Relationship between Wujiaochang Wanda Plaza and Daning International Commercial Plaza site plans—drawn by the author.

(3) Street Area Ratio (Area Density)

The street area ratio refers to the proportion of street or road area within a given unit area. Within the context of block-style commercial complexes' external spaces, the author regards it as the coverage of these areas. This value is intricately linked to both street density and the development intensity of the plot. Since it involves unified development within a plot, building density directly impacts the size of external spaces in block-style commercial complexes. For this study, the author selected a 25% street coverage rate as the street area ratio for the spatial prototype model.

(4) Building Height

Building height has an impact on urban microclimate, primarily influencing the wind environment and the shielding of thermal radiation. Considering the principle of commercial value, high-rise commercial blocks with a height exceeding 24 m are rarely encountered. Therefore, this study will adopt 24 m as the building height for the space prototype design.

(5) Number of Street Crossings

In view of the sample analysis of several typical commercial districts in Shanghai, there are mostly 3–8 street intersections (Figure 10). Therefore, in this study, the author will select 3–8 street intersections with the same street density to design spatial prototype models with a different number of intersections.

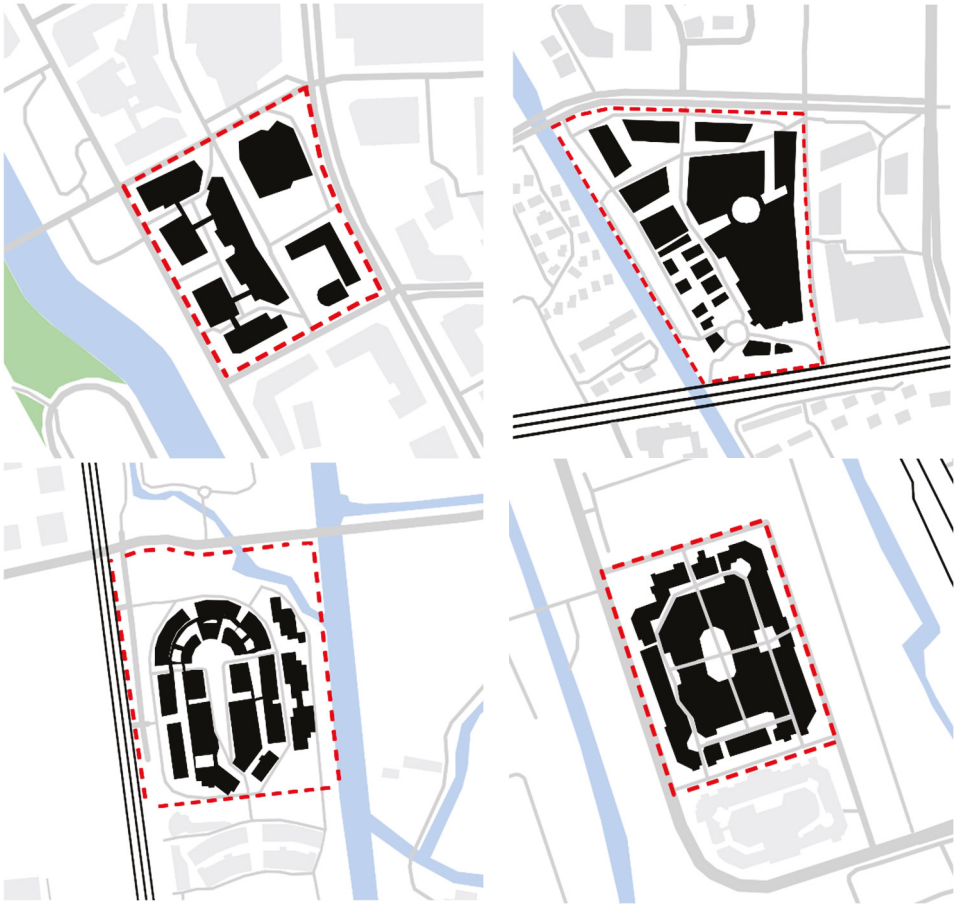


Figure 10. Upper left: site plan of Hongqiao Tiandi commercial street district; **upper right**: site plan of Qibao Square commercial street district; **bottom left**: site plan of Bailian Outlet commercial street district; **bottom right**: site plan of Florence Town commercial street district—drawn by the author.

(6) Street Direction

Dr. Wang Zhen from Huazhong University of Science and Technology discusses the thermal comfort and orientation of two spatial prototypes (long street short street and long lane short street). In this study, based on the investigation of street density and the number of intersections, the author will examine their orientations and compare the overall thermal comfort of three street layout directions: 0°, 45°, and 90°.

3.4.2. Model Construction

Combining the design basis of the original model mentioned above, the author presents the following spatial prototype model (Figure 11).

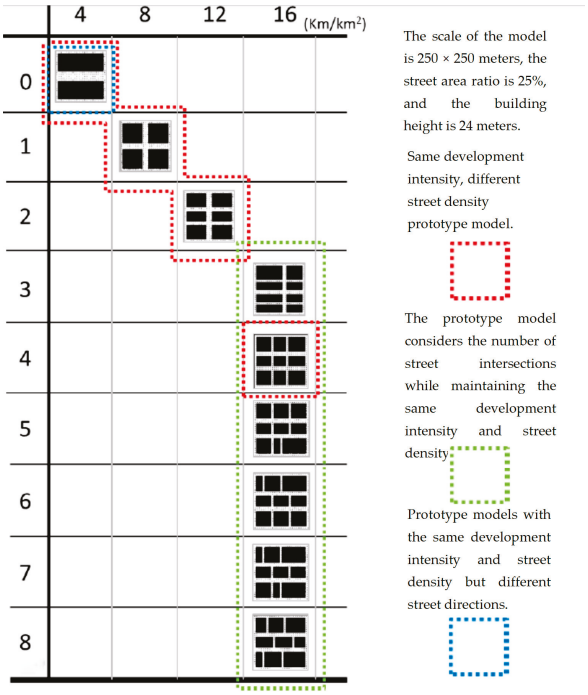


Figure 11. Spatial prototype diagram—drawn by the author.

4. Analysis and Results

The discussion regarding the business hours of the block-style commercial complex in Shanghai has been mentioned earlier. Therefore, in this section, the selected prototype model was simulated using meteorological data from a sunny and hot day in Shanghai on 5 August 2022. The simulation period for air temperature, wind speed, humidity, mean radiant temperature (MRT), and Predicted Mean Vote (PMV) in the outer space of the prototype model was set at 16:00. Through comparative studies, relevant data were obtained.

To facilitate data statistics and readers' comprehension, these prototype models are labeled with numbers. The first digit represents the simulation from different perspectives. For instance, the study on the correlation between street density and thermal comfort is labeled as 1, the study on the number of street intersections and thermal comfort is labeled as 2, and the study on the correlation between street direction and thermal comfort is labeled as 3. The second digit is 0 for division purposes. The third number represents different prototype models, starting at 1 and gradually increasing with the rise in street density and the number of street entrances. In the study of street direction, three or four digits represent the angle between the original model and the east–west direction (clockwise is positive, counterclockwise is negative, and the model with a street density of 4 km/km^2 is defined as the original model 3000).

4.1. Thermal Comfort Analysis of Different Commercial Street Densities

4.1.1. Overall Comparative Analysis of Thermal Comfort in the External Space of the Model

Figure 12 shows the modeling of prototype models with street densities of 4 km/km^2, 8 km/km^2, 12 km/km^2, and 16 km/km^2 in Envi-met.

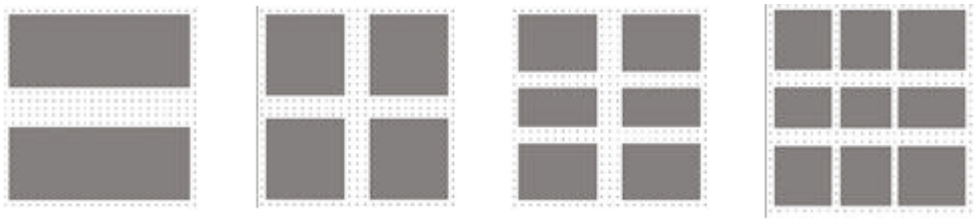


Figure 12. The prototype models with street densities of 4 km/km^2, 8 km/km^2, 12 km/km^2, and 16 km/km^2 were modeled in Envi-met, and their corresponding model numbers were 101, 102, 103, and 104, respectively—drawn by the author.

With the increase in street density, the lower MRT area of the outer space of models 102, 103, and 104 will increase, primarily distributed within their street space.

The overall MRT trend among the four models is basically the same. The maximum MRT difference in the outer space of the four models also occurred between 14:00 and 15:00, starting to decrease at 18:00, with the MRT difference becoming less apparent by 23:00. By comparing the charts of air temperature, wind speed, and humidity, it can be seen that MRT has a greater relationship with solar radiation and a higher correlation with air temperature. With the increase in street density, MRT decreases during daytime hours, while during the night, MRT values tend to be uniform (Figures 13 and 14).

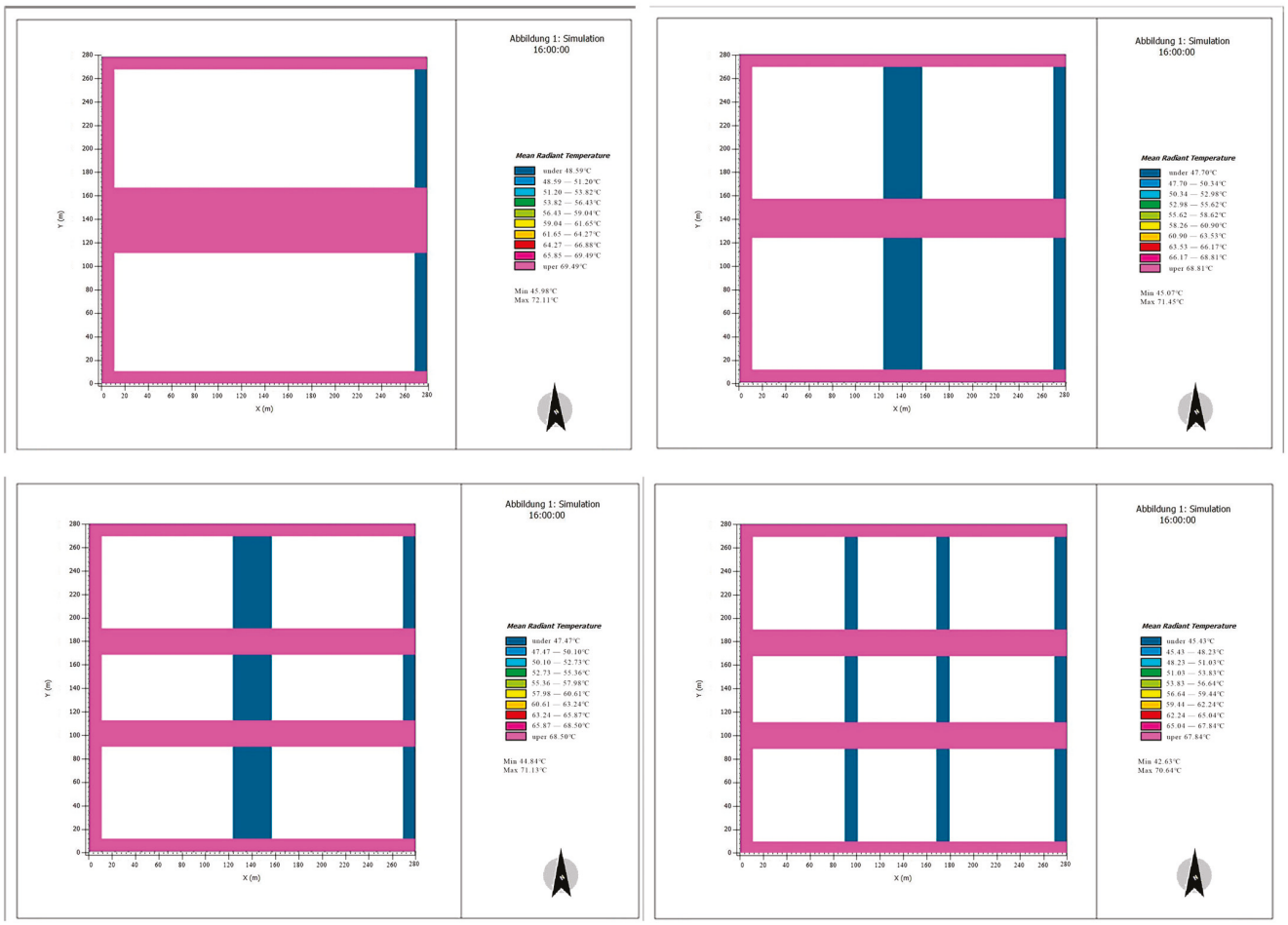


Figure 13. MRT (°C) distribution of prototype model 101–104 in outer space (at 16:00, 1.2 m above ground)—drawn by the author.

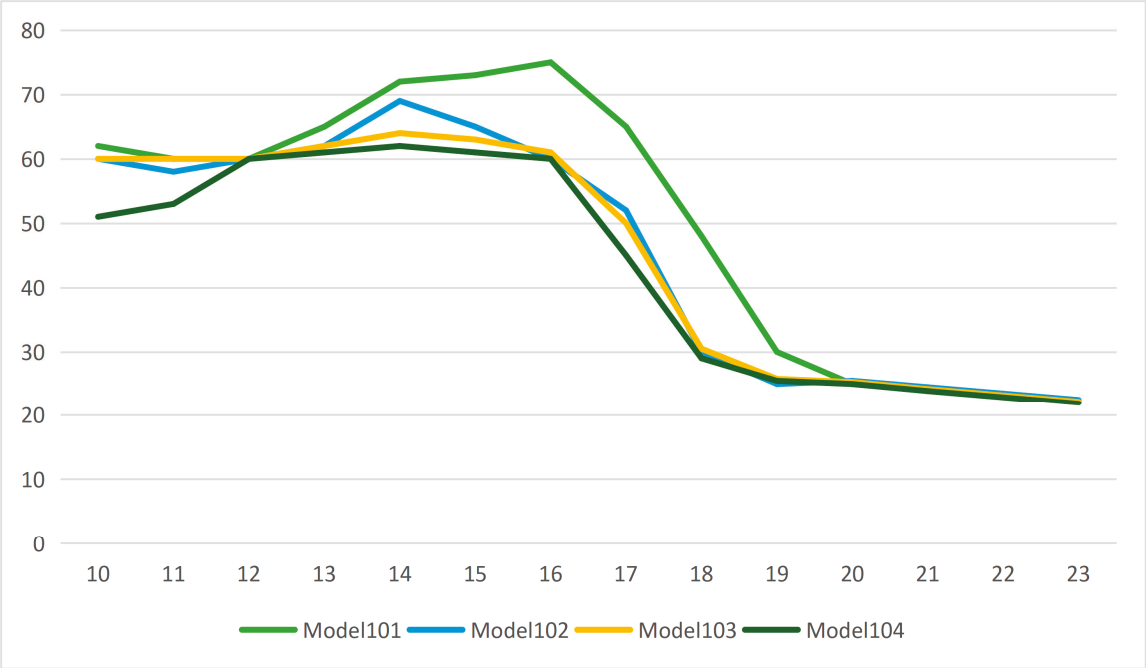


Figure 14. Comparison of MRT (°C) values of prototype model 101–104 (10:00–23:00, 1.2 m above ground)—drawn by the author.

In general, the correlation between the change in MRT and street scale was significant during the daytime, with a low correlation observed between MRT and street scale at night. In other words, the higher the street density, the lower the MRT during the daytime. However, compared to model 103, there is no significant decrease in MRT in model 104. Thus, within a certain range of street density increase, the MRT value of its external space decreases significantly. When this range is exceeded, the MRT value does not decrease significantly with the increases in street density.

4.1.2. Thermal Comfort Analysis Conclusion of Street Density in Different External Spaces

According to the simulation data statistics, street density is correlated with the temperature, wind speed, humidity, and MRT of the outer space. The temperature, wind speed, MRT, and PMV show an inverse correlation, meaning that an increase in street density will decrease the air temperature, wind speed, MRT, and PMV. The influence of street density on humidity was not obvious during the day but showed a certain inverse correlation at night. That is, with the increase in street density, the relative humidity would decrease slowly, resulting in higher values.

4.2. Thermal Comfort Analysis of Different Commercial Street Intersections

4.2.1. Overall Comparative Analysis of Thermal Comfort in the External Space of the Model

Figure 15 shows the modeling of prototype models with different street intersections.

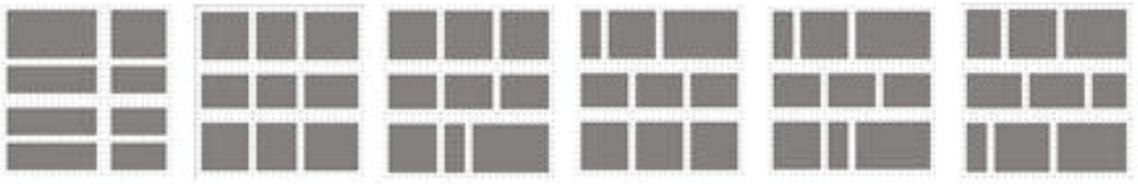


Figure 15. The prototype models of street intersections 3, 4, 5, 6, 7, and 8 were modeled in Envi-met, and the corresponding model numbers were 201, 202, 203, 204, 205, and 206, respectively—drawn by the author.

In general, the correlation between MRT changes and street intersections is significant during the day but low at night. In other words, MRT decreases with the increase in the number of street intersections during the daytime. However, in model 205, MRT does not decrease significantly; it may even increase. This suggests that within a certain range, the MRT value of the external space decreases noticeably with the increase in the number of street intersections, but this is not absolute. The reason, combined with wind speed and humidity, can be speculated as low wind speed hindering thermal comfort (Model 205 has the lowest average wind speed throughout the day). When this range is exceeded, the MRT value does not decrease significantly with the increase in street density (Figures 16 and 17).

4.2.2. Conclusion of Thermal Comfort Analysis on the Number of Intersections in Different External Spaces

Through data statistics, we know that the number of street intersections has a certain correlation with the wind speed, humidity, and MRT of the external space, with a general trend inversely correlated with temperature. However, there are local differences in the data, and the possible causes need to be further verified.

4.3. Thermal Comfort Analysis of Different Commercial Street Directions

4.3.1. Overall Comparative Analysis of Thermal Comfort in the External Space of the Model

It can be clearly seen from the figure that prototype model 30–45, which deviates from the dominant summer wind direction, exhibits a large area of lower MRT in the outer space, primarily distributed within the street space (Figure 18).

In general, there was a significant correlation between MRT changes and street direction during the day. At night, the correlation between MRT and street orientation is low. That is, the MRT value is low when the street direction aligns with the dominant summer wind direction during the daytime (Figure 19).

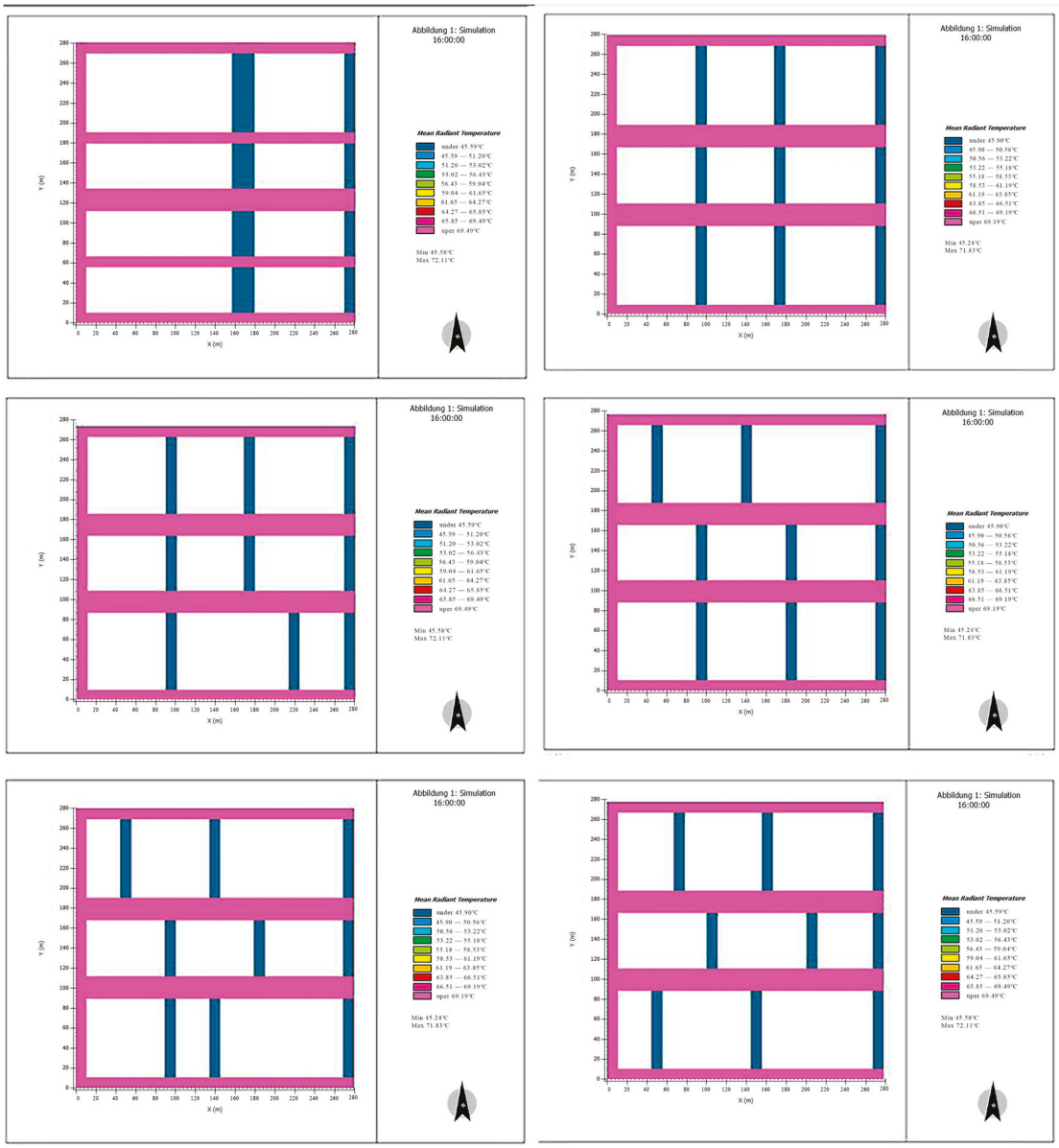


Figure 16. Prototype model 201–206 External space MRT (°C) distribution map (16:00, 1.2 m above ground)—drawn by the author.

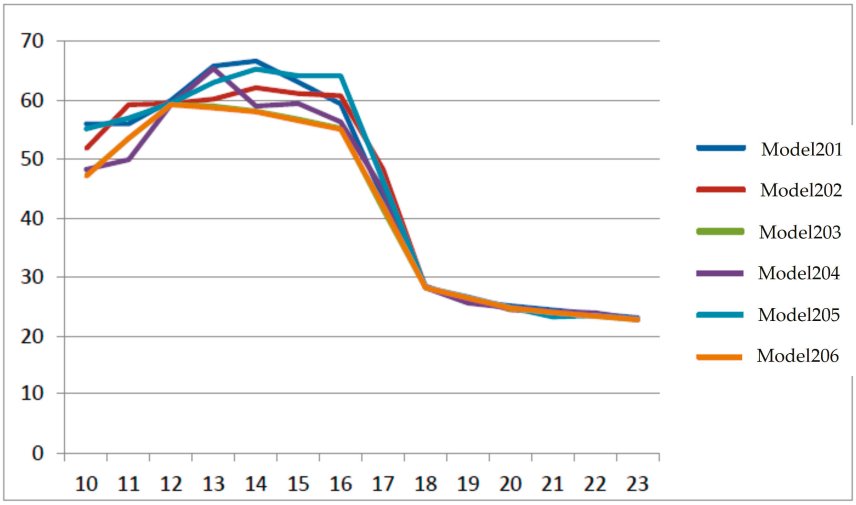


Figure 17. Comparison of MRT (°C) values of prototype model 201–206 (10:00–23:00, 1.2 m above ground)—drawn by the author.

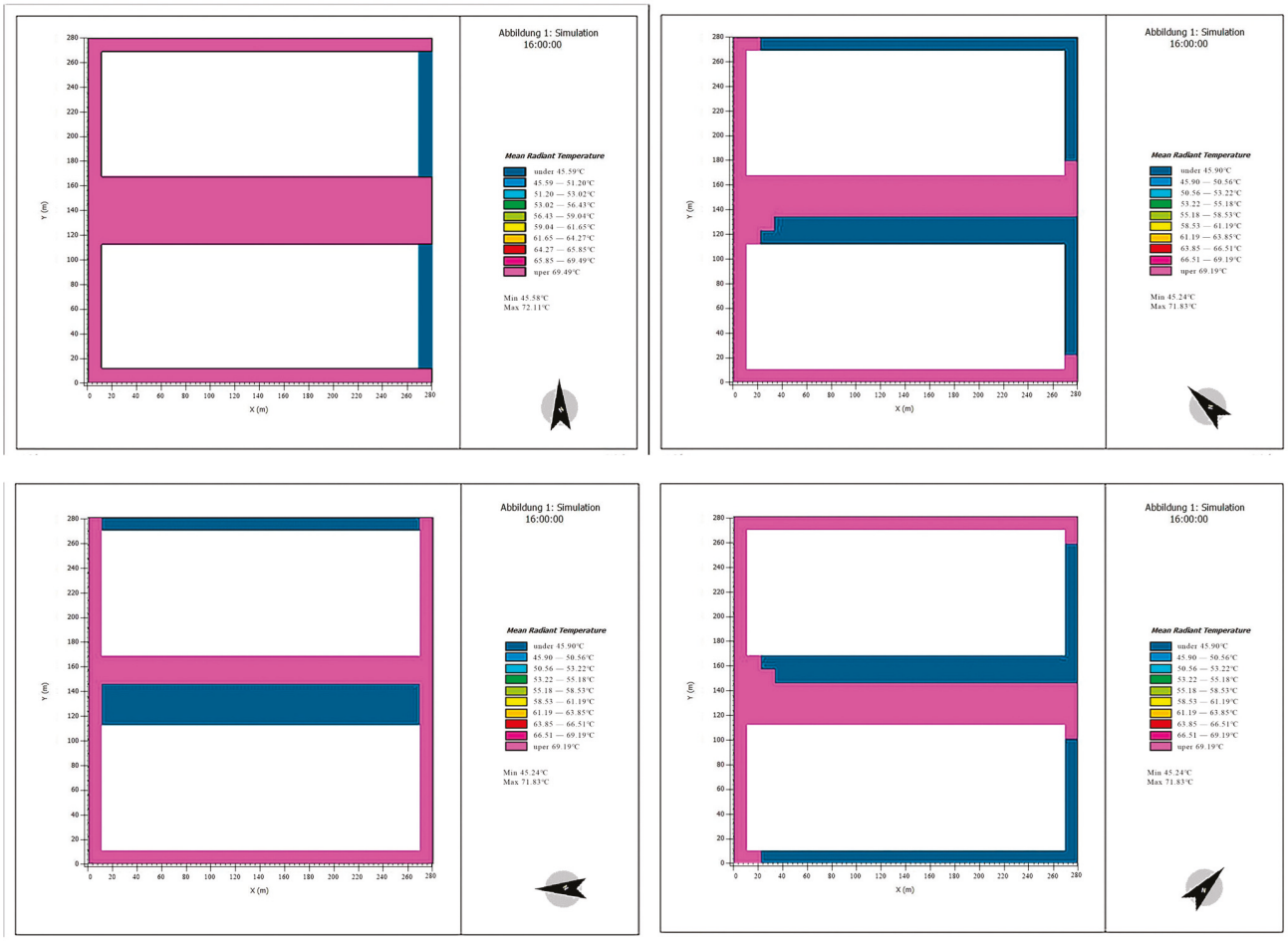


Figure 18. Prototype model 3000-30-45 MRT (°C) distribution map in outer space. (16:00, 1.2 m above ground)—drawn by the author.

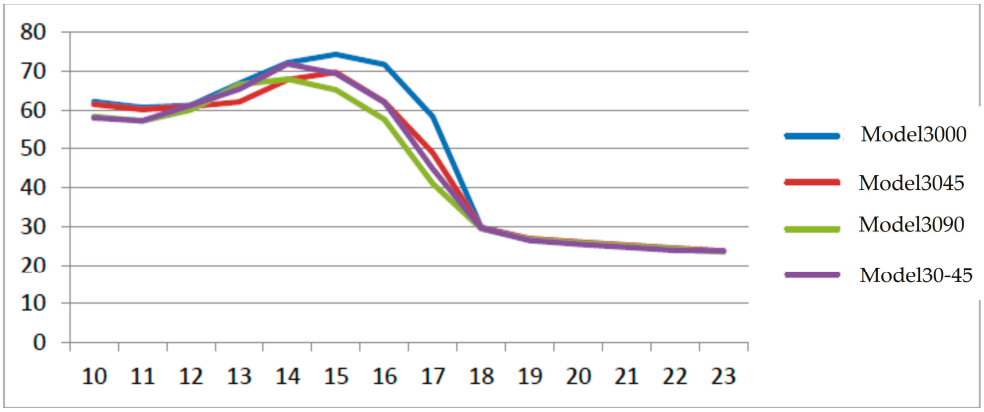


Figure 19. Numerical comparison of MRT (°C) in the outer space of prototype model 3000-30-45 (10:00–23:00, 1.2 m above ground)—drawn by the author.

4.3.2. Thermal Comfort Analysis Conclusions of Street Directions in Different External Spaces

According to the statistics of the model data, we can conclude that the outer space of the prototype model conforming to the dominant summer wind direction is related to wind speed, humidity, MRT, and PMV, but it has no significant correlation with temperature. In other words, in the outer space of the prototype model conforming to the dominant summer wind direction, humidity and wind speed increase, and MRT will decrease relatively. In general, different street directions will affect the amount of solar radiation, meaning that north–south streets experience greater thermal comfort improvements due to the increased shading from the podium in the afternoon.

4.4. Thermal Comfort Analysis After Model Optimization

Based on the three sets of numerical computer simulations from different perspectives mentioned above, it can be concluded that street density, the number of street intersections, and the direction of streets within the block all have an impact on the thermal comfort of the human body.

Based on the conclusions above, the author designs a new optimized prototype model and simulates it using numerical computer simulation, data sorting, and analysis to verify the research findings.

This optimized model is named prototype model 207, with street density, street intersection number, and street direction still serving as its shape control indices. According to the experimental conclusions in Sections 4.1–4.3 the author defines the above three quantitative indicators as follows:

(1) The street density is set to 12 km/km^2.

(2) While maintaining the street density in the external space, the street layout is adjusted to create more street intersections. The number of street intersections in this optimization model is 6.

(3) The main street layout is oriented north–south to better align with the dominant wind direction in Shanghai during the summer, thus increasing average wind speed and enhancing heat convection and diffusion. Additionally, the podium building on the west side provides shadow areas in the afternoon when solar radiation is intense, effectively reducing direct solar radiation.

After the author defined the quantitative indices, the shape of the optimized model resembled that of prototype model 204 (Figure 20), which also explains why prototype model

204 had a better thermal comfort evaluation index. After determining the quantitative indicators, its spatial morphology is shown as follows (Figure 21):

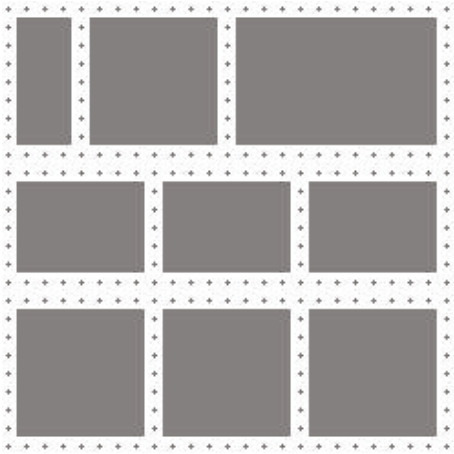


Figure 20. Prototype model 204 Schematic modeling in Envi-met—drawn by the author.

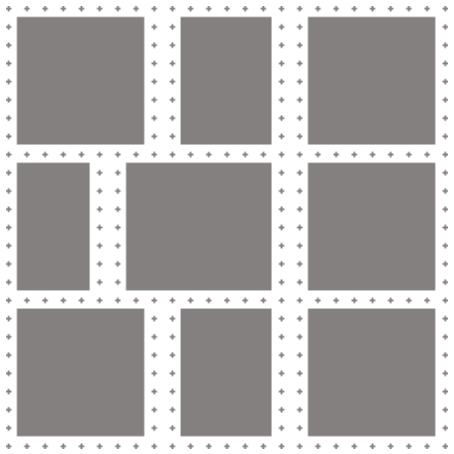


Figure 21. The optimized prototype model 207 is modeled in Envi-met—drawn by the author.

The spatial structure of this model is very similar to that of prototype model 204, but there are slight differences in terms of quantitative indicators from prototype model 204:

(1) The street density did not change and was 12 km/km^2.

(2) The number of street intersections has not changed, both being 6.

(3) The main direction of the street has been adjusted, from two east–west street spaces in prototype model 204 to two north–south street spaces.

Thermal Comfort Analysis of an Optimized Model

The same basic data for numerical simulation were used to simulate the optimized model using a computer. The emphasis was placed on sorting out the Average Radiation Temperature (MRT) index, and the data were compared with that of prototype model 204.

Figure 22 displays the mean radiant temperature (MRT) distribution of prototype model 204 and optimized model 207 at 16:00. From these two images, the MRT distribution during this time can be readily observed. The MRT distribution in the external space of optimized model 207 is noticeably larger than that of prototype model 204, with the majority concentrated in the north–south street space.

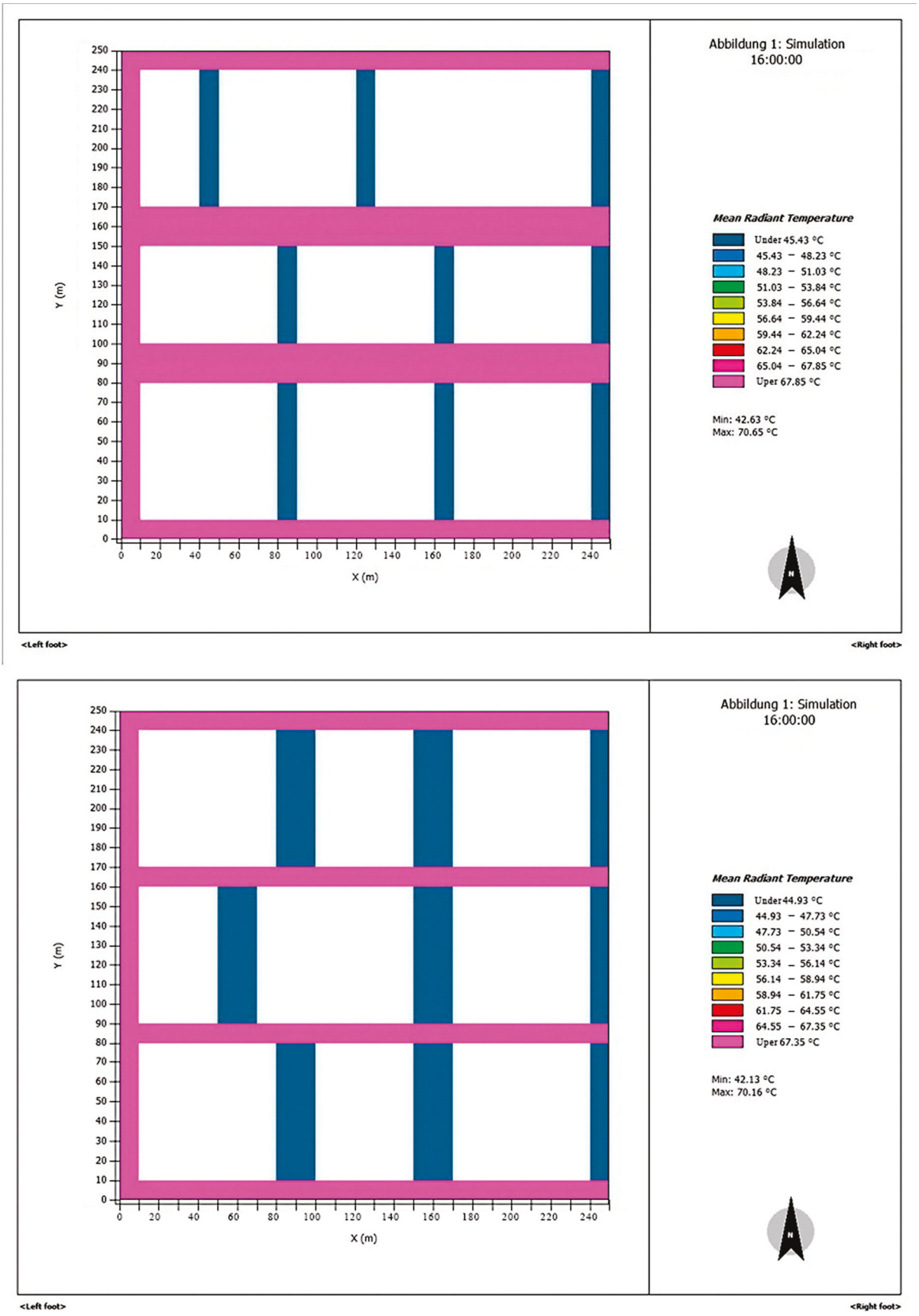


Figure 22. MRT (°C) distribution of prototype model 204 (**top**) and optimized model 207 (**bottom**). (16:00, 1.2 m above ground)—drawn by the author.

Figure 23 presents a numerical comparison of MRT values in the outer space from prototype model 101 to model 104, spanning from 10:00 to 23:00. Upon comparison, it is evident that the overall trend of MRT between the two models is similar. However, the MRT value of the optimized model 207 is significantly lower than that of the prototype model.

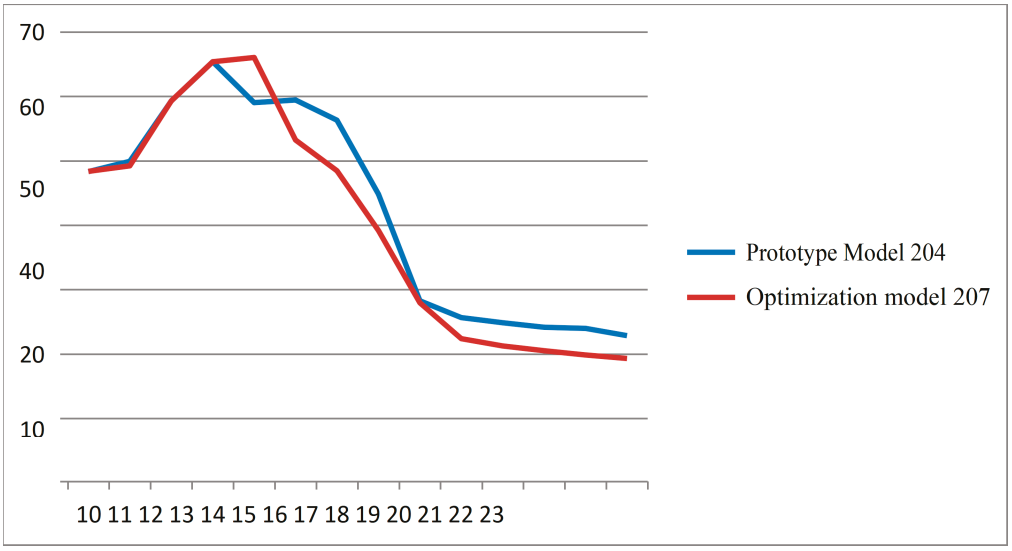


Figure 23. Comparison of external space MRT (°C) between prototype model 204 and optimized model 207—drawn by the author.

Moreover, optimized model 207 exhibits a larger shaded area in the external space, resulting in reduced solar radiation exposure and consequently a lower average radiation temperature—a factor closely linked to human thermal comfort.

In conclusion, variations in MRT are influenced not only by street density, the number of street intersections, and street orientation, but also by the amount of solar radiation received.

5. Discussion and Conclusions

5.1. Research Conclusions

5.1.1. Block Form Control Factors of Block-Style Commercial Complex

This paper compiles and organizes related concepts of streets and blocks in urban road traffic planning. It selects three control factor indicators of block shape that can be quantitatively studied: street density, number of street intersections, and street direction within blocks, as the variables for this study.

These three quantitative indicators can serve as reference points for architects and urban designers during the spatial form design stage of block-style commercial complexes, aiming to enhance human thermal comfort. They can also function as criteria for evaluating thermal comfort in existing block-style commercial complexes.

Based on the author's actual investigation and analysis of numerical computer simulation data, it is evident that these three quantitative indicators possess a certain degree of universality. They are closely intertwined with spatial form design practices within the disciplines of architecture and urban design. Moreover, these three quantitative indicators are intricately linked to human thermal comfort.

5.1.2. The External Space of a Block-Style Commercial Complex Is Based on the Design Strategy of Thermal Comfort Enhancement

Based on the numerical computer simulation and data collection presented in this paper, along with the architectural design characteristics of block-style commercial complexes, the following design strategies for improving thermal comfort can be proposed. These strategies can serve as a reference for architects and urban designers during the preliminary decision-making stage of design:

(1) The length of street spaces and street density within the block can be moderately increased to enhance the thermal comfort of the external space. The suggested street density value is 12 km/km^2. For instance, in a 250 × 250 m block plot, cutting four streets across would notably enhance the thermal comfort of its external space. Additionally, from an architectural perspective, forming a block shape similar to the nine-palace format by cutting four streets can ensure the commercial building area and maintain its commercial value.

(2) Given the predetermined street density of the external space of the block-style commercial complex, the street spaces can be appropriately repositioned to create more street intersections, thus enhancing the thermal comfort of the external space. The recommended number of street intersections is 6-8.

(3) The main street space of the block-style commercial complex should be oriented in the north–south direction. This arrangement serves two purposes: firstly, it aligns with the prevailing wind direction in Shanghai during the summer, thereby increasing the average wind speed and accelerating heat convection and diffusion. Secondly, it allows the podium on the west side of the building to create shaded areas in the afternoon when solar radiation is high and the air temperature is elevated, reducing direct solar radiation and improving the overall thermal comfort of the block space.

The synergistic effects of the three control factors (street density, intersection count, and orientation) demonstrate a non-linear enhancement pattern on thermal comfort. Specifically:

- Low-density blocks (street density <10 km/km^2) show limited improvement even with optimal orientation, indicating a threshold effect of street network complexity.
- Moderate-to-high density (12–14 km/km^2) combined with 6–8 intersections achieves peak thermal performance, with significant reductions in MRT translating to improved PET values.
- A north–south orientation enhances wind-driven cooling effects in high-density configurations, while east–west orientations increase solar radiation gains.

This trend highlights that morphological optimization requires balanced coordination between geometric parameters and climatic responsiveness, with diminishing returns observed beyond critical thresholds (e.g., street density > 15 km/km^2).

5.2. Discussion on the Shortcomings of the Research

As discussed earlier, human thermal comfort is influenced by numerous factors. This study attempts to consider air temperature, relative humidity, and average wind speed. However, from the perspective of architecture and urban design, the focus lies primarily on the block form. Factors such as underlying surface material, building interface material, vegetation planting within the block, air flow within street spaces, and particle diffusion levels can all impact human thermal comfort through radiation and convection [16]. This study solely examines the impact of the building industry on human thermal comfort

within the block without considering the combined effects of multiple factors on human thermal comfort in external spaces.

This research lays a foundation for integrating dynamic environmental factors into the design of block-style commercial complexes. Future research should prioritize the following directions to enhance practical applications of dynamic simulations:

1. Real-time monitoring and adaptive design: Integrate IoT sensors and real-time climate data with AI-driven models to dynamically optimize spatial configurations, balancing thermal comfort and energy efficiency.
2. Multi-factor synergistic analysis: Simulate interactions among vegetation, water features, building materials, and human activities, leveraging machine learning to identify synergistic cooling strategies.
3. Climate change resilience: Incorporate long-term climate projections (e.g., extreme heat, shifting wind patterns) into thermal comfort evaluations to ensure design robustness under global warming.
4. User-centric behavioral modeling: Integrate pedestrian flow dynamics and virtual reality (VR) tools to align spatial configurations with activity patterns and thermal demands.

Dynamic impact analysis will transcend static evaluations, offering actionable insights for designing adaptive, sustainable, and human-centric commercial complexes capable of maintaining comfort and functionality amid evolving climatic and usage challenges.

The data that support the findings of this study are available from the corresponding author upon reasonable request.

Author Contributions: Methodology, Y.Z. and Y.H.; Investigation, E.N.; Resources, J.Z.; Data curation, E.N.; Writing—original draft, E.N.; Writing—review & editing, Y.Z. and Y.H.; Project administration, J.Z. All authors have read and agreed to the published version of the manuscript.

Funding: This research received no external funding.

Data Availability Statement: Data are contained within the article.

Conflicts of Interest: Author Jiang Zhu was employed by the company Zhengzhou Zhengdong High tech Industrial Development Co., Ltd. The remaining authors declare that the research was conducted in the absence of any commercial or financial relationships that could be construed as a potential conflict of interest.

References

1. Ali-Toudert, F.; Ali-Toudert, F. Dependence of Outdoor Thermal Comfort on Street Design in Hot and Dry Climate. Ph.D. Thesis, Universität Freiburg, Freiburg im Breisgau, Germany, 2005.
2. Ali-Toudert, F.; Djenane, M.; Bensalem, R.; Mayer, H. Outdoor thermal comfort in the old desert city of Beni-Isguen, Algeria. *Clim. Res.* **2005**, *28*, 243–256. [CrossRef]
3. *ANSI/ASHRAE Standard 55-1992*; Thermal Environmental Conditions for Human Occupancy. ASHRAE: Peachtree Corners, GA, USA, 1992.
4. Bruse, M.; Fleer, H. Simulating surface–plant–air interactions inside urban environments with a three dimensional numerical model. *Environ. Model. Softw.* **1998**, *13*, 373–384. [CrossRef]
5. Chen, T.Y.; Huang, C.S.; Sung, W.P. Improving summer outdoor comfort in metropolitan park: A data-driven approach using AI, experimental and design analysis. *J. Meas. Eng.* **2025**, *13*, 3–7. [CrossRef]
6. Bulcao, C.F.; Frank, S.M.; Raja, S.N.; Tran, K.M.; Goldstein, D.S. Relative contribution of core and skin temperatures to thermal comfort in humans. *J. Therm. Biol.* **2000**, *25*, 147–150. [CrossRef]
7. Ding, W.; Tong, Z. An approach for simulating the street spatial patterns. *Build. Simul.* **2011**, *4*, 321–333. [CrossRef]
8. Fanger, P.O. *Thermal Comfort. Analysis and Applications in Environmental Engineering*; Danish Technical Press: Copenhagen, Denmark, 1970.

9. Hao, T.; Huang, J.; He, X.; Li, L.; Jones, P. A machine learning-enhanced design optimizer for urban cooling. *Indoor Built Environ.* **2023**, *32*, 355–374. [CrossRef]
10. Höppe, P. The physiological equivalent temperature—A universal index for the biometeorological assessment of the thermal environment. *Int. J. Biometeorol.* **1999**, *43*, 71–75. [CrossRef] [PubMed]
11. Mahgoub, M.H.; Hamza, D.N.; Dudek, D.S. Microclimatic Investigation of Two Different Urban Forms in Cairo, Egypt: Measurements and Model Simulations. In Proceedings of the Building Simulation Cairo 2013—Towards Sustainable & Green Built Environment, Cairo, Egypt, 23–24 June 2013.
12. Cuce, P.M.; Cuce, E.; Santamouris, M. Towards Sustainable and Climate-Resilient Cities: Mitigating Urban Heat Islands Through Green Infrastructure. *Sustainability* **2025**, *17*, 1303. [CrossRef]
13. Li, H.; Zhang, W.; Wang, F. Evaluation and optimization of thermal comfort in urban outdoor spaces in hot summer and cold winter climate zones: A case study of central Shanghai. *Jianzhu Kexue* **2022**, *38*, 45–54. (In Chinese)
14. Zhao, Y.; Zhao, K.; Ge, J. Predicting the temperature distribution of a non-enclosed atrium and adjacent zones based on the Block model. *Build. Environ.* **2022**, *214*, 108952. [CrossRef]
15. Meta, H. *Space, Density and Urban Form*; Technique University of Delft: Delft, The Netherlands, 2009.
16. Yuan, S. Quantitative Analysis of Urban Street Network Spatial Form. Ph.D. Thesis, Tianjin University, Tianjin, China, 2012. (In Chinese)

Disclaimer/Publisher's Note: The statements, opinions and data contained in all publications are solely those of the individual author(s) and contributor(s) and not of MDPI and/or the editor(s). MDPI and/or the editor(s) disclaim responsibility for any injury to people or property resulting from any ideas, methods, instructions or products referred to in the content.

buildings

MDPI

Review

Optimizing Energy Efficiency: Louver Systems for Sustainable Building Design

Waseem Iqbal [1], Irfan Ullah [2], Asif Hussain [3], Meeryoung Cho [4], Jongbin Park [5], Keonwoo Lee [6] and Seoyong Shin [7,*]

[1] Department of Computer Science, School of Systems and Technology, University of Management and Technology, C-II, Johar Town, Lahore 54770, Pakistan; waseem.iqbal@umt.edu.pk
[2] Hong Kong Applied Science and Technology Research Institute, 2 Science Park East Avenue, Hong Kong Science Park, Shatin, Hong Kong, China; irfan@solarlits.com
[3] Department of Electrical Engineering, School of Engineering, University of Management and Technology, C-II, Johar Town, Lahore 54770, Pakistan; asif.hussain@umt.edu.pk
[4] Digital Lighting Research Division, Korea Photonics Technology Institute, 108 Chumdanbencheo-ro, Gwangju 61007, Republic of Korea; cnscmr@kopti.re.kr
[5] Green Energy Division, KIEL Institute, 261 Doyak-ro, Bucheon 14523, Republic of Korea; koreabini@kiel.re.kr
[6] New & Renewable Energy Center, Korea Energy Agency, 323 Jongga-ro, Ulsan 44538, Republic of Korea; keonwoo@energy.or.kr
[7] Department of Information and Communication Engineering, College of ICT Convergence, Myongji University, 116 Myongji-ro, Yongin 17058, Republic of Korea
* Correspondence: sshin@mju.ac.kr

Abstract: As the global focus on sustainability intensifies, architects and engineers are increasingly seeking innovative passive strategies to improve building energy efficiency. Among these strategies, the strategic integration of louvers has garnered significant attention due to their potential to optimize building envelope performance and reduce energy consumption. Louvers effectively manage solar heat gain, mitigating the impact of extreme temperatures on indoor spaces. Consequently, louvers reduce the reliance on active HVAC systems, leading to notable energy savings and a decreased carbon footprint. This paper presents a comprehensive review of the role of louvers in enhancing building energy efficiency, highlighting their designs, efficiency, and improvement suggestions. Moreover, this review article addresses potential challenges related to louver design, such as balancing the trade-off between solar heat gain and daylighting and how to optimize louver configurations for specific building types. Approaches to overcome these challenges, including advanced modeling techniques and parametric design, are also explored to assist architects and designers in achieving the most energy-efficient outcomes.

Keywords: louvers; daylight harvesting; energy-saving; ventilation; passive cooling; energy efficiency

1. Introduction

Global energy consumption comprises a wide range of activities, including industrial processes, transportation, residential usage, buildings, and commercial sectors [1–3]. As of now, global energy consumption stands at 445 EJ, reflecting a 15% increase over the last decade [4]. With continued population growth and economic development, energy demand has steadily risen and is projected to exceed 530 EJ by 2050 [4]. Among the major consumers, the industrial, building, and transportation sectors account for the largest share of electricity usage.

According to the World Energy Outlook, the building sector consumed approximately 120 EJ of energy in 2023 [4]. Electricity demand in buildings has grown significantly from 9637 TWh (2010) to 12,594 TWh (2021) and is expected to rise to 15,850 TWh by 2050 [5]. This rise is accompanied by a 4% increase in building energy demand and a 5% rise in CO_2 emissions since 2020 [6]. Approximately 37% of global operational energy and process-related CO_2 emissions are associated with the buildings and construction industry. Historically, fossil fuels have dominated the global energy mix, accounting for 80% of energy consumption in 2023 [4]. However, efforts are underway to reduce this dependence, with projections indicating a decline to 58% by 2050 under the STEPS scenario [4]. To address environmental concerns and promote sustainability, 560 GW of renewable energy capacity was added to the global energy mix in 2023 [4]. This shift reflects a growing emphasis on incorporating renewable energy alternatives to mitigate environmental impacts and ensure long-term sustainability [7,8].

Despite these advancements, governments, households, and businesses face challenges in investing in building decarbonization due to the unpredictability of global energy prices and rising interest rates. Reports suggest that the building and construction sector is not currently on track to achieve decarbonization by 2050. However, transitioning to a low-carbon economy is essential to achieving Sustainable Development Goals (SDGs) [9]. Energy supplied by renewable sources was documented at 74 EJ in 2021 and is expected to increase to 215 EJ by 2050 [5]. Monitoring and managing global energy consumption are crucial endeavors, as they play a pivotal role in shaping the world's economic trajectory, environmental impact, and efforts to combat climate change. Sustainable practices, energy efficiency measures, and innovative technologies are essential for meeting future energy demands while minimizing adverse effects on the planet [10–12].

Energy Saving in Buildings

Energy in buildings can be optimized and saved using efficient lighting sources and appliances, onsite renewable production and use, improvements in existing building stock, and new buildings with high energy performance [13,14]. Combining renewable energy sources with energy-efficient practices is key to creating sustainable and eco-friendly buildings that meet their energy needs while minimizing environmental impact [15]. The importance of sunlight for the energy needs of a building cannot be overstated [16]. Sunlight, as a readily available and renewable energy source, plays a vital role in reducing a building's reliance on conventional power grids [17,18]. Properly harnessing sunlight through strategically placed windows and solar panels can significantly contribute to passive heating, daylighting, and natural ventilation, thereby decreasing the demand for artificial lighting and cooling systems [19,20]. As a result, different research have been carried out focusing on relevant techniques [21], encompassing blinds [22,23], louvers [24,25], awnings [26], and light shelves [27]. Among these components, louver systems find extensive application in buildings due to their unique designs, exceptional efficiency, and high-performance capabilities [28]. In [29], a louver system reduced cooling energy consumption by 27% and achieved 80% energy saving in lighting requirements. Furthermore, the energy savings were also analyzed at 30%, 50%, 70%, and 100% opening of louvers.

2. Louvers in Buildings

Some common applications of louver systems in building design and architecture include sun shading, ventilation, daylighting, heating and cooling, privacy and security, rain and weather protection, aesthetic and architectural design, noise control, mechanical equipment screening, and sustainable building design. Overall, louver systems are versatile

architectural features that serve both functional and aesthetic purposes in modern building design, contributing to energy efficiency, occupant comfort, and visual appeal. Figure 1 shows an adjustable louver to control blinds' number, angle, and width for optimizing daylight and thermal comfort under diverse climatic conditions. The parameters affected the shading density, daylight transmission deep inside the building, and structural stability of the louver [30].

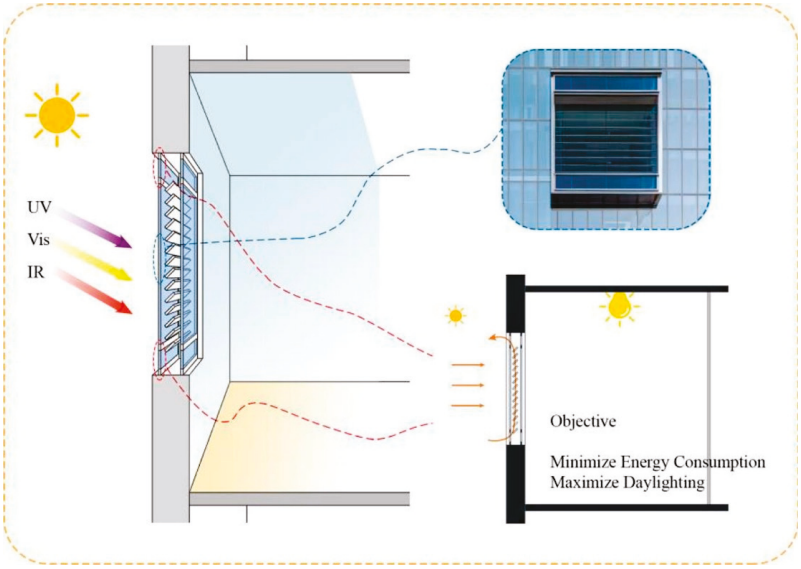


Figure 1. Showing a schematic of the center-mounted louver configuration on a window [30].

2.1. Illumination

2.1.1. Daylighting

Louver systems are designed to manage the direction, intensity, and distribution of daylight, enhancing the overall illumination while minimizing glare and heat gain. By harnessing daylight, buildings can reduce their dependence on artificial lighting during daylight hours, leading to significant energy savings and lower utility costs [31]. Incorporating louver systems for daylighting aligns with sustainable building practices, as it reduces the building's environmental footprint by decreasing energy consumption and reliance on non-renewable resources. Furthermore, by carefully positioning louvers, glare from direct sunlight can be minimized, creating a more visually comfortable and productive environment for occupants [32]. Access to natural light has also been linked to improved mood, productivity, and overall well-being of occupants. Louver systems contribute to creating a more pleasant and health-supportive indoor environment. An innovative optical louver design was proposed to achieve better daylighting that also reduced the annual electrical energy cost as compared to the conventional blinds [24]. DF, DA, and UDI are the most widely used metrics to assess the daylight in a building. DF is the ratio of illuminance available inside the building over the illuminance available outside under the sky, as mentioned in Equation (1) [33]. A DF less than 2 required artificial lighting, while values of DF between 2 and 5 did not require any artificial lighting. When the DF was greater than 5, it caused visual discomfort and temperature issues [33]. UDI is preferred over DF and DA for more clarity and climate-based modeling because it contains hourly data of sun orientation [34,35].

Based on illuminance, daylight is divided into three categories: <100 lux, 100–2000 lux, and >2000 lux. Artificial lighting is required for an illuminance range of <100 lux, while 100–2000 lux is acceptable and does not require any artificial lighting. However, the illumi-

nance >2000 lux creates thermal discomfort, necessitating cooling measures. UDI is based on an illuminance range of 100–2000 lux for the offices and buildings [34]. A computer-assisted simulation was performed by adjusting louver types and input parameters to improve DF up to 5% [33]. The results showed that daylight simulation assisted in improving the overall performance and helped to finalize the design in the early stages of building construction. Daylight simulation improved illuminance by 79.48%, 80%, and 146.26% in Sydney, Birmingham, and Jakarta, respectively [36]. Further, simulations were carried out to improve the daylight and energy savings using louver systems [37]. The simulation was carried out using Daysim and Trnsys simulation software to find out optimal angles for the louver. A unique design, split louver with parametric control, achieved illuminance of 150–700 lux in the month of June in Amman, Jordan [38]. To generate the weather data of Amman, an epw format was used with the help of Ladybug (plugin/toolkit) with Grasshopper software, and Honeybee (plugin/toolkit) was used to further connect the Daysim and Radiance software for daylighting simulations. The split louver improved illuminance in the front and back of the room compared to the conventional single louver.

Four different types of shading devices, such as venetian blinds, horizontal louvers, light shelves, and egg crates, were simulated to reduce energy consumption in South Korea [39]. The overhang-shaped louver and egg crate performed better than other shading devices to reduce cooling energy consumption by about 51% to 54%. Further, egg crate reduced the electric lighting energy consumption by 15%. An innovative kinetic louver system was used to improve daylighting and reduce energy consumption by reducing the electrical lighting consumption by about 99% compared to the ASHRAE 90.1 standard's lighting profile [40]. In [41], the author improved the indoor daylight environment using electrochromic-applied kinetic louvers where LEED v4.1 daylight option 2 criteria was achieved for visible light transmission of 40–45%. In [42], a louver-based shading system was compared by investigating length, depth, and count in three different cities in Canada. Table 1 presents a comprehensive summary of studies conducted on louver systems from 1962 to 2024, highlighting advancements in daylighting performance. It includes information on the year and country of each study, the simulation tools or experimental methods used, and the key findings related to daylighting improvements. The data covers a wide range of simulation software, such as Grasshopper, Radiance, EnergyPlus, DAYSIM, and others, as well as experimental approaches involving physical prototypes and algorithms. Key observations include enhancements in daylighting metrics such as UDI, daylight factors, visual comfort, energy savings, and innovative louver designs, demonstrating their potential for improving indoor lighting and energy efficiency in diverse climatic and geographical contexts. Figure 2 illustrates reflective slats that adapt to the sun's position throughout the day and year. The automated louver was simulated to determine the parameters for slat rotation and a full-system rotation [43].

$$DF = \frac{Inside\ illuminance}{Outside\ illuminance} \times 100 \quad (1)$$

Table 1. Summary of louver system studies: year, country, tools/methods, and key daylighting observations.

Year	Country	Simulation Tools	Experiment	Improvements (%)	Key Findings
1962 [44]	USA	Mathematical model	×	-	• Achieved a 50% light transmittance for north-facing and south-facing orientations • Observed a low transmittance of 10% for east-facing buildings, which was unsatisfactory

Table 1. *Cont.*

Year	Country	Simulation Tools	Experiment	Improvements (%)	Key Findings
2015 [45]	USA	Hybrid ray tracing	✓	-	• Analyzed daylight glare probability and illuminance • Used HDR cameras and calibrated photometers alongside simulations for data collection • Glare equation could lead to inaccuracies in extreme brightness conditions, requiring adjustments
2016 [33]	Korea	Grasshopper, Rhinoceros, DIVA, NURBS	×	5 (DF)	• Improved performance incorporating genetic algorithm-based input parameters • Galapagos optimization is less optimal for small datasets
2017 [46]	UK	Grasshopper, Radiance, DAYSIM, EnergyPlus,	×	80 (Daylighting)	• Compared the daylighting performance of parametric and conventional systems • Limited energy savings in winter due to weak radiations
2017 [37]	Spain	SketchUp, DAYSIM, TRNSYS	×	40 (UDI)	• Reduced high solar gain for the south-oriented building • Achieved UDI improvements at angles of $-30°$and $30°$
2017 [47]	USA	Radiance, EnergyPlus	×	43 (Daylighting)	• Used synthetic and measured data to save lighting load • Achieved optimum improvements at vertical angles of incidence from $18°$ to $35°$ • Micro-structured prismatic louvers caused glare for seated positions looking directly at the window
2018 [48]	Chile, Canada, China, USA	Radiance, EnergyPlus SketchUp, Groundhog, WINDOW	×	63 (Daylighting)	• Improved energy saving by optimizing louver spacing • High perforation rates caused glare in some locations • Simulations were carried out in specific office locations; performance could vary in different climate conditions
2020 [49]	Israel	Radiance, DAYSIM, Rhinoceros, Grasshopper,	×	51 (UDI)	• Dynamic louver design increased illuminance compared to static louver • Limited performance on specific window orientations and is influenced by seasonal variations
2020 [50]	Poland	De Luminae, SketchUp	×	-	• Improved daylighting in a fully glazed south-oriented façade located at $51°$ • The impact of shading on thermal comfort, cooling, and heating loads was not discussed
2020 [51]	Taiwan	EnergyPlus	×	-	• Achieved better daylighting using roller shades • Tested for south and west façade orientations, limiting their applicability in other orientations

Table 1. *Cont.*

Year	Country	Simulation Tools	Experiment	Improvements (%)	Key Findings
2020 [52]	USA	EnergyPlus	×	-	• Improved daylighting using kinetic control strategy and multi-objective optimization technique • In some cases, static louvers performed better compared to dynamic louvers, highlighting the need for context-specific optimization
2020 [53]	Indonesia	Radiance, DAYSIM, Rhinoceros, Grasshopper	×	-	• Thermal comfort should also be analyzed in addition to visual comfort for better adaptability • Tested in tropical climate, findings may not be directly applicable to buildings in colder or temperate climates
2020 [54]	Egypt	Radiance, DAYSIM, Rhinoceros, Grasshopper	×	90 (Daylighting)	• Reflective slats improved floor illuminance to 300–500 lux • Only tested for south-oriented office and hot arid climate, limiting its applicability
2021 [55]	UK	Radiance, Rhinoceros, Grasshopper, Ladybug, Honeybee	✓	-	• Integrated simulations, Arduino, motors, and illuminance sensors, with prototypes tested at 1:20 and 1:1 scales, but under controlled conditions • If sensors are miscalibrated or if there is error in the input data, the louver adjustments may not perform as expected
2021 [56]	Indonesia	EnergyPlus, Rhinoceros, Grasshopper, LadyBug, Honeybee	×	16.78 (UDI)	• L-shaped mini louvers improved UDI levels compared to overhangs • These louvers can be easily retrofitted into both new and existing buildings, requiring minimal maintenance • L-shaped aluminum louvers are lightweight, inexpensive, and widely available
2022 [36]	Australia, the UK, and Indonesia	EnergyPlus, Radiance	×	79, 80, 146	• Analyzed the effect of louver spacing and blade size using the MOO technique • Daylighting improvements were a tradeoff between cooling energy reduction, requiring careful balancing.
2022 [38]	Jordan	Grasshopper, Radiance, DAYSIM, EnergyPlus, Ladybug, Honeybee	×	-	• Achieved illuminance of 150–750 lux using split louver with parametric control • Maintained a glare-free ambiance
2022 [57]	Jordan	Grasshopper, Ladybug, and Honeybee	×	50	• Achieved a daylight uniformity of 0.6 • Achieved UDI for 50% of the floor area in office hours • Achieved UDI for 90% of the floor area at noon only
2022 [41]	Korea	Rhino 6′s, Grasshopper, Radiance	×	75 (UDI)	• Achieved UDI improvements using an electrochromic louver system • Dependent on a mixed-humid climate and a visible light transmittance range of 20−70%, limiting the system's practicality

Table 1. *Cont.*

Year	Country	Simulation Tools	Experiment	Improvements (%)	Key Findings
2022 [58]	China	Radiance, EnergyPlus	×	23 (UDI)	• Achieved 23% and 68% improvements in UDI level and glare discomfort in comparison with double glazing • Achieved a 29% improvement in UDI compared to the metal louvers
2023 [59]	China	Ladybug and Honeybee	×	2.5 (UDI)	• Tested on a west-facing school building in cold and severe cold regions • Egg crate louvers were most effective in Beijing and Lanzhou, while horizontal louvers performed best in Urumqi
2023 [60]	Indonesia	Ant Colony Optimization (ACO) algorithm	×	-	• Achieved better indoor lighting by maintaining a distance of 0–18 cm between the window and louvers • Conducted sensitivity tests on five design parameters: reflection coefficient, distance, depth, rotation angle, and number of louvers to improve daylighting
2023 [61]	Jordan	Grasshopper, Rhino, Radiance, Daysim, EnergyPlus	×	90 (UDI)	• Achieved a desirable UDI level at 90% of the workplace • Achieved illuminance uniformity of 0.7 using PV-integrated split louvers
2023 [62]	USA	DIVA, Grasshopper	×	14 (Daylight)	• Designed a dynamic louver system for high-rise buildings • Analyzed the system based on solar irradiance and daylighting as performance metrics
2024 [29]	South Korea	DIALUX evo, Rhinoceros	×	80 (Daylight)	• Improvements in daylighting and visual comfort. • Reduced cooling energy consumption of 27% at 50% louvers opening
2024 [63]	China	EnergyPlus, Radiance, Grasshopper, Rhinoceros	×	97 (UDI)	• Achieved uniformity level of 0.6 • Achieved a UDI level of 97% by optimizing slat angle
2024 [64]	USA	EnergyPlus, Rhino	×	-	• Achieved desirable illuminance level using PV-integrated louver system • Illuminance level, DA, and visual comfort were used as performance metrics to improve illuminance
2024 [65]	Japan	-	✓	-	• Control heat gain using slat angles • Minor discrepancy in minute-by-minute predictions, especially when louvers open after a temperature drop
2024 [40]	Denmark	Rhinoceros, Honeybee, Grasshopper, and Ladybug	×	99 (Daylighting)	• Improve daylighting for South, East, and West orientations using kinetic louvers • Reduction in electrical lighting energy usage from 14.22 to 0.2 kWh/m^2 per year for south-facing

Table 1. *Cont.*

Year	Country	Simulation Tools	Experiment	Improvements (%)	Key Findings
2024 [66]	USA	Rhinoceros, Honeybee, Grasshopper, and Ladybug	×	75 (daylighting)	• Enhance energy performance, particularly daylighting using prismatic-vertical louvers • It caused overlit conditions near windows during some times of the year
2024 [67]	South Korea	Designbuilder, Revit and Twinmotion	✓	64	• Achieved daylighting and electrical power generation efficiency of 64% using a PV-integrated automatic louver system • Daylighting improvements caused a 6% increase in cooling loads

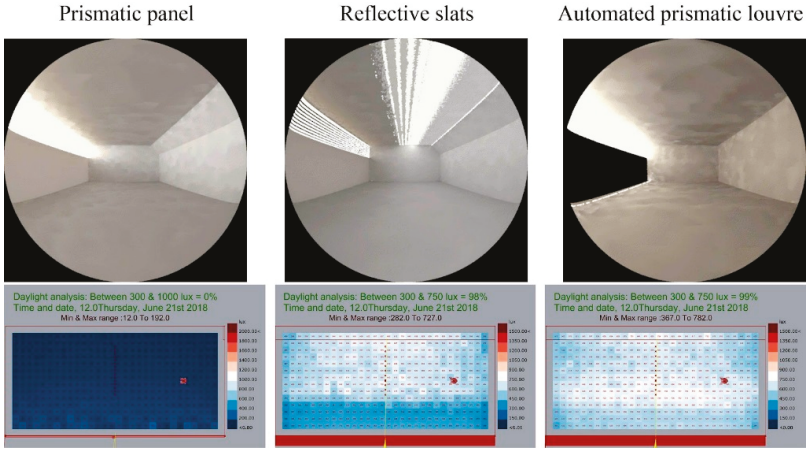


Figure 2. Radiance maps illustrate daylight distribution for the prismatic panel, reflective slats, and automated prismatic louver, generated through daylight analysis [43].

2.1.2. Hybrid Lighting

Louver systems have been integrated with other daylight harvesting technologies, such as sensors and automated controls, to optimize the use of natural light throughout the day. These systems may adjust the angle of the louvers based on the position of the sun, time of day, and interior lighting needs. A sensor-based innovative design was proposed to improve the indoor light uniformity and energy savings (e.g., daylighting, heating, and cooling) up to 13.9% and 49.7%, respectively [28]. In New Cairo, prismatic panels and automated louvers were used to improve the daylight and visual comfort indoors [43]. The sunlight was reflected by prismatic louvers towards the ceiling and then redirected towards the floor to improve light distribution and comfort. The proposed system was tested using Grasshopper, Radiance software with the help of the Ladybug and Honeybee toolkit. An experiment was conducted using louvers integrated with LED dimming control in Jincheon-gun, Chungcheongbuk-do, Korea, to save lighting energy consumption of 85% [68]. In this experiment, concentrated louvers were used, which reflected the light towards the indoor setup with a reflectance of 90%. A sensor-based setup was used to dim the LED light intensity, which maintained 300 lux only instead of a constant lighting approach. In [69], a sensor-based horizontal louver system was designed to improve daylighting and energy savings for museum space in Poland. Figure 3 shows an experimental study on indoor illuminance and lighting energy-saving for a south-facing window with horizontal fixed louvers. Louvers with high reflective material having a reflectance of over 90% at an angle of 60° were tested [68].



(**a**) (**b**) (**c**)

Figure 3. Louvers-based external experimental setup: (**a**) external view, (**b**) internal view, (**c**) illuminance sensor [68].

2.2. Heating and Cooling

Energy consumption (e.g., heating, cooling, and lighting) and discomfort hours are quite important for the HVAC systems and optimized windows in high-rise buildings [70,71]. Excessive daylight can lead to higher indoor temperatures [72,73], which in turn increases the cooling load on air conditioning systems and results in elevated energy consumption and potentially higher utility bills. Furthermore, excessive daylight can create glare issues, making it uncomfortable for occupants and potentially hindering their productivity [74]. Louvers are strategically positioned to block or allow sunlight into a building [75]. During hot summer days, angled louvers can block direct sunlight from entering, reducing solar heat gain, and helping to keep the interior cooler [76]. In the winter, properly oriented louvers can allow sunlight to enter and contribute to passive solar heating, reducing the need for artificial heating.

A study was conducted in Sydney, Jakarta, and Birmingham, which showed the improvements in cooling energy consumption of 2.99%, 3.26%, and 28%, respectively, using the MOO technique [36]. The results showed that cooling energy consumption varies with the climate and energy requirements of a building. A louver-based system was proposed to find out the optimal angle, which saved the cooling demand of 68% [37]. The proposed system showed better improvements in cooling energy consumption at the north and south orientations at louvers angles of 60° and −60°, respectively. However, the system showed poor results for daylighting that increased the electrical load. Furthermore, the system achieved an equilibrium for the visual comfort, daylighting, and cooling demand at an angle of 30° and −30°. In Canada [42], a study was conducted to optimize and compare the performance of louver systems by changing the depth, count, and angles of the louver slats. Louvers were optimized by changing their angle to minimize the thermal energy consumption for different Korean regions [77]. In Australia, a case study was conducted, which saved building energy up to 38 MWh/annum with the help of open louvers [78]. A novel louver-based design was proposed to improve energy efficiency and thermal performance by analyzing different fin configurations with varying redirection louvers in domestic and transport air conditioning applications [79]. In [80], the TRNSYS and MATLAB-based simulation results showed solar heat gain of 17.7% in winter, which also saved 33.8% heating energy. A survey [81] is also conducted by the scholar of Greece to provide a review based on passive cooling strategies for the building envelopes. The authors concluded that mechanical ventilation systems with better heat recovery, cool-colored material, and green facades improved thermal performance and visual comfort. Furthermore, such cooling strategies could reduce urban heat by lowering peak temperatures. In Malaysia, a recent study focused on energy and thermal performance achieved superior results, with significant reductions in energy consumption and cooling load, alongside improved daylighting

distribution and thermal comfort [82]. Table 2 showcases a variety of studies that employed simulation tools such as TRNSYS, IES-VR, RADIANCE, DAYSIM, and SketchUp to assess how louver systems influence energy performance. The findings from these studies indicate energy savings ranging from 17.7% to 80%, influenced by factors such as the building's orientation and design features. These outcomes underscore the significant role shading devices play in enhancing thermal efficiency and lowering energy usage. Figure 4 shows horizontal and vertical louvers for a double-skin façade office building. The horizontal and vertical blades were placed near the outer layer at right angles and 45 degrees, respectively, for better performance [83].

Table 2. Presenting Global studies on heating and cooling improvements using louvers: simulation tools, experimental methods, and key findings.

Year	Country	Simulation Tools	Experiment	Energy Savings	Key Findings
2001 [84]	Italy	TRNSYS	×	-	• Evaluated the effect of fixed horizontal louvers on south-facing windows in summer • Analyzed the reduction in cooling load and overall annual energy consumption • Need to incorporate dynamic control strategies and other louver designs to compare results for better generalizability
2010 [85]	UAE	IES-VR	×	28.57, 30.31, and 34.02, respectively	• Analyzed key variables included slat tilt angles, shading coefficients, and the location of light dimming sensors. • Attained energy savings for the E, W, and S orientations showed varying percentages, respectively • No analysis shown for cooler climates, where heating is required
2017 [46]	UK	RADIANC, DAYSIM	×	80	• The automatically-controlled louver system performed better in S and S-W orientation • The system's reliance on direct sunlight limits its effectiveness in regions with low winter solar radiation
2017 [37]	Spain	SketchUp, DAYSIM, and TRNSYS	×	68	• Recommended horizontal louvers for southwest facades and vertical louvers for east-facing facades • Improved cooling but drastically reduced daylight exposure under certain conditions
2018 [48]	Chile, Canada, China, USA	Radiance, EnergyPlus SketchUp, Groundhog, WINDOW	×	63	• Improved energy savings at 120 mm louver spacing • Energy savings were decreased by increasing the louver spacing • Observed a trade-off between cooling efficiency and visual comfort
2020 [86]	Japan	CFD	✓	-	• Louvers and windows are spaced at 1–2.8 m apart • Experimental and simulation results were compared, revealing a temperature difference of less than 1° • Assumptions of fully open windows and simulations in a humid subtropical climate (Kumagaya), limiting its adaptability

Table 2. *Cont.*

Year	Country	Simulation Tools	Experiment	Energy Savings	Key Findings
2020 [52]	USA	EnergyPlus	×	-	• Proposed multi-objective optimization technique for climate adaptive buildings • Reduction in cooling load using radiation parameters • No simulations were conducted for cold or mixed climates, which limits its generalizability
2021 [56]	Indonesia	EnergyPlus, Rhino, Grasshopper, LadyBug,	×	18	• Reduction in cooling load using L-shaped mini louvers for different orientations (E, W, N, S) • Tested only for cooling needs in Jakarta's tropical climate, limiting its applicability to heating demand and other climates
2023 [80]	China	TRNSYS, MATLAB	×	33.8	• Reduced heating energy consumptions by high solar heat gain • The system's performance is limited to winter conditions and heating energy only
2023 [59]	China	Ladybug	×	2.5	• Enhancement in thermal comfort using an external louver-based system for a west facing building setup • Findings are based on non-air-conditioned buildings only; no analysis was conducted for HVAC setup.
2023 [87]	China	CFD	×	-	• Analyzed heat transfer pattern using vertical louver only, limiting its performance for other designs • Optimized heat coefficients with the help of louver's angle and width • Used Wind Velocity (U_{10}) standard, real time wind speed and direction could vary, affecting the result
2023 [88]	China	Numerical Analysis	×	-	• Optimized thermal performance and airflow by varying the louver's inclination angle • Achieved optimal performance at louvers angle of 90°
2023 [89]	Indonesia	THERB	×	23	• Improved annual energy savings and indoor temperature by optimizing louver's area and insulation • Combined solution performed better to reduce cooling demand
2023 [60]	Indonesia	Ant Colony Optimization (ACO) algorithm	×	-	• Proposed an Ant Colony Optimization algorithm to improve energy consumption in buildings • Achieved energy savings in daylighting, heating, and cooling • Limited to Jakarta, Indonesia only, results could vary in dynamic weather variations and unforeseen building behaviors
2023 [90]	China	CFD	×	-	• Fast prediction of glazing temperature • Cavity heat transfer contributes 58−62% of solar heat

Table 2. *Cont.*

Year	Country	Simulation Tools	Experiment	Energy Savings	Key Findings
2023 [91]	China	Rhino, Grasshopper, Ladybug, and Honeybee plug-ins	×	35	• Fulfilled the energy demand of 46% by PV integration • Reduced cooling load and thermal discomfort hours by 35% and 404, respectively
2024 [29]	South Korea	DIALUX evo and Rhino	×	27	• Achieved 27.02% total energy savings at 50% opening • Higher louver openings improved the cooling, but modest overall savings
2024 [92]	Portugal	SEnergEd	×	-	• HVAC energy use varies by building type and climate. • Recommended T_{air} optimization strategy for cooling • Recommended PMV setpoints optimization for heating
2024 [93]	Japan	-	✓	9.3	• Horizontal louvers achieved better energy savings compared to vertical louvers • Adjustable PV-integrated louvers improved electricity generation
2024 [94]	China	CFD, COMSOL	×	-	• Compared the performance of louvers and circular hole covers to improve cooling • Optimized louver angle and cover distance to reduce energy consumptions
2024 [64]	USA	Rhino	×	-	• Reduction in energy consumption in warm climates • Maintained proper lighting levels using PV louvers
2024 [82]	Malaysia	Rhino, Grasshopper, Ladybug, Honeybee, and genetic algorithm	×	26.2	• Reduced cooling load using dynamic louvers integrated with a double-glazed façade • Reduced thermal dissatisfaction by 28.72% • Heating analysis is not conducted
2024 [67]	South Korea	Designbuilder, Revit, and Twinmotion	✓	64	• Achieved accumulative electricity generation of 64% using PV-integrated louvers • The system reduced heating energy, while daylighting louvers increased cooling loads by up to 6%

2.3. Ventilation

Louvers are adjusted to allow or restrict airflow into a building. During hot weather, opening the louvers allows fresh air to enter and promotes natural ventilation, helping to cool down the interior without relying solely on air-conditioning systems. In colder weather, louvers can be closed or adjusted to reduce heat loss, thus improving energy efficiency. A wind-tunnel test was conducted in a factor building to assess ventilation [95]. In [96], soffit louvers were used to stop the intrusion of wind-driven force in hip and gable roof buildings. The University of Southampton has conducted an experiment for cross-ventilation, which examined various louver openings, including the center, lower, and upper sections, and compared scenarios with and without louvers. Results indicated

that the highest flow rate occurred at the upper part of the façade, while the maximum air exchange efficiency (AEE) of 45% was achieved with the louvers opened at the center [97]. The natural airflow was increased, and simulations were conducted to analyze the louver system using CFD techniques [83]. Horizontal louvers showed better results and were preferred over the vertical louvers.

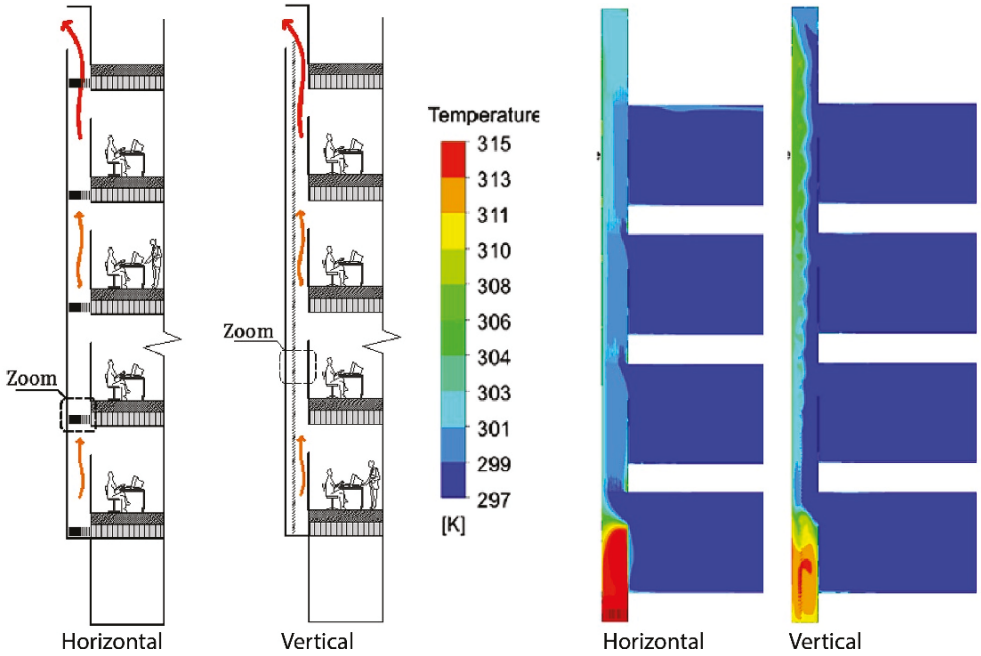


Figure 4. Illustrating a double skin façade with horizontal and vertical louvers and showing temperature contours of the office building [83].

In one study, [98], a windcatcher-louver system was designed to improve natural ventilation. The highest wind speed was achieved to optimize the angle of attack (8°) of the airfoil. The natural airflow increased up to 14% by optimizing the louver's angle at 45° [99]. A case study has shown improvements in heating energy only. On the other hand, airflow and ventilation reduce infection using semi-shaded openings along with external louvers, resulting in an infection rate of 26.17% [100]. A recent study was conducted in Portugal to assess the HVAC energy needs using SEnergEd software for the residential and commercial buildings [92]. The energy demands of cooling and heating were observed with the different climate changes. Various studies have explored ventilation performance using a mix of experimental setups and simulation tools as shown in Table 3. Different simulation methods included software such as TRNSYS, CFD with advanced turbulence models (e.g., RNG, SST, RSM), and Star-CCM+, as well as virtual assistants such as Google Assistant. Experimental approaches involved wind-tunnel tests, rain impact studies, and practical investigations conducted at institutions such as the University of Southampton. Figure 5 shows the geometry of the louver and boundary conditions around the building to perform velocity and heat transfer simulation on the building façade and louver surfaces [71].

Table 3. Summary of Global Investigations on Ventilation Improvements Using Software and Hardware Configurations.

Year	Country	Simulation Tools	Experiment	Improvements (%)	Key Findings
2005 [101]	Italy	TRNSYS, LOOPDA	×	8	• Utilized the stack effect for ventilation to prevent overheating, particularly in summer • Reduced cooling energy demand by 8% through nighttime ventilation • Tested in a Mediterranean climate (Cavaso del Tomba, Italy), limiting the findings of the double-skin façade system, which may vary in hotter or colder climates
2008 [95]	Republic of Korea	×	✓	-	• Improved ventilation by setting the outer louver at 90° and the inner louver angle at −70° • Real time factors such as wind direction, velocity, and outdoor conditions vary dynamically and were not fully analyzed in the wind tunnel test
2017 [96]	USA	×	✓	-	• Used Soffit louvers for hip and gable roof buildings • Closed vents affected the net mean and peak pressure coefficients
2019 [97]	England	CFD, RANS turbulence models; RNG, SST, RSM	✓	45	• Achieved higher volume flow rate with the louver openings at the upper side • Obtained AEE of 45% with the louver openings at the center • Valid for isothermal conditions only, and the impact of heat or temperature-driven ventilation was not addressed
2020 [83]	Iran	CFD, Google Assistant, Amazon Alexa, or Apple Siri	×	-	• Natural air flow and ventilation increased in a five-story office building • Horizontal louvers showed better results compared to vertical louvers
2020 [98]	Korea	CFD, Star-CCM+	×	-	• Achieved the highest wind speed at an 8° angle of attack using windcatcher-louvers • Enhanced indoor air quality by reducing the fine particle concentration by 37.5% • Limited wind directions (0° and 90°)
2020 [102]	Jordan	CFD	×	96.6	• Ventilation system met the standard (CO concentration < 50 ppm, ACH > 2.7) • IAQ results showed a maximum deviation of 1.5 ppm, with an error of 3.4%
2021 [99]	Australia	CFD	×	14	• Airflow increased around 14% at a louver angle of 45° • Focused on solar altitude angles, while other factors such as wind direction, building orientation, and internal thermal loads were not considered
2022 [100]	China	CFD	×	-	• Improvements in energy saving for heating only • Louvers showed a decrease in airflow and ventilation • Increased infection risk by 26.17% due to shading

Table 3. *Cont.*

Year	Country	Simulation Tools	Experiment	Improvements (%)	Key Findings
2022 [103]	China	CFD	✓	-	• Enhanced the indoor air quality by fully opening slats • Windward louvers preferred over leeward ones
2022 [104]	Malaysia	CFD	×	53.4	• Optimization of louver angle and position for ventilation • Achieved a high AEE of 53.4% at a louver angle of 15° • Achieved a low AEE of 20% at a louver angle of 0°
2023 [88]	China	Numerical Analysis	×	6.25	• Achieved ventilation rate from −16.45% to 6.25%. • Showed better improvements at a louver angle of 90°
2023 [90]	China	CFD	✓	-	• Fast prediction of ventilation and heat • The proposed theoretical model could replace time-consuming simulations
2023 [105]	Iran	Simulation	×	-	• Vertical louvers showed maximum AEE at low wind speeds (1 m/s), and louver angle of 15° • Horizontal louvers showed maximum AEE at higher wind speeds (2–3 m/s), and louvers had an angle of 15°
2024 [106]	USA	Large Eddy	✓	-	• Cut paper (kirigami) design was preferred for adaptive ventilation, offering an alternative to traditional louvers • Idealized box models and controlled wind tunnels may not capture the full range of variable outdoor conditions, limiting their scope and adaptability
2024 [92]	Portugal	SEnergEd	×	-	• Showed improvements in ventilation and thermal energy • PMV and T_{air} set points affected the ventilation efficiency • Mediterranean climate zones may not be directly applicable to regions with extreme climates (either very hot or cold)

2.4. PV Integrated Louvers

For PV-based renewable energy systems, PV [107], floating PV [108], CPV [109,110], and CSP [111] are widely used to meet energy needs. PV integrated louver systems combine two important functions in building design: PV electricity generation and sun-shading through louver structures [112]. These innovative systems offer a dual-purpose solution that maximizes the benefits of solar energy while enhancing the building's energy efficiency and occupant comfort [113]. PV integrated louver systems incorporate solar panels into the design of louver structures. These solar panels capture sunlight and convert it into electricity, which is used to power the building's electrical systems, reducing reliance on conventional grid power and lowering utility costs.

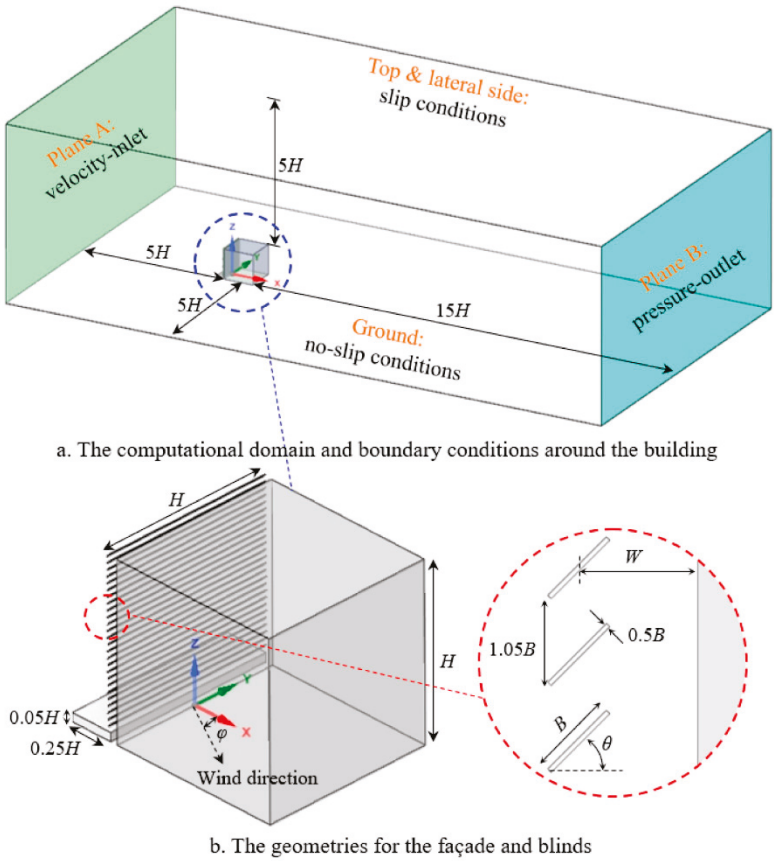


Figure 5. Showing boundary conditions, louvers geometry, wind direction, and slip conditions to optimize the airflow [71].

The PV-integrated louver system helped with electricity production, passive cooling, and lowering carbon footprints [114,115]. To predict PV output, work plane illuminance, and daylight glare index, an ANN model was used to save energy up to 1.88 kWh. Further, a case study using a naturally ventilated double PV window was conducted in China, which generated 18,917 kWh of electricity [116]. A sun-tracked PV-integrated shading design was presented, which achieved 50% more electricity generation in comparison with the static PV-integrated building envelope [117]. However, it also provided 115% of the energy demand in temperate and arid climates for an office room. A PV-louvered window design [118] was proposed, which enhanced the daylight time up to 85%. Further, it also increased the electricity revenue due to the production of electrical energy using sunlight. A novel PV-integrated double-glazed façade system [119] was tested that saved 25% of energy. In [93], a PV-integrated horizontal louver system has shown an improvement of 9.3%, while vertical louvers were less effective by producing only 7.3% of electrical energy. Seventeen various sites in the USA were analyzed using PV-integrated building envelopes to predict the illuminance and heating and cooling load. The proposed design saved energy, which was a sustainable building strategy for a south-facing building envelope [64]. Recent research [120] added a value to existing literature, which proposed a design to maximize the energy generation on a building façade using PV panels. In [61], the transparent PV-integrated louver system was used to improve daylighting by testing PV glass transmittances of 30%, 50%, and 70%. To reduce daylight glare, PV glass transmittances of 30% and 50% were used. Furthermore, a semi-transparent PV window was used to optimize the energy consumption and thermal comfort hours [121], which showed improvements of 65.7% and 5%, respectively. In one study, [67], a servo motor-based control strategy was

used to optimize the performance of a PV integrated louver system, which showed 65% power generation performance. The proposed study suggested 2-axis and 3-axis louver systems to enhance the louver's performance. A case study conducted in Zhengzhou, China, demonstrated a 35% reduction in cooling load and energy generation, meeting 46% of the total energy requirements of the test room [91]. The integration of PV louvers in buildings has significantly demonstrated energy saving as well as energy generation by optimizing indoor illumination and ventilation. Figure 6 shows three different types of PV-based façade shading systems. Maximum array power per module was calculated to compare the performance of each shading system. A horizontal louver system having a vertical cell orientation produced higher power. For the vertical louver system, the horizontal cell gave higher power. For the diamond pattern louver system, the -45° cell produced higher power than other orientations [122].

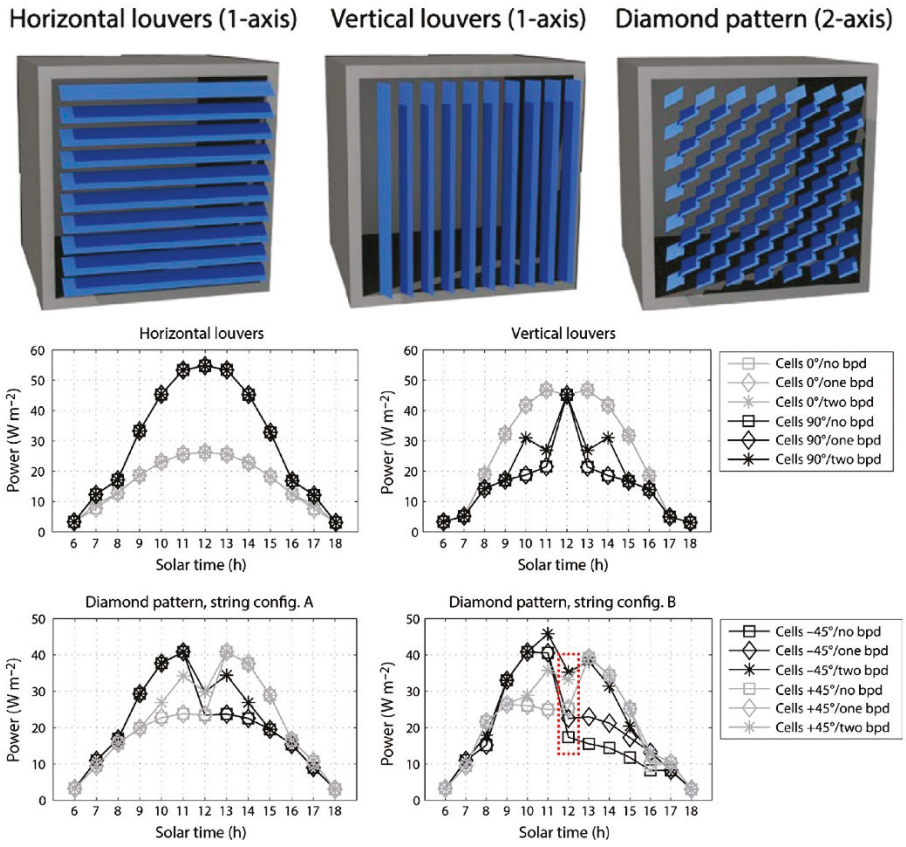


Figure 6. Different PV-integrated louver configurations for optimizing solar energy output [122].

3. Louver Designs

A louver system consists of adjustable slats, allowing for precise control over the amount of sunlight entering the building. This system enables occupants to optimize natural lighting while preventing excessive heat gain during hot periods, promoting a more energy-efficient and comfortable indoor environment. By integrating sunlight and a louver system, buildings can enhance their sustainability, reduce energy consumption, and contribute positively to the overall green building movement. Louver systems can add an aesthetic touch to building facades while serving a functional purpose. The patterns created by louver arrangements can be architecturally pleasing, enhancing the overall design. There are different classifications of louver systems based on shapes, angles, and objectives [28,33,123]. Figure 7 illustrates four different shading devices_ horizontal louvers,

vertical louvers, egg crate shading, and baffle shading_ to study thermal comfort in the interior. The design variables for each louver system were parameterized through the Grasshopper software. The study concluded that fixed louvers significantly performed well for both thermal comfort and daylighting [59].

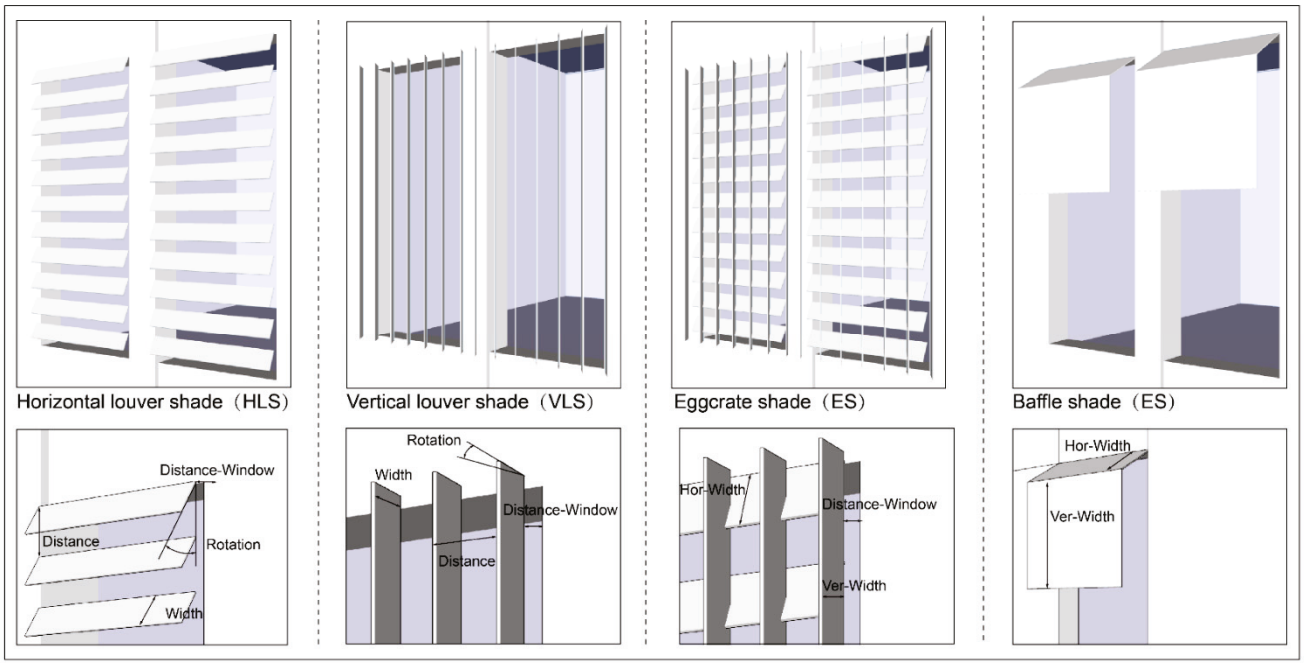


Figure 7. Different louver designs to optimize the daylighting, ventilation, heating, and cooling [59].

3.1. Vertical Louver

The vertical louver systems consist of vertical slats without any snow load. However, the view is not much clearer as compared to the horizontal louver systems. They have been classified as vertical fin and overhanging vertical fins. Table 4 outlines how different countries have applied vertical louver systems to improve building performance. In the USA [44], louvers with transmittance higher than 50% were used effectively, while orientations facing east or west showed less than 10% transmittance, which is not ideal for window installation. In Jordan [124], horizontal and vertical louvers were tested at an angle of 0° and 45°, and vertical louvers were preferred over horizontal ones for south-facing buildings. In Portugal [125], a case study was conducted to explore the impact of slat angles (10–90°) on energy savings in various regions. The UAE favored dynamic louvers at a wide range of angles, as opposed to static ones. In the UK [46], parametric control was the choice for improving daylight in office spaces. In [37], louvers were adjusted to a length of 1 m and a spacing of 0.5 m. Louver angles of 60° and −60° achieved better reductions in cooling energy demand facing north- and south, respectively, but enhanced the use of electrical lighting energy due to poor daylight at these specific orientations. A study in Israel [49] achieved the highest UDI levels with fixed, movable, and automated designs. In Iran, horizontal and vertical louvers were used to enhance natural airflow and heat transfer rate [83]. Horizontal louvers achieved a high ventilation rate. In Poland, authors have focused on visual comfort and UDI levels in vertical shading systems. A case study was conducted in Japan that demonstrated a 7.3% and 9.3% increase in electricity production with a vertical and horizontal louver system [93]. Horizontal louvers were preferred over vertical louvers. Despite having shadows on the louvers, optimum spacing was maintained to achieve the improvements in electricity generation.

Table 4. Vertical louver designs depicting performance metrics, orientations, and angles across various applications.

Year	Country	Slat Angle	Orientation	Key Findings
1962 [44]	USA	-	N	• Vertical louvers performed better for buildings facing north • Achieved transmittance >50%
1962 [44]	USA	-	E/W	• Resulted in transmittance <10% if avoiding sunlight • Not a recommended orientation (E/W) for window installation
2010 [124]	Jordan	0°, 45°	S	• Vertical louvers performed better compared to horizontal louvers • Regression analysis was used to correlate the shading device positions with lighting levels and achieved better results at 0° • Findings may not apply universally to other climates except Mediterranean climate (Amman, Jordan)
2010 [125]	Portugal	10°−90°, with a difference of 10°.	E, W	• Preferred vertical louvers for E-W facades • Limited to single zone building model, which may not fully capture the complexities of multi-zone or larger buildings
2010 [85]	UAE	−80°, −60°, −40°, −20°, 0°, 20°, 40°, 60°, 80°	E, W	• Preferred dynamic louver system over static louver system • Vertical louvers at 20° achieved energy savings of 26% and 25.97% for E and W orientations, receptively
2017 [46]	UK	15°	S, S-W	• Compared and preferred parametric control-based louvers over aluminum-based vertical louvers • Spacing and depth of 15 cm for each vertical louver is maintained
2017 [37]	Spain	−60°, −30°, 0°, 30°, 60°	E	• Louver length and spacing of 1 m and 0.5 m were chosen, respectively • Preferred vertical louvers in the east façade • Dynamic louvers were not considered, limiting the scope of the findings
2020 [49]	Israel	-	N-W, N-W, and S-W	• Improvements in daylighting by 7.62% • Showed better improvements in the N-W orientations • Preferred dynamic louvers compared to static louvers
2020 [83]	Iran	0°	-	• Increased airflow and heat transfer rate • Preferred horizontal louvers compared to vertical louvers
2020 [50]	Poland	15°, 30°, 45°, 60°	S	• Achieved improvements in visual comfort and UDI level • De Luminae and SketchUp simulation tools were used
2023 [87]	China	-	-	• Analyzed the heat transfer coefficients • Deployed Newton's cooling equation and CFD simulation

Table 4. *Cont.*

Year	Country	Slat Angle	Orientation	Key Findings
2023 [105]	Iran	15°, 30°, 45°	-	• Vertical louvers showed maximum AEE at low wind speeds (1 m/s), and louver angle of 15° • Horizontal louvers showed maximum AEE at higher wind speeds (2–3 m/s), and louvers had an angle of 15°
2024 [93]	Japan	-	-	• Showed improvements of 7.3% in electricity production using PV-integrated vertical louvers • PV-integrated horizontal louvers showed better results
2024 [66]	USA	-	-	• Achieved daylighting improvements of 75% for east-facing using a prismatic-vertical louver system • Despite its benefits, the system led to overlit areas near the windows

3.2. Horizontal Louver

The horizontal louver systems provide free air movement with horizontal slats. They provide a clear view, unlike vertical louver systems. However, the snow load is experienced in horizontal louver systems. Further, they have been classified as horizontal single blades, overhang horizontal louvers, and overhand multiple blades. In [37], 68% energy was saved with the help of a horizontal louver system. A study was conducted to assess the performance of daylight, which showed that the illuminance level was decreased at louvers angles of 15° and 30° [126]. Furthermore, the horizontal louvers design has provided better daylighting with a slat angle of 0°. Different geometrical designs of ceilings were optimized to enhance the daylight performance. Table 5 presents horizontal louver designs, highlighting key parameters such as slat angles, orientations, and energy performance outcomes across different countries.

Table 5. Horizontal louver designs highlighting slat angles, orientations, and energy performance across countries.

Year	Country	Design	Slat Angle	Orientation	Key Findings
1962 [44]	USA	Flat	0°	S	• Horizontal louvers are most effective for south-facing facades • Tilt angle, aperture sizes, and the solar position were optimized to analyze the transmittance
2001 [84]	Italy	Flat/external	0°, 30°, 45°, 60°, and 90°	S	• Reduction in cooling load for summers, while allowing some passive solar gain in winter • Not fully applicable to tropical, desert, or extreme cold climates, where different shading strategies were required
2009 [126]	UK	Flat/external	0°	-	• Louvers integrated with curved and chamfered ceilings significantly improved daylighting • Other geometries such as arched ceilings or dynamic ceiling systems were not explored

Table 5. *Cont.*

Year	Country	Design	Slat Angle	Orientation	Key Findings
2010 [124]	Jordan	Flat/external	0°, 45°	S	• Vertical louvers reduced energy consumption by 40% compared to no shading • Tested on south-facing facades, limiting their applicability to buildings with different orientations
2010 [125]	Portugal	Flat/external	10°, 20°, 30°, 40°, 50°, 60°, 70°, 80°, 90°	S	• Preferred horizontal louvers for south facades • Limited to single zone building model, which may not fully capture the complexities of multi-zone or larger buildings
2010 [85]	UAE	Flat/external	−80°, −60°, −40°, −20°, 0°, 20°, 40°, 60°, 80°	S	• Dynamic louver design was preferred • Energy saving of 31.28% at −20 for S orientation • Highest energy saving of 34.02% at south orientation using dynamic louvers
2016 [33]	Korea	External	-	S	• Preferred horizontal louvers over vertical louvers • Higher weight for input parameters
2017 [37]	Spain	Flat/external	0°	S	• Preferred horizontal louvers for south orientation • Reduced cooling energy demand of 68%
2019 [127]	Chile, Canada, USA	Curved/External	30°, 45°, 60°	-	• Improved energy savings and visual comfort • Fixed louvers with a 60° title angle performed best for the W-facing building • A limitation of this study is the exclusion of a hybrid control setup, as fixed louvers outperformed dynamic systems in certain cases
2020 [49]	Israel	External	-	N-W, W, and W, respectively	• Horizontal louvers achieved 1–2% higher UDI levels compared to diagonal louvers under certain conditions • Heating and cooling were not considered, and the results are based on a Mediterranean climate, limiting broader applicability
2020 [83]	Iran	Flat	0°	-	• Increased airflow and heat transfer rate • Horizontal louvers showed better results
2021 [69]	Poland	Flat	60°	S-W	• Saved 1215 h/yr of artificial lighting • Limited to horizontal louvers; other shading strategies are not tested • Roof aspects and ceiling geometry were not considered
2022 [58]	China	-	7°	-	• Combined system achieved better daylight distribution compared to metal louvers • No assessment conducted for thermal analysis and energy efficiency

Table 5. *Cont.*

Year	Country	Design	Slat Angle	Orientation	Key Findings
2023 [105]	Iran	Flat	15°, 30°, 45°	-	• Horizontal louvers achieved better results at 15° • In-depth daylighting and thermal analysis were not considered
2024 [63]	China	Flat	0°	E, S-E, S, S-W, and W-oriented	• Horizontal louvers showed less energy savings as compared to trapezoid louvers • Achieved a daylighting uniformity of 0.6
2024 [68]	Korea	Flat	0°	-	• Louver's upper slat optimized at 0° horizontal • Not analyzed the effect of the summer season on energy savings
2024 [92]	Portugal	External, fixed	0°	-	• Energy needs were observed for different climate conditions using fixed horizontal louvers • Simulations are based on hypothetical scenarios, so real-world variables might differ
2024 [93]	Japan	-	-	-	• PV-integrated horizontal louvers enhanced electricity production by 9.3% • Preferred horizontal compared to vertical louvers • The analysis is conducted in a specific climate (Japan), and the results may not be directly applicable to buildings in other regions

3.3. Innovative Louvers

There are distinct architectural elements (e.g., egg crate, diagonal louvers, trapezoids, overhangs, and baffle louvers) commonly utilized in building design to control light, airflow, and privacy. The egg crate design [39] features a grid-like pattern resembling the structure of an egg carton, characterized by a series of square or rectangular openings. This configuration effectively diffuses and distributes light while maintaining a degree of privacy. Diagonal louvers [49], on the other hand, are slanted elements that can be adjusted to control the angle and intensity of sunlight entering a space. Their adjustable nature allows for dynamic modulation of natural light throughout the day, reducing glare and minimizing heat gain. Overhang louvers are horizontal projections that extend outward from a building's facade. They serve as a shading device, effectively blocking direct sunlight from entering a space during peak daylight hours, which aids in maintaining a comfortable and energy-efficient interior environment. Each of these architectural features represents a thoughtful approach to balancing the interplay between natural elements and the built environment, enhancing both aesthetic appeal and functional performance in architectural design. A trapezoid louver system was tested under different orientations [63], which saved energy and showed better results in comparison with the horizontal, vertical, diagonal, and egg crate louver systems. A novel design [128] was presented, which consisted of a vertical greening shading device using climbing plants. It was compared with the louver system, and the proposed design achieved a 2.6° lower temperature. In [56], an L-shaped louver system was tested in different orientations (E, W, N, S) in Jakarta, which improved the daylighting and energy savings with a payback year < 1.

4. Louver System Control

4.1. Fixed Control

A fixed louver system consists of non-adjustable angled slats or blades that are permanently set in a fixed position. These louvers are designed to provide a consistent and predetermined level of shading and daylighting. Fixed louvers are often positioned at a specific angle to allow a certain amount of natural light to enter the building while minimizing direct sunlight and excessive heat. They are commonly used in building facades and windows to control daylighting and improve energy efficiency, as given in Table 6.

Table 6. Performance of fixed control louvers for sustainable building energy performance.

Year	Country	Slat Angle	Orientations	Key Findings
2001 [84]	Italy	0°, 30°, 45°, 60°, and 90°	S	• Improvements in thermal performance using fixed horizontal louvers with varying slat lengths and tilt angles • Dynamic control strategies integrated with other louver designs (e.g., vertical, egg crate) were not tested
2009 [126]	UK	0°	-	• Daylight performance was improved by modifying the ceiling geometry
2010 [85]	UAE	−20°, 20°	S, E/W	• Dynamic louvers were preferred instead of static louvers
2020 [49]	Israel	-	S, S-E, E, N-E, N, NW, W, and SW, respectively.	• UDI levels of 35.73, 33.83, 36.65, 37.78, 39.49, 41.27, 39.47, and 39.58 were achieved, respectively, using horizontal design • Horizontal louvers performed best in the N, N-W, W, and S-W orientations
2020 [49]	Israel	-	S, S-E, E, N-E, N, N-W, W, and S-W, respectively.	• UDI levels of 35.65, 35.04, 36.79, 37.21, 38.64, 39.94, 37.58, and 37.70 were achieved, respectively, using vertical design • Vertical louvers performed lower than diagonal and horizontal louvers
2023 [59]	China	-	W	• The proposed shading system improved thermal comfort by a factor of 1.5–2.5
2024 [63]	China	45°	-	• A UDI level of 92 and a DA of 67 were achieved
2024 [92]	Portugal	0°	-	• A novel louver system was designed to improve energy requirements

4.2. Moveable Control

Moveable louver systems, also known as adjustable or operable louvers, consist of slats or blades that can be adjusted or moved to control the amount of daylight, natural ventilation, and solar heat entering a building [99], as discussed in Table 7. These louvers are often manually operated but can also be motorized for easier control and convenience. Occupants can adjust the angle of the louvers to optimize natural light while minimizing glare and heat gain.

Table 7. Performance of moveable louvers with different orientations.

Year	Country	Angle	Orientation	Key Findings
2020 [49]	Israel	-	S, S-E, E, N-E, N, N-W, W, and S-W, respectively	UDI levels of 37.33, 34.19, 36.67, 37.81, 40.23, 41.75, 41.93, and 41.30 were achieved, respectively using horizontal design.
2020 [49]	Israel	-	S, S-E, E, N-E, N, N-W, W, and S-W, respectively.	UDI levels of 37.20, 35.87, 36.82, 37.21, 38.64, 40.54, 38.84, and 39.76 were achieved, respectively, using vertical louver design.

4.3. Automated Control

A hybrid louver system combines elements of both fixed and moveable louvers to provide a versatile daylighting solution. Typically, this involves installing fixed louvers with movable sections or panels integrated within the system. The fixed louvers provide a consistent shading effect, while the moveable sections allow for adaptability and finer control over daylight levels. Table 8 provides a summary of automatic louver control methods applied across different buildings and countries. It includes various control techniques such as dynamic systems with sensor-based controls, simple controls, and parametric controls, implemented in office, residential, and other types of buildings. The remarks highlight the impact of these control methods on energy efficiency, daylighting, and overall building performance. Parametric control in louvers is a dynamic control strategy that adjusts the orientation, tilt angle, or position of the louvers based on various parameters, such as the solar position, time of day, season, occupants, and weather conditions. A parametric control-based louver system behaves differently depending on the presence or absence of occupants. When no occupants were present, the parametric louvers redirected sunlight to the PV module for electricity generation. In the presence of occupants, the louvers adjusted to secure the necessary illuminance for lighting [67]. Figure 8 shows a flowchart to optimize visual comfort and energy efficiency using multi-objective optimization for an external shading device. The optimal design reduced the discomfort glare by 49% to 53% and the annual load by 100 kWh [129]. Figure 9 illustrates a sensor-based dynamic louver system that integrates real time outdoor conditions to optimize indoor daylighting, heating, cooling, and overall energy management [85]. The dynamic system effectively reduced both lighting and cooling loads.

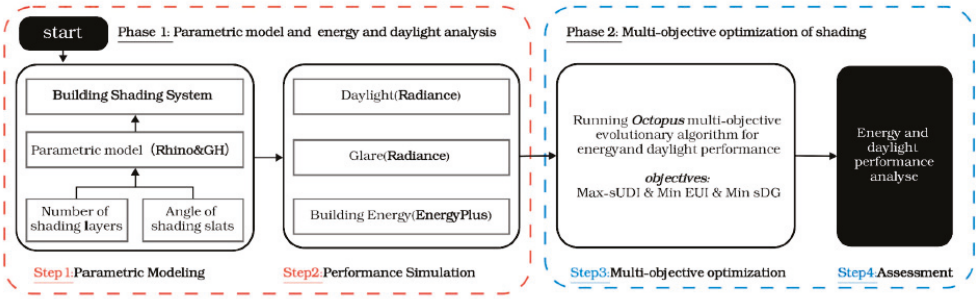


Figure 8. Simulation layout for a parametric control-based louver system [129].

Table 8. Building louvers with automatic control mechanisms to enhance energy efficiency and daylighting performance.

Year	Country	Control method	Building	Key Findings
2010 [85]	UAE	Sensor-based	Office	A dynamic louver system was proposed and compared with sensor-based dimming light techniques
2017 [47]	USA	Prismatic	Office	The proposed system achieved energy savings of 43% and was tested at different louvers angles

Table 8. *Cont.*

Year	Country	Control method	Building	Key Findings
2020 [49]	Israel	Simple control	Office	UDI increased up to 51% in N-W orientation
2020 [43]	Egypt	Parametric	Virtual room	A case study in New Cairo to improve daylighting
2020 [51]	Taiwan	Sensor-based	Office	Radiance-based strategy is used to optimize the daylighting and glare control
2020 [52]	USA	Parametric	Office	Climate adaptive envelope achieved less cooling load and better daylighting in hot and humid climates
2020 [53]	Indonesia	Parametric	Office	The proposed study enhanced daylighting performance and was tested in a south orientation
2020 [54]	Egypt	Parametric	Office	This study was conducted in an office room in New Cairo that used an automatic louver system
2021 [55]	UK	Parametric	Office	Illuminance of 300–500 lux was achieved.
2021 [69]	Poland	Sensor-based	Museum	An energy savings of 118 kWh/yr was achieved
2022 [38]	Jordan	Parametric	Office	Split louvers were used to improve daylighting
2022 [57]	Jordan	Parametric slat angle	Office	The proposed system used a slat angle to parametrically control the louvers
2023 [61]	Jordan	Parametric	Office	Transparent PV panels were used to enhance energy generation and improve daylighting
2023 [121]	China	Rule-based strategy	Office	Semi-transparent PV windows were used to improve thermal comfort hours (up to 5%) and energy savings of 65% (W orientation)
2023 [91]	China	Parametric	Office	The proposed louver system effectively reduced the cooling load of a west-facing building
2023 [62]	USA	Parametric	Office	Louvers were tested at different angles to achieve the optimum results
2023 [130]	China	Parametric	Office	Photovoltaic louvers and prismatic design achieved 22.8% energy savings
2024 [68]	Korea	Sensor-based	Office	Daylighting was improved using sensor-based LED dimming control of the louver system
2024 [65]	Japan	Sensor-based	Office	The slat angle, opening, and closing of a louver system are managed by a solar collector, having very less error
2024 [40]	Denmark	Parametric	Office	The proposed louver-based system improved visual comfort and electrical lighting energy utilization
2024 [66]	USA	Sensor-based	Office	An Arduino microcontroller was used to test the performance of vertical louvers
2024 [67]	South Korea	Sensor-based	Office	An illuminometer, thermocouple, servo motor, controller, and energy sensors were used to control the louvers

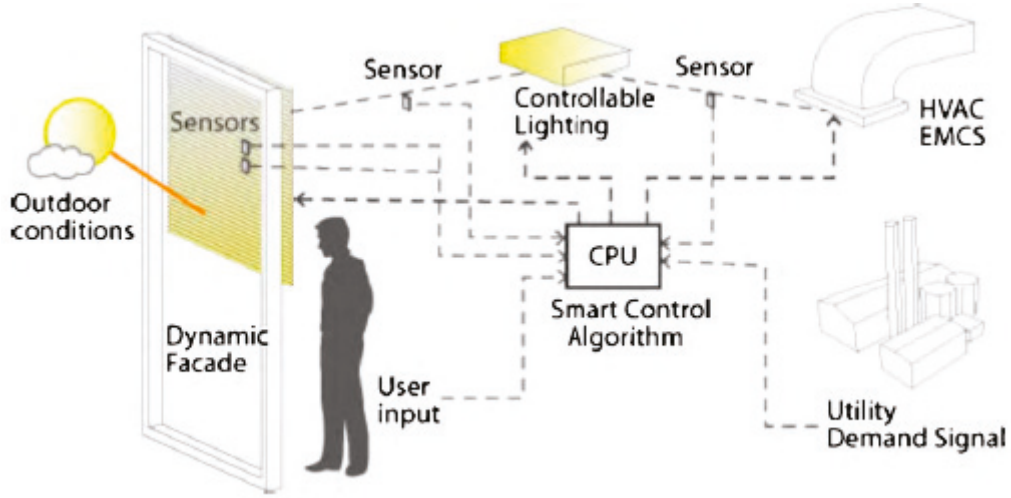


Figure 9. Showing a schematic diagram of a dynamic louver system [85].

5. Materials

The choice of material for louvers significantly impacts their durability, performance, and maintenance needs. Each material used in louver systems—aluminum, plastic, glass, and wood—offers distinct advantages and considerations for improving building energy efficiency. Aluminum with insulating cores provides a robust solution with high durability and low maintenance. It is frequently used in both residential and commercial applications. The natural oxide layer on aluminum provides excellent protection against rust and degradation, and its low density makes handling and installation easier. Additionally, aluminum can be easily fabricated into various shapes and finishes through processes such as powder-coating or anodizing.

While plastic louvers offer cost-effective, lightweight options with customizable insulation. Glass louvers with low-E coatings or double glazing contribute to thermal performance and natural lighting, albeit at a higher cost and with greater maintenance needs. Wooden louvers provide natural insulation and aesthetic appeal but require regular upkeep to maintain their performance. The choice of material depends on various factors, including the building's design requirements, environmental conditions, budget, and desired energy efficiency outcomes, as presented in Table 9. By carefully selecting and applying the appropriate material, building owners and designers can effectively enhance energy performance and achieve sustainable building goals. Figure 10 shows the split louver for balance distribution of daylight in the interior using different shapes of upper section slats and controlling the orientation of the lower section slats [61].

Table 9. Different louver materials and their impact on durability, performance, and energy efficiency.

Year	Country	Material	Reflectance	PV-Integrated	Key Findings
2017 [46]	UK	Mirror	75%	×	• Mirrored louvers enhanced daylight deep inside the office room • Electrochromic window maintaining desired illuminance levels
2017 [119]	China	Glass	-	✓	• PV blinds enhanced energy efficiency and maintained indoor visual comfort • Lowered the solar heat gain and reduced indoor cooling power consumption
2020 [83]	Iran	Glass for windows and plastic for louvers	-	×	• Horizontal louvers provided higher temperatures. • Vertical louvers maintained lower temperatures while providing weaker airflow
2020 [49]	Israel	Diffused metal	0.175	×	• Dynamically adjusted louver of diffuse metal increased UDI by 51% • Horizontal louvers performed better than vertical and diagonal louvers
2022 [41]	Korea	Electrochromic (smart glass)	20−70%	×	• Maximized performance by dividing the electrochromic louvers into 10–15 parts • Achieved LEED criteria at visible light transmittance of 40–45%
2023 [61]	Jordan	Glass	50−70%	✓	• Significantly enhanced daylight distribution and improved uniformity to 70% • PV glass having transmittance of 30–50% reduced glare

Table 9. *Cont.*

Year	Country	Material	Reflectance	PV-Integrated	Key Findings
2024 [29]	South Korea	Aluminum	90%	×	• Aluminum louvers with high reflectance boosted indoor illumination • Highest cooling energy savings at 30% louver opening
2024 [67]	South Korea	Aluminum	90%	✓	• Integrated louver and PV modules achieved an efficiency of 64% • Limited efficiency due to 1-axis louver

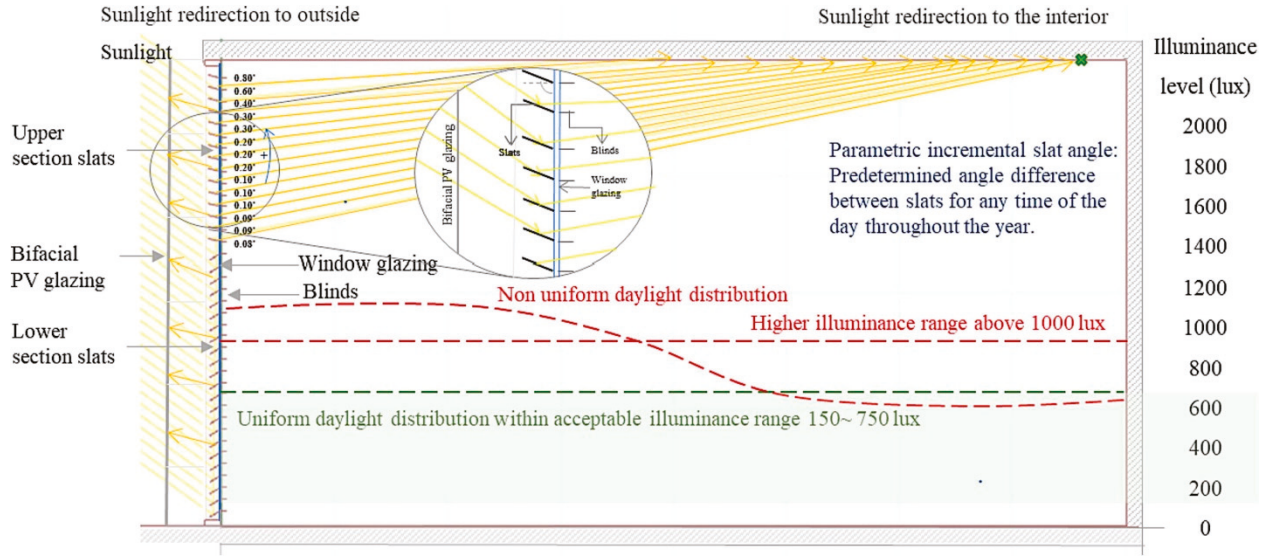


Figure 10. Showing a PV-integrated semitransparent louver system to analyze the effect of slat orientation and PV glass to improve daylighting [61].

6. Results and Discussion

The results emphasize the versatility and efficiency of various louver systems in optimizing energy performance across diverse climates and building types, as discussed in Table 10. Fixed horizontal louvers showed exceptional cooling performance, achieving up to 70% energy savings in hot-summer Mediterranean offices. Both internal and external systems improved ventilation by 12–60% in factory settings, depending on the climate. Vertical and dynamic designs demonstrated strong illuminance control, with improvements up to 39.8% in subtropical arid regions and 34.02% in arid deserts.

Advanced configurations, such as PV-integrated and parametric controlled louvers, achieved remarkable results, with illuminance improvements reaching 100% in subtropical arid climates and 90% in arid and Mediterranean regions. External and horizontal systems contributed significantly to both cooling and illuminance in offices, while trapezoid and curved designs enhanced energy efficiency in mid-latitude and subarctic regions. Dynamic and automatic louvers proved effective in museums and virtual office settings, optimizing both daylighting and thermal comfort. The study highlights how tailored louver designs, including vertical, horizontal, PV-integrated, and trapezoidal shapes, can address specific building energy needs while adapting to diverse climatic conditions.

Table 10. Overview of energy savings and performance improvements across different building types and climates.

Year	Type	Energy Savings/ Improvements	Illuminance/Heat/Ventilation	Building	Climate
2001 [84]	Fixed, horizontal	70	Cooling	Office	Hot-summer Mediterranean
2005 [101]	External and internal	12	Ventilation	Factory	Mediterranean
2008 [95]	External, Internal	60	Ventilation	Factory	Temperate
2010 [124]	Vertical	39.8	Illuminance	Office	Subtropical arid
2010 [85]	External, dynamic, horizontal, vertical	34.02, 30.31, 28.57	Illuminance	Office	Arid desert
2016 [33]	Horizontal	5	Illuminance	Office	Dry-winter humid continental
2017 [37]	External, Horizontal, Vertical	68	Cooling	Office	Mediterranean
2017 [47]	Vertical	39–43	Daylighting	Office	Warm-summer Mediterranean
2018 [48]	External	63	Illuminance and cooling	Office	Continental semiarid, tropical, humid subtropical
2020 [49]	External, dynamic, horizontal, vertical, and diagonal	51	Illuminance	Office	Mediterranean
2020 [98]	External, horizontal, vertical	37.5	Ventilation	Office	Temperate
2020 [83]	Internal, external, horizontal, and vertical	-	Ventilation	Office	Hot and arid
2021 [99]	External, movable	14	Ventilation	Office	Semi-arid, temperate
2021 [56]	External	18	Illuminance and cooling	Office	Tropical
2021 [69]	Horizontal, automatic	30.2	Illuminance	Museum	Moderate
2022 [38]	Parametric control	100	Illuminance	Virtual office	Subtropical arid
2022 [104]	-	53.4	Ventilation	Office	Tropical
2023 [59]	External	2.6	Illuminance and thermal	School office	Severe cold and cold
2023 [89]	External	23	Cooling	Residential	Tropical
2023 [61]	PV-integrated and retro-shaped	90	Illuminance	Office	Arid, desert, Mediterranean
2023 [121]	PV-integrated	65.7	Illuminance, heating, and cooling	Office	Humid subtropical
2023 [91]	Parametric	46	Illuminance, heating, and cooling	Office	Humid subtropical
2024 [29]	Curved	27	Illuminance and cooling	Office	Mid-Latitude
2024 [63]	Trapezoid	44	Illuminance	Office	Subarctic and tropical
2024 [68]	External, horizontal	85	Illuminance	Office	Humid continental
2024 [92]	External, horizontal, and fixed.	-	HVAC	Residential & commercial	Temperate Mediterranean
2024 [93]	Vertical, horizontal	7.3, 9.3	Heating and cooling	Office	Subarctic-subtropical
2024 [64]	PV-integrated, external	-	Illuminance, heating, and cooling	Office	ASHRAE
2024 [40]	Parametric, Kinetic	99	Illuminance	Office	Temperate
2024 [67]	Automatic, Sensor-based	65	Illuminance, heating, and cooling	Office	Humid temperate

Louver systems also have certain limitations that can influence their performance and practicality. Advanced systems, such as automated or dynamic louvers, often entail high installation and operational costs, along with the need for regular maintenance to prevent mechanical failures or wear and tear, particularly in external applications. Designing

optimal configurations for specific climates and building types can be complex, requiring sophisticated modeling tools and expertise. Additionally, in extreme climates, louvers alone may not provide sufficient thermal regulation, necessitating supplementary active systems such as HVAC. Material selection is another critical factor, as durability varies—wood may deteriorate in humid conditions, while metal systems could exacerbate heat transfer if not adequately insulated. Fixed louvers also lack adaptability to changing weather conditions or sun angles, reducing their efficiency, while automated systems may rely on sensors prone to malfunction or requiring frequent calibration. Moreover, louvers can present aesthetic or structural challenges, potentially conflicting with architectural styles or local codes, and their energy-saving potential often involves trade-offs with natural daylighting, which can increase dependence on artificial lighting. These challenges highlight the need for innovative designs, advanced materials, and adaptable control mechanisms to maximize the benefits of louver systems in sustainable building practices.

7. Conclusions

This study underscores the vital role of louvers in promoting sustainable building design by enhancing energy efficiency and minimizing environmental impact. It examined various louver control methods, including fixed, movable, and automatic systems, alongside design configurations such as vertical, horizontal, and egg crate styles for varying climate conditions, from subtropical to arid regions. The analysis of their performance across different orientations highlighted their effectiveness in optimizing daylighting, ventilation, heating, and cooling, contributing to significant energy savings.

The studies on louver designs and orientations conducted across various countries from 1962 to 2024 highlighted the critical influence of design parameters, such as slat angles (ranging from -90° to 80°), orientations (e.g., south, east, west, and southeast-facing facades), and louver configurations on achieving energy efficiency, visual comfort, and airflow improvements. Various studies were found to optimize performance based on climatic conditions and building orientations where horizontal louvers, typically installed in equatorial or temperate regions, were most effective in reducing solar heat gain and glare for buildings with high solar altitudes, such as those with south-facing facades. Addition of automated design could significantly improve their performance for dynamic climates. Other louver designs were orientation-dependent to reduce glare and thermal discomfort.

Various control strategies for louvers were evaluated alongside these design configurations, highlighting their unique advantages and limitations. Fixed louvers, while providing basic shading, were constrained by their static nature and inability to adapt to changing environmental conditions, and they produced glare and heat when poorly integrated with buildings. In contrast, moveable louvers offered enhanced flexibility, improved daylighting, and moderate energy savings, proving effective across diverse orientations and climates, especially in office settings. However, automatic louvers, including parametric, PV-integrated, and dynamic systems, significantly outperformed traditional fixed control strategy and designs in energy savings, daylight optimization, and adaptability. Parametrically controlled louvers demonstrated exceptional flexibility by adjusting slat angles based on solar conditions, as seen in studies reporting enhanced daylighting and reduced cooling loads. PV-integrated louvers added an energy generation feature, which also maintained the thermal and visual comfort. Dynamic louvers, such as sensor-based and climate-adaptive systems, further improved energy efficiency by optimizing shading and ventilation in real time, effectively addressing diverse climatic and building demands. The optical design of louvers should be carefully designed for providing uniform illumination deep inside buildings. In addition, efficient coating materials having reflection, refraction, absorption,

and scattering properties can increase efficiency by providing high illuminance, low glare, and low heat penetration inside buildings without blocking views.

The study explored the adaptability of louvers in diverse building types and climates, emphasizing the impact of material selection on durability, performance, and maintenance. By addressing design challenges and employing advanced modeling techniques, this review offers valuable guidance for optimizing louver configurations to achieve superior energy efficiency and sustainability. Incorporating dynamic and sensor-based louvers capable of adjusting in real time to changing solar angles and weather conditions will foster a more responsive indoor environment. Additionally, facade designs should consider hybrid louver systems—combining horizontal, vertical, and diagonal elements—to optimize solar control across various orientations. Materials with high thermal resistance and durability should be employed to generate renewable energy while maintaining shading and thermal comfort. By aligning louver innovations with regional climatic demands and sustainable building practices, future construction can achieve significant energy savings, enhanced comfort, and reduced environmental impact.

In summary, this study offers a comprehensive review of louver performance across different climates and various architectural building types. Future research should focus on evaluating simulated louver designs through practical implementations. Additionally, integrating louvers into the façade design offers challenges, such as design complexity, climate dependency, building orientation, sizing, and cost, which need to be investigated considering diverse approach, local conditions, and building requirements. To find the effectiveness of integrating PV with louvers, adaptive designs for various louver types need to be experimented with for sustainable development. Future research should explore advanced louver designs considering AI-based control methods for optimizing performance using weather, energy demand, and illumination data. The aforementioned research needs for optimizing louvers will have an impact on sustainable building design.

Author Contributions: Conceptualization, W.I., I.U. and A.H.; Writing—Original Draft, Methodology, Writing—review and editing, W.I., I.U. and A.H.; Visualization, Validation, Data curation, and Resources, J.P. and K.L.; Supervision, I.U. and S.S.; Funding acquisition, Project Administration, M.C. All authors have read and agreed to the published version of the manuscript.

Funding: This work was supported by the Technology Innovation Program (20020705, Development of international standard for solar collecting system's BIM data) funded by the Ministry of Trade, Industry & Energy (MOTIE, Korea).

Conflicts of Interest: The authors declare no conflicts of interest.

Nomenclature

ACH	Air Changes per Hour
AEE	Air Exchange Efficiency
BIPV	Building-integrated photovoltaic
CFD	Computational fluid dynamics
CPV	Concentrator photovoltaic
DF	Daylight factor
DA	Daylight autonomy
EJ	Exajoule
HVAC	Heating, ventilation, and air conditioning
h/yr	Hours per year

IEA	International Energy Agency
IoT	Internet of Things
IAQ	Indoor air quality
T_{air}	Indoor air temperature
KWh	Kilowatt-hour
MWh	Megawatt-hour
MJ	Multi-junction
MOO	multi-objective optimization
POE	Primary optical element
PV	Photovoltaic
RER	Renewable energy resource
PMV	Predicted Mean Vote
PIV	Particle Image Velocimetry
PPM	Parts Per Million
TWh	Terawatt-hour
UDI	Useful daylight illuminance
E	East
W	West
N	North
S	South
E-W	East-West
S-E	SouthEast
N-E	NorthEast
N-W	NorthWest
S-W	SouthWest
Stated Policies Scenario	STEPS

References

1. Xu, T.; Zhang, Y.; Shi, L.; Feng, Y.; Zhang, C. A comprehensive evaluation framework of energy and resources consumption of public buildings: Case study, People's Bank of China. *Appl. Energy* **2023**, *351*, 121869.
2. Schweizer, M.; Stöckl, M.; Tutunaru, R.; Holzhammer, U. Influence of heating, air conditioning and vehicle automation on the energy and power demand of electromobility. *Energy Convers. Manag. X* **2023**, *20*, 100443. [CrossRef]
3. Xu, C.; Gao, Y.; Qin, Z.; Li, Z.; Pan, S.; Qi, L. Historical characteristics and projection of global renewable energy consumption. *Renew. Energy* **2024**, *121222*, 234.
4. IEA. *World Energy Outlook 2024*; International Energy Agency (IEA): Paris, France, 2024.
5. IEA. *World Energy Outlook 2022*; International Energy Agency (IEA): Paris, France, 2022.
6. UNEP. *2022 Global Status Report for Buildings and Construction: Towards a Zero Emission, Efficient and Resilient Buildings and Construction Sector*; United Nations Environment Programme (UNEP): Nairobi, Kenya, 2022.
7. Ahmad, J.; Imran, M.; Khalid, A.; Iqbal, W.; Ashraf, S.R.; Adnan, M.; Ali, S.F.; Khokhar, K.S. Techno economic analysis of a wind-photovoltaic-biomass hybrid renewable energy system for rural electrification: A case study of Kallar Kahar. *Energy* **2018**, *148*, 208–234.
8. Yolcan, O.O. World energy outlook and state of renewable energy: 10-Year evaluation. *Innov. Green Dev.* **2023**, *2*, 100070.
9. Erdogan, S.; Pata, U.K.; Solarin, S.A. Towards carbon-neutral world: The effect of renewable energy investments and technologies in G7 countries. *Renew. Sustain. Energy Rev.* **2023**, *186*, 113683.
10. Chen, Y.; Ren, Z.; Peng, Z.; Yang, J.; Chen, Z.; Deng, Z. Impacts of climate change and building energy efficiency improvement on city-scale building energy consumption. *J. Build. Eng.* **2023**, *78*, 107646.
11. Elmalky, A.M.; Araji, M.T. Computational procedure of solar irradiation: A new approach for high performance façades with experimental validation. *Energy Build.* **2023**, *298*, 113491.
12. Pilechiha, P.; Mahdavinejad, M.; Rahimian, F.P.; Carnemolla, P.; Seyedzadeh, S. Multi-objective optimisation framework for designing office windows: Quality of view, daylight and energy efficiency. *Appl. Energy* **2020**, *261*, 114356.
13. IPCC. *AR6 Climate Change 2022: Mitigation of Climate Change*; Intergovernmental Panel on Climate Change (IPCC): Geneva, Switzerland, 2022.

14. He, Q.; Tapia, F.; Reith, A. Quantifying the influence of nature-based solutions on building cooling and heating energy demand: A climate specific review. *Renew. Sustain. Energy Rev.* **2023**, *186*, 113660.
15. Restrepo, S.A.; Morcillo, J.; Castaneda, M.; Zapata, S.; Aristizábal, A.J. Experimental research on the performance of a BIPV system operating in Girardot, Colombia. *Energy Rep.* **2023**, *9*, 194–204.
16. Yue, Y.; Yan, Z.; Lei, F.; Qin, G. Promoting solar energy utilization: Prediction, analysis and evaluation of solar radiation on building surfaces at city scale. *Energy Build.* **2024**, *319*, 114561. [CrossRef]
17. Li, C.; Zhang, W.; Tan, J.; Liu, W.; Lyu, Y.; Tang, H. Energy performance of an innovative bifacial photovoltaic sunshade (BiPVS) under hot summer and warm winter climate. *Heliyon* **2023**, *9*, e18700. [CrossRef] [PubMed]
18. Tang, H.; Wu, J.; Chen, W.; Li, C. Building energy saving of a rotatable radiative cooling-photovoltaic system by alternate utilization of solar energy and radiative cooling. *Energy Build.* **2024**, *316*, 114350. [CrossRef]
19. Tian, J.; Ooka, R. Evaluation of solar energy potential for residential buildings in urban environments based on a parametric approach. *Sustain. Cities Soc.* **2024**, *106*, 105350. [CrossRef]
20. Abdelmaksoud, W.A. Solar energy utilization for underfloor heating system in residential buildings. *Energy Rep.* **2024**, *12*, 979–987. [CrossRef]
21. Zhang, X.; Lau, S.-K.; Lau, S.S.Y.; Zhao, Y. Photovoltaic integrated shading devices (PVSDs): A review. *Sol. Energy* **2018**, *170*, 947–968. [CrossRef]
22. Gunay, H.B.; O'Brien, W.; Beausoleil-Morrison, I.; Gilani, S. Development and implementation of an adaptive lighting and blinds control algorithm. *Build. Environ.* **2017**, *113*, 185–199.
23. Albatayneh, A. Optimising the Parameters of a Building Envelope in the East Mediterranean Saharan, Cool Climate Zone. *Buildings* **2021**, *11*, 43. [CrossRef]
24. Konis, K.; Lee, E.S. Measured daylighting potential of a static optical louver system under real sun and sky conditions. *Build. Environ.* **2015**, *92*, 347–359.
25. Eltaweel, A.; Su, Y.; Mandour, M.A.; Elrawy, O.O. A novel automated louver with parametrically-angled reflective slats; design evaluation for better practicality and daylighting uniformity. *J. Build. Eng.* **2021**, *42*, 102438. [CrossRef]
26. Rossi, F.; Cardinali, M.; Giuseppe, A.D.; Castellani, B.; Nicolini, A. Outdoor thermal comfort improvement with advanced solar awnings: Subjective and objective survey. *Build. Environ.* **2022**, *215*, 108967.
27. Lee, H.; Han, S.; Seo, J. Light Shelf Development Using Folding Technology and Photovoltaic Modules to Increase Energy Efficiency in Building. *Buildings* **2022**, *12*, 81. [CrossRef]
28. Jung, S.-Y.; Han, S.; Lee, M.-G.; Lee, H. Development of a Solar Tracking-Based Movable Louver System to Save Lighting Energy and Create a Comfortable Light Environment. *Buildings* **2022**, *12*, 2017. [CrossRef]
29. Kieu, N.-M.; Ullah, I.; Park, J.; Bae, H.; Cho, M.; Lee, K.; Shin, S. The Energy Saving Potential in an Office Building Using Louvers in Mid-Latitude Climate Conditions. *Buildings* **2024**, *14*, 512. [CrossRef]
30. Ma, Q.; Ma, H.; Wan, Z.; Wang, Z.; Wei, X. Effect of Ventilation Strategies of Center-Mounted Louver Ventilation Window on Building Energy Consumption and Daylighting. *Sustainability* **2025**, *17*, 670. [CrossRef]
31. Konis, K.; Selkowitz, S. *Effective Daylighting with High-Performance Facades: Emerging Design Practices*; Springer: Berlin/Heidelberg, Germany, 2017.
32. Matin, N.H.; Eydgahi, A.; Gharipour, A. Sustainable Design: Minimizing Discomfort Glare Through Data-Driven Methods for Responsive Facades. *Sustainability* **2025**, *17*, 783. [CrossRef]
33. Lee, K.S.; Han, K.J.; Lee, J.W. Feasibility Study on Parametric Optimization of Daylighting in Building Shading Design. *Sustainability* **2016**, *8*, 1220. [CrossRef]
34. Nabil, A.; Mardaljevic, J. Useful daylight illuminances: A replacement for daylight factors. *Energy Build.* **2006**, *38*, 905–913.
35. Bournas, I. Daylight compliance of residential spaces: Comparison of different performance criteria and association with room geometry and urban density. *Build. Environ.* **2020**, *185*, 107276.
36. Khidmat, R.P.; Fukuda, H.; Paramita, B.; Koerniawan, M.D. The optimization of louvers shading devices and room orientation under three different sky conditions. *J. Daylight.* **2022**, *9*, 137–149. [CrossRef]
37. Hernández, F.F.; López, J.M.C.; Suárez, J.M.P.; Muriano, M.C.G.; Rueda, S.C. Effects of louvers shading devices on visual comfort and energy demand of an office building. A case of study. *Energy Procedia* **2017**, *140*, 207–216.
38. Alsukkar, M.; Hu, M.; Gadi, M.; Su, Y. A Study on Daylighting Performance of Split Louver with Simplified Parametric Control. *Buildings* **2022**, *12*, 594. [CrossRef]
39. Lim, T.; Yim, W.S.; Kim, D.D. Evaluation of Daylight and Cooling Performance of Shading Devices in Residential Buildings in South Korea. *Energies* **2020**, *13*, 4749. [CrossRef]

40. Hosseini, S.M.; Heiranipour, M.; Wang, J.; Hinkle, L.E.; Triantafyllidis, G.; Attia, S. Enhancing Visual Comfort and Energy Efficiency in Office Lighting Using Parametric-Generative Design Approach for Interactive Kinetic Louvers. *J. Daylight.* **2024**, *11*, 69–96.
41. Kim, J.-H.; Han, S.-H. Indoor Daylight Performances of Optimized Transmittances with Electrochromic-Applied Kinetic Louvers. *Buildings* **2022**, *12*, 263. [CrossRef]
42. Rafati, N.; Hazbei, M.; Eicker, U. Louver configuration comparison in three Canadian cities utilizing NSGA-II. *Build. Environ.* **2023**, *229*, 109939.
43. Eltaweel, A.; Mandour, M.A.; Lv, Q.; Sua, Y. Daylight Distribution Improvement Using Automated Prismatic Louvre. *J. Daylight.* **2020**, *7*, 84–92. [CrossRef]
44. Moon, P.; Spencer, D.E. Optical transmittance of louver systems. *J. Frankl. Inst.* **1962**, *273*, 1–24.
45. Konstantzos, I.; Tzempelikos, A.; Chan, Y.-C. Experimental and simulation analysis of daylight glare probability in offices with dynamic window shades. *Build. Environ.* **2015**, *87*, 244–254. [CrossRef]
46. Eltaweel, A.; Su, Y. Evaluation of Suitability of a Parametrically Controlled Louvers for Various Orientations throughout a Year Comparing to an Existing Case. *Buildings* **2017**, *7*, 109. [CrossRef]
47. McNeil, A.; Lee, E.S.; Jonsson, J.C. Daylight performance of a microstructured prismatic window film in deep open plan offices. *Build. Environ.* **2017**, *113*, 280–297.
48. Uribe, D.; Bustamante, W.; Vera, S. Potential of perforated exterior louvers to improve the comfort and energy performance of an office space in different climates. *Build. Simul.* **2018**, *11*, 695–708.
49. Grobman, Y.J.; Austern, G.; Hatiel, Y.; Capeluto, I.G. Evaluating the Influence of Varied External Shading Elements on Internal Daylight Illuminances. *Buildings* **2020**, *10*, 22. [CrossRef]
50. Brzezicki, M.; Regucki, P. Optimization of useful daylight illuminance vs. drag force for vertical shading fins/panels. *Sci. Technol. Built Environ.* **2020**, *27*, 367–376.
51. Do, C.T.; Chan, Y.-C. Evaluation of the effectiveness of a multi-sectional facade with Venetian blinds and roller shades with automated shading control strategies. *Sol. Energy* **2020**, *212*, 241–257.
52. Kim, H.; Clayton, M.J. A multi-objective optimization approach for climate-adaptive building envelope design using parametric behavior maps. *Build. Environ.* **2020**, *185*, 107292.
53. Khidmat, R.P.; Ulum, M.S.; Lestari, A.D.E. Façade Components Optimization of Naturally Ventilated Building in Tropical Climates through Generative Processes. Case study: Sumatera Institute of Technology (ITERA), Lampung, Indonesia. In Proceedings of the IOP Conference Series: Earth and Environmental Science (EES), Lampung, Indonesia, 1 July 2020.
54. Eltaweel, A.; Su, Y.; Lv, Q.; Lv, H. Advanced parametric louver systems with bi-axis and two-layer designs for an extensive daylighting coverage in a deep-plan office room. *Sol. Energy* **2020**, *206*, 596–613.
55. Eltaweel, A.; Su, Y.; Hafez, M.; Eltaweel, W. An automated louver with innovative parametrically-angled reflective slats: Prototyping and validation via using parametric control in Grasshopper along with Arduino board. *Energy Build.* **2021**, *231*, 110614.
56. Suryandono, A.R.; Hariyadi, A.; Fukuda, H. Economic Assessment of L-Shaped Minilouvers for Reducing Cooling Energy and Improving Daylight Condition in Offices: A Simulation Study in Jakarta. *Sustainability* **2021**, *13*, 4021. [CrossRef]
57. Alsukkar, M.; Hu, M.; Eltaweel, A.; Su, Y. Daylighting performance improvements using of split louver with parametrically incremental slat angle control. *Energy Build.* **2022**, *274*, 112444.
58. Fang, J.; Zhao, Y.; Tian, Z.; Lin, P. Analysis of dynamic louver control with prism redirecting fenestrations for office daylighting optimization. *Energy Build.* **2022**, *262*, 112019.
59. Liu, Y.; Wang, W.; Li, Z.; Song, J.; Fang, Z.; Pang, D.; Chen, Y. Daylighting Performance and Thermal Comfort Performance Analysis of West-Facing External Shading for School Office Buildings in Cold and Severe Cold Regions of China. *Sustainability* **2023**, *15*, 14458. [CrossRef]
60. Chen, T.-C.; Dwijendra, N.K.A.; Parwata, I.W.; Candra, A.I.; Din, E.M.T.E. Multi-Objective Optimization of External Louvers in Buildings. *Comput. Mater. Contin.* **2023**, *75*, 1305–1316.
61. Alsukkar, M.; Hu, M.; Alkhater, M.; Su, Y. Daylighting performance assessment of a split louver with parametrically incremental slat angles: Effect of slat shapes and PV glass transmittance. *Sol. Energy* **2023**, *264*, 112069.
62. Jahanara, A.; Suk, J.Y. Parametric Design and Analysis of Dynamic Louver for Optimized Daylighting in High-Rise Office Buildings. In Proceedings of the 28th Conference on Computer Aided Architectural Design Research in Asia (CAADRIA), Ahmedabad, India, January 2023.
63. Ibrahim, A.; Alsukkar, M.; Dong, Y.; Hu, P. Improvements in energy savings and daylighting using trapezoid profile louver shading devices. *Energy Build.* **2024**, *321*, 114649.

64. Hossei, H.; Kim, K.H. Comprehensive analysis of energy and visual performance of building-integrated photovoltaics in all ASHRAE climate zones. *Energy Build.* **2024**, *317*, 114369.
65. Togashi, E.; Muramatsu, H.; Nakagawa, J.; Yamada, K. Modeling a solar shading system that controls heat gain by using solar energy to change louver slat angles. *Energy Build.* **2024**, *319*, 114518.
66. Haghani, M.; Place, W.; Buckner, G.D. Daylighting Performance of Innovative Sun-Tracking Prismatic Vertical Louvers (Pvl) System: A Comparative Study. *SSRN* **2024**. [CrossRef]
67. Jun, Y.-J.; Han, T.-G.; Song, Y.-H.; Park, K.-S. A study on the enhancement of energy efficiency and indoor environment through the integration of solar photovoltaic modules in daylighting louver systems. *Sol. Energy* **2024**, *282*, 112931.
68. Lee, J.H.; Kang, J.-S. Study on Lighting Energy Savings by Applying a Daylight-Concentrating Indoor Louver System with LED Dimming Control. *Energies* **2024**, *17*, 3425. [CrossRef]
69. Brzezicki, M. An Evaluation of Annual Luminous Exposure from Daylight in a Museum Room with a Translucent Ceiling. *Buildings* **2021**, *11*, 193. [CrossRef]
70. Zhao, J.; Du, Y. Multi-objective optimization design for windows and shading configuration considering energy consumption and thermal comfort: A case study for office building in different climatic regions of China. *Sol. Energy* **2020**, *206*, 997–1017. [CrossRef]
71. Ma, R.; Tao, S.; Li, Z.; Yuan, Y.; Jiang, F. Investigation on Forced Convective Heat Transfer at the Building Façade with Louver Blinds under Different Wind Directions. *Buildings* **2022**, *12*, 1096. [CrossRef]
72. Dong, Q.; Li, S.; Han, C. Numerical and experimental study of the effect of solar radiation on thermal comfort in a radiant heating system. *J. Build. Eng.* **2020**, *32*, 101497.
73. Xue, Y.; Liu, W. A Study on the Optimization of Atrium Daylight and Energy Performance through Skylight and Shading Design in Commercial Buildings in Cold Zones. *Buildings* **2023**, *13*, 228. [CrossRef]
74. Zomorodian, Z.S.; Tahsildoost, M. Assessing the effectiveness of dynamic metrics in predicting daylight availability and visual comfort in classrooms. *Renew. Energy* **2019**, *134*, 669–680.
75. Rababa, W.; Asfour, O.S. Façade Retrofit Strategies for Energy Efficiency Improvement Considering the Hot Climatic Conditions of Saudi Arabia. *Appl. Sci.* **2024**, *14*, 10003. [CrossRef]
76. Li, X.; Shi, W.; Liu, Y.; Zhang, N. Optimization Strategy for Thermal Comfort in Railway Stations above Ground Level in Beijing. *Buildings* **2024**, *14*, 2843. [CrossRef]
77. Choe, S.-J.; Han, S.-H. Energy Balance Data-Based Optimization of Louver Installation Angles for Different Regions in Korea. *Energies* **2022**, *15*, 9214. [CrossRef]
78. Ahmed, N.A.; Wongpanyathaworn, K. Optimising Louver Location to Improve Indoor Thermal Comfort based on Natural Ventilation. *Procedia Eng.* **2012**, *49*, 169–178. [CrossRef]
79. Saleem, A.; Kim, M.-H. Airside Thermal Performance of Louvered Fin Flat-Tube Heat Exchangers with Different Redirection Louvers. *Energies* **2022**, *15*, 5904. [CrossRef]
80. Bai, M.; Wang, F.; Liu, J.; Wang, Z. Thermal effects validation on solar louver module applying to active solar house in winter. *Energy Build.* **2023**, *291*, 113093.
81. Kitsopoulou, A.; Bellos, E.; Tzivanidis, C. An Up-to-Date Review of Passive Building Envelope Technologies for Sustainable Design. *Energies* **2024**, *17*, 4039. [CrossRef]
82. Bahdad, A.A.; Taib, N.; Allahaim, F.S.; Ajlan, A.M. Parametric Optimization Approach to Evaluate Dynamic Shading Within Double-Skin Insulated Glazed Units for Multi-Criteria Daylighting Performance in Tropics. *J. Daylight.* **2024**, *11*, 349–371.
83. Pourshab, N.; Tehrani, M.D.; Toghraie, D.; Rostami, S. Application of double glazed façades with horizontal and vertical louvers to increase natural air flow in office buildings. *Energy* **2020**, *200*, 117486.
84. Datta, G. Effect of fixed horizontal louver shading devices on thermal perfomance of building by TRNSYS simulation. *Renew. Energy* **2001**, *23*, 497–507.
85. Hammad, F.; Abu-Hijleh, B. The energy savings potential of using dynamic external louvers in an office building. *Energy Build.* **2010**, *42*, 1888–1895.
86. Rio, M.A.D.; Asawa, T.; Hirayama, Y. Modeling and Validation of the Cool Summer Microclimate Formed by Passive Cooling Elements in a Semi-Outdoor Building Space. *Sustainability* **2020**, *12*, 5360. [CrossRef]
87. Tao, S.; Yu, N.; Jiang, F.; Su, X.; Zhao, K. Correlations for forced convective heat transfer coefficients at the windward building façade with vertical louvers. *Build. Environ.* **2023**, *242*, 110611.
88. Deng, W.; Sun, F.; Wang, R.; He, K. Influence mechanism of the louver on the thermal performance of the mechanical draft wet cooling tower. *Appl. Therm. Eng.* **2023**, *230*, 120640.
89. Iqbal, M.; Ozaki, A.; Choi, Y.; Arima, Y. Performance Improvement Plan towards Energy-Efficient Naturally Ventilated Houses in Tropical Climate Regions. *Sustainability* **2023**, *15*, 12173. [CrossRef]

90. Tao, Y.; Yan, Y.; Chew, M.Y.L.; Tu, J.; Shi, L. A theoretical model of natural ventilation enhanced by solar thermal energy in double-skin façade. *Energy* **2023**, *276*, 127534.
91. Liang, X.; Zhang, H.; Sun, B. Parametric design of photovoltaic louver integrated shading devices for west facade windows of office buildings in central China. *J. Asian Archit. Build. Eng.* **2024**, *24*, 924–938.
92. Raimundo, A.M.; Oliveira, A.V.M. Assessing the Impact of Climate Changes, Building Characteristics, and HVAC Control on Energy Requirements under a Mediterranean Climate. *Energies* **2024**, *17*, 2362. [CrossRef]
93. Ito, R.; Lee, S. Development of adjustable solar photovoltaic system for integration with solar shading louvers on building façades. *Appl. Energy* **2024**, *359*, 122711.
94. Wu, J.; Wang, L.; Hong, T.; Hu, Q.; Wang, W. Revealing and optimizing the design of cover installation for outdoor units of air conditioners through CFD simulations and thermodynamic modeling. *J. Build. Eng.* **2024**, *87*, 109014.
95. Kang, J.-H.; Lee, S.-J. Improvement of natural ventilation in a large factory building using a louver ventilator. *Build. Environ.* **2008**, *43*, 2132–2141.
96. Arch, G.; Hajra, B.; Moravej, M.; Zisis, I.; Irwin, P.; Chowdhury, A.G.; Suaris, W. An experimental study to assess the effect of soffit louvered vents on wind loads and wind driven rain intrusion on low rise buildings. *Sustain. Cities Soc.* **2017**, *34*, 43–55.
97. Kosutova, K.; Hooff, T.V.; Vanderwel, C.; Blocken, B.; Hensen, J. Cross-ventilation in a generic isolated building equipped with louvers: Wind-tunnel experiments and CFD simulations. *Build. Environ.* **2019**, *154*, 263–280.
98. Yang, Y.K.; Kim, M.Y.; Song, Y.W.; Choi, S.H.; Park, J.C. Windcatcher Louvers to Improve Ventilation Efficiency. *Energies* **2020**, *13*, 4459. [CrossRef]
99. Tao, Y.; Fang, X.; Setunge, S.; Tu, J.; Liu, J.; Shi, L. Naturally ventilated double-skin façade with adjustable louvers. *Sol. Energy* **2021**, *225*, 33–43. [CrossRef]
100. Zheng, J.; Tao, Q.; Chen, Y. Airborne infection risk of inter-unit dispersion through semi-shaded openings: A case study of a multi-storey building with external louvers. *Build. Environ.* **2022**, *225*, 109586. [CrossRef] [PubMed]
101. Ballestini, G.; Carli, M.D.; Masiero, N.; Tombola, G. Possibilities and limitations of natural ventilation in restored industrial archaeology buildings with a double-skin façade in Mediterranean climates. *Build. Environ.* **2005**, *40*, 983–995. [CrossRef]
102. Al-Waked, R.; Yassin, A.; Adwan, A.; Mostafa, D.B. Effects of Cross Level Air Interaction within Multilevel Underground Carparks on Indoor Air Quality. *Fluids* **2020**, *5*, 177. [CrossRef]
103. Jiang, F.; Tao, S.; Tao, Q.; Li, Z.; Yuan, Y.; Zheng, J. The effect of louver blinds on the wind-driven cross ventilation of multi-storey buildings. *J. Build. Eng.* **2022**, *54*, 104614.
104. Tai, V.C.; Kai-Seun, J.W.; Mathew, P.R.; Moey, L.K.; Cheng, X.; Baglee, D. Investigation of varying louver angles and positions on cross ventilation in a generic isolated building using CFD simulation. *J. Wind. Eng. Ind. Aerodyn.* **2022**, *229*, 105172. [CrossRef]
105. Rahimi, R.; Hassanzadeh, R. Impacts of horizontal and vertical louvers on the natural cross-ventilation performance of a generic building. *Int. J. Vent.* **2023**, *23*, 51–74.
106. Stein-Montalvo, L.; Ding, L.; Hultmark, M.; Adriaenssens, S.; Bou-Zeid, E. Kirigami-inspired wind steering for natural ventilation. *J. Wind. Eng. Ind. Aerodyn.* **2024**, *246*, 105667. [CrossRef]
107. Cui, W.; Peng, X.; Yang, J.; Yuan, H.; Lai, L.L. Evaluation of Rooftop Photovoltaic Power Generation Potential Based on Deep Learning and High-Definition Map Image. *Energies* **2023**, *16*, 6563. [CrossRef]
108. Nguyen, N.-H.; Le, B.-C.; Bui, T.-T. Benefit Analysis of Grid-Connected Floating Photovoltaic System on the Hydropower Reservoir. *Appl. Sci.* **2023**, *13*, 2948. [CrossRef]
109. Iqbal, W.; Ullah, I.; Shin, S. Nonimaging High Concentrating Photovoltaic System Using Trough. *Energies* **2023**, *16*, 1336. [CrossRef]
110. Iqbal, W.; Ullah, I.; Shin, S. Optical Developments in Concentrator Photovoltaic Systems—A Review. *Sustainability* **2023**, *15*, 10554. [CrossRef]
111. Mutume, B. A feasibility assessment of utilizing concentrated solar power (CSP) in the Zimbabwean regions of Hwange and Lupane. *Heliyon* **2023**, *9*, e18210. [CrossRef]
112. Mandalaki, M.; Tsoutsos, T. *Solar Shading Systems: Design, Performance, and Integrated Photovoltaics*; Springer: Berlin/Heidelberg, Germany, 2020.
113. Baghdadi, A.; Abuhussain, M. In-Depth Analysis of Photovoltaic-Integrated Shading Systems' Performance in Residential Buildings: A Prospective of Numerical Techniques Toward Net-Zero Energy Buildings. *Buildings* **2025**, *15*, 222. [CrossRef]
114. Jung, S.K.; Kim, Y.; Moon, J.W. Performance Evaluation of Control Methods for PV-Integrated Shading Devices. *Energies* **2020**, *13*, 3171. [CrossRef]
115. Hasan, H.S.; Hwang, H. Economic Feasibility Assessment of Motorized PV Louver System Considering the Near Shading Parameter, Array Incidence Losses and Other Environmental Factors. *World J. Eng. Technol.* **2024**, *12*, 540–551. [CrossRef]

116. Guo, W.; Kong, L.; Chow, T.; Li, C.; Zhu, Q.; Qiu, Z.; Li, L.; Wang, Y.; Riffat, S.B. Energy performance of photovoltaic (PV) windows under typical climates of China in terms of transmittance and orientation. *Energy* **2020**, *213*, 118794. [CrossRef]
117. Svetozarevic, B.; Begle, M.; Jayathissa, P.; Caranovic, S.; Shepherd, R.F.; Nagy, Z.; Hischier, I.; Hofer, J.; Schlueter, A. Dynamic photovoltaic building envelopes for adaptive energy and comfort management. *Nat. Energy* **2019**, *4*, 671–682. [CrossRef]
118. Chen, H.; Cai, B.; Yang, H.; Wang, Y.; Yang, J. Study on natural lighting and electrical performance of louvered photovoltaic windows in hot summer and cold winter areas. *Energy Build.* **2022**, *271*, 112313. [CrossRef]
119. Luo, Y.; Zhang, L.; Wang, X.; Xie, L.; Liu, Z.; Wu, J.; Zhang, Y.; He, X. A comparative study on thermal performance evaluation of a new double skin façade system integrated with photovoltaic blinds. *Appl. Energy* **2017**, *199*, 281–293.
120. Reffat, R.; Ezzat, R. Maximizing solar energy generation: Guidelines for optimizing photovoltaic panel placement on building facades. *Archnet-IJAR Int. J. Archit. Res.* **2024**. [CrossRef]
121. Tan, Y.; Peng, J.; Wang, M.; Luo, Y.; Song, A.; Li, N. Comfort assessment and energy performance analysis of a novel adjustable semi-transparent photovoltaic window under different rule-based controls. *Build. Simul.* **2023**, *16*, 2343–2361.
122. Hofer, J.; Groenewolt, A.; Jayathissa, P.; Nagy, Z.; Schlueter, A. Parametric analysis and systems design of dynamic photovoltaic shading modules. *Energy Sci. Eng.* **2016**, *4*, 134–152.
123. Riviere, G.; Malet-Damour, B. Developing a new decision support tool for sizing louvers in hot and humid climates concerning light efficiency and building energy gain. In Proceedings of the Building Simulation 2023: 18th Conference of IBPSA 2023, Shanghai, China, 4 September 2023.
124. Alzoubi, H.H.; Al-Zoubi, A.H. Assessment of building façade performance in terms of daylighting and the associated energy consumption in architectural spaces: Vertical and horizontal shading devices for southern exposure facades. *Energy Convers. Manag.* **2010**, *51*, 1592–1599.
125. Palmero-Marrero, A.I.; Oliveira, A.C. Effect of louver shading devices on building energy requirements. *Appl. Energy* **2010**, *87*, 2040–2049.
126. Freewan, A.A.; Shao, L.; Riffat, S. Interactions between louvers and ceiling geometry for maximum daylighting performance. *Renew. Energy* **2009**, *34*, 223–232.
127. Uribe, D.; Vera, S.; Bustamante, W.; McNeil, A.; Flamant, G. Impact of different control strategies of perforated curved louvers on the visual comfort and energy consumption of office buildings in different climates. *Sol. Energy* **2019**, *190*, 495–510.
128. Bao, S.; Zou, S.; Zhao, M.; Chen, Q.; Li, B. Experimental Study on the Modular Vertical Greening Shading in Summer. *Int. J. Environ. Res. Public Health* **2022**, *10*, 11648.
129. Zheng, Y.; Wu, J.; Zhang, H.; Lin, C.; Li, Y.; Cui, X.; Shen, P. A novel sun-shading design for indoor visual comfort and energy saving in typical office space in Shenzhen. *Energy Build.* **2025**, *328*, 115083.
130. Ma, Q.; Ran, S.; Chen, X.; Li, L.; Gao, W.; Wei, X. Study on the effect of photovoltaic louver shading and lighting control system on building energy consumption and daylighting. *Energy Sources Part A Recovery Util. Environ. Eff.* **2023**, *45*, 10873–10889. [CrossRef]

Disclaimer/Publisher's Note: The statements, opinions and data contained in all publications are solely those of the individual author(s) and contributor(s) and not of MDPI and/or the editor(s). MDPI and/or the editor(s) disclaim responsibility for any injury to people or property resulting from any ideas, methods, instructions or products referred to in the content.

buildings

MDPI

Article

A Comparative Analysis of Advanced Glazing Technologies for Energy-Efficient Buildings in Jeddah City, Saudi Arabia

Mohammed M. Gomaa [1,2], Amr Sayed Hassan Abdallah [3], Mohammed A. Aloshan [3,*] and Ayman Ragab [2]

[1] Department of Architecture, School of Engineering, Computing& Design, Dar Al-Hekma University, Jeddah 22246, Saudi Arabia; mgomaa@dah.edu.sa
[2] Department of Architectural Engineering, Faculty of Engineering, Aswan University, Aswan 81542, Egypt; ayman.ragab@aswu.edu.eg
[3] Department of Architectural Engineering, Imam Mohammad Ibn Saud Islamic University (IMSIU), Riyadh 11432, Saudi Arabia; asabdullah@imamu.edu.sa
* Correspondence: mamoshan@imamu.edu.sa

Abstract: This study employs Design Builder software to evaluate advanced glazing technologies for enhancing the thermal performance of residential buildings in Jeddah, Saudi Arabia. Recognizing the energy inefficiencies caused by adopting Western architectural styles unsuited to local climatic conditions, and given that buildings consume 44% of national energy, we conducted a systematic parametric analysis to isolate the effects of key glazing parameters. The study examines six polycarbonate (PC) configurations and three critical comparative cases: (1) a selective double-glazed unit representing a new baseline glazing; (2) a low-U configuration to isolate thermal insulation effects; and (3) a low-SHGC configuration to evaluate solar heat gain mitigation independently. These controlled comparisons address a critical research gap by decoupling the traditionally confounded impacts of U-value and SHGC in hot climates. The simulations reveal that the 36 mm aerogel glazing (U = 0.9 W/m^2·K, SHGC = 0.3) reduces cooling demand by 48.6% annually compared to single-pane glazing while maintaining indoor temperatures at 30.09 °C versus 38.43 °C at baseline. Notably, the findings demonstrate that 87% of these savings derive from SHGC reduction, with only 3.02 percentage points attributable to U-value improvements. The selective DGU benchmark delivers 85% of aerogel's benefits at 40% lower cost, establishing it as a practical solution for most applications. These findings provide evidence-based guidance for Saudi Vision 2030's sustainability goals, emphasizing that while aerogel glazing excels in extreme solar exposures, strategic SHGC optimization in conventional glazing can achieve the most energy savings in hot climates.

Keywords: polycarbonate glazing; energy efficiency; thermal performance; aerogel insulation; net zero energy buildings

1. Introduction

Rapid modernization in Saudi Arabia has shifted towards Western architectural styles, often neglecting indigenous designs' traditional and socio-cultural context. This has resulted in questionable urban development patterns and a construction boom focused on client preferences over environmental considerations. Consequently, most houses suffer from poor insulation and a heavy reliance on air conditioning, exacerbating the energy challenges imposed by Saudi Arabia's harsh, hot, and dry climate [1]. The building sector,

responsible for nearly 44% of the nation's energy consumption, presents a significant opportunity for efficiency improvements. With a rapidly growing population and ambitious homeownership goals outlined in Saudi Vision 2030, the residential sector remains at the forefront of this challenge. However, conventional housing designs prioritize client preferences over energy performance, creating a need for innovative solutions.

Glazing in windows significantly affects the energy needed for cooling in buildings in hot, arid regions. Numerous advanced materials for building envelopes have been explored and introduced to reduce energy consumption. Among these, nanomaterials such as silica aerogels have garnered significant attention due to their unique properties [2–5]. Simultaneously, PC multi-panels have become increasingly popular in commercial and industrial building applications owing to their lightweight design, durability, and resistance to fire, weather, and UV radiation. These air-filled structural units, composed of multiple layers of PC sheets, are valued for their thermal insulation properties, ability to diffuse light, and ease of installation. The incorporation of interlock junctions in their design further enhances their thermal and optical performance, making them a versatile and efficient choice for modern construction needs [6]. These panels are increasingly used in fenestration systems, continuous windows, roofs, and walls, offering various geometric configurations, colors, and thicknesses. Notably, PC panels are more cost effective than traditional glazing systems and, when properly designed, can significantly enhance thermal performance, reducing energy costs in public buildings [7].

In a prior study [8], the thermal and optical behavior of these panels was evaluated. The results showed that while the optical properties of PC panels exhibit stronger angular dependence than conventional glass units, they still provide effective light diffusion, reducing glare and improving visual comfort. The joints between panels were found to impact performance, with variations depending on the number of layers and sample characteristics. Although PC panels exhibit lower light transmittance (approximately 30% less than double glazing units, DGUs), their thermal performance remains competitive, with U-values ranging from 1.2 to 1.9 W/m^2 K—comparable to DGUs [8].

For applications requiring higher thermal insulation, granular silica aerogels can be incorporated into the air gaps of PC panels. Aerogels are nanostructured materials characterized by high porosity (>90%) and low density (80–200 kg/m^3), with thermal conductivity ranging from 0.012 to 0.023 W/m K depending on granule size [9,10]. These properties make aerogels a "superinsulation" material, suitable for various energy-efficient building solutions, including opaque applications like concrete and plasters [11], flexible blankets [12], and translucent systems such as high-performance windows [13–15]. However, granular aerogels in glazing systems prevent direct visibility, offering only diffuse light transmittance, which helps reduce glare. While the thermal, optical, and acoustic performances of aerogel-based glazing systems have been extensively studied [16–18], research on aerogel-filled PC systems remains limited.

Buratti et al. [19] investigated the thermal and optical properties of a double-glazing system (DGUs) with a 15 mm layer of granular silica aerogel. The results showed a 63% reduction in thermal transmittance (U-value of 1.0–1.1 W/m^2 K) compared to air-filled DGUs, alongside a light transmittance of 0.57, representing a 30% reduction. Increasing the aerogel thickness to 60 mm further improved the U-value to 0.3 W/m^2 K [19]. However, light transmittance decreases by approximately 20% for every 10 mm increase in aerogel thickness [14]. The particle size of aerogel granules also significantly influences optical and thermal performance [9,12,17].

In humid subtropical climates, Huang and Niu [20] demonstrated that aerogel glazing systems could reduce the annual space cooling load by about 4% in commercial

buildings in Hong Kong, comparable to shading-type low-emissive glazing. Similarly, Ihara et al. [21] found that granular aerogel glazing used as spandrels reduced energy demand in cooling-dominated climates like Tokyo and Singapore. However, in heating-dominated climates such as Oslo, aerogel glazing systems underperformed compared to triple glazing, suggesting that a combination of aerogel and triple glazing could be more effective. Buratti et al. [22] further confirmed the energy-saving potential of aerogel glazing systems, achieving 60–70% energy savings in refurbishing a building in Perugia, Italy. Dowson et al. [23] conducted an experimental study on two prototype PC panels filled with granular aerogel (6 mm and 10 mm thicknesses). Installed in an office building in London, the panels demonstrated a 73% heat flux reduction for the 6 mm aerogel panel and 80% for the 10 mm panel. Light transmittance values were 58% and 51% for the 6 mm and 10 mm panels, respectively, compared to 73% for single glazing. These findings highlight the potential of aerogel-filled PC panels in retrofit applications.

Despite extensive research on façade design and energy performance, there remains a significant gap in the evaluation of the application of advanced materials, such as PC panels integrated with nanogel technology, in Saudi Arabia. This study bridges this gap by employing dynamic simulations to optimize glazing assembly designs incorporating these innovative materials. Focusing on a typical residential building in Jeddah—a city characterized by high cooling demands—this research aims to assess the effects of various nanogel-filled PC glazing configurations on annual cooling loads, energy consumption, and CO_2 emissions. The study also endeavors to determine the optimal glazing designs that reduce cooling requirements, enhance thermal comfort, and improve energy efficiency while minimizing carbon emissions. Furthermore, the research aims to provide detailed performance data and design recommendations to support adopting PC–nanogel glazing systems in future residential developments across Saudi Arabia. The anticipated outcomes of this research hold significant potential to influence building design strategies in Saudi Arabia, promoting the reduction of thermal discomfort and energy use in residential buildings. Aligning with the sustainability goals outlined in Saudi Vision 2030, this research may pave the way for adopting innovative facade technologies, ultimately transforming modern housing and contributing to a more sustainable future for the Kingdom.

2. Materials and Methods

2.1. Study Area

Jeddah City, located in the western region of Saudi Arabia, is characterized by a hot and humid climate. Geographically, the city lies at a latitude of 27.5° N, approximately 600 km northwest of Riyadh, the capital of Saudi Arabia, as depicted in Figure 1. The climate in Jeddah is classified as BWh, according to the Köppen–Geiger system, indicating a hot desert climate [24]. Jeddah City is in the hot–dry maritime subzone, characterized by a hot and dry climate. This climate zone exhibits several distinct features: the summers are notably hot and dry, with dry bulb temperatures (DBTs) often exceeding 43 °C, and the average maximum DBT reaches approximately 40 °C. The average monthly DBT is around 33 °C, while the wet-bulb temperature (WBT) averages 16.5 °C. The average relative humidity hovers around 19%. Additionally, Jeddah experiences an annual mean wind speed of 3.39 m/s, contributing to generally calm weather conditions throughout the year. Seasonal variations in climatic conditions are evident, with June recording peak average high temperatures of 33.5 °C, compared to cooler average lows of 25.7 °C in January. Annual precipitation levels are minimal, ranging from 1 mm to 19 mm, with the least rainfall occurring in June and the most during winter [25].

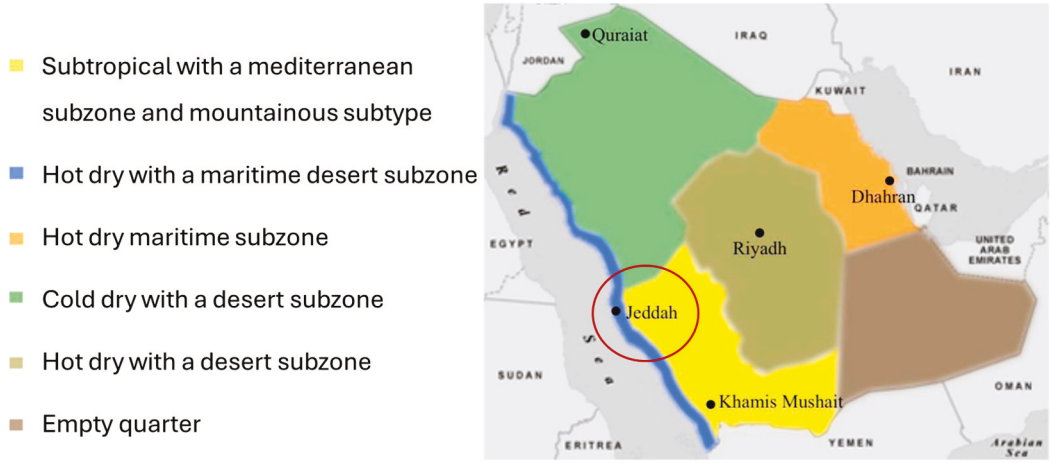


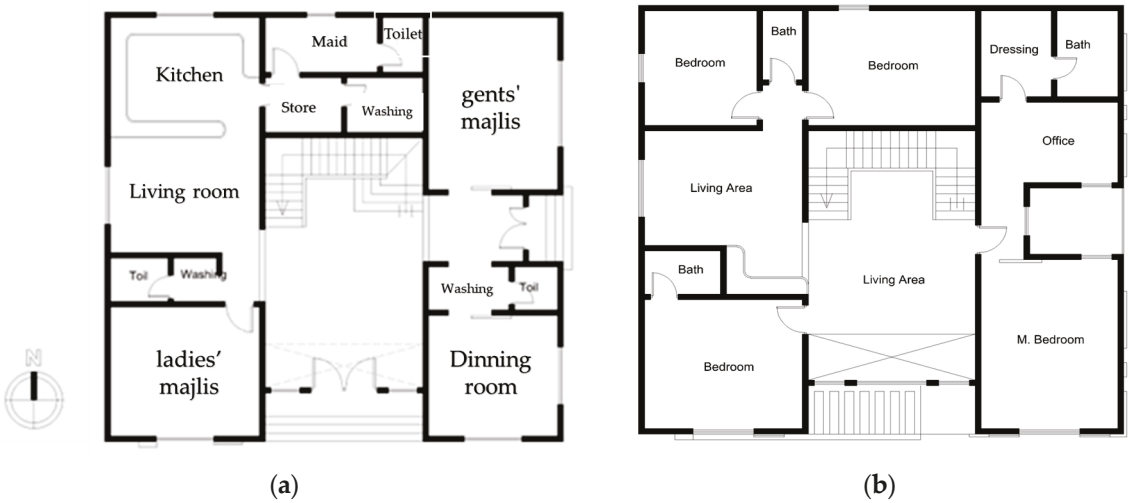
Figure 1. Geographic location of Jeddah, Saudi Arabia, and the climatic zoning of the country [26].

These severe climate conditions require heavy reliance on air conditioning systems to maintain indoor comfort, emphasizing the need for energy-efficient building designs. However, window glazing systems in buildings across Saudi Arabia often lack sufficient insulation, a shortfall rooted in conventional construction practices. Given the critical impact of climatic factors on building energy performance, analyzing glazing systems must account for these variables. The poor thermal performance of glazing systems in Jeddah contributes to increased cooling energy demands and highlights the necessity for improvements in building envelopes. Enhancing glazing configurations with advanced materials offers an opportunity to address this challenge by reducing energy consumption while improving thermal comfort.

2.2. Study Model Characteristics

Environmental factors, particularly temperature and humidity, significantly influence building energy demands. In regions with hot and arid climates like Jeddah, Saudi Arabia, cooling requirements dominate energy consumption. Therefore, selecting window glazing materials with enhanced thermal insulation properties is essential in reducing energy usage for cooling and heating purposes.

To address this issue, the current research focuses on assessing cooling energy requirements for a typical family residence in Jeddah, Saudi Arabia, utilizing innovative, advanced PC windows. The residential model chosen for evaluation represents a two-story building with a total floor area of 240 m^2, designed to accommodate a family of up to ten individuals. The architectural design of the model is represented in Figure 2. It is important to note that this model is representative of the prevalent housing structures found throughout Jeddah and adheres to the construction techniques specified in the Saudi Building Code (SBC), which includes guidelines for achieving thermal insulation [27]. The building model incorporates characteristic construction elements, including 30 cm brick walls with a 2 cm cement plaster layer on each side, achieving a thermal transmittance (U-value) of 1.61 W/m^2 K. The roof structure consists of 12 cm of insulated slabs layered with 2 cm of bitumen, 5 cm of insulated foam, 7 cm of sloped ordinary concrete, 6 cm of sand, 2 cm of cement mortar, and 2 cm of cement tiles, resulting in a U-value of 0.47 W/m^2 K. The baseline glazing comprises single-pane windows with a U-value of 5.6 W/m^2 K and a Solar Heat Gain Coefficient (SHGC) of 0.85, configured at a 14% window-to-wall ratio.



(**a**) (**b**)

Figure 2. The residential building model: (**a**) first floor; (**b**) second floor.

2.3. Modeling and Simulation Steps

Throughout the evaluation process, consideration was given to Jeddah's hot desert climate, designated as BWh according to the Köppen–Geiger climate classification. The specific geographical coordinates of Jeddah City (16°54′34.8588″ N and 42°34′4.4472″ E) were considered. A detailed simulation was developed, which precisely accounted for the thermal conductivity of each building material and the composition of the window layers. The building's design was input as 2D DXF files, enabling the software to generate a comprehensive 3D model.

Accurate weather data are a cornerstone of reliable building energy simulations. While Design Builder software (version 5.0.0.105) offers a default 2002 EPW (EnergyPlus Weather) file for Jeddah's climate zone obtained from the U.S. Department of Energy's (DOE) website, this study prioritized the use of more recent and localized data to ensure model precision. Following the recommended practices established in previous research [28–31], we utilized weather data from 2024 obtained from the King Abdullah University of Science and Technology (KAUST) weather station. While typical meteorological year (TMY) data are commonly used for building performance simulations as they represent long-term climate patterns, we selected a single-year dataset for this study to capture recent climatic trends and potential anomalies that may not be reflected in standardized TMY files. This approach was adopted because (1) the study focuses on evaluating current thermal performance under potentially changing climate conditions and (2) the selected year exhibited weather patterns consistent with the region's observed climate shifts in recent years. The dataset was carefully validated against historical records to ensure its representativeness despite the shorter timeframe.

The data acquisition and processing procedures adhered to the following steps:

1. EPW File Conversion: The original EPW file from the DOE website was first converted to a CSV (comma-separated values) format to extract the necessary data seamlessly.
2. Data Retrieval from Weather Station: Key meteorological variables, including dry-bulb temperature, relative humidity, global radiation, wind speed, and wind direction, were extracted from the CSV file, representing actual measurements from the local weather station.
3. Dew Point and Direct Radiation Calculation: To complement the acquired data, dew point and direct radiation values were calculated using Element software (version 1.0.6).

4. EPW File Generation: The final step involved incorporating the extracted and calculated data into a newly generated EPW file, adhering to the EnergyPlus weather file format.
5. Integration into Design Builder: The updated EPW file was subsequently imported into Design Builder, serving as the foundation for weather data within the simulation environment.

This meticulous approach to weather data handling ensures the model's alignment with the specific climate conditions of Jeddah in 2024, fostering more accurate and meaningful energy performance predictions. Using contemporary and site-specific data mitigates the potential discrepancies that could arise from relying on outdated or generalized weather datasets, ultimately enhancing the reliability and relevance of the simulation results.

Multiple outputs were derived using various performance metrics, including reductions in cooling load (kWh), annual energy consumption (kWh/year), CO_2 emissions mitigation (kg/year), monthly energy savings, and overall improvement rates relative to conventional glazing systems. The simulation was enhanced by adding data related to the PC windows and the building's operational dynamics, encompassing heating, airflow, and lighting. Table 1 thoroughly outlines the input parameters and building characteristics employed in the calculations.

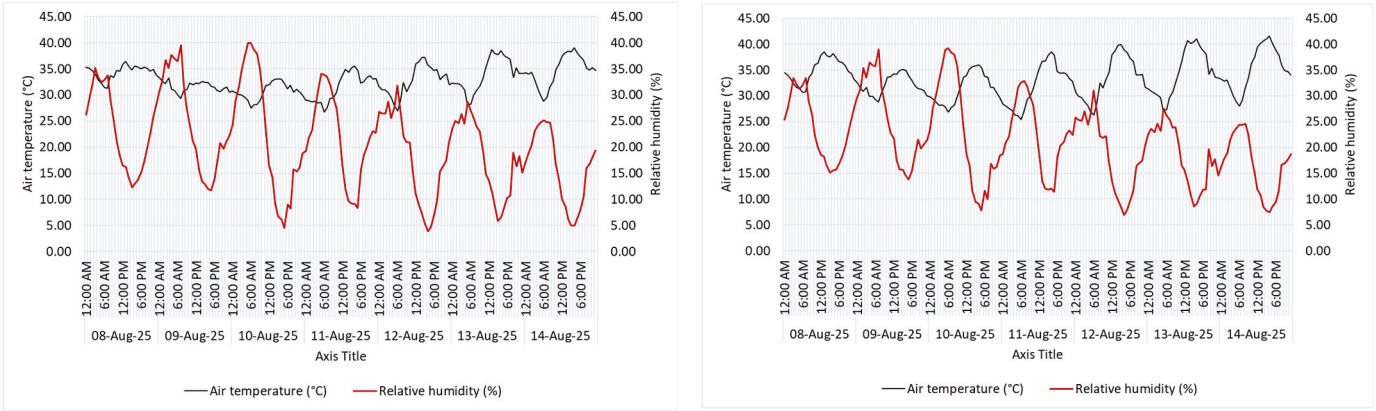
Table 1. Assumptions, boundary conditions, and characterization of building simulation data.

Item	Specification
Geographic location	Jeddah City, Saudi Arabia
Climate	Hot desert climate (BWh) according to the Köppen–Geiger system; hot and dry maritime subzone
Data source and year of simulation	(KAUST) weather station, 2024
Building type	Family residence
Floor area (m^2)	272
No. of floors	Ground floor and first floors
Floor height (m)	3.5
Orientation	Northeast
Occupancy	Six people
Window glazing	6 mm single clear glazing
Window-to-wall ratio	14%
Lighting (Lux)	400
HVAC	Split wall mounted
Lighting power (LED)	Gents' and ladies' majlis: 152 W each; living/dining: 200 W; bedrooms: 152 W; kitchen: 120 W; toilets: 20 W
Equipment load (TV/VCR, PC)	Gents' and ladies' majlis: 5 W/m^2 each; living/dining: 7 W/m^2; bedrooms: 7 W/m^2; kitchen: 30 W/m^2 [29]
Cooling/heating setpoints (°C)	24 °C/16 °C

2.4. Field Measurements

Figure 3 illustrates the variations in air temperature and relative humidity over seven days in two different settings. In Figure 3a, representing the gents' majlis, air temperature fluctuates between approximately 23 °C during the early morning and 44 °C during midday, reflecting the impact of solar radiation on indoor conditions. Correspondingly, relative humidity ranges from about 15% at midday to 40% in the early morning, showing a strong inverse relationship with air temperature. The observed decrease in humidity during peak

temperatures can be attributed to the increased air capacity to hold moisture at higher temperatures. At the same time, the reverse trend during cooler hours is likely due to reduced evaporation and lower moisture-holding capacity.



(**a**) (**b**)

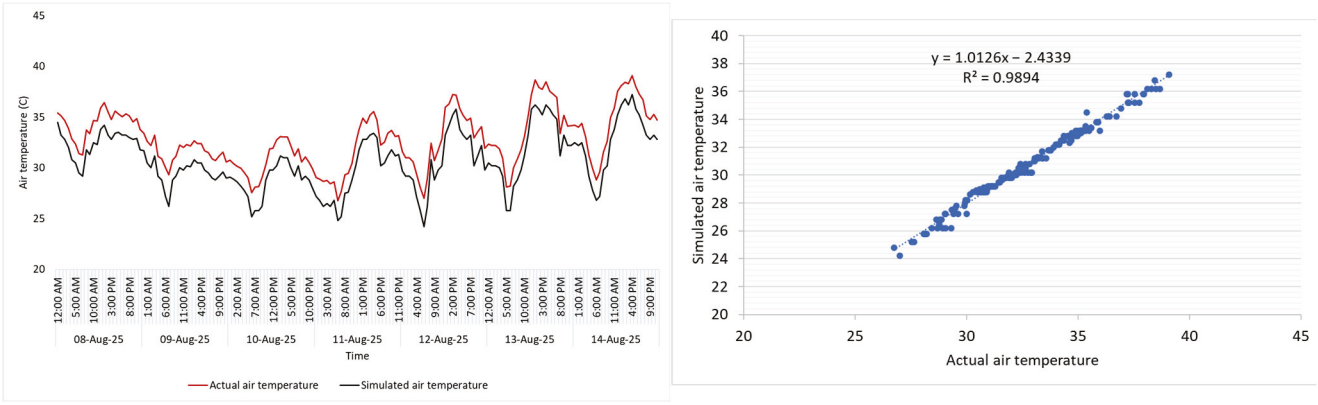
Figure 3. The field measurements in terms of air temperature and relative humidity for (**a**) gents' majlis and (**b**) ladies' majlis.

Figure 3b, representing the ladies' majlis, demonstrates similar trends but with slight differences in magnitude. Air temperatures range from approximately 24 °C to 43 °C, and relative humidity varies between 16% and 39%, indicating a marginally narrower range of variation compared to the gents' majlis. These differences could be linked to variations in insulation, ventilation, or the proximity of the space to external heat sources. The diurnal nature of the fluctuations in both spaces underscores the influence of external climatic conditions and solar radiation.

2.5. Model Validation

Validating the model is a critical step before advancing to further analyses, as it ensures reliability and minimizes discrepancies between predicted and actual performance. Verifying the house model's accuracy involved comparing simulated outputs against measured data. This validation was carried out in two distinct steps: first, a check of thermal performance, and second, an analysis of energy use. The thermal validation specifically examined how closely the model's temperature forecasts matched actual indoor temperatures during occupancy periods. Meanwhile, energy consumption validation examined the accuracy of the modeled energy use by comparing the predicted total energy consumption with actual electricity bill data. The thermal validation was carried out in August 2023 when the ladies' and gents' majlis were used. To record indoor temperature variations, iButton data loggers (DS1921H-F5 Thermochron) (Analog Devices, CA, USA) were deployed, capturing hourly temperature readings throughout the study period.

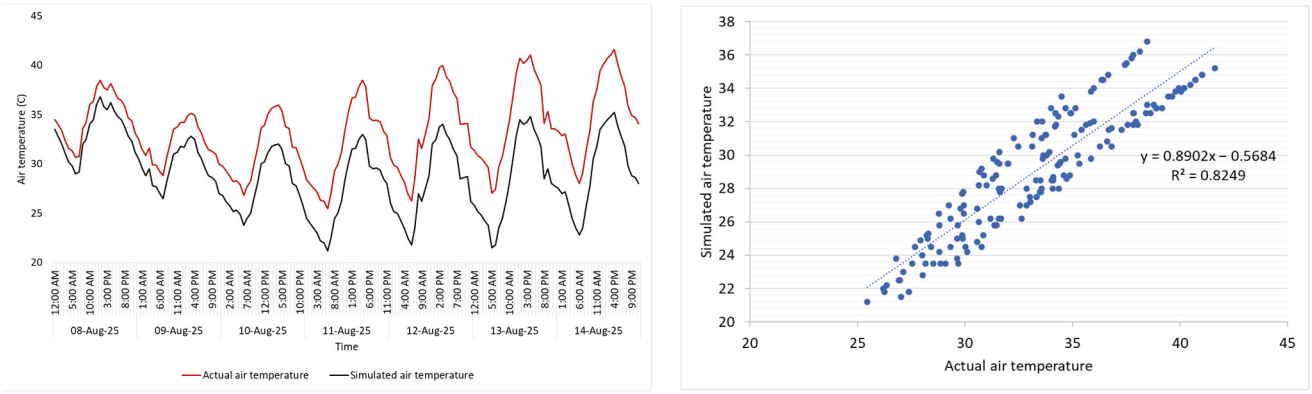
The validation results demonstrate the robust performance of the temperature simulation model for both the gents' and ladies' majlis. In the gents' majlis (Figure 4), the simulated and observed temperature profiles exhibit strong agreement throughout the validation period. The model accurately captures peak and trough variations, with minimal deviations occurring only under extreme thermal conditions. Statistical analysis reveals an exceptionally high coefficient of determination ($R^2 = 0.9894$), confirming near-perfect predictive accuracy. The regression equation ($y = 1.0126x - 2.4339$) indicates a marginal overprediction at lower temperatures but maintains high reliability across the operational range.



(**a**) (**b**)

Figure 4. Model validation results for air temperature in the gents' majlis. (**a**) observed versus simulated temperature profiles. (**b**) scatter plot demonstrating the predictive accuracy of the simulation.

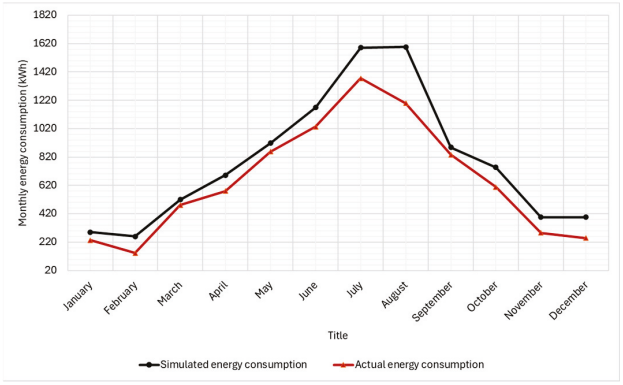
For the ladies' majlis (Figure 5), the model similarly achieves strong agreement, though minor discrepancies arise during periods of significant thermal fluctuation. The scatter plot yields an R^2 of 0.8249, indicating slightly reduced but still robust predictive performance compared to the gents' majlis. The regression relationship ($y = 0.9802x - 0.5684$) suggests a slight underestimation at higher temperatures. The performance variation between the two spaces may stem from differences in occupancy dynamics, thermal load distribution, or ventilation characteristics.



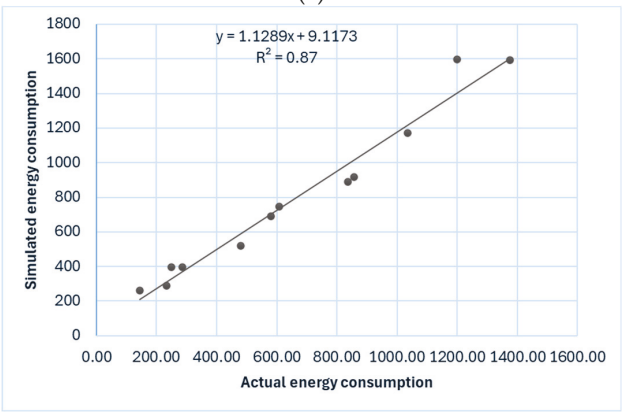
(**a**) (**b**)

Figure 5. Model validation results for air temperature in the ladies' majlis. (**a**) observed versus simulated temperature profiles. (**b**) scatter plot demonstrating the predictive accuracy of the simulation.

Figure 6 compares the simulated indoor temperatures with actual measurements for the ladies' and gents' majlis. The results indicate a strong alignment between the two datasets. A statistical evaluation was conducted to quantify the differences, revealing R^2 values of 0.72 for the ladies' majlis and 0.874 for the gents' majlis. The notable discrepancy observed in the thermal performance of the ladies' majlis can be attributed to its southern and western orientation, which is more exposed to solar heat gain compared to the northern and eastern orientation of the gents' majlis. This difference in exposure results in higher thermal loads on the ladies' majlis facades, contributing to greater deviations between measured and simulated temperatures. Despite being subjected to identical external weather conditions, the orientation of the ladies' majlis amplifies its vulnerability to solar radiation, particularly during peak afternoon hours when the west-facing facade experiences direct sunlight.



(**a**)



(**b**)

Figure 6. Validation for the energy consumption (**a**) comparison between actual and simulated output; (**b**) correlation between actual values and their corresponding simulated values.

Furthermore, the model's energy efficiency, which considered the combined consumption of HVAC, lighting, and miscellaneous equipment, was validated by comparing the simulated energy totals against real-world electricity bill data. The estimated energy consumption was derived from the building's lighting system, material properties, climate control settings, and environmental conditions. Following ASHRAE Guideline 14 standards, the model's accuracy was validated using the Coefficient of Variation of Root Mean Square Error CV(RMSE) and Normalized Mean Bias Error (NMBE). These metrics were chosen for their reliability as standardized performance indicators. The guideline recommends thresholds of 30% for CV(RMSE) and 10% for NMBE for monthly calibration, ensuring the model's calibration aligns with established accuracy criteria [32].

Monthly energy consumption values from the simulation were then compared with recorded electricity usage, as illustrated in Figure 6a. The model's performance was assessed following ASHRAE Guideline 14, utilizing CV(RMSE) and NMBE as evaluation metrics. The CV(RMSE) was determined to be 22.4%, well within the recommended threshold of 30% for monthly calibration, indicating an acceptable level of variability in prediction errors. In contrast, the NMBE was calculated at −18.6%, surpassing the guideline's 10% benchmark and indicating a systematic trend of overprediction. This bias was particularly evident during winter months, such as February and December, potentially reflecting an overestimation of heating loads or infiltration rates. Despite the deviation in NMBE, the model demonstrated a robust R^2 value of 0.87 and compliance with the CV(RMSE) criterion, affirming its overall reliability for energy performance evaluation (Figure 6b). The differences between actual and simulated energy consumption can largely be attributed to assumptions made in the simulation model, particularly regarding occupancy schedules.

These assumptions were based on typical Saudi household routines but may not fully reflect actual occupant behavior. Further refinement of thermal assumptions could help mitigate the identified bias.

2.6. Thermal Properties of the Proposed Advanced Glazing Options

This research investigates the effect of various glazing configurations on the cooling energy requirements of a typical residential building in Jeddah. The thermal characteristics of the construction materials used in the simulations were obtained from the guidelines outlined in the Saudi Building Code (SBC-602) [33]. The specifications of the nanogel were derived from the previous literature [2] with slight adjustments. Figure 7 illustrates cross-sectional diagrams of the six analyzed PC window configurations. The configurations analyzed include a baseline case (BC) featuring standard clear glass and six optimized options (O1–O6), which integrate advanced technologies such as PC glazing with air gaps and aerogel-based glazing. Table 2 provides a comprehensive overview of the specifications for each configuration, outlining their thermal properties and design features. The BC serves as a reference point, utilizing standard clear glass without any advanced thermal insulation features. This glazing type is characterized by high thermal transmittance and a high SHGC, making it less effective at mitigating heat gains. It is used as the benchmark to evaluate the thermal performance enhancements offered by the other configurations. The PC glazing configurations (O1–O3) are designed to improve thermal performance by incorporating two layers of PC separated by air gaps of varying thickness. These air gaps function as insulating layers, reducing heat transfer through the glazing. O1 incorporates a 12 mm air gap, resulting in modest improvements in thermal insulation compared to the baseline case. O2 features a 24 mm air gap, which provides enhanced insulation and greater energy savings. O3 utilizes the largest air gap (36 mm), delivering the most effective thermal insulation among the PC options.

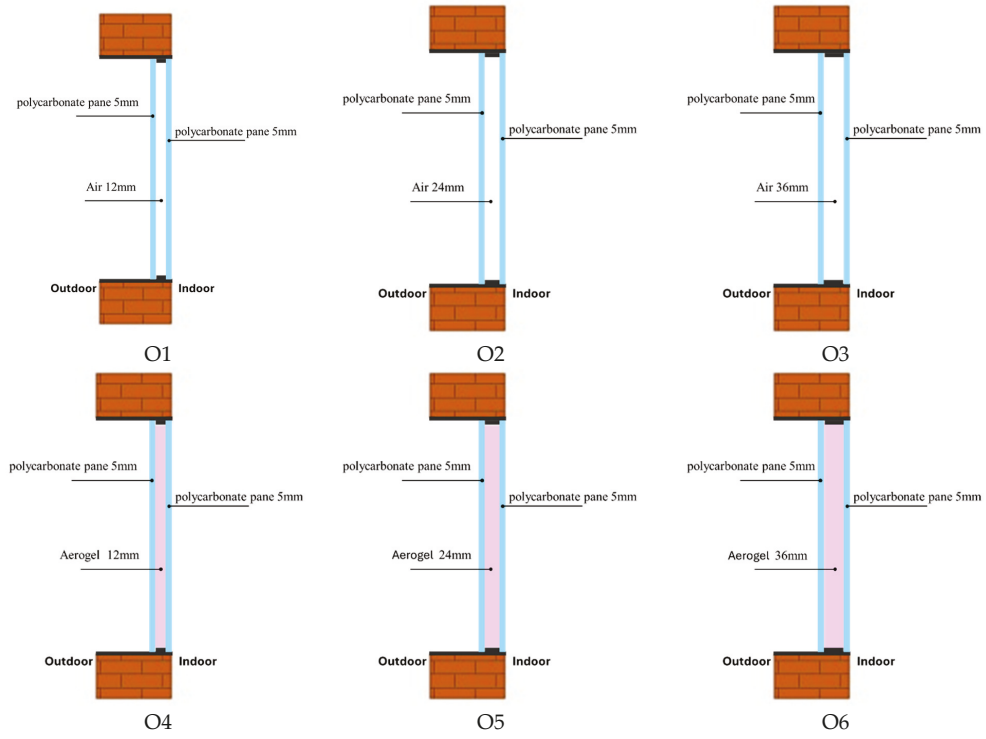


Figure 7. Cross-sectional diagrams of window configurations.

Table 2. Specifications of advanced glazing configurations for windows.

Options	Configuration	(U-Value) [W/m^2·K]	SHGC	VLT [%]
BC	One 5 mm thick PC pane	5.6	0.85	90
O1	Two 5 mm thick PC panes separated by a 12 mm air gap	2.9	0.69	75
O2	Two 5 mm thick PC panes separated by a 24 mm air gap	2.5	0.6	71
O3	Two 5 mm thick PC panes separated by a 36 mm air gap	2	0.55	63
O4	Two 5 mm thick PC panes separated by a 12 mm aerogel	1.42	0.44	55
O5	Two 5 mm thick PC panes separated by a 24 mm aerogel	1.15	0.37	43
O6	Two 5 mm thick PC panes separated by a 36 mm aerogel	0.9	0.3	38

The aerogel-based glazing configurations (O4–O6) utilize aerogel, a highly porous material known for its extremely low thermal conductivity, to maximize thermal insulation. These configurations demonstrate superior energy performance compared to the baseline case and the PC alternatives. O4 features a 12 mm aerogel layer, significantly improving insulation compared to the baseline case and PC configurations. O5 doubles the aerogel thickness to 24 mm, further enhancing insulation and achieving substantial energy savings throughout the year. O6 represents the most advanced configuration, with a 36 mm aerogel layer offering the highest level of insulation and the lowest cooling energy requirements. Each glazing configuration was evaluated based on its thermal transmittance (U-value), SHGC, and visible light transmission (VLT). These parameters determine the glazing's ability to regulate heat transfer, minimize solar heat gain, and maintain adequate natural light levels indoors. Advanced configurations, particularly O5 and O6, are likely enhanced with low-emissivity coatings and optimized insulation properties, enabling superior thermal performance. This systematic analysis provides valuable insights into the potential of advanced glazing technologies to improve energy efficiency and reduce cooling loads in hot climates like Jeddah.

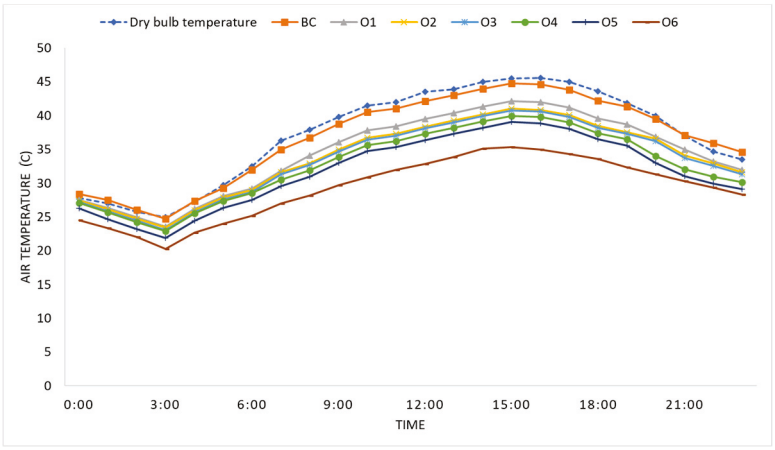
Then, further investigation has been conducted to explore the effect of both U-value and SHGC on cooling energy demand separately. In this regard, a selective double-glazed unit (DGU) (U = 1.5 W/m^2·K, SHGC = 0.35) has been set as a baseline benchmark to be compared to a low-U configuration (U = 0.7 W/m^2·K, SHGC = 0.35) and a low-SHGC configuration (U = 1.5 W/m^2·K, SHGC = 0.25). All these alternatives were evaluated in comparison to the most optimal solution identified during the initial phase of the investigation.

3. Results

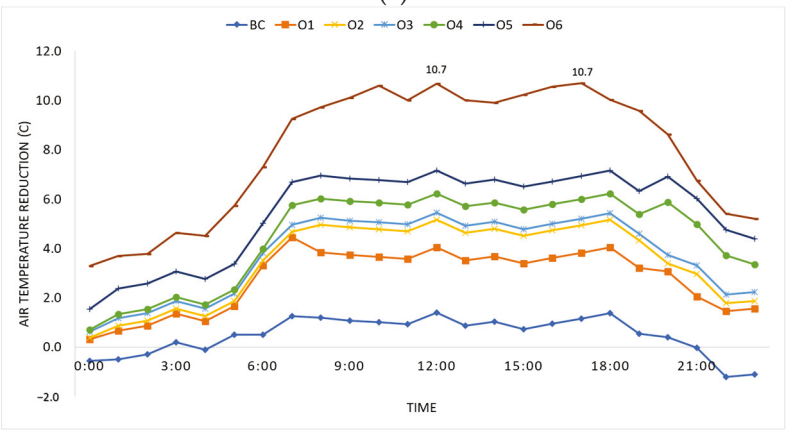
A representative Saudi residential building in Jeddah was simulated to evaluate the thermal performance of PC window glazing. The case of BC is employed as a reference for comparative analysis. Subsequent investigations isolated the effects of U-value and solar heat gain coefficient (SHGC) on cooling energy demand. A selective DGU served as the baseline, against which two variations were tested: (1) a low-U configuration and (2) a low-SHGC configuration. These were compared to the optimal solution identified in preliminary simulations.

3.1. The Influence of the Proposed Advanced Glazing Options on Indoor Air Temperature

The ladies' majlis was selected to examine the impact of the proposed glazing options due to its high occupancy during daytime compared to other spaces. Additionally, its southern orientation results in continuous exposure to direct solar radiation throughout the day, making it a suitable candidate for evaluating thermal performance and glazing effectiveness. The results demonstrate significant improvements in indoor thermal performance for all investigated glazing options (O1–O6) compared to the base case (BC), as shown in Figure 8a. The base case, featuring a standard clear PC, exhibits the highest indoor air temperatures across all hours, reflecting its high U-value and SHGC. Optimized options, however, progressively reduce indoor temperatures, with the most substantial reductions achieved by the aerogel-based configurations (O4–O6). At peak outdoor temperature (around 15:00), the base case records an indoor air temperature of 45.53 °C. O1 reduces this to 44.81 °C (0.72 °C reduction), while the maximum temperature reduction of 10.7 °C was recorded for O6, occurring at 12:00 and 17:00 (Figure 8b). During early morning (03:00), when outdoor temperatures are lower, O6 still shows a notable improvement, reducing indoor temperatures from 24.94 °C (BC) to 20.30 °C, a 4.64 °C reduction (18.6%). Over the day, BC's average indoor air temperature is approximately 38.43 °C. In contrast, O6 achieves an average temperature of 30.09 °C, translating to a daily reduction of 8.34 °C, or approximately 21.7%. PC options (O1–O3) also offer meaningful improvements, with daily average reductions ranging from 2.86 °C for O1 (7.4%) to 4.73 °C for O3 (12.3%).



(**a**)



(**b**)

Figure 8. Hourly thermal performance in the ladies' majlis: (**a**) indoor air temperature; (**b**) the air temperature reduction compared to the BC.

PC glazing with air gaps (O1–O3) provides incremental enhancements, with larger air gaps (e.g., 36 mm in O3) yielding more effective insulation. This results in temperature reductions of up to 5.47 °C at specific hours. Aerogel-based glazing (O4–O6) significantly outperforms PC options owing to its superior thermal insulation properties. For instance, O6 consistently maintains indoor temperatures below 33 °C throughout the late afternoon, a critical period for occupant comfort. The data underscores the critical role of advanced glazing systems in mitigating indoor heat gains during hot summer days. While PC options provide moderate enhancements, aerogel-based glazing demonstrates the highest efficacy, with O6 showing an average temperature reduction exceeding 20% relative to the base case. These results highlight the potential of advanced glazing technologies in enhancing indoor thermal comfort in hot climates like Jeddah.

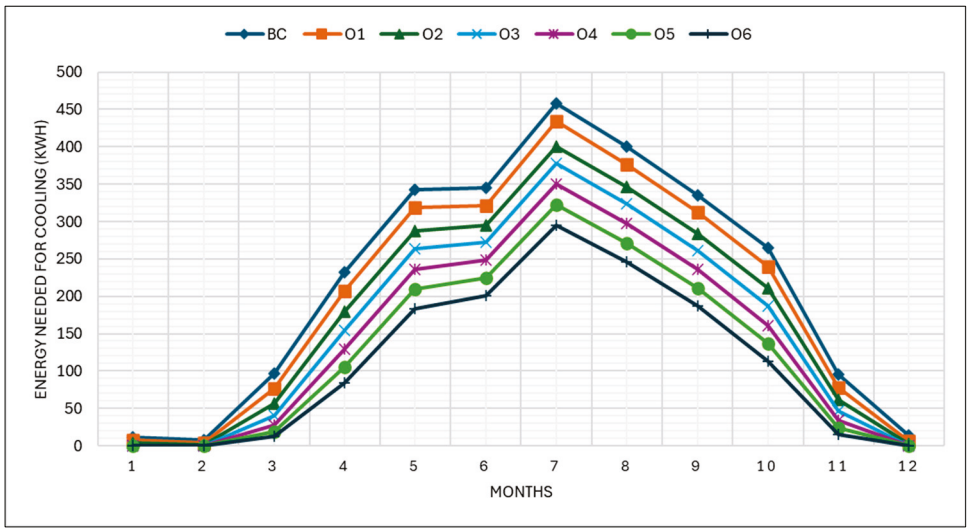
3.2. Evaluating the Impact of PC Windows on Cooling Energy Consumption

The study examines the impact of different glazing configurations (BC, O1–O6) on the cooling energy requirements of a typical family residence in Jeddah, highlighting their performance across monthly and annual scales. Cooling energy demand exhibits substantial variation throughout the year, with peak values observed during the summer months (May to August) and minimum levels during winter (November to February), as shown in Figure 9a. Using standard clear glass, the base case (BC) consistently records the highest energy demand, reaching approximately 458 kWh in July. This indicates the limitations of traditional clear glass in reducing solar heat gains in Jeddah's hot climate.

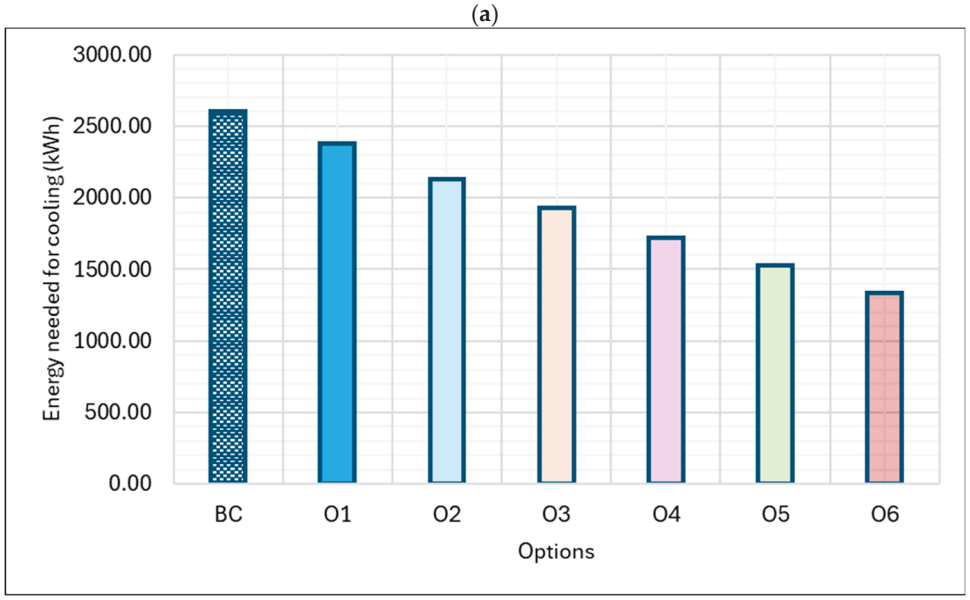
PC glazing (O1–O3), featuring air gaps of different thicknesses, shows noticeable energy efficiency improvements compared to the base case. O1, which has a 12 mm air gap, reduces monthly energy demand by 5–10%, while O2 (24 mm air gap) and O3 (36 mm air gap) provide reductions of up to 20–25% during the summer. These findings emphasize the importance of increasing air gap thickness to enhance thermal insulation. Superior performance is observed in aerogel-based glazing configurations (O4–O6), which outperform the PC alternatives. O6, with a 36 mm aerogel layer, achieves the lowest cooling energy demand, reducing peak summer consumption by approximately 35% compared to the base case.

On an annual scale, cooling energy demand consistently decreases as glazing configurations advance from BC to O6. The base case registers the highest annual cooling energy requirement at 2602.27 kWh, while O6 demonstrates the most significant reduction, requiring only 1337.63 kWh (Figure 9b). This substantial decrease underscores the effectiveness of advanced glazing technologies in mitigating heat gain through windows, thereby reducing cooling loads throughout the year. Aerogel-based options consistently maintain the lowest energy requirements, even during winter when cooling demands are naturally lower.

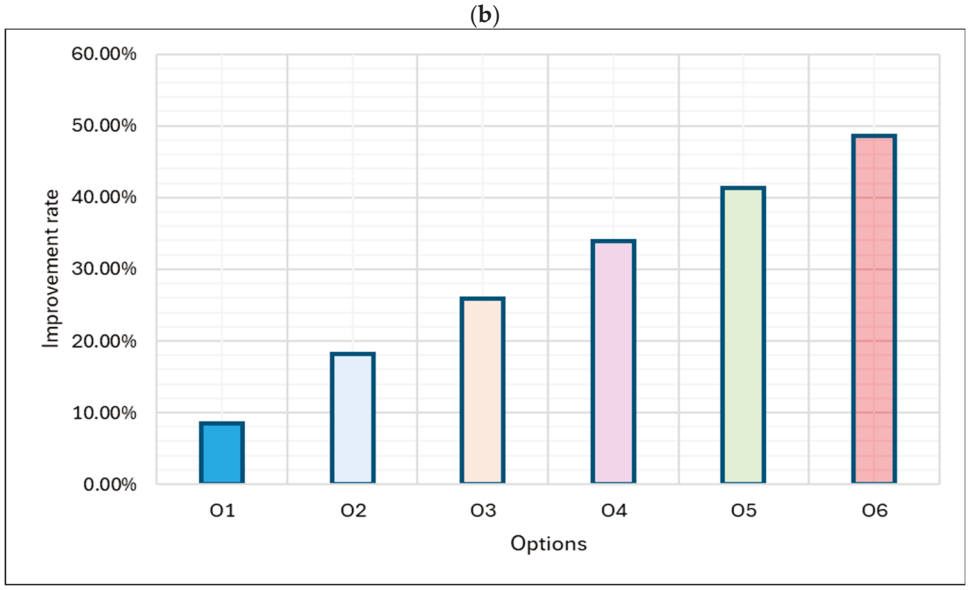
The improvement rate, expressed as the percentage reduction in energy demand relative to the base case, highlights the progressive benefits of optimized glazing technologies. O1 achieves a modest improvement rate of 8.47%, indicating limited thermal performance enhancement compared to BC. Improvement rates increase with advanced configurations, with O2, O3, and O4 achieving 18.22%, 25.93%, and 33.84%, respectively. Aerogel-based options O5 and O6 exhibit the highest improvement rates, achieving reductions of 41.37% and 48.60%, respectively (Figure 9c). These results emphasize the significant energy savings associated with high-performing glazing systems.



(**a**)



(**b**)

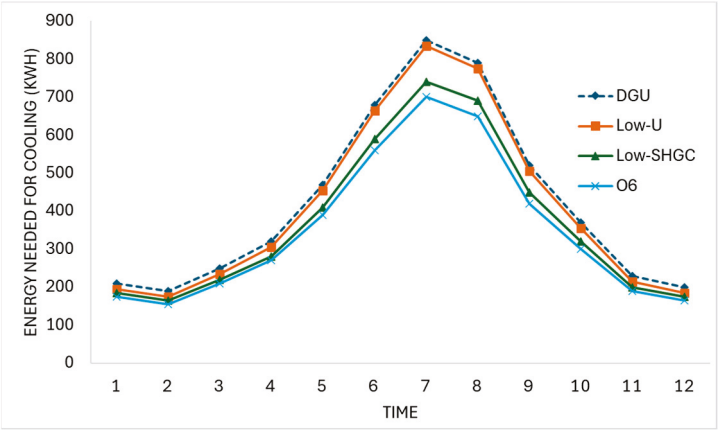


(**c**)

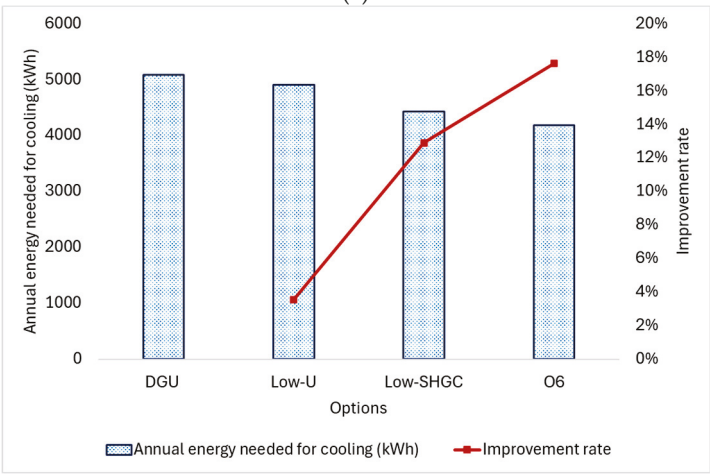
Figure 9. The energy required for cooling: (**a**) monthly results; (**b**) annual results; (**c**) improvement rate.

The superior performance of advanced glazing options can be attributed to their ability to regulate solar heat gain, thermal transmittance (U-value), and visible light transmission. The considerable difference between BC and O6 reflects the combined optimization of these parameters. O5 and O6 likely incorporate low-emissivity coatings and advanced insulation layers, which minimize energy transfer and enhance thermal comfort. While premium solutions like O5 and O6 align with energy-efficient design principles, their feasibility depends on initial costs, material availability, and local climatic conditions. Intermediate options (O2–O4) provide cost-effective alternatives, demonstrating that incremental enhancements in glazing specifications contribute to measurable energy savings while reducing operational costs and carbon emissions.

To elucidate the individual contributions of U-value and SHGC to cooling energy demand, this study expanded its analysis by comparing the most effective option (O6) with four critical window configurations. These include a baseline selective DGU ($U = 1.5\ W/m^2 \cdot K$, SHGC = 0.35), representing commercially available low-emissivity glazing; a low-U configuration ($U = 0.7\ W/m^2 \cdot K$, SHGC = 0.35), designed to evaluate thermal insulation effects; a low-SHGC configuration ($U = 1.5\ W/m^2 \cdot K$, SHGC = 0.25), which isolates the influence of solar heat gain reduction; and an aerogel-enhanced glazing system O6 ($U = 0.9\ W/m^2 \cdot K$, SHGC = 0.3) that combines both attributes. As illustrated in Figure 10a, the analysis revealed distinct trends in monthly and annual cooling energy requirements.



(**a**)



(**b**)

Figure 10. Comparative cooling energy performance: (**a**) monthly energy demand; (**b**) annual savings and the rate of improvement.

The results demonstrate that SHGC is the dominant factor influencing thermal performance in hot climates. The low-SHGC configuration achieved cooling energy savings of 12–18% compared to the baseline DGU, closely matching the performance of the aerogel system despite the latter's superior U-value (Figure 10b). This finding underscores that SHGC reduction accounts for approximately 80% of the total cooling energy savings, with U-value improvements contributing a modest 2–5% increment. The baseline selective DGU delivers 80% of the energy benefits of the aerogel glazing at a substantially lower cost, establishing it as a practical and cost-effective solution for most applications.

Nevertheless, the aerogel glazing exhibits a notable trade-off. Its lower U-value leads to a 25% reduction in nocturnal cooling capacity compared to conventional glazing, potentially increasing mechanical cooling demand during early morning hours. These results affirm that prioritizing SHGC optimization has the most significant impact on energy savings in hot climates, while U-value enhancements provide secondary benefits.

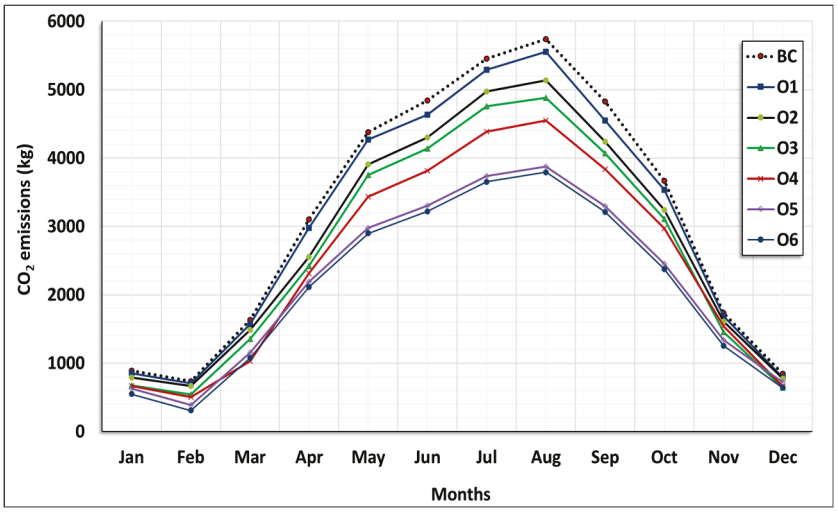
3.3. The Effects of Proposed Advanced Glazing Options on the Operational CO_2 Emissions

Figure 11a showcases monthly CO_2 emissions for the base case (BC) and six optimized options (O1–O6) across all months for the investigated building in Jeddah. The annual emissions for BC total 37,859 kg CO_2, serving as the reference point for assessing the improvements achieved by the optimized options. Across all options, a consistent reduction in emissions is observed, with O6 achieving the highest improvement rate of 33.7%, corresponding to an annual CO_2 reduction of 12,754.3 kg compared to BC.

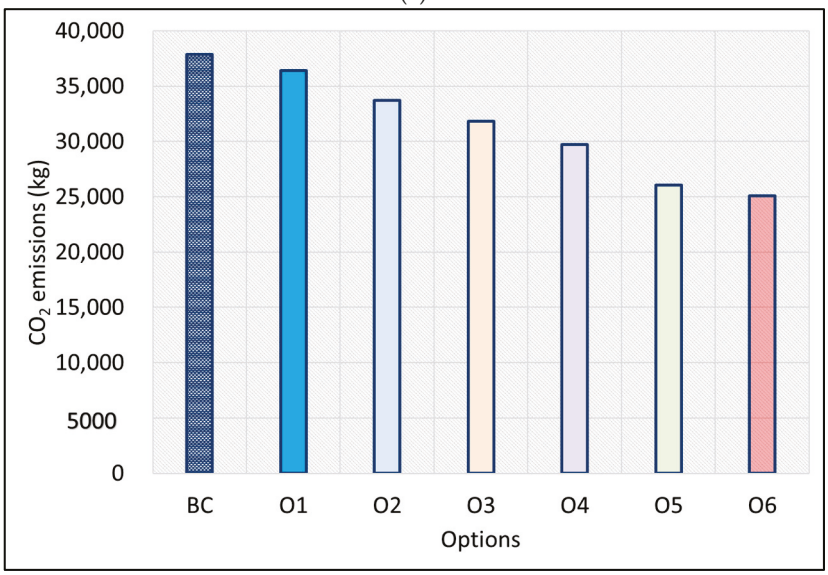
Examining the monthly performance, the optimized options demonstrate varying levels of effectiveness. For January, the CO_2 reduction ranges from 39.90 kg in O1 (a 4.47% reduction) to 342.61 kg in O6 (a 38.42% reduction). In July, a peak cooling demand month, BC emits 5451.36 kg CO_2, whereas O6 achieves a substantial reduction of 1795.59 kg (32.96% reduction), underscoring the effectiveness of O6 in high-demand months. The improvement trend remains consistent throughout the summer, with August showing reductions from 187.7 kg in O1 (3.27% improvement) to 1946.71 kg in O6 (33.9% improvement). These figures highlight the superior performance of O6 in minimizing emissions during critical periods of cooling demand.

On an annual scale, all options achieve significant cumulative reductions, as shown in Figure 11b. O1 reduces emissions by 1447.87 kg (3.8% improvement), indicating modest gains over BC. Meanwhile, O4, with an annual reduction of 8144.28 kg, achieves a notable 21.5% improvement. The impact of O6 is particularly noteworthy, as it combines efficiency enhancements across all months to deliver the most pronounced reductions (Figure 11c). These results reflect the scalable benefits of each option and emphasize the substantial potential of advanced strategies like those employed in O6.

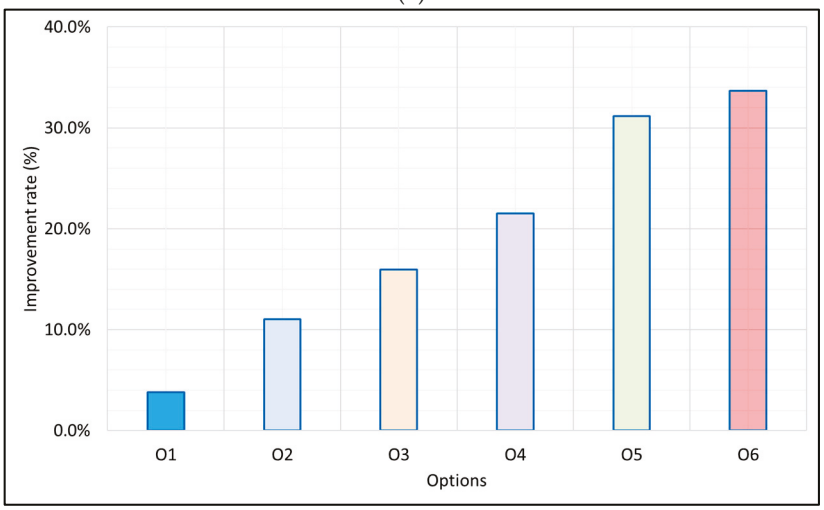
The analysis demonstrates a clear hierarchy of CO_2 emission reductions across the six options. While all options achieve meaningful improvements over the base case, O6 stands out as the most effective solution, offering the highest monthly and annual reductions. The results highlight the critical role of adopting advanced energy efficiency measures to mitigate CO_2 emissions in high-demand climates like Jeddah's, contributing to sustainable environmental goals. These findings underscore the importance of scaling up interventions such as those exemplified by O6 to maximize emissions reduction potential across diverse contexts.



(**a**)



(**b**)



(**c**)

Figure 11. CO_2 emissions: (**a**) monthly amount; (**b**) annual amount; (**c**) improvement rate.

The analysis of annual energy consumption and CO_2 emissions across various glazing configurations reveals significant improvements in energy efficiency and environmental

impact. The base case (BC) exhibited the highest energy consumption at approximately 2602.27 kWh and CO_2 emissions of 37,859.27 kg, underscoring the inefficiency of standard glazing in hot climates. In contrast, advanced options (O1 to O6) demonstrated progressively lower energy needs and emissions, with O6 achieving a remarkable energy saving of 1264.65 kWh (48.60% improvement) and a CO_2 reduction of 12,754.30 kg (33.69%). The regression analysis indicated a strong correlation between energy savings and CO_2 reduction, with an R-squared value of 0.9863, suggesting that 98.63% of the variability in CO_2 reductions can be attributed to energy savings (Figure 12). The derived regression equation showed that each kilowatt-hour saved corresponds to an approximate reduction of 11.25 kg in CO_2 emissions, emphasizing the effectiveness of advanced glazing technologies. These findings support the integration of innovative glazing materials in residential buildings, particularly in regions like Jeddah, Saudi Arabia, aligning with the sustainability goals outlined in Saudi Vision 2030. Future research should focus on the long-term performance of these technologies and their combined effectiveness with other energy-saving measures.

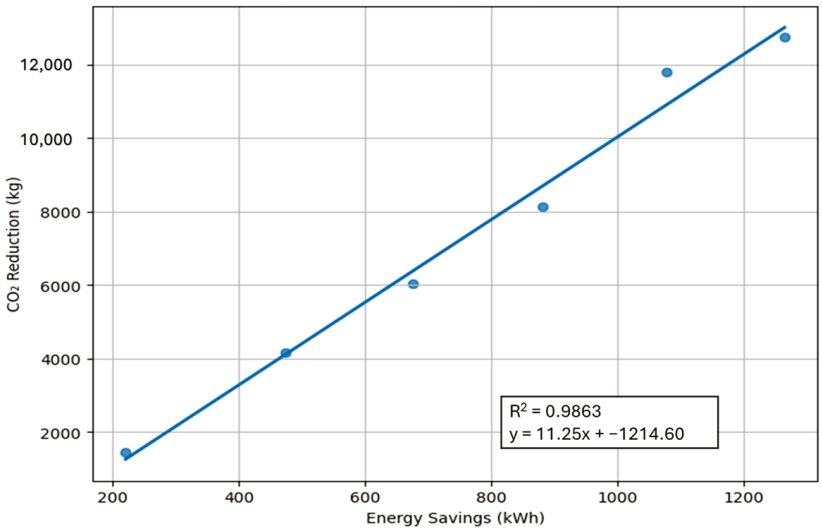
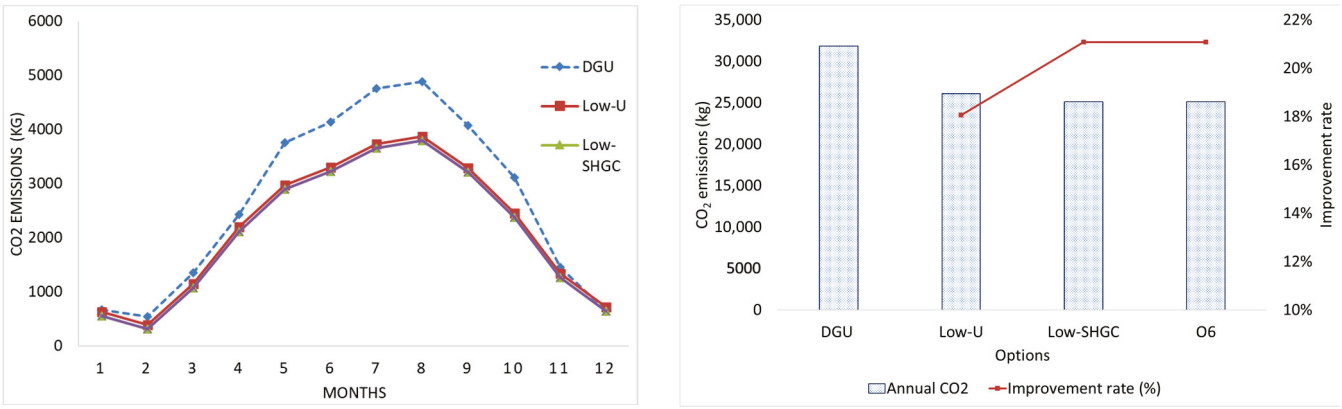


Figure 12. The correlation between energy savings and CO_2 reduction.

To enhance the study and provide more nuanced insights, a comparative analysis of CO_2 emissions was conducted to isolate the individual contributions of U-value and SHGC. The comparative CO_2 emissions analysis (Figure 13) reveals critical insights into the monthly and annual glazing performance in Jeddah's climate. The findings demonstrate that SHGC reduction drives the majority of performance gains in hot climates. The low-SHGC configuration achieved a 21.08% annual reduction in emissions, closely matching the performance of the aerogel-enhanced glazing, while the low-U configuration achieved a lower reduction of 18.06%. This 3.02 percentage point difference underscores the diminishing returns of U-value improvements below 1.5 $W/m^2 \cdot K$, particularly during cooling-dominated periods when SHGC contributes approximately 87% of emissions reductions. The baseline selective DGU emerges as a practical and cost-effective benchmark. It delivers 85% of the annual CO_2 emissions savings attributed to the aerogel glazing at a significantly lower cost. Moreover, its moderate U-value facilitates nocturnal heat dissipation, an essential factor for buildings located in climates with significant diurnal temperature variations.



(**a**) (**b**)

Figure 13. Comparative CO_2 emissions analysis: (**a**) monthly emissions distribution across glazing configurations; (**b**) annual emissions totals and improvement rates relative to the baseline DGU.

4. Discussion

This study thoroughly assesses advanced glazing technologies and their influence on the energy performance of residential buildings in Jeddah, Saudi Arabia. The results indicate a distinct advantage of using innovative glazing solutions compared to conventional methods in this hot climatic region. Analysis of indoor air temperatures revealed a significant reduction in heat gain when employing advanced glazing systems, particularly those integrating aerogels. A decrease of more than 20% in average daily indoor temperature, relative to the base case, was observed with the most efficient configuration (O6), highlighting the effectiveness of aerogel as a high-performance insulation component. This superior performance directly results from aerogel's unique nanostructure, which effectively minimizes all three heat transfer mechanisms while maintaining adequate visible light transmission [34]. These findings align with prior research confirming aerogel's effectiveness in reducing cooling loads in hot climates [2,35–38]. While PC glazing with air gaps (O1–O3) also improved thermal performance, the temperature reduction was less pronounced, suggesting that increasing air gap thickness enhances insulation but not to the extent achieved by aerogel.

Further evaluation of cooling energy consumption reinforced the benefits of advanced glazing. A progressive reduction in monthly and annual cooling energy demand was observed as configurations advanced from the base case to optimized solutions. Notably, O6 exhibited the highest energy savings, highlighting its potential to significantly lower cooling energy requirements in residential buildings. This result aligns with broader research advocating advanced materials to enhance energy efficiency [37–40]. The observed improvement in energy efficiency with increased air gap thickness in PC glazing is consistent with thermal insulation principles, where air gaps act as barriers to heat transfer. Additionally, the study quantified the effect of advanced glazing on CO_2 emissions, a crucial factor in climate change mitigation. The findings revealed a direct correlation between energy savings and CO_2 emission reductions, with O6 achieving the most substantial annual decrease in emissions. The high R-squared value confirms this relationship, emphasizing the environmental advantages of energy-efficient glazing technologies. The derived regression equation, which estimates CO_2 reduction per kWh saved, is a valuable metric for evaluating the environmental impact of energy conservation strategies in buildings. For Saudi Arabia's oil-dependent electricity sector, where each kWh saved prevents approximately 0.7 kg of CO_2 emissions [41], these findings underscore the critical role of building technologies in national climate mitigation strategies. Model validation

using field measurements and electricity bill data enhances the reliability of the study's conclusions. Minor discrepancies between simulated and actual energy consumption were primarily due to assumptions regarding occupancy schedules, a standard limitation in building energy simulations.

Additionally, this study conclusively demonstrates that in Jeddah's hot, arid climate, SHGC optimization yields substantially greater energy and emissions savings than U-value improvements, with SHGC reductions accounting for 87% of cooling energy savings. The selective double-glazed baseline configuration (U = 1.5 W/m^2 K, SHGC = 0.35) delivered 85% of the aerogel glazing's performance at a lower cost, while the low-SHGC option (U = 1.5 W/m^2 K, SHGC = 0.25) achieved comparable CO_2 reductions (21.08%) to the aerogel system, confirming SHGC's dominant role in thermal performance. Notably, the aerogel glazing's superior U-value (0.9 W/m^2 K) reduced nocturnal cooling capacity by 25%, revealing an important trade-off for naturally ventilated designs. These findings establish that for cooling-dominated climates, glazing specifications should prioritize SHGC reduction below 0.3 while maintaining U-values around 1.5 W/m^2 K for optimal cost-performance balance, providing critical guidance for energy codes and sustainable building design in alignment with Saudi Vision 2030 objectives.

The socio-economic feasibility of implementing these advanced glazing solutions in Jeddah requires careful consideration of cost, maintenance, and market readiness. While aerogel-integrated glazing (O6) demonstrates exceptional thermal performance, its high initial cost and specialized installation requirements may limit widespread adoption to high-budget or government-supported projects. DGU presents a balanced middle-ground option, offering substantial energy savings at relatively moderate costs and with familiar installation protocols that align with local construction practices. Polycarbonate (PC) glazing systems with air gaps (O1–O3) emerge as the most immediately viable solution for mass-market adoption, given their competitive pricing, ease of maintenance, and established supply chains in the region. However, our findings suggest that the long-term energy savings of aerogel solutions could justify their higher upfront costs, particularly for projects targeting net-zero energy performance. Strategic policy interventions, such as subsidies for high-performance glazing or green building certification requirements, could accelerate market acceptance of these technologies while supporting Saudi Arabia's Vision 2030 sustainability objectives.

Despite its robust findings, this study has certain limitations. The analysis was restricted to a specific residential building model in Jeddah, potentially limiting the generalizability of results to other building types or climates. Furthermore, the long-term durability and economic viability of advanced glazing technologies were not explicitly examined. Future research could expand on these aspects by investigating diverse building typologies, conducting long-term energy performance monitoring, and performing comprehensive cost-benefit analyses. This study provides strong evidence supporting the efficacy of advanced glazing technologies in enhancing energy efficiency and reducing CO_2 emissions in Jeddah's residential buildings. The findings hold significant implications for building design and policy, particularly in alignment with Saudi Vision 2030's sustainability objectives. Implementing such innovations can contribute to a more sustainable built environment while mitigating the environmental impact of the construction sector.

5. Conclusions

This study presents a systematic analysis of glazing performance in hot, arid climates by evaluating the individual effects of U-value and SHGC through simulation-based investigations. Key conclusions include the following:

- The optimal aerogel glazing configuration, O6, achieved a 48.6% reduction in annual cooling energy consumption, accompanied by a 33.7% decrease in CO_2 emissions while maintaining indoor temperatures 8.3 °C (21.7%) cooler compared to conventional locally used glazing.
- The selective DGU baseline (U = 1.5 W/m^2 K, SHGC = 0.35) established a reliable performance benchmark for comparative analysis, revealing that low-U glazing (U = 0.7 W/m^2 K, SHGC = 0.35) provided moderate energy savings with marginal SHGC trade-offs, while low-SHGC glazing (U = 1.5 W/m^2 K, SHGC = 0.25) was more effective, contributing to 87% of cooling energy savings.
- SHGC reduction emerged as the dominant factor in mitigating cooling loads under extreme climatic conditions, highlighting its critical role in glazing optimization for energy-efficient building design in hot, arid regions.

These findings advance sustainable building design by (1) resolving the confounding effects of U-value and SHGC through controlled parameter variation, (2) providing climate-specific evidence that SHGC optimization should precede U-value improvements, and (3) offering validated performance benchmarks for Saudi Vision 2030's energy efficiency targets. The methodology and results presented here create a framework for evidence-based glazing selection in hot climates while highlighting the need for future research on real-world performance validation and integration with passive cooling strategies. This work particularly emphasizes that while advanced aerogel systems show superior performance, strategic SHGC management in conventional glazing can achieve the most energy savings in typical residential applications.

Author Contributions: Conceptualization, A.R. and M.M.G.; methodology, M.A.A. and A.S.H.A.; software, A.R., M.A.A. and A.S.H.A.; validation, A.S.H.A., M.M.G. and A.R.; formal analysis, A.R. and M.A.A.; investigation, A.S.H.A. and A.R.; resources, M.A.A. and M.M.G.; data curation, A.S.H.A.; writing—original draft preparation, A.S.H.A., M.M.G. and A.R.; writing—review and editing, M.A.A. and M.M.G.; visualization, A.S.H.A. and A.R.; project administration, M.A.A. and A.S.H.A.; funding acquisition, M.A.A. and A.S.H.A. All authors have read and agreed to the published version of the manuscript.

Funding: This work was supported and funded by the Deanship of Scientific Research at Imam Mohammad Ibn Saud Islamic University (IMSIU) (grant number IMSIU-DDRSP2503).

Data Availability Statement: The original contributions presented in this study are included in the article. Further inquiries can be directed to the corresponding author.

Conflicts of Interest: The authors declare no conflicts of interest.

References

1. Saleh, M.A.E. The Integration of Tradition and Modernity: A Search for an Urban and Architectural Identity in Arriyadh, The Capital of Saudi Arabia. *Habitat Int.* **1998**, *22*, 571–589. [CrossRef]
2. Abdelrady, A.; Abdelhafez, M.H.H.; Ragab, A. Use of insulation based on nanomaterials to improve energy efficiency of residential buildings in a hot desert climate. *Sustainability* **2021**, *13*, 5266. [CrossRef]
3. Jelle, B.P.; Hynd, A.; Gustavsen, A.; Arasteh, D.; Goudey, H.; Hart, R. Fenestration of today and tomorrow: A state-of-the-art review and future research opportunities. *Sol. Energy Mater. Sol. Cells* **2012**, *96*, 1–28. [CrossRef]
4. Koebel, M.; Rigacci, A.; Achard, P. Aerogel-based thermal superinsulation: An overview. *J. Sol-Gel Sci. Technol.* **2012**, *63*, 315–339. [CrossRef]
5. Ye, H.; Meng, X.; Long, L.; Xu, B. The route to a perfect window. *Renew. Energy* **2013**, *55*, 448–455. [CrossRef]
6. Chevalier, B.; Hutchins, M.; Maccari, A.; Olive, F.; Oversloot, H.; Platzer, W.; Polato, P.; Roos, A.; Rosenfeld, J.; Squire, T.; et al. Solar energy transmittance of translucent samples: A comparison between large and small integrating sphere measurements. *Sol. Energy Mater. Sol. Cells* **1998**, *54*, 197–202. [CrossRef]

7. Chinnappan, T.; CM, R.; Dhairiyasamy, R.; Rajendran, S. Comparative Analysis of Polycarbonate and Glass Cover Configurations for Enhanced Thermal Efficiency in Flat Plate Solar Collectors for Water Heating. *J. Sol. Energy Res.* **2024**, *9*, 1794–1810.
8. Moretti, E.; Zinzi, M.; Belloni, E. Polycarbonate panels for buildings: Experimental investigation of thermal and optical performance. *Energy Build.* **2014**, *70*, 23–35. [CrossRef]
9. Buratti, C.; Merli, F.; Moretti, E. Aerogel-based materials for building applications: Influence of granule size on thermal and acoustic performance. *Energy Build.* **2017**, *152*, 472–482. [CrossRef]
10. Moretti, E.; Merli, F.; Cuce, E.; Buratti, C. Thermal and acoustic properties of aerogels: Preliminary investigation of the influence of granule size. *Energy Procedia* **2017**, *111*, 472–480. [CrossRef]
11. Buratti, C.; Moretti, E.; Belloni, E. Aerogel plasters for building energy efficiency. *Nano Biotech Based Mater. Energy Build. Effic.* **2016**, 17–40. [CrossRef]
12. Cuce, E.; Cuce, P.M.; Wood, C.J.; Riffat, S.B. Toward aerogel based thermal superinsulation in buildings: A comprehensive review. *Renew. Sustain. Energy Rev.* **2014**, *34*, 273–299. [CrossRef]
13. Buratti, C.; Moretti, E. Silica nanogel for energy-efficient windows. In *Nanotechnology in Eco-Efficient Construction*; Elsevier: Amsterdam, The Netherlands, 2013; pp. 207–235.
14. Buratti, C.; Moretti, E. Nanogel windows. In *Nearly Zero Energy Building Refurbishment: A Multidisciplinary Approach*; Springer: Berlin, Germany, 2013; pp. 555–582.
15. Buratti, C.; Moretti, E.; Belloni, E. Nanogel windows for energy building efficiency. In *Nano and Biotech Based Materials for Energy Building Efficiency*; Springer: Berlin, Germany, 2016; pp. 41–69.
16. Buratti, C.; Moretti, E. Glazing systems with silica aerogel for energy savings in buildings. *Appl. Energy* **2012**, *98*, 396–403. [CrossRef]
17. Gao, T.; Jelle, B.P.; Ihara, T.; Gustavsen, A. Insulating glazing units with silica aerogel granules: The impact of particle size. *Appl. Energy* **2014**, *128*, 27–34. [CrossRef]
18. Reim, M.; Beck, A.; Körner, W.; Petricevic, R.; Glora, M.; Weth, M.; Schliermann, T.; Fricke, J.; Schmidt, C.; Pötter, F. Highly insulating aerogel glazing for solar energy usage. *Sol. Energy* **2002**, *72*, 21–29. [CrossRef]
19. Buratti, C.; Moretti, E.; Zinzi, M. High energy-efficient windows with silica aerogel for building refurbishment: Experimental characterization and preliminary simulations in different climate conditions. *Buildings* **2017**, *7*, 8. [CrossRef]
20. Huang, Y.; Niu, J.-L. Application of super-insulating translucent silica aerogel glazing system on commercial building envelope of humid subtropical climates–Impact on space cooling load. *Energy* **2015**, *83*, 316–325. [CrossRef]
21. Ihara, T.; Gao, T.; Grynning, S.; Jelle, B.P.; Gustavsen, A. Aerogel granulate glazing facades and their application potential from an energy saving perspective. *Appl. Energy* **2015**, *142*, 179–191. [CrossRef]
22. Buratti, C.; Belloni, E.; Palladino, D. Evolutive Housing System: Refurbishment with new technologies and unsteady simulations of energy performance. *Energy Build.* **2014**, *74*, 173–181. [CrossRef]
23. Dowson, M.; Harrison, D.; Craig, S.; Gill, Z. Improving the thermal performance of single-glazed windows using translucent granular aerogel. *Int. J. Sustain. Eng.* **2011**, *4*, 266–280. [CrossRef]
24. Peel, M.C.; Finlayson, B.L.; McMahon, T.A. Updated world map of the Köppen-Geiger climate classification. *Hydrol. Earth Syst. Sci.* **2007**, *11*, 1633–1644. [CrossRef]
25. Abdullah, M.M.A.; Youssef, A.M.; Nashar, F.; AlFadail, E.A. Statistical analysis of rainfall patterns in Jeddah City, KSA: Future impacts. In *Rainfall-Extremes Distribution Properties*; IntechOpen: London, United Kingdom, 2019; pp. 17–33.
26. Alrashed, F.; Asif, M. Analysis of critical climate related factors for the application of zero-energy homes in Saudi Arabia. *Renew. Sustain. Energy Rev.* **2015**, *41*, 1395–1403. [CrossRef]
27. Aldersoni, A.; Albaker, A.; Alturki, M.; Said, M.A. The Impact of Passive Strategies on the Overall Energy Performance of Traditional Houses in the Kingdom of Saudi Arabia. *Buildings* **2022**, *12*, 1837. [CrossRef]
28. Gomaa, M.M.; El Menshawy, A.; Nabil, J.; Ragab, A. Investigating the Impact of Various Vegetation Scenarios on Outdoor Thermal Comfort in Low-Density Residential Areas of Hot Arid Regions. *Sustainability* **2024**, *16*, 3995. [CrossRef]
29. Mohamed, A.F.; Gomaa, M.M.; Amir, A.A.; Ragab, A. Energy, thermal, and economic benefits of aerogel glazing systems for educational buildings in hot arid climates. *Sustainability* **2023**, *15*, 6332. [CrossRef]
30. Tarek, D.; Ahmed, M.M.; Hussein, H.S.; Zeyad, A.M.; Al-Enizi, A.M.; Yousef, A.; Ragab, A. Building envelope optimization using geopolymer bricks to improve the energy efficiency of residential buildings in hot arid regions. *Case Stud. Constr. Mater.* **2022**, *17*, e01657. [CrossRef]
31. Mahmoud, H.; Ragab, A. Impact of urban geometry on cooling loads in Egypt: Case study: A social residential compound in New Aswan city. In Proceedings of the 2020 9th International Conference on Power Science and Engineering (ICPSE), London, UK, 23–25 October 2020; pp. 71–75.

32. Refrigerating American Society of Heating; Engineers Air-Conditioning. *ASHRAE Guideline 14-2023: Measurement of Energy, Demand, and Water Savings*; ASHRAE: Atlanta, GA, USA, 2023.
33. Saudi Building Code National Committee. Saudi Building Energy Conservation Code—Residential SBC 602. 2018. Available online: https://sbc.gov.sa/ar/_layouts/15/SBC.buildingcode/freebrowsingcode.aspx (accessed on 15 December 2023).
34. Baetens, R.; Jelle, B.P.; Gustavsen, A. Aerogel insulation for building applications: A state-of-the-art review. *Energy Build.* **2011**, *43*, 761–769. [CrossRef]
35. Mohamed, A.F.; Amir, A.A.; Ragab, A. The effect of aerogel glazing on daylight and heat gain in school buildings in hot and dry climate. In *Environment, Development and Sustainability*; Springer: Berlin, Germany, 2024; pp. 1–22. [CrossRef]
36. Mahmoud, A.R. Investigating the impact of different glazing types on the energy performance in hot arid climate. *J. Adv. Eng. Trends* **2022**, *42*, 69–84. [CrossRef]
37. Mujeebu, M.A.; Ashraf, N.; Alsuwayigh, A.H. Effect of nano vacuum insulation panel and nanogel glazing on the energy performance of office building. *Appl. Energy* **2016**, *173*, 141–151. [CrossRef]
38. Mujeebu, M.A.; Ashraf, N.; Alsuwayigh, A. Energy performance and economic viability of nano aerogel glazing and nano vacuum insulation panel in multi-story office building. *Energy* **2016**, *113*, 949–956. [CrossRef]
39. Abdelhafez, M.H.H.; Aldersoni, A.A.; Gomaa, M.M.; Noaime, E.; Alnaim, M.M.; Alghaseb, M.; Ragab, A. Investigating the thermal and energy performance of advanced glazing systems in the context of Hail City, KSA. *Buildings* **2023**, *13*, 752. [CrossRef]
40. Aly, A.M.; Hassn, M.H.; Rady, Y.R.A.; Mohammed, A.T. The effect of using nano-materials in external openings on energy consumption in hot desert climate. *JES—J. Eng. Sci.* **2020**, *48*, 468–477. [CrossRef]
41. Dechamps, P. The IEA World Energy Outlook 2022–a brief analysis and implications. *Eur. Energy Clim. J.* **2023**, *11*, 100–103. [CrossRef]

Disclaimer/Publisher's Note: The statements, opinions and data contained in all publications are solely those of the individual author(s) and contributor(s) and not of MDPI and/or the editor(s). MDPI and/or the editor(s) disclaim responsibility for any injury to people or property resulting from any ideas, methods, instructions or products referred to in the content.

buildings

MDPI

Article

Computational Evaluation of a Biomimetic Kinetic Façade Inspired by the Venus Flytrap for Daylight and Glare Performance

Fataneh Farmani [1], Seyed Morteza Hosseini [2,*], Morteza Khalaji Assadi [3] and Soroush Hassanzadeh [4]

[1] Kish International Campus, University of Tehran, Kish 39982-79416, Iran
[2] Department of Architecture, Design and Media Technology, Aalborg University Copenhagen, A.C. Meyers Vænge 15, 2450 Copenhagen, Denmark
[3] Faculty of Architecture, University of Tehran, Tehran 14174-66191, Iran; morteza.khalaji@guest.ut.ac.ir
[4] Department of Architecture and Environmental Design, Iran University of Science and Technology (IUST), Tehran 16846-13114, Iran
* Correspondence: smho@create.aau.dk

Abstract: Centralized daylight control has been extensively studied for its ability to optimize useful daylight while mitigating glare in targeted areas. However, this approach lacks a comprehensive visual comfort framework, as it does not simultaneously address spatial glare distribution, uniform high useful daylight levels across all sensor points, and overheating prevention through regulated annual solar exposure. Nevertheless, decentralized control facilitates autonomous operation of the individual façade components, addressing all the objectives. This study integrates a biomimetic functional approach with building performance simulations by computational design to evaluate different kinetic façade configurations. Through the implementation of parametric modeling and daylight analysis, we have identified an optimal angular configuration (60° for the focal region, 50° for the non-focal region) that significantly increases building performance. The optimized design demonstrates substantial improvements, reducing excessive sunlight exposure by 45–55% and glare incidence by 65–72% compared to other dynamic solutions. The recommended steeper angles achieve superior performance, maintaining high useful daylight illuminance (UDI > 91.5%) while dramatically improving visual comfort. Sensitivity analysis indicates that even minor angular adjustments (5–10°) can induce a 10–15% variation in glare performance, emphasizing the necessity of precise control mechanisms in both focal and non-focal regions of the façade. These findings establish a framework for creating responsive building façades that balance daylight provision with occupant comfort in real-time operation.

Keywords: biomimetic kinetic façade; daylight performance; Venus flytrap; visual comfort; decentralized strategies

1. Introduction

People spend a significant amount of time indoors, where daylighting plays a crucial role in illuminating the space and contributing to the comfort and well-being of occupants [1,2]. The façade acts as an interface that regulates energy flows between indoor and outdoor environments [3–5]. Acting as a mediator between the interior and exterior, the building skin selectively filters external influences, blocking unfavorable ones while

allowing beneficial impacts to enhance indoor environmental quality [6,7]. Demands for diverse building performances have driven a shift from static to dynamic forms in façade design [8,9], as well as to dynamic, technology-driven forms incorporating adaptive features, like integrated sensors and biomimetic designs [7,10]. Variable skins now employ reflective [11–13], transmissive [14,15], and shading capabilities [16,17] to regulate light interaction with indoor spaces, fulfilling functional and control-oriented objectives. Several methodologies have been developed to enhance the responsiveness of kinetic skins to climate change [18–20].

In recent years, biomimicry has gathered significant attention from both industry and academia for its role in developing innovative building technologies inspired by adaptive geometries and mechanisms found in nature [21–25]. Janine [26] defines biomimicry as "the science of studying and imitating nature's designs to address human challenges". For instance, Lidia Badarnah introduced the concept of a "*living envelope*", a bio-inspired system that dynamically responds to environmental stimuli changes to ensure occupant comfort [27]. Similarly, kinetic façades, including biomimetic designs, represent unconventional systems capable of altering their configuration, transforming their structure over time to adapt to changing conditions [2,28,29]. For example, Hosseini et al. (2020) [30] developed a kinetic façade which proposed real-time daylight control management based on sun positioning and occupant movement. A related study drew inspiration from tree morphology to develop a multilayered kinetic façade. While complex geometry enhanced visual comfort and daylight performance, it did not account for occupant positioning in determining centralized versus decentralized control strategies [24]. In contrast, Hosseini et al. (2024) [15] proposed a periodic interactive region inspired by the nanostructure of butterfly wings. Their study emphasized the performance differences between complex and simplified forms, highlighting the importance of focal regions, but overlooked the potential control benefits of non-focal areas in improving overall visual comfort and daylight distribution.

Since the concept of kinetic façades combines elements from nature, technology, and architecture, nature offers a valuable source of inspiration for building sustainable solutions [31]. There are practical examples of integrating movement and materials to develop centralized kinetic façades, such as the Arab World Institute and Al-Bahar Towers [32,33] (Figure 1). While this control system performs adequately in meeting users' visual comfort requirements, it fails to simultaneously provide a glare-free view and excellent daylight performance for all points in the space while reducing solar gains to avoid overheating. Facade centralized systems make decisions based on single sensor points (areas), often neglecting the impact on other areas, resulting in responses that are not adaptive for the entire space. Therefore, it is crucial to review the literature and investigate the performance of centralized and decentralized systems to propose a new form and kinetic control system for façades.

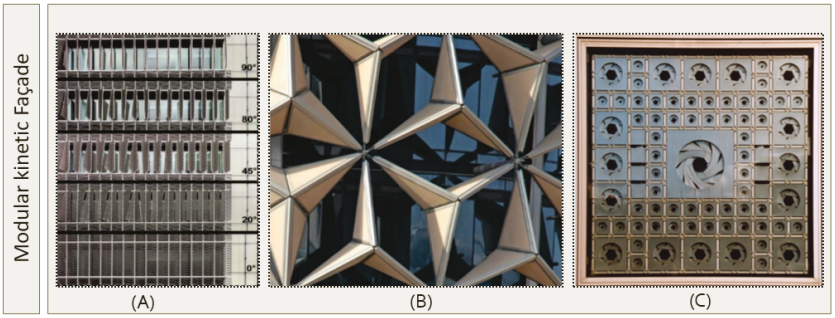


Figure 1. (**A**) Thysse Krupp cube, (**B**) Al-Bahar Towers, and (**C**) Arab World Institute [30,34].

The literature predominantly analyzes centralized control systems using parametric adjustments. However, the impact of decentralized systems, which allow modules at non-focal regions to operate independently under real-time control, has been largely overlooked. Upon closer examination, the logic control of decentralized systems and precise angular adjustments have been mostly unexplored in the context of unconventional façades. This logic can operate in real-time, responding to changes in user and sun positions to enhance visual comfort and daylight performance.

The study aims to answer the following questions:

- How can a decentralized control strategy for unconventional façades improve daylight and enhance visual comfort?
- To what extent does the kinetic façade form generation and precision of angle control improve the occupants' daylight performance and visual comfort?

2. Literature Review

This section comprises two parts, namely (1) the state-of-the-art in kinetic façades (unconventional) and (2) biomimetic insights for kinetic and decentralized movements. In the first section, the study investigates the state-of-the-art of kinetic façades, with a focus on daylighting functions, to identify research gaps and potential developments. The second part will examine potential functional convergence in biological analogies and provides biomimetic examples for interactive and decentralized movements.

2.1. The State-of-the-Art in Kinetic Façades (Unconventional)

Recently, nature-inspired ideas have emerged as a valuable source for developing adaptive façade concepts. For example, the Flectofin™ project, inspired by the Strelitzia reginae flower, features a hinge-less louver system that rotates its lamina 90 degrees when an external force applied to the spine induces bending stresses [35,36]. Temperature changes activate the lamina's displacements [36] (Figure 2a). Another project is Achim Menges's meteorosensitive pavilion, HygroSkin, as shown in Figure 2b [37]. Plywood planar sheets are elastically bent to create a conical product for the project's envelope, which is humidity-sensitive and may open and close independently in response to weather variations. These ideas represent high potential for energy efficiency and adaptability, utilizing the biomimetic approach [37–40].

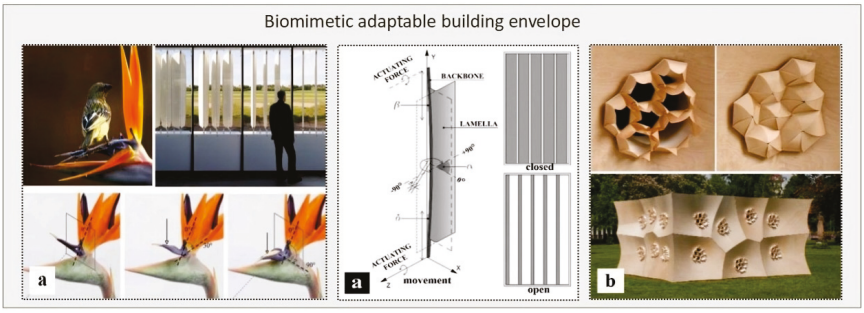


Figure 2. Examples of biomimetic adaptable building envelope projects: (**a**) Flectofin [35] and (**b**) Hygroskin [37].

Table 1 reviews recent research studies, covering topics including mechanisms, geometric forms, adaptation, environmental triggers, materials, functions, users' detection and estimations, and control strategies. These systems have been explored in various building types and climates, comprising solar-responsive wall surfaces and intelligent systems, shading and blind systems, and unconventional façade designs [8,41]. Similarly, studies by Soliman

and Bo [42] and Kuru et al. [43] introduced adaptive façades designed to address multiple functions, including thermoregulation and energy efficiency through daylight control in real-time operation. Most studies have concentrated on tropical, humid subtropical, and desert climates, highlighting the potential of kinetic façades to enhance visual comfort and daylight performance across diverse weather conditions. While parametric design, simulation, and building performance analysis are widely adopted, biomimetic strategies [2] and multiobjective optimization [42] are emerging as valuable methodologies in adaptive façade research. This evolution underscores the need to integrate biomimicry with computational design workflows [44]. Tools, such as Rhino, Grasshopper, and Ladybug Tools, commonly used in conjunction with Radiance and Energy Plus, enable detailed daylight and visual comfort analyses, supporting this integrated approach [29,45]. Although various kinetic mechanisms, such as rotation, sliding, and 3D transformations using hexagonal or rectangular modules, have been explored, there remains significant potential to integrate movement with complex three-dimensional geometries to enhance daylighting control performance.

Table 1. Review of characteristics based on forms, control logic, and function of daylighting and kinetic façade. Climate—tropical rainforest: Af, humid continental: Dfb, humid continental climate: Dwa, temperate: Cfb, humid subtropical climate: Cfa, warm desert: BWh, marine west coast: Cfb, mild and semi-humid: Csa, monsoonal humid subtropical climate: Cwa, tropical savanna: Aw, semi-arid: BSh, and tropical and subtropical steppe: BSK. Method—parametric design: PD, parametric simulation: PS, building performance simulation: BPS, biomimetic: B, general morphological analysis: GMA, fabrication: F, multiobjective optimization: MOO, survey: S, machine learning: ML, sensitivity analysis: SA, finite element analysis: FEA, genetic algorithms: GAs, systematic methodology: SM, conceptual design kinetic strategy: CDKS, daylight performance (electrical): DPE, computer-aided design: CAD, and cold rolling method: CRM. Tools/software—Ladybug Tools: LB, DIVA: D, Climate Studio: CS, Design Builder: DB, Parametric Modeling Rhinoceros: RH, Grasshopper: GH, WUFI Plus: WP, Energy Plus: EP, Radiance: R, Galapagos: GP, Honeybee: HB, and SimScale: SS. Movement type—flap: F, fold: Fo, rotate: R, retractable: Ret, rolling: Ro, pivot: P, slide: S, scale: Sc, swelling and shrinking: SS, curve: C, three-dimensional: 3D, two-dimensional: 2D, Karamba 3D, periodic geometrical change: PGC, periodic interactive region: PIR, parameters identification: PI, and control strategy: CS. Geometric form—complex form: CF, hierarchical structure: HS, roller blind: RB, Venetian blind: VB, primary shape: PS, circular shape: CP, hyperbolic paraboloid shape: HPS, transitory sensitive area: TSA, and section shape: SS. Grid—rectangular: R, triangular, T, and hexagonal: H. Material—constant: C, smart material: SM, visible transmittance: VT, openness factor: OF, colorful glass: CG, photochromic glazing: PG, opaque material: OM, and shape memory materials: SMMs. Functions—thermoregulation: T, daylight performance: DP, energy efficiency: EE, energy production: EP, aesthetic: A, glare protection: GP, sufficient supply of daylight: SSD, real-time daylight control: RTDC, visual contact to exterior: VCE, visual occupants' behavior: OP, daylight coefficient: DC, multiple occupants: MO, visual comfort: VC, and daylight glare probability: DGP. User detection and estimation—single user: SU, multiple users: MU, space: S, postures: P, one position: OP, and multiple positions: MP. Environmental trigger—sun: S and temperature: T. Control Logic—decentralized control: DC, centralized control: CC, interactive to environment: IE, and interactive to user: IU.

Kinetic Strategy	Climate	Methodology	Software	Movement Mechanism	Form/Grid	Material	Function	User Detection and Estimation	Influential Parameters	Environmental Trigger	Control Logic
Light-responsive kinetic façade (2024)	Cfb	PD, PS, BPS, B	LB, RH, GH, R	S, 3D	HS, CF/R	SM	DP, GP, RTDC, SSD	SU, MP	Identification of focal and peripheral regions on the façade	S	DC, IU

Table 1. *Cont.*

Kinetic Strategy	Climate	Methodology	Software	Movement Mechanism	Form/Grid	Material	Function	User Detection and Estimation	Influential Parameters	Environmental Trigger	Control Logic
Parametric façade design (2024)	_	GAs, SM	GH, GP	S, 3D	T, S, H	_	DP, VOB	SU	geometric patterns and the position of the supports in façade design	T	IU
Real-time daylight control (2024)	Bsh	PD, PS, BPS, B	LB, RH, GH, R	PGC, PIR	CP, HPS	_	DP, DC, SSD, GP	MU, P	Kinetic façade draws inspiration from the nano-scale structure and kinetic behavior of the Morpho butterfly wing	S	IU
Parametric-generative kinetic façade (2024)	Bsh	PS, B, PD, DPE	D, LB, HB	R, PI, CS	R, TSA	OM	EE, MO, DP, GP	MU	Interactive kinetic louver coupled with electric lighting	S	IU, GEL, IL, DC, IE
Variable building skin with solar-concentrating technology (2024)	Cwa	PM, PS, BPS, MOO	LB, RH, GH, R	R, 3D	CF/H	VT	DP, GP, RTDC, SSD, EP	SU, MP	Integrating hexagonal module with a Fresnel lens to concentrate solar rays, sun tracking system	S	DC, IE
Multifunctional adaptive building envelope (2023)	BWH	B, BPS	DB	SS, R, Fo, 3D	CF/H	PG	T, RTDC, EE	S	Foldable surfaces with hexagonal shapes, multiple layers, self-shading features, and symmetrical triangular fins	T	DC, IE
Flexible adaptive shading façade (2023)	Dwa	B, PD, BPS, FEA, F		C, 3D	CF/H	SM	DP, RTD	S	Real-time façade shape change, flexural hexagonal shapes	S	CC, IE
Interactive kinetic façade (2022)	BWh	B, GMA, PM, PS, BPS, MOO	LB, RH, GH, R	R, Sc, S, 3D	CF, HS/H	CG	DP, GP, SSD, RTDC	SU, MP	Geometrical changes (different depths and scales), composition of colored glass, periodic changes based on sun-timing positions and user positions	S	DC, IU
Occupant-centric adaptive façade design (2022)	Dwa	S, PM, BPS, ML, MOO	LB, RH, GH, R, EP	R, 3D	CF, HS/R	VT	DP, T, GP, SSD, RTDC, EE	SU, P, OP	Posture definition, adjusting shading unit, sun angle, and temperature	S	CC, IU
Multiobjective optimization (2022)	Aw, Cfa, Cfa, Dfb, BSk	PS, MOO, SA	RH, GH, CS, R, EP	Ro, 2D	RB	VT, OF	DP, T, GP, SSD, RTDC, EE, VCE	S	Window to wall ratio, glazing, blind, fully opened or fully closed without intermediate change	S	CC, IE

Table 1. *Cont.*

Kinetic Strategy	Climate	Methodology	Software	Movement Mechanism	Form/Grid	Material	Function	User Detection and Estimation	Influential Parameters	Environmental Trigger	Control Logic
Advanced control of indoor and outdoor Venetian blinds (2022)	Csa	PD, PS, MOO	LB, RH, GH, R	R, 3D	VB/R	VT	DP, GP, SSD, VCE	MU, MP	Integration of interior light shelves and exterior venetian blind, independently adjustable tilt angles of multiple sections of thw façade	S	DC, IU
Form-finding of kinetic façades (2022)	Csa	PD, PS, MOO	LB, RH, GH, R	R, S, 3D	PS/R	C	DP	S	Shape changes, tessellated form	S	CC, IE
Bio-inspired kinetic façade (2021)	BWh	B, PM, PS, BPS	D, RH, GH, R	R, S, 3D	CF, HS/R	VT	DP, GP, SSD, RTDC	MU, MP	Dynamic transitory-sensitive area, symmetrical element, hierarchical arrangement, immediate reconfiguration	S	DC, IU
Biomimetic kinetic shading façade (2021)	BWh	B, PM, PS, BPS	D, RH, GH, R	C, 3D	CF/R	_	DP, GP, SSD, RTDC	SU, OP	Multilayered skin, kinetic curvature movement, intersected element	S	IE
Adaptive shading control (2021)	Af, BSh, Cfb, BWh, Csa, Dfb	PM, PS, BPS	LB, RH, GH, R, EP	R, 3D	VB/R	VT	DP, T, GP, SSD, RTDC, EE	S	Climate zone, window-to-wall ratio, building orientation, shading control strategy and its activation threshold, rotation range from 0° to 90°	T	CC, IE
Bio-curvilinear shading device (2024)	BWh, Csa	CAD, B	IDA ICE	_	SS	OM	EE	S	Sensitivity analysis for optimum depth and interval values	T	IE
Vertical fin shading system (2024)	Dfb	PD, PS, BPS	RH, GH, LB,	R, 3D	SS	_	EE, DGP, DP,	MU, MP	Vertical fins rotate (closed and open) according to the illuminance level at the work plane	T	IE, IU
Design of a responsive façade for occupant visual comfort in different latitudes (2024)	Bsh, Bwh, Dfb	PD, PS, BPS	RH, GH, LB,	Sc, 3D	H	_	vc	MU, MP	Uses inclined walls to enhance visual comfort and adequate natural light	S, T	IE, IU
Kinetic module using bimetal (2024)	Cfa	PS, CRM	_	Sc, 3D printed	CF, T	SM	EE	MU	Different openings for the biomodules; rotation of up to 90° allows ventilation	T	IE

Given that visual comfort is closely tied to users' detection-estimation and light level preferences within space, some studies have missed the essential role of users in the façade design process. For instance, Le et al. [46] explored adaptive façades with roller blinds, but

their study was limited to fully open or closed configurations, disregarding users' positions. However, there are few studies on decentralized control [31,47,48]. They considered the role of multiple users in an office, each with different light preferences. For example, recent studies developed decentralized control systems primarily focused on the shapes of focal areas [49,50]. However, the examination of controlling non-focal areas in terms of size and rotating angles, and their integration with the focal region, remains unclear. Furthermore, a detailed study of decentralized control with simultaneous adjustment of both focal and non-focal region components has not yet been conducted [29]. Specifically, the potential improvement in spatial disturbing glare through this control system has not been considered. In addition, a study proposed a biomimetic shading system for improving energy efficiency and daylight performance [29]. However, the evaluation relied solely on spatial daylight autonomy (sDA) as the performance metric, without considering other critical indicators, such as annual sunlight exposure (ASE), useful saylight illuminance (UDI), or the glare indices, which are essential for a comprehensive daylight and visual comfort assessment.

2.2. Biomimetic Insights for Kinetic and Decentralized Movements

The Venus flytrap possesses high-speed responsive systems, serving as a source of inspiration for rapid sensing and actuating functions. A *hydroelastic curvature* mechanism facilitates the movement of water between different leaf layers, enabling rapid closure within a fraction of a second [51]. These mechanisms can be utilized to prevent glare while allowing sufficient daylight to enter the room in daylighting systems. Its sensitive hairs can detect mechanical stimuli and transmit a signal for immediate buckling in its bistable lobes, resulting in an exceptionally rapid closure time of less than 100 milliseconds [52]. This combination of sensing and actuating prevents any possible delays, as the mechanical stimuli directly release pre-stored elastic energy through "*hydroelastic curvature*" [53,54]. Precedent studies indicate that a single touch can trigger two distinct action options under identical conditions, which changed the traditional perception of the trap's mechanism [55]. This fast and accurate response procedure to environmental stimuli is aligned with the goals of kinetic façades to improve daylight performance and visual comfort by adapting to ever-changing daylight conditions [56].

Moreover, the plant can count and memorize several stimuli and plan for multiple possible actions for full trap closure and the digestive process [57]. This intelligent decision making allows the system to navigate complex scenarios and effectively differentiate between genuine stimuli and false triggers [57,58]. Principles inspired by the Venus flytrap in kinetic façades involve the integration of rapid movement, responsive opening and closing, and advanced sensing and triggering mechanisms. The Venus flytrap's rapid trap closure, triggered by mechanical or electrical stimuli, can inspire kinetic façade designs [59, 60]. There is strong potential to develop a new generation of kinetic façades by examining the Venus flytrap's control logic and rapid actuation mechanisms, as well as by applying its distinctive three-dimensional geometry. This research aims to integrate biomimetic principles with computational design to explore innovative kinetic façade solutions inspired by the Venus flytrap's responsive behavior.

3. Methods

This study integrates a biomimetic functional approach with building performance simulations using computational design to evaluate different kinetic façade configurations using four interconnected phases (Figure 3). The process begins with Section 3.1, focusing on the speed of response to daylight change and sensing, and actuation to visual discomfort

challenges to identify a proper biological analogy. It then progresses to Section 3.2, which examines the morphology and kinetic behavior of the Venus flytrap to extract biomimetic principles. The outcomes of this step are based on the biomimetic literature review in the introduction section of "Section 2.2". The third component, Section 3.3 (Design Solution Development), addresses both the mechanism aspects (rapid closure and transitory sensitive area) and form considerations (rotation of form and reversible motion). This step is crucial for developing a concept of a new kinetic façade and identifying its kinetic component variables. The methodology concludes with Section 3.4, which involves conducting daylight performance and visual comfort evaluation, then using inverse design and parametric exploration to find the optimal solutions. This comprehensive framework represents an organized biomimetic approach to solving design challenges by translating biological principles from the Venus flytrap into functional adaptive systems (Figure 3).

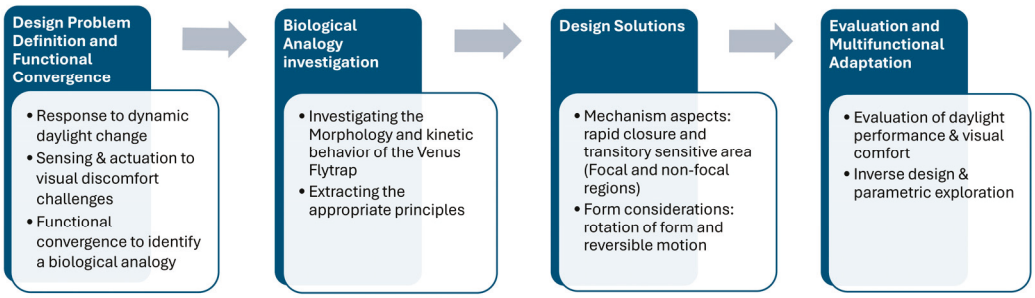


Figure 3. Integrating a biomimetic functional approach with building performance simulations by computational design for kinetic façade design. Source: authors' own creation.

3.1. Design Problem Definition and Functional Convergence

Dynamic daylight can cause visual discomfort for users due to real-time changes in direction and intensity. Consequently, adaptive façades must respond promptly to mitigate these challenges. This issue should be addressed by developing effective forms, movement, and control logic for the façades. A similar function of opening and closing shading systems in buildings can be observed in the Venus flytrap, which rapidly closes its lobes based on quick decision making regarding the position and situation of prey on the inner side of the lobes. A climate-adaptive façade should respond in real time to dynamic daylight. Investigating its forms and kinetic behavior can yield innovative solutions for the next generation of adaptive façades. This procedure provides a meaningful exploration to identify an appropriate biological analogy for further investigations into morphology and kinetic behavioral levels (Figure 4).

Design Problem	Buildings	Biological Analogy
Response to dynamic Daylight Change & Visual Discomfort Challenges	Shading Device	Venus Flytrap
	Functions: Opening and Closing, Adaptive Control	Functions: Open and close, Rapid movement, Sensitivity and Responsive control

Functional Convergence

Figure 4. Design problem definition and functional convergence to identify the proper biological analogy.

3.2. Biological Analogy Investigation

An examination of the Venus flytrap's sensing and actuation processes shows that its rapid response is closely linked to its unique morphology and dynamic movement

mechanisms. It possesses lobe structures and utilizes snap-buckling movements to facilitate opening and closing actions. From a behavioral perspective, the Venus flytrap can simultaneously detect the positions of multiple prey, memorize several stimuli, and implement periodic shape changes through a fast-triggering mechanism, enabling the planning of multiple actions to capture all prey. Indeed, it demonstrates intelligent decentralized control for immediate closure triggering by localized sensitive hairs (Figure 5). Translating this principle to a kinetic façade, each module functions as an independent unit, equipped with local sensors and actuators. A decentralized system can explore the façade surface and control kinetic elements within the focal area and the non-focal area individually. Based on the feedback from internal sensors about visual discomfort and the lack of useful daylight, the module quickly shifts from an open to a closed state, like how a Venus flytrap snaps shut (Figure 6). This procedure improves daylight performance with all possible positions in space while avoiding discomfort from glare (Figure 7).

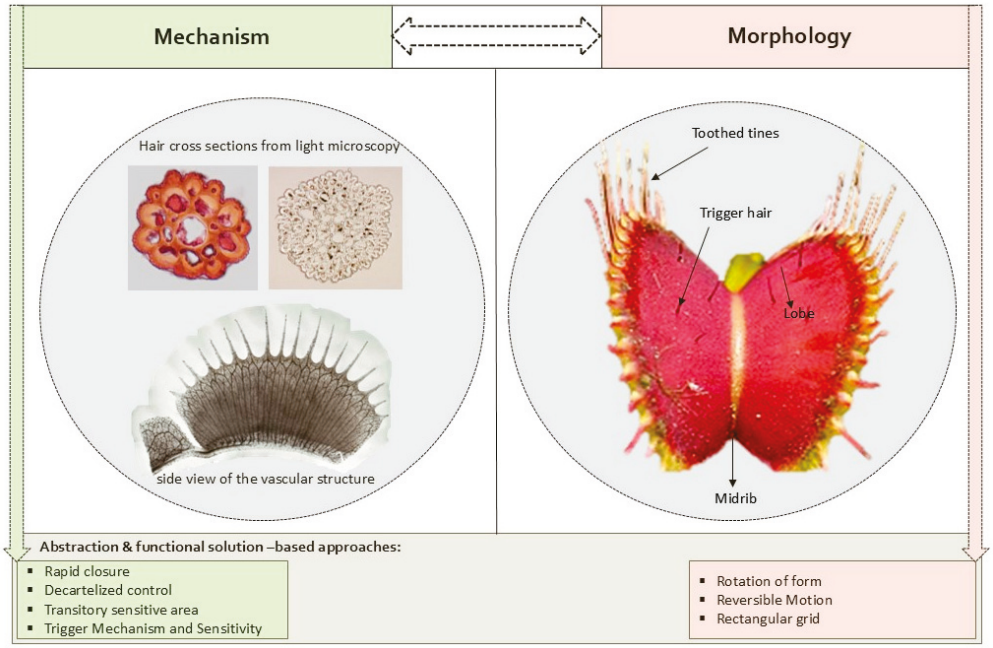


Figure 5. Biomimicry concepts inspired by the form and movement of the Venus flytrap, adapted from [61].

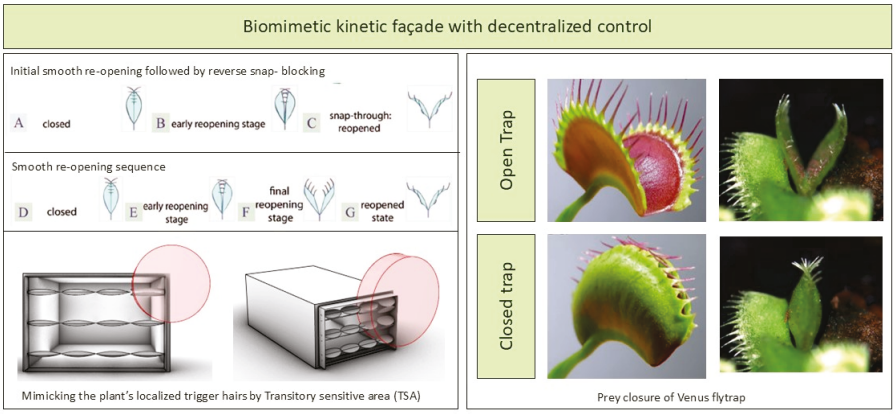


Figure 6. Decentralized control with biomimetic façade approaches based on the Venus flytrap's mechanism, adapted from [62].

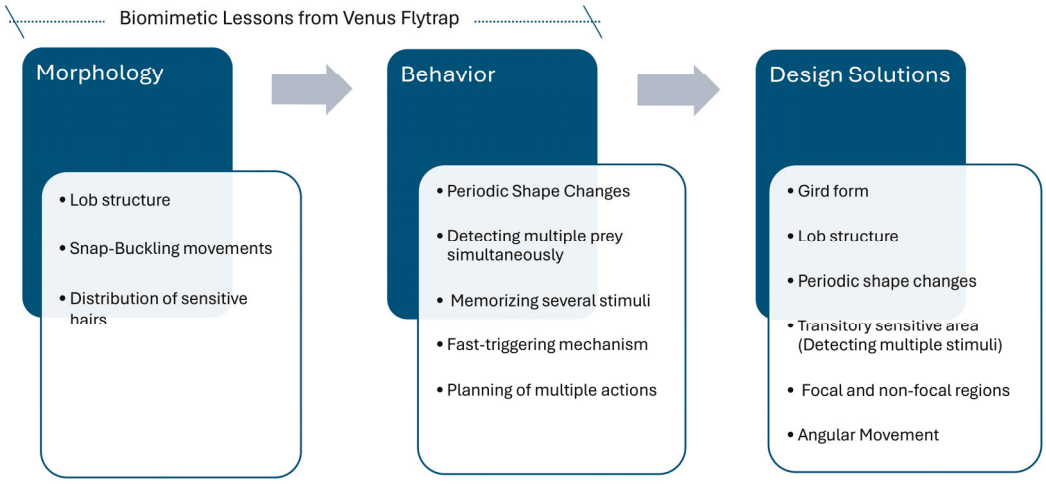


Figure 7. Investigation of Venus flytrap morphology and behavior to detect design solutions. Source: authors' own creation.

3.3. Design Solution Development

The façade design utilizes a lobe structure form, allowing for dynamic angular adjustments to the dynamic characteristics of daylight. The Venus flytrap's intelligent mechanism utilizes sensitive hairs to detect the precise positions of prey in real-time within the leaf area, triggering rapid and precise enclosure. This responsive mechanism inspires the concept of a transitory sensitive area [48], where multiple sensors on a façade enable decentralized movement, enhancing visual comfort and daylight performance for users. First, a grid was initially established 50 cm from the building façade to position the biomimetic shade sails. Following this, fixed shading planes were designed around the windows located on the eastern, western, and upper sides of the building. Finally, biomimetic shade sails were placed in the center of each section of the grid (Figure 8). The dynamic positions of occupants and the timing of sunlight involve creating a system that connects the sun's position at different times with the locations of users within the space. This process also includes identifying key attraction points by determining where the user's lines of sight intersect with the façade's surface (Figure 9).

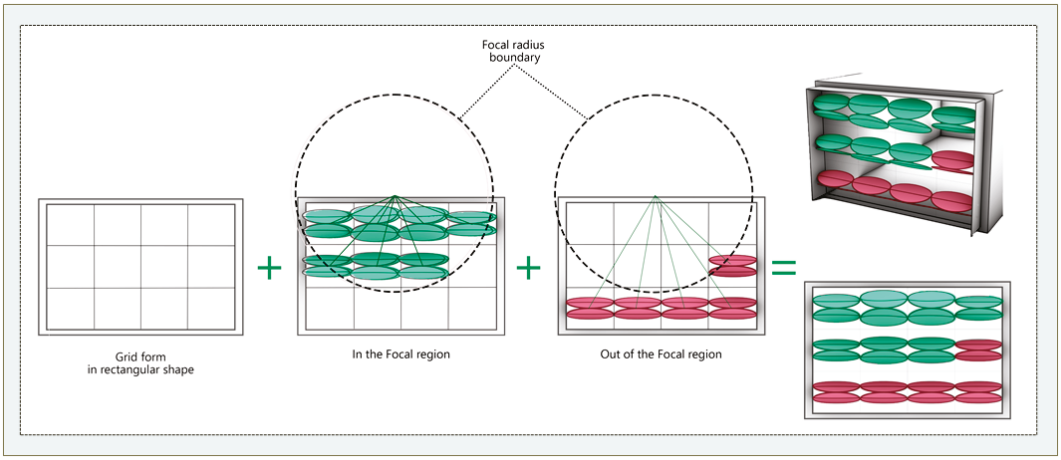


Figure 8. A combination of a grid layout and a focal radius boundary is used for simulating the angle design. Source: authors' own creation.

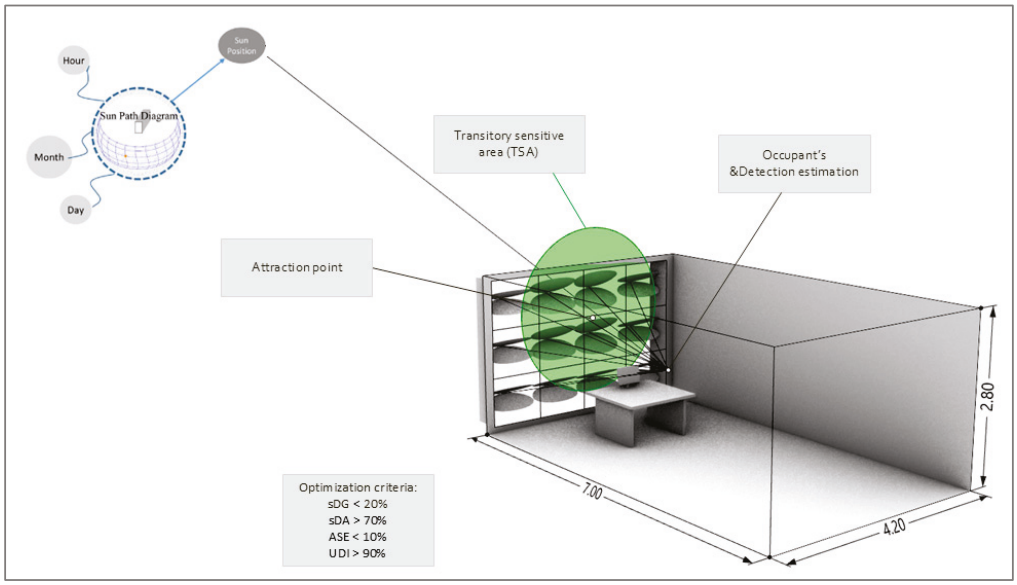


Figure 9. Sunlight exposure and the occupants' position affect the façade shape changes in a transitory sensitive area (TSA) based on optimization criteria.

3.4. Evaluation and Multifunctional Adaptation

The designed kinetic façade offers real-time daylight control to enhance daylight performance and improve occupants' visual comfort. This section describes the use of climate-based and illuminance metrics to establish the criteria for daylight performance simulation, which are based on the guidelines for predicting daylight performance [63]. The study conducts comprehensive parametric simulations to analyze the daylight performance of various kinetic façades, focusing on their ability to enhance visual comfort. The analysis employs Rhino 8, Grasshopper, Climate Studio, and Design Explorer to assess daylight performance. These powerful tools enable an in-depth examination of daylight performance at the office [64,65]. The study uses daylight performance simulations to evaluate the kinetic façade solutions according to climate-based daylight modeling metrics, including spatial daylight autonomy (sDA), useful daylight illuminance (UDI), annual sun exposure (ASE), and spatial disturbing glare (sDG).

A point is considered "daylit" if its sDA value is 50% or higher, indicating that it meets a threshold of 300 lux [65]. Useful daylight illuminance (UDI) is an annual illuminance metric that categorizes daylight levels in a space, considering illuminance ranges between 100–3000 lux as desirable for most tasks, while values below 100 lux are insufficient and values above 3000 lux may cause visual discomfort [66]. Annual sunlight exposure (ASE) is a metric used to assess the percentage of space that receives excessive direct sunlight, which can lead to visual discomfort and increased cooling loads. "*It is defined as the percent of an analysis area that exceeds a specified direct sunlight illuminance level (typically 1000 lux) for more than a specified number of hours (usually 250 h) per year*" [67].

Glare is a sensation experienced when a bright light source appears in the field of vision, surpassing the brightness to which the eyes have adjusted [68]. DGP is a metric that has gained popularity in recent years, as indicated by various sources. It uses CCD camera-based luminance mapping technology to evaluate glare. DGP values are categorized into four groups, namely imperceptible, perceptible, disturbing, and intolerable (45–100). "Spatial Disturbing Glare (sDG): The percentage of views across the regularly occupied floor area that experience Disturbing or Intolerable Glare (DGP > 38%) for at least 5% of occupied hours" [69].

This assessment was conducted over an entire year, using hourly time intervals that commonly used the daylight coefficient (DC) method. The method simulates various daylight scenarios, using the following formula:

$$E = DC \times S$$

The resulting illuminance matrix (E) is obtained by multiplying the DC matrix with the sky matrix. The DC matrix describes the relationship between the virtual sensor points (n) and the 145 sky patches, while the sky matrix (S) contains the luminance values for each sky patch at every hour of the year. The DC matrix is derived from a computationally intensive lighting simulation. Once this matrix is established, the process of calculating illuminances involves the relatively quick multiplication of matrices. Both climate-based daylight modeling (CBDM) and radiance-based techniques are grounded in the Radiance software (version 5.4) platform and feature specific modifications of the DC method [65] (Table 2).

Table 2. Ambient parameters for radiance were utilized in the simulation. Source: authors' own creation.

Method	Ambient Bounces (-ab)	Ambient Divisions (-ad)	Ambient Super Samples (-as)	Ambient Accuracy (-aa)	Ambient Resolution (-ar)	Limit Weight (-lw)
Daylight Coefficient	6	4096	512	0.15	512	0.002

Multiple input parameters can lead to different design alternatives that need to be evaluated based on design goals. The inverse design diagram (Figure 10) represents how input and output parameters interact in a brute-force algorithmic search to identify the optimal set of solutions. Building on the exploration size established in previous phases, this research utilizes a brute-force algorithm to explore all potential solutions precisely.

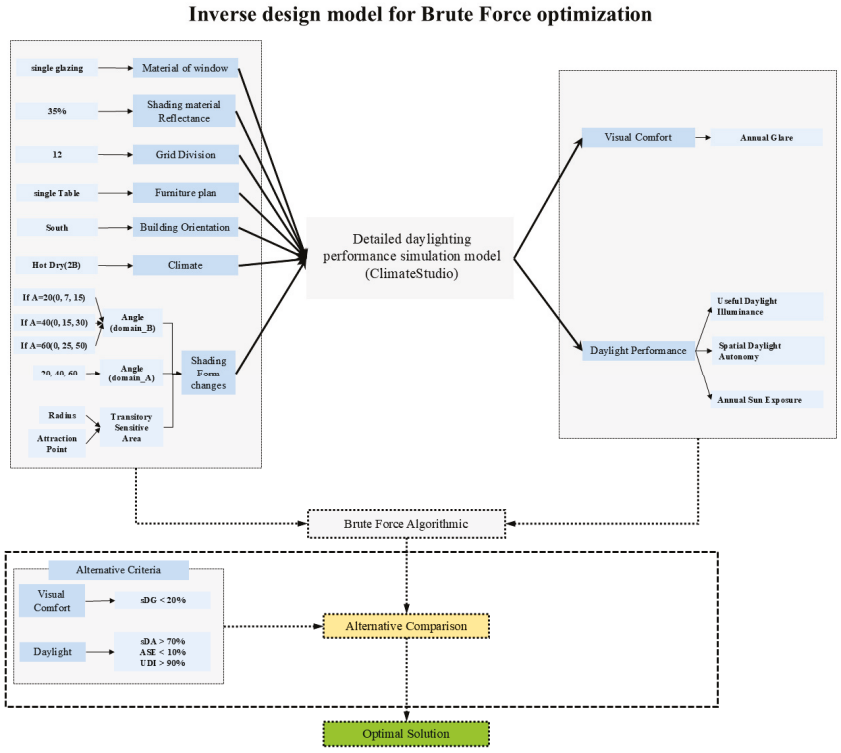


Figure 10. An inverse design model for the optimization of the kinetic façade with Venus flytrap design principles using a brute force algorithm and a design explorer.

The next step involves conducting a benchmarking process, prioritizing an sDG of less than 20% while ensuring that UDI is greater than 90% and sDA exceeds 70% to identify the optimal solutions [63].

4. Case Study

The simulation experiment was conducted for an office building located in Yazd, Iran, which experiences a hot desert climate (BWh) with clear skies, according to the Köppen climate classification. The region's weather data were obtained from the Energy Plus website. The weather file was organized by the countries defined by the World Meteorological Organization to indicate local climate conditions accurately. The file output provides key environmental indicators, including global solar radiation, global horizontal illuminance, and dry bulb temperature (Figure 11). Daylight-based metrics are calculated annually for each unique façade configuration. A grid was created to position the bio-imitation awnings 50 cm away from the building façade. The model depicted a single-zone office space located on the first floor of the reference building, measuring 4.20 m in depth, 7.00 m in width, and 2.80 m in height based on a standard office layout. It is important to note that the interior walls, roof, and floor were considered adiabatic surfaces. The south-facing wall features a window-to-wall ratio (WWR) of 85%, which is subject to variation depending on the applied shading strategies. For the daylight simulation, we assumed there was one occupant in the space (Figure 12A). Figure 12B illustrates the height of the user's view toward the outside and its relationship to the sun's position, which helps determine the location of the attraction point. The height of the task area for the simulation was set at 0.8 m for illuminance and 1.20 m for glare analysis. Table 3 provides information about the optical properties of material surfaces. Parametric and environmental analysis software, including Rhinoceros, Grasshopper, and Climate Studio, were used for conducting daylight performance and visual comfort evaluation (Table 3).

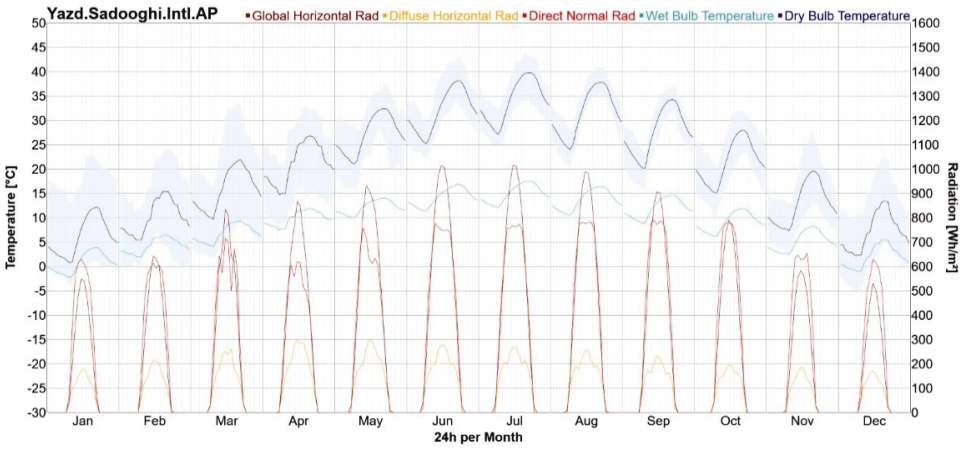


Figure 11. Diurnal averages of weather environmental indicators.

Table 3. Model description, including parameters related to fixed conditions, driving conditions, time, climate, energy, and daylight.

Performance Criteria			
Parameters	**Name**	**Unit**	**Range**
Daylight Related Parameters	Useful daylight Illuminance	Lux	[100−3000]
	Spatial daylight autonomy	Percentage	[0−100]
	Annual Sun Exposure	Percentage	[0−100]

Table 3. *Cont.*

Performance Criteria			
Parameters	**Name**	**Unit**	**Range**
Visual Comfort	Annual Glare	Percentage	[0 − 100]
Model Driving Parameters	Shading Form change (TSA)	m	[0.5−1−1.5−2−2.5−3−3.5−4−4.5−5−5.5−6]
	Shading Form Angle(domain_A)	Degrees	20, 40, 60
	Shading Form Angle(domain_B)	Degrees	If domain_A = 20(0, 7, 15) If domain_A = 40(0, 15, 30) If domain_A = 60(0, 25, 50)
Model fixed Parameters	Grid Division	Integer	12
	Glazing Ratio	Percentage	90
	Window Material	user−defined	Single−Low−E
	Task Area Height	m	0.76
	View Area Height	m	1.20
	Space Width	m	4.2
	Space Length	m	7
	Space High	m	2.8
	Shading device Reflectance	Percentage	35
	Int. Wall Reflectance	Percentage	50
	Int. Ceiling Reflectance	Percentage	80
	Int. Floor Reflectance	Percentage	20
	Ext. Ground Reflectance	Percentage	20
Time Parameters	Month	Integer	6−9−12
	Day	Integer	21
	Hour	Integer	9−12−15
Climate Parameters	Weather File for analysis	user−defined	Hot Dry

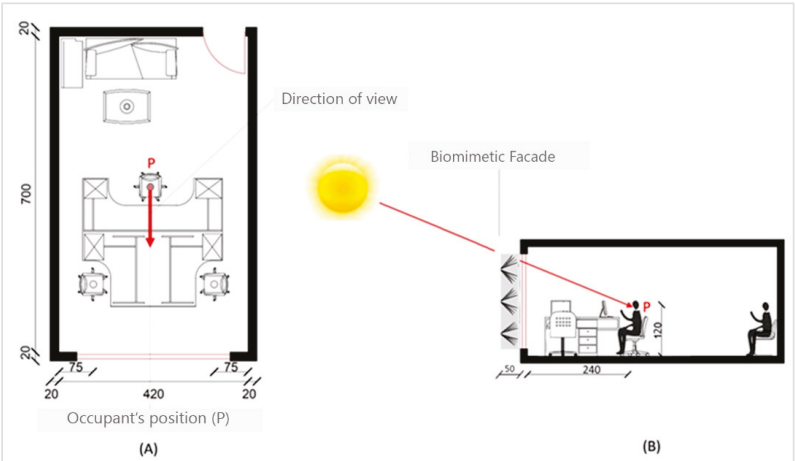


Figure 12. Test room definition (**A**): Plan view of test room, dimensions of room and occupant positions (**B**): Identification of attraction points and occupant's direction of view.

Daylight Simulation Validation

To validate the accuracy of the simulation, annual daylight simulations were conducted using the same case study room of Hosseini et al. (2020) [30]. The simulation results for sDA, UDI, ASE, and sDG were compared across both studies for various window-to-wall ratios ranging from 20% to 95% in 5% intervals, maintaining identical optical properties and office dimensions (Figure 13). The comparison utilized the normalized mean bias error (NMBE) for evaluation. According to ANSI/ASHRAE Standard 140 [70], a model is considered calibrated if the NMBE is within ±10% for the hourly data or ±5% for the monthly data. The comparison results indicated that all NMBE values fell within the acceptable range of less than 5%, specifically −3.36%, 0.83%, −0.41%, and 1.75% for sDA, ASE, UDI, and sDG, respectively. Therefore, our daylight simulation was validated.

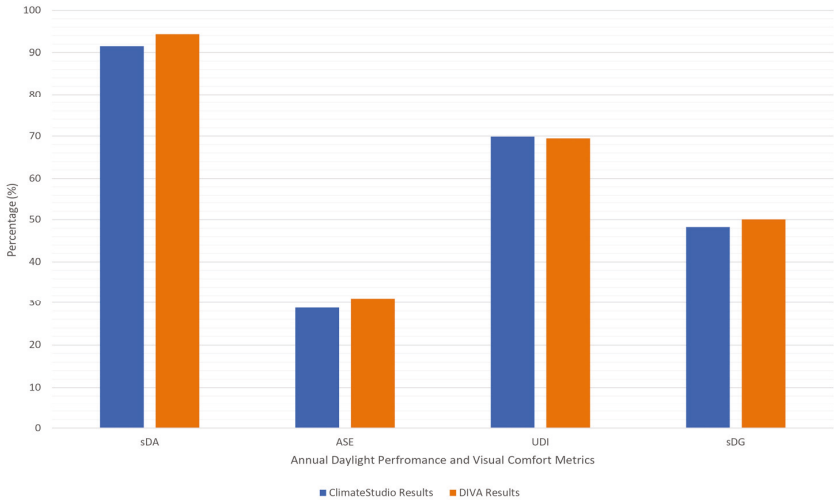


Figure 13. The average performance metrics of sDA, ASE, UDI, and sDG for validating the case study based on the DIVA results from Hosseini et al. (2020) [30].

5. Results

Figure 14 illustrates a parametric exploration of a biomimetic interactive kinetic façade utilizing a transitory sensitive area based on a climate-based daylight modeling metric. The figure employs parallel coordinate plots to represent various design parameters and performance outputs along vertical axes. The design parameters include month, hour, TSA (transitory sensitive area), angle domain A (focal region), and angle domain B (outside the focal region). The outputs comprise daylight performance metrics, namely sDA (spatial daylight autonomy) and UDI (useful daylight illuminance), while the visual comfort metrics include ASE (annual sunlight exposure) and sDG (spatial daylight glare). These metrics are used to evaluate the quality of daylighting. The bottom diagram shows a filtered set of design solutions based on the following criteria: sDA > 70%, ASE < 10%, UDI > 90%, and sDG < 20%. This procedure facilitates the collection of ideal solutions for data analysis and result interpretation, as shown in Figure 14.

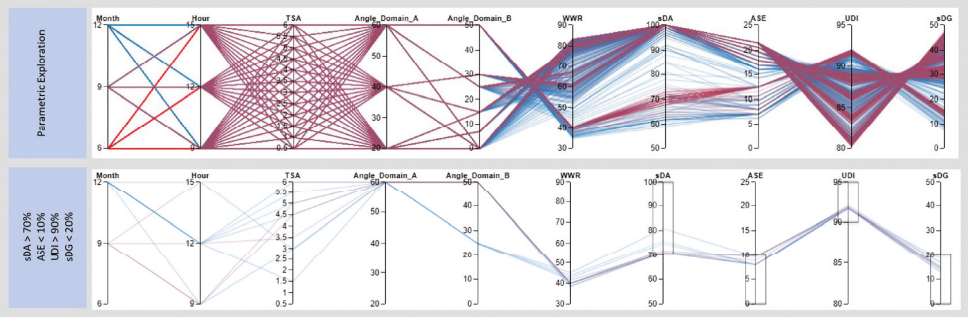


Figure 14. Parametric exploration of a biomimetic, interactive kinetic façade utilizing a transitory sensitive area based on a climate-based daylight modeling metric.

5.1. Performance Analysis Across Angle Domains (A: In the Focal Region, B: Outside the Focal Region) Based on Daylight Performance and Visual Comfort Metrics for TSAs of 0.5, 1, 1.5, and 2

The analysis of angular domains A and B reveals significant performance variations across different configurations due to changes within the focal region (A) and outside the focal region (B). Figure 15 presents a detailed examination of how changes in TSA radius from 0.5 to 2 across these angular domains influence key daylight metrics, including spatial daylight autonomy (sDA), annual sunlight exposure (ASE), useful daylight illuminance (UDI), and spatial daylight glare (SDG).

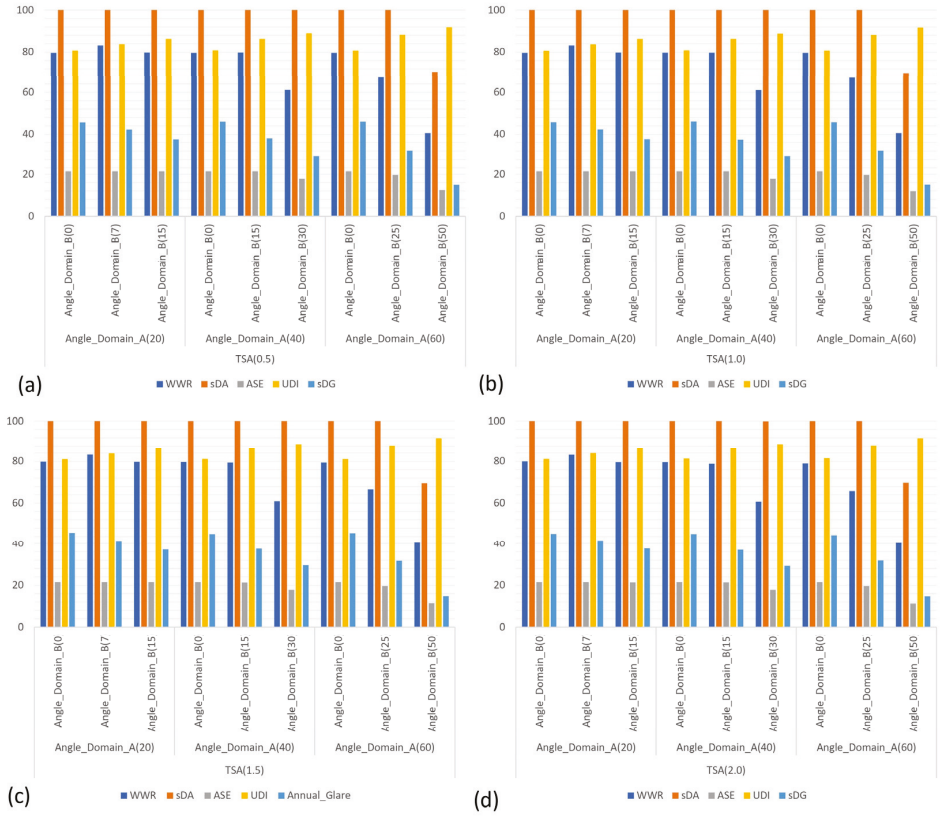


Figure 15. A comparison of average daylight and visual comfort performance across different angle domains (A: in the focal region, B: outside the focal region) for TSAs radius of (**a**): 0.5, (**b**): 1, (**c**): 1.5, and (**d**): 2, and their effects on variations in the sDA, ASE, UDI, SDG metrics and the amount of WWR.

Several combinations of Angle_Domain_A (focal region) and Angle_Domain_B (outside the focal region) under a TSA of 0.5 have shown different impacts on daylight per-

formance and visual comfort (Figure 15a). Most of the combinations reach an sDA of 100%, except for (A60/B50), which drops to 70.56%. Nevertheless, this solution shows exceptional performance with the highest UDI of 91.83%, while decreasing the ASE to 12.5% and avoiding the risk of glare and overheating. The sDG value of 15.02% indicates the high performance of the steeper angles in providing visual comfort as well.

Conducting a daylighting analysis for TSA: 1 (Figure 15b), based on the performance targets (sDA > 75% and UDI > 75%), reveals that all cases meet the criteria, except A60/B50 with an sDA of 70%. As this case reaches the maximum UDI of 91.71%, we can neglect the shortage of 5% in the sDA percentage. In terms of visual comfort, no solution fully meets both ASE < 10% and sDG < 15% simultaneously. The A60/B50 solution comes closest with an ASE of 11.9% (just above the 10% target) and an sDG of 15.07% (marginally exceeding the 15% limit).

Considering the solutions based on a TSA of 1.5 (Figure 15c) reveals an underlying trade-off between daylight performance and visual comfort across different angular configurations. While nearly all solutions meet daylight performance criteria, visual comfort is only met by the steepest angular domain. A60/B50 meets the glare mitigation criteria (sDG < 15%), whereas other configurations fail to avoid glare, with sDG values ranging from 29.60% to 45.77%.

Regarding a TSA of 2 (Figure 15d), the best daylight performance is identified at Angle_Domain_A at 20° or 40° in conjunction with Angle_Domain_B at 0° or 15°, where UDI ranges from 81.09% to 86.44% and sDA remains at 100%. However, these solutions exceed the recommended threshold for ASE and sDG, indicating suboptimal visual comfort quality. The best glare control is achieved with Angle_Domain_A at 60° and Angle_Domain_B at 50°, but this compromises daylight performance (sDA: 69.78%). A balanced option is Angle_Domain_A at 40° and Angle_Domain_B at 30°, where sDG is 29.28% and sDA remains high (99.89%). Overall, combinations with lower Angle_Domain_B values (e.g., 0–15°) provide strong daylight performance but require additional glare control measures.

5.2. Performance Analysis Across Angle Domains (A: In the Focal Region, B: Outside the Focal Region) Based on Daylight Performance and Visual Comfort Metrics for TSAs of 2.5, 3, 3.5, and 4

Figure 16 analyzes the impact of varying TSA radii (2.5 to 4) across different angular domains on the critical daylight performance measures of sDA and UDI and on the visual comfort measures of ASE and SDG. Figure 16a (TSA: 2.5) demonstrates that changing angle domains A (focal region) and B (outside the focal region) substantially affects daylight and visual comfort metrics. Angular changes in both domains result in a UDI ranging from 80.27% to 88.81% while maintaining sDA at 100%.

In terms of visual comfort, ASE remains below 21.43% in most cases, exceeding the target of <10%, while sDG (annual glare) ranges from 27.23% to 46.54%, far above the desired <15%. This indicates that while daylight performance is strong, the glare control is insufficient, especially as Angle_Domain_B increases. The best daylight performance is achieved with Angle_Domain_A at 20° and Angle_Domain_B at 0° or 7°, where sDA and UDI exceed 75%, but glare (sDG) remains problematic (39.4–46.32%). A reduction in glare highly depends on increasing the angle domains A and B with angle ranges of 40° to 60° and 30° to 50°, respectively.

UDI values range from 81.54% to 91.75% with an sDA of 100% for a TSA of 3 (Figure 16b), indicating the high performance of the solutions in meeting daylighting requirements. However, ASE values vary from 17.66% to 21.43%, which implies a risk of excessive sunlight and potential glare. In terms of visual comfort and glare control, spatial daylight glare (sDG) decreases as the angle of domain B increases, showing improved glare

control. Specifically, sDG ranges from 44.59% to 14.37%. The lowest sDG value of 14.37% is observed when Angle_Domain_A is 60° and Angle_Domain_B is 50°. This highlights that larger angles for domain B are effective in reducing glare, bringing it closer to the recommended 15% threshold.

Overall, while the configurations effectively provide high daylight levels, optimizing the angles, especially increasing domain B, is essential to mitigate glare and enhance visual comfort. Analysis of angle domains A and B indicates consistently strong daylight performance, with spatial daylight autonomy (sDA) frequently reaching 100% (based on a TSA of 3.5, as in Figure 16c). The UDI values exceed the required 75%, demonstrating effective daylight distribution ranging from 81.94% to 91.68%. However, ASE values ranging from 10.12% to 21.43% indicate a risk of overheating and potential discomfort. Glare control can be improved through increasing the angular domain of the non-focal region (B), which reduces glare from 44.59% to 13.70%.

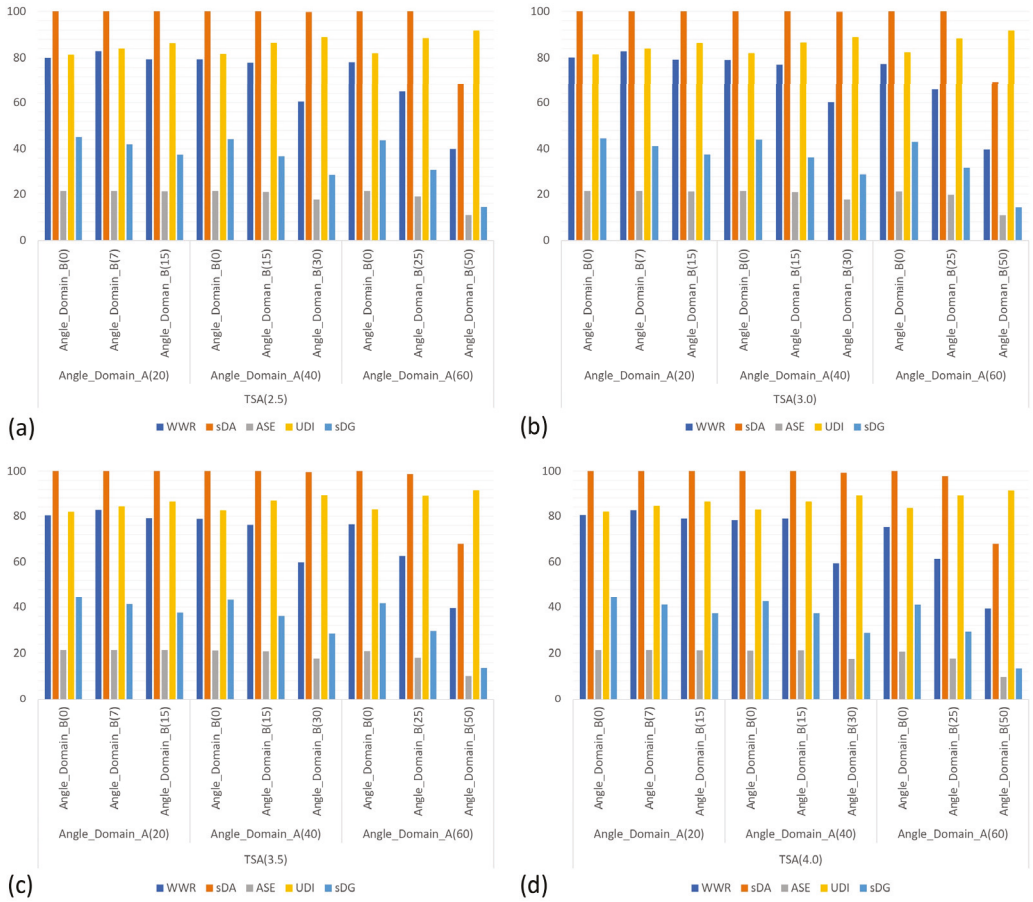


Figure 16. A comparison of the average daylight and visual comfort performance across different angle domains (A: in the focal region, B: outside the focal region) for TSAs radius of (**a**): 2.5, (**b**): 3, (**c**): 3.5, and (**d**): 4, and their effects on variations in sDA, ASE, UDI, and SDG metrics and the amount of WWR.

Similarly, the interaction of focal and non-focal regions (A and B) based on a TSA of 4 (Figure 16d) demonstrates effective daylight performance. In contrast, ASE values typically exceed the recommended 10%, fluctuating between 17.56% and 21.43%, indicating a risk of overheating and potential glare. However, as the angle of domain B increases, the sDG values decrease, resulting in improved visual comfort. The sDG values range from 44.28% to 13.48%. Notably, the lowest sDG (13.48%) occurs when Angle_Domain_A is 60° and

Angle_Domain_B is 50°, confirming that larger domain B angles effectively reduce glare to below the target of 15%.

5.3. Performance Analysis Across Angle Domains (A: In the Focal Region, B: Outside the Focal Region) Based on Daylight Performance and Visual Comfort Metrics for TSAs of 4.5, 5, 5.5, and 6

Analyzing the performance of the combined angle domains A and B based on a TSA of 4.5 (Figure 17a) indicates strong daylight performance, with an sDA of 99.44% to 100% and a UDI between 82.32% and 91.69%. In terms of visual comfort, an improvement can be identified as the sDG and ASE values decrease from 44.11% to 12.98% and 21.43% to 9.92%, respectively. Notably, several solutions reach the desired sDG of less than 15%, indicating successful management of potential glare. Similar results have been observed for a TSA of 5 (Figure 17b). Daylighting performance is generally excellent, with sDA and UDI values consistently high, ranging from 99.33% to 100% and 82.40% to 91.50%, respectively, which suggests that a larger area receives useful daylight. However, visual comfort varies. ASE values range from 9.62% to 21.43%, indicating a risk of excessive sunlight and potential glare in some configurations, as the target is below 10%. sDG values decrease as angle domain B increases, moving from 43.32% to 12.98%, demonstrating better glare control with a larger angle domain B. Notably, several configurations achieve sDG values below the 15% threshold, showing effective glare management.

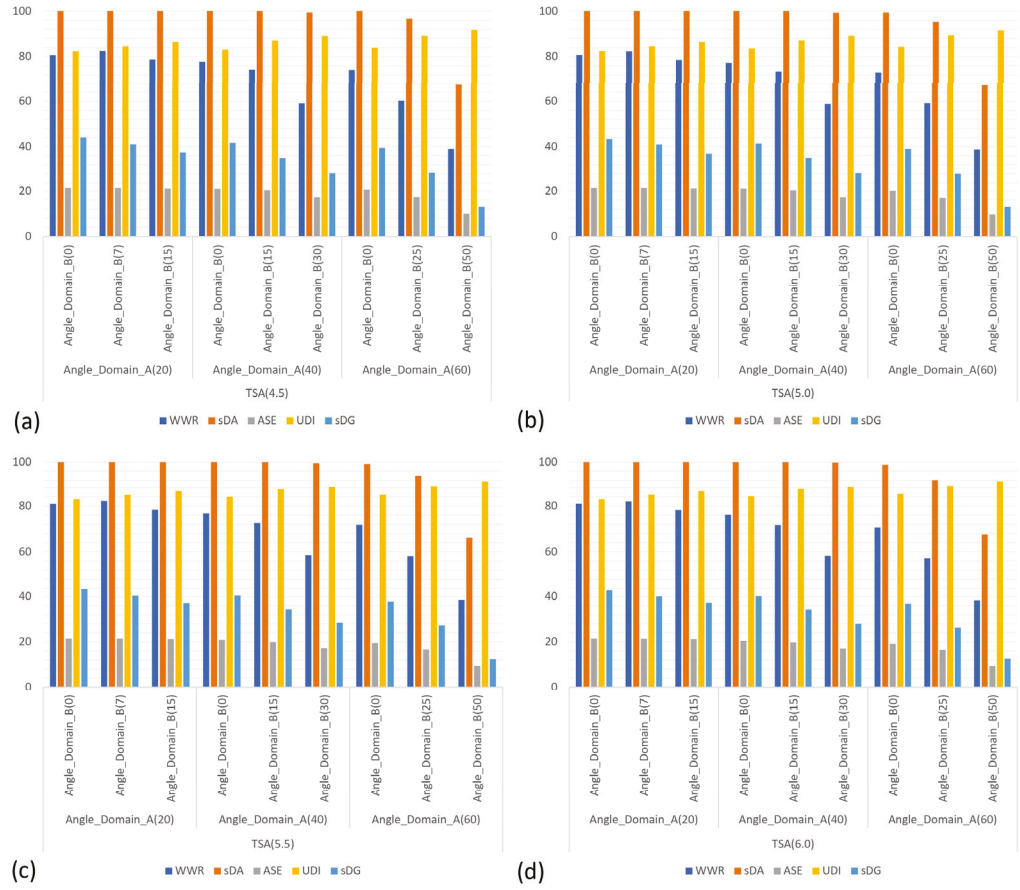


Figure 17. A Comparison of average daylight and visual comfort performance across different angle domains (A: in the focal region, B: outside the focal region) for TSAs radius of (**a**): 4.5, (**b**): 5, (**c**): 5.5, and (**d**): 6, and their effects on variations in sDA, ASE, UDI, SDG metrics, and the amount of WWR.

For a TSA of 5.5 (Figure 17c), daylight performance is evaluated as generally strong with an sDA of 100% and a UDI of 91.55%. The visual comfort can vary, with ASE values

between 9.42% and 21.43%, indicating a risk of excessive sunlight, and sDG values between 12.4% and 43.51%. Many alternatives achieve sDG values below the target point of 15%, highlighting that the larger angular domain of the non-focal region (B) is an effective medium for managing glare.

The integration of angle domains A and B based on a TSA of 6 (Figure 17d) suggests that applying the highest angle domains (A: 60° and B: 50°) provides high daylight performance with an sDA of 98.77% and a UDI of 91.51%. Visual comfort, however, shows variability; ASE values range from 9.32% (angle domain A at 60° and angle domain B at 50°) to 21.43% (angle domain A at 20° and angle domain B at 0°), indicating potential issues with excessive sunlight. sDG values decrease as angle domain B increases, demonstrating improved glare control, from 42.78% (angle domain A at 20° and angle domain B at 0°) to 12.58% (angle domain A at 60° and angle domain B at 50°). Notably, several configurations achieve sDG values below the 15% target, indicating effective glare management with a larger angle domain B.

5.4. The Best Biomimetic Kinetic Façade Solutions Based on the Daylight Performance and Visual Comfort Analysis

According to Figure 18, the biomimetic kinetic façades with angle domains A (60°) and B (50°) outperform most of the solutions due to daylight performance criteria. The results show that while all TSA scenarios reach the acceptable sDA values, the UDI of 91.55% struggles to provide a high level of useful daylight in space. In terms of the visual comfort, ASE values are steadily below 10% (ranging from 7.14% to 9.82%), meeting the target of ASE < 10%. Furthermore, sDG values ranging from 12.83% to 14.96% confirm that the façade successfully balances daylight penetration with visual comfort (Figure 19).

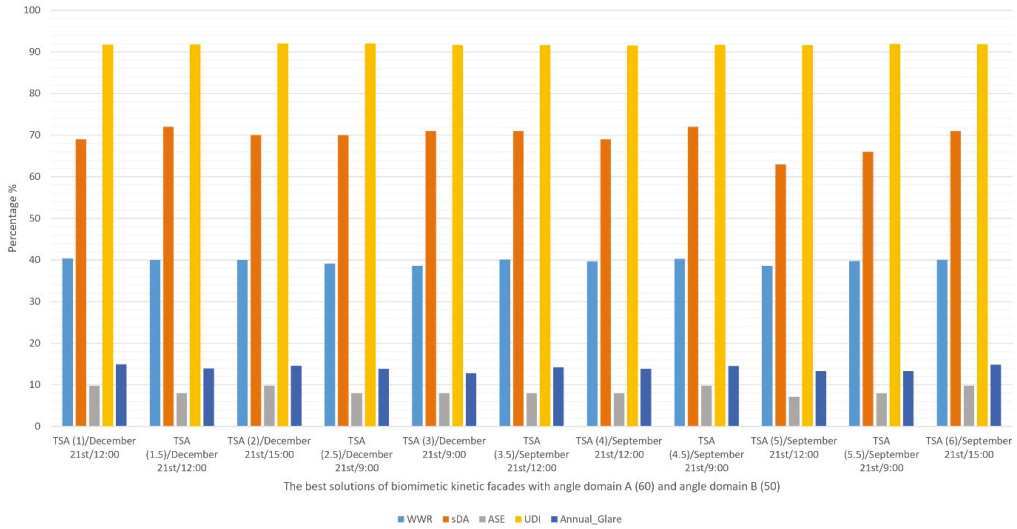


Figure 18. A comparative analysis of WWR, sDA, ASE, UDI, and SDG metrics for the best solutions of biomimetic kinetic façades with angle domain A (60) and angle domain B (50).

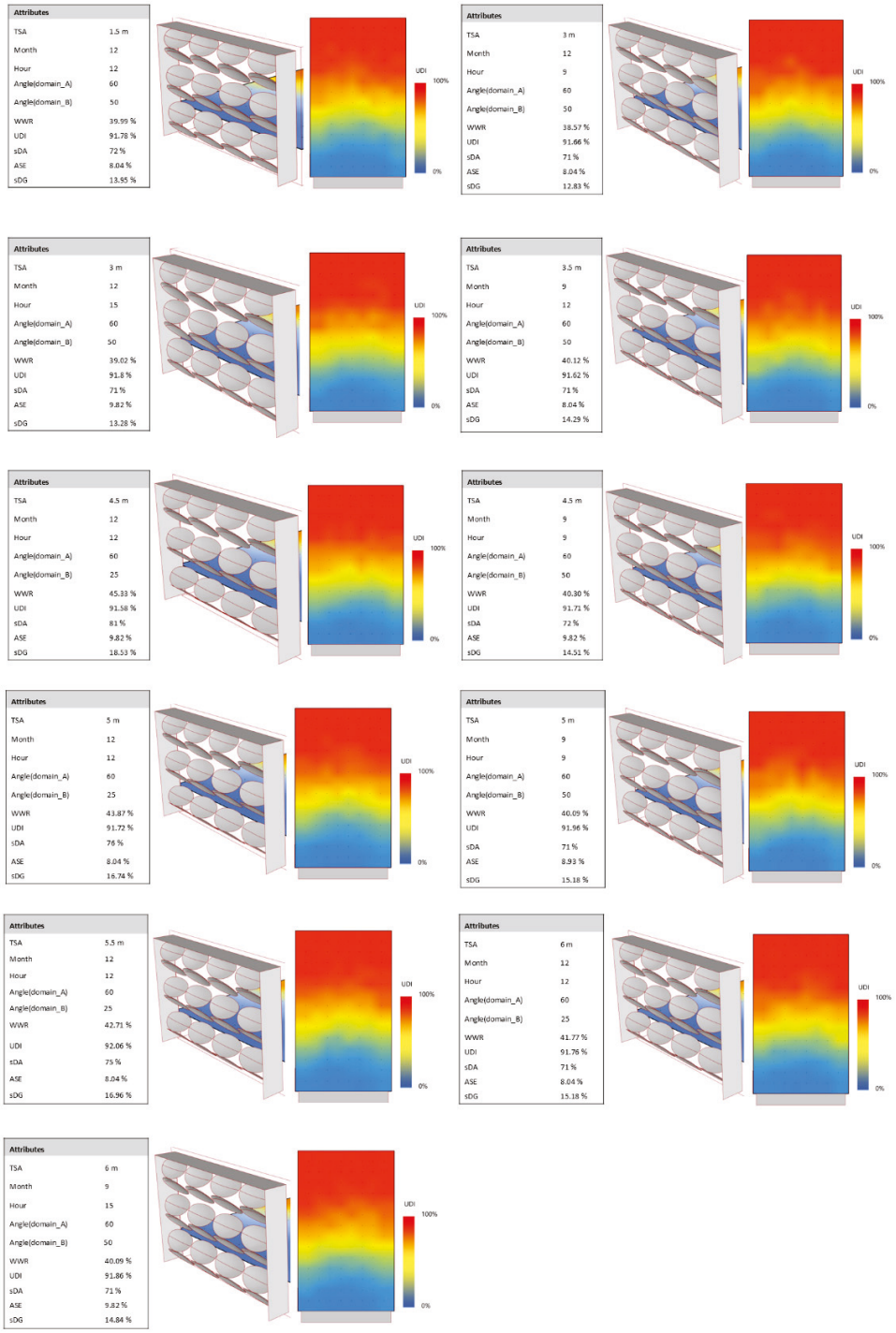


Figure 19. Visualization of the best solutions in meeting the requirements of daylight performance and visual comfort.

Table 4 presents the averages, standard deviations, and the upper and lower bands with a 95% confidence interval for the WWR, sDA, ASE, UDI, and sDG of the biomimetic kinetic façades with angle domain A (60) and angle domain B (50). The average values for sDA, ASE, UDI, and sDG are 68.55%, 10.59%, 91.68%, and 13.88%, respectively. In terms of daylight performance, sDA and UDI exhibited significant differences in their standard deviation (SD) values, with 3.47 for sDA and 0.3 for UDI. This indicates that UDI values are closely clustered around the mean, with lower and upper bands of 0.27 and 0.35,

respectively. In contrast, sDA values show greater variability, suggesting a less consistent performance, with lower and upper bands of 3.06 and 4.0, respectively.

Table 4. Standard deviations and the upper and lower bands with a 95% confidence interval for the WWR, sDA, ASE, UDI, and sDG of the biomimetic kinetic façades with angle domain A (60) and angle domain B (50) daylight.

	WWR	sDA	ASE	UDI	sDG
Average	39.59	68.55	10.59	91.68	13.88
Standard deviation	1.53	3.47	2.36	0.30	1.98
Lower band	1.35409	3.06	2.08	0.27	1.75
Upper band	1.772382	4.01	2.72	0.35	2.29

Regarding visual comfort, the SD values for ASE and sDG indicate moderate fluctuations and variability. Considering the upper and lower bands, we are 95% confident that the true average glare (sDG) and annual sunlight exposure (ASE) fall within the ranges of 12.13% to 16.17% and 8.51% to 13.31%, respectively.

6. Discussion

The parametric analysis of biomimetic kinetic façades with angle domains A (focal region) and B (outside the focal region) under various radii of TSA reveal that logic-based control strategies can significantly enhance both daylight performance and visual comfort through dynamic façade adjustments. The most optimal solution integrates focal and non-focal regions through angle domains A (60°) and B (50°). This kinetic form meets the requirements of visual comfort by having an ASE below 10% (9.32–11.9%) and an sDG below 15% (12.4–15.07%). It shows a 45–55% enhancement in sunlight exposure control and a 65–72% reduction in glare compared to baseline configurations. This result confirms the critical role of TSA and angular optimization in providing high amount of useful daylight without glare and overheating in the office space, aligning with the results of Kamalabadi et al. (2025) [9] and Hosseini et al. (2024) [15]. Another study by Hosseini et al. (2024) [50] utilized the TSA concept with a similar methodology. However, they did not account for angular shape changes in non-focal areas, leading to a lack of consideration for spatial disturbing glare (sDG). In a similar study by Sankaewthong et al. 2022 [2], the authors applied the angular changes in kinetic components without considering the TSA control. Although the kinetic façade obtained a high performance for the daylight factor and LEED criteria, it could not provide any evidence for visual comfort improvements. Ashraf and Abdin (2024) [29] developed a biomimetic shading façade that achieved a sDA of 97%. Building on this benchmark, the current study introduces a novel system that simultaneously regulates focal and non-focal regions through the angular movements of a three-dimensional form inspired by the Venus flytrap. This design similarly reaches an sDA close to 97%. Beyond sDA, this study also assessed UDI and ASE, highlighting the façade's capacity to provide ample useful daylight while effectively limiting exposure to direct sunlight. Additionally, the system records an sDG index of 12.4%, indicating that more than 87% of the occupied area remains free from glare. These performance indicators, including UDI, ASE, and sDG, were not addressed in the aforementioned study, thereby emphasizing the improved daylighting efficiency and visual comfort achieved by our proposed design. In addition, this study demonstrates the significance of three-dimensional forms derived from natural analogs in enhancing performance. These findings align with those of Hosseini et al. (2019) [71], who reported improved daylighting and

visual comfort resulting from the transition from two-dimensional to three-dimensional shape transformations.

The system's daylight performance shows interesting trade-offs between different angular configurations. While moderate angles (A20°/B0°) achieve perfect spatial daylight autonomy (sDA) at 100%, they underperform in terms of glare control. Conversely, steep angles (A60°/B50°) show a 28–31% reduction in sDA (69–72%) but significantly improve useful daylight illuminance (UDI) by 5–10%, reaching values above 91.5%.

The decentralized strategy and the precision of angle control play critical roles in system performance. Specifically, minor adjustments to the non-focal angle domain (B), ranging from 5 to 10°, have been observed to result in significant alterations to glare performance, with estimated variances ranging from 10 to 15%. This underscores the paramount importance of maintaining precise angle control. To illustrate this point, consider the following example: an increase in angle domain B from 30° to 50° results in a reduction in sDG of approximately 15%. Conversely, a decrease in angle domain A from 60° to 40° leads to an enhancement of sDA by approximately 30%, though this is accompanied by a 20–25% increase in glare risk. The findings indicate that the implementation of an adaptive control strategy, characterized by the dynamic modulation of steep angles (A60°/B50°) during periods of glare susceptibility and moderate angles (A20–40°/B0–15°) to ensure uniform daylight distribution, would lead to optimal performance.

6.1. A Simple Decision-Making Framework

This study proposes a simplified decision-making framework based on decentralized control logic. At the core of this system is the transitory sensitive area (TSA), a dynamic zone on the façade that shifts in response to the changing positions of both the sun and occupants. By adjusting its size and location, the TSA defines focal and non-focal regions across the façade. The focal region primarily supports individual visual comfort and daylight performance, while the non-focal region manages the remaining interior areas.

The control logic is adaptable to multiple users simultaneously and supports a broad range of window-to-wall ratios (WWRs), from 35% to 83%, with optimal performance typically observed between 38% and 46%. This flexibility allows the system to tailor WWR configurations based on user preferences, balancing daylight access, glare control, and outdoor views. In some cases, users may accept a degree of glare in exchange for maintaining visual connection with the exterior. The framework can be adapted to various scenarios by modifying the TSA's position and extent, as well as by adjusting the angular behavior of the kinetic façade components in both focal and non-focal regions individually.

The Al Bahr Towers represent a real-world application of three-dimensional shape transformation using angular movements controlled through a decentralized system, aimed at enhancing visual comfort and daylight performance for occupants. While both the Al Bahr Towers and the current study employ decentralized control and dynamic geometry, the results presented here indicate higher performance. This improvement is attributed to the system's ability to independently and precisely adjust angular movements in both focal and non-focal regions simultaneously.

6.2. Correlation Matrix

As illustrated by the correlation matrix in Figure 20, there is a discernible distinction between the impact of Angle_Domain_A (focal region) and Angle_Domain_B (outside the focal region) on daylight performance and visual comfort metrics. For the assessment of daylight performance, Angle_Domain_B exhibits a robust negative correlation with sDA (-0.76), signifying that an increase in focal angles results in a reduction in spatial daylight

autonomy, which may consequently lead to suboptimal daylight conditions in specific areas. Conversely, it exhibits a robust positive correlation with UDI (0.88), signifying that the exterior of the focal region substantially enhances the useful daylight illuminance, thereby fostering balanced daylight distribution. Conversely, Angle_Domain_A demonstrates a moderate negative correlation with sDA (−0.46), signifying a reduction in daylight sufficiency by the focal region, albeit to a lesser extent. It also exhibits a weak positive correlation with UDI (0.41), suggesting only a marginal enhancement in daylight uniformity compared to the non-focal region.

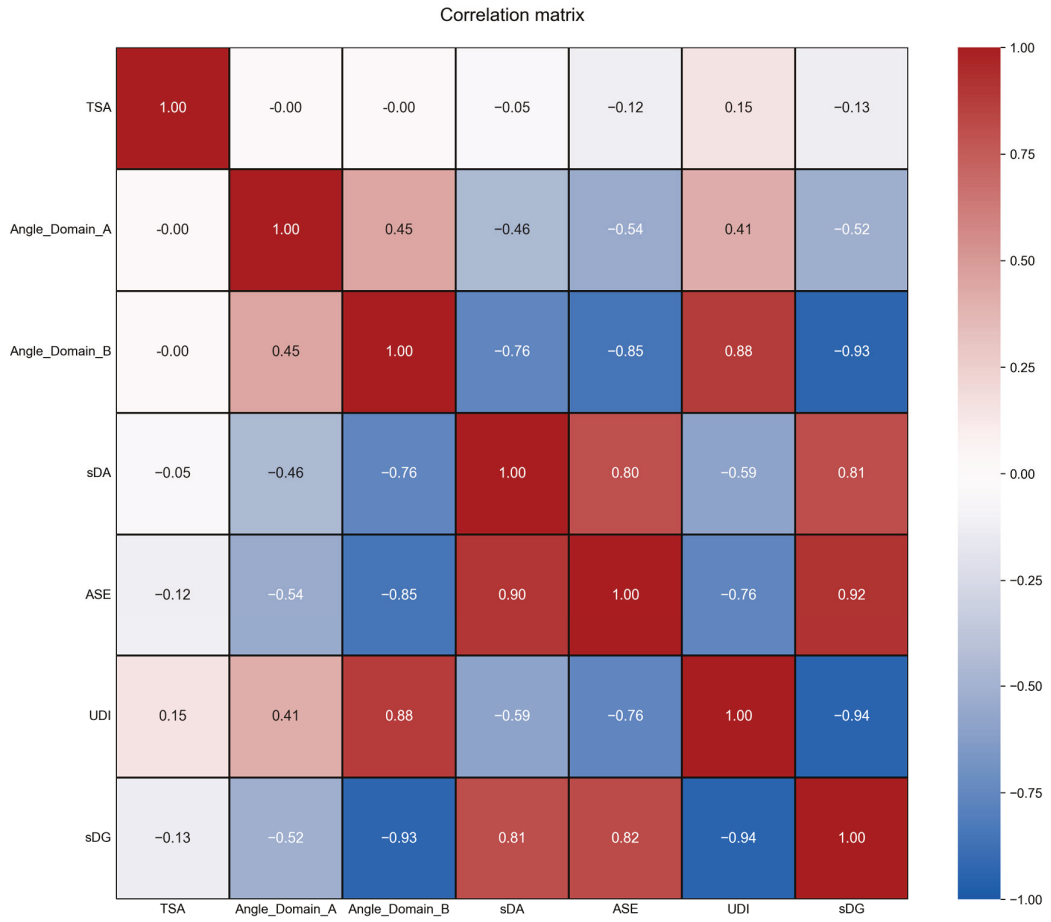


Figure 20. Correlation matrix for considering the effects of TSA and angle domains A (focal region) and B (outside the focal region) on the visual comfort and daylight performance metrics.

In consideration of visual comfort, Angle_Domain_B exhibits a robust negative correlation with ASE (−0.85) and an exceedingly robust negative correlation with SDG (−0.93). This indicates that an increase in non-focal angles leads to a substantial reduction in excessive solar exposure and glare, thereby enhancing visual comfort. These findings underscore the critical role of Angle_Domain_B in ensuring visual comfort in peripheral regions. Angle_Domain_A, on the other hand, shows a moderate negative correlation with ASE (−0.54) and with SDG (−0.52), suggesting some reduction in solar exposure and eliminating glare, though less pronounced than in the non-focal region. In summary, while the non-focal region strongly influences both daylight uniformity and visual comfort, the focal region collaborates in minimizing glare, complementing the non-focal region's performance. This finding demonstrates the effectiveness of incorporating both focal and non-focal regions in dynamic façades to enhance performance, as evidenced by Kamalabadi et al. (2025) [9] and

Sommese et al. (2024) [49]. However, this study emphasizes the crucial role of controlling the non-focal region to achieve the most optimal solutions.

6.3. Limitations

Conducting daylight performance and visual comfort analysis using complex façade forms is computationally expensive. Due to the limitations of hardware and simulation time, we ran preliminary tests to identify potential angle domains for this investigation. This approach ensured that we could explore all possible solutions by varying the window-to-wall ratios, providing different amounts of daylight within the spaces while evaluating visual discomfort. In addition, we need to mention that the focus of this study was the development of the concept through a combination of the biomimetic approach and computational design. The next phase would be rationalization of the concept to address practical implementation challenges, such as mechanical durability, maintenance requirements, or cost implications. As a result, this will require interdisciplinary collaboration from material science, mechanical, structural, and robotic engineers. While factors, such as orientation, climate variation, and different building functions, can significantly influence performance outcomes, these variables fall outside the scope of the current research. As such, we have acknowledged this limitation and recommended these aspects for future investigation in the corresponding section.

7. Conclusions

This study addresses a gap in the literature, which has predominantly focused on centralized control systems, by exploring the potential of decentralized systems in which modules within non-focal regions operate independently in real time. Drawing inspiration from the Venus flytrap's rapid, localized response to stimuli and its distinctive three-dimensional form, the research integrates biomimetic principles with computational design to develop a kinetic façade capable of independently controlling elements across both focal and non-focal regions.

The parametric analysis of biomimetic kinetic façades, encompassing angle domains A (focal region) and B (outside the focal region) across various radii of TSA, demonstrates that decentralized control strategies can markedly enhance daylight performance and visual comfort through dynamic façade modulation. The most efficient configuration integrates angle domain A (60°) with angle domain B (50°), yielding substantial advancements in visual comfort metrics. This optimal arrangement sustains the annual sunlight exposure (ASE) below 10% and spatial daylight glare (sDG) below 15%, signifying a 45–55% enhancement in sunlight exposure management and a 65–72% diminution in glare relative to baseline configurations. Precision in angular control emerges as a pivotal determinant of system efficacy. The results indicate that an adaptive decentralized control of angle domains, dynamically oscillating between steep angles (A60°/B50°) during glare-prone intervals and moderate angles (A20–40°/B0–15°) for uniform daylight distribution, would optimize overall performance.

There are potential lighting energy savings and a cooling load increases to consider in a future study, which will require conducting a co-simulation optimization to come up with solutions that are energy efficient as well. Another avenue for future development involves fabricating a pilot system to assess mechanical durability, maintenance requirements, and cost implications. Additionally, conducting post-evaluations of the system using IoT technologies will enable precise adjustments and enhance performance in response to continuously changing climatic conditions. In addition, this study highlights the critical role of three-dimensional forms found in natural analogs in achieving high-performance

outcomes. Future research could delve deeper into the morphological characteristics of these natural forms, with a focus on geometric optimization of the modules, as well as exploring practical aspects, such as fabrication techniques and prototyping strategies.

Author Contributions: Conceptualization, F.F. and S.M.H.; methodology, F.F., S.M.H. and S.H.; software, F.F., S.M.H. and S.H.; validation, F.F., S.M.H. and S.H.; formal analysis, F.F., S.M.H. and S.H.; investigation, F.F. and S.M.H.; data curation, F.F. and S.M.H.; writing—original draft preparation, F.F. and S.M.H.; writing—review and editing, F.F., S.M.H. and M.K.A.; visualization, F.F., S.M.H. and S.H.; supervision, S.M.H. and M.K.A. All authors have read and agreed to the published version of the manuscript.

Funding: This research received no external funding.

Data Availability Statement: The data that support the findings of this study are available on request from the corresponding author (SMHO).

Acknowledgments: This study forms part of our contribution to the project titled "EUDP 2023-I Participation in IEA SHC Task 70/EBC Annex 90: Low Carbon, High Comfort Integrated Lighting".

Conflicts of Interest: The authors declare no conflict of interest.

References

1. Taherkhani, R.; Aziminezhad, M. Human-Building Interaction: A Bibliometric Review. *Build. Environ.* **2023**, *242*, 110493. [CrossRef]
2. Sankaewthong, S.; Horanont, T.; Miyata, K.; Karnjana, J.; Busayarat, C.; Xie, H. Using a Biomimicry Approach in the Design of a Kinetic Façade to Regulate the Amount of Daylight Entering a Working Space. *Buildings* **2022**, *12*, 2089. [CrossRef]
3. Sadineni, S.B.; Madala, S.; Boehm, R.F. Passive Building Energy Savings: A Review of Building Envelope Components. *Renew. Sustain. Energy Rev.* **2011**, *15*, 3617–3631. [CrossRef]
4. Dehghan Lotfabad, A.; Hosseini, S.M.; Dabove, P.; Heiranipour, M.; Sommese, F. Impacts of Vertical Greenery on Outdoor Thermal Comfort and Carbon Emission Reduction at the Urban Scale in Turin, Italy. *Buildings* **2025**, *15*, 450. [CrossRef]
5. Zaina, S.M.; Fadli, F.; Hosseini, S.M. Evaluation of smart irrigation systems in hot-arid climates for green roofs and walls: Case of Doha, Qatar. *Smart Sustain. Built Environ.* **2022**, *11*, 346–367. [CrossRef]
6. Loonen, R.C.G.M.; Trčka, M.; Cóstola, D.; Hensen, J.L.M. Climate Adaptive Building Shells: State-of-the-Art and Future Challenges. *Renew. Sustain. Energy Rev.* **2013**, *25*, 483–493. [CrossRef]
7. Shi, F.; Zheng, Y.; Ma, Y. A study of the bionic design of a climate-adaptability building surface. *South Archit.* **2023**, *2*, 22–32.
8. Loonen, R.C.G.M. Bio-Inspired Adaptive Building Skins. In *Biotechnologies and Biomimetics for Civil Engineering*; Pacheco Torgal, F., Labrincha, J.A., Diamanti, M.V., Yu, C.-P., Lee, H.K., Eds.; Springer International Publishing: Cham, Switzerland, 2015; pp. 115–134. ISBN 978-3-319-09287-4.
9. Kamalabadi, S.T.; Hosseini, S.M.; Azmoodeh, M. Integration of Bio-Inspired Adaptive Systems for Optimizing Daylight Performance and Glare Control. *J. Build. Eng.* **2025**, *105*, 112415. [CrossRef]
10. Guo, Z.; Ma, Y. Exploration of a Dynamic Building Skin System Responding to Light Environment Information. In Proceedings of the 7th International Conference on Architecture, Materials and Construction, Lisbon, Portugal, 27–29 October 2021; Mendonça, P., Cortiços, N.D., Eds.; Springer International Publishing: Cham, Switzerland, 2022; pp. 91–97.
11. Zocchi, G.; Hosseini, M.; Triantafyllidis, G. Exploring the Synergy of Advanced Lighting Controls, Building Information Modelling and Internet of Things for Sustainable and Energy-Efficient Buildings: A Systematic Literature Review. *Sustainability* **2024**, *16*, 10937. [CrossRef]
12. Sabry, H.; Sherif, A.; Gadelhak, M.; Aly, M. Balancing the Daylighting and Energy Performance of Solar Screens in Residential Desert Buildings: Examination of Screen Axial Rotation and Opening Aspect Ratio. *Sol. Energy* **2014**, *103*, 364–377. [CrossRef]
13. Meerbeek, B.; te Kulve, M.; Gritti, T.; Aarts, M.; van Loenen, E.; Aarts, E. Building Automation and Perceived Control: A Field Study on Motorized Exterior Blinds in Dutch Offices. *Build. Environ.* **2014**, *79*, 66–77. [CrossRef]
14. Shahin, H.S.M. Adaptive Building Envelopes of Multistory Buildings as an Example of High Performance Building Skins. *Alex. Eng. J.* **2019**, *58*, 345–352. [CrossRef]
15. Hosseini, S.M.; Heidari, S.; Attia, S.; Wang, J.; Triantafyllidis, G. Biomimetic Kinetic Façade as a Real-Time Daylight Control: Complex Form versus Simple Form with Proper Kinetic Behavior. *Smart Sustain. Built Environ.* 2024; *ahead of print*. [CrossRef]

16. Fang, J.; Zhao, Y.; Tian, Z.; Lin, P. Analysis of Dynamic Louver Control with Prism Redirecting Fenestrations for Office Daylighting Optimization. *Energy Build.* **2022**, *262*, 112019. [CrossRef]
17. Masoud, S.; Zamani, Z.; Hosseini, S.M.; Attia, S. A Review of Factors Affecting the Lighting Performance of Light Shelves and Controlling Solar Heat Gain. *Buildings* **2024**, *14*, 1832. [CrossRef]
18. Eltaweel, A.; Su, Y.; Lv, Q.; Lv, H. Advanced Parametric Louver Systems with Bi-Axis and Two-Layer Designs for an Extensive Daylighting Coverage in a Deep-Plan Office Room. *Sol. Energy* **2020**, *206*, 596–613. [CrossRef]
19. Tian, Z.; Zhao, Y.; Fang, J.; Kong, Z. AStudy of Daylight Glare Evaluation with Prism Daylighting Redirecting Fenestrations. *J. Build. Eng.* **2023**, *71*, 106428. [CrossRef]
20. Zhu, L.; Shao, Z.; Sun, Y.; Soebarto, V.; Gao, F.; Zillante, G.; Zuo, J. Indoor Daylight Distribution in a Room with Integrated Dynamic Solar Concentrating Facade. *Energy Build.* **2018**, *158*, 1–13. [CrossRef]
21. Shao, Z.; Wang, B.; Xu, Y.; Sun, L.; Ge, X.; Cai, L.; Chang, C. Dynamic Concentrated Solar Building Skin Design Based on Multiobjective Optimization. *Buildings* **2022**, *12*, 2026. [CrossRef]
22. Rizi, R.A.; Eltaweel, A. A User Detective Adaptive Facade towards Improving Visual and Thermal Comfort. *J. Build. Eng.* **2021**, *33*, 101554. [CrossRef]
23. López, M.; Rubio, R.; Martín, S.; Croxford, B. How Plants Inspire Façades. From plants to architecture: Biomimetic principles for the development of adaptive architectural envelopes. *Renew. Sustain. Energy Rev.* **2017**, *67*, 692–703. [CrossRef]
24. Hosseini, S.M.; Fadli, F.; Mohammadi, M. Biomimetic Kinetic Shading Facade Inspired by Tree Morphology for Improving Occupant's Daylight Performance. *J. Daylighting* **2021**, *8*, 65–82. [CrossRef]
25. Pawlyn, M. *Biomimicry in Architecture*, 2nd ed.; RIBA Publishing: London, UK, 2016; ISBN 978-1-85946-628-5.
26. Benyus, J.M. *Biomimicry: Innovation Inspired by Nature*, 2nd ed.; Harper Perennial: New York, NY, USA, 2002; ISBN 978-0-06-053322-9.
27. Badarnah, L. Towards the LIVING Envelope: Biomimetics for Building Envelope Adaptation. Ph.D. Thesis, Delft University of Technology, Delft, The Netherlands, 2012.
28. Romano, R.; Aelenei, L.; Aelenei, D.; Mazzucchelli, E.S. What Is an Adaptive Façade? Analysis of Recent Terms and Definitions from an International Perspective. *J. Facade Des. Eng.* **2018**, *6*, 65–76. [CrossRef]
29. Ashraf, N.; Abdin, A.R. Biomimetic Design Synthesis and Digital Optimization of Building Shading Skin: A Novel Conceptual Framework for Enhanced Energy Efficiency. *Energy Build.* **2024**, *323*, 114824. [CrossRef]
30. Hosseini, S.M.; Mohammadi, M.; Schröder, T.; Guerra-Santin, O. Integrating Interactive Kinetic Façade Design with Colored Glass to Improve Daylight Performance Based on Occupants' Position. *J. Build. Eng.* **2020**, *31*, 101404. [CrossRef]
31. Hosseini, S.M.; Heidari, S. General Morphological Analysis of Orosi Windows and Morpho Butterfly Wing's Principles for Improving Occupant's Daylight Performance through Interactive Kinetic Façade. *J. Build. Eng.* **2022**, *59*, 105027. [CrossRef]
32. Imani, M.; Donn, M.; Balador, Z. Bio-Inspired Materials: Contribution of Biology to Energy Efficiency of Buildings. In *Handbook of Ecomaterials*; Martínez, L.M.T., Kharissova, O.V., Kharisov, B.I., Eds.; Springer International Publishing: Cham, Switzerland, 2019; pp. 2213–2236. ISBN 978-3-319-68255-6.
33. Lurie-Luke, E. Product and Technology Innovation: What Can Biomimicry Inspire? *Biotechnol. Adv.* **2014**, *32*, 1494–1505. [CrossRef]
34. Kuipers, N. FROM STATIC TO KINETIC—The Potential of Kinetic Façades in Care-Hotels.AE-Intecture-Stud. 2015. Available online: https://www.academia.edu/24258545/FROM_STATIC_TO_KINETIC_-_The_potential_of_kinetic_fa%C3%A7ades_in_care-hotels (accessed on 20 January 2025).
35. Lienhard, J.; Schleicher, S.; Poppinga, S.; Masselter, T.; Milwich, M.; Speck, T.; Knippers, J. Flectofin: A Hingeless Flapping Mechanism Inspired by Nature. *Bioinspir. Biomim.* **2011**, *6*, 45001. [CrossRef]
36. Poppinga, S.; Masselter, T.; Lienhard, J.; Schleicher, S.; Knippers, J.; Speck, T. Plant Movements As Concept Generators For Deployable Systems In Architecture. *WIT Trans. Ecol. Environ.* **2010**, *138*, 403–409. [CrossRef]
37. Krieg, O.D. HygroSkin—Meteorosensitive Pavilion. In *Advancing Wood Architecture*; Routledge: Oxfordshire, UK, 2016; ISBN 978-1-315-67882-5.
38. Menges, A. Biomimetic Design Processes in Architecture: Morphogenetic and Evolutionary Computational Design. *Bioinspir. Biomim.* **2012**, *7*, 15003. [CrossRef]
39. Knippers, J.; Gabler, M.; La Magna, R.; Waimer, F.; Menges, A.; Reichert, S.; Schwinn, T. From Nature to Fabrication: Biomimetic Design Principles for the Production of Complex Spatial Structures. In *Proceedings of the Advances in Architectural Geometry 2012*; Hesselgren, L., Sharma, S., Wallner, J., Baldassini, N., Bompas, P., Raynaud, J., Eds.; Springer: Berlin/Heidelberg, Germany, 2013; pp. 107–122.

40. Menges, A. Integrative Design Computation: Integrating Material Behaviour and Robotic Manufacturing Processes in Computational Design for Performative Wood Constructions. In *Integration Through Computation—Proceedings of the 31st Annual Conference of the Association for Computer Aided Design in Architecture*; ACADIA: Fargo, ND, USA, 2011; pp. 72–81. [CrossRef]
41. Kim, H.; Clayton, M.J. A Multi-Objective Optimization Approach for Climate-Adaptive Building Envelope Design Using Parametric Behavior Maps. *Build. Environ.* **2020**, *185*, 107292. [CrossRef]
42. Soliman, M.E.; Bo, S. An Innovative Multifunctional Biomimetic Adaptive Building Envelope Based on a Novel Integrated Methodology of Merging Biological Mechanisms. *J. Build. Eng.* **2023**, *76*, 106995. [CrossRef]
43. Kuru, A.; Oldfield, P.; Bonser, S.; Fiorito, F. Biomimetic Adaptive Building Skins: Energy and Environmental Regulation in Buildings. *Energy Build.* **2019**, *205*, 109544. [CrossRef]
44. Bui, D.K. Improving Building Energy Efficiency: Biomimetic Adaptive Façade and Computational Data-Driven Approach. Ph.D. Thesis, The University of Melbourne, Parkville, Australia, 2020.
45. Goharian, A.; Mahdavinejad, M.; Ghazazani, S.; Hosseini, S.M.; Zamani, Z.; Yavari, H.; Ghafarpoor, F.; Shoghi, F. Designing Adaptability Strategy to a Novel Kinetic Adaptive Façade (NKAF); Toward a Pioneering Method in Dynamic-Objects Daylight Simulation (Post-Processing). *J. Daylighting* **2025**, *12*, 69–90. [CrossRef]
46. Le, D.M.; Park, D.Y.; Baek, J.; Karunyasopon, P.; Chang, S. Multi-Criteria Decision Making for Adaptive Façade Optimal Design in Varied Climates: Energy, Daylight, Occupants' Comfort, and Outdoor View Analysis. *Build. Environ.* **2022**, *223*, 109479. [CrossRef]
47. Wang, Y.; Han, Y.; Wu, Y.; Korkina, E.; Zhou, Z.; Gagarin, V. An Occupant-Centric Adaptive Façade Based on Real-Time and Contactless Glare and Thermal Discomfort Estimation Using Deep Learning Algorithm. *Build. Environ.* **2022**, *214*, 108907. [CrossRef]
48. Hosseini, S.M.; Mohammadi, M.; Schröder, T.; Guerra-Santin, O. Bio-Inspired Interactive Kinetic Façade: Using Dynamic Transitory-Sensitive Area to Improve Multiple Occupants' Visual Comfort. *Front. Archit. Res.* **2021**, *10*, 821–837. [CrossRef]
49. Sommese, F.; Hosseini, S.M.; Badarnah, L.; Capozzi, F.; Giordano, S.; Ambrogi, V.; Ausiello, G. Light-Responsive Kinetic Façade System Inspired by the Gazania Flower: A Biomimetic Approach in Parametric Design for Daylighting. *Build. Environ.* **2024**, *247*, 111052. [CrossRef]
50. Hosseini, S.M.; Heiranipour, M.; Wang, J.; Hinkle, L.E.; Triantafyllidis, G.; Attia, S. Enhancing Visual Comfort and Energy Efficiency in Office Lighting Using Parametric-Generative Design Approach for Interactive Kinetic Louvers. *J. Daylighting* **2024**, *11*, 69–96. [CrossRef]
51. Markin, V.S.; Volkov, A.G.; Jovanov, E. Active Movements in Plants: Mechanism of Trap Closure by Dionaea Muscipula Ellis. *Plant Signal Behav.* **2008**, *3*, 778–783. [CrossRef]
52. Lin, Y.; Zhang, C.; Tang, W.; Jiao, Z.; Wang, J.; Wang, W.; Zhong, Y.; Zhu, P.; Hu, Y.; Yang, H.; et al. A Bioinspired Stress-Response Strategy for High-Speed Soft Grippers. *Adv. Sci.* **2021**, *8*, 2102539. [CrossRef]
53. Guo, Q.; Dai, E.; Han, X.; Xie, S.; Chao, E.; Chen, Z. Fast Nastic Motion of Plants and Bioinspired Structures. *J. R. Soc. Interface* **2015**, *12*, 20150598. [CrossRef] [PubMed]
54. Zeng, X.; Wang, Y.; Morishima, K. Asymmetric-Bifurcation Snapping, All-or-None Motion of Venus Flytrap. *Sci. Rep.* **2025**, *15*, 4805. [CrossRef] [PubMed]
55. Burri, J.T.; Saikia, E.; Läubli, N.F.; Vogler, H.; Wittel, F.K.; Rüggeberg, M.; Herrmann, H.J.; Burgert, I.; Nelson, B.J.; Grossniklaus, U. A Single Touch Can Provide Sufficient Mechanical Stimulation to Trigger Venus Flytrap Closure. *PLoS Biol.* **2020**, *18*, e3000740. [CrossRef] [PubMed]
56. Yunitsyna, A.; Sulaj, E. Daylight Optimization of the South-Faced Architecture Classrooms Using Biomimicry-Based Kinetic Facade Shading System. *J. Daylighting* **2025**, *12*, 1–20. [CrossRef]
57. Bemm, F.; Becker, D.; Larisch, C.; Kreuzer, I.; Escalante-Perez, M.; Schulze, W.X.; Ankenbrand, M.; de Weyer, A.-L.; Krol, E.; Al-Rasheid, K.A.; et al. Venus Flytrap Carnivorous Lifestyle Builds on Herbivore Defense Strategies. *Genome Res.* **2016**, *26*, 812–825. [CrossRef]
58. Li, J.; Tian, A.; Sun, Y.; Feng, B.; Wang, H.; Zhang, X. The Development of a Venus Flytrap Inspired Soft Robot Driven by IPMC. *J. Bionic. Eng.* **2023**, *20*, 406–415. [CrossRef]
59. Volkov, A.G.; Harris, S.L.; Vilfranc, C.L.; Murphy, V.A.; Wooten, J.D.; Paulicin, H.; Volkova, M.I.; Markin, V.S. Venus Flytrap Biomechanics: Forces in the Dionaea Muscipula Trap. *J. Plant Physiol.* **2013**, *170*, 25–32. [CrossRef]
60. Volkov, A.G.; Adesina, T.; Markin, V.S.; Jovanov, E. Kinetics and Mechanism of Dionaea Muscipula Trap Closing. *Plant Physiol.* **2008**, *146*, 694–702. [CrossRef]
61. Wang, B.; Hou, Y.; Zhong, S.; Zhu, J.; Guan, C. Biomimetic Venus Flytrap Structures Using Smart Composites: A Review. *Materials* **2023**, *16*, 6702. [CrossRef]
62. Durak, G.M.; Speck, T.; Poppinga, S. Shapeshifting in the Venus Flytrap (Dionaea Muscipula): Morphological and Biomechanical Adaptations and the Potential Costs of a Failed Hunting Cycle. *Front. Plant Sci.* **2022**, *13*, 970320. [CrossRef]

63. Reinhart, C. Daylight Performance Predictions. In *Building Performance Simulation for Design and Operation*; Routledge: Oxfordshire, UK, 2019; ISBN 978-0-429-40229-6.
64. Reinhart, C.F.; Walkenhorst, O. Validation of Dynamic RADIANCE-Based Daylight Simulations for a Test Office with External Blinds. *Energy Build.* **2001**, *33*, 683–697. [CrossRef]
65. Brembilla, E.; Mardaljevic, J. Climate-Based Daylight Modelling for Compliance Verification: Benchmarking Multiple State-of-the-Art Methods. *Build. Environ.* **2019**, *158*, 151–164. [CrossRef]
66. Nabil, A.; Mardaljevic, J. Useful Daylight Illuminance: A New Paradigm for Assessing Daylight in Buildings. *Light. Res. Technol.* **2005**, *37*, 41–57. [CrossRef]
67. American, A.N. *ANSI/IES LM-83-23 Approved Method: IES Spatial Daylight Autonomy (SDA) and Annual Sunlight Exposure (ASE)*; Illuminating Engineering Society: New York, NY, USA, 2022.
68. Wienold, J.; Christoffersen, J. Evaluation Methods and Development of a New Glare Prediction Model for Daylight Environments with the Use of CCD Cameras. *Energy Build.* **2006**, *38*, 743–757. [CrossRef]
69. Reinhart, C.F.; Wienold, J. The Daylighting Dashboard—A Simulation-Based Design Analysis for Daylit Spaces. *Build. Environ.* **2011**, *46*, 386–396. [CrossRef]
70. Nouri, A.; Frisch, J.; van Treeck, C. Statistical Methodologies for Verification of Building Energy Performance Simulation. *IBPSA* **2021**, *17*, 1719–1726.
71. Hosseini, S.M.; Mohammadi, M.; Guerra-Santin, O. Interactive Kinetic Façade: Improving Visual Comfort Based on Dynamic Daylight and Occupant's Positions by 2D and 3D Shape Changes. *Build. Environ.* **2019**, *165*, 106396. [CrossRef]

Disclaimer/Publisher's Note: The statements, opinions and data contained in all publications are solely those of the individual author(s) and contributor(s) and not of MDPI and/or the editor(s). MDPI and/or the editor(s) disclaim responsibility for any injury to people or property resulting from any ideas, methods, instructions or products referred to in the content.

buildings

MDPI

Article

Improvement of Vernacular Building Spaces for Human Thermal Comfort in Hot Arid Climate of Egypt

Amr Sayed Hassan Abdallah [1,*], Uthman Abdullah Alamri [1], Randa Mohamed Ahmed Mahmoud [2] and Mohamed Hssan Hassan Abdelhafez [3]

[1] Department of Architectural Engineering, College of Engineering, Imam Mohammad Ibn Saud Islamic University (IMSIU), Riyadh 11432, Saudi Arabia; uaalamri@imamu.edu.sa
[2] Department of Architecture, Faculty of Engineering, Assiut University, Assiut 71516, Egypt; randa.m@aun.edu.eg
[3] Department of Architectural Engineering, College of Engineering, University of Hail, Hail 81422, Saudi Arabia; mo.abdelhafez@uoh.edu.sa
* Correspondence: asabdullah@imamu.edu.sa

Abstract: Inner courtyards have been traditionally used as passive strategy in vernacular buildings in desert climates. This paper presents a study conducted to investigate indoor and outdoor thermal comfort of two vernacular buildings in the hot arid climate of Upper Egypt and proposes an improved solution for courtyards to achieve sustainable development of current vernacular houses and apply the same in the arid climate zone of Egypt. The thermal comfort of vernacular building spaces was evaluated based on using field measurements during the hot season and improvement for courtyards based on ENVI-met V5.6.1 simulation model using three scenarios. Two vernacular buildings (Hassan Fathy and Nubian house) were selected to represent the traditional buildings south of Egypt. The study found that using adobe bricks with high thermal mass in vernacular buildings maintained lower indoor temperature with a range of 2.7 °C to 6.7 °C compared to outdoor temperature; this is considered effective thermal insulation. Meanwhile under extreme hot conditions, courtyard temperature inside the vernacular house was 0.3 K higher than the outdoor. This is not sufficient to maintain indoor thermal comfort without integrating passive solutions inside courtyards. In addition, applying the hybrid solution with big dense trees in the courtyards achieved a significant reduction in PET ranging from 4.2 °C and 5.7 °C; shading the widest area of courtyards and allowing for family activities. The study provided techniques and methodology for the middle courtyard of vernacular buildings, demonstrating how improvement achieves thermal comfort and sustainable development required in the 21st century in Upper Egypt, and can be applied to other vernacular houses in different desert cities in southern Egypt.

Keywords: vernacular house; outdoor thermal comfort; PET; improvement solutions

1. Introduction

There are several studies focused on assessing the improvement of indoor thermal comfort in vernacular buildings besides its efficiency in saving energy consumption. For example, Heidari and Davtalab [1] have evaluated the thermal effect of KharKhona on the indoor thermal comfort of a room in a vernacular house in Sistan region, Iran. They reported a reduction in PET, the Predicted Mean Vote (PMV), and standard effective temperature (SET): 7.69 °C, 1.39, and 3.98 °C, respectively. Moreover, Zou et al. [2] assessed the

indoor overheating degree and indoor overheating hours to analyze the thermal environment in vernacular buildings in China. The results showed that the indoor overheating degree improved from 0.7 °C to 1.5 °C inside the case study, and indoor overheating hours were enhanced by a ratio of 40–70%. Fernandes et al. [3] have evaluated the thermal performance of a rammed earth building located in southern Portugal. It was found that thermal comfort had improved to grade "Comfortable" by utilizing shading and natural ventilation devices. Chang et al. [4] studied the impact of building spaces on the thermal environment in vernacular buildings in China, by conducting an occupancy survey. The results indicated that the acceptable air temperature ranged from 23.3 °C to 24.9 °C in summer, and from 18.3 °C to 23.4 °C in winter, and that is available in vernacular buildings compared to modern buildings in the same location. Nevertheless, He et al. [5] assessed the influence of two climate-responsive strategies of vernacular buildings in China on energy consumption by using DesignBuilder software v6.1.8.021. The two strategies employed were multilayer spaces and integrated building envelopes, and their energy-saving rate was 23.7% and 38.3%, respectively. Bayoumi [6] analyzed the Nubian vernacular system in Nubian houses in Aswan, Egypt for applying this system in contemporary buildings to improve passive cooling and thermal comfort, as well as decreasing energy consumption. Also, Du et al. [7] have conducted field measurements of vernacular building microclimate and compared the measurements with dynamic thermal and CFD simulation results. Hence, the simulations could predict the building microclimate successfully. Furthermore, a set of studies has assessed the effect of vernacular buildings on outdoor thermal comfort. For example, Diz-Mellado et al. [8] have assessed the effect of urban courtyards in vernacular centers of a Mediterranean city. It was found that the number of comfort hours (physiological equivalent temperature index) increased by 27%. In contrast, global cooling demand was reduced by 31% using shading devices and courtyards. Davtalab and Heidari [9] have investigated the impact of Kharkhona (an architectural element) on outdoor thermal comfort in the vernacular region of Iran. The results revealed that the physiological equivalent temperature (PET) index was reduced by 9.34 °C. Thus, Kharkhona can be used as a natural ventilation strategy and be more efficient than the vegetation strategy. Xu et al. [10] have studied the factors that influence thermal comfort in vernacular dwellings in Southwest China. It was found that the narrow design of alleys in vernacular dwellings played a main role in reducing the indoor heat gain by 58%. Consequently, it was recommended to integrate the vernacular urban design concepts with modern urban fabric. Also, most studies agree that vernacular buildings in hot regions of the Middle East achieve good thermal comfort using passive design [11–14]. Abdulkareem [12] shows that courtyard houses create cooler microclimates than surrounding streets, especially in late afternoon and evening. Haseh et al. [13] found that greenery covering more than 50% of the courtyard can improve thermal comfort in hot dry Isfahan. Later studies on Fathy's Nubian house used architecture design and elements for achieve thermal comfort. A review on vernacular architecture and Indoor Environmental Quality (IEQ) notes vernacular elements tend to improve satisfaction with thermal comfort and overall IEQ [14].

On the other hand, several scientific studies have compared the indoor thermal performance in vernacular and modern buildings, or different types of vernacular buildings. For instance, Mangeli et al. [15] have proposed a framework to compare vernacular buildings' parameters (rock-cut houses) with contemporary buildings' parameters in Iran and estimated the energy consumption. The result of the PMV index in rock-cut houses and modern houses were 0.61 and 0.77, respectively. Further, energy consumption was zero in rock-cut houses against 7.7 KW daily in modern houses. Also, Widera [16] evaluated the thermal environment of vernacular dwellings in western sub-Saharan Africa and compared

its results with modern houses in the same location. The results indicated that the user thermal comfort was accepted by 70% in vernacular dwellings (air temperature 26–30 °C), in contrast to 20% in modern houses. Additionally, the concentrations of CO_2 increased to 1800–1900 ppm because of the lack of adequate ventilation. Chkeir et al. [17] analyzed thermal comfort parameters and conducted an occupancy survey in two traditional and contemporary houses in Lebanon. The results revealed that the thermal performance in a traditional house is better than in a contemporary one and, consequently, in energy consumption because of using courtyards, natural ventilation, and special architectural elements (narrow and tall windows, porous and light-colored materials, three arch motifs). Also, Toe and Kubota [18] have compared the vernacular cooling techniques in two traditional houses in Malaysia and two other traditional shophouses in China. It was found that, in all four cases, the courtyards assisted in reducing the indoor air temperature in rooms adjacent to the courtyards by 5 °C. Chandel et al. [19] have reviewed the vernacular architectural features that can be adapted in contemporary buildings to keep pace with current lifestyles for improving indoor thermal comfort conditions and energy efficiency. The results indicated that the critical features are built mass design, building and roof materials, orientation, construction techniques, space planning, openings, sunspace provision, and earth as a floor with thermal insulation property. There are many studies on this approach, such as Salameh et al. [20] and Hassan et al. [21].

Moreover, some studies have addressed improvement solutions for vernacular buildings. For example, Zheng et al. [22] have proposed optimization strategies, such as adopting insulating glass windows and increasing the insulation materials of the envelope, to improve indoor thermal comfort in vernacular dwellings in China. The results of the simulation process using DesignBuilder indicated an improvement in thermal environment grade of 4.7%. Also, Abdel Kader and Hassan [23] have improved the model of modern Nubian houses in Aswan, Egypt, to enhance indoor thermal performance using Autodesk Simulation CFD software 2024. So, the results revealed that the air temperature decreased by 2.8 K and the inner ventilation was enhanced to reach 0.9 m/s. Evola et al. [24] have proposed modern envelope solutions for a vernacular house located in Catania, Italy to improve indoor thermal comfort. The modern envelope solutions were (a) a double leaf of bricks, and (b) installing insulation material on the inner and outer walls. It was found that the envelope of the double leaf of bricks decreased the inner air temperature by 1 °C. Conversely, the insulation material caused overheating in the inner spaces.

According to the vernacular buildings analyses in the previous studies, despite the importance of indoor passive strategies for enhancing thermal comfort, the courtyards of these buildings often face environmental challenges such as overheating in summer, limited shading in some spaces, etc. Therefore, this study will investigate the indoor and outdoor thermal comfort of two vernacular houses in Aswan City, Egypt. Based on the field studies and a questionnaire, the vernacular houses' occupants report that courtyards are considered the main place to practice the most important daily family activities in addition to being a source of indoor spaces' ventilation. Furthermore, some studies have investigated the outdoor thermal comfort in the vernacular buildings and proposed new improvement solutions for their courtyards. As observed, there is a problem with high air temperature and outdoor discomfort inside the courtyard, which causes heat stress for the residents. Thus, there is a necessity to propose passive solutions for the courtyards in the vernacular houses, such as shading and vegetation, besides the indoor passive strategies (thick walls, vaults, and domes). Consequently, the air temperature and outdoor thermal comfort will be improved to allow family activities to be performed comfortably during the day and the night. Hence, the main objective of this study is to analyze the indoor and

outdoor thermal comfort of two vernacular buildings in the hot arid climate of Upper Egypt. In addition, the thermal influence of a set of improvement solutions on the thermal comfort of vernacular houses' courtyards will be investigated. The novelty of this study lies in its integrated assessment of both indoor and outdoor thermal comfort in vernacular houses, an area rarely explored, combined with the development and simulation of context-specific passive courtyard enhancement strategies for hot arid regions.

2. Case Study Location and Description

2.1. Hassan Fathy House, New Gourna, Luxor

New Gourna, a village located near Luxor on the west bank of the Nile River, represents a practical case of community development utilizing locally available resources and traditional techniques. In 1945, the Egyptian government entrusted Hassan Fathy to design New Gourna, as shown in Figure 1 [25]. Luxor, located in Egypt at a latitude of 25°7′ N and a longitude of 32°64′ E, experiences maximum temperatures ranging from 41 °C to 44 °C and minimum temperatures between 4 °C and 7 °C. New Gourna, planned by Hassan Fathy, was officially inaugurated by the Egyptian government in 1945 [26]. The project was completely constructed using traditional building techniques and materials, such as adobe-baked mud bricks. Influenced by Nubian and Gourna architectural styles, Fathy adopted mud bricks to construct enclosed courtyards and arched roofings [25]. The main characteristics of New Gourna Village include its innovative reinterpretation of historic urban and architectural environments, the appropriate use of local materials and techniques, and its noticeable sensitivity to climatic conditions [27]. Fathy adapted traditional house designs for New Gourna to address the needs of contemporary farmers. These designs focused mainly on reducing the number of exterior openings, with a central courtyard serving as the house's "lung," providing natural ventilation to the rooms. Fathy brought back to life the courtyard house as a culturally relevant alternative rooted in Arab traditions [25]. His design decisions were informed, and influenced, by his extensive knowledge of traditional architecture, which guided the adaptation of dwellings to the local climate. Fathy's sustainable practices were not just about urban planning, encompassing the organization, scaling, and alignment of streets, as well as the integration of courtyards in both residential and urban designs. He avoided construction methods adopted in developed countries, as they were beyond the financial capabilities of people living in rural areas in Egypt. Instead, he looked for affordable materials and construction methods, such as mudbrick and vaulted or domed roofs. Figure 2a illustrates the architectural layout of a Hassan Fathy house, which includes:

a. The Entrance Lobby: Positioned at the center of the main facade, leading directly to the courtyard.
b. The courtyard: The central space where most family activities occur, connecting the various rooms of the house. It features a large, open, unroofed area.
c. Bedrooms: Two rooms.
d. The Kitchen: A small, often overlooked area.
e. The Toilets: Located inside the house.

2.2. The Nubian House, West Sohail, Aswan

Aswan, located in Egypt at a latitude of 24°09′ N and a longitude of 32°9′ E (Figure 1), experiences maximum temperatures ranging from 42 °C to 45 °C and minimum temperatures between 7 °C and 10 °C. According to the Köppen–Geiger classification (BWh), Aswan has a hot, dry desert climate. The "B" category denotes arid or semi-arid regions characterized by high evaporation rates, while "W" signifies a desert climate. The com-

bination "BW" indicates a dry desert climate, with the "h" for hot climate. The average annual temperature in Aswan is approximately 18 °C [28].

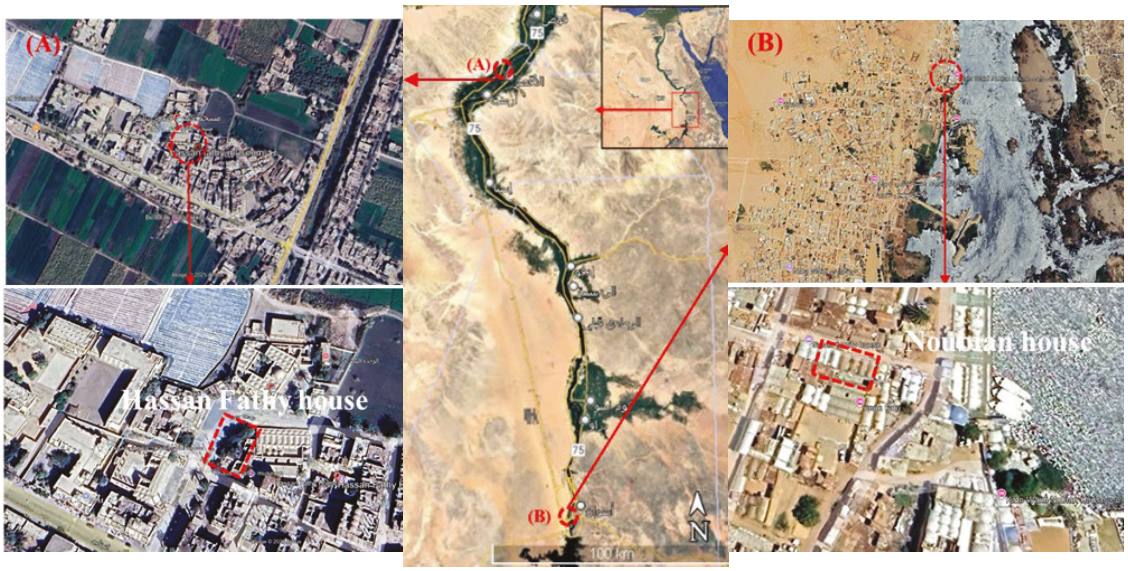


Figure 1. The satellite image of (**A**) Hassan Fathy House, New Gourna, Luxor, with (**B**) Nubian House, West Sohail, Aswan (Author).

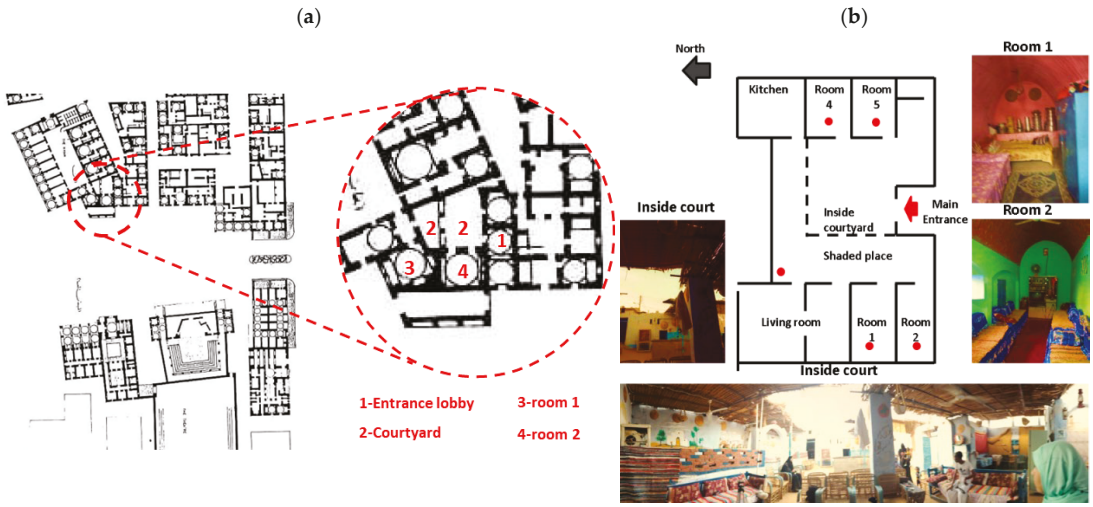


Figure 2. Location of measurements of the two vernacular dwellings, (**a**) four locations inside the Hassan Fathy House, New Gourna, (**b**) five locations inside the Nubian house in West Suhail, Aswan (the authors).

The Nubian houses in Aswan were constructed using mud bricks, which remain one of the most significant examples of indigenous building materials. These homes, built by the Nubians, demonstrate eco-friendly design. Environmentally sustainable practices and climate-responsive architecture contribute to creating a low-cost, comfortable indoor environment [29]. Figure 2b illustrates the layout of a Nubian house, which includes:

(a) The Main Entrance: Positioned in the center of the house's main facade, leading directly to the courtyard or, in some cases, to a lobby before the courtyard.
(b) The Main Courtyard: The central space where most family activities occur, connecting the various rooms of the house. Measuring 8 × 7 m, it is a large, open, unroofed area, with a portion covered by a semi-shaded structure made of palm leaves.

(c) Bedrooms: Four rooms located on the east and west sides of the house. Their doors open to the courtyard, and small ventilation windows beneath the vaults draw air from the courtyard into the rooms [30].
(d) The Kitchen: Comprising two rooms, their traditional design includes a dome covering and an open vent at the top for ventilation [6].
(e) Toilets: Located inside the house without dedicated ventilation solutions.

3. Methodology

As shown in the previous section, two vernacular houses in the south of Egypt have been chosen to investigate indoor and outdoor thermal comfort. The selected case studies are located in low-density areas, which indeed influences thermal comfort by allowing greater exposure to solar radiation and reduced mutual shading between buildings. In the analysis, building density was controlled by accurately representing the surrounding built environment in the simulation models and ensuring that the same contextual conditions were maintained across all improvement scenarios. Furthermore, courtyards in Upper Egyptian vernacular architecture are uniquely adapted to extreme heat and aridity, where their enclosed geometry and shaded surfaces reduce daytime heat accumulation and promote cooler nighttime temperatures. Their performance is further enhanced by locally available materials, such as mudbrick and limestone, which possess high thermal mass and naturally regulate indoor–outdoor temperature fluctuations. Accordingly, the methodology of this study was proposed, as detailed in Figure 3. Thus, the framework of the methodology consists of three main stages as follows:

(a) The first stage is the experimental results of the field measurements inside the two vernacular houses, comparing the two houses' measurements and validating the modeling results.
(b) The second stage is simulating the courtyards of the two vernacular houses using ENVI-met software to assess and visualize the air temperature, relative humidity (RH), wind speed (WS), and mean radiant temperature (T_{mrt}). Then, Rayman software v1.2 was used to calculate the Physiological Equivalent Temperature (PET) as the outdoor thermal comfort index.
(c) The third stage is applying the three improvement solutions to improve the outdoor thermal comfort in the courtyards and determine the optimal solution for each vernacular house.

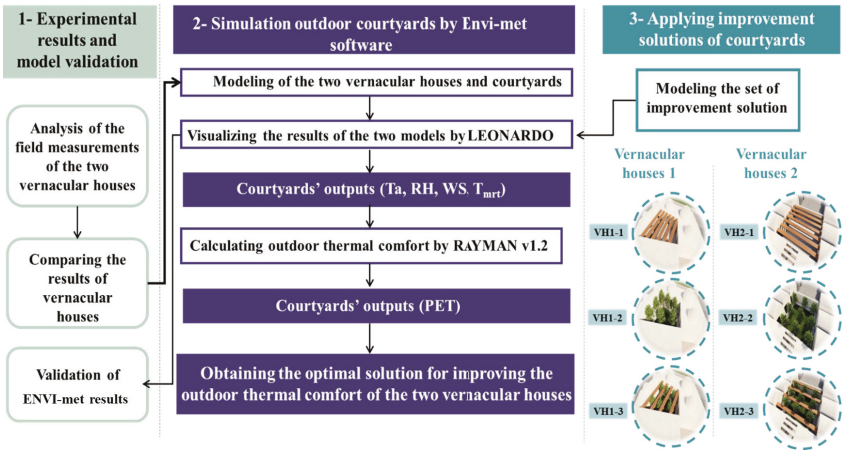


Figure 3. The methodology framework.

Consequently, by conducting the proposed methodology, the study could achieve its goals in investigating the thermal influence of a set of improvement solutions on the outdoor thermal comfort of vernacular houses' courtyards, to improve the outdoor thermal comfort and allow family activities to be performed comfortably during day and night. The study provided information to use improved courtyards of vernacular house as a solution strategy for residential houses in the hot arid climate of Upper Egypt.

3.1. Modeling Vernacular Houses by ENVI-Met and Validation

The models of the New Gourna vernacular house (VH1) and the Nubian vernacular house (VH2) have been built using ENVI-met V5.6.1 software to predict the thermal performance and outdoor thermal comfort inside their courtyards, as elaborated in Figure 4. All meteorological inputs for the ENVI-met model, including wind speed and direction, temperature, humidity, and radiation, were obtained from the METAR dataset of Luxor International Airport (ICAO: HELX). Relying on the two models' characteristics in Table 1, the size of the ENVI-met net was 30 × 24 × 20 for the X, Y, and Z dimensions, respectively. Firstly, the field measurements of Ta, RH inside the two courtyards were monitored using a Thermo Recorder model TR72Ui on 26 April 2016 inside VH1, and on 17 May 2017 inside VH2. Measurement was conducted using data logger with time interval 30 s. The measurement devices were calibrated based on other measurement devices in the lab with accuracy (±1%RH, ±0.1 °C–10 to 95% RH and 0 to 50 °C). Secondly, the field measurements of the two cases were compared with the simulation results to validate the results of the Envi-met model. Consequently, the Coefficient of Determination (R2) for Ta was calculated as 0.96 and 0.91, in VH1 and VH2, respectively, as clarified in Figure 5. According to the good performance of the correction and determination of the coefficient, ENVI-met results are reliable in predicting the thermal performance of the two courtyards in the vernacular houses. The validation of MRT in thermal comfort was not included in this study due to limitations in the available field measurement equipment. Importantly, MRT was fully calculated within the ENVI-met simulations and incorporated into the PET evaluation. In hot-arid climates, several studies have shown that when MRT cannot be measured, air temperature is commonly used as the primary validation parameter because under highly ventilated and low-humidity conditions, operative temperature tends to converge toward air temperature [31,32]. Therefore, using air temperature as the main validation metric represents a reasonable and widely adopted approximation.

Table 1. The characteristics of the two vernacular houses for ENVI-met modeling and validation.

The Characteristics	New Gourna Vernacular House (VH1)	Nubian Vernacular House (VH2)
Area of Study	192 m^2	270 m^2
Building dimensions	12 × 16 m	15 × 18 m
Building Height	4 m	4 m
Courtyard dimensions	9 × 10 m	7 × 8 m
Aspect ratio (H/W)	0.4	0.5
Building Material	Clay + Yellow painted	Clay + Yellow painted
Building Albedo	0.3	0.3
Courtyard ground material	loamy	loamy
Courtyard ground Albedo	0.02	0.02

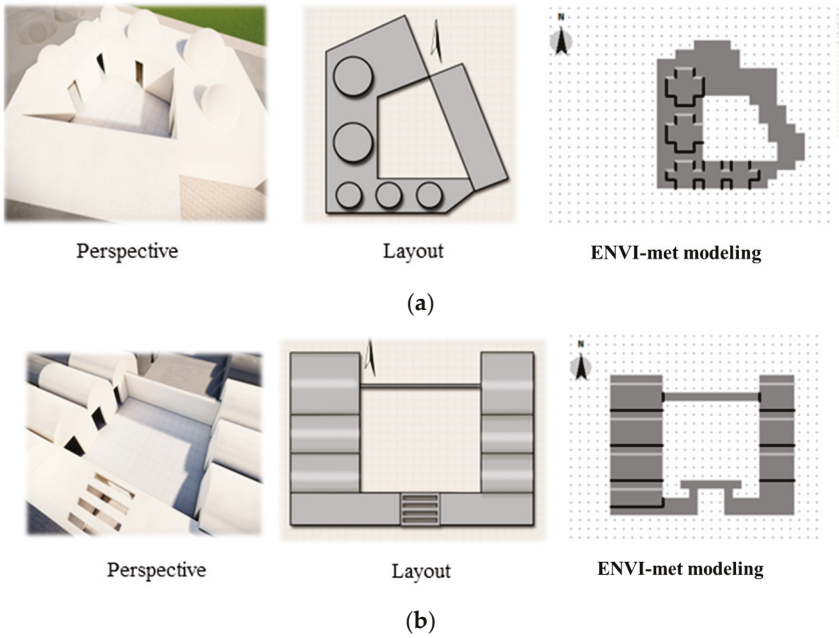


Figure 4. The modeling of the vernacular houses; (**a**) VH1, and (**b**) VH2.

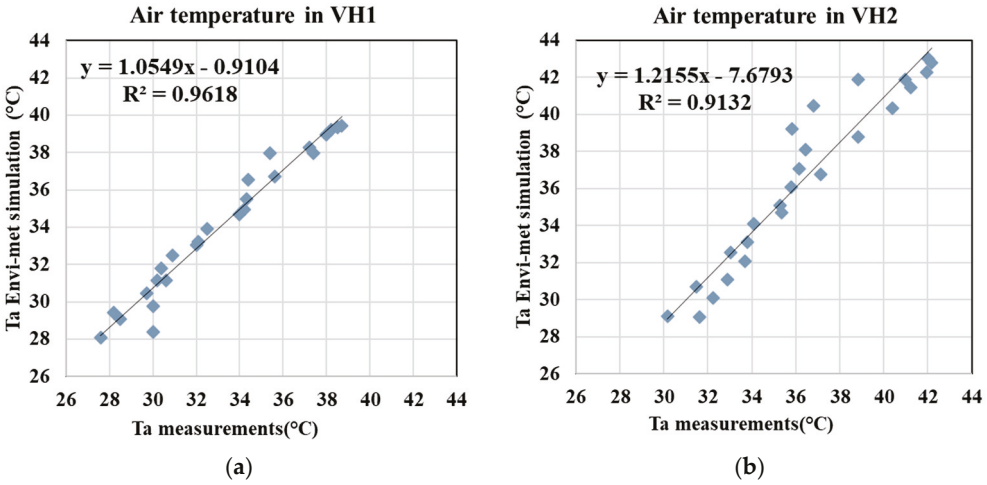


Figure 5. Linear regression of air temperature in (**a**) VH1 and (**b**) VH2.

3.2. The Improvement Solutions of the Vernacular Houses' Courtyards

Figure 6 clarifies the proposed improvement solutions for each vernacular house to improve outdoor thermal comfort. It can be observed that the proposed solutions for the VH1 and VH2 are (a) adding semi-shading by 50% (VH1-1, VH2-1), (b) vegetation solution and adding grass area and trees (VH1-2, VH2-2), and (c) hybrid semi-shading and vegetation (VH1-3, VH2-3). The impact of vegetation on human activity space was addressed by selecting vegetation densities and shading ratios (50%) that enhance thermal comfort without obstructing circulation or usable outdoor areas. Vegetation was positioned along the courtyard perimeter and in non-central zones, ensuring that shading benefits were achieved while maintaining an open, functional activity space for users. In this study, a set of Ficus trees were chosen for vegetation solutions because they are common in the area. Additionally, all proposed solutions remain fully affordable because they rely solely on simple vegetation arrangements and lightweight wooden shading elements, which require minimal cost and maintenance. These proposed solutions have proven their effectiveness in improving outdoor thermal comfort in different types of buildings [33–39].

Consequently, the air temperature and outdoor thermal comfort improve to allow family activities to be performed comfortably during the day and the night.

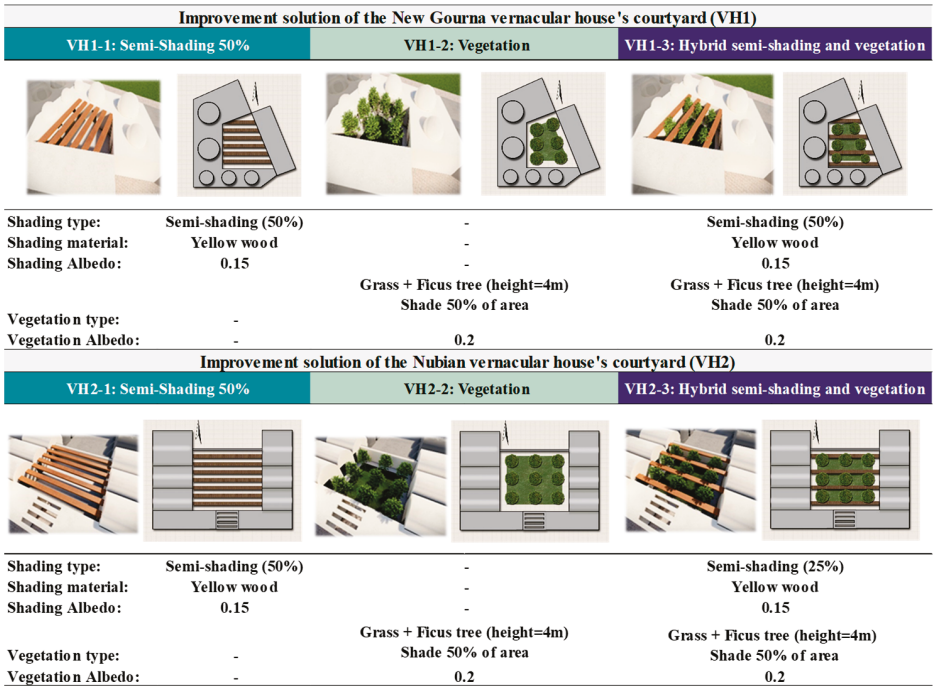


Figure 6. Description of the improvement solutions.

The proposed methodology has a set of potentials as detailed below:

(a) Analyzing the indoor and outdoor thermal comfort of two different vernacular houses.
(b) Proposing diverse improvement solutions to improve outdoor thermal comfort, such as vegetation, shading, and hybrid solutions.
(c) The flexibility of applying the methodology to other vernacular houses, or any house with a courtyard in different desert cities in southern Egypt.
(d) The application of the methodology in two different courtyards with different shapes and H/W ratios so it can be applied to other houses.
(e) The ability to upgrade, to investigate the influence of the improvement solutions through the climate change issue.

Despite that, the study recognizes a set of shortcomings of the methodology:

(a) The methodology ignored other improvement solutions such as albedo.
(b) The study focused only on the semi-shading solution with a ratio of 50% and ignored other ratios, shapes, and materials of the shading system, as well as the effect of surface temperature of the courtyard.
(c) The methodology focused on one-floor vernacular houses with courtyards and ignored other types of vernacular houses.

4. Results and Discussion

4.1. Indoor Thermal Environment Analysis

Figure 7 presents the results of indoor temperature and relative humidity monitoring in Hassan Fathy House from 22 to 28 April. The data revealed that indoor temperatures ranged from 25 °C to 39 °C. Most indoor temperatures exceeded the upper limit of the Adaptive Comfort Standard (ACS) of ANSI/ASHRAE/IES 90.2-2022 [40] (maximum temperature: 32.5 °C). The entrance lobby, Room 1, and Room 2 have effectively mitigated the indoor

climate, maintaining temperatures below the maximum outdoor levels. Air temperature has been identified as a critical factor influencing indoor thermal comfort. Maarof's [37] studies have demonstrated that changes in air temperature can significantly affect an individual's comfort level. Relative humidity (RH) was also monitored, with results from 24 April showing that while outdoor conditions were extremely dry (average 4%), the indoor RH levels in the entrance lobby, Room 1, and Room 2 were 27%, 17%, and 28%, respectively. Although still relatively low, these indoor RH levels were more comfortable compared to the courtyard, where the RH was 5%. The design of Hassan Fathy House focused on effective cooling and necessary heating by strategically distributing rooms and orienting interior spaces toward the sun.

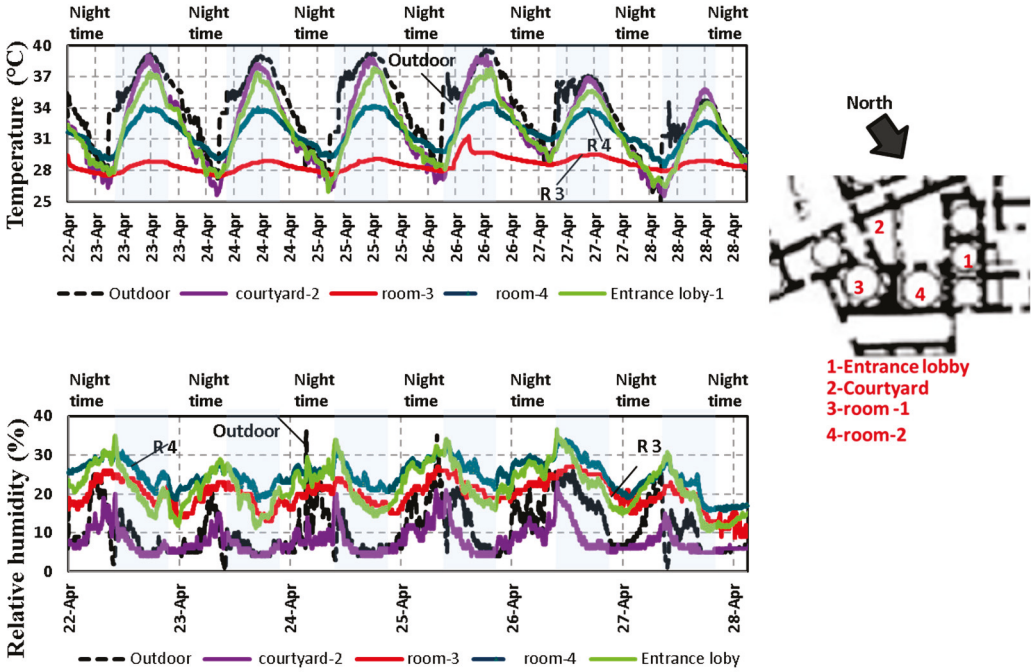


Figure 7. Temperature profile of three locations in the Hassan Fathy House relative to outdoor and courtyard temperature during April 2017.

Figure 8 presents the results of indoor temperature and relative humidity monitoring in the Nubian house from 5 to 23 May. Analysis was performed using dry-bulb air temperature measurements; these values were used due to the limitations of the available monitoring equipment. According to the data, indoor temperatures in the Nubian house ranged from 23 °C to 44 °C. During the day, although all indoor temperatures exceeded the upper limit of the ACS, Rooms 1, 2, 4, and 5 managed to mitigate the indoor climate below the maximum outdoor temperatures. Relative humidity (RH) data from 7 May showed that in dry outdoor conditions (average 25%), the indoor RH levels in Rooms 1, 2, 4, and 5 were 13%, 8%, 20%, and 13%, respectively. Thus, the indoor RH levels were less comfortable, except for the courtyard, where the RH was 26%.

Figure 8 illustrates the temperature patterns of different points in the Hassan Fathy House (the entrance lobby, courtyard, Room 1, and Room 2) from 26 to 29 April. Generally, the temperature curve shows an increase during the day and a decrease at night. On the 26 April, indoor temperatures ranged from 25 °C to 39.1 °C, with the lowest temperatures in Room 3 (28 °C to 32 °C). The highest temperature recorded was 37.5 °C in the entrance lobby, with a relative humidity of 17%. The courtyard temperature reached 39.1 °C with 4% humidity, while the outdoor temperature reached 39.5 °C with 6% humidity. This

indicates that the room temperatures were 1.6 °C lower than the courtyard and 2 °C lower than the outdoor temperature. On the 28 April, the courtyard temperature exceeded 36 °C with 5% humidity, while the outdoor temperature was 34.9 °C with 5% humidity. This suggests that the courtyard's exposure to solar radiation increased its temperature by 1.1 °C compared to the outdoor temperature. The absence of green elements in the courtyard contributed to higher indoor temperatures. These findings agree with the results of Mousli & Semprini [41], who stated that activating a fountain in the courtyard reduced temperatures by at least 1 °C.

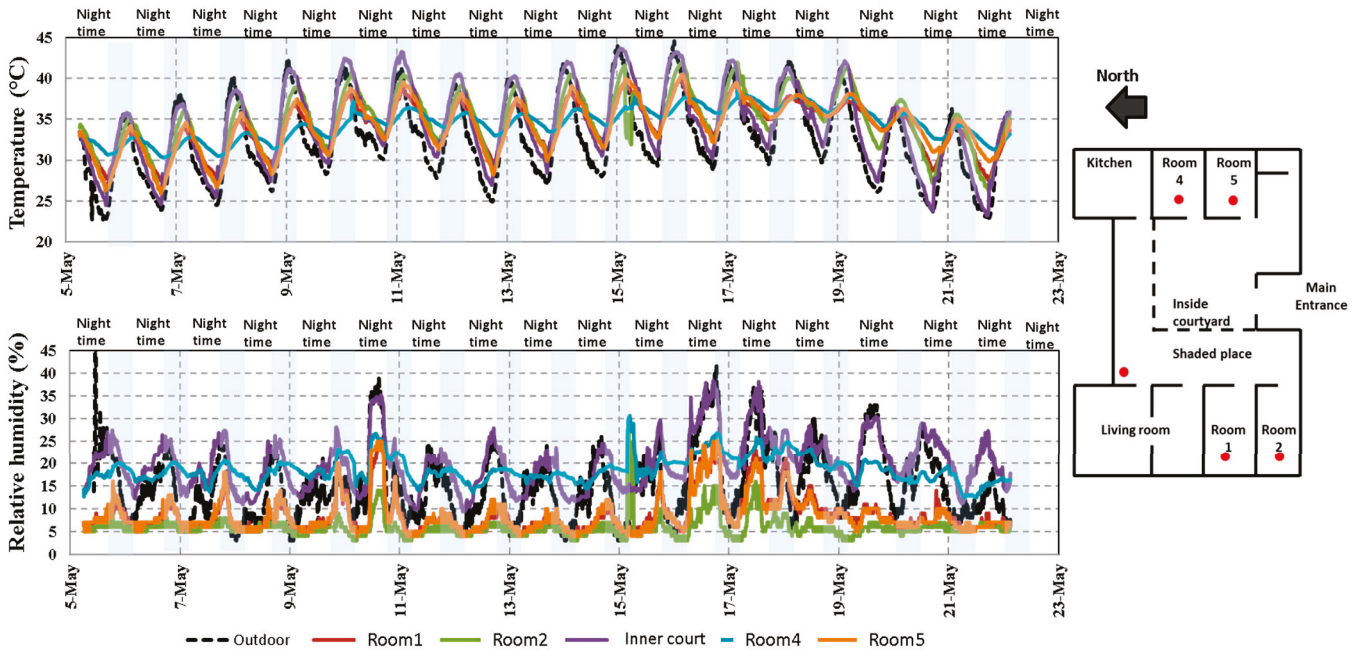


Figure 8. Temperature profile of four locations in the Nubian house relative to outdoor and courtyard temperature during May 2017.

On the 27 April, the highest temperature in Room 3 was 29 °C with 28% humidity, while the courtyard temperature was 35 °C with 10% humidity, and the outdoor temperature reached 37 °C with 20% humidity. This indicates that Room 3 was 6 °C cooler than the courtyard and 8 °C cooler than the outdoor temperature, highlighting the significant effect of thermal insulation caused by the adobe bricks used in the Hassan Fathy House.

4.2. Thermal Comfort and Materials

In the Hassan Fathy House, the indoor temperatures at the four measurement points (entrance lobby, courtyard, Room 1, and Room 2) complied with the 90% acceptability upper limits of the ACS, with a maximum temperature of 32.5 °C. It should be noted that the adaptive comfort limits in ASHRAE Standard 55-2023 [42] are defined in terms of operative temperature, not air temperature. In our study, however, the indoor values obtained from the data loggers represent dry-bulb air temperature. Because vernacular buildings in hot-arid regions typically have thick adobe walls, low air movement, and limited radiant temperature differences, the operative temperature is usually very close to the air temperature. For this reason, using air temperature as an approximation is considered reasonable and is consistent with previous field studies conducted in similar climates. The upper comfort limit of 32.5 °C reported in the results was calculated using the Adaptive Comfort Model in ASHRAE 55-2023—Section 5.4.2.2, which defines the upper 80% acceptability limit as $T_{upper} = 0.31 \times T_{pma(out)} + 21.3$. Applying this formula to the

prevailing mean outdoor temperature measured during the monitoring period yielded a comfort threshold of approximately 32.5 °C. For clarity, all thermal comfort evaluations in this study are based on ASHRAE 55-2023, as shown in Figure 9. The use of materials with high thermal mass, such as stone, clay, and straw, helped maintain lower temperatures due to their physical properties—0.72 kJ/kg·k and 2000 kg/m^3 for specific heat and density [6]. Studies have shown that buildings constructed with materials of low thermal conductivity, such as wood in the roof, provide strong thermal comfort [43]. However, the relative humidity (RH) in the Hassan Fathy House ranged between 5% and 30%, falling outside the ASHRAE thermal comfort range (30–60%), except for 26 and 27 April in the entrance lobby and Room 4.

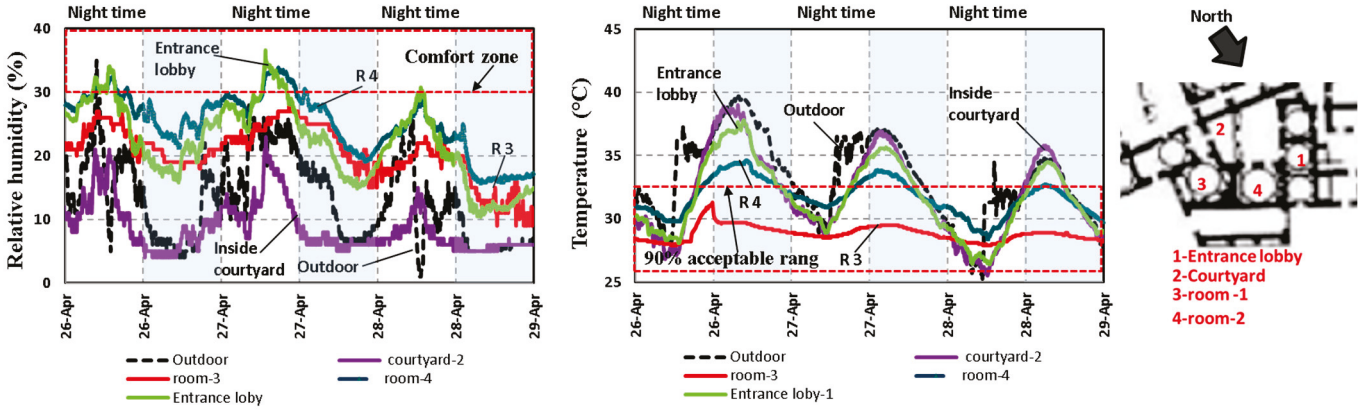


Figure 9. The temperature pattern of the Hassan Fathy House with different measurement locations (the authors).

Figure 10 shows the temperature patterns of different points in the Nubian house (Room 1, Room 2, courtyard, Room 4, and Room 5) from 13 May to 17 May. Indoor temperatures ranged from 28 °C to 44.7 °C, with the lowest temperatures in Room 3 (28 °C to 32 °C). This is attributed to:

1. The use of mud bricks, a mixture of mud and gravel, which provides effective insulation.
2. Wall thickness of 500 mm, which helps maintain cooler room temperatures in hot climates [6].
3. Narrow, elevated openings that reduce heat exposure and sun glare while preserving privacy.
4. Triangular slots in parapets and vaults that facilitate natural ventilation and reduce heat absorption [44].
5. Timberless vaults made of earth bricks and mortar [6].

The results indicate a rise in temperature inside Room 2 during the day, with a peak of 42 °C and a relative humidity level of 10%. Meanwhile, the courtyard recorded a temperature of 43 °C with a relative humidity of 35%, while the outdoor temperature reached 44 °C with a relative humidity of 26%. It can be observed that the temperature in Room 2 was 1 K lower than that of the courtyard and 2 K higher than the outdoor temperature. Further, the air temperature in the courtyard was 1 K lower than the outdoor temperature. On 13 May, the temperature in Room 4 dropped to 36.5 °C with 16% humidity, while the courtyard temperature was 42 °C with 12.5% humidity, and the outdoor temperature was 41.7 °C with 16.5% humidity. This indicates that Room 4 was 5.5 °C cooler than the courtyard and 5.2 °C cooler than the outdoor temperature, demonstrating the effectiveness of solar protection and natural ventilation. These results are consistent with those of Clark [45] and El Azhary et al. [46] regarding the importance of solar protection and ventilation in

moderating indoor temperatures. The air temperature in the courtyard was observed to be 0.3 K higher than the outdoor temperature, highlighting the significant influence of solar radiation on the courtyard, which led to an increase in its temperature relative to the outdoor environment. As for relative humidity (RH), the results indicated that the Nubian house generally fell outside the ASHRAE thermal comfort range of 30–60%, with RH levels ranging between 4% and 30%. However, exceptions were noted on 16 and 17 May the courtyard, as well as on May 15th in Room 4, where RH levels were within a more comfortable range, as illustrated in Figure 10.

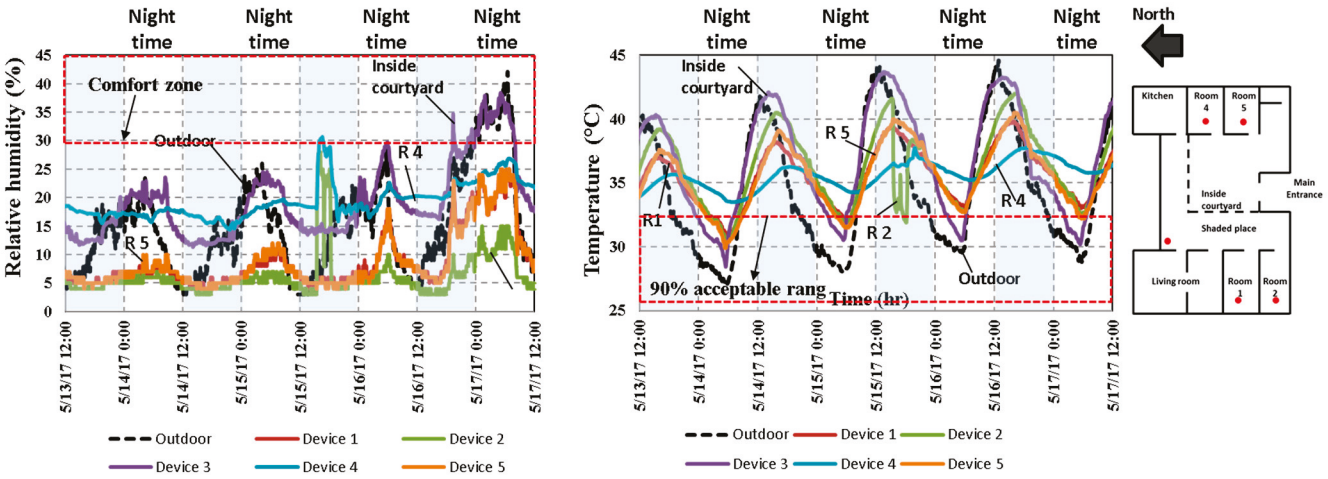


Figure 10. The temperature pattern of the Nubian house, West Sohail, Aswan with different measurement locations (the authors).

Figure 11 shows the regression lines between outdoor and indoor temperatures for both the Hassan Fathy House and the Nubian house. The graph shows significant linear relationships, with high R^2 values. In the Hassan Fathy House, the R^2 value for Room 1 was 0.2385, indicating a weak relationship between indoor and outdoor temperatures. In contrast, the R^2 value for Room 2 was 0.617, indicating a strong relationship. In the Nubian house, the R^2 values for Rooms 1, 2, and 3 were 0.6171, 0.6928, and 0.5334, respectively, indicating significant linear relationships. However, the correlation coefficient for Room 4, which overlooks the courtyard, was very low (0.2021). This proves that vernacular houses (The Nubian house and Fathy house) can adapt to their local climate. These findings are consistent with previous studies [47].

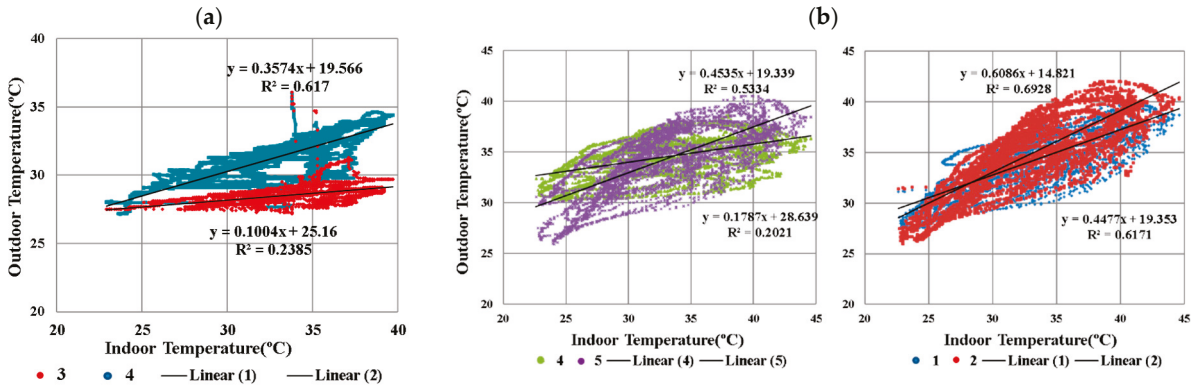


Figure 11. The regression lines between daily outdoor and indoor temperatures, (**a**) Fathy House in two points (Entrance lobby, Courtyard), and (**b**) Nubian house in four points (room 1, room 2, room 4, room 5).

4.3. Evaluation of Indoor and Outdoor Thermography Environment and Temperature Distribution

Thermal imaging helps analyze surface temperature differences in various materials and the effects of shading techniques. It assists architects and engineers in identifying materials and methods that reduce heat absorption [32]. Thermal imaging was conducted using a FLIR (C2) camera, and images were processed using FLIR tools software 6.4. The procedure was made to assess thermal comfort levels for both indoor and outdoor areas. Figure 12a shows a thermal image of the exterior façade of the Nubian house. The floor and wall surface temperatures exceeded 40.5 °C. The red bricks used in the domes provided less thermal insulation than the mud bricks used in the rest of the structure, resulting in higher temperatures. Figure 12b shows the average air temperature distribution inside Hassan Fathy House, ranging from 30 °C to 34.1 °C. This indicates a temperature reduction of 2.7 °C to 6.7 °C compared to the exterior facade, highlighting the thermal insulation effect of adobe bricks. Also, the emissivity values range for brick and painted wall (beige color) are 0.90~0.93 and 0.80~0.90, respectively.

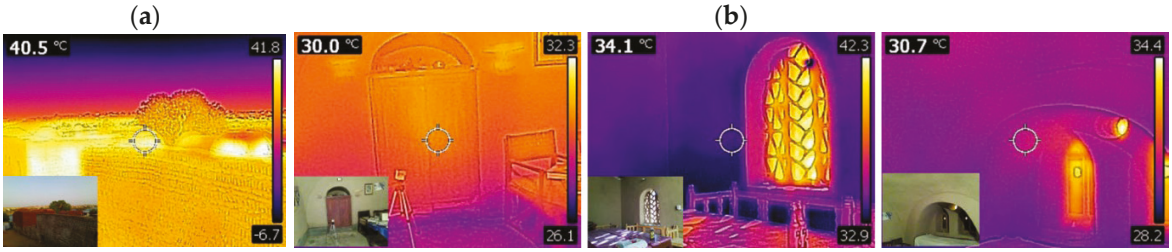


Figure 12. The thermal image for the two vernacular dwellings, (**a**) Nubian house in West Suhail, Aswan (**b**) Hassan Fathy house in Gourna, Luxor.

Data monitoring, during the hot summer months of April and May in the Hassan Fathy House and the Nubian house, showed that indoor temperatures were significantly lower than outdoor temperatures. The Hassan Fathy House performed better in maintaining temperatures close to the comfort range. Fathy's design, incorporating natural ventilation systems, demonstrates a high degree of adaptability to the Egyptian arid climate [25]. Both houses, with their thick walls and use of local materials like adobe bricks, provide effective thermal insulation. The study concludes that traditional construction methods and materials play a significant role in moderating indoor environments in extreme climates, aligning with previous research [28,44,48,49].

4.4. ENVI-Met Simulation Results of the Courtyards Improvement Solutions

4.4.1. Evaluation of Air Temperature

Figure 13a illustrates the variation in Ta inside the courtyard of VH1 for the base case and improvement solutions from 6:00 am on the 26 April to 6:00 am to the 27 April. In the base case (VH1), Ta reached the highest value at 15:00, and it was 39.4 °C. It can be observed that using semi-shading with a ratio of 50% (solution VH1-1) caused a slight temperature reduction in the early hours. The range of Ta reduction is from 1 °C to 2.42 °C. By applying the VH1-2 solution of adding trees, the highest Ta value was reduced to 37.7 °C. The peak reduction in Ta took place by applying the hybrid solution VH1-3 at 15:00, and it was 2.8 °C. Also, the Ta reduction ranged from 2.3 °C to 3.4 °C over the day. Hence, that result is compatible with the result of Mahmoud and Abdallah (2022) [37] who found that adding a 50% semi-shading caused a reduction of 1.5 °C, but the hybrid scenario was the highest reduction up to around 5 °C.

In addition, in VH2 Ta values were from 29 °C to 42.9 °C on 17th and 18 May as shown in Figure 13b. Applying a semi-shading 50% solution (VH2-1) contributed to reducing Ta by 1.0 °C at the hottest hour 15:00. All day long, the reduction ranged from 0.7 °C to 2.0 °C. Nevertheless, the vegetation in the VH2-2 solution assisted in reducing the Ta by 2.9 °C, as in from 17:00 to 4:00. Meanwhile, a significant reduction in air temperature occurred by applying the hybrid improvement solution. Further, the Ta declined from 42.9 °C in the base case to 40.9 °C in the hybrid solution at the hottest hour 15:00. Moreover, the reduction in Ta was observed over the hours, while the reduction ranged between 1.7 °C and 3.2 °C. This is evidence of the efficiency and effectiveness of the hybrid solution in reducing Ta and improving outdoor thermal comfort accordingly.

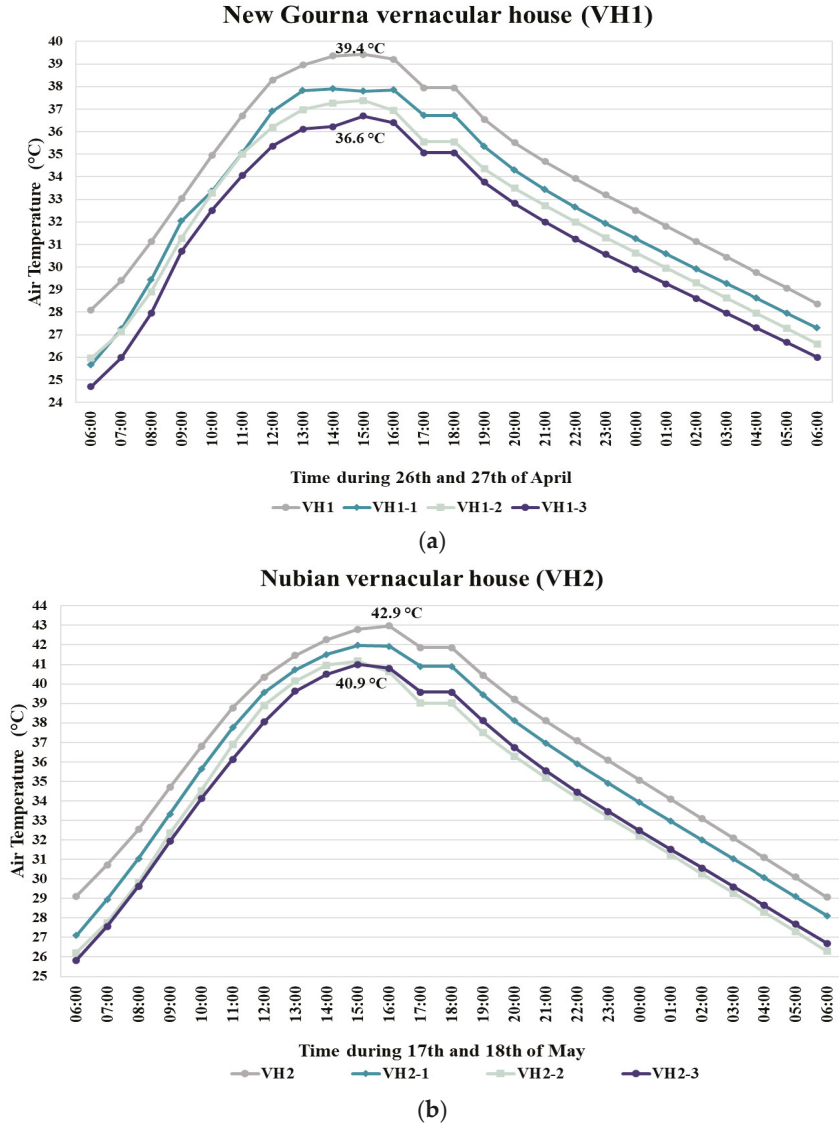


Figure 13. Air temperature inside the courtyard of the base cases and improvement solutions in: (**a**) New Gourna vernacular house (VH1), and (**b**) Nubian vernacular house (VH2).

4.4.2. Evaluation of the T_{mrt}

Mean Radiant Temperature (T_{mrt}) is a crucial indicator for assessing urban radiant and thermal environments. Therefore, the calculated MRT is used to determine the physiologically equivalent temperature (PET) in the RayMan model. Although the earlier discussion focused on mean radiant temperature (MRT), it is equally important to relate these results

to operative temperature, which is the key comfort indicator used in ASHRAE Standard 55. Operative temperature reflects how people actually experience the thermal environment, as it combines both the air temperature and the radiant temperature of surrounding surfaces. In the vernacular buildings examined in this study, the indoor conditions are shaped by thick adobe walls, limited air movement, and relatively uniform surface temperatures. These factors reduce differences between MRT and air temperature, meaning that the operative temperature tends to be very close to the measured air temperature. For this reason, air temperature provides a reasonable and practical approximation of operative temperature in this hot-arid context, and this relationship helps to interpret the comfort findings discussed in this paper. As illustrated in Figure 14a, the three improvement solutions caused a high reduction in the T_{mrt} in the courtyard of VH1. That is a result of shading almost of the courtyard area. In the base case of VH1, the peak of T_{mrt} was obtained at 14:00 and was 78.3 °C. Conversely, the highest value of T_{mrt} by applying VH1-1, VH1-2, and VH1-3 was 54.2 °C, 53.7 °C, and 52.2 °C, respectively. Furthermore, the reduction by applying VH1-1 semi-shading solution reached 29.2 °C during the daytime hours. In contrast to the nighttime hours, the T_{mrt} increased by a range from 0.5 °C to 2.8 °C because of the absorption and emission coefficients of the materials from which the shading is made, and are not present in the base case. Furthermore, by applying VH1-2 vegetation solution, the reduction of T_{mrt} goes up to 29.3 °C. Meanwhile, the VH1-3 hybrid solution assisted in dropping T_{mrt} by a range from 3 °C to 30.5 °C during the daytime hours.

Figure 14b shows the T_{mrt} values of VH2, whilst the peak value was 82.4 °C at 14:00. After applying VH2-1 semi-shading solution, the T_{mrt} values were reduced up to 27.5 °C. On the other hand, the reduction of T_{mrt} in the VH2-2 vegetation solution was the lowest between solutions—24.5 °C. Because the type of trees used could not cover the wide courtyard with an area of 56 m^2, it was recommended to use a big dense tree in the courtyard of the Nubian house. Even though, by applying the VH2-3 hybrid solution, the peak reduction of T_{mrt} was 33.4 °C at 8:00 am, and it was 25.1 °C at the hottest hour 14:00. LEONARDO as a results visualization tool of ENVI-met software was used to obtain thermal distribution maps of T_{mrt} of VH1, VH2, and their improvement solutions at 11:00, 14:00, and 17:00 as shown in Figures 15 and 16. One can observe numerically and graphically the significant decrease of T_{mrt} values in the courtyards of the two vernacular houses, as a result of applying the improvement solutions that led to improved outdoor thermal comfort.

4.4.3. Evaluation of the PET

PET results for the two vernacular houses and the improvement solutions were obtained using LEONARDO outputs and RayMan outputs. The human-related parameters used in the PET calculations were defined in accordance with standard thermal comfort guidelines. These included clothing insulation (0.5–0.9 clo, depending on the season), metabolic rate (1.2 met for light activity), user profile (adult occupants), posture (standing), and activity and behavior (standing still) for ensuring reproducibility and accurate interpretation of the results. Firstly, the PET values of VH1′s courtyard are clarified in Figure 17a, while the range of PET values was between 21.4 °C and 58.2 °C. After applying VH2-1 semi-shading solution, PET dropped from 3 °C to 4.4 °C to reach the highest value is 55 °C at 13:00. As well as VH2-2 vegetation solution contributed to reducing PET by 3.6 °C to 5.1 °C. Above that, the peak of PET reduction ranging from 4.2 °C and 5.7 °C has been obtained by applying the hybrid solution of semi-shading and trees. Consequently, a hybrid solution is the most suitable solution to improve outdoor thermal comfort over the day hours to allow family activities to be performed comfortably.

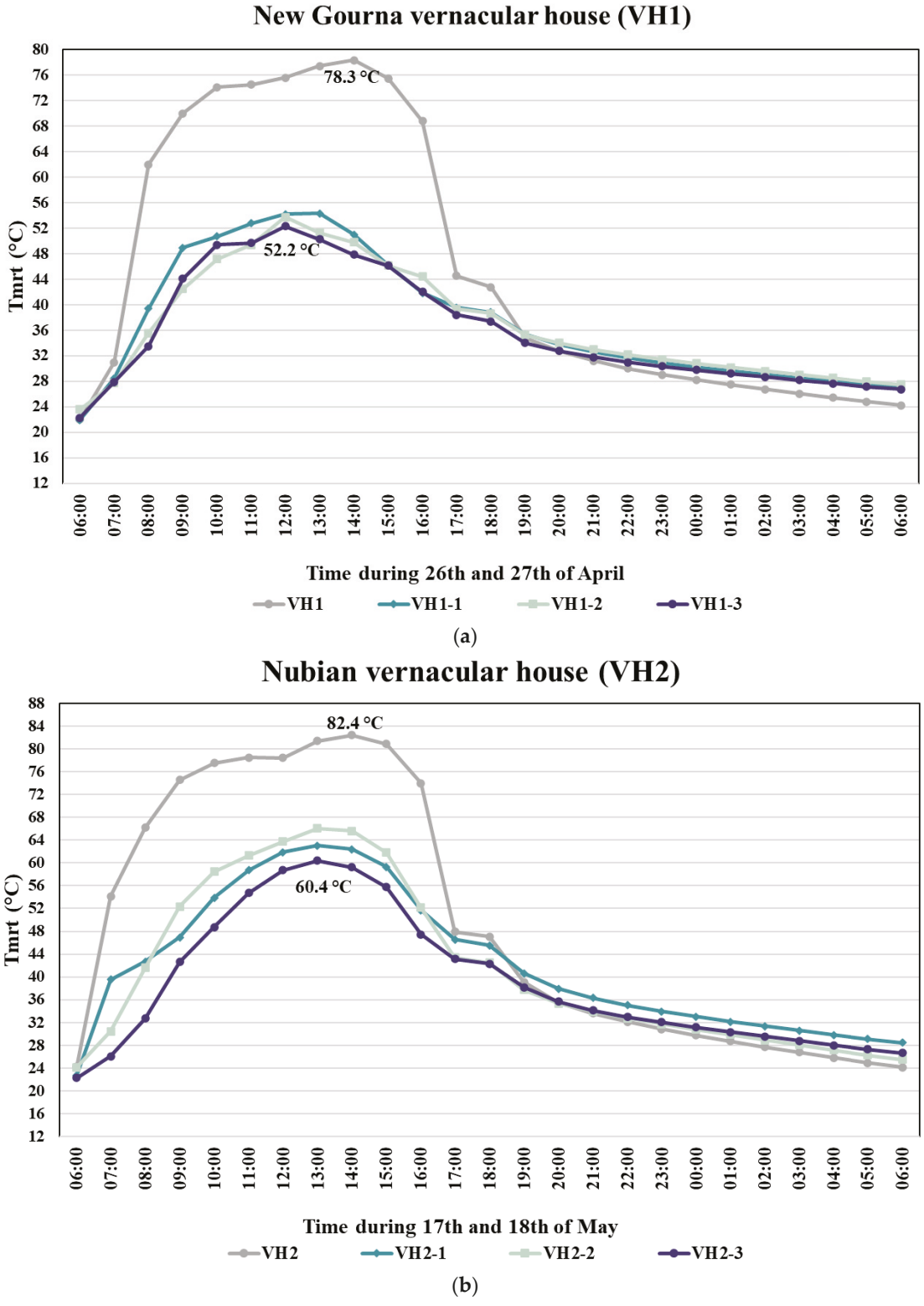


Figure 14. T_{mrt} values inside the courtyard of the base cases and improvement solutions in (**a**) New Gourna vernacular house (VH1), and (**b**) Nubian vernacular house (VH2).

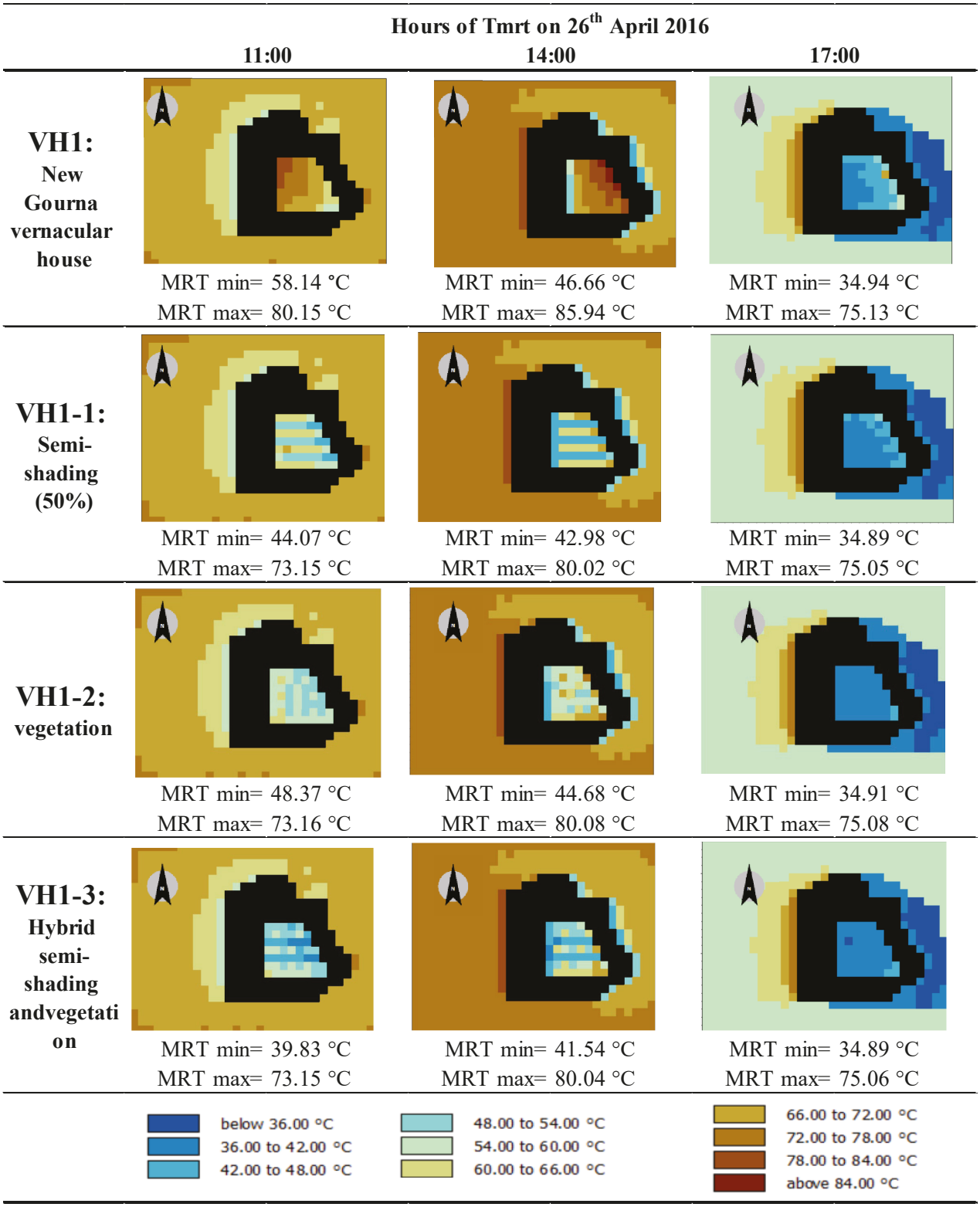


Figure 15. The Thermal distribution map of the Gourna vernacular house (VH1) at 11:00, 14:00, and 17:00.

Due to simulating and calculating the PET in the VH2's courtyard, it can be observed that the high PET values reached 61.4 °C at 14:00, as illustrated in Figure 17b. After applying the VH2-1 semi-shading solution, PET reached 58.8 °C at the hottest hour, 14:00, whilst the reduction range was between 1.8 °C and 4.2 °C. Likewise, PET dropped from 3.2

°C to 6.0 °C by adding trees as in the VH2-2 solution. Additionally, the VH2-2 vegetation solution caused the lowest PET values during the night after 18:00. Furthermore, the hybrid solution (VH2-3) contributed to reducing PET to 59.7 °C at 14:00 and by the range between 3.1 °C and 7.3 °C. It can be concluded that by applying the hybrid solution of semi-shading and trees, the widest area of the courtyard was shaded. This has noticeably reduced the air temperature and mean radiant temperature and improved the outdoor thermal comfort.

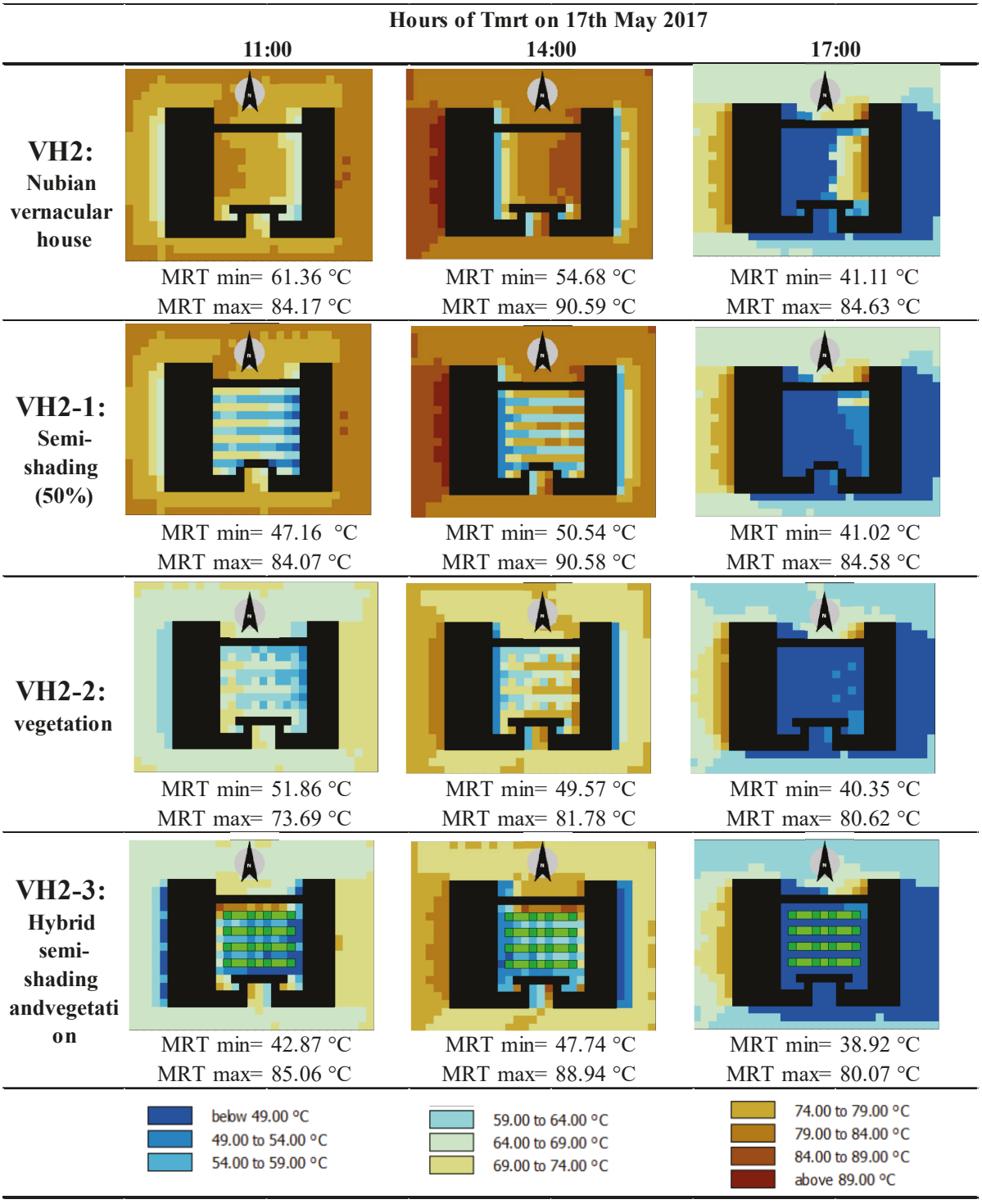


Figure 16. The Thermal distribution map of the Nubian vernacular house (VH2) at 11:00, 14:00, and 17:00.

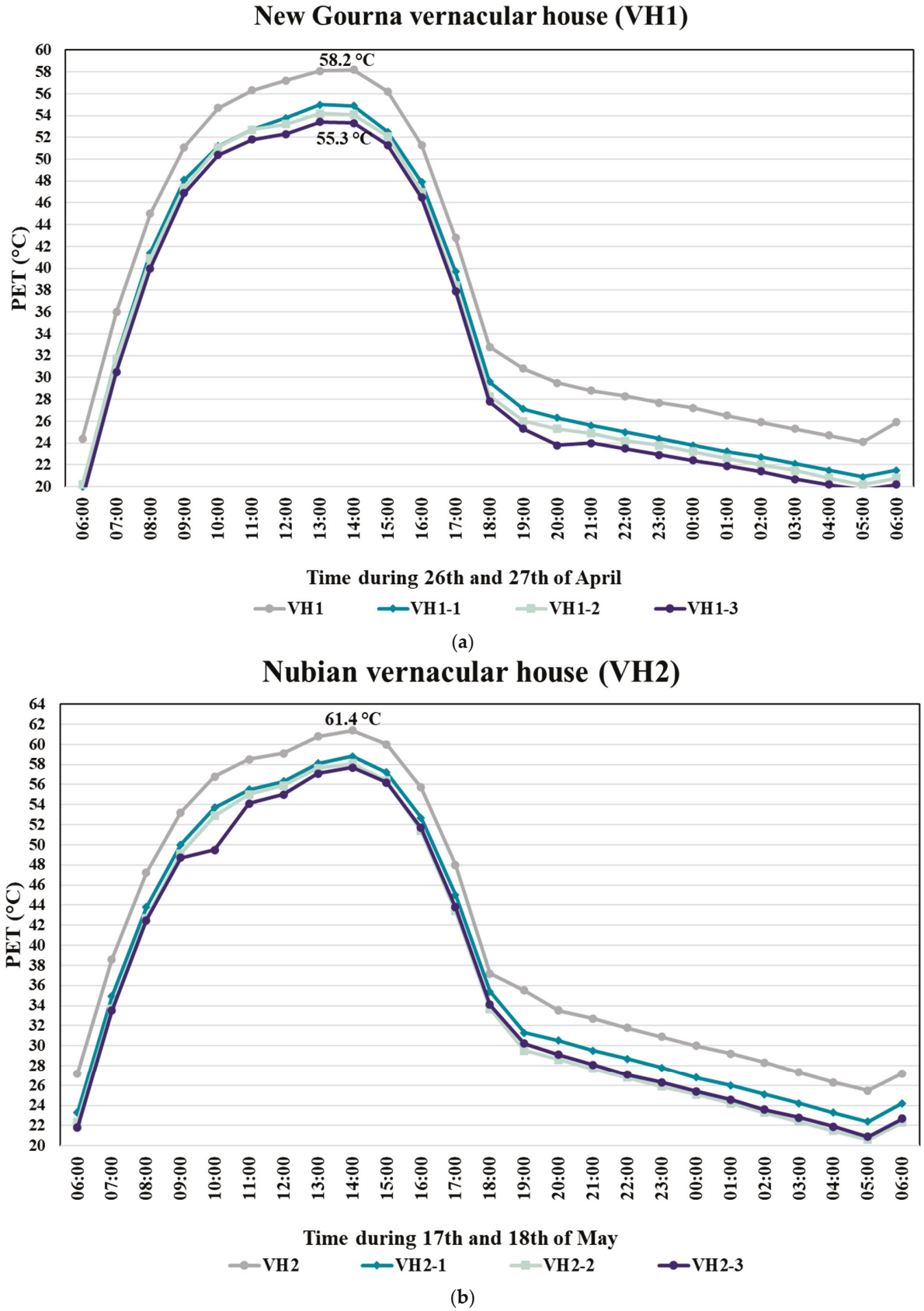


Figure 17. PET values inside the courtyard of the base cases and improvement solutions in: (**a**) New Gourna vernacular house (VH1), and (**b**) Nubian vernacular house (VH2).

Eventually, the limitations of this study are clarified as follows:

(a) Improvement strategies were limited to specific shading and vegetation options, excluding other shading ratios, materials, or cooling methods.
(b) The study focused only on one-floor vernacular houses and two case studies.
(c) Field measurements covered short time periods and may not represent full seasonal conditions.
(d) Courtyard surface temperature effects and a wider range of vegetation types were not examined.
(e) MRT was not validated due to equipment limitations, and only air temperature was used for model validation.
(f) The study did not evaluate other potentially influential solutions such as high-albedo surfaces, evaporative cooling elements, or courtyard surface material modifications.
(g) Only one shading configuration was studied (50% semi-shading). Other shading ratios, materials, geometries, and dynamic shading systems were not investigated.

5. Conclusions

The purpose of this study was to investigate indoor and outdoor thermal comfort of two vernacular buildings in the hot arid climate of Upper Egypt and propose improved solution for courtyards to achieve sustainable development of current vernacular houses and apply the same in the arid climate zone of Egypt. The results from the measurements and simulation can be summarized as follows:

- Using adobe bricks as a material for traditional and vernacular buildings south of Egypt is considered as effective thermal insulation that moderates indoor environments in extreme climates, and lowers indoor temperature by 2.7 °C to 6.7 °C.
- Using inner courtyards without any passive solutions achieved high air temperature due to the significant influence of solar radiation on the courtyard; 0.3 K higher than the outdoor temperature.
- Significant reductions for Ta and PET values are achieved through providing hybrid shading in the courtyards of the vernacular buildings, ranging from 2.3 °C to 3.4 °C over the day, and 4.2 °C and 5.7 °C for air temperature and PET, respectively.
- Inner courtyards with shading and big dense trees achieve thermal comfort and allow family activities to be performed comfortably.

In conclusion, the study demonstrated that implementing a hybrid strategy of semi-shading structures combined with trees provides the largest shaded coverage across the courtyard. This approach has significantly lowered both air temperature and the mean radiant temperature, thereby enhancing outdoor thermal comfort. Consequently, such improvements can motivate Egyptian families to engage more actively in courtyard activities, while also contributing to a noticeable reduction in indoor temperatures in the arid climates of Upper Egypt.

Author Contributions: Conceptualization, A.S.H.A. and R.M.A.M.; methodology, A.S.H.A. and R.M.A.M.; software, R.M.A.M.; validation, R.M.A.M.; formal analysis, A.S.H.A. and R.M.A.M.; investigation, A.S.H.A. and R.M.A.M.; resources, A.S.H.A. and R.M.A.M.; data curation, A.S.H.A. and R.M.A.M.; writing—original draft preparation, A.S.H.A. and R.M.A.M.; writing—review and editing, A.S.H.A., R.M.A.M., M.H.H.A. and U.A.A.; visualization, R.M.A.M.; supervision, A.S.H.A.; project administration, U.A.A.; funding acquisition, U.A.A. All authors have read and agreed to the published version of the manuscript.

Funding: This work was supported and funded by the Deanship of Scientific Research at Imam Mohammad Ibn Saud Islamic University (IMSIU) (grant number IMSIU-DDRSP2503).

Data Availability Statement: The original contributions presented in this study are included in the article. Further inquiries can be directed to the corresponding authors.

Conflicts of Interest: The authors declare that they have no known competing financial interests or personal relationships that could have appeared to influence the work reported in this paper. There are no conflicts of interest.

References

1. Heidari, A.; Davtalab, J. Effect of Kharkhona on thermal comfort in the indoor space: A case study of Sistan region in Iran. *Energy Build.* **2024**, *318*, 114431. [CrossRef]
2. Zou, Y.; Guo, J.; Xia, D.; Lou, S.; Huang, Y.; Yang, X.; Zhong, Z. Quantitative analysis and enhancement on passive survivability of vernacular houses in the hot and humid region of China. *J. Build. Eng.* **2023**, *71*, 106431. [CrossRef]
3. Fernandes, J.; Silva, S.M.; Mateus, R.; Teixeira, E.R. Analysis of the Thermal Performance and Comfort Conditions of Vernacular Rammed Earth Architecture from Southern Portugal. *Ref. Modul. Mater. Sci. Mater. Eng.* **2020**, *4*, 1–10. [CrossRef]
4. Chang, S.; He, W.; Yan, H.; Yang, L.; Song, C. Influences of vernacular building spaces on human thermal comfort in China's arid climate areas. *Energy Build.* **2021**, *244*, 110978. [CrossRef]
5. He, W.; Wu, Z.; Jin, R.; Liu, J. Organization and evolution of climate responsive strategies, used in Turpan vernacular buildings in arid region of China. *Front. Archit. Res.* **2023**, *12*, 556–574. [CrossRef]
6. Bayoumi, O.A.M. Nubian Vernacular architecture & contemporary Aswan buildings' enhancement. *Alex. Eng. J.* **2018**, *57*, 875–883. [CrossRef]
7. Du, X.; Bokel, R.; Dobbelsteen, A.V.D. Building microclimate and summer thermal comfort in free-running buildings with diverse spaces: A Chinese vernacular house case. *Build. Environ.* **2014**, *82*, 215–227. [CrossRef]
8. Diz-Mellado, E.; L'opez-Cabeza, V.P.; Roa-Fern'andez, J.; Rivera-G'omez, C.; Gal'an-Marín, C. Energy-saving and thermal comfort potential of vernacular urban block porosity shading. *Sustain. Cities Soc.* **2023**, *89*, 104325. [CrossRef]
9. Davtalab, J.; Heidari, A. The Effect of Kharkhona on Outdoor Thermal Comfort in Hot and Dry Climate: A Case Study of Sistan Region in Iran. *Sustain. Cities Soc.* **2021**, *65*, 102607. [CrossRef]
10. Xu, Y.; Yang, Z.; Zheng, X.; Ren, J.; Feng, C.; Tang, M. Thermal environments of vernacular dwellings and the adjacent alley in summer: An experimental study in Southwest China. *Build. Environ.* **2024**, *261*, 111634. [CrossRef]
11. Reynolds, N.Y. Architecture design for procuring thermal comfort: Hassan Fathy, Nubia and desert building. *Int. J. Islam. Archit.* **2024**, *13*, 361–391.
12. Haval, A.A. Thermal comfort through the microclimates. Acritical review of the middle-eastern courtyard house as a climatic response. *Procedia Soc. Behav. Sci.* **2016**, *216*, 662–674.
13. Haseh, H.R.; Khakzand, M.; Ojaghlou, M. Optimal thermal characteristics of the courtyard in the hot and arid climate of Isfahan. *Building* **2018**, *8*, 166. [CrossRef]
14. Shetty, S.; Patil, S. Vernacular architecture and indoor environmental satisfaction: Asystematic review of influencing factors. *Architecture* **2025**, *5*, 87. [CrossRef]
15. Mangeli, M.; Aram, F.; Abouei, R. Energy consumption and thermal comfort of rock-cut and modern buildings. *Heliyon* **2024**, *10*, e34217. [CrossRef]
16. Widera, B. Comparative analysis of user comfort and thermal performance of six types of vernacular dwellings as the first step towards climate resilient, sustainable and bioclimatic architecture in western sub-Saharan Africa. *Renew. Sustain. Energy Rev.* **2021**, *140*, 110736. [CrossRef]
17. Chkeir, A.; Bouzidi, Y.; El Akili, Z.; Charafeddine, M.; Kashmar, Z. Assessment of thermal comfort in the traditional and contemporary houses in Byblos: A comparative study. *Energy Built Environ.* **2024**, *5*, 933–945. [CrossRef]
18. Toe, D.H.C.; Kubota, T. Comparative assessment of vernacular passive cooling techniques for improving indoor thermal comfort of modern terraced houses in hot–humid climate of Malaysia. *Sol. Energy* **2015**, *114*, 229–258. [CrossRef]
19. Chandel, S.S.; Sharma, V.; Marwah, B.M. Review of energy-efficient features in vernacular architecture for improving indoor thermal comfort conditions. *Renew. Sustain. Energy Rev.* **2016**, *65*, 459–477. [CrossRef]
20. Salameh, M.; Mushtaha, E.; El Khazindar, A. Improvement of thermal performance and predicted mean vote in city districts: A case in the United Arab Emirates. *Ain Shams Eng. J.* **2023**, *14*, 101999. [CrossRef]
21. Hassan, A.M.; Lee, H.; Ohb, S. Challenges of passive cooling techniques in buildings: A critical review for identifying the resilient technique. *J. Teknol.* **2016**, *78*, 149–162. [CrossRef]
22. Zheng, W.; Wei, F.; Su, S.; Cai, J.; Wei, J.; Hua, R. Effect of the envelope structure on the indoor thermal environment of low-energy residential building in humid subtropical climate: In case of brick–timber vernacular dwelling in China. *Environ. Technol. Innov.* **2022**, *28*, 102884. [CrossRef]

23. Abdel Kader, H.S.; Hassan, M.H. Improving the thermal performance of modern nubian house (wadi karkar as a case study). *JES Assiut Univ. Fac. Eng.* **2017**, *45*, 545–557. [CrossRef]
24. Evola, G.; Marletta, L.; Natarajan, S.; Patane, E.M. Thermal inertia of heavyweight traditional buildings: Experimental measurements and simulated scenarios. *Energy Procedia* **2017**, *133*, 42–52. [CrossRef]
25. Ferruses, I.J.; Dols, S.A.; Gago, C.C. Sustainable Approaches Employed in Settlements Designed by Hassan Fathy: Lessons from New Gourna and New Baris in Egypt. *J. Int. Soc. Study Vernac. Settl.* **2024**, *11*, 194–208. [CrossRef]
26. Attia, S. The Earth Construction Fallacy: Hassan Fathy's New Gourna Revisited. In Proceedings of the PLEA Conference (Re) Thinking Resilience, Wroclaw, Poland, 26 June 2024.
27. Hamouchene, H. *Dismantling Green Colonialism: Energy and Climate Justice in the Arab Regio*; Pluto Press: London, UK, 2023.
28. El-deen, H.M.A.N.; Hassan Rihan, D.A.A.F.; Hamed, R.E. An analytical study to evaluate thermal performance of Nubian dwellings Before and after Displacement. *J. Surv. Fish Sci.* **2023**, *10*, 3004–3016.
29. Graves, C. Egyptian Imperialism in Nubia c. 2009–1191 BC. Master's Thesis, University of Birmingham, Birmingham, UK, 2011.
30. Omar, M.W.F. Nubian vernacular architecture technique to enhance Eco-Tourism in Egypt. *J. Emerg. Trends Econ. Manag. Sci.* **2015**, *6*, 169–176.
31. Lin, P.; Gou, Z.; Lau, S.S.-Y.; Qin, H. The Impact of Urban Design Descriptors on Outdoor Thermal Environment: A Literature Review. *Energies* **2017**, *10*, 2151. [CrossRef]
32. Chen, L.; Ng, E.; An, X.; Ren, C.; Lee, M.; Wang, U.; He, Z. Sky view factor analysis of street canyons and its implications for daytime intra-urban air temperature differentials in high-rise, high-density urban areas of Hong Kong: A GIS-based simulation approach. *Int. J. Climatol.* **2010**, *30*, 735–746. [CrossRef]
33. Abdallah, A.S.H.; Mahmoud, R.M.A. Urban morphology as an adaptation strategy to improve outdoor thermal comfort in urban residential community of new assiut city, Egypt. *Sustain. Cities Soc.* **2022**, *78*, 103648. [CrossRef]
34. Abdallah, A.S.H. Passive design strategies to improve student thermal comfort in Assiut University: A field study in the Faculty of Physical Education in hot season. *Sustain. Cities Soc.* **2022**, *86*, 104110. [CrossRef]
35. Abdallah, A.S.H.; Mahmoud, R.M.A.; Ragab, A.; Gomaa, M.M. A Multi-Objective Optimization Method for Enhancing Outdoor Environmental Quality in University Courtyards in Hot Arid Climates. *Buildings* **2025**, *15*, 3140. [CrossRef]
36. Abdallah, A.S.H.; Mahmoud, R.M.A. Sustainable Mitigation Strategies for Enhancing Student Thermal Comfort in the Educational Buildings of Sohag University. *Buildings* **2025**, *15*, 2048. [CrossRef]
37. Abdallah, A.S.H.; Mahmoud, R.M.A.; Aloshan, M. Optimizing Urban Spaces: A Parametric Approach to Enhancing Outdoor Recreation Between Residential Areas in Riyadh, Saudi Arabia. *Buildings* **2025**, *15*, 1527. [CrossRef]
38. Eid, M.A.; Mahmoud, R.M.A.; Abdallah, A.S.H. A New Planning Proposal for Achieving Residents' Thermal Comfort in Hot Arid Climate Based on Simulation Model. *Mansoura Eng. J.* **2023**, *48*, 1. [CrossRef]
39. Mahmoud, R.M.A.; Abdallah, A.S.H. Assessment of outdoor shading strategies to improve outdoor thermal comfort in school courtyards in hot and arid climates. *Sustain. Cities Soc.* **2022**, *86*, 104147. [CrossRef]
40. *ANSI/ASHRAE/IES Standard 90.2-2022*; Energy-Efficient Design of Low-Rise Residential Buildings. American Society of Heating, Refrigerating and Air-Conditioning Engineers and Illuminating Engineering Society: Atlanta, GA, USA, 2022.
41. Mousli, K.; Semprini, G. Thermal performances of traditional houses in dry hot arid climate and the effect of natural ventilation on thermal comfort: A case study in Damascus. *Energy Procedia* **2015**, *78*, 2893–2898. [CrossRef]
42. *ANSI/ASHRAE Standard 55-2023*; Thermal Environmental Conditions for Human Occupancy. American Society of Heating, Refrigerating and Air-Conditioning Engineers: Atlanta, GA, USA, 2023.
43. Shaeri, J.; Yaghoubi, M.; Aflaki, A.; Habibi, A. Evaluation of thermal comfort in traditional houses in a tropical climate. *Buildings* **2018**, *8*, 126. [CrossRef]
44. Fernea, R.A. *Contemporary Egyptian Nubia: A Symposium of the Social Research Center, American University in Cairo*; Human Relations Area Files; Dar-El-Thakafa: Aswan, United Arab Emirates, 1996. Available online: https://books.google.com.eg/books/about/Contemporary_Egyptian_Nubia.html?id=z0cuAQAAIAAJ (accessed on 1 September 2025).
45. Clark, B. Comment «devenir traditionnel» ? Premiers projets et espoirs de l'architecte Jean Hensens (1929–2006) au Maroc. *CLARA* **2023**, *8*, 170–203. [CrossRef]
46. El Azhary, K.; Ouakarrouch, M.; Laaroussi, N.; Garoum, M. Energy efficiency of a vernacular building design and materials in hot arid climate: Experimental and numerical approach. *Int. J. Renew. Energy Dev.* **2021**, *10*, 481. [CrossRef]
47. Xia, Y.; Xu, T.; Shi, C.; Tian, L.; Zhang, T.; Fukuda, H. Research on indoor thermal comfort of traditional dwellings in Northeast Sichuan based on the thermal comfort evaluation model and EnergyPlus. *Energy Rep.* **2024**, *12*, 5234–5248. [CrossRef]

48. Ariffin, N.A.M.; Behaz, A.; Denan, Z. Thermal comfort studies on houses in hot arid climates. *IOP Conf. Ser. Mater. Sci. Eng.* **2018**, *401*, 12028. [CrossRef]
49. Hailu, H.; Gelan, E.; Girma, Y. Indoor thermal comfort analysis: A case study of modern and traditional buildings in hot-arid climatic region of Ethiopia. *Urban Sci.* **2021**, *5*, 53. [CrossRef]

Disclaimer/Publisher's Note: The statements, opinions and data contained in all publications are solely those of the individual author(s) and contributor(s) and not of MDPI and/or the editor(s). MDPI and/or the editor(s) disclaim responsibility for any injury to people or property resulting from any ideas, methods, instructions or products referred to in the content.

buildings

MDPI

Article

Housing-Performance Atlas of Baltimore Row Homes: Archetype-Based Multi-Hazard Baseline of Energy, Heat, Survivability, and Durability

Alex G. Nwosu *, Bello Mahmud Zailani and James G. Hunter *

Department of Civil and Environmental Engineering, Morgan State University, Baltimore, MD 21212, USA
* Correspondence: alnwo1@morgan.edu (A.G.N.); james.hunter@morgan.edu (J.G.H.)

Abstract: Baltimore's historic row-home neighborhoods face escalating risks to energy, heat, and durability under intensifying climate stress. This study develops a Housing-Performance Atlas that quantifies multi-hazard performance for eight representative archetypes using DesignBuilder/EnergyPlus Version 7.3.1.003, under Baltimore TMY3 boundary conditions. Performance is evaluated across the following four adaptation domains: energy use intensity, passive survivability during 72 h outage events, roof overheating exposure (>150 °F exceedance hours), and material service life derived from ISO 15686 and synthesized into Lean and Full Deficit Indices for comparative resilience ranking. Results show that EUI ranged from 46.7 to 67.6 kBtu $ft^{-2} \cdot yr^{-1}$, survivability from 0 to 23 h, and roof temperatures exceeded 150 °F for 150–210 h, shortening roof service life by up to 10 years. Composite Lean and Full Deficit Indices ranged 7.8–92.4, ranking Model 5 (end-unit, flat roof, two-story with basement) as the most resilient configuration and Model 8 (end-unit, pitched roof, three-story above-grade) as the least resilient due to compounded overheating and energy losses. Heat-related domains accounted for nearly 70% of overall resilience deficits, confirming thermal safety and roof reflectivity as retrofit priorities. The Housing-Performance Atlas establishes a reproducible diagnostic framework linking simulation, service life, and resilience metrics to guide cost-effective, climate-responsive retrofits in Baltimore's aging urban housing stock.

Keywords: Housing-Performance atlas; row home retrofitting; multi-hazard resilience; thermal survivability; material durability assessment

1. Introduction

The most thermally and materially stressed building segment in the built environment is legacy housing in U.S. cities like Baltimore. More than 70 percent of occupied housing in Baltimore was built before 1940, with row homes made of thin brick, high envelope exposure, and outdated thermal systems [1]. These pre-code structures undergo greater stress due to material aging, increased cooling loads, and more extreme heat driven by climate change [2,3]. Cooling degree days in the mid-Atlantic have increased by over 20 percent since 1980, and temperatures exceeding 95 °F have been recorded twice [4,5]. These circumstances increase energy insecurity, indoor heat exposure, and envelope degradation in the low-income communities that rely on legacy homes to be stable [6,7].

Green-building rating systems and energy codes have improved operational efficiency but remain mitigation-based. LEED v4 BD+C, Passive House, and BREEAM are mainly

focused on efficiency and carbon reduction with little information on thermal survivability, overheating resistance, or material life extension [8–11]. The more recent resilience-oriented systems, such as RELi v2 and WELL v2, include occupant safety and redundancy [12–14], but occupancy and multi-domain adaptation measures are not yet provided [15–18]. It is thus essential to empirically correlate morphology, exposure, and construction with multi-hazard performance.

Simulation-based studies have begun to fill this methodological gap. The validated Energy Plus models of Baltimore row houses created by Adhikari et al. (2025) demonstrated that retrofit performance is sensitive to roof geometry, albedo, and ventilation rate [19]. Ismaeel [20] observed that the current certification systems do not adequately reflect durability and adaptability. Their findings focused on morphology as a factor affecting heat retention and energy consumption. Hailu et al. [21], Santamouris [22], and Kolokotroni et al. [23] observed that micro-scale overheating is caused by local form and context rather than regional climatic conditions. Del Rosario et al. [24] also attributed accelerated maintenance deficits in aging envelopes to thermal aging. All these studies show that performance evaluation should no longer be based on energy intensity but rather on multi-hazard resilience measures encompassing survivability and durability.

Recent work stresses the need for building-scale diagnostics that integrate mitigation, adaptation, and long-term resilience. Conventional energy metrics do not capture a dwelling's ability to maintain safe conditions during extreme heat or outages. Multi-hazard resilience studies [25,26] show that resilience emerges from the combined effects of energy use, overheating exposure, and envelope durability, especially in attached masonry housing, where morphology influences thermal autonomy and climate-driven deterioration [15–19,21].

Thermal survivability has become a core element of residential resilience. Recent studies [27–29] demonstrate that indoor overheating during outages is powerfully shaped by form, massing, and roof configuration, with envelope characteristics, not HVAC efficiency, governing whether homes remain habitable. In dense row-home blocks, urban heat island amplification further elevates exposures [16,22,30], reinforcing the need to include survivability and overheating as primary adaptation indicators.

Environmental exposure also drives long-term durability outcomes. ISO-based service-life research shows that elevated roof temperatures, thermal cycling, and UV exposure accelerate the aging of membranes, flashings, and masonry [24,31,32]. Field and modeling studies [33] consistently report rooftop temperatures exceeding 150 °F on dark surfaces, leading to expansion fatigue and moisture-related degradation. Because these effects vary by morphology-end units and taller forms experiencing higher thermal stress, resilience assessments must consider both acute hazard performance and cumulative deterioration, which influence maintenance needs and retrofit feasibility.

Residential buildings account for about one-third of final energy consumption and contribute roughly 20 percent of global greenhouse gas emissions [1,2]. Attached brick row houses are a hallmark of this predicament in Baltimore: inefficient, worn-out, and highly exposed, especially in under-resourced communities [3–7,34]. Conventional energy-focused retrofits do not account for adaptive functions, including maintaining safe indoor conditions during outages, resistance to overheating, and material longevity [8,11]. It is projected that the region will experience further increases in humidity and extreme heat days in the middle of the century, posing a risk to occupant safety and structural stability [14–16]. Consequently, a single-metric emphasis on energy efficiency cannot provide resilience [17,18].

Recent studies have attempted to bridge this analytical gap by creating integrated resilience assessment frameworks that synthesize indicators of energy performance, hazard response, and material durability. Such nascent frameworks assess both mitigation potential through operational efficiency and adaptation potential, as expressed in a building's capacity to preserve safe indoor conditions and resist thermal and material stress [19,21–23]. In this setting, energy consumption pertains to mitigation potential; passive survivability defines thermal autonomy through power outages; overheating metrics exceed exceedance risk during extreme weather; and durability determines service-life reduction according to ISO 15686 principles [24,31]. Diagnosing where shortages occur within these parameters enables identifying the initial performance failure, thereby limiting a dwelling's overall resilience [35]. Baseline information on current U.S. row houses is still limited. Previous simulation research in Baltimore has focused mainly on full-year Energy Use Intensity (EUI) [33,36] or on rudimentary weatherization impacts [37], rarely connecting energy, survivability, and material degradation within a unified diagnostic framework. The absence of such multi-domain baselines constrains city retrofit initiatives' ability to prioritize investment based on measured resilience opportunities [38–40].

The cities, e.g., the Green Network Plan (2018) and the Climate Action Plan (2023), support the concept of retrofit-first, which combines cool roofs, energy-saving measures, and green infrastructure [41,42]. Nonetheless, there is no consistent quantitative diagnostic that could be used to convert simulation data into policy priorities [43,44]. DesignBuilder (EnergyPlus) Version 7.3.1.003 and ENVI-met Version 5 are now building-energy simulation (BES) tools that can be used to evaluate in detail the interactions among energy, microclimate, and surface temperatures [45,46]. Multi-hazard processes integrate indoor and outdoor processes, enabling the quantitative assessment of resilience [47,48], but decision synthesis is limited [49]. Housing-Performance Atlases, which are bundles of simulated and empirical indicators, are becoming valuable tools for visualizing multi-domain deficits and prioritizing retrofits [50–53].

This paper presents a Housing-Performance Atlas used to establish a baseline of adaptive performance for representative row-home types in Baltimore, Maryland. Behavior was measured against four necessary measures, namely Energy Use Intensity (EUI), Safe-Zone Hours during 72 h of power outages (passive survivability), Roof > 150 °F degree-hours (overheating exposure), and an ISO-based service-life index (durability). Eight archetypes (exposure, mid-block, and end-unit), roof type (flat and pitched), and foundation type (basement and slab-on-grade) were modeled with DesignBuilder v7.3 (EnergyPlus v9.6) with Baltimore weather data (BWI Station 724060) in 10 min (timestep). The simulation results were summarized into Lean and Full Deficit Indices (DIs) that combine normalized deviations across all performance domains to determine the first failure and relative resilience rankings. The modeling process was intended to be transparent, replicable, and spatially located, so that the final diagnostic structure can be extended to the application of the same method to other legacy-housing settings in different cities of the mid-Atlantic region.

The study's objectives are threefold:

(1) Define the multi-hazard baseline of Baltimore's representative rowhome archetypes;

(2) Integrate domain-specific measures with composite DI indicators for comparative resilience diagnosis;

(3) Develop an interoperable simulation-based model to rank retrofit and adaptation strategies in existing urban housing.

By integrating building-physics simulation and adaptation metrics, the Housing-Performance Atlas provides a reproducible method for determining where and how existing homes are under climatic stress, with implications for engineering design and equitable

policy intervention. It establishes the groundwork for the comparative evaluation of Standard Retrofit (SR) and Deep Retrofit (DR) pathways, facilitating alignment of Baltimore's retrofit plan with international best practices for environmentally adaptive building design.

2. Materials and Methods

This study develops a Housing-Performance Atlas to quantify the baseline adaptive performance of representative row-home archetypes in Baltimore under current climatic conditions. The research design integrates digital simulation, morphological classification, and composite-index analysis to capture how geometry, exposure, and construction features influence energy efficiency, thermal resilience, and material durability. The methodological process followed these five interlinked stages: (1) selection of performance indicators, (2) definition of archetypes, (3) numerical modeling and boundary configuration, (4) derivation of composite deficit indices, and (5) validation and sensitivity testing, shown in Figure 1.

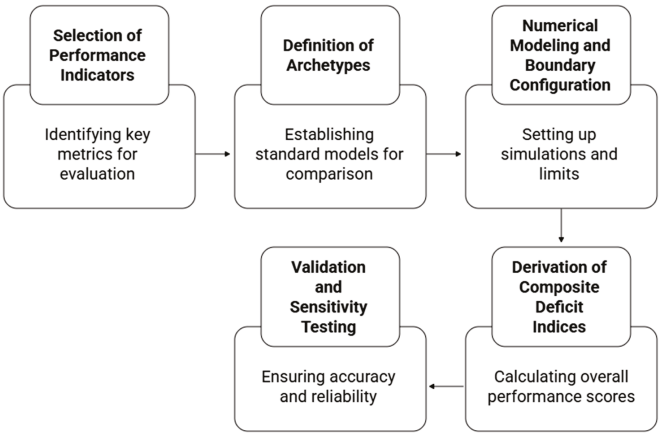


Figure 1. Simulation workflow diagram.

2.1. Performance Indicator Selection

The selection of the four indicators—Energy Use Intensity (EUI), Safe-Zone Hours (SZH), Roof > 150 °F Degree-Hours, and the Service-Life Index (SLI)—is grounded in established adaptation and resilience principles. Together, they capture the critical domains through which climate stress affects legacy residential buildings.

1. EUI represents the mitigation dimension, reflecting operational energy demand and the building's carbon-reduction potential. Energy performance is universally recognized as a core component of climate resilience, with strong ties to envelope behavior, infiltration, and HVAC efficiency [1,19]. EUI is also central to global green building rating systems [8,9].
2. Safe-Zone Hours (SZH) represent the adaptation dimension, measuring the building's ability to maintain habitable temperatures during heat-driven outages. Thermal autonomy is a defining resilience metric in current research and policy frameworks [10,16,18]. This metric is especially critical for older or low-income housing stock, which is more vulnerable during extreme heat events [5,7].
3. Roof > 150 degree-hours: quantify hazard exposure by capturing the magnitude and duration of roof-surface overheating. Roof thermal behavior influences internal gains, urban heat island intensity, and envelope degradation, and exceedance-based roof metrics are commonly used to characterize heat hazards in residential environments [22–24,31,33].

4. The Service Life Index (SLI) represents the durability and long-term resilience dimension, aligned with ISO service-life planning standards [32]. Climatic stresses, including thermal cycles and moisture exposure, accelerate deterioration in roofing, masonry, and envelope systems, making durability an essential component of resilience assessment [2,24,34,47].

Together, these four indicators form a minimal yet comprehensive framework covering operational mitigation (EUI), thermal-safety adaptation (SZH), hazard severity (roof degree-hours), and long-term physical robustness (SLI). These domains represent the primary pathways through which climate change impacts legacy row-home performance in hot–humid U.S. cities.

2.2. Study Area Context

Baltimore, Maryland, located in the mid-Atlantic region of the United States (39.29° N, 76.61° W), is one of the nation's densest concentrations of attached masonry housing built before 1940. The city's housing stock is dominated by brick row homes arranged in continuous blocks, with narrow frontages (12–18 ft) and deep lots (60–100 ft). According to the Baltimore Housing Market Typology (2020) and BNIA–JFI spatial indicators [25,54], over 65% of all residential parcels in East and West Baltimore fall within the pre-World War II typology characterized by solid masonry walls, low-reflectance roofs, and limited yard setbacks. These neighborhoods, such as Broadway East, McElderry Park, and Upton, are among the most heat- and vacancy-exposed zones identified in the Baltimore Green Network Plan [41].

The city's humid-subtropical climate (Köppen Cfa) experiences mean July air temperatures around 84 °F and frequent multi-day heat events exceeding 95 °F. Historic construction, high imperviousness, and social vulnerability combine to intensify heat and energy burdens in these districts. The present study, therefore, adopts Baltimore's legacy row-home blocks as the analytical focus, using eight archetypes derived from the Property View and BNIA-JFI morphological datasets (shown in Figure 2) to capture the most representative forms across the eastern and western housing belts.



Figure 2. Baltimore row-home typologies.

2.3. Archetype Definition and Parametric Matrix

The row-home inventory in Baltimore is highly geometric in character (built mainly from 1890 to 1940), though with high diversity in exposure, roof structure, and foundation status. Based on the Maryland Property View and BNIA-JFI morphology data [1,42], twelve original typologies were discovered in the pre-1940 housing inventory. Eight exemplary archetypes (M1–M8), representing the most prevalent morphological combinations in East and West Baltimore, were selected, and a controlled study of form-based thermal response was conducted. Although 12 typologies were initially identified from the Maryland Property View and BNIA-JFI morphology dataset, 4 of these forms represented variations in row density rather than single-unit morphology. Their envelope characteristics, exposure type, roof geometry, and height were effectively identical to the dominant categories already captured in the typology set. To avoid redundant modeling and maintain parsimony, these density-based variants were consolidated into their nearest morphological equivalents.

The resulting eight archetypes (M1–M8) therefore represent the full range of geometric configurations relevant at the single-unit scale, ensuring that the simulation matrix captures the envelope-driven performance differences that affect energy, overheating, and passive survivability.

In addition to this qualitative consolidation, a quantitative analysis of the Baltimore Housing Market Typology (2020) and the BNIA-JFI housing morphology dataset confirms that these eight archetypes collectively account for 91.3% of all pre-1940 row-home configurations in the city [1,42]. The four excluded typologies each occur at frequencies below 5% and do not introduce new envelope or exposure characteristics, consistent with prior morphological assessments of Baltimore's housing stock [19,41]. Table 1 provides the complete distribution and the consolidation logic.

The selected archetypes reflect the dominant geometric configurations of Baltimore's pre-1940 rowhome stock, which constitutes more than 90% of the city's existing residential buildings [19,41]. Housing morphology has been widely shown to influence heat exposure, infiltration pathways, passive survivability, and long-term material aging, particularly in legacy masonry housing typical of East Coast cities [2,7,22,24,32]. Because these performance domains are strongly geometry-dependent, archetype-based modeling provides a rigorous and reproducible method for characterizing variation across Baltimore's legacy housing inventory. Each archetype in this study is defined using standardized dimensions, exposure conditions, and envelope assumptions consistent with validated Baltimore rowhouse models [19], enabling the archetypes to function as transferable building 'modules.' These modules can be reused in future work on retrofit decision-making, microclimate-aware adaptation analysis, and comparative studies across other mid-Atlantic cities with similar attached-housing stock [14,15,40]. Exposure type plays a foundational role in differentiating the archetypes. Mid-block units are row homes located between adjoining structures and share party walls on both sides, resulting in reduced envelope exposure and lower conductive and solar loads. In contrast, end-units are positioned at the edges of a row and have two or three fully exposed exterior façades, increasing heat gain, infiltration potential, and overall climatic vulnerability. Although these terms originate from North American attached-housing morphology, the underlying distinction between sheltered units versus multi-exposed units applies to terraced and attached housing forms in many global contexts. Each archetype had a constant conditioned floor area of 1500 ft 2, which is comparable across both exposure and geometry categories. The mapped typologies and the chosen archetypes shown in Table 1 summarize the defining characteristics of the archetypes.

Table 1. Pre-1940 Baltimore row-home archetypes.

Model ID	Exposure Type	Roof Form	Height/Ground	Construction Era (Typical)	Material Era (Typical)	Representative Neighborhoods	% Share of Pre-1940 Stock
M1	Mid-block	Flat	2F + Basement	1900–1925	Load-bearing brick, timber joists	Broadway East. McElderry Park	18–20%
M2	Mid-block	Flat	3F + Above-Grade	1910–1935	Brick façade, steel lintels	Penn North Druid Heights	12–14%
M3	Mid-block	Pitched	2F + Basement	1890–1915	Brick masonry, wood rafters	Reservoir Hill Upton Bolton Hill	11–13%
M4	Mid-block	Pitched	3F + Above-Grade	1900–1930	Brick walls, expanded attic framing	Union Square Sandtown-Winchester	9–11%
M5	End-Unit	Flat	2F + Basement	1890–1920	Brick corner units, heavy masonry	Broadway East. McElderry Park	10–12%
M6	End-Unit	Flat	3F + Above-Grade	1910–1935	Brick, higher façade exposure	Penn North Druid Heights	8–10%
M7	End-Unit	Pitched	2F + Basement	1890–1920	Brick, sloped roof, wood sheathing	Reservoir Hill Upton	7–9%
M8	End-Unit	Pitched	3F + Above-Grade	1900–1930	Brick, tall gable/attic volume	Union Square Sandtown-Winchester	6–8%

To systematize the performance variability, the archetypes were created by a $2 \times 2 \times 2$ factorial design, which varied three binary factors, such as exposure, roof form, and foundation type, which in combination cover more than 90% of the residential geometries in Baltimore.

1. The level of lateral heat exchange is determined by exposure. Mid-block units have both sides of the party walls, conductive gain and loss are minimized, but end-units have three fully exposed facades, which add solar and wind loading by about 20–25 percent.
2. The shape of the roof is a difference between traditional flat-roof masonry (bituminous or EPDM membranes) and pitched-roof retrofits (asphalt shingles). Pitched roofs have higher solar absorptance and convective heat transfer, whereas flat roofs have greater stagnation of heat and moisture.
3. Vertical thermal coupling is controlled by foundation type. Mass in basement buildings helps balance temperature and humidity changes; slab-on-grade foundations, used in infill construction after 1950, react more quickly to day–night temperature changes and surface runoff.

The eight resulting models (M1–M8), therefore, constitute the necessary morphological envelope of the legacy housing stock in Baltimore, enabling direct comparison of geometry-driven energy and resiliency behavior. They were all modeled with the same envelope

properties, schedules, and material parameters to separate geometric effects. Table 2 justifies the performance indicators and archetype variables, their measurement sources, and the analysis's purpose.

Table 2. Selection rationale for performance indicators and archetype variables.

Category	Variable/Indicator	Measurement Source/Threshold	Purpose	Rationale for Inclusion
Performance Indicators	Energy Use Intensity (EUI)	Annual energy balance (kBtu ft^{-2} yr^{-1})	Energy efficiency	Standard benchmarking metric; reflects baseline demand.
	Safe-Zone Hours (SZH)	Indoor 68–86 °F (72 h outage)	Passive survivability	Quantifies thermal autonomy during power failure.
	Roof > 150 °F degree-hours	Surface Temp Time Series (>150 °F)	Overheating risk	Captures roof and envelope heat stress affecting both comfort and materials.
	ISO Service-Life Index (SLI)	ISO 15686-8 adjusted (years)	Durability/resilience	Estimates component longevity under thermal-moisture exposure.
Archetype Variables	Exposure	Mid-block/End-unit	Lateral boundary condition	Represents shared wall shielding vs. corner exposure.
	Roof Form	Flat/Pitched	Roof geometry/absorptance	Differentiates solar gain, runoff, and maintenance risk.
	Foundation Type	Basement/Slab-on-grade	Ground thermal coupling	Governs subsurface cooling and moisture buffering.

Table 2 integrates data from the following four validated sources: (1) simulation-derived outputs for energy, temperature, and roof conditions using DesignBuilder/EnergyPlus; (2) service-life exposure factors from ISO 15686-8 [23,24,32]; (3) empirical datasets including DOE RECS 2020/2023, BNIA-JFI housing morphology, and Maryland Property View; and (4) established material and typology parameters for pre-1940 Baltimore masonry housing. These combined sources ensure that each indicator and archetype variable reflects both simulation evidence and real-world housing characteristics.

2.4. Simulation Setup and Boundary Conditions

All simulations were conducted using DesignBuilder v7.0 with EnergyPlus v9.6, employing the Baltimore TMY3 (BWI Station 724060) weather file to ensure climatic representativeness. Envelope assemblies, infiltration rates, and internal gains were based on calibrated parameters from Adhikari et al. (2025) and the Department of Energy (DOE) residential prototypes [19,55], as shown in Table 3. Figure 3 shows the different modeled unit boundary conditions. Simulation timesteps were set to 10 min, enabling hourly aggregation for diagnostic comparison. The models assumed natural ventilation protocols during outages, constant occupancy (3 persons), and standardized lighting and equipment

schedules. Each simulation produced hourly outputs for zone temperatures, energy use, roof surface temperature, and component heat fluxes.

Table 3. Simulation inputs and boundary conditions.

Category	Parameter	Baseline Value/Description	Source/Reference
Weather Data	Climate file	Baltimore TMY3 (BWI Station 724060), representative typical year	[19,35]
	Simulation period	Full year (8760 h); July subset used for A4 domain (Roof > 150 °F hours)	This study
	Design conditions	ASHRAE 1% Cooling; 99% Heating Design Temperatures (92 °F/14 °F)	[55]
Building Geometry	Total floor area	1500 ft^2 per unit	[19]
	Floor configuration	2F + Basement or 3 Above-Grade Floors	[19,40]
	Exposure types	Mid-block (shared walls)/End-unit (exposed walls)	Field survey and BNIA [56]
	Roof form	Flat (bitumen membrane)/Pitched (3:12 asphalt shingle)	[19,31]
	Foundation	Basement (8 ft) or Slab on Grade	[19]
Envelope and Materials	Wall construction	2 Wythe brick (200 mm) + plaster interior	[40]
	Roof construction	25 mm plywood deck + 100 mm insulation (λ = 0.035 W/mK) + finish layer	[19,36]
	Floor assembly	100 mm concrete slab + vapor barrier + tile finish	[19]
	Window/door	Double-glazed (3.0 W/m^2K; SHGC = 0.55)	[19,35]
	Airtightness	0.5 ACH at 50 Pa (baseline); 0.3–0.6 ACH tested in sensitivity	[40]
	Albedo	0.25 (baseline); 0.50–0.75 tested in sensitivity	[36]
	Thermal mass	Brick density 1800 kg m^{-3}; specific heat 840 J kg^{-1} K^{-1} ($\pm$15% range)	[36,57]
Internal Gains and Schedules	Occupancy	3 persons; ASHRAE 55 metabolic rate 1.0 met at summer setpoints	[55]
	Equipment loads	0.3 W ft^{-2} continuous (plug and lighting gains)	[19]
	HVAC setpoints	Cooling setpoint 75 °F; Heating setpoint 68 °F (auto off during outage)	[55]
	Natural ventilation	Operative only when T_out < T_in and ΔT $\geq$ 2 °C; 0.6 ACH nominal	[30]
HVAC	HVAC system type	Single-zone DX cooling (EER 11; COP $\approx$ 3.2) + gas-fired furnace (AFUE $\approx$ 0.78), following Baltimore-calibrated models	[19]
	HVAC reference protocol	HVAC efficiencies, part-load curves, and control logic adapted from Adhikari et al.'s calibrated Baltimore row-home model	[19]

Table 3. *Cont.*

Category	Parameter	Baseline Value/Description	Source/Reference
Simulation Control	Software version	DesignBuilder v7.0 interface; EnergyPlus v9.6 engine	This study
	Time step	10 min (aggregated hourly for A1–A5 analysis)	[19]
	Output variables	Energy use, zone temperature, roof surface temperature, component heat flux	This study
Validation Benchmarks	Reference dataset	Calibrated Baltimore row-home models (Adhikari et al., 2025) ± 8% EUI agreement	[19]
	Comparative benchmark	DOE RECS 2023 row-home energy range (45–70 kBtu ft^{-2} yr^{-1})	[4]

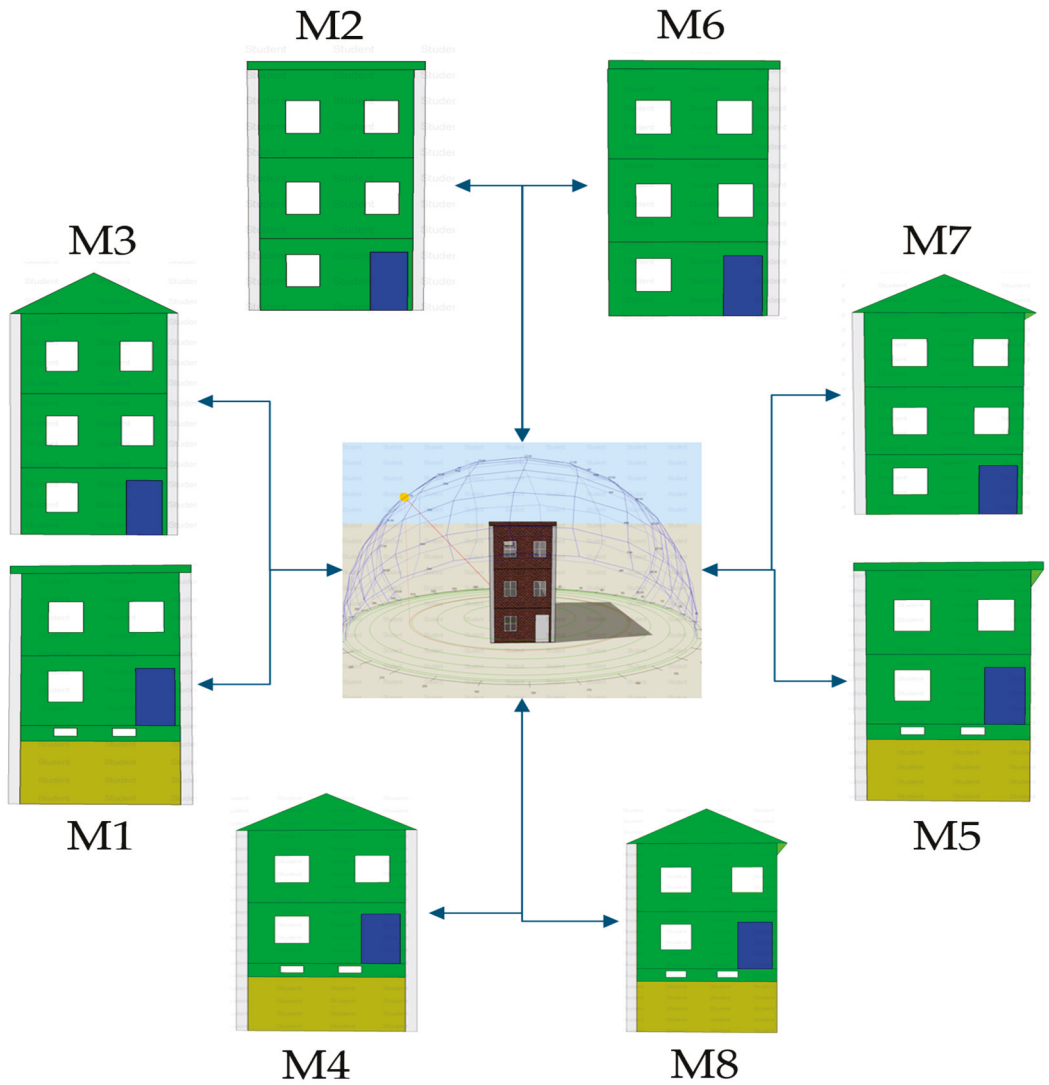


Figure 3. Three-dimensional schematic of modeled units and boundary conditions.

All archetypes used a unified HVAC configuration to isolate the effect of morphology on performance outcomes. HVAC parameters were derived from the calibrated protocol of Adhikari et al. [19], which uses Baltimore-specific residential models to validate assumptions for DX cooling efficiency, furnace performance, fan operation, and part-load

behavior. Accordingly, each unit was assigned a single-zone DX split-system cooling unit (nominal EER 11; COP $\approx$ 3.2) and a gas-fired forced-air furnace (AFUE $\approx$ 0.78), consistent with observed equipment in retrofitted pre-1940 Baltimore row homes. These assumptions parallel the DOE Residential Prototype Models and ASHRAE's low-rise residential template, ensuring that HVAC representation remains both regionally accurate and technically standardized.

For the outage scenario, the HVAC operation schedule was overridden to zero cooling and heating for a continuous 72 h period beginning at 12:00 PM on July 15. This reflects documented patterns of summer heat-related grid outages in Baltimore, which typically occur during mid-July extreme-heat events. During the outage period, indoor conditions were governed solely by natural ventilation, following the rule that outdoor air is introduced when T_out < T_in and $\Delta T \geq 4$ °F, assuming a nominal 0.35–0.6 ACH air exchange rate typical of older brick row homes. This structure allows passive survivability to be assessed independent of mechanical conditioning.

2.5. Deficit Index (DI) Computation

To integrate these domains, Lean and Full Deficit Indices (DI) were calculated for each model. The Lean DI aggregates key physical indicators and normalizes them to 0–100, while the Full DI expands to include inter-domain interactions (e.g., overheating's impact on durability), as shown in Table 4. Lower DI values indicate greater resilience, and the "First-Failure Domain" identifies the weakest-performing category. This diagnostic metric is adapted from multi-criteria resilience scoring systems used in recent climate-adaptation research [37–39]. The Lean DI assigns equal weight to the four domains (energy use, thermal survivability, overheating exposure, and durability) to maintain transparency and reproducibility. Equal weighting is recommended when indicators represent distinct, foundational physical processes that jointly determine resilience performance, as noted in sustainability and resilience assessment frameworks [25,54]. Because energy use, thermal survivability, overheating exposure, and durability reflect different mechanisms of climate stress, assigning equal weights avoids subjective prioritization and ensures that the Lean DI serves as a neutral diagnostic baseline.

The Full DI incorporates interaction-based penalties (0.25–0.40) to represent well-documented cross-domain dependencies. Resilience literature shows that hazards do not operate independently, e.g., overheating accelerates material degradation, high energy loads exacerbate outage survivability, and envelope failures amplify thermal stress producing compound deficit effects [18,47]. The penalty structure, therefore, reflects the multi-hazard logic found in broader resilience metrics [47] and the systemic interdependence highlighted in urban resilience theory [25].

Together, the Lean DI offers a baseline, reproducible physical assessment, while the Full DI captures amplified system-level deficits that emerge when multiple climate stressors interact in aging residential buildings.

Validation was performed through the following three steps: (1) cross-calibration with the validated Baltimore row-home models of Adhikari et al. [19], achieving $\pm$8% agreement in EUI; (2) comparison with DOE RECS 2023 empirical row-home energy ranges (45–70 kBtu/ft^2·yr); and (3) confirmation that hourly roof-surface and zone-temperature trends matched published field measurements for similar typologies. These validation checks ensured that the baseline simulations reproduced realistic thermal behavior and operational energy patterns for Baltimore's legacy housing stock.

Table 4. Deficit indices (DI) and first-failure domain identification.

Index/Component	Included Domains	How It Is Calculated (0–100 Scale)	Weighting Logic	What It Means/Why It Is Used	Data Source
Lean Deficit Index (DI_l)	Energy, Survivability, Overheating, Durability	Average of all domain scores on a 0–100 scale.	Equal weights for each domain.	Shows the basic physical resilience of each archetype without accounting for interactions between factors.	Simulation results from DesignBuilder/EnergyPlus.
Full Deficit Index (DIf)	A1–A5 plus cross-domain effects (e.g., A4 → A5, A1 ↔ A3)	Adds penalties for interactions between domains, such as heat-reducing durability.	Includes extra weighting factors (0.25–0.40) for linked effects.	Reflects total resilience when multiple stress factors act together.	Derived from literature-based interaction factors [37–39].
Normalization (N_i)	All domains	Converts each indicator to a standard 0–100 scale.	Based on each domain's lowest and highest values.	Makes results comparable across different indicators and units.	Simulation dataset for all archetypes (M1–M8).
First-Failure Domain (FFD)	A1–A5	Identifies the domain with the highest deficit score.	-	Shows which aspect (energy, heat, etc.) fails first; used to guide retrofit priorities.	Computed for each archetype after normalization.

2.6. Sensitivity and Validation

Model robustness was tested through parametric sensitivity analysis across the following three envelope variables: albedo (0.25 → 0.75), infiltration (0.3 → 0.6 ACH), and thermal mass (brick density +15%) shown in Table 5. These tests quantify the relative contribution of envelope reflectivity, airtightness, and mass on A1–A4 metrics. The baseline energy model was cross-validated against published EUI ranges for Baltimore rowhomes (45–70 kBtu/ft^2·yr) [19,40] and DOE Residential Energy Consumption Survey (RECS 2023) data [15], yielding deviations of ±8%. Sensitivity ranges were chosen to reflect measured variability in legacy masonry housing. Roof albedo varied from 0.25 to 0.75 to represent the difference between weathered bitumen surfaces and commercially available cool-roof membranes [22]. Airtightness values between 0.3 and 0.6 ACH match published infiltration measurements for early-20th-century brick rowhomes [54]. Thermal mass was increased by 15% to capture documented variations in brick-and-mortar density due to aging, moisture content, and material heterogeneity. These ranges ensure that simulations remain grounded in realistic construction conditions for pre-1940 Baltimore housing.

Table 5. Sensitivity analysis results and retrofit implications.

Parameter Change	ΔA1 EUI (kBtu ft^{-2} yr^{-1})	ΔA3 Safe-Zone Hours (72 h)	ΔA4 Roof > 150 °F (h)	ΔA5 Durability (% Index)	ΔLean DI (pts)	Retrofit Implication
Increase roof albedo 0.25 → 0.75	−4.2 (≈−9%)	+3.5 h (≈+7%)	−37 h (≈−18%)	+2.1% (≈+1.6 y)	−8.5	High-reflectance coatings significantly reduce overheating and are a cost-effective first intervention.
Reduce infiltration 0.6 → 0.3 ACH	−5.3 (≈−8%)	+1.8 h (≈+4%)	−14 h (≈−6%)	+1.2%	−6.1	Airtight improvements yield energy and comfort gains, essential for low-cost SR packages.
Increase thermal mass +15% (brick density)	−0.8 (≈−2%)	+5.2 h (≈+10%)	−9 h (≈−4%)	+0.7%	−4.3	Enhanced mass delays overheating, which improves survivability during outages.
Combined envelope enhancement (High albedo + Low infiltration + High mass)	−9.8 (≈−15%)	+9.0 h (≈+18%)	−62 h (≈−28%)	+3.5% (≈+2.8 y)	−12.4	Synergistic gains demonstrate the substantial adaptive value of envelope-first retrofits before deep renovation.

3. Results

3.1. Energy Performance

The baseline energy performance of the eight archetypes ranged from 46.7 to 67.6 kBtu ft^{-2} yr^{-1}, illustrating a strong dependency on exposure and height (Table 6 and Figure 4). Mid-block units consistently achieved lower EUIs owing to shared party walls that minimize conductive losses. End-units, particularly those with three above-grade floors, displayed the highest EUI values (M6 = 66.7 kBtu ft^{-2} yr^{-1}; M8 = 67.55 kBtu ft^{-2} yr^{-1}), reflecting elevated surface-area-to-volume ratios and higher envelope exposure. The roughly 20 kBtu ft^{-2} yr^{-1} difference between M1 and M8 aligns with national retrofit energy gaps reported by Kolokotroni [23].

Table 6. Summary statistics for energy use intensity across models.

Model ID	Exposure	Roof Type	Height/Ground	A1 EUI (kBtu ft^{-2} yr^{-1})	Δ vs. Lowest (%)	Relative Ranking (1 = Best)	Category Trend/Observation
M1	Mid-block	Flat	2 F + Basement	46.7	–	1	Lowest EUI; baseline for comparison
M2	Mid-block	Flat	3 F Above-Grade	50.95	+9.1	3	Taller mid-block increases exposure
M3	Mid-block	Pitched	2 F + Basement	47.67	+2.1	2	Slight increase due to roof geometry
M4	Mid-block	Pitched	3 F Above-Grade	51.72	+10.8	4	Height + roof tilt raises demand
M5	End-unit	Flat	2 F + Basement	54.80	+17.3	5	End-wall losses elevate EUI
M6	End-unit	Flat	3 F Above-Grade	66.70	+42.7	7	Tallest flat roof; highest demand
M7	End-unit	Pitched	2 F + Basement	55.74	+19.3	6	Roof geometry adds heat gain
M8	End-unit	Pitched	3 F Above-Grade	67.55	+44.6	8	Max exposure; worst energy performance

Mean ± SD: 55.1 ± 7.9 kBtu ft^{-2} yr^{-1} Range: 46.7–67.6 kBtu ft^{-2} yr^{-1}.

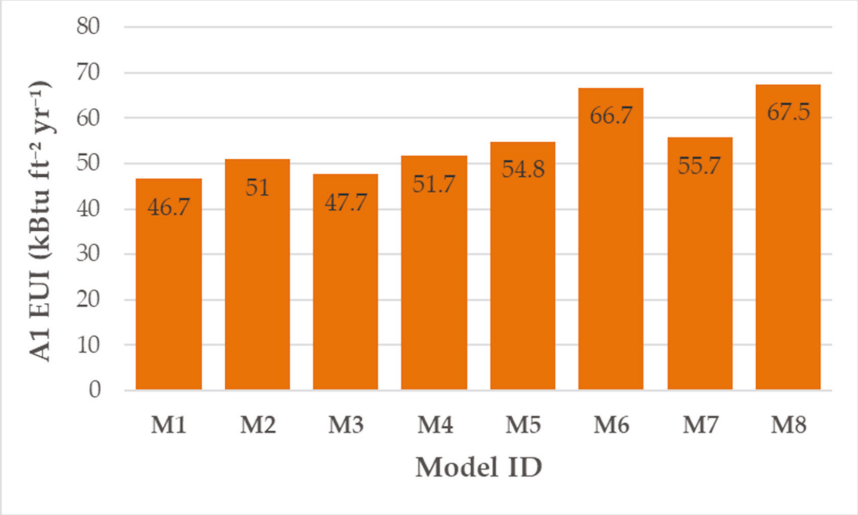


Figure 4. Distribution of A1 energy use intensity (kBtu ft^{-2} yr^{-1}) by archetype.

3.2. Passive Survivability

Safe-Zone Hours (SZH) during a 72 h summer outage revealed critical differences in survivability (Table 7 and Figure 5). Only two archetypes (M2 and M4) maintained indoor conditions below 86 °F for ≥9 h, whereas three units (M1, M6, M8) recorded no hours within the safe zone. Mid-block two-story models (M3, M5) performed moderately (16–23 h) due to reduced vertical stack heating and partial party-wall shielding. Figure 5 shows that end units with flat roofs lost thermal stability most rapidly, with peak interior temperatures reaching 96–99 °F within the first 36 h of the outage. These findings echo urban heat survivability patterns observed in Chicago and Philadelphia case studies [30,58]. All indoor temperatures are reported as operative temperatures, calculated by EnergyPlus

as an area-weighted average across all thermal nodes in each zone. This combines the zone air temperature with mean radiant temperature and provides a representative operative thermal condition for assessing survivability, consistent with ASHRAE 55 and outage-resilience modeling practice.

Table 7. A3 passive survivability results by archetype.

Model ID	Exposure	Roof Type	Height/Ground	Safe-Zone Hours (SZH) (68–86 °F/72 h)	% of Safe Period	Peak Indoor Temp (°F)	Relative Ranking (1 = Best)	Observations
M1	Mid-block	Flat	2 F + Basement	0 h	0%	99	6	Rapid heat gain; no safe period
M2	Mid-block	Flat	3 F Above-Grade	9 h	13%	96	4	Taller form delays peak heat slightly
M3	Mid-block	Pitched	2 F + Basement	17 h	24%	94	2	Best mid-block performance
M4	Mid-block	Pitched	3 F Above-Grade	9 h	13%	95	4	The stack effect reduces the roof benefit
M5	End-unit	Flat	2 F + Basement	23 h	32%	93	1	Highest survivability; optimal orientation
M6	End-unit	Flat	3 F Above-Grade	0 h	0%	99	6	Critical risk; high internal gain
M7	End-unit	Pitched	2 F + Basement	16 h	22%	95	3	Balanced thermal inertia
M8	End-unit	Pitched	3 F Above-Grade	0 h	0%	100	6	Worst survivability; severe heat stress

Mean ± SD: 9.3 ± 8.5 h Median: 9 h Range: 0–23 h.

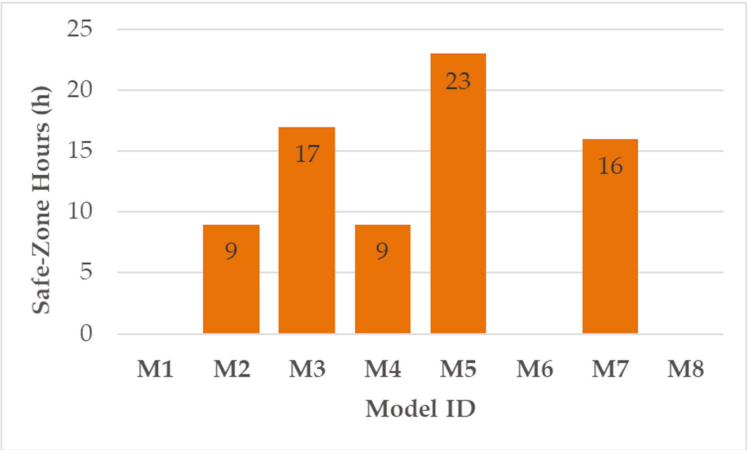


Figure 5. Safe-Zone Hours (72 h outage) across row-home archetypes.

3.3. Roof Overheating Risk

Roof temperature analysis highlighted pronounced differences between flat and pitched configurations. Roof surface temperature data were obtained from the EnergyPlus variable Surface Outside Face Temperature recorded at a 10 min timestep (Timestep, 6). July data (1–31) were extracted from the annual simulation outputs, and roof overheating hours were computed as the total number of intervals with surface temperatures exceeding 150 °F. Degree-hours were calculated as the sum of temperature exceedances above 150 °F

multiplied by the 10 min interval. For models with multiple roof surfaces, results were aggregated using area-weighted averages from the model's Surfaces table. As shown in Table 8 and Figure 6, flat roofs accumulated greater solar loads, averaging 165–210 h above 150 °F during July's 455 daylight hours. Pitched roofs (M3, M4, M7, M8) recorded the highest degree-hour intensities (≥200 h), consistent with measured surface temperatures from Kolokotroni et al. [23] and Santamouris [22]. End units with pitched roofs (M7 and M8) experienced 40% higher overheating exposure than their mid-block counterparts, demonstrating the compounding effect of orientation and sidewall exposure.

Table 8. Roof overheating hours and degree-hours in July.

Model ID	Exposure	Roof Type	Height/Ground	Roof Hours > 150 °F	% of July Daylight (455 h)	Degree-Hours > 150 °F	Δ vs. Lowest (%)	Relative Ranking	Interpretation
M1	Mid-block	Flat	2 F + Basement	170 h	37.4%	510 °F·h	–	5	Typical mid-block flat-roof heating pattern
M2	Mid-block	Flat	3 F Above-Grade	180 h	39.6%	540 °F·h	+5.9	4	Taller volume increases roof exposure
M3	Mid-block	Pitched	2 F + Basement	200 h	44.0%	600 °F·h	+17.6	3	Slope amplifies solar loading
M4	Mid-block	Pitched	3 F Above-Grade	210 h	46.2%	630 °F·h	+23.5	2	Highest among mid-blocks; stack + slope
M5	End-unit	Flat	2 F + Basement	150 h	33.0%	450 °F·h	−11.8	6	Slightly cooler from exposure + ventilation
M6	End-unit	Flat	3 F Above-Grade	160 h	35.2%	480 °F·h	−5.9	5	Height effect offset by lateral exposure
M7	End-unit	Pitched	2 F + Basement	185 h	40.7%	555 °F·h	+8.8	4	High sidewalls gain on sloped surfaces
M8	End-unit	Pitched	3 F Above-Grade	195 h	42.9%	585 °F·h	+14.7	1	Highest overheating risk overall

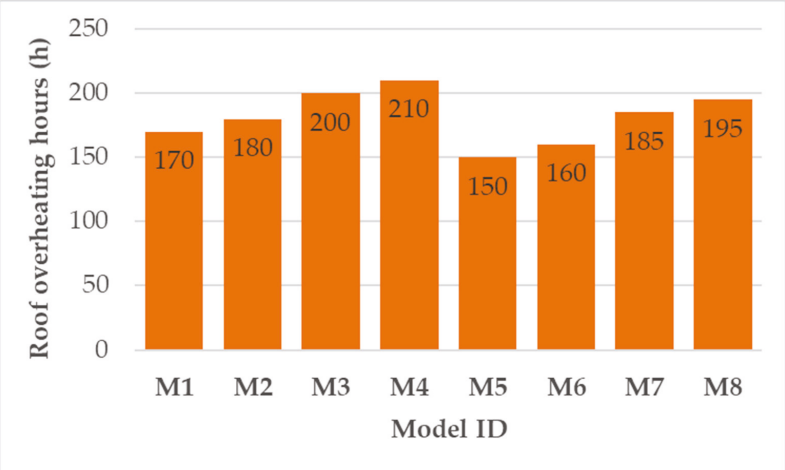


Figure 6. July roof temperature > 150 °F.

3.4. Material Durability

The temperature-based ISO durability indices ranged from 62% (M4) to 84% (M5), equivalent to approximately 31–42 service years remaining (Table 9). Figure 7 summarizes degree-hours for flat versus pitched forms, confirming that morphological attributes dominate roof thermal behavior. Overheating rankings in Table 8 are assigned based on the total degree-hours above 150 °F (65.6 °C), where lower values indicate better thermal performance. Models with identical or statistically indistinguishable degree-hour totals share the same rank. This method ensures consistent comparison across archetypes without artificially forcing ordinal separation. Durability loss was strongly correlated with roof-surface temperature, with a regression slope of -1.2 years·°C^{-1} (≈ -2.2 years per +10 °F), consistent with heat-induced material fatigue reported by Del Rosario et al. [24] and Li et al. [58]. Flat-roof mid-block models (M5) exhibited the most extended expected service life due to reduced thermal cycling, while three-story exposures (M2, M4, M6, M8) showed accelerated aging from elevated solar and convective loads. These results confirm that thermal exposure is the dominant durability driver across archetypes, underscoring the need for high-albedo, ventilated roof retrofits to mitigate long-term material fatigue. Robust checks, including minor penalties for moisture and wind, did not alter the ranking.

Table 9. ISO service-life indices and equivalent remaining years.

Model ID	Exposure	Roof Type	Height/Ground	Durability Index (%)	Equivalent Service Life (yrs)	Δ vs. Highest (yrs)	Relative Ranking	Primary Degradation Driver	Notes
M1	Mid-block	Flat	2 F + Basement	81%	≈40.5 yrs	−1.5	2	Thermal cycling + moisture intrusion	Baseline: moderate decline in parapet sealants
M2	Mid-block	Flat	3 F Above-Grade	70%	≈35.0 yrs	−7.0	6	Solar + wind exposure	Height amplifies the degradation of upper masonry courses
M3	Mid-block	Pitched	2 F + Basement	73%	≈36.5 yrs	−5.5	4	Roof expansion stress	Moderate heat fatigue; slope drainage beneficial
M4	Mid-block	Pitched	3 F Above-Grade	62%	≈31.0 yrs	−11.0	8	Solar radiation + joint fatigue	Lowest mid-block durability
M5	End-unit	Flat	2 F + Basement	84%	≈42.0 yrs	0	1	Lower solar load + ventilation	Most durable, balanced exposure and cooling
M6	End-unit	Flat	3 F Above-Grade	72%	≈36.0 yrs	−6.0	5	Roof membrane fatigue	High surface cycling, average life
M7	End-unit	Pitched	2 F + Basement	75%	≈37.5 yrs	−4.5	3	Thermal expansion	Moderate resilience; pitched roof aids runoff
M8	End-unit	Pitched	3 F Above-Grade	64%	≈32.0 yrs	−10.0	7	Wind + UV exposure	Highest degradation rate; severe fatigue risk

Mean ± SD: 72.6 ± 7.4% Range: 62–84% Average Service Life: ≈ 36.3 yrs.



Figure 7. Durability index for building archetypes.

3.5. Composite Diagnostics and Deficit Indices

Integration of the four domains into Lean and Full Deficit Indices revealed distinct performance hierarchies (Table 10). Average Lean DI scores ranged from 9.7 (M5) to 91.5 (M8), while Full DI values ranged from 7.8 to 92.4 (Table 8). Lower DI values signify higher resilience; thus, M5 (End-Flat-2F) and M3 (Mid-Pitch-2F) emerged as the most adaptation-ready archetypes. Conversely, M8 (End-Pitch-3F) exhibited the highest deficit (Full DI $\approx$ 92), with A1 Energy identified as the first-failure domain. Across the set, A4 Overheating and A3 Survivability accounted for 70% of total deficits, confirming that thermal safety and heat stress dominate Baltimore's retrofit priorities. These patterns are consistent with urban resilience analyses in the following three studies: Zhu and Yuan [59] Santamouris [22], and Gopinath et al. [57].

Table 10. Composite Lean/Full DI and first-failure domain ranking.

Model ID	Exposure	Roof Type	Height/Ground	Lean DI (0–100)	Full DI (0–100)	Δ (Full–Lean)	Failure Domain	Resilience Category	Notes
M1	Mid-block	Flat	2 F + Basement	36.7	50.4	+13.7	A3 Survivability	Moderate	Balanced baseline; fails under outage conditions
M2	Mid-block	Flat	3 F Above-Grade	48.7	50.5	+1.8	A5 Durability	Moderate	Height stress raises material fatigue
M3	Mid-block	Pitched	2 F + Basement	41.0	39.7	−1.3	A4 Overheating	High	Stable; minor roof overheating risk
M4	Mid-block	Pitched	3 F Above-Grade	71.2	69.2	−2.0	A4 Overheating	Low	Stack and slope exacerbate heat stress
M5	End-unit	Flat	2 F + Basement	9.7	7.8	−1.9	A1 Energy	Very High	Best-performing archetype; retrofit-ready baseline
M6	End-unit	Flat	3 F Above-Grade	66.8	71.5	+4.7	A3 Survivability	Low	Heat gain from roof and sidewalls; outage-vulnerable
M7	End-unit	Pitched	2 F + Basement	43.3	41.6	−1.7	A4 Overheating	High	Moderate adaptation capacity; thermal penalty limited
M8	End-unit	Pitched	3 F Above-Grade	91.5	92.4	+0.9	A1 Energy	Very Low	Highest deficit; unsuitable without deep retrofit

3.6. Sensitivity Outcomes

Sensitivity tests (Table 11) demonstrated that increasing roof albedo from 0.25 to 0.75 reduced A4 degree-hours by ≈18% and extended service life by ≈1.6 years. Lowering infiltration from 0.6 to 0.3 ACH decreased EUI by ≈8%, while raising thermal mass by 15% increased safe-zone hours by ≈5 h under outage conditions. The combined retrofit scenario ("high albedo + low infiltration + mass increase") improved Lean DI by ≈12 points, confirming that envelope enhancements can partially offset morphological disadvantages. These parametric findings corroborate global evidence that simple envelope interventions yield high adaptive value relative to cost [36,37]. Sensitivity results reveal that archetypes with the highest geometric exposure, specifically the end-unit and three-story configurations (M6 and M8), exhibited the strongest response to envelope modifications. Increasing roof albedo and reducing infiltration produced 20–28% reductions in roof degree-hours and 6–10% decreases in annual energy demand for these units. In contrast, mid-block units with basements (M1 and M3) showed comparatively modest changes (<10% across metrics) due to reduced surface-area exposure and thermal buffering from sub-grade mass. These trends confirm that more exposed geometries benefit disproportionately from simple envelope retrofits, a pattern now highlighted in Table 11.

Table 11. Sensitivity analysis summary and retrofit implications.

Scenario ID	Parameter Modified	Adjustment Range	Δ EUI (%)	Δ SZH (h)	Δ Roof > 150 °F (%)	Δ Service Life (yrs)	Δ Lean DI (points)	Key Observation	Retrofit Implication
S1	Roof Albedo	0.25 → 0.75	−4.2	+2.5	−18.0	+1.6	−5.8	High-reflectivity measures reduce roof overheating by ~20%.	Apply white or cool-roof coatings for low-cost mitigation.
S2	Infiltration Rate	0.6 → 0.3 ACH	−8.0	+1.0	−4.5	+0.7	−3.9	Airtight envelopes improve energy efficiency; minor overheating offset.	Implement blower-door-guided sealing; maintain ventilation control.
S3	Thermal Mass	+15% wall density	−1.5	+5.0	−2.3	+0.8	−2.1	Increased heat capacity extends safe-zone duration by 4–6 h.	Add internal mass (gypsum/brick linings) for passive heat buffering.
S4	Combined Envelope Upgrade	S1 + S2 + S3	−12.0	+8.0	−22.0	+2.5	−12.4	An integrated envelope retrofit provides synergistic benefits across domains.	Bundle roof, sealing, and mass measures as the Standard Retrofit (SR) kit.

4. Discussion

The findings of the Housing-Performance Atlas confirm that legacy Baltimore row homes are operating at the edge of climatic vulnerability, where minor geometric or exposure variations can significantly alter adaptive capacity. Energy, thermal, and durability results are widely dispersed across the archetypes, indicating that efficiency metrics do not adequately reflect the housing stock's resilience. Across all eight configurations, the Energy Use Intensity ranged from 46.7 to 67.6 kBtu $ft^{-2} \cdot yr^{-1}$. However, safe-zone survivability hours during a 72 h outage ranged from 0 to 23 h, and roof overheating lasted 150–210 h at 150 °F. These nonlinear discrepancies confirm the new view that adaptation performance cannot be replaced by operational energy savings in hot–humid urban climates [1,56].

The data show that morphology regulates resilience more than construction age or material type. Mid-block units have the advantage of shared party walls that reduce conductive gain and loss, and end-units have approximately 25% higher EUI and four times less survivability. Basement conditions consistently improve performance across three areas—energy, survivability, and durability—by 6 to 10 percent, with thermal inertia that attenuates diurnal variations. On the other hand, height and roof pitch increase envelope exposure and radiant absorption, thereby increasing overheating and service-life loss. The worst performer, M8 (end-unit, pitched roof, 3F above-grade), has all the undesirable characteristics: maximum exposure, minimum sub-grade mass, and high thermal surface area, leading to a Full DI of 92% and energy and durability failures.

Adaptation hierarchies are also further explained by the distribution of first-failure domains. The most common primary deficit was roof overheating, then survivability, energy, and durability. This result highlights the fact that the operative limit of habitability during extreme events is not determined by energy efficiency but by thermal safety. The practical application of retrofit sequencing would thus require interventions that address surface temperature and indoor safe-zone stability, followed by incremental energy savings. These results align with the adaptive-mitigation ladder proposed by Aruta et al. [52], in which heat resilience serves as the basis for the next stage of efficiency gains.

The material durability results also support this interdependence. The service-life index ranged from 31 to 42 years, indicating that roof life could be reduced by 10 years under high-exposure conditions. A 10 °F rise in average roof-surface temperature was associated with a loss of service life of about 2.5 years, consistent with ISO 15686-8 exposure factors and empirical data on bituminous membranes [3]. These correlations underscore that the concept of durability is thermally mediated: the very processes that threaten occupants by exposing them to heat are also those that accelerate envelope decay. Therefore, there is no way to consider adaptation without accounting for asset management.

Composite Lean and Full Deficit Indices are concise measures of multi-domain resilience. The values of lean DI were 9.7–91.5, and Full DI were 7.8–92.4. The ranking M5 (best) > M3 > M7 > M2 > M1 > M4 > M6 > M8 (worst) represents a near-logarithmic deterioration in performance with increasing exposure. The extremely low DI of M5 (end-unit flat + basement) indicates the stabilizing effect of sub-grade coupling and compact geometry. The second-best competitor, M3 (mid-block pitched + basement) is a compromise of moderate energy consumption and regulated overheating of the roof. On the other hand, the tall end-units (M6, M8) reveal the compounding effect of amplified heat and the rapid degradation of materials, proving that vertical extension without simultaneous envelope upgrades undermines resilience.

The fact that thermal domains (A3 + A4) account for 70 percent of total DI variance confirms that the adaptation deficit in Baltimore is mainly heat-related. Heat gain, survivability, and degradation pathways are determined by microclimatic context and geometry, even with the exact envelope specifications. The trends align with the city-level results reported by Santamouris [22], where local form is more significant than material conductivity in defining the intensity of heat risk [4,5]. The Atlas maps these lessons to the building level, offering a scalable method for quantifying retrofit prioritization.

From a policy standpoint, the Atlas transforms abstract resilience concepts into actionable diagnostics. Lean/Full DI thresholds can delineate Retrofit Triage Bands:

Tier 1 (Standard Retrofit) DI < 40 → low-cost envelope and ventilation upgrades;

Tier 2 (Deep Retrofit) 40–70 → comprehensive insulation, cool-roof, and HVAC electrification;

Tier 3 (Standard Retrofit + Green Infrastructure) > 70 → combined building + green-infrastructure interventions.

This stratification aligns with the European Renovation Passport logic [6] and can be implemented in the Baltimore Climate Plan to distribute incentives based on need and potential impact.

The distribution of high-DI archetypes across space organically defines the dimensions of equity. End-unit conditions are prevalent along block edges and vacant-lot perimeters, which overlap with historically disinvested neighborhoods, including Broadway East and Upton. Therefore, the lack of thermal and durability is associated with socio-economic deprivation, which supports the trends of environmental injustice reported in U.S. legacy cities [7]. The Atlas thus goes beyond technical assessment to provide a diagnosis of spatial resilience inequity, which equips municipalities with a data-driven instrument for equitable adaptation investment.

Implications of retrofit design engineering are also clear. A 30–35% reduction in degree-hours and 8–10-year service life increases with increasing roof solar reflectance (0.35–0.70) and halved infiltration (AH = 1.0–0.5) to lower EUI and safe-zone hours by 10 and 4 percent, respectively. These relationships determine the roof's reflectivity, airtightness, and controlled ventilation as the first-order, cost-effective resilience gains.

The Atlas methodologically confirms that high-resolution simulation is a plausible proxy for empirical diagnostics when field data are scarce. Model robustness is ensured by calibration to metered energy use ($\pm$8%) and by consistency between EnergyPlus temperature patterns. However, its limitations also become apparent in the analysis. The external factors to the model are occupant behavior, moisture transport, long-term degradation kinetics, and subsequent stages; they shall incorporate sensor-based validation and cost-carbon coupling to increase its predictive fidelity.

In general, the Atlas supports urban-housing adaptation as an objective engineering approach rather than a qualitative policy goal. It brings building physics into the decision-making process and equity planning by capturing the interplay among energy, heat, survivability, and durability through a single diagnostic lens. The resulting hierarchy, in which thermal safety overrides efficiency, indicates a fundamental shift like retrofits in legacy cities: not lower kilowatt-hours but safer degrees Fahrenheit. This diagnostic can be incorporated into municipal programs to help Baltimore shift its energy-focused compliance toward truly climate-responsive, equitable housing performance.

5. Conclusions

This study established a Housing-Performance Atlas for Baltimore's legacy row homes, providing a multi-domain diagnostic that integrates energy, survivability, overheating, and durability under present-day climate conditions. Using DesignBuilder v7.0 (EnergyPlus v9.6) simulations and Baltimore TMY3 boundary data, eight archetypes were evaluated through the A1–A5 + C adaptation framework. Results reveal that form, exposure, and ground coupling govern resilience more strongly than material specification or construction age. Energy Use Intensity ranged from 46.7 to 67.6 kBtu ft^{-2} yr^{-1}, yet thermal survivability ranged from 0 to 23 h and roof overheating persisted 150–210 h above 150 °F, confirming the weak correlation between efficiency and safety.

Composite Lean and Full Deficit Indices (DI = 7.8–92.4) captured resilience gradients across archetypes. The most resilient configuration, M5 (end-unit flat + basement), achieved the lowest DI ($\approx$8), while the least resilient, M8 (end-unit pitched + 3F above-grade), recorded DI $\approx$ 92. Thermal domains accounted for roughly 70% of total deficits, establishing overheating and survivability as the dominant failure modes in Baltimore's aging housing stock. These findings redefine retrofit sequencing as follows: thermal-safety stabilization and roof-temperature control must precede energy-efficiency upgrades. The

Atlas, therefore, functions as both a research tool and a decision-support mechanism, enabling municipalities to prioritize limited retrofit funding toward geometries and neighborhoods where adaptation returns are greatest.

The study also advances methodological transparency by translating complex simulation outputs into a clear, reproducible index structure. The integration of service-life modeling (ISO 15686) with heat-exceedance metrics bridges building physics, asset management, and resilience policy, supporting Baltimore's transition from energy-centric codes to climate-responsive redevelopment. Beyond its local relevance, the Atlas framework is transferable to similar mid-Atlantic cities characterized by attached masonry housing and growing urban-heat burdens.

Limitations

While the Housing-Performance Atlas establishes a reproducible baseline, several limitations remain. The simulations represent steady-occupancy and controlled-behavior conditions, excluding stochastic effects such as window operation, thermostat settings, and shading behavior, which can significantly influence survivability and overheating outcomes. Material durability estimations rely on ISO 15686 exposure factors rather than long-term empirical degradation data, potentially under- or overestimating service-life reductions under urban heat-island conditions. The study also omits stormwater and cost/carbon (+C) domains, which will be addressed in subsequent research phases to capture the full spectrum of adaptation co-benefits and to integrate standard retrofitting with green infrastructure pathways. Moreover, validation was limited to cross-comparison with benchmarked metered data; future work should incorporate in situ temperature and humidity sensors to calibrate real-time resilience performance. Despite these constraints, the diagnostic reliability of $\pm 8\%$ for energy predictions and the consistent qualitative heat-mapping patterns confirm the robustness of the framework for comparative analysis and methodological replication.

Author Contributions: Conceptualization: A.G.N. Methodology: A.G.N., B.M.Z. and J.G.H.; Validation: A.G.N. and B.M.Z.; Formal analysis: A.G.N.; Investigation: A.G.N. and B.M.Z.; Resources: A.G.N.; Data curation: A.G.N.; Writing—original draft preparation: A.G.N.; Writing—review and editing: A.G.N., B.M.Z. and J.G.H.; Visualization: A.G.N. and B.M.Z.; Supervision: J.G.H.; Project administration: A.G.N.; Funding acquisition: J.G.H. All authors have read and agreed to the published version of the manuscript.

Funding: This research was supported by the Baltimore Social-Environmental Collaborative (BSEC) project funded by DOE BER under Contract DE-FOA-0002581.

Data Availability Statement: The raw data supporting the conclusions of this article will be made available by the authors on request.

Acknowledgments: We thank the Department of Civil Engineering at Morgan State for academic and administrative support. Special appreciation is extended to the Baltimore Social–Environmental Collaborative (BSEC), notably the Building and Energy Team, for their insights and collaboration. Additional thanks go to the reviewers whose constructive feedback helped enhance the quality and clarity of this manuscript.

Conflicts of Interest: The authors declare that they have no conflicts of interest.

References

1. International Energy Agency (IEA). *World Energy Outlook 2023*; IEA: Paris, France, 2023. [CrossRef]
2. Waddicor, D.A.; Fuentes, E.; Sisó, L.; Salom, J.; Favre, B.; Jiménez, C.; Azar, M. Climate Change and Building Ageing Impact on Building Energy Performance and Mitigation Measures Application: A Case Study in Turin, Northern Italy. *Build. Environ.* **2016**, *102*, 13–25. [CrossRef]
3. Taki, A.; Zakharanka, A. The Impact of Degradation on a Building's Energy Performance. *Sustainability* **2023**, *15*, 1145. [CrossRef]
4. Miranda, N.D.; Lizana, J.; Sparrow, S.N.; Zachau-Walker, M.; Watson, P.A.G.; Wallom, D.C.H.; Khosla, R.; McCulloch, M. Change in Cooling Degree Days with Global Mean Temperature Rise Increasing from 1.5 °C to 2.0 °C. Nat. *Sustainability* **2023**, *6*, 1326–1330. [CrossRef]
5. Spangler, K.R.; Wellenius, G.A. Spatial Patterns of Recent US Summertime Heat Trends: Implications for Heat Sensitivity and Health Adaptations. *Environ. Res. Commun.* **2020**, *2*, 035002. [CrossRef] [PubMed]
6. Siegel, E.L.; Lane, K.; Yuan, A.; Smalls-Mantey, L.A.; Laird, J.; Olson, C.; Hernández, D. Energy Insecurity Indicators Associated with Increased Odds of Respiratory, Mental Health, and Cardiovascular Conditions. *Health Aff.* **2024**, *43*, 260–268. [CrossRef] [PubMed]
7. Sakka, A.; Santamouris, M.; Livada, I.; Nicol, F.; Wilson, M. On the Thermal Performance of Low Income Housing during Heat Waves. *Energy Build.* **2012**, *49*, 69–77. [CrossRef]
8. Doan, D.T.; Ghaffarianhoseini, A.; Naismith, N.; Zhang, T.; Ghaffarianhoseini, A.; Tookey, J. A Critical Comparison of Green Building Rating Systems. *Build. Environ.* **2017**, *123*, 243–260. [CrossRef]
9. Sánchez Cordero, A.; Gómez Melgar, S.; Andújar Márquez, J.M. Green Building Rating Systems and the New Framework Level(s): A Critical Review of Sustainability Certification within Europe. *Energies* **2020**, *13*, 66. [CrossRef]
10. Siu, C.Y.; O'Brien, W.; Touchie, M.; Armstrong, M.; Laouadi, A.; Gaur, A.; Jandaghian, Z.; Macdonald, I. Evaluating Thermal Resilience of Building Designs Using Building Performance Simulation—A Review of Existing Practices. *Build. Environ.* **2023**, *234*, 110124. [CrossRef]
11. Awadh, O. Sustainability and Green Building Rating Systems: LEED, BREEAM, GSAS and Estidama—Critical Analysis. *J. Build. Eng.* **2017**, *11*, 25–29. [CrossRef]
12. Felicioni, L.; Lupíšek, A.; Gaspari, J. Exploring the common ground of sustainability and resilience in the building sector: A systematic literature review and analysis of building rating systems. *Sustainability* **2023**, *15*, 884. [CrossRef]
13. Bi Obam Assoumou, S.S.; Zhu, L.; Khayeka-Wandabwa, C. Healthy building standards, their integration into green building practices and rating systems for one health. *Discov. Sustain.* **2025**, *6*, 796. [CrossRef]
14. Singh, P.; Amekudzi-Kennedy, A.; Ashuri, B.; Chester, M.; Labi, S.; Wall, T.A. Developing adaptive resilience in infrastructure systems. *Int. J. Disaster Resil. Built Environ.* **2023**, *8*, 26–47. [CrossRef]
15. Dong, B.; Liu, Y.; Fontenot, H.; Ouf, M.; Osman, M.; Chong, A.; Qin, S.; Salim, F.; Xue, H.; Yan, D.; et al. Occupant behaviour modelling methods for resilient building design, operation and policy at urban scale: A review. *Appl. Energy* **2021**, *293*, 116856. [CrossRef]
16. Saifudeen, A.; Khan, I.; El-Shimy, M.; Alajmi, A.; Algarni, A.; Alhejji, M. Adaptation of buildings to climate change: An overview. *Front. Built Environ.* **2024**, *10*, 1327747. [CrossRef]
17. Khoja, A.; Danylenko, O. Charting climate adaptation integration in smart building rating systems: A comparative study. *Front. Built Environ.* **2024**, *9*, 1333146. [CrossRef]
18. Krelling, A.F.; Wu, Y.; Malik, J.; Wei, M.; Perry, C.; Lamberts, R.; Yan, D.; Hong, T. Thermal resilience of buildings and communities. *Annu. Rev. Environ. Resour.* **2025**, *50*, 1–26. [CrossRef]
19. Adhikari, R.; Sui, J.; Yang, Y.; O'Donnell, J.; Hewitt, N.; Zuo, W. Energy Efficiency and Thermal Resilience Analysis for Row Houses Using Representative Building Energy Models. *Build. Environ.* **2025**, *282*, 113229. [CrossRef]
20. Ismaeel, W.S.E. The Dynamics of Sustainable Material Selection for Green-Certified Projects. *Buildings* **2023**, *13*, 2077. [CrossRef]
21. Hailu, H.; Gelan, E.; Girma, Y. Indoor Thermal Comfort Analysis: A Case Study of Modern and Traditional Buildings in Hot-Arid Climatic Region of Ethiopia. *Urban Sci.* **2021**, *5*, 53. [CrossRef]
22. Santamouris, M. Recent progress on urban overheating and heat island research: Integrated assessment of the energy, environmental, vulnerability and health impact synergies with global climate change. *Energy Build.* **2020**, *207*, 109482. [CrossRef]
23. Kolokotroni, M.; Zune, M.; Gratton, P.; Tun, T.P.; Christantoni, I.; Tsakanika, D. Impact of the urban environment on the thermal performance and environmental quality of residential buildings: A case study in Athens. *Energies* **2025**, *18*, 2062. [CrossRef]
24. Ortega Del Rosario, M.D.L.Á.; Beermann, K.; Chen Austin, M. Environmentally Responsive Materials for Building Envelopes: A Review on Manufacturing and Biomimicry-Based Approaches. *Biomimetics* **2023**, *8*, 52. [CrossRef]

25. Sharifi, A.; Yamagata, Y. Resilience-Oriented Urban Planning. In *Resilience-Oriented Urban Planning—Theoretical and Empirical Insights*; Yamagata, Y., Sharifi, A., Eds.; Lecture Notes in Energy; Springer: Cham, Switzerland, 2018; Volume 65, pp. 3–27. [CrossRef]
26. Cimellaro, G.P.; Reinhorn, A.M.; Bruneau, M. Framework for Analytical Quantification of Disaster Resilience. *Eng. Struct.* **2010**, *32*, 3639–3649. [CrossRef]
27. Luo, M.; Wang, Z.; Ke, K.; Cao, B.; Zhai, Y.; Zhou, X. Human metabolic rate and thermal comfort in buildings: The problem and challenge. *Build. Environ.* **2018**, *131*, 44–52. [CrossRef]
28. Zhang, Y.; Wang, W.; Xie, J.; Lei, Y.; Cao, J.; Xu, Y.; Bader, S.; Bowen, C.; Oelmann, B. Enhanced variable-reluctance energy harvesting for self-powered monitoring. *Appl. Energy* **2022**, *321*, 119402. [CrossRef]
29. Zou, Y.; Wu, Z.; Li, B.; Jia, Y. Cooling Energy Challenges in Residential Buildings During Heat Waves: Urban Heat Island Impacts in a Hot-Humid City. *Buildings* **2024**, *14*, 4030. [CrossRef]
30. Moret Rodrigues, A.; Santos, M.; Gomes, M.G.; Duarte, R. Impact of Natural Ventilation on the Thermal and Energy Performance of Buildings in a Mediterranean Climate. *Buildings* **2019**, *9*, 123. [CrossRef]
31. Bano, F. Roofing systems and energy efficiency in low-rise buildings. *Energy Build.* **2024**, *329*, 113321. [CrossRef]
32. *ISO 15686-1:2020*; Buildings and Constructed Assets—Service Life Planning—Part 1: General Principles and Framework. International Organization for Standardization: Geneva, Switzerland, 2020.
33. Zhao, Q.; Myint, S.W.; Wentz, E.A.; Fan, C. Rooftop Surface Temperature Analysis in an Urban Residential Environment. *Remote Sens.* **2015**, *7*, 12135. [CrossRef]
34. Berdahl, P.; Akbari, H.; Levinson, R.; Miller, W.A. Weathering of Roofing Materials—An Overview. *Constr. Build. Mater.* **2008**, *22*, 423–433. [CrossRef]
35. Wang, W.L.; Toftum, J.; Olesen, B.W. Determination of Individual Building Performance Targets for Smart Retrofitting of Residential Buildings. *J. Sustain. Built Environ.* **2022**, *14*, 100859.
36. Ozcan-Deniz, G.; Fryer, R.; De Castro Amorim Ferreira, A. The Design of Net-Zero-Energy Affordable Housing in Philadelphia. *Designs* **2018**, *2*, 26. [CrossRef]
37. Wilson, C.; Dowlatabadi, H. Models of Decision Making and Residential Energy Use. *Annual Review of Environment and Resources* **2007**, *32*, 169–203. [CrossRef]
38. Liyanage, D.R.; Hewage, K.; Hussain, S.A.; Razi, F.; Sadiq, R. Climate adaptation of existing buildings: A critical review on planning energy retrofit strategies for future climate. *Renew. Sustain. Energy Rev.* **2024**, *199*, 114476. [CrossRef]
39. Joo, M.R.; Sinha, R. Performance-based selection of pathways for enhancing built infrastructure resilience. *Sustain. Resilient Infrastruct.* **2023**, *8*, 532–554. [CrossRef]
40. Rezvani, S.M.H.S.; Falcão, M.J.; Komljenović, D.; de Almeida, N.M. A systematic literature review on urban resilience enabled with asset and disaster risk management approaches and GIS-based decision support tools. *Appl. Sci.* **2023**, *13*, 2223. [CrossRef]
41. City of Baltimore Department of Planning. *Baltimore Green Network Plan 2018*; Baltimore City Department of Planning: Baltimore, MD, USA, 2018. Available online: https://planning.baltimorecity.gov/green-network-plan (accessed on 17 October 2025).
42. City of Baltimore Office of Sustainability. *Baltimore Climate Action Plan Update 2023*; Baltimore Office of Sustainability: Baltimore, MD, USA, 2023. Available online: https://www.baltimoresustainability.org/plans/climate-action-plan/ (accessed on 17 October 2025).
43. Kong, L.; Mu, X.; Hu, G.; Zhang, Z. The application of resilience theory in urban development: A literature review. *Environ. Sci. Pollut. Res. Int.* **2022**, *29*, 49651–49671. [CrossRef]
44. Hassan, A.N.M.; Hachem-Vermette, C. A Data-Driven Decision-Making Tool for Prioritizing Resilience Strategies in Cold-Climate Urban Neighborhoods. *Energies* **2025**, *18*, 5421. [CrossRef]
45. Sezer, N.; Yoonus, H.; Zhan, D.; Wang, L.; Hassan, I.G.; Rahman, M.A. Urban microclimate and building energy models: A review of the latest progress in coupling strategies. *Renew. Sustain. Energy Rev.* **2023**, *184*, 113577. [CrossRef]
46. Fahmy, M.; Sharples, S.; Eltrapolsi, A. Dual Stage Simulations to Study the Microclimatic Effects of Trees on Thermal Comfort in a Residential Building, Cairo, Egypt. In Proceedings of the Building Simulation 2009: 11th Conference of IBPSA 2009, Glasgow, UK, 27–30 July 2009; pp. 1730–1736.
47. Bianchi, S.; Matteoni, M.; Kim, K.; Koniari, A.M.; Koning, K.; Costache, R.; Ciobotaru, N.; Luna-Navarro, A.; Peng, Z.; Ciurlanti, J.; et al. Resilience Readiness Levels for Buildings: Establishing Multi-Hazard Resilience Metrics and Rating Systems. *Int. J. Disaster Risk Reduct.* **2025**, *128*, 105746. [CrossRef]
48. Al Assaad, D.; Sengupta, A.; Breesch, H. A Novel Quantitative Assessment Framework of the IAQ Resilience of Buildings. *Build. Environ.* **2023**, *243*, 110669. [CrossRef]
49. Elkady, S.; Hernantes, J.; Labaka, L. Decision-making for community resilience: A review of decision support systems and their applications. *Heliyon* **2024**, *10*, e33116. [CrossRef] [PubMed]

50. Johansson, T.; Olofsson, T.; Mangold, M. Development of an energy atlas for renovation of the multifamily building stock in Sweden. *Appl. Energy* **2017**, *203*, 723–736. [CrossRef]
51. Eriksson, P.; Johansson, T. Towards differentiated energy renovation strategies for heritage-designated multifamily building stocks. *Heritage* **2021**, *4*, 4318–4334. [CrossRef]
52. Aruta, G.; Ascione, F.; Bianco, N.; Bindi, L.; Iovane, T. Energy Classification of Urban Districts to Map Buildings and Prioritize Energy Retrofit Interventions: A Novel Fast Tool. *Appl. Energy* **2025**, *377*, 124664. [CrossRef]
53. Chen, Y.; Hong, T.; Piette, M.A. City-Scale Building Retrofit Analysis: A Case Study Using CityBES. In Proceedings of the 15th International Conference International Building Performance Simulation Association 2017, San Francisco, CA, USA, 7–9 August 2017; pp. 259–266. [CrossRef]
54. Berardi, U. Sustainability assessments of buildings, communities, and cities. In *Assessing and Measuring Environmental Impact and Sustainability*; Klemeš, J.J., Ed.; Butterworth-Heinemann: Oxford, UK, 2015; pp. 497–545. [CrossRef]
55. *Standard 55-2017*; Thermal Environmental Conditions for Human Occupancy. ANSI/American Society of Heating, Refrigerating and Air-Conditioning Engineers (ASHRAE): Atlanta, GA, USA, 2017.
56. Intergovernmental Panel on Climate Change (IPCC). *AR6 Synthesis Report 2023*; IPCC: Geneva, Switzerland, 2023.
57. Gopinath, S.; Kumar, A.; Lavanya, E. Thermal Properties of Multiple-Wythe Masonry Overlayed with Textile Reinforced Concrete Sandwich Panels. *Sādhanā* **2023**, *48*, 39. [CrossRef]
58. Li, W.; Xu, X.; Yao, J.; Chen, Q.; Sun, Z.; Makvandi, M.; Yuan, P.F. Natural Ventilation Cooling Effectiveness Classification for Buildings. *Sci. Rep.* **2024**, *14*, 66684. [CrossRef]
59. Zhu, W.; Yuan, C. Urban heat health risk assessment in Singapore to support resilient urban design—by integrating urban heat and the distribution of the elderly population. *Cities* **2023**, *132*, 104103. [CrossRef]

Disclaimer/Publisher's Note: The statements, opinions and data contained in all publications are solely those of the individual author(s) and contributor(s) and not of MDPI and/or the editor(s). MDPI and/or the editor(s) disclaim responsibility for any injury to people or property resulting from any ideas, methods, instructions or products referred to in the content.

buildings

MDPI

Article

Low-Carbon Climate-Resilient Retrofit Pilot: Construction Report

Hamish Pope *, Mark Carver and Jeff Armstrong

Natural Resources Canada, CanmetENERGY, Ottawa, ON K1A 1M1, Canada;
mark.carver@nrcan-rncan.gc.ca (M.C.); jeff@coldclimatebuilding.ca (J.A.)
* Correspondence: hamish.pope@nrcan-rncan.gc.ca

Abstract: Deep retrofits are one of the few pathways to decarbonize the existing building stock while simultaneously improving climate resilience. These retrofits improve insulation, airtightness, and mechanical equipment efficiency. NRCan's Prefabricated Exterior Energy Retrofit (PEER) project developed prefabricated building envelope retrofit solutions to enable net-zero performance. The PEER process was demonstrated on two different pilot projects completed between 2017 and 2023. In 2024, in partnership with industry partners, NRCan developed new low-carbon retrofit panel designs and completed a pilot project to evaluate their performance and better understand resiliency and occupant comfort post-retrofit. The Low-Carbon Climate-Resilient (LCCR) Living Lab pilot retrofit was completed in 2024 in Ottawa, Canada, using low-carbon PEER panels. This paper outlines the design and construction for the pilot, including panel designs, the retrofitting process, and post-retrofit building and envelope commissioning. The retrofitting process included the design and installation of new prefabricated exterior retrofitted panels for the walls and the roof. These panels were insulated with cellulose, wood fibre, hemp, and chopped straw. During construction, blower door testing and infrared imaging were conducted to identify air leakage paths and thermal bridges in the enclosure. The retrofit envelope thermal resistance is RSI 7.0 walls, RSI 10.5 roof, and an RSI 3.5 floor with 0.80 $W/m^2 \cdot K$ U-factor high-gain windows. The measured normalized leakage area @10Pa was 0.074 cm^2/m^2. The net carbon stored during retrofitting was over 1480 kg CO_2. Monitoring equipment was placed within the LCCR to enable the validation of hygrothermal models for heat, air, and moisture transport, and energy, comfort, and climate resilience models.

Keywords: embodied carbon; building envelope; prefabrication; sustainable materials; energy efficiency; deep-energy retrofit

1. Introduction

The need for sustainable, efficient, and resilient buildings has become paramount. As we confront the challenges posed by climate change, population growth, and urbanization, retrofitting existing structures to meet modern standards has emerged as a crucial strategy. The existing building stock worldwide represents a significant portion of the global energy consumption and carbon emissions. Many of these buildings were constructed decades ago, lacking the energy-efficiency standards and environmental considerations that are now integral to sustainable development goals. Retrofitting these structures presents an opportunity to enhance overall building performance and occupant comfort, reduce energy consumption, lower carbon emissions, and improve the climate resilience of the built environment. Retrofitting also extends the service life of the current building, which avoids emissions from demolition and new construction.

The building industry contributes 40% of the world's carbon emissions, and residential buildings account for roughly 25% of global energy consumption [1,2]. Carbon emissions from buildings can be categorized into operational emissions, which include heating, cooling, and other energy demands, and embodied emissions, which result from the production, manufacturing, and transport of building materials. In Canada, building operations comprised 18% of the greenhouse gas emissions in 2021, with space heating accounting for 59% of the emissions [3–7]. Embodied carbon from building construction comprised 4% of Canada's greenhouse gas emissions in 2021 [6]. If no changes are made to the materials and construction methods used, embodied carbon is expected to comprise half of the building sector emissions as building performance improves [1]. The Government of Canada aims to achieve net-zero carbon emissions by 2050, which will require reductions in both operational and embodied carbon.

To achieve these emission reductions, deep retrofits are required [8]. Such retrofits include upgrading the building envelope, installing energy-efficient HVAC systems, and integrating renewable energy technologies. Using low-carbon building materials and low-GWP refrigerants will ensure that the upfront emissions are minimized. Many retrofits undertaken in Canada are small-scale and/or completed piecemeal (adding attic insulation, insulating an unfinished basement from the interior, air sealing around new windows, etc.) [9,10]. While these unsystematic approaches can reduce operational emissions, they often lead to discontinuity of the air barrier and/or thermal bridging [9,10]. Another issue with the piecemeal approach is that it increases the amount of time occupants are disrupted and invariably increases the overall cost of the work. There is also a lack of skilled trades in Canada, and this deficit in the trades is expected to increase in the coming years [11–13]. Canada faces a potential recruitment shortfall of almost 30,000 workers by 2027 [14].

One way to scale up retrofits with reduced labour is to use prefabrication. Prefabricated industrialized building retrofits involve the use of standardized components manufactured offsite and assembled onsite, offering numerous advantages over traditional construction methods. These include accelerated construction, reduced waste, and improved quality control. While retrofits can be completed from the interior, the use of exterior retrofits allows occupants to remain in a building during construction. This is particularly appealing as most buildings that require deep retrofits are currently occupied.

There are already several completed projects (mainly in Europe) that have undertaken prefabricated exterior deep-energy retrofits. They have helped to pave the way forward on accomplishing similar retrofits in Canada. Many of these projects focused on low-income housing buildings as these structures often had simple geometry, poor energy efficiency, and a single owner (allowing multiple similar buildings to be retrofitted at once) [12,15–17].

One of the most well-known deep retrofitting projects is Energiesprong, based in the Netherlands [16,18]. This project, funded by the Dutch government, helped to develop the deep retrofit market in the Netherlands by providing retrofit solutions including highly insulated panels, electrification and renewables, and prefabrication [18]. Through successful pilots and aggregation of buildings to be retrofitted, a market for prefabricated exterior retrofitted panels for buildings was developed. This project outlined the business case for owners, showing that retrofitting could be financed through energy savings over the course of 30–40 years. Energiesprong now supports market development teams in various countries to replicate their process [18].

The retrofitting process starts with building capture using photogrammetry, or laser scanning to obtain accurate dimensions of the building. This building capture data is then uploaded to a building information modelling (BIM) tool to convert the raw data into workable shop drawings [13,19,20]. These shop drawings need to account for the locations

of rough openings, maximum dimensions for shipping, pick points, etc. The panels can then be fabricated using various levels of automation, ranging from manual to semi-automated to fully automated. Many early-stage projects tended towards more manual approaches while prototyping designs and building up demand [16]. For installation, many projects used cranes and lifts to install panels to reduce installation time and disruption when compared to the use of scaffolding [16,17]. Any mechanical retrofits are then completed on the interior, swapping out the older system for a new one.

NRCan's Prefabricated Exterior Energy Retrofit (PEER) project devised and showcased a method for large-scale comprehensive building retrofits utilizing prefabricated panels, adapting Energiesprong to the Canadian context [9]. The R&D adapted existing panel designs, intended for new construction, to suit retrofits, aiming for swift industry adoption. These initial panels utilized commonly available and well-understood building materials. Through this project, a pilot was completed to test out a nailbase (rigid foam laminated to oriented strand board) panel design and a woodframe stand-off panel design. Following the success of the pilot, a four-unit building was retrofitted with SIP panels, and fifty-nine units were retrofitted with stand-off woodframe panels.

In 2023, CanmetENERGY initiated a new project aimed at integrating carbon-storing materials into enclosure assemblies suitable for factory production. While some such materials, like cellulose insulation, are proven and widely available, others are still undergoing development and require thorough testing to ascertain their performance and instill confidence in their application.

1.1. The Pilot

The Low-Carbon Climate-Resilient (LCCR) Living Lab pilot was a PEER-style retrofit of an office trailer located in Ottawa, Canada. The panel designs included low-carbon materials such as straw, cellulose, hemp, and wood fibre [9]. Construction involved the addition of exterior retrofitted panels for the walls and roof, new windows, and a new HVAC system. The intent of retrofitting was to create a living lab that provides office space while data is being collected. Two different companies fabricated the panels, one insulating with dense-pack cellulose and the other insulating with dense-pack chopped straw. All the roof panels and half the wall panels were insulated using dense-pack cellulose, while the other half of the wall panels were insulated using dense-pack chopped straw. This allowed for two different low-carbon materials to be tested, and it also provided an opportunity to assess constructability with two different panel fabricators. This pilot focused on adapting the previous retrofit designs to work with carbon-storing materials and trialing novel installation methods. Data and insights on the design, fabrication, and installation process were collected. The building was modelled to assess the improved thermal performance, amount of carbon stored, and associated costs.

1.2. Original Structure

The original structure was an old office trailer (Figure 1). In preparation for the renovation, the trailer was moved into position, and the trailer chassis was removed and replaced with four steel beams supported by helical piles. The insulation under the floor of the trailer was limited and in need of replacement. Joist cavities were insulated with RSI 4.9 (R-28) mineral wool batts, and RSI 1.8 (R-10) high-density EPS foam was placed under the framing to support the batt insulation and further insulate the floor. Plywood sheathing was then installed outboard of the foam insulation and taped to serve as the primary airtight layer of the floor system and to protect the assembly from pests. Finally, the

existing leaking cladding was removed, and the building was wrapped in a self-adhered vapour-open water-resistive barrier (WRB) to protect it until the retrofitting occurred.



Figure 1. LCCR original structure (**left**); LCCR before panel installation (**right**).

2. Materials and Methods

2.1. Design Stage

2.1.1. Building Capture and Model Creation

To design panels, accurate building dimensions were required. Even for a simple building, there are several dimensions that need to be captured accurately to ensure that panels fit when they arrive onsite. The building was measured using Light Detection and Ranging (LiDAR), photogrammetry, and hand measurements, and a point cloud of the building was developed (Figure 2). From the point cloud, the locations of points of interest (such as the corners of the building and rough openings) can be determined, and a model of the building can be created, which will in turn allow shop drawings to be designed. One comment that arose from the project partners and from others with experience using point clouds for retrofits was that the person manipulating the point clouds should be the same person creating the shop drawings. This is because some adjustments, assumptions, and fine-tuning are required when manipulating the point clouds and creating the shop drawings, so having the same person or firm perform both tasks reduces the impact of compounding errors.

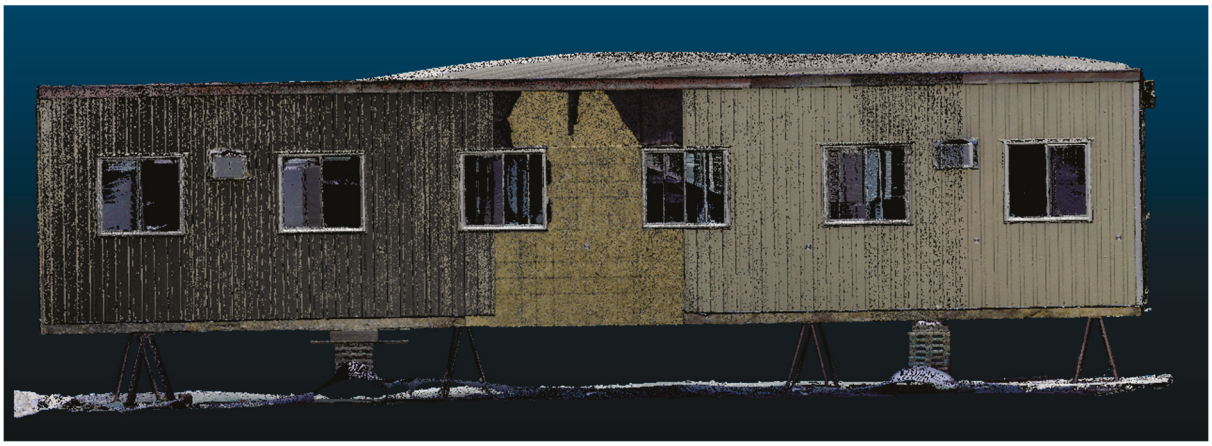


Figure 2. Original building point cloud.

Once all the building dimensions were confirmed, 3D models were created in Revit and SketchUp. The building dimensions were shared with the panel fabricators, and the 3D model was used for developing and illustrating construction details.

2.1.2. Panel Designs Developed

The panel design for this project was geared towards Part 9 residential buildings in the National Building Code of Canada. These residential buildings are 3 stories or less in height and under 600 m^2 building area [21]. With these types of buildings, the panels are not required to support the building structure itself and only need to be able to support their own weight. In regard to fire performance, Part 9 buildings are allowed to be built out of combustible construction, so no fire testing was conducted. As the original structure had no below-grade foundation (as it was set on beams supported by piles), no below-grade retrofit was included in this project.

The retrofit design called for R40 (RSI 7.0) walls and R60 (RSI 10.5) roof post-retrofit. As the biogenic insulating materials used had lower thermal performance than traditional materials such as foam insulation, a deeper panel was required. To achieve this, panel designs were developed using I-joists as framing members to provide a deep "outlooker" cavity (Figure 3). I-joists are available in long straight lengths and offer a deep cavity with minimal thermal bridging, which makes them well suited for thick insulation panels. The framing cavities were dense-packed with chopped straw or cellulose. Wood fibre board insulation was used to insulate the web cavity at panel edges and in small cavities where dense packing would be difficult. The wall panels used 9 $\frac{1}{2}''$ (241 mm) I-joists, and the roof panels used 14″ (356 mm) I-joists.

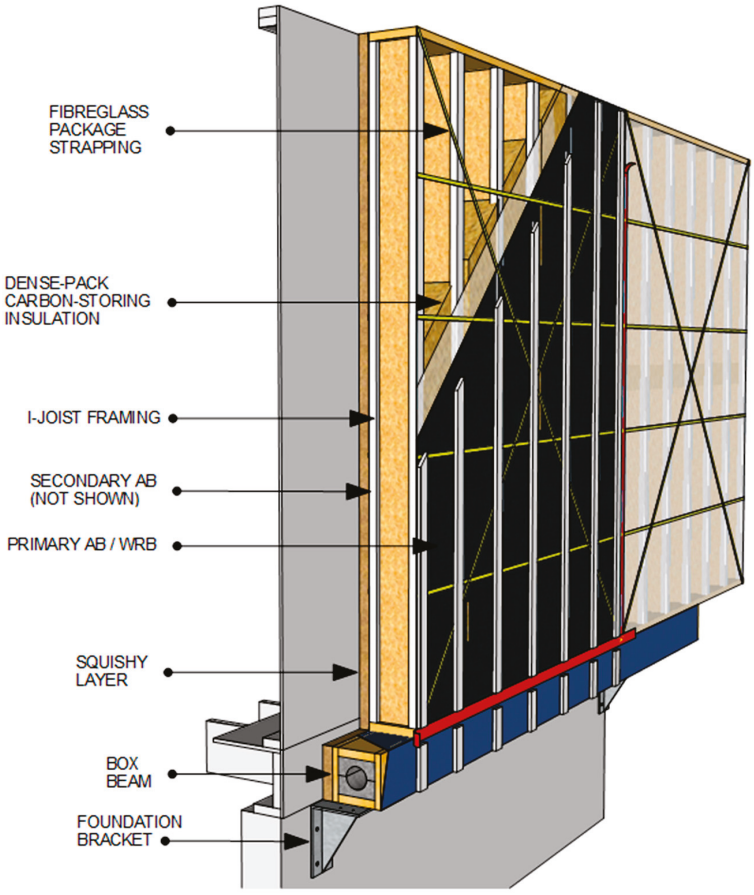


Figure 3. Retrofit panel design.

As the wall panels were not structural, and drying potential was a concern with biogenic materials, it was decided that the wall panels would be constructed without sheathing, and packing straps (which could be removed, if necessary, after the install) would be used to keep the panels from racking during transportation and installation. Without sheathing, the panels were less stiff, but they had increased drying potential. The panels included a primary Air Barrier and Water Resistive Barrier (AB/WRB) on the outside face, and a secondary AB/WRB on the inside face of the panel. These barriers helped to make the new structure more airtight and watertight and protected the moisture-sensitive biogenic cavity insulation during transit.

Steel brackets were used to support the panels (Figure 3). Normally, such brackets would be connected to the foundation, but, in the case of the LCCR, which sits on steel beams, the brackets were connected to the existing floor system rim. Insulated box beams span between brackets and support the panels (Figure 3). The box beams allow the brackets to be placed at regular intervals, which in turn allows the panel widths to be more flexible. The box beams could also be installed without the use of a crane, which can help to minimize the amount of time a crane is required onsite. The box beams can also include an MEP (mechanical, electrical, and plumbing) chase. The box beams were designed to be constructed with laminated strand lumber (LSL) rimboard web and dimensional lumber flanges, insulated with a two-piece Graphite Polystyrene (GPS) foam core, with an optional machined hole in the centre.

Because few existing buildings are perfectly level, plumb, and square, retrofitting projects present a greater amount of design uncertainty for prefabrication than for new construction. A variety of measures were implemented to increase tolerance and ensure the final retrofitted panels would fit. A 2″ (51 mm) hemp batt insulation was used as a "squishy" interface layer between the existing building and panels. This "squishy layer" would be installed on the structure or on the panels and was planned to be compressed to roughly 1″ (25 mm) to accommodate any irregularities in the building and to ensure the panels remain plumb.

As there is also some uncertainty laterally, a nominal 1″ (25 mm) gap was designed between panels. This gap could expand or shrink by $\frac{1}{2}$″ (13 mm) to increase the lateral tolerance when aligning the panels. This gap was filled with a 2″ (51 mm) hemp batt insulation, which could be compressed to size, as well as a gasket material to help air seal the vertical panel joint (Figure 4). To increase tolerance and to make it easier to align the panels to existing rough openings, the panel's window rough openings were shrunk by $\frac{1}{2}$″ (13 mm) on all 4 sides. The door rough opening was not shrunk, so this panel needed extra care when being installed. The other panels could be aligned around the door panel to ensure a good fit.

As the existing structure had a low-slope roof, roof panels were designed to span the whole width of the building, and additional overhangs were added. A 2 × 4 registration block was fastened to the underside of the roof panels to catch a 2 × 8 sleeper pre-installed on the existing roof (Figure 5). This facilitated panel alignment during installation. As the roof panels are unventilated and insulated with biogenic insulation, they are reliant on a very airtight installation to ensure warm moisture-laden air is not introduced into the assembly, where it could condense with no real drying mechanism. As the retrofitted roof panels were installed over the existing continuous modified bitumen roofing membrane, it is unlikely that interior air would reach the panels.

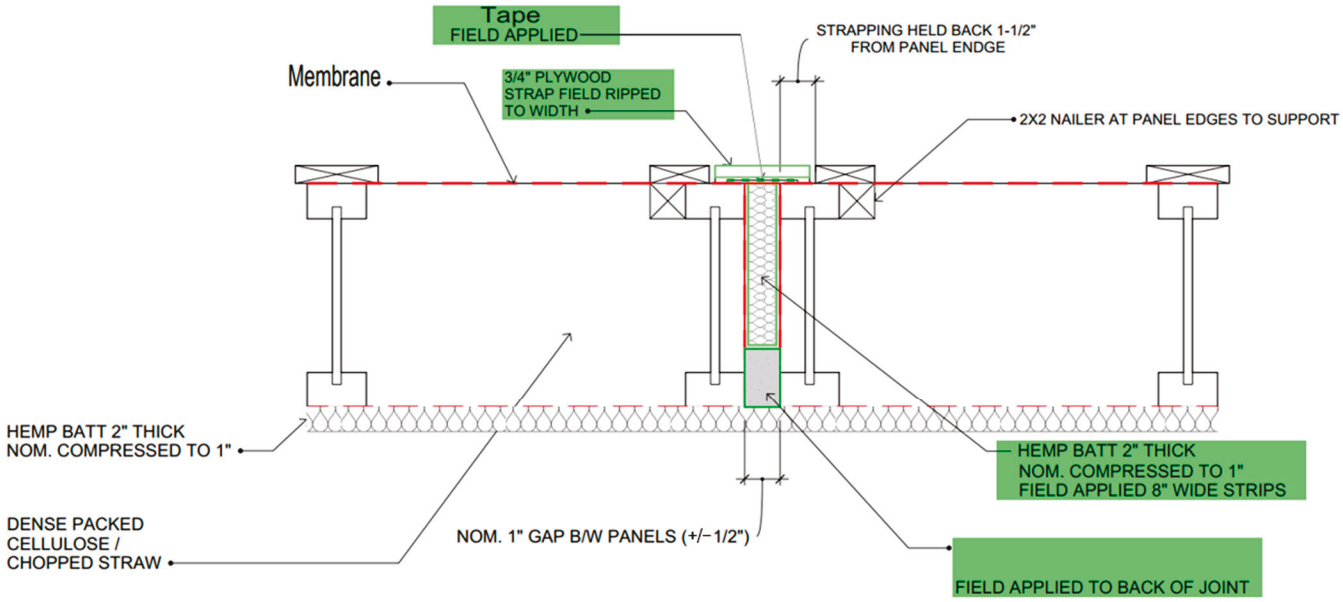


Figure 4. Vertical panel joint detail (plan view). Green items installed on site.

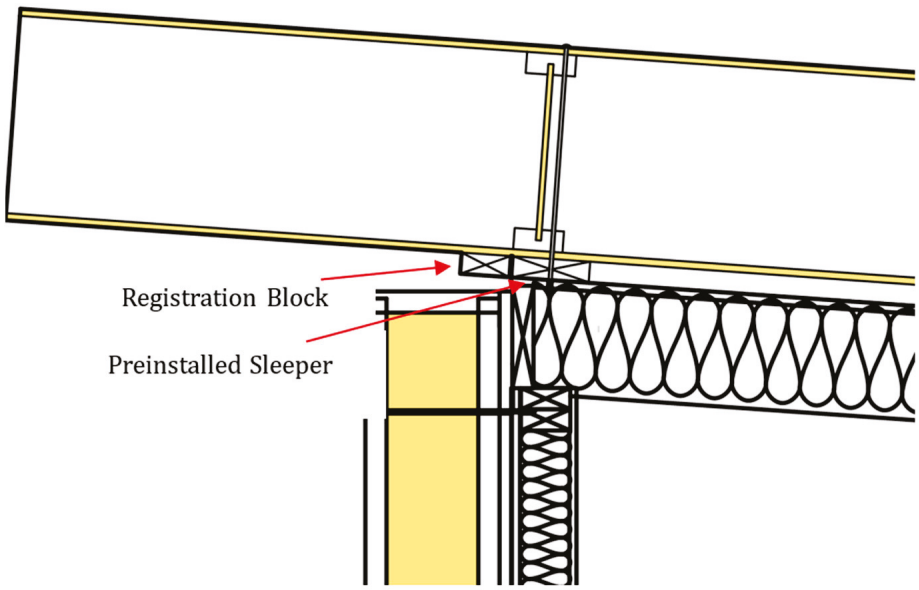


Figure 5. Roof panel installation detail, registration block, and sleeper.

2.2. Fabricator Work

2.2.1. Shop Drawings Were Developed

Both panel fabricators developed their own shop drawings for their respective panels, using their typical software and processes (Figure 6). To develop the shop drawings, fabricators first needed to determine panel sizes and layout, location of structural members and blocking, the location of rough openings within panels, etc. The final shop drawings included pick points for handling the panels, the centre of mass, as well as the location of framing and blocking.

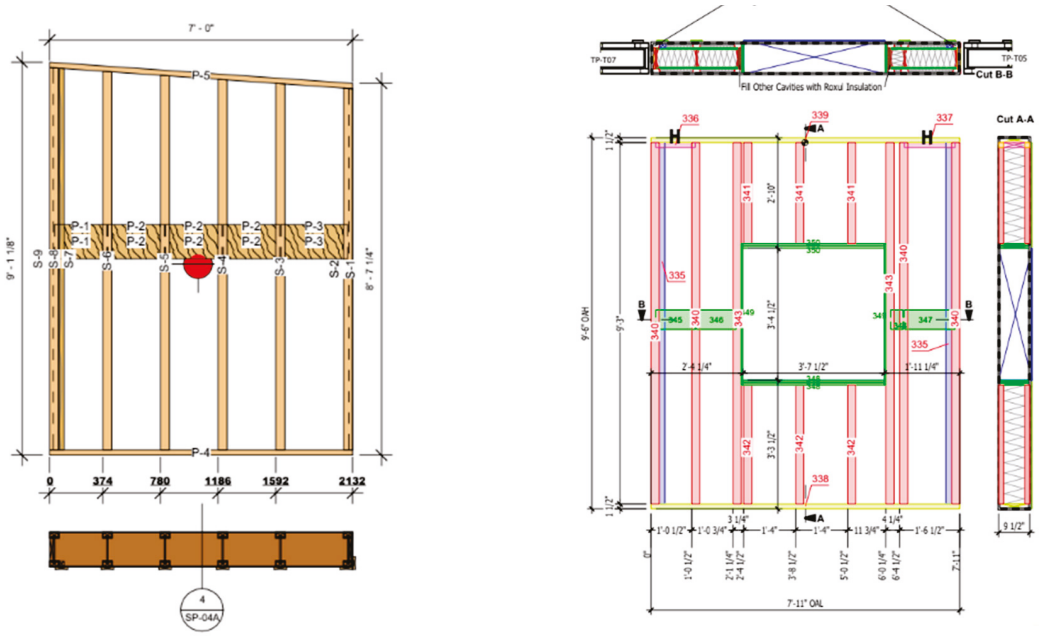


Figure 6. Fabricator shop drawings.

2.2.2. Panel Fabrication

The panels were prefabricated offsite by two different manufacturers. The cellulose panels were connected using structural screws, with extra reinforcement around the pick points. The straw panels used nails, and there was no reinforcement around the pick points. Once framed, one side of the panel was covered in membrane. For the cellulose panels, an insulation retention mesh was placed on the other side of the panels, and cellulose was blown in, and then the WRB was added to finish wrapping the whole panel. For the chopped straw panels, no mesh was used, and initially the panel was fully closed with airtight WRB membrane before insulating. This prevented the escape of air while insulating, causing blow-out. The second attempt involved pre-filling the cavities with chopped straw to prevent buildup of air. Once the panels were insulated and sealed, the window opening rough sills were flashed, and the panels were strapped.

While the fabricators were able to prefabricate the panels offsite, the process was still mostly manual. With higher demand for prefabricated retrofits, investments in automated machinery would become more economically viable.

2.2.3. Panels Loaded and Shipped

Part of the prefabrication process was to determine how best to lay out panels for transportation, so they fit efficiently (Figure 7). Panel heights (and sometimes widths) are dictated by the trucking restrictions. Keeping a panel height below 8’6 is required for panels that are being shipped horizontally [22,23]. If the panels are being shipped vertically, then the maximum panel height can be higher, depending on the height of the trailer that will be delivering it and local vehicle height restrictions [23]. Panels can be shipped horizontally if there are no windows, but, if windows or doors are pre-installed (factory installed), they need to be shipped vertically to reduce the likelihood of damage. Efficiency in stacking the panels is important to reduce the overall shipping costs. Ideally, the load order is the inverse of the desired install order. Panels can be loaded and unloaded with either a crane or a forklift with fork extensions.



Figure 7. Delivered panels.

2.3. Onsite Work

2.3.1. Building Preparation

The wall AC units, light fixtures, and attached deck were removed, and the penetrations were sealed. The old windows were left in place, but the trim was removed. In a typical structure, the existing cladding might need to be removed, but it is also possible for the panels to be installed over existing cladding with an appropriate squishy layer capable of accommodating the dimensional differences in the cladding. Installing the panels over existing cladding would also require that the substrates of the assembly are still in good condition (no mold, damage, etc.).

2.3.2. Brackets and Box Beam Installed

After the building preparation, the brackets and the box beams were installed. The brackets were positioned using a laser level and fastened with structural screws to the existing floor system. Next, the box beams were placed level on the brackets and fastened through the bottom of the bracket screws. The squishy layer was placed between the box beam and existing building and compressed during the alignment process. The box beam was then taped to the WRB to air seal the beam to the backup wall and to flash the hemp squishy layer temporarily (Figure 8).



Figure 8. Box beam installation.

The box beams were fabricated longer than required so they could be cut to size onsite. In a larger-scale project or if box beam retrofits become more commonplace, box beams could be prefabricated in set sizes and produced in bulk quantities. These box beams could then be shipped before the panels arrive so that the entire building could be prepared without using any crane time.

2.3.3. Wall Panel Installation—Hemp Squishy Layer

The 4′x′8′x2″ thick hemp batt squishy layer was tacked in place on the existing sheathing using 2″ staples. The hemp was cut using a track saw as it is too tough to be cut with an insulation knife. The hemp had to be installed on the day the panels were installed as it could not get wet, and if it was to be left out with potential wind more staples would have been required to tack it in place. The hemp layer was 2″ (51 mm) with a 35 kg/m^3 density. The intent was to compress it by 1″ (25 mm) nominally during the panel installation. This ended up being difficult as the hemp was not easy to compress at this density.

2.3.4. Wall Panel Installation—Crane

The panels were lifted by crane (Figure 9). The panels themselves had D-rings pre-installed to make hoisting them fast and simple. A bead of durable airtight adhesive was placed on the box beam to connect the secondary airtight plane at the interior panel face [24]. Panel registration was performed by aligning panel rough stud openings (RSOs) with existing RSOs. The vertical panel joints could easily grow or shrink as necessary.



Figure 9. Wall panel installation.

A long prybar was used move the panels fore and aft (Figure 10), and rachet straps attached to the D-rings were used to pull the top of the panel into place. Aligning the panels took more time and required excessive racking force from the prybar since the

hemp batt placed between panels was more difficult to compress than expected. The straw panels' studs were connected to plates with nails, and it appears that the nails were sheared through the force applied to move the panels into position. The cellulose panels had screws connecting the framing, and they were able to withstand the forces used to pry the panels into position. It is expected that using a "panel puller" tool would have resulted in the same issue. A better solution would be specifying a more compressible material for the vertical panel joint or filling the joint after the panels are installed.



Figure 10. Prybar panel adjustment.

Once the panels were aligned properly, they were screwed into place at the top and the bottom. The panels were toe-screwed into the box beam at the bottom and connected into the top plate of the building using long stainless-steel screws with washers to prevent them from pulling through.

Stainless steel screws were specified for their lower thermal conductivity, but these have a relatively high cost (CAD 2.5–CAD 4/screw) and still result in some minor thermal bridging (Chi-values of roughly 0.000224 W/K). Using brackets connected at the panel edges that would later be concealed would be more cost-effective and would reduce thermal bridging. As an added advantage, if all connections could be made at panel joints, panels could be factory-clad more readily.

Most of the panels were of a similar size, being roughly 8 feet wide. These panels took a 3-person crew roughly 15–20 min each to install (rigging, hoisting, positioning, and fastening each panel, and preparing the joint for the next panel). Two of the panels were larger (~16 ft long). It was assumed that the larger panels would take roughly the same amount of time to install, but there were some difficulties with adjusting the larger panels to make them flush. They took 30–35 min, with most of that being panel adjustment time. The squishy layer had a significant impact on panel adjustment time, so it is likely that the time would be reduced with a less dense material/simpler detail.

2.3.5. Panel Joints

The vertical panel joints were detailed after the first panel was installed (Figure 11). A compressible foam gasket was placed at the back of the panel joint to air seal. The rest of the joint was filled with hemp insulation prior to placing the next panel. The second panel would then be pulled or pried into position, compressing the gasket and the hemp to the $1'' +/- \frac{1}{2}''$ spacing (25 mm +/− 13 mm). The vertical panel joints were then taped and strapped with field-ripped plywood to fit.



Figure 11. Vertical panel joint viewed from above.

The box beam-to-panel joints did not have any squishy layer or gasket, and the panels were simply placed directly on top of the box beam. A bead of caulking was placed at the back of the box beam to help seal the joint. At the front of the box beam-to-panel joint, the joint was taped. One fabricator left a flap of WRB at the bottom of the panel, which allowed proper shingling of the WRB to shed water without relying on the leading edge of a taped WRB connection. Once D-rings were removed, a transition membrane was used to connect the WRB/AB at the top of the panels to the existing modified bitumen roofing (which was treated as the airtight layer for the roof).

2.3.6. Roof Panel Installation

There were 2 × 8 sleepers installed on the long edges of the existing roof. Further, 2″ thick hemp batts were laid on the roof to fill the cavity between the existing roof and the new roof panels. The roof panels had 4 pick points with D-rings so they were able to be lifted evenly. The registration block at the bottom of the panel lined up with the upper sleeper to align the panels together (Figure 12). Similar to the wall panels, ratchet straps were used to pull the panels into position. The roof panels were butted together flush with no hemp or gasket between them. The panels were fastened to the existing structure with long screws into the sleepers. The D-rings were then removed and holes taped, and the joints between panels were taped.



Figure 12. Roof panel installation.

2.3.7. Window Installation

The old windows were removed just before the new windows were installed. The panel rough openings had already been taped and flashed, and the new windows were set at the mid-depth of the panel. The rough openings were shimmed.

Air-sealing details using a tape and a gasket were trialed (Figure 13). For the taped method, the windows were taped all around the interior edge and along 3 sides of the exterior (bottom left open for drainage). The windows were connected to the RSO (rough stud opening) with screws through the frame, and the tape was connected to the air barrier membrane that was returned into the window openings, The head and jamb rough opening cavities were insulated with canned polyurethane foam.



(**a**) (**b**)

Figure 13. (**a**) Taped window detail; (**b**) gasket window detail.

For the gasket method, the gasket was placed around the perimeter of windows. The window was then connected to the RSO with screws through the frame and screwed into place. The gasket then expanded to fill the gap between the window frame and the RSO.

For all windows, bug screen was installed to terminate the rain screen cavity above and below the window, and aluminum sill flashing was installed. The windows were finished with jamb extensions on the exterior and interior and a picture frame casing on the inside.

2.3.8. Penetrations

The prefabricated panels had penetration holes for electrical and internet cables predrilled, and conduit was placed through and sealed. The larger penetrations for ERV and heat pump line set were left as uninsulated boxes so that conduit could be placed through after panel installation and sealed (Figure 14). Ideally, penetrations are located ahead of time so that they can be precisely located in the shop drawings and fabricated to the exact dimensions. The locations of new penetrations need to be determined within the existing building, and this may not be simple to locate once the panels are installed. One method of locating new penetrations would be to drill pilot holes through the structure from the interior or indicate positions using targets that will appear in LiDAR scans or photo surveys. This will make determining the locations more accurate as measurements for panels are taken from the outside of the structure, but existing framing and equipment placement are usually only located from the interior.

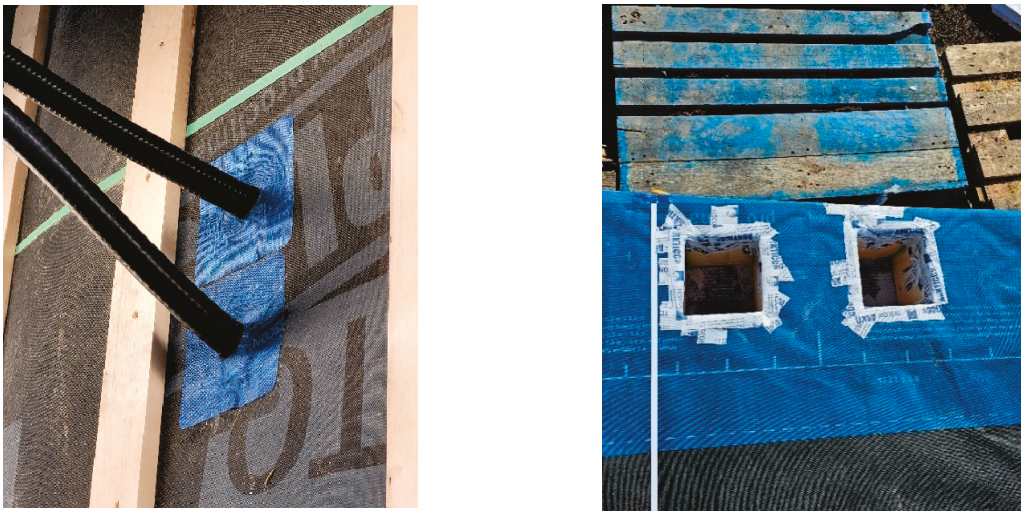


Figure 14. Penetration details.

2.3.9. Interior and Exterior Finishing

On the building interior, the windows and door were trimmed. On the exterior, the horizontal and vertical cladding, soffit, and facia were installed. One comment that arose was a need for a better nailing surface for the facia boards, which could have been fixed by either installing 2x rims or by using a facia material that was able to span the full depth of the panel in one piece (Figure 15). A new metal roof was installed, with a watertight and vapour-impermeable membrane to project the roof. The majority of the onsite time for the project was for the finishing process as the site preparation and panel installation took about a week and the finishing took roughly 3–4 weeks.



Figure 15. Finished building.

2.3.10. Mechanical Installation

An ERV was installed and ducted to provide ventilation air to all three rooms as the new building would be too airtight to rely on natural ventilation. For heating and cooling, a low-GWP heat pump was installed, and transfer grills were installed in the interior doors to provide better air flow (Figure 16).



(**a**) (**b**)

Figure 16. Mechanical systems: (**a**) heat pump and (**b**) ERV.

2.4. Modelling and Monitoring Methods

2.4.1. Thermal Performance Methodology

A blower door test was performed before retrofitting to establish a baseline, and a second blower door test was performed after the retrofitting process to measure the improvement in air tightness. The thermal performance and air tightness of the pre- and post-retrofit structure were modelled using HOT2000. This model was used to determine the air change rate, normalized leakage area, thermal resistance, design heat loss, and thermal energy demand intensity. The clear field thermal resistance, as well as Ψ-values of the linear thermal bridges and X-values of the point thermal bridges were calculated using Flixo Energy 8.2 modelling software. Thermal imaging was also conducted to qualitatively identify any thermal bridges or defects within the post-retrofit assembly.

2.4.2. Embodied Carbon Methodology

For this study, Environmental Product Declarations (EPDs) were used to calculate upfront greenhouse gas emissions associated with manufacturing materials (often simply "embodied carbon"). EPDs often report emissions in a variety of functional units (i.e., kg of CO_2e per mass of the materials, volume of the material, assembly area, RSI/m^2, R10/100 m^2, etc.). In the case of this report, the total kg CO_2e emissions were estimated, and the average amount per m^2 of wall panel area is provided.

The embodied carbon of the panel designs was estimated using the Material Carbon Emissions Estimator (MCE2) tool. The MCE2 is a free tool developed by Natural Resources Canada and Builders for Climate Action [25]. This tool works similarly to a National Database in that it provides cradle-to-gate information on various building materials. This means the embodied carbon calculations include extraction/harvesting, manufacturing, and all of the transportation involved right up until the material is delivered to site. The source of the data is derived from EPDs, and the data is local to Canada. Users can input the materials they are looking to incorporate in their building to estimate the total embodied carbon. This tool is helpful for comparing the estimated embodied carbon emissions for various options.

2.4.3. Cost Analysis

Exact costing for pilot projects has some difficulties due to the smaller scale and the novel nature of the projects. Estimates for the labour and material costs were collected from the fabricators for the offsite work, and data on the onsite labour and materials were collected. As this is one of several prefabricated pilot projects, the cost/m^2 of the past pilots was compared to the current pilot, as well as contractor estimates for conducting similar deep retrofits onsite and estimates for fully new construction.

2.4.4. Monitoring Plan

As the building was retrofitted with two different sets of panels, there were two sets of sensors placed within the new retrofitted panels (one in a cellulose panel and one in a straw panel). These sensors were capable of measuring temperature, wood moisture, and relative humidity. Each panel had three sensors, placed on the panel interior, panel exterior, and centre of the I-joist (Figure 17). There were also sensors placed inside the existing wall, in line with the new panels, and on the interior of the rooms. This allows for a better understanding of heat flow and drying through the assembly. The moisture sensors in particular are needed to ensure that the new panel design does not create any issues with drying to the exterior, and that no part of the assembly is at a point where mold growth is likely to occur.

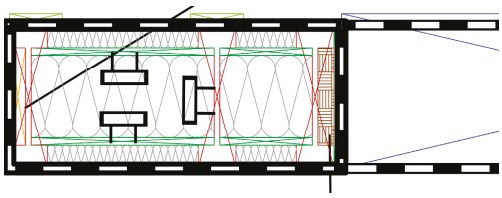


Figure 17. Sensor locations within retrofitted panels (plan view).

Sensors for energy monitoring were also installed so that the amount of heating and cooling energy could be compared for each change to the windows (either when window sashes were swapped to a different solar heat gain coefficient or if shading was included in

the future). This would allow for a comparison regarding the impact of these windows on the energy use for both the heating and cooling seasons.

One aspect of climate resilience is a building's ability to remain safe and comfortable during power outages or equipment failure. To determine this building's resilience, the heating and cooling were shut off during long unoccupied periods during the hottest and coldest periods of the year to determine the indoor floating temperature. The temperature was compared to the safe conditions' thresholds and exterior temperature to see how long the interior space would remain safe to occupants. For the cooling season, the maximum safe temperature is defined as 26 °C [26]. For the heating season, the safe temperature for comfort is 18 °C, and for long-term safety it is 16 °C [27].

3. Results

3.1. Panel Design

The sheathing-less I-joist panel design was a viable way of producing a thick insulated panel. The panels arrived without significant racking, and the lack of sheathing had no major impact on the installation process. In relation to cost and time, however, both fabricators mentioned that I-joists were more expensive, and they were not as straight and simple to work with as had been anticipated. For this reason, the fabricators suggested modifying the design to a double-stud wall design, which they could fabricate easily and more cost-effectively while still maintaining a thick cavity for blown in insulation.

One question about the panel design that arose involved the necessity of the two air barriers. Having the panels fully wrapped with the membrane made shipping and storing the panels outside uncovered possible as they were fully protected. As moisture ingress into biogenic materials is a major concern, this is a great benefit. The two air barriers also helped to increase the air tightness of the building. Some of the issues of having the panels fully wrapped were the added material cost, labour, and embodied carbon. The membrane has a cost and embodied carbon associated with it, and fully wrapping the panels takes additional time as the panels need to be flipped to allow for proper fastening.

In addition to the membrane itself, this method requires a gasket material at the back of the panel joints to keep the back air barrier continuous. If only one air barrier was needed, this gasket could potentially be avoided, saving material cost, labour, and embodied carbon. However, with the front membrane as the only air barrier, it would have a higher likelihood of damage while installing the panels and cladding and would likely lead to a less airtight building.

3.2. Panel Construction

An outline of the fabrication steps for a cellulose panel can be found in Table 1. It provides a list of the steps in the process, the estimated amount of time to complete each step, and a picture. These estimates are rough and based on a 7′11″ (2.4 m) wide and 9′6″ (2.9 m) tall panel, but they provide a good baseline to compare time for offsite construction to onsite construction. The overall time for panel construction was roughly 16 people-hrs, or 2.29 people-hrs/m^2.

The panel manufacturers both commented that, while a sheathing-less panel was possible to construct, and the sheathing-less panels were able to be transported without significant racking, the panels took more time and labour to construct, which outweighed any cost savings from not using sheathing. The lack of sheathing required more care to be taken to keep the panels square, and it also limited where the membrane could be attached to the panels. There were also issues with controlling the bulging of insulation once dense-packed, which would have been simpler to accomplish with sheathing (such as

in a structurally insulated panel). For the straw panels in particular, there were problems with insulating as the manufacturer did not typically use an insulation retention mesh, and, without the rigidity of sheathing, the staples holding the membrane blew out.

Table 1. Construction steps and labour time.

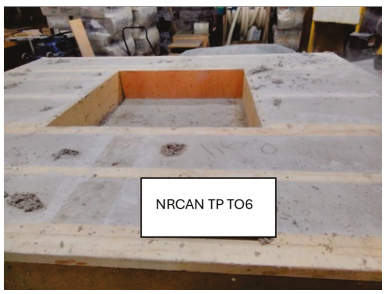
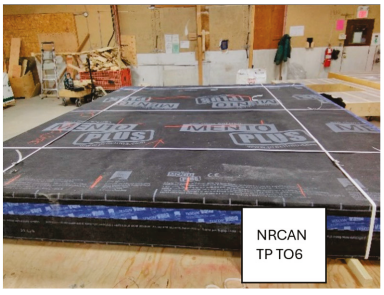
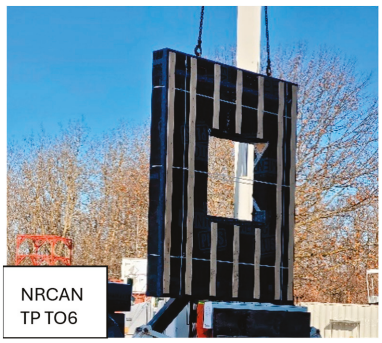
Step	Time (People-Hours)	Picture
Processing/ripping plates and RSO plywood and cutting members to length	0.75 hr × 2ppl =1.5 ppl-hrs	
Assembling frames and installing blocking	5 hrs × 2 ppl =10 ppl-hrs	
Installing insulating mesh on both panel faces	0.75 hrs × 1 ppl =0.75 ppl-hrs	
Blowing in insulation to required density	0.75 hr × 1 ppl =0.75 ppl-hr	
Installing AB/WRB to fully wrap the panel	1.5 hrs × 1 ppl =1.5 ppl-hrs	

Table 1. *Cont.*

Step	Time (People-Hours)	Picture
Installing strapping on the panel's exterior side	0.5 hr × 1 ppl =0.5 ppl-hr	
Installing industrial package strapping/final Q/A	1 hr × 1 ppl =1 ppl-hr	
TOTAL	16 people-hours	

Possible alternative designs to retain insulation while still promoting outward drying include let-in bracing, perforated sheathing (i.e., pegboard), or wood fibre board sheathing (which has a higher vapour permeance than OSB or plywood).

3.3. Installation

3.3.1. Box Beam

The box beams were a success, and they simplified panel installation. The contractors installing the panels found it much easier to install and prepare the box beams first, and then the panel installation/alignment process was more streamlined. As the crane time is costly, work that can be completed to make the installation with the crane faster helps to reduce the cost. As the box beam design relies on the thickness of the panel and is cut to size onsite, fabricators can begin making box beams while the panel designs are being finalized. This can reduce some of the lead time with projects.

3.3.2. Squishy Layer

The squishy layer installed between the panels and the original structure and within the panel joints worked, but there were some lessons learned to improve the process in future projects.

The hemp batt material was stiffer than expected and took more work to compress. This slowed down the installation process in some cases when panels needed to be adjusted. A lower-density material (25 kg/m^3 or less) or a thicker hemp layer compressed less would improve panel installation; however, a lower-density material may not hold its shape and may tear when fastened.

The squishy layer was installed on the original structure before the panels were installed, which took some time. The squishy layer could have been pre-installed on the panels; however, as there was no sheathing, it would have been more difficult to attach it to the panels. If this pre-installation were completed by the fabricators, there is also a chance that the squishy layer may become damaged during shipping. For these reasons, installing this layer on the original structure was the optimal choice. However, for taller buildings or buildings with cladding still intact, pre-installing this layer on the panels would likely be the better choice.

The hemp batts that were used are not meant to experience high volumes of water. As such, the installation of the hemp had to be completed close to when the panels were being installed. A hydrophobic material that can tolerate moisture would be beneficial in case it needed to be left exposed overnight or for an extended period of time. A hydrophobic material would likely also be needed if the squishy layer was to be pre-installed on the panels as there is a higher likelihood of it getting wet during shipping or storage onsite.

3.3.3. Panel Installation and Joints

The gasket material used to air-seal the back of the panel joint was quite expensive, had a high embodied carbon content, and it took additional time to apply it to the joint. The self-adhered gasket material also had issues adhering at lower temperatures and when it was applied to the full vertical length of the panel (the weight of the gasket caused it to peel off the panel in some instances). Alternatives that were considered were to provide an intentionally large gap between panels, which would allow for manual taping at the back of the panel. The larger gap could then be filled with a thicker compressible batt material (such as the hemp).

3.3.4. Roof Panels

The registration blocks made panel alignment much faster, and panel adjustment was also much simpler. Once the first panel was set in place, all the subsequent panels could be placed rather quickly. As the roof panel joints were all butted together (no gasket or insulation needed to be installed between panels), a roof panel was installed in about 10 min, roughly half the time of a wall panel. This could be accomplished because the roof had no penetrations that needed to be worked around, and the final overhand depth was flexible.

3.3.5. Windows

Two different air-sealing methods were trialed, and each had its own pros and cons relating to cost, installation, and thermal performance. The gasket material was about four times as expensive as the tape. The windows chosen had a low-profile design, which made taping difficult and required some trial and error to navigate corners. The tape also provided limited dimensional tolerance during the window installation. For the gasket option, the installation was fast and simple. The gasket provided some tolerance to adjust the position of the window in the RSO ($+/-\ 3/16''$ (5 mm)). With the gasket method, it would be possible to pre-install windows in the shop with the gasket and adjust them slightly once they arrive onsite. This would provide the field crew with a bit more flexibility to adjust window position. Through thermal imaging (Figure 18), it was found that the tape and spray foam performed better thermally than the gasket. The reduction in thermal performance could potentially be mitigated by using a wider gasket.

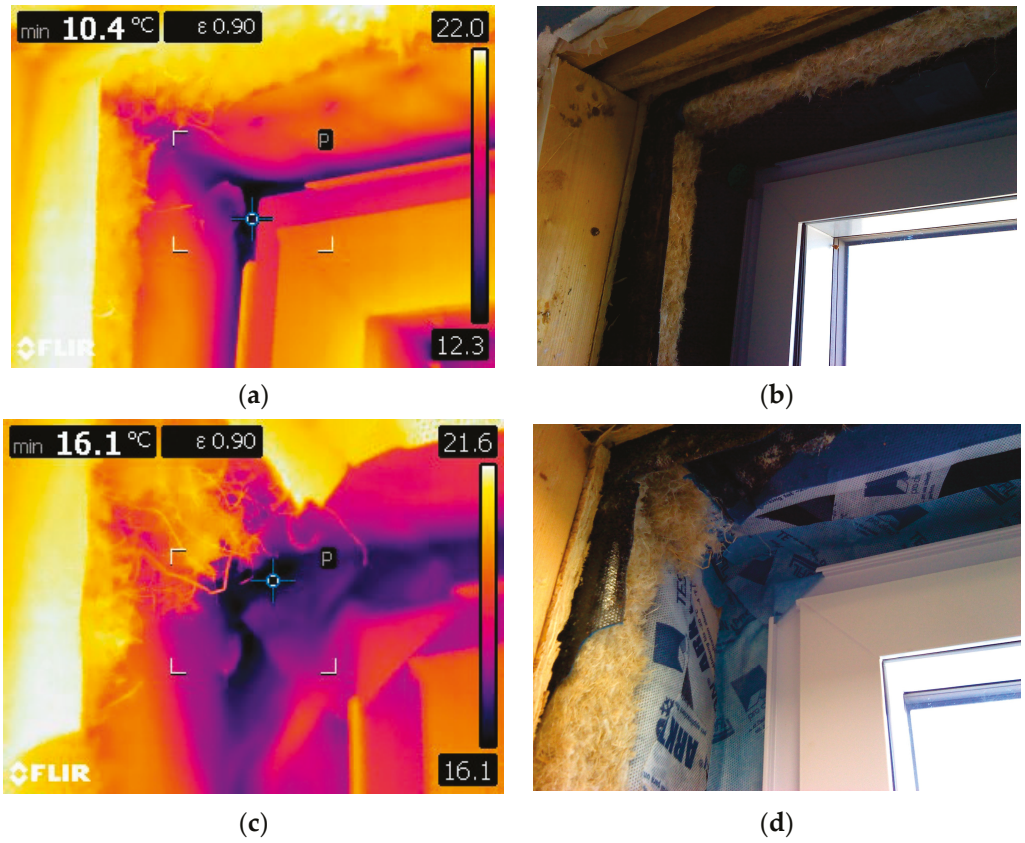


Figure 18. Thermal imaging of the gasket method (**a**,**b**) as well as the taped method (**c**,**d**).

3.4. Thermal Performance

The retrofitting thermal results are summarized in Table 2. One focus of the retrofitting process was to improve the air tightness. Each of the panels was airtight, and every joint was taped and sealed. The number of penetrations was minimized to reduce air leakage. The pre- and post-retrofit building was modelled using HOT2000 V11.12 modelling software. The post-retrofit had a measured air change rate of 0.26 ACH@50Pa and a normalized air leakage area (NLA) of 0.074 cm^2/m^2. Typical air tightness for buildings ranges around 11–3 ACH@50Pa for buildings built pre-1946 to 2011, respectively [28]. While the national building code of Canada does not mandate air tightness, for new construction in Canada, under 3 ACH@50Pa is considered good, with high-performance homes like Passive House aiming below 0.6 ACH@50Pa [21,29].

Table 2. Building modelling thermal results.

Performance Metric		Baseline	Retrofit	% Improvement
Air Change Rate (ACH@50Pa)		7.20	0.26	96
Normalized Leakage Area @10Pa (cm^2/m^2)		1.03	0.07	93
Thermal Resistance (R-Value [RSI])	Walls	13 [2.3]	40 [7.0]	308
	Roof	20 [3.5]	60 [10.6]	300
Design Heat Loss (−25 °C) W		3380	1610	52
Thermal Energy Demand Intensity (kWh/m^2a)		260	8.0	97

Another project goal was to increase the thermal resistance of the walls and roof. New construction in Canada typically aims for above R20 walls and R30 roofs. For this project, the goal was R40 (RSI 7.0) for the walls and R60 (RSI 10.6) for the roof, and this goal was achieved (the chopped straw walls reached R40, and the cellulose wall panels performed slightly above R40). The overall thermal energy demand intensity (TEDI) was decreased by 97%, to approximately 8.0 kWh/m^2a, which is within the typical net-zero or PHIUS performance range for most Canadian climate zones.

To determine the thermal performance of individual assembly pieces, thermal models were created using Flixo Energy 8.2. This included calculating the performance of the two different panel types, as well as accounting for the various linear and point thermal bridges (Ψ-values and X-values). The linear thermal bridges included the window-to-wall interface, the vertical panel joints, and the box beams. The point thermal bridges included the long screws, as well as the brackets that were used to support the box beams. The results can be found in Table 3. The vertical panel joint was found to be below 0.01 W/m·K; therefore, it can be considered thermal bridge-free. The box beam and windows were found to contribute some thermal bridging, accounting for roughly 2.7% and 5% decreases in overall thermal resistance, respectively. The foundation brackets were found to have a small amount of thermal bridging, and the long screws were found to have a negligible amount of thermal bridging. As they had low X-values and limited quantities used, their impact on the overall thermal performance was limited. If more brackets or screws were required to fasten panels into place, their impact could become more significant.

Table 3. Thermal performance of enclosure by assembly.

Clear Field	**Thermal Resistance**		**Surface Area**		**% Area**	**% Heat Flow**
Assembly	**(m^2·K/W)**	**(hr·ft^2·°F/BTU)**	**(m^2)**	**(ft^2)**		
Floor	5.4	30.9	50.4	542	22.7%	29.8%
Cellulose Insulated Roof	12.5	71.2	50.4	542	22.7%	12.9%
Cellulose Insulated Walls	8.2	46.5	55.7	600	23.7%	22.8%
Straw Insulated Walls	8.0	45.4	55.7	600	23.7%	23.4%
Linear Thermal Bridges	Ψ-value		Total Length		% Area	% Heat flow
	(W/m·K)	(BTU/hr·ft·°F)	(m)	(ft)		
Window-to-wall interface	0.038	0.0220	6.5625	21	2.8%	2.7%
Vertical panel Joint	0.004	0.0023	39.4	126	1.0%	1.0%
Box Beam	0.018	0.0104	42.5	136	4.5%	4.4%
Point Thermal Bridges	X-value		Quantity		% Area	% Heat flow
	(W/K)	(BTU/hr·°F)				
Foundation Bracket	0.0063	0.011648448	8		-	2.7%
Long Screws	0.00022	0.000406771	28		-	0.3%

To gather qualitative information on thermal bridging and to obtain a visual representation of heat flow through the building, a thermal imaging camera was used (Figure 19). The interior of the building was set to 21 °C, and the exterior temperature was −4 °C. The thermal imaging clearly showed some thermal bridging along the framing (as is to be expected). The panel joints and the box beam did not demonstrate any thermal bridging. The window-to-wall interface had some thermal bridging, although the difference in emissivity of the glass does account for part of the temperature difference in the images.

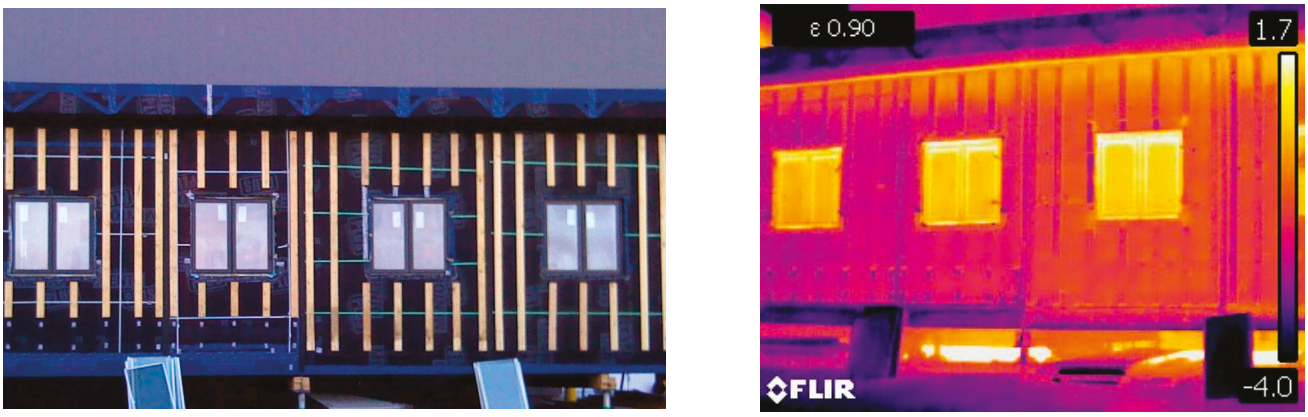


Figure 19. Thermal imaging of the building after panel installation.

3.5. Embodied Carbon

A total of 1480 $kgCO_2e$ net carbon storage was achieved during retrofitting from the addition of the new envelope panels and box beams. The contributions of each element can be found in Figure 20. When comparing different panel designs, it can be helpful to take an average value/m^2 of panel area to make the comparison simpler. In this case, the cellulose wall panels stored 12 $kgCO_2e/m^2$, the cellulose roof panels stored 17 $kgCO_2e/m^2$, and the straw wall panels stored 34 $kgCO_2e/m^2$ (Figure 21).

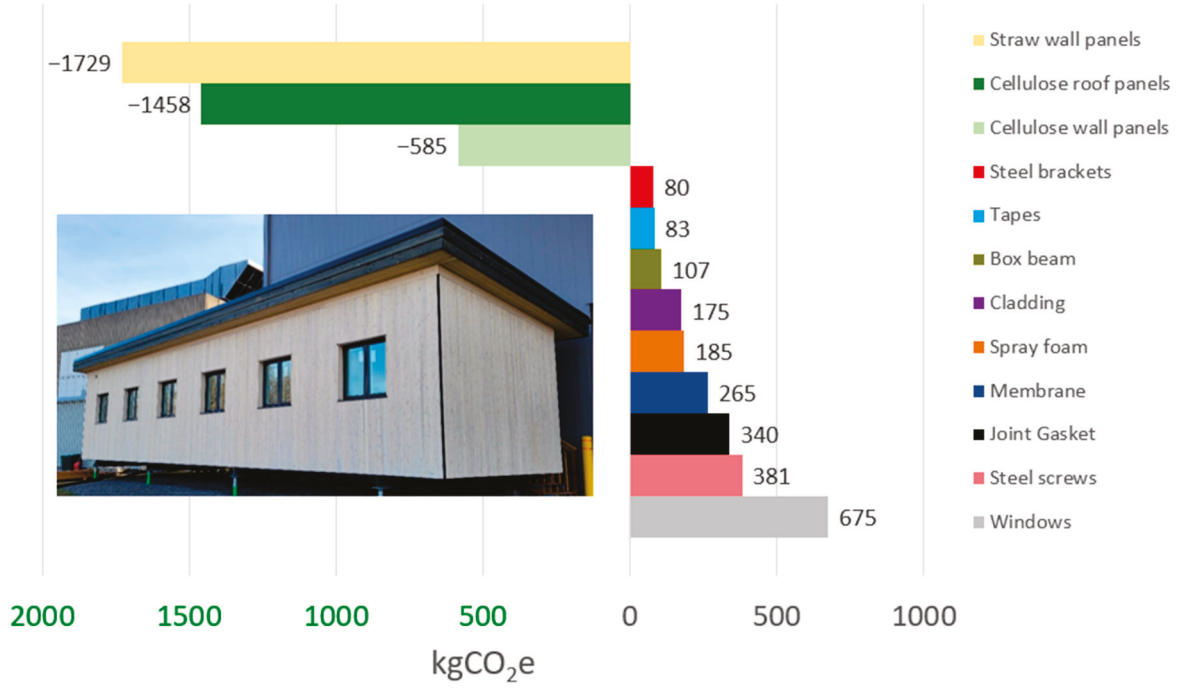


Figure 20. Whole-building enclosure retrofit embodied carbon ($kgCO_2e$).

It is worth noting that the building components with the highest impact on the embodied carbon are not necessarily those with the largest volume/area. The windows have a large impact on the embodied carbon, especially when combined with the spray foam needed to seal/insulate around the windows. The joint gasket material and membranes are also a large source of embodied carbon, which is another reason to eliminate the secondary air barrier. If only a single air barrier is needed, it would remove all the embodied carbon from the joint gaskets and halve the embodied carbon from the membranes. The steel

screws also accounted for a large portion of the embodied carbon. This could be reduced slightly by not using stainless steel screws, or it could potentially be reduced more significantly by designing a method of attaching the panels that could be conducted with shorter screws.

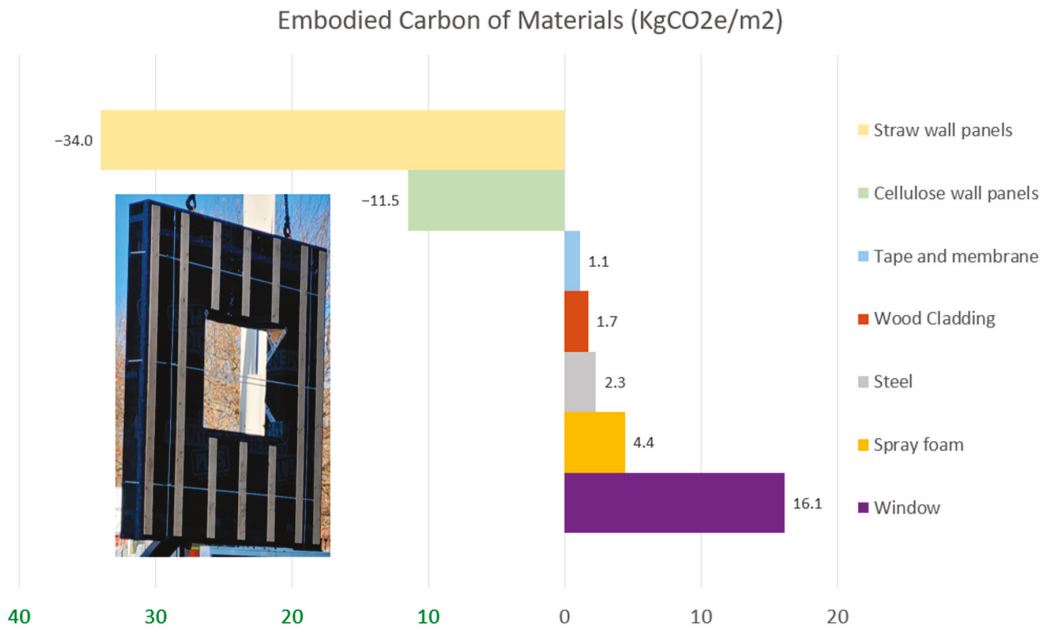


Figure 21. Embodied carbon of materials per m^2 of panel area (for a typical 7 m^2 (75 ft^2) panel).

3.6. Costing

When looking into the costing of such a pilot, it is important to see how the costs break down in terms of the offsite labour cost, the onsite labour cost, and the material cost. The costs of each item can be found in Figure 22. The siding accounted for a large portion of the onsite labour, so, if there is a way to install siding offsite, it could have significant time and labour savings. However, with the current design, installing siding offsite would likely increase the total labour costs as the joints would need special care. In terms of materials, the straw insulation is less expensive than the cellulose, so the straw panels have a lower panel cost.

Figure 23 compares past PEER panel designs (adjusted for inflation) with this project's panel design. These values calculated include all the materials and labour that went into constructing and installing the retrofitted panels (with some omissions noted). The figure also includes estimates for the costs of conducting a similar retrofit with existing onsite methods, or the cost of a new build. It is important to note that these estimates do not account for costs associated with design, which would likely be higher for the prefabricated approaches.

For the past projects, the prices were adjusted for inflation using the building construction price index [30]. For the site-built retrofit, the material costs would be similar to the prefabricated approaches, although increased waste onsite would somewhat increase the cost. The larger cost difference is related to setting up and tearing down equipment, as well as the increased labour cost of onsite work as it is less efficient compared to work completed in a factory and may be impacted by the weather. For new construction, the costs are higher still as there are even more materials that need to be purchased, and structural aspects need to be considered. New construction also requires finishing the interior, which adds a

significant cost. As more retrofitting projects are completed, the estimates of overall costs will become more exact.

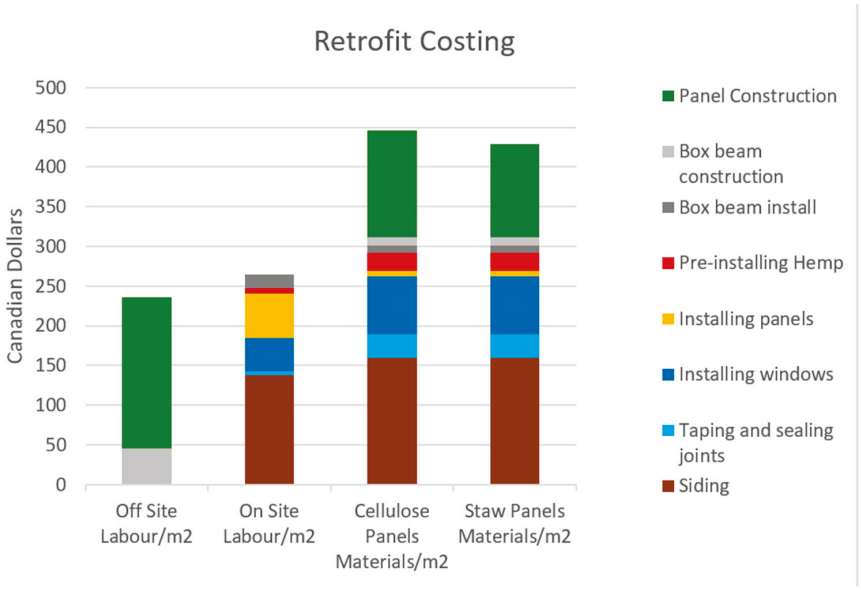


Figure 22. Labour and material costs (CAD/m^2 panel area).

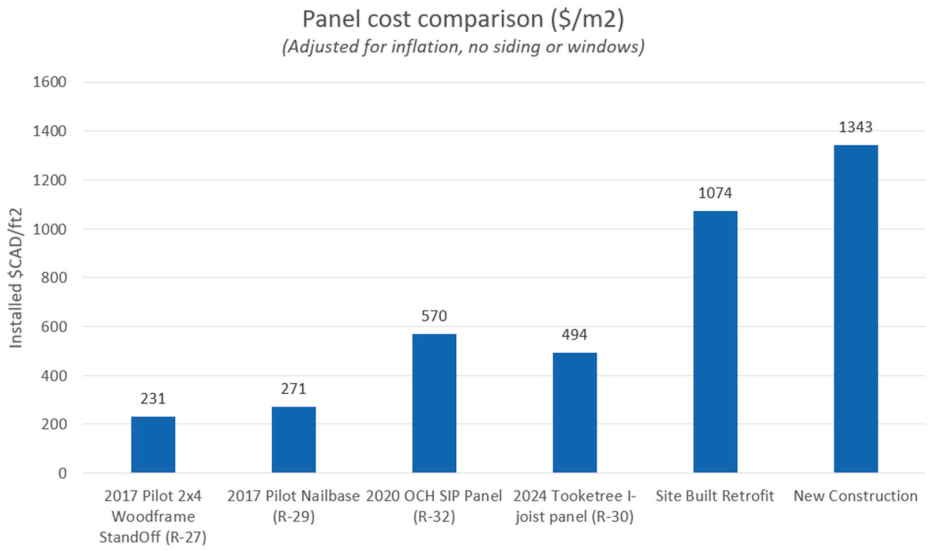


Figure 23. Cost comparison of past deep retrofit approaches compared to estimates for a similar site-built retrofit and new construction.

4. Conclusions

- The sheathing-less I-joist panel design was found to be viable for lowrise residential buildings. The panels arrived without significant racking, and the lack of sheathing had no major impact on the installation process. As the I-joists were expensive, the fabricators suggested using a double-stud wall design, which they could fabricate easily and more cost-effectively.
- Both fabricators mentioned that sheathing-less panels took more time to prepare, and that including sheathing should save time and money (even when accounting for the additional materials).

- The box beams were a success and simplified the panel installation. The contractors installing the panels found it much easier to install and prepare the box beams first, and then the panel installation and alignment process was more streamlined.
- A lower-density squishy layer is required to make panel installation easier. This could be accomplished by using a lower-density material or using a thicker hemp batt and planning for it to compress less.
- Flat roof panels with registration blocks can be installed quite quickly. The first panel takes the most time to install correctly, but once installed, the other panels can be quickly placed, adjusted, and installed.
- The thermal air tightness and thermal performance of the building were significantly improved post-retrofit. Thermal bridging was modelled, and Ψ-values of the linear thermal bridges and X-values of the point thermal bridges were calculated.
- A total of 1480 kgCO_2e net carbon storage was achieved during retrofitting from the addition of the new envelope panels and box beams.
- The cost of labour and materials for the retrofitting process was outlined and compared to other retrofitting projects, onsite construction, and new construction.
- The prefabricated wall panels have been instrumented, as well as the interior of the building itself. The thermal and hygrothermal performance of the wall panels will be monitored. The interior conditions of the building will be monitored to study occupant comfort and climate resilience. At certain points during the winter and summer, the power will be shut off to determine the building's ability to maintain safe living conditions during an extended power outage.

Author Contributions: Writing—original draft, H.P.; writing—review and editing, supervision, and project administration, M.C.; conceptualization, J.A. All authors have read and agreed to the published version of the manuscript.

Funding: This research received no external funding.

Data Availability Statement: The original contributions presented in this study are included in the article. Further inquiries can be directed to the corresponding author(s).

Conflicts of Interest: The authors declare no conflicts of interest.

References

1. Actions for a Zero Carbon Built Environment. Architecture 2030. 2023. Available online: https://architecture2030.org/why-the-building-sector/ (accessed on 7 July 2023).
2. Wang, Y.; Ma, M.; Zhou, N.; Ma, Z. Paving the way to carbon neutrality: Evaluating the decarbonization of residential building electrification worldwide. *Sustain. Cities Soc.* **2025**, *130*, 106549. [CrossRef]
3. Government of Canada. *Canada's 2030 Emissions Reduction Plan*; Environment and Climate Change Canada: Gatineau, QC, Canada, 2022.
4. Natural Resources Canada. National Energy Use Database (NEUD) Comprehensive Energy Use Database. 2019. Available online: https://oee.nrcan.gc.ca/corporate/statistics/neud/dpa/data_e/databases.cfm?attr=0 (accessed on 2 January 2024).
5. HOME. Government of Canada. 2024. Available online: https://data-donnees.az.ec.gc.ca/data/substances/monitor/canada-s-greenhouse-gas-emissions-projections/Current-Projections-Actuelles/GHG-GES/detailed_GHG_emissions_GES_detaillees.csv (accessed on 7 July 2024).
6. The Canada Green Buildings Strategy: Transforming Canada's Buildings Sector for a Net-Zero and Resilient Future. Government of Canada, 8 July 2024. Available online: https://natural-resources.canada.ca/transparency/reporting-and-accountability/plans-and-performance-reports/departmental-strategies/the-canada-green-buildings-strategy-transforming-canadas-buildings-sector-for-net-zer/26065 (accessed on 20 July 2024).

7. Residential Sector Canada Table 2: Secondary Energy Use and GHG Emissions by End-Use. Natural Resources Canada. 2024. Available online: https://oee.nrcan.gc.ca/corporate/statistics/neud/dpa/showTable.cfm?type=CP&sector=res&juris=ca&year=2021&rn=2&page=0 (accessed on 22 July 2024).
8. BERTIM Consortium. BERTIM—Innovative wood prefabrication for energy efficient renovations: Project results booklet. European Union Horizon 2020 Research and Innovation Programme. 2019.
9. CanmetENERGY. *Prefabricated Exterior Energy Retrofit (PEER) Project Guide*; Natural Resources Canada: Ottawa, ON, Canada, 2023.
10. TAF the Atmospheric Fund. *The Case for Deep Retrofits*; The Atmospheric Fund: Toronto, ON, Canada, 2020.
11. Government of Canada Promotes in-Demand Skilled Trades as a First-Choice Career Path. Government of Canada, 3 January 2022. Available online: https://www.canada.ca/en/employment-social-development/news/2022/01/skills-trade.html (accessed on 2 August 2023).
12. Affordable and Adaptable Public Buildings Through Energy Efficient Retrofitting. CORDIS EU Research Results. 2018. Available online: https://cordis.europa.eu/project/id/609060/reporting (accessed on 1 January 2023).
13. New Easy to Install and Manufacture PRE-Fabricated Modules Supported by a BIM based Integrated Design ProceSS. CORDIS EU Research Results. 2020. Available online: https://cordis.europa.eu/article/id/413460-old-meets-new-sustainable-retrofit-of-buildings-through-prefabricated-panels (accessed on 1 January 2023).
14. BuildForce Canada. *Construction and Maintenance Looking Forward*; BuildForce Canada: Ottawa, ON, Canada, 2022.
15. Industrialised Energy Efficient Retrofitting of Resident Buildings in Cold Climates. CORDIS EU Research Results. 2022. Available online: https://cordis.europa.eu/project/id/260058 (accessed on 1 January 2023).
16. Make Net Zero Energy Refurbishments for Houses a Mass Market Reality. CORDIS EU Research Results. 2021. Available online: https://cordis.europa.eu/project/id/696186/reporting (accessed on 1 January 2023).
17. Multifunctional Energy Efficient Façade System for Building Retrofitting. CORDIS EU Research Results. 2017. Available online: https://cordis.europa.eu/project/id/285411/reporting (accessed on 1 January 2023).
18. Energiesprong. What Is Energiesprong. Energiesprong. 2025. Available online: https://www.energiesprong.org/what-is-energiesprong (accessed on 18 September 2025).
19. Building Energy Renovation Through Timber Prefabricated Modules. CORDIS EU Research Results. 2022. Available online: https://cordis.europa.eu/project/id/636984 (accessed on 1 January 2023).
20. Holistic Energy-Efficient Retrofitting of Residential Buildings. CORDIS EU Research Results. 2015. Available online: https://cordis.europa.eu/article/id/159896-energyefficient-technology-demonstrated-in-13-old-buildings (accessed on 1 January 2023).
21. National Research Council Canada. *National Building Code of Canada: 2020*; National Research Council of Canada: Ottawa, ON, Canada, 2022.
22. Guide to Oversize/Overweight Vehicles and Loads. Ontario. 2022. Available online: https://www.ontario.ca/page/guide-oversizeoverweight-vehicles-and-loads#:~:text=width%20of%203.70%20m%20on,height%20maximum%20of%204.26%20m (accessed on 6 June 2024).
23. Mott, H. The good, the bad, and the hygge: Designing for prefab from a manufacturer's perspective. In *Passive House Canada Prefab Symposium*; Passive House Canada: Victoria, BC, Canada, 2022.
24. Proclima. System Products. Proclima. Available online: https://proclima.com/products (accessed on 12 December 2024).
25. Material Carbon Emissions Estimator (MCE2). Government of Canada, 11 July 2022. Available online: https://natural-resources.canada.ca/maps-tools-and-publications/tools/modelling-tools/material-carbon-emissions-estimator/24452 (accessed on 8 July 2023).
26. BC Building Codes and Standards Branch. BC Codes 2024. 2024. Available online: https://www2.gov.bc.ca/gov/content/industry/construction-industry/building-codes-standards/bc-codes/2024-bc-codes (accessed on 5 September 2025).
27. Jevons, R.; Carmichael, C.; Crossley, A.; Bone, A. Minimum indoor temperature threshold recommendations for English homes in winter—A systematic review. *Public Health* **2016**, *136*, 4–12. [CrossRef] [PubMed]
28. Purdy, J.; Parekh, A. Building Envelope Thermal and Air Leakage Characteristics of Canadian Housing. In *CCBST 2017*; Vancouver, BC Building Envelope Council: Delta, BC, Canada, 2017.
29. Passive House Requirements. Passive House. 2025. Available online: https://passiv.de/en/02_informations/02_passive-house-requirements/02_passive-house-requirements.htm (accessed on 20 September 2025).
30. Statistics Canada. Building Construction Price Index. Statistics Canada. 2025. Available online: https://www150.statcan.gc.ca/n1/en/surveys/2317 (accessed on 7 January 2025).

Disclaimer/Publisher's Note: The statements, opinions and data contained in all publications are solely those of the individual author(s) and contributor(s) and not of MDPI and/or the editor(s). MDPI and/or the editor(s) disclaim responsibility for any injury to people or property resulting from any ideas, methods, instructions or products referred to in the content.

buildings

MDPI

Article

Developing a BIM-Integrated Framework for Embodied Carbon Assessment in Developing Countries: A Systematic Review and Expert Validation Study for Sri Lanka

Ahmed Hagras *, Talpe Pandithawattage Anuradha Lasantha Piyasena, Amalka Nawarathna, Marianthi Leon, Ana Karina Silverio and Abhinesh Prabhakaran

School of Architecture and Environment, College of Arts, Technology and Environment, University of the West of England (UWE), Bristol BS16 1QY, UK; anuradha.piyasena@gauntfrancis.co.uk (T.P.A.L.P.); amalka.nawarathna@uwe.ac.uk (A.N.); marianthi.leon@uwe.ac.uk (M.L.); karina.silverio@uwe.ac.uk (A.K.S.); abhi.prabhakaran@uwe.ac.uk (A.P.)

* Correspondence: ahmed.hagras@uwe.ac.uk

Abstract

Construction is responsible for 40% of global carbon emissions, yet embodied carbon (EC) assessment is rarely integrated into standard building design workflows in developing countries. This research presents and validates a BIM-integrated EC assessment framework specifically adapted to Sri Lanka, utilising the government's Building Standard Rates (BSR) as the foundation for material quantity and cost data. The streamlined workflow combines Revit, Dynamo, and Excel to automate EC calculations across lifecycle stages A1–C4, informed by a systematic review of 75 peer-reviewed articles (2017–2025) and validation through structured interviews with five experienced domain professionals. Results demonstrate that BSR, when supplemented with material densities and transport data, enables automated EC calculations for typical building materials and construction elements. Expert validation confirmed strong technical feasibility, economic viability, and scalability. The framework offers significant advantages over manual approaches by automating EC quantification and reducing software licensing requirements compared to proprietary LCA tools. The framework's modular design and transparent methodology make it generalisable for other developing economies with similar government construction documentation systems, providing practitioners and policymakers with a practical, cost-effective pathway to embedding life cycle assessment into standard construction practice.

Keywords: building information modelling (BIM); life cycle assessment (LCA); embodied carbon; sustainable construction; developing countries; Sri Lanka; BIM-LCA integration

1. Introduction

1.1. The Global Construction Sector and Its Carbon Footprint

The construction industry is one of the most significant contributors to global carbon emissions, accounting for a substantial portion of worldwide greenhouse gas (GHG) emissions across the complete lifecycle of built assets. Recent evidence indicates that the built environment accounts for approximately 38–40% of global GHG emissions across the full life cycle, encompassing embodied carbon in materials, construction activities, operational energy use, and end-of-life processes [1,2]. This substantial contribution highlights the sector's crucial role in global decarbonisation efforts and underscores the urgent need for comprehensive carbon assessment methodologies.

Moreover, the construction sector places great importance on embodied carbon (EC), the greenhouse gas emissions generated throughout a building's life cycle, including manufacturing, construction, maintenance, and dismantling. Even new, energy-efficient buildings can account for up to 50% of their carbon footprint, making it responsible for approximately 10% of global energy-related CO_2 emissions [3]. Therefore, reducing EC is crucial for achieving sustainability and climate goals [4]. EC calculations are vital for developing countries like Sri Lanka for several reasons. The results of these calculations provide crucial insight into the environmental impact of construction projects [5]. Construction plays a pivotal role in Sri Lanka's dynamic landscape, marked by rapid economic growth [6]. Thus, to mitigate environmental harm, it is essential to understand the concept of EC. Further, Sri Lanka can effectively reduce emissions by quantifying EC, thereby promoting sustainable development. Additionally, there is an increasing emphasis on environmentally responsible projects, as mandated by international agreements and investors, as well as commercial buildings, hotels, and apartments [7].

1.2. The Sri Lankan Construction Sector: Economic Significance and Environmental Imperatives

In Sri Lanka, the construction industry is crucial to the economy and also contributes significantly to the country's greenhouse gas emissions. The sector has consistently contributed significantly to Gross Domestic Product (GDP), typically between 6% and 7% over the past decade [8].

From an environmental standpoint, the Sri Lankan construction sector has a significant impact on national emissions through embodied carbon in materials and construction processes. Studies employing lifecycle methodologies and input-output analytical techniques have quantified the sector's carbon footprint, designating construction as a major emitter within the national economy [9]. Case study research focusing on specific building components and lifecycle boundary definitions has demonstrated how design choices, material selections, and assessment methodologies influence embodied carbon estimates, emphasising the practical significance of carbon accounting for policy-relevant decarbonisation strategies [10,11].

As a result, by conducting EC calculations, Sri Lanka can align itself with global standards, rendering it more appealing for international collaborations, funding, and partnerships. Furthermore, understanding and accounting for EC can foster technological innovation and spur the development of local industries [12]. This approach can encourage the adoption of cleaner and more efficient technologies, creating opportunities for local businesses to prosper by offering sustainable solutions. EC holds excellent value for Sri Lanka's sustainability. There is also increasing interest among researchers in contributing to investigations on EC estimation across various entities, and many researchers are participating in these studies.

An example of this is the comprehensive evaluation conducted by Nawarathna et al. [12], which analysed twenty different case studies of office buildings. Similarly, Kumanayake, Luo, and Paulusz [13] and residential structures in Sri Lanka. Moreover, Kumari et al. [14] highlight the importance of EC evaluation in high-rise buildings in Sri Lanka. Collectively, these studies underscore the need for more precise calculations and shorter assessment times to enhance acceptance in Sri Lanka.

1.3. Building Information Modelling and Life Cycle Assessment Integration: Digital Tools for Carbon Management

This concept of Building Information Modelling (BIM) integrated EC assessment has gained momentum primarily in developed nations [15]. BIM technology is integrated with LCA methodologies to gauge buildings' carbon emissions [16]. This amalgamation offers enhanced accuracy and substantial time savings in the assessment process [17]. BIM-LCA

https://doi.org/10.3390/buildings16040814

integration involves the streamlined amalgamation of data, real-time calculations, and interactive visualisation of carbon emissions. According to Xu et al. [16], this integrated solution significantly automates the EC assessment process by transferring accurate material information to the LCA tool, thereby improving the efficiency of EC calculations. In Sri Lanka, the construction sector is increasingly recognising the benefits of BIM, such as enhanced project efficiency, decreased errors, and improved collaboration [18]. Moreover, the number of educational programs focused on BIM technology is increasing, and the number of adept professionals is also rising [19]. This burgeoning expertise indicates a progressing preparedness for a more holistic integration of BIM. Numerous projects in Sri Lanka have commenced utilising BIM, showcasing successful outcomes and inspiring further exploration of its potential [7]. The country is witnessing a shift in market demand, with clients and stakeholders recognising the value that BIM can bring to construction projects, thus fostering a favourable environment for its acceptance. Unfortunately, there is a notable scarcity of comprehensive, scholarly studies on EC assessment integrated with BIM in Sri Lanka [10]. This absence of extensive research is a matter of concern and urgency, demanding immediate attention. It is imperative to underscore the pressing need to develop and implement research initiatives that focus on integrating EC assessment within the Sri Lankan context using BIM.

1.4. The Sri Lankan Building Standard Rates: A Foundation for Localised Carbon Assessment

Within the Sri Lankan construction context, the Building Schedule of Rates (BSR), issued annually by the Building Department, represents an established institutional framework with significant potential for integration into embodied carbon assessment processes. The BSR serves as the longstanding standard work norm governing materials, equipment, and labour costs across construction projects, providing comprehensive specifications for diverse building elements through standardised item codes, descriptions, and measurement units [20]. Engineering professionals throughout Sri Lanka routinely consult the BSR for cost estimation, making it a familiar and accessible reference framework across the construction industry.

The structural characteristics of the BSR offer unique opportunities to integrate embodied carbon. Each BSR item comprises detailed material breakdowns that specify constituent materials and quantities, information generated during initial rate preparation processes. By systematically associating Embodied Carbon Factors (ECFs) with these material breakdowns, it becomes feasible to derive item-specific carbon intensities expressed in standardised units (e.g., $kgCO_2e$ per cubic meter or per linear meter). This approach would establish a comprehensive, Sri Lanka-specific material database aligned with existing industry practices, potentially facilitating embodied carbon calculations without requiring substantial modifications to established professional practices.

The BSR-based approach to embodied carbon assessment offers several strategic advantages within the Sri Lankan context. First, it leverages an existing institutional infrastructure familiar to construction professionals, which may potentially reduce barriers to adoption. Second, it aligns carbon assessment with established cost-estimation processes, enabling the integrated consideration of economic and environmental factors. Third, it provides a standardised framework for carbon quantification across projects, supporting consistency and comparability, which are essential for benchmarking and policy implementation. However, realising this potential requires systematic development of ECFs appropriate to Sri Lankan material production contexts, validation of database accuracy, and integration with digital modelling tools such as BIM platforms.

https://doi.org/10.3390/buildings16040814

1.5. Research Gaps and the Imperative for BIM-Integrated Embodied Carbon Assessment in Sri Lanka

Although embodied carbon assessment is essential and more people worldwide are utilising BIM-LCA integration methods, significant gaps remain in research and implementation within the Sri Lankan construction industry. A primary limitation recognised in Sri Lankan embodied carbon research is the lack of a national standard for carbon measurement, along with restricted access to localised, material-specific data. This deficiency hinders consistency in assessments and cross-project comparability. This data and governance gap is a significant bottleneck to efforts to measure and reduce embodied carbon at scale. It slows down both research and real-world use [13].

The lack of capacity, training, and institutional support makes it even more challenging to utilise LCA and embodied carbon methods effectively in Sri Lanka's construction industry. Research has identified skill deficiencies and organisational preparedness issues that hinder the extensive implementation of carbon assessment methodologies in construction design and decision-making processes [21,22]. These limitations are especially evident given the sector's growth trajectory and diversification, which simultaneously increased demand for comprehensive carbon accounting while exerting pressure on companies to innovate and compete amid resource constraints [23].

Furthermore, there is an evident lack of thorough academic research on BIM-integrated embodied carbon assessment in Sri Lanka [10]. International literature demonstrates the technical feasibility and considerable advantages of integrating BIM-LCA. Concurrently, Sri Lankan research has highlighted the sector's economic importance and has initiated efforts to quantify embodied carbon. However, the systematic integration of BIM methodologies with localised carbon assessment frameworks, especially by leveraging established institutional infrastructure such as the BSR, has yet to be thoroughly investigated.

This research gap is troubling because the sector has a significant impact on the economy and the environment. BIM-LCA has been shown to improve the accuracy and efficiency of assessments, and Sri Lanka has promised to be more environmentally friendly under international frameworks. Accordingly, this paper aims to bridge the existing research gap in EC calculation by utilising BIM in the specific context of Sri Lanka. By developing a comprehensive framework, it seeks to contribute to the field by serving as a foundation for future studies. The purpose of this paper is to pave the way for further research and exploration in this area by taking this critical step forward. Moreover, this research addresses this gap through the following objectives in the next section.

Given the absence of a national methodology, database, or digital workflow for embodied carbon assessment in Sri Lanka, the development of a foundational framework is an essential prerequisite to any empirical or project-level validation. Many developing countries follow this staged pathway, first establishing methodological clarity and industry-aligned structures before progressing into case studies or pilot implementations. This study deliberately focuses on conceptualising and validating a BIM-integrated EC assessment approach, which is suggested as an initial phase and will subsequently involve pilot applications and comparative analyses in future research studies. As observed in similar developing-country contexts, early stages of framework creation rely on small panels of domain experts to ensure methodological coherence, after which broader industry consultation follows. This study intentionally follows that sequence.

1.6. Research Objectives

Primary Objective: Develop a pragmatic BIM-integrated framework for EC assessment tailored to Sri Lankan construction industry characteristics, utilising indigenous data sources and accessible software tools.

https://doi.org/10.3390/buildings16040814

Specific Objectives:

1. Critically analyse existing BIM-LCA integration methodologies through a systematic literature review, identifying key parameters, tools, databases, and implementation approaches.
2. Evaluate Sri Lanka's BSR document as a potential indigenous data source for EC calculations.
3. Design a comprehensive framework integrating BSR data with BIM parametric modelling approaches using Revit ver. 2024.0 and Dynamo ver. 2.17.0.3472.
4. Validate framework feasibility and applicability through expert consultation with Sri Lankan construction industry professionals.
5. Identify implementation barriers and propose strategies to overcome challenges specific to developing-country contexts.

2. Materials and Methods

This study employed the systematic literature review (SLR) methodology in conjunction with an expert interview to validate the proposed framework [24]. A Complete overview of the research methodology is illustrated in Figure 1.

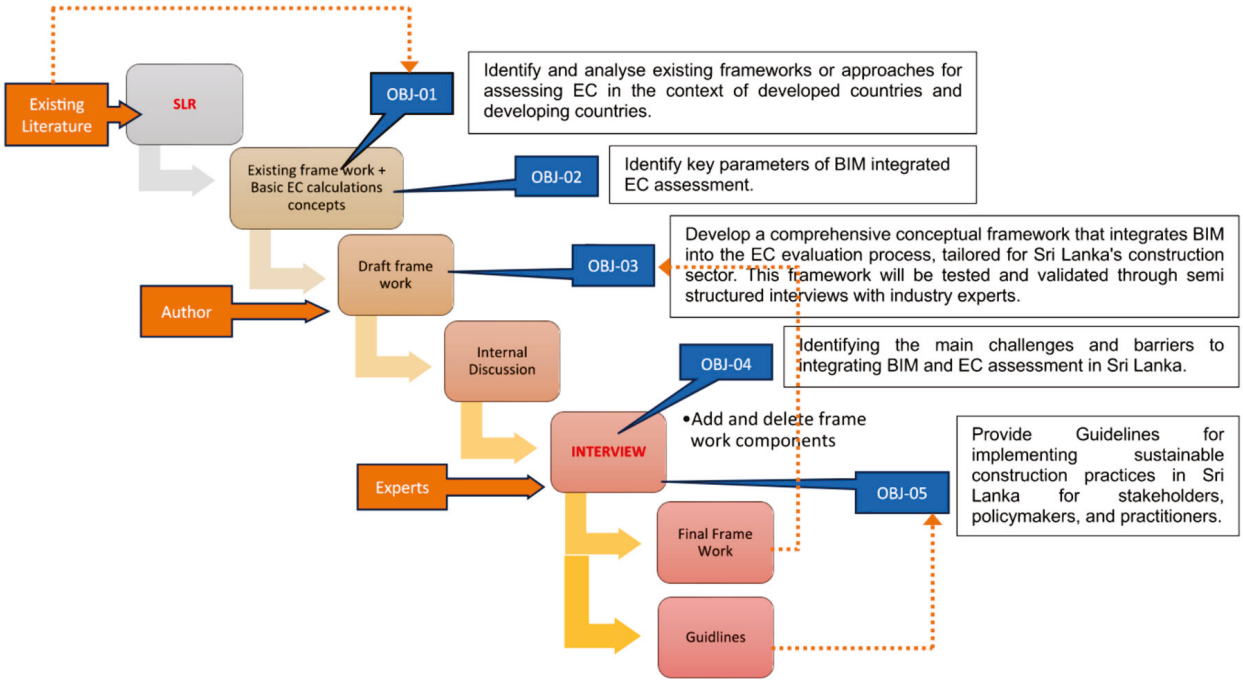


Figure 1. Research methodology.

2.1. Systematic Literature Review (SLR)

A SLR has been employed as our primary methodology, adhering to the Preferred Reporting Items for Systematic Reviews and Meta-Analyses (PRISMA) framework [25] for comprehensive reporting. This approach was chosen for its widespread acceptance in the built environment field, ensuring objectivity, precision, and comprehensiveness [26]. Given the study's objective to formulate a conceptual framework for integrating BIM into EC assessment within the Sri Lankan context, SLR proved suitable for exploring the latest BIM integration technologies [27]. Following a four-step process adapted from Rabiser, Grünbacher, and Dhungana [24], the SLR utilised Scopus, known for its extensive archive and reputation as the largest global repository of peer-reviewed publications across business, management, construction management, and engineering [28].

https://doi.org/10.3390/buildings16040814

2.1.1. Search Strategy

The identification of relevant articles began with selecting an appropriate database and keywords, as outlined by Deng and Smyth [29]. Utilising specific keywords, the study focused on terms such as BIM, "Embodied carbon," EC, "Carbon Assessment," LCA, "Life cycle assessment," "Calculation methodology," "Embodied carbon in building services," "Material selection," "Embodied carbon emission," EPD, and "Environmental product declaration." These terms were combined using "AND," "OR," and "AND NOT" operators. After iterative attempts and experiments, the final search term for Scopus articles emerged as: "(TITLE-ABS-KEY (BIM) AND TITLE-ABS-KEY ("Embodied carbon*") OR TITLE-ABS-KEY (EC) OR TITLE-ABS-KEY ("Carbon assessment*") OR TITLE-ABS-KEY (LCA) OR TITLE-ABS-KEY ("Life cycle assessment*") OR TITLE-ABS-KEY ("Calculation methodology") OR TITLE-ABS-KEY ("Embodied carbon in building services") OR TITLE-ABS-KEY ("Material selection") OR TITLE-ABS-KEY ("Embodied carbon emission*") OR TITLE-ABS-KEY ("EPD*") OR TITLE-ABS-KEY ("Environmental product declaration") AND NOT TITLE-ABS-KEY ("Operational carbon") OR TITLE-ABS-KEY ("OC") OR TITLE-ABS-KEY ("Life cycle cost")) AND PUBYEAR > 2016 AND PUBYEAR < 2026 AND (LIMIT-TO (SUBJAREA, "ENGI") OR LIMIT-TO (SUBJAREA, "ENVI") OR LIMIT-TO (SUBJAREA, "MULT")) AND (LIMIT-TO (DOCTYPE, "ar")) AND (LIMIT-TO (LANGUAGE, "English"))".

It is important to note that Scopus categorises "Articles in Press," "Online First," and "Early Access" publications using the upcoming calendar year as their official publication year. As a result, peer-reviewed articles that were fully available during the search window (late 2024) were indexed as 2025 publications.

In line with developments in BIM–LCA integration research, the literature search was limited to publications from 2017 onward. Studies before 2017 predominantly addressed BIM or LCA in isolation and seldom explored automated workflows or database-integrated carbon assessment methods, which only began to mature in the late 2017s [26,27]. Recent reviews highlight 2017–present as the period when BIM-enabled embodied carbon methodologies significantly expanded in technical scope and maturity [30]. Scopus was selected as the primary database due to its wide, multidisciplinary coverage of engineering, construction management, and sustainability research, and because it is the most commonly used database in systematic reviews within the built-environment domain [28]. Nevertheless, we recognise that relying on a single index may exclude relevant publications from other databases, and we have explicitly acknowledged this limitation.

2.1.2. Selection Criteria

To conduct a thorough literature review on EC assessment and BIM within the engineering domain, this study meticulously followed the PRISMA Statement [31] as illustrated in Figure 2. The search scope encompassed engineering, environmental science, and multidisciplinary fields, with a focus on articles published exclusively in English. Articles published between 2017 and 2025 were considered, deliberately excluding those published before 2017 to capture recent advancements. Despite adopting a broad international perspective, the study identified only a limited number of articles from developing nations. The exclusion process during the preliminary search phase systematically removed 475 research articles due to factors such as non-English language, irrelevant subject areas, and non-peer-reviewed formats, including books, book chapters, conference papers, and reviews, as illustrated in Figure 1. The emphasis on peer-reviewed papers aligns with the need for rigour and accuracy, as highlighted by Thelwall [32], ensuring the inclusion of reliable information in the study. Ultimately, 329 records were identified for the subsequent stages of the review.

https://doi.org/10.3390/buildings16040814

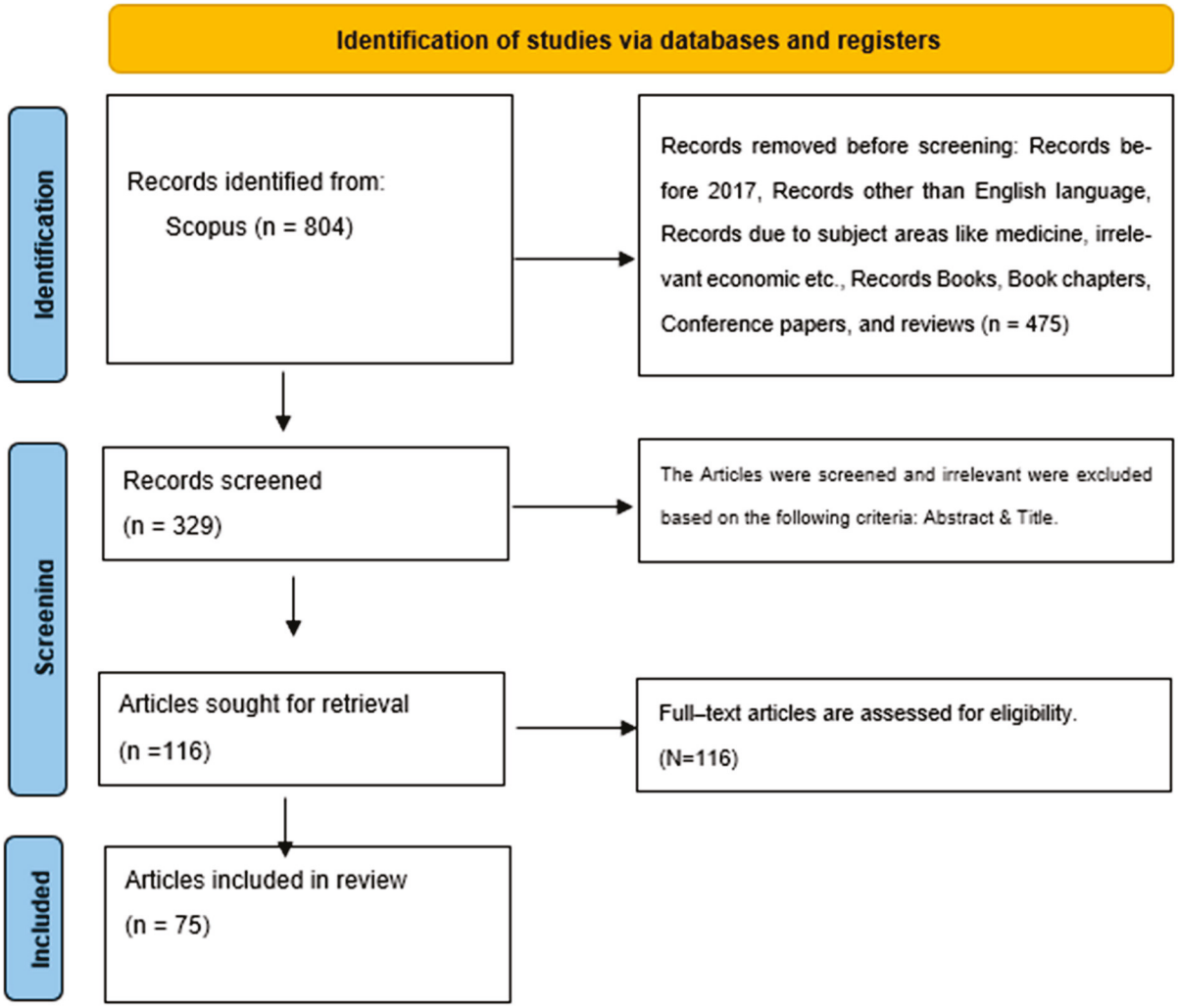


Figure 2. Statement under PRISMA Framework.

2.1.3. Quality Assessment

To ensure the review's integrity, a meticulous examination was conducted to identify potential duplications. Abstracts underwent a comprehensive scrutiny, refining articles for academic calibre and relevance. A subsequent phase involved a detailed screening of each scholarly article. Articles focusing on cost aspects, energy, thermal analysis, building facades, and demolition waste were excluded from the study. In this screening, an additional 253 articles were removed, comprising 213 from title and abstract screening and 40 from full-text screening, as they did not contribute substantively to the study's objectives. After rigorous application of inclusion and exclusion criteria, 75 articles were selected, meeting the standards for the review process.

2.2. Expert Interview Design and Protocol

Drawing insights from the SLR guided by PRISMA guidelines, a conceptual framework tailored to the unique context of SL was formulated. To validate its relevance and comprehensiveness, an expert survey was conducted using the approach of Rabiser, Grünbacher, and Dhungana [24]. Five esteemed Sri Lankan experts, each holding a doctoral degree, brought over a decade of invaluable experience in BIM-LCA to the interviews. Their extensive expertise, marked by advanced academic qualifications and years of professional practice, ensured a nuanced and comprehensive evaluation of the BIM-integrated carbon assessment framework. The interview questionnaire covered demographics, understand-

https://doi.org/10.3390/buildings16040814

ing of the framework, comparison of the application to existing methods, and barriers to adoption. Expert suggestions prompted modifications, refining the framework to meet specific requirements and addressing potential misunderstandings that arose during the interview process.

The expert validation stage in this study was not to achieve statistical representativeness but to ensure methodological and technical validation of the proposed BIM–BSR integrated framework. Consistent with qualitative design science and early-stage BIM–LCA research, small expert panels (typically 3–8 members) are recognised as an appropriate method for verifying conceptual soundness [33] before empirical testing. In the Sri Lankan context, the availability of professionals with combined expertise in BIM, LCA, and embodied carbon is limited; therefore, the five doctoral-level experts selected represent a significant proportion of the national knowledge base in this specialised domain. Their role was to evaluate the framework's feasibility and ensure alignment with real industry workflows, for which depth of expertise is more critical than sample size.

2.3. Data Analysis

The analysis unfolds in three stages. Firstly, SLR findings are scrutinised, employing VOSviewer (V1.6.20) for literature clustering [34], which identifies primary areas within the BIM-LCA integrated assessment process. The co-occurrence analysis using VOSviewer reveals crucial parameters [35]. In the second step, a co-occurrence analysis of terms is conducted, extracting key variables for calculating correlation coefficients [23] using the ATAtab online tool [36]. Positive and negative correlations indicate relationships, and "p" values determine significance. Preparation of Scatter plot charts based on these variables further enhances understanding [37], contributing to the BIM-integrated LCA framework for EC assessment tailored for the Sri Lankan context. In the subsequent phase, expert interview transcripts are manually coded to identify themes [38] that discuss views and framework elements. The final analysis stage comprehensively evaluates SLR and interview data, using overlapping scatterplots to synthesise insights [37] and draw conclusions from the integrated examination of both sources.

The research design follows a sequential, staged methodology commonly adopted in the development of national LCA frameworks in data-limited environments. Due to the lack of Sri Lankan-specific EC datasets, the absence of EC factors within the BSR, and the inconsistent availability of BIM-based material breakdowns, it was methodologically necessary to first establish the conceptual and data-integration framework before attempting a pilot case study. This staged approach ensures that subsequent applications are grounded in a validated, industry-aligned structure rather than relying on ad hoc or incomplete data inputs.

3. Results

3.1. General Features

A total of 22 papers appeared in the year 2025 from 75 publications generated by the SLR (see Figure 3). The number of papers in 2025 constitutes 29.3% of the total number of papers since 2017. BIM-LCA has been increasingly integrated into EC evaluations based on the data. In 2024 and 2025, 20 and 22 papers were published, respectively, indicating an increasing interest in the field.

https://doi.org/10.3390/buildings16040814

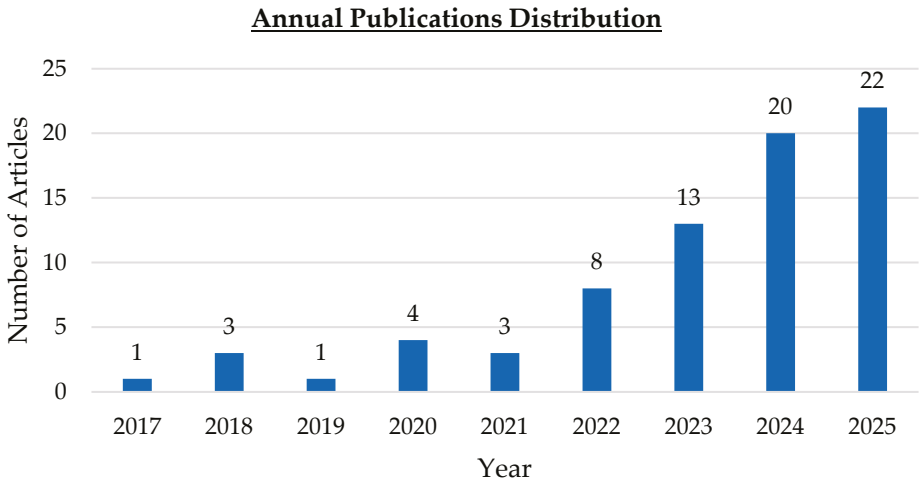


Figure 3. Annual Publication distribution.

The noticeable number of papers dated 2025 stems from Scopus's indexing protocol, which assigns Early Access and Articles in Press to the forthcoming publication year.

Out of the 75 examined publications, 81.3% identified as case study-based studies and only 18.67% (14 papers) were identified as concept papers (Figure 4). Case study Publications are mainly distributed throughout the five continents: Africa, Asia, Europe, North America, and South America (Figure 5). China, India, and Iran are among the major contributors to Asia. China has undertaken the most research endeavours (Figure 6).

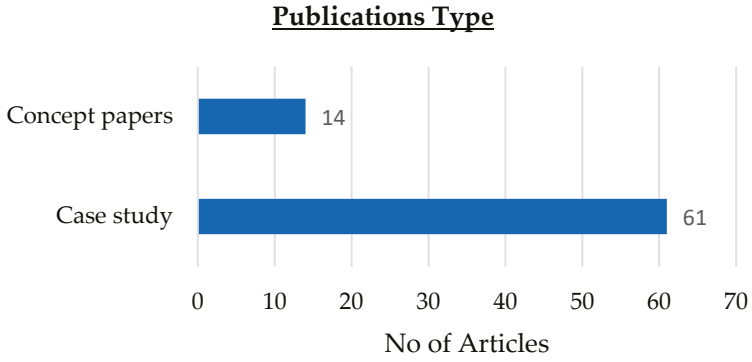


Figure 4. Publication distribution among Case Study papers and concept papers.

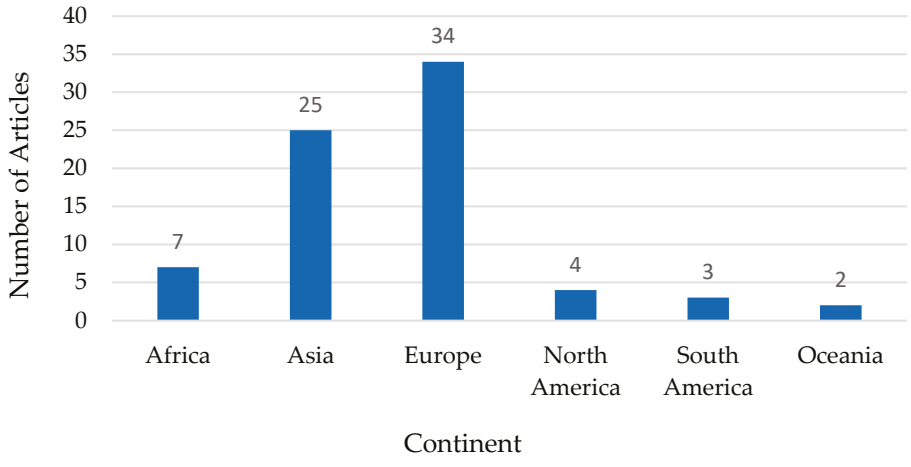


Figure 5. Publication distribution among different Continents.

https://doi.org/10.3390/buildings16040814

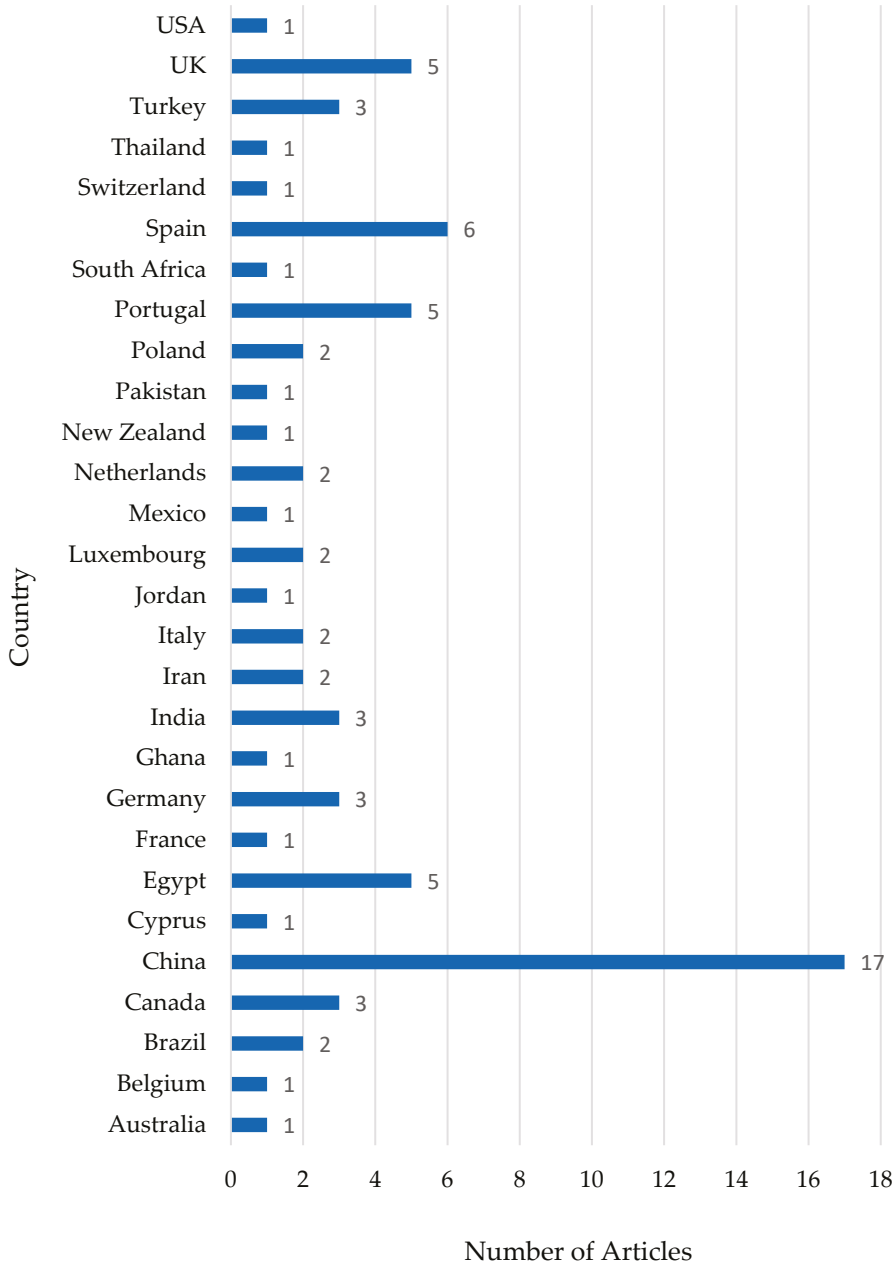


Figure 6. Publication distribution among different Countries.

3.2. BIM-LCA Base Embodied Carbon Assessment Key Parameters

Utilising the VOSviewer clustering method in bibliometric research enables the analysis and visualisation of scientific publications. This approach effectively delineates key ideas within short-listed papers [39]. In the identified literature clusters, three prominent groups emerge: the BIM cluster, the application cluster, and the information cluster (Figure 7). Terms co-occurrence and content analysis of these clusters reveal their significant contributions to BIM-LCA-based EC assessment, encompassing data preparation, integration, assessment, and visualisation. The information cluster primarily focuses on terms related to databases, Environmental Product Declaration (EPD)s, and ECFs. The BIM cluster revolves around terms associated with feeding data into BIM models using auxiliary tools and standard documents. Meanwhile, the application cluster emphasises key terms related to LCA tools, scripting languages, ultimately leading to the assessment and visualisation aspects of the research.

https://doi.org/10.3390/buildings16040814

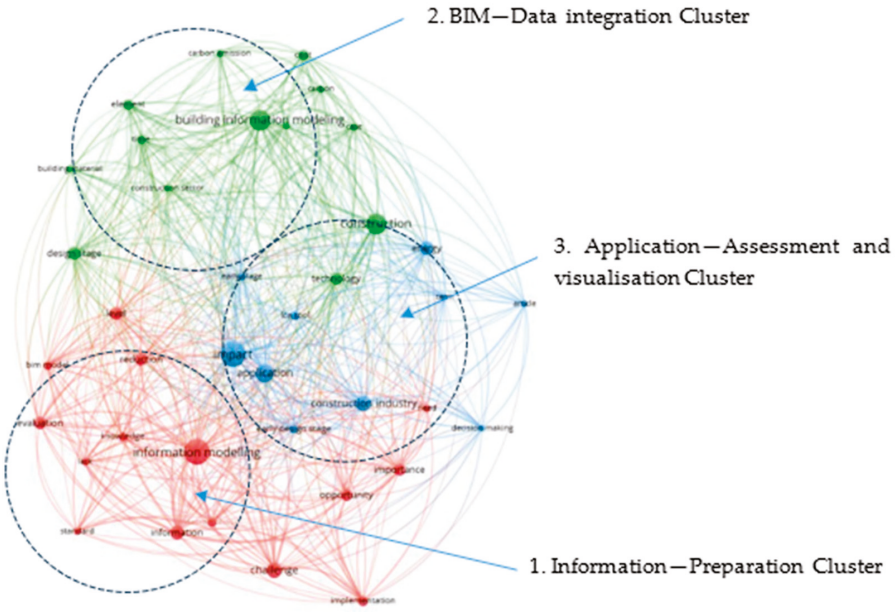


Figure 7. Key cluster arrangement of the literature.

From the Scopus database, a term co-occurrence map was generated using VOSviewer. The number of occurrences represents the term's importance. Those are helping to identify key parameters. Extracted from titles and abstracts, these terms are weighted based on word frequency, and a relevance score is calculated to select the most significant terms (Figure 8). The recurring terms in the extracted papers are considered key parameters for BIM-LCA integrated EC assessments, and their contributions are detailed in Table 1, with their meaningful conversions listed below as P1 to P8, as follows:

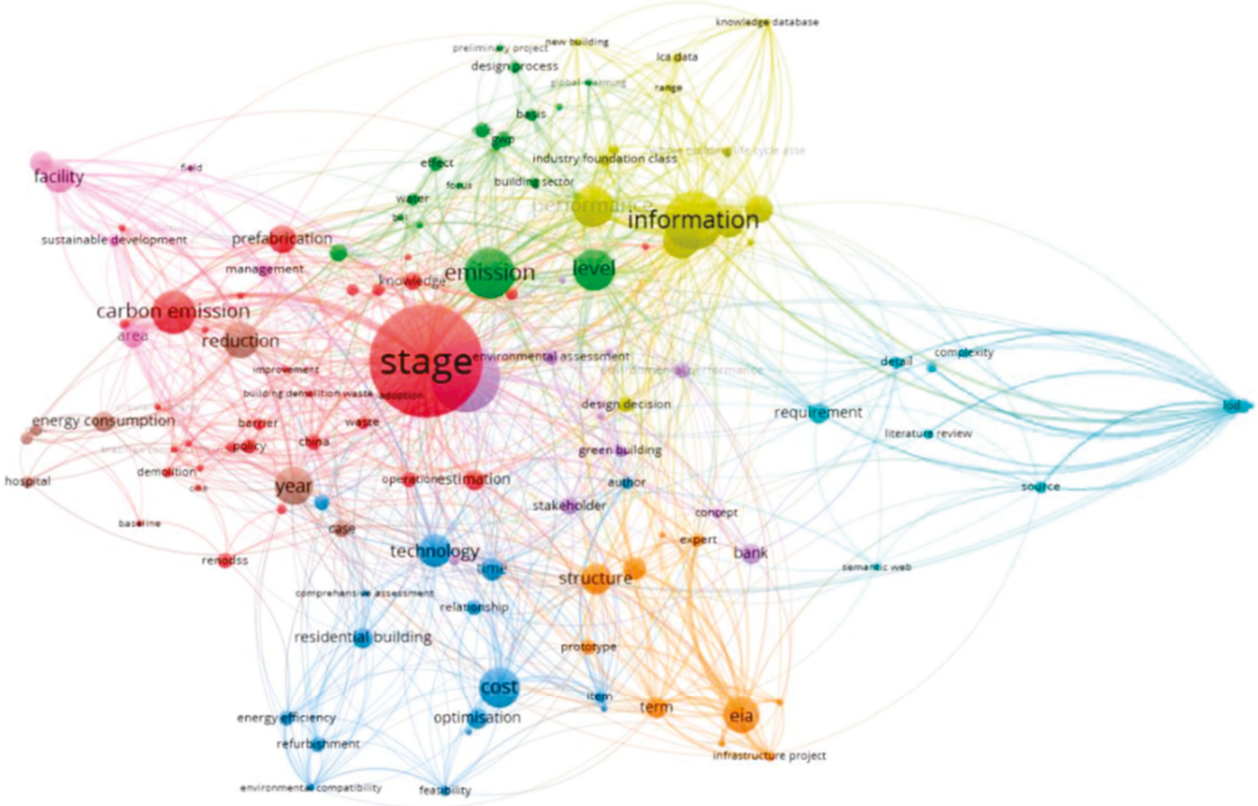


Figure 8. Terms Co-Occurrence map to identify Key parameters.

https://doi.org/10.3390/buildings16040814

- P1-BIM Model Geometry,
- P2-Material Information,
- P3-LCA Data,
- P4-Transportation Data,
- P5-Building Use and End-of-Life Considerations,
- P6-Data Interoperability,
- P7-Data Accuracy and Precision,
- P8-Energy Performance Data.

Table 1. Publication distribution among Key parameters.

No	Research Paper	P1-BIM Model Geometry	P2-Material Information	P3-LCA Data	P4-Transportation Data	P5-Building Use and End-of-Life Considerations	P6-Data Interoperability	P7-Data Accuracy and Precision	P8-Energy Performance Data
1	Chen et al. [40]	x	x	x			x	x	
2	Soust-Verdaguer et al. [41]	x	x	x			x	x	
3	Xu, Chen and Kim [42]	x	x	x	x		x	x	
4	Wu et al. [43]	x	x	x	x		x	x	
5	Xu et al. [44]	x	x	x	x		x	x	
6	Borkowski et al. [45]	x	x	x			x		
7	Li et al. [46]	x	x	x	x	x			x
8	Baskaran, Chockkalingam and Senthil Muthalvan [47]	x	x	x	x			x	
9	Li et al. [30]	x	x	x	x	x			x
10	Sistos-Sescosse et al. [48]	x	x	x			x	x	
11	Xiang, Li and Li [49]	x	x	x			x	x	
12	Strelets et al. [50]	x	x	x			x	x	
13	Gu et al. [51]	x	x	x			x	x	
14	Fernández Rodríguez et al. [52]	x	x	x			x	x	
15	Al-Zrigat [53]	x	x	x		x	x	x	x
16	Mohammed, Elmasoudi and Ghannam [54]	x	x	x	x		x	x	x
17	Ferreira, Costa and Silvestre [55]	x	x	x		x	x	x	
18	Ding et al. [56]	x	x	x	x		x	x	
19	Lv [57]	x	x	x				x	
20	Safari and Ghandehariun [58]	x	x	x	x	x	x	x	

https://doi.org/10.3390/buildings16040814

Table 1. *Cont.*

No	Research Paper	P1-BIM Model Geometry	P2-Material Information	P3-LCA Data	P4-Transportation Data	P5-Building Use and End-of-Life Considerations	P6-Data Interoperability	P7-Data Accuracy and Precision	P8-Energy Performance Data
21	Samniang et al. [59]	x	x	x	x		x	x	
22	Pandimani, Bilgates and Raviteja [60]	x	x	x	x	x	x	x	x
23	Yardımcı, Colak Demirel and Ertosun Yıldız [61]	x	x	x	x		x	x	
24	Kathiravel and Feng [62]	x	x	x	x		x		
25	Aragón and Alberti [63]	x		x			x	x	
26	Parece, Resende and Rato [64]	x	x	x			x	x	
27	Abdelaal et al. [65]	x	x	x	x		x	x	
28	Ali [66]	x	x	x	x				
29	Manifold et al. [67]	x	x	x	x		x	x	
30	Gao et al. [68]	x	x	x	x				
31	Atik, Aparisi and Raslan [69]	x	x	x		x	x	x	
32	Ullah et al. [70]	x	x		x	x	x	x	x
33	Han et al. [71]	x	x	x	x				
34	Płoszaj-Mazurek and Ryńska [1]	x	x	x					x
35	Yavan, Maalek and Toğan [72]	x	x	x			x		
36	Eslami et al. [73]	x	x	x	x		x	x	
37	Kylili et al. [74]	x	x						
38	Lima et al. [2]	x	x	x			x		
39	Topraklı [75]	x	x	x	x	x	x		
40	Danso et al. [76]	x					x		
41	Sugiyama, Rodrigues and Rodrigues [77]	x	x	x			x	x	
42	Ma, Azari and Elnimeiri [78]	x	x	x	x	x	x	x	
43	Forth, Abualdenien and Borrmann [79]	x	x	x	x	x	x	x	x
44	Boje et al. [80]	x	x	x	x	x		x	x
45	Di Santo et al. [81]	x	x	x	x	x			x
46	Arvizu-Piña et al. [82]	x	x	x	x	x	x	x	x
47	Yevu et al. [83]	x	x	x			x	x	x
48	Hunt and Osorio-Sandoval [84]	x	x	x	x	x	x		

https://doi.org/10.3390/buildings16040814

Table 1. *Cont.*

No	Research Paper	P1-BIM Model Geometry	P2-Material Information	P3-LCA Data	P4-Transportation Data	P5-Building Use and End-of-Life Considerations	P6-Data Interoperability	P7-Data Accuracy and Precision	P8-Energy Performance Data
49	Mowafy, Mohamed El Zayat and Marzouk [85]	x	x	x	x	x		x	
50	Feng et al. [86]	x	x	x	x			x	x
51	Serrano-Baena et al. [87]	x	x	x	x	x	x	x	x
52	Guignone et al. [88]	x	x	x		x	x		x
53	Bernardette Soust-Verdaguer, Jose Antonio Gutiérrez and Llatas [89]	x	x	x	x		x	x	x
54	Klumbyte et al. [90]	x	x	x	x	x	x	x	x
55	Deng and Lu [91]	x	x	x	x	x	x		
56	Tavares and Freire [92]	x	x	x	x		x	x	
57	Soust-Verdaguer et al. [93]	x	x	x	x	x		x	x
58	Onososen and Musonda [94]	x	x	x		x			x
59	Viscuso et al. [95]	x	x	x	x	x	x	x	x
60	Li et al. [96]	x	x	x	x		x	x	x
61	Alotaibi et al. [97]	x	x	x	x	x	x		x
62	Abdelaal and Guo [98]	x	x	x		x	x	x	x
63	Morsi et al. [99]	x	x	x	x	x			
64	Sameer and Bringezu[100]	x	x	x	x			x	
65	Alwan et al. [101]	x	x	x	x	x	x	x	x
66	Sobhkhiz et al. [102]	x	x	x	x	x	x	x	x
67	Hao et al. [103]	x	x	x	x	x	x		x
68	van Eldik et al. [104]	x	x	x	x			x	
69	Durão et al. [105]	x	x	x		x	x	x	x
70	Hollberg, Genova and Habert [106]	x	x	x	x	x	x		x
71	Santos et al. [107]	x	x	x	x		x	x	x
72	Nizam, Zhang and Tian [108]	x	x	x	x	x		x	
73	Bueno and Fabricio [109]	x	x	x		x	x		x
74	Eleftheriadis, Duffour and Mumovic [110]	x	x	x	x			x	x
75	Najjar et al. [111]	x	x	x	x	x	x	x	x

Note: "x" indicates that the corresponding parameter was addressed or considered in the respective study.

https://doi.org/10.3390/buildings16040814

3.3. BIM Tools

In the 75 articles, Revit was used as a BIM tool in 72% of the cases. On the other hand, Chinese researchers have used modelling software such as GTJ2018 and GGJ2013. In particular, two researchers chose Rhino for modelling. Many research papers have used the Dynamo plugin (15%) in conjunction with Revit (Figure 9).

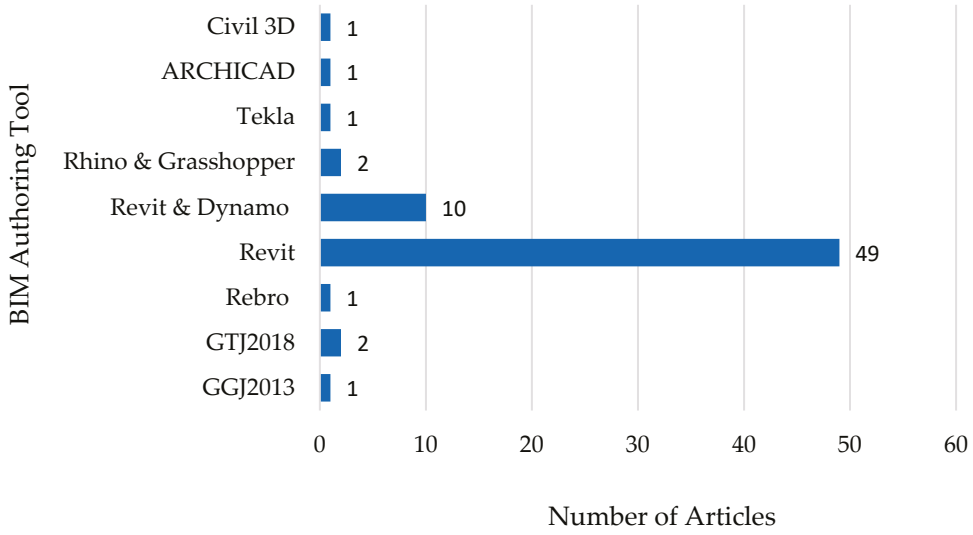


Figure 9. Publication distribution among BIM authoring tools.

There exist BIM tools beyond Autodesk products, specifically GGJ2013, GTJ2018, and Rhino. Their distribution is represented in the selected research papers.

3.4. LCA Tools

Several LCA tools have been employed in diverse research endeavours. The use of Excel sheets as the primary LCA tool stands out as a widely adopted approach, appearing in 12 of the shortlisted papers. Tally and OneClickLca follow closely as the second-most popular tools, each contributing 7 and 10 research articles (Figure 10). All other identified tools are outlined in the figure below, with their utilisation being minimal across the shortlisted research articles.

3.5. System Boundaries and Life Cycle Stages

Within the EC assessment process, there are four fundamental system boundaries. A1–A3 are cradle to gate boundaries, A1–A5 are cradle to handover boundaries, A1–A5, B1–B5, C1–C4 are cradle to grave boundaries, and A1–A5, B1–B5, C1–C4, and D are cradle to cradle boundaries. Among the chosen research studies, the most commonly employed system boundaries are cradle-to-gate and cradle-to-grave (25.4% in each case), as illustrated in Figure 11.

3.6. LCA Database

Figure 12 portrays the quantity of scholarly articles that are in opposition to the specific database employed by each research. Ecoinvent is widely acknowledged as the most important database among researchers (15.4%). Following closely behind are the EPD and Local datasets, which are utilised by a significant proportion of research endeavours (13.84%). OneClickLCA also enjoys considerable popularity (12.3%). A small number of studies employ multiple data sources, encompassing BEDEC, ICE, and ÖKOBAUDAT.

https://doi.org/10.3390/buildings16040814

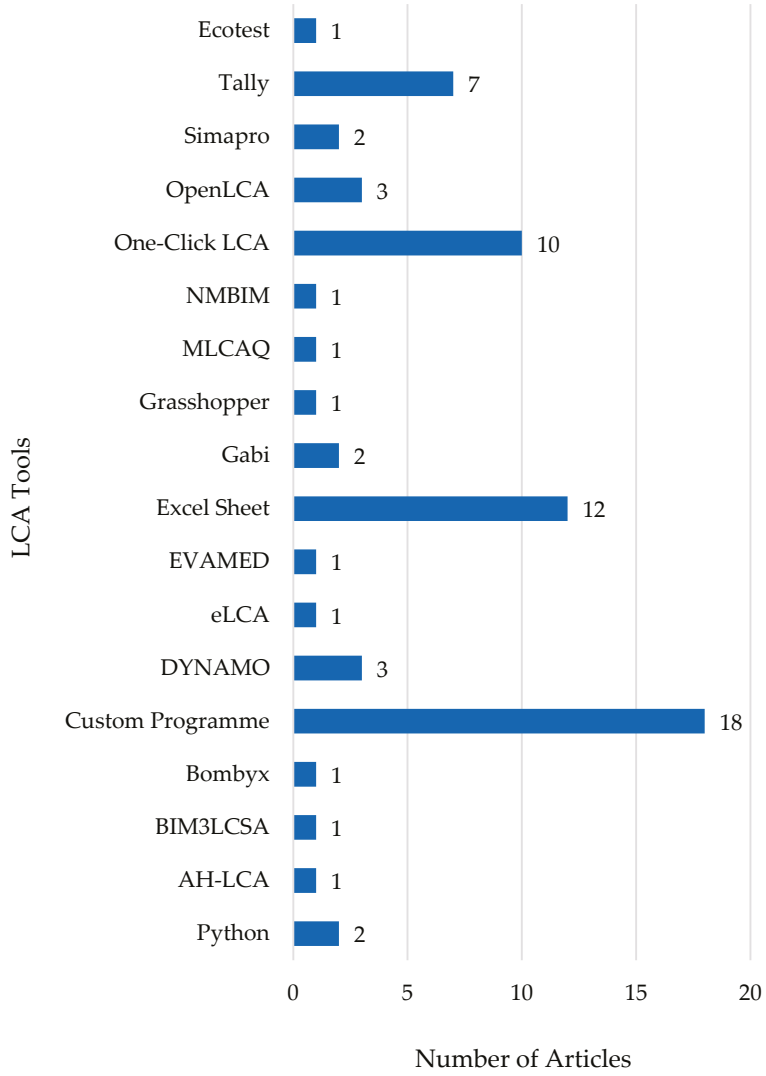


Figure 10. LCA tools and program distribution among Research papers.

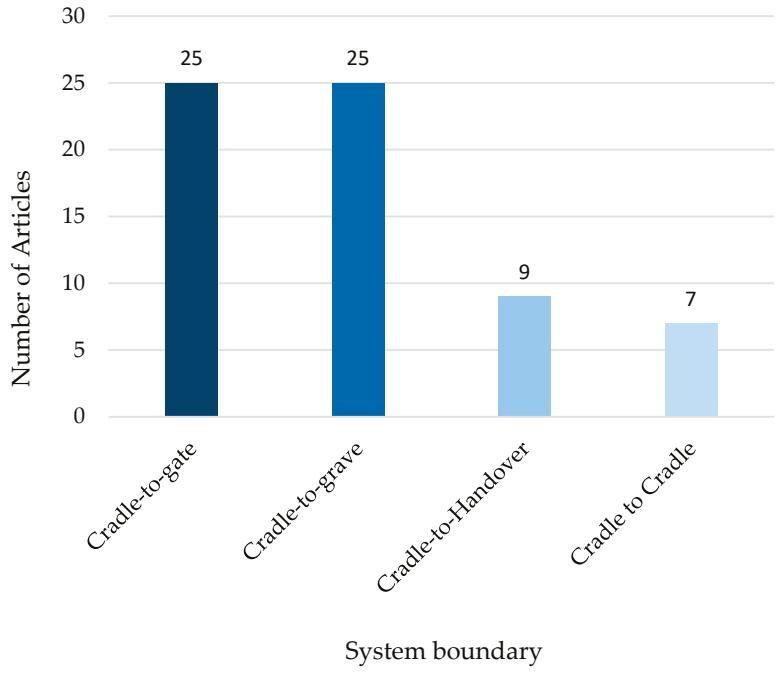


Figure 11. System Boundaries distribution among Publications.

https://doi.org/10.3390/buildings16040814

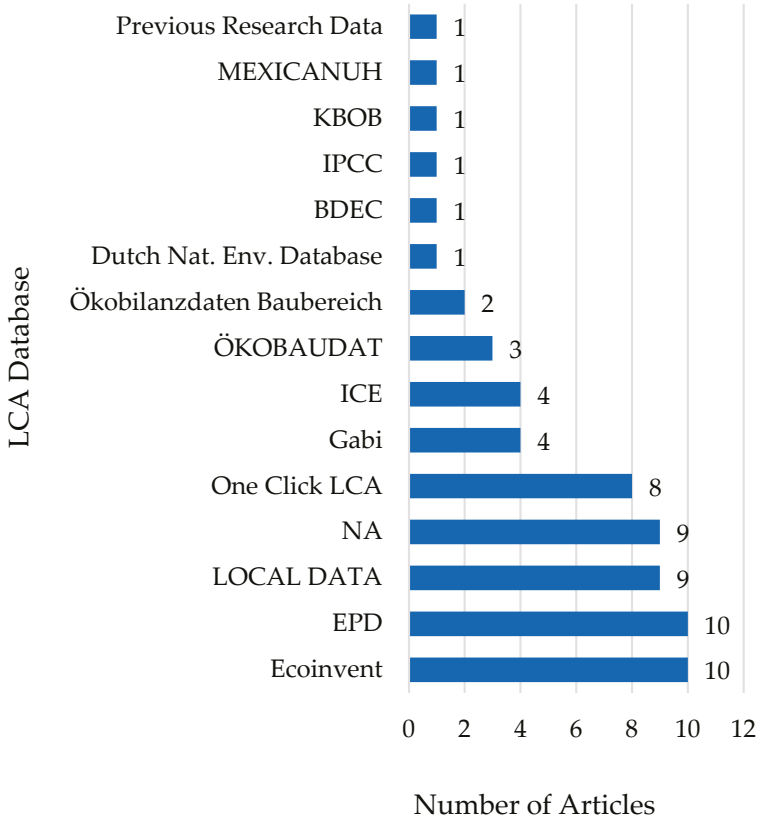


Figure 12. LCA Database distribution among Publication.

3.7. Statistical Associations Between Key Variables of the Initial Framework

This study examines the relationships among core variables characterising BIM–LCA practices in the reviewed literature. The variables of interest, such as BIM software, LCA tools, LCA databases, life-cycle stage boundaries, and country of origin, are nominal categorical data. Accordingly, associations among them were analysed using the Chi-square test of independence together with Cramér's V, which quantifies the strength of association on a scale from 0 (no association) to 1 (perfect association).

The purpose of this analysis is to understand structural patterns in international BIM–LCA workflows and to identify methodological clusters that inform the development of the proposed framework.

For each pair of variables, a contingency matrix was generated to capture the frequency of category co-occurrence within the literature sample. The Chi-square test of independence was used to assess whether the observed distributions deviated from what would be expected under statistical independence. Cramér's V was subsequently calculated as an effect-size indicator appropriate for nominal data, providing an interpretable measure of association strength. Heatmaps were then used to visualise the co-occurrence patterns (Figures 13–16), enabling precise identification of clustering tendencies across categories.

A strong association was observed between BIM software and LCA tools (Cramér's V = 0.693), indicating that tool selection within BIM–LCA workflows is highly ecosystem-dependent rather than random. The heatmap (Figure 13) reveals clear clustering patterns: Revit shows dominant co-occurrence with One-Click LCA, Tally, OpenLCA, GaBi, and Excel-based workflows, reflecting its position as the primary BIM environment in current practice. Revit and Dynamo instances cluster strongly with DYNAMO and, to a lesser extent, with Excel-based custom scripts, demonstrating the integration of parametric workflows with LCA modelling. Rhino and Grasshopper pair well with custom programmes, highlighting their use in computational and research-oriented LCA pipelines. Less fre-

https://doi.org/10.3390/buildings16040814

quently used BIM tools such as Tekla, Civil 3D, ARCHICAD, and Rebro each display sparse but identifiable associations with a limited set of LCA tools, suggesting specialised application contexts. Overall, these patterns illustrate that BIM–LCA integration is shaped by established software ecosystems, in which each BIM platform tends to align with a characteristic set of LCA tools.

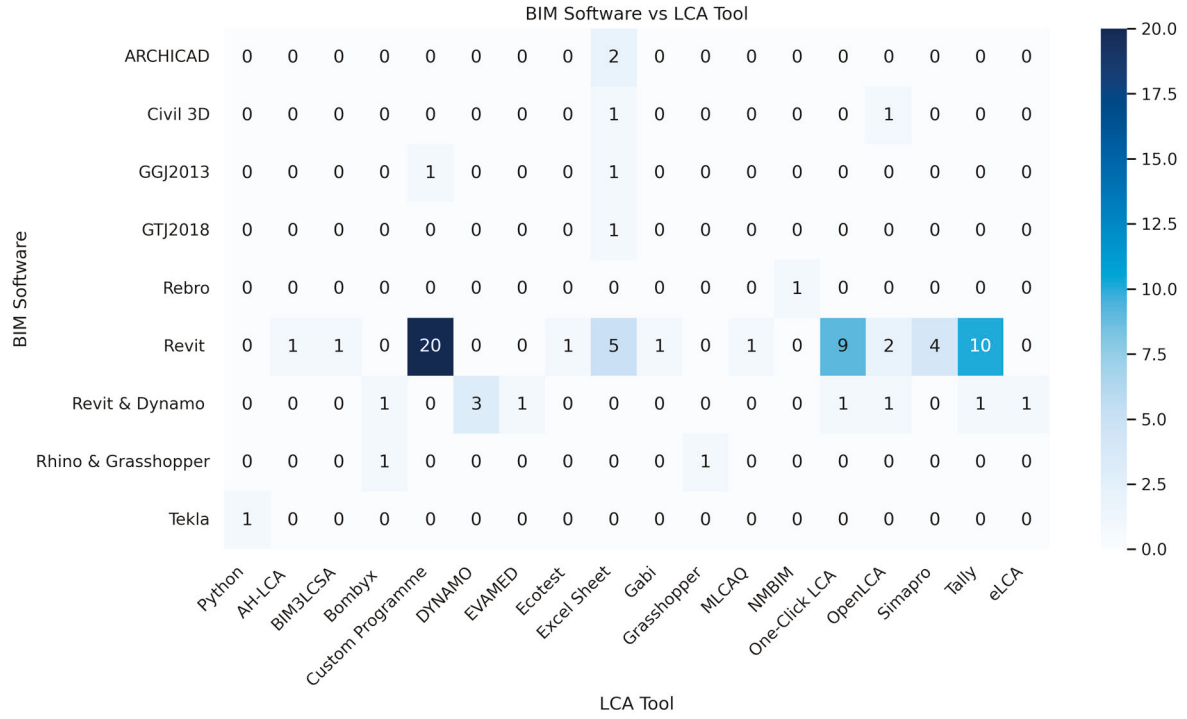


Figure 13. Heatmap of BIM Software and LCA tools.

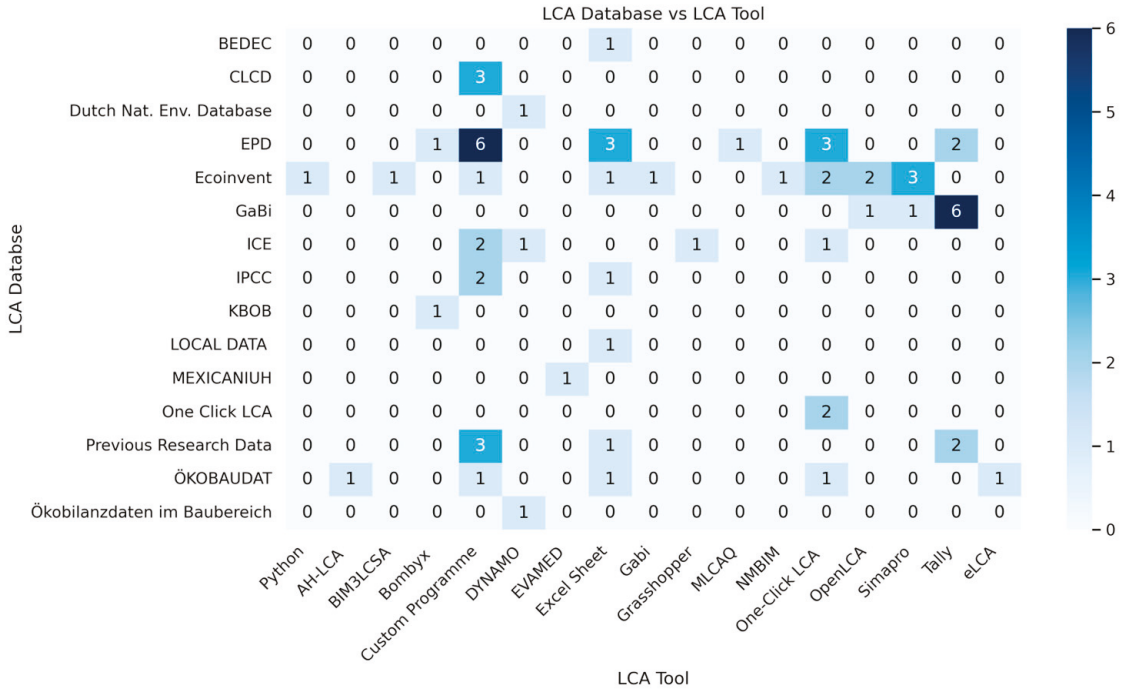


Figure 14. Heatmap of LCA databases and LCA tools.

https://doi.org/10.3390/buildings16040814

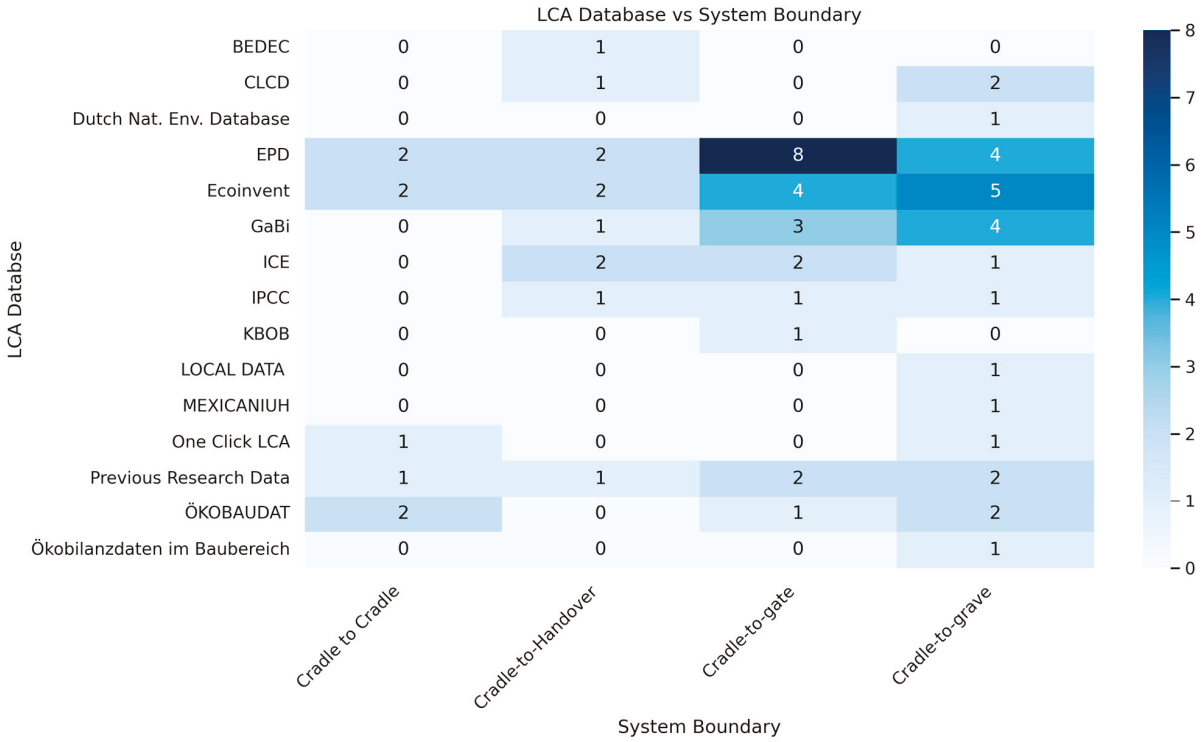


Figure 15. Scatter plot diagram of LCA databases and Life Cycle stages.

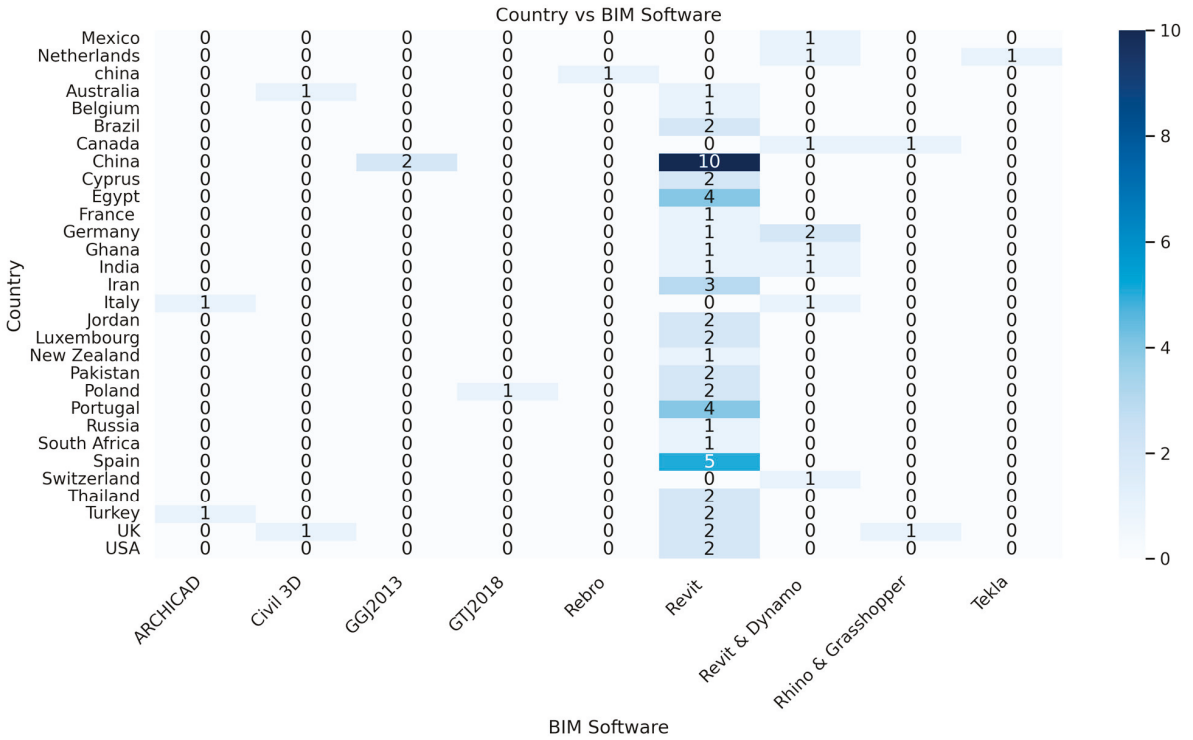


Figure 16. Scatter plot diagram of Country and BIM software.

A moderate association was identified between LCA databases and LCA tools (Cramér's V = 0.559). Figure 14 shows that several databases display strong preferences for specific tools; for example, Ecoinvent frequently appears alongside OpenLCA and One-Click LCA, while GaBi is used primarily with Tally and SimaPro, and EPDs recur in Excel-based and custom-programme assessments. This pattern indicates that database

https://doi.org/10.3390/buildings16040814

selection is mainly shaped by the technical architecture and default configurations of each LCA tool, rather than by fully open user-defined choices.

A weak association was identified between LCA databases and the life-cycle stages used in studies (Cramér's V = 0.396). As shown in Figure 15, some databases tend to appear more frequently in cradle-to-gate analyses (e.g., ICE, GaBi), while others (such as Ecoinvent and EPD datasets) occur across a wide range of system boundaries, including cradle-to-grave and cradle-to-handover. This suggests that the methodological scope adopted in LCA studies is influenced only to a limited extent by database selection, with system-boundary choices remaining primarily driven by research aims rather than database constraints.

Country of origin is strongly associated with the BIM software used in a study (Cramér's V = 0.680). Figure 16 highlights clear geographical patterns: Revit dominates across most regions (China, Germany, Portugal, UK), Rhino and Grasshopper appear mainly in research-oriented contexts, and specialised tools such as GTJ2018, Rebro, or Civil 3D are used only within specific national or institutional settings. These preferences reflect established market presence, training culture, national standards, and institutional procurement practices.

Across all variable pairs, the results demonstrate that BIM–LCA workflows exhibit recognisable ecosystems of practice. BIM software, LCA tools, and LCA databases show moderate-to-strong co-occurrence patterns, while system boundary choices display weaker alignment with database selection. National contexts also contribute to a structured pattern of methodological use, particularly in shaping preferences for BIM software. These insights reveal a global BIM–LCA landscape defined by characteristic toolchains, influenced by interoperability conventions, database availability, and country-specific norms. Together, these patterns provide an empirical foundation for understanding prevailing workflows and identifying integration challenges. They also offer essential evidence for designing a context-sensitive BIM–EC assessment framework.

The associations identified in the statistical analysis indicate that BIM–LCA configurations follow recognisable patterns shaped by tool compatibility, database ecosystems, and regional practices. These structural tendencies informed several strategic decisions in developing the proposed BIM–EC assessment framework. First, the dominance of Revit and its strong association with multiple LCA tools support its selection as the anchor BIM environment for the framework. Second, the moderate coupling between LCA tools and their corresponding databases underscores the need for a database-aware integration strategy that ensures material mappings and environmental datasets remain coherent across tools. Third, the strong influence of country context on BIM software usage underlines the necessity for local adaptation, enabling the framework to accommodate Sri Lankan datasets, regulatory conditions, and construction practices.

These considerations shaped the workflow architecture, particularly the use of Dynamo scripts for automation, structured Excel-based mapping sheets for transparency, and compatibility with widely adopted database formats. Collectively, these design choices ensure that the framework is both internationally informed and locally applicable. As a result, the framework can flexibly respond to varying project requirements while maintaining methodological consistency for embodied carbon assessment.

Based on the initial insights from the SLR and statistical analysis, Figure 17 presents the primary framework for assessing EC through the integration of BIM and LCA. This framework delineates three key stages: preparation, data integration, and assessment and visualisation. A detailed exploration of these stages and processes will be undertaken in the next section.

https://doi.org/10.3390/buildings16040814

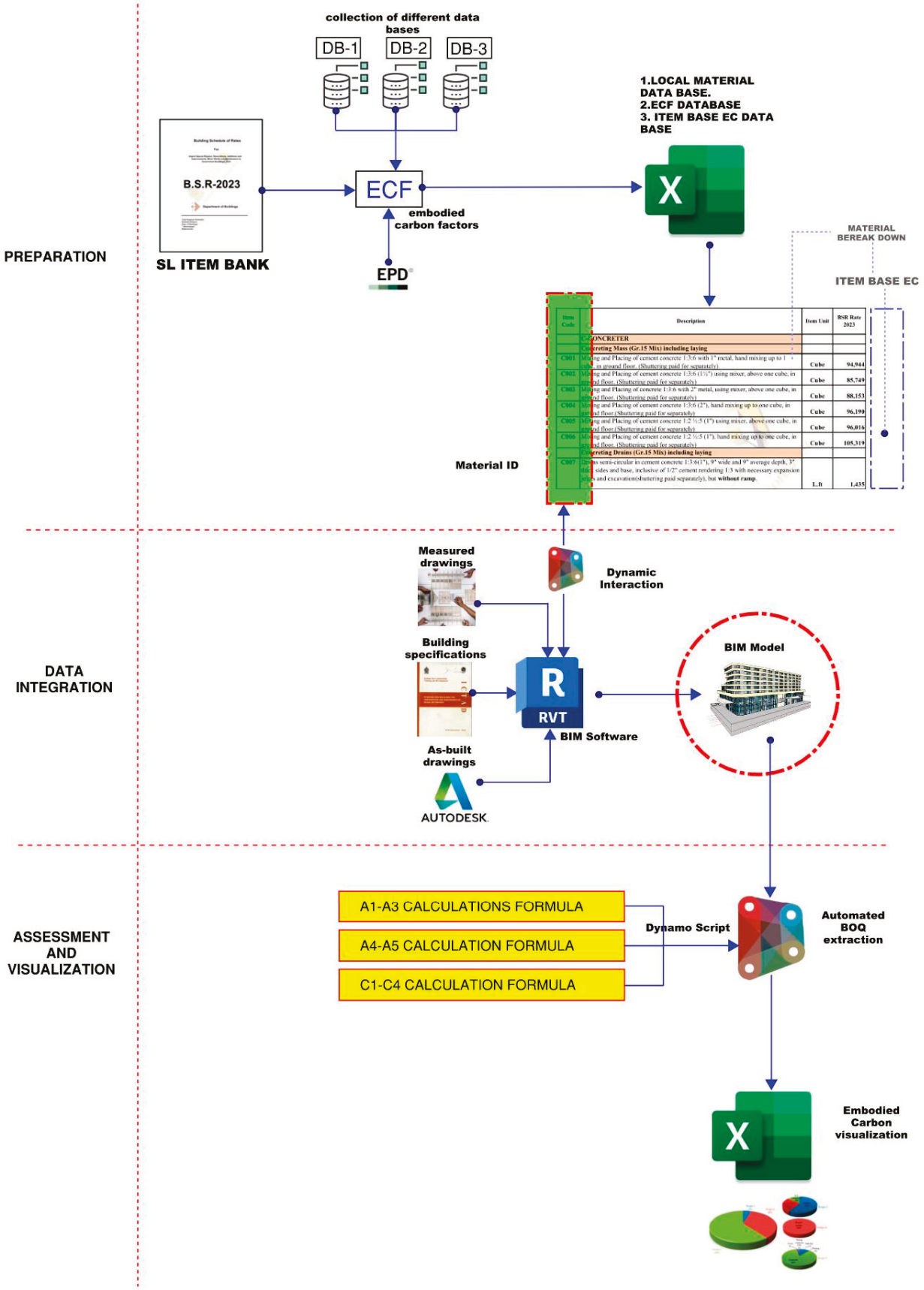


Figure 17. Initial BIM-integrated EC assessment framework.

https://doi.org/10.3390/buildings16040814

3.8. Expert Interview Findings

Five experts were interviewed to gather insights and feedback on the developed BIM-LCA integrated framework for assessing environmental compliance in the context of SL.

According to Williams and Lee [112], experts, defined as 'knowledge specialists,' possess technical expertise within a specific field. Von Soest [113] employed expert interviews to bridge gaps between expert insights and literature findings. The framework, presented for verification, underwent scrutiny through open-ended questions organised into five sections (Appendix A). Recorded interviews (anonymised as IN1 to IN5) were transcribed and thematically analysed (Appendix B) to ensure relevance and identify modifications, maintaining participant anonymity while enhancing the framework's validity. Summary of analysis illustrated in Figure 18.

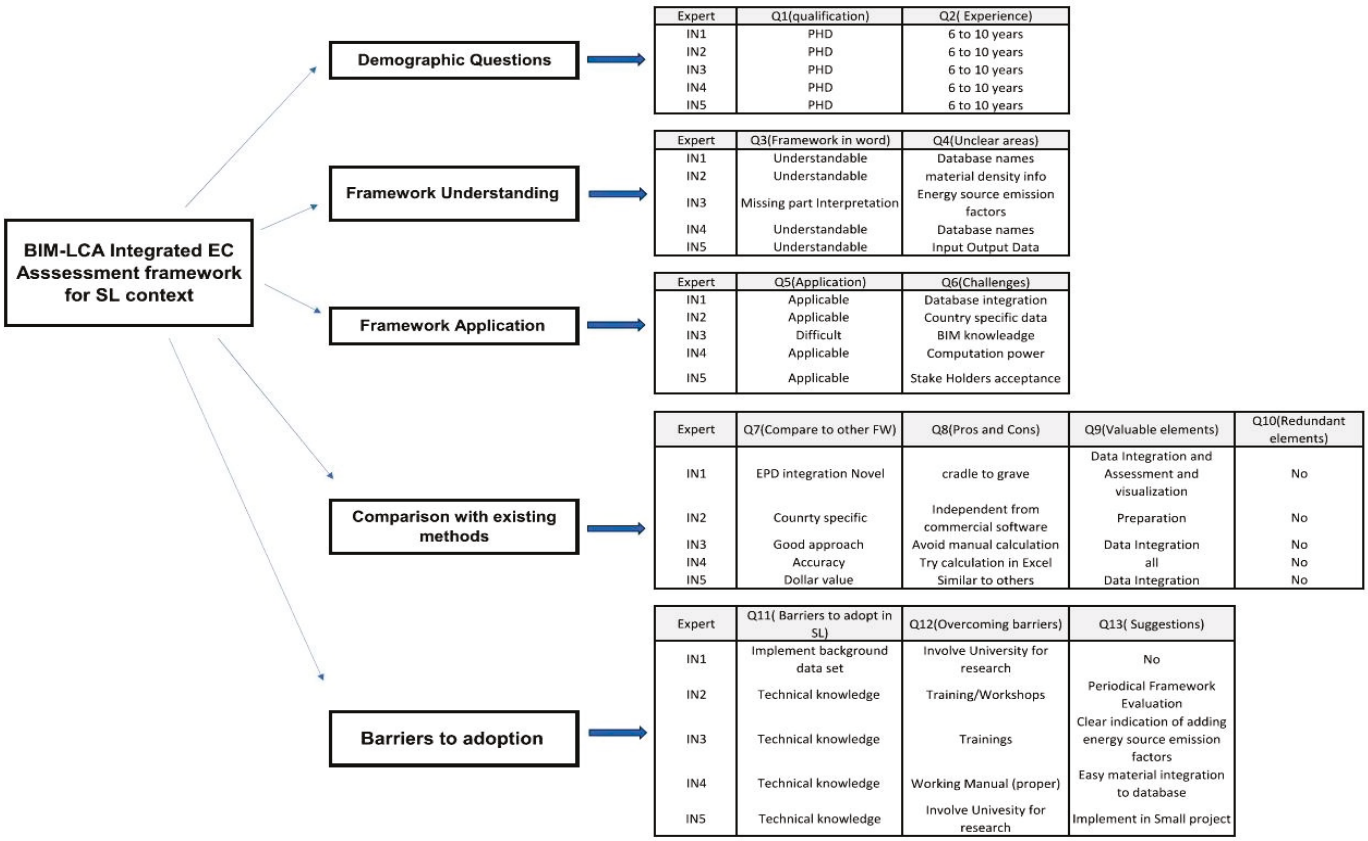


Figure 18. Thematic Analysis Results against the initial framework.

4. Discussion

Synthesising SLR findings and expert insights yields a comprehensive framework specifically adapted to the characteristics of the Sri Lankan construction industry (see Figure 19). This framework addresses the central research question: How can embodied carbon assessments be integrated within BIM frameworks in the Sri Lankan context?

https://doi.org/10.3390/buildings16040814

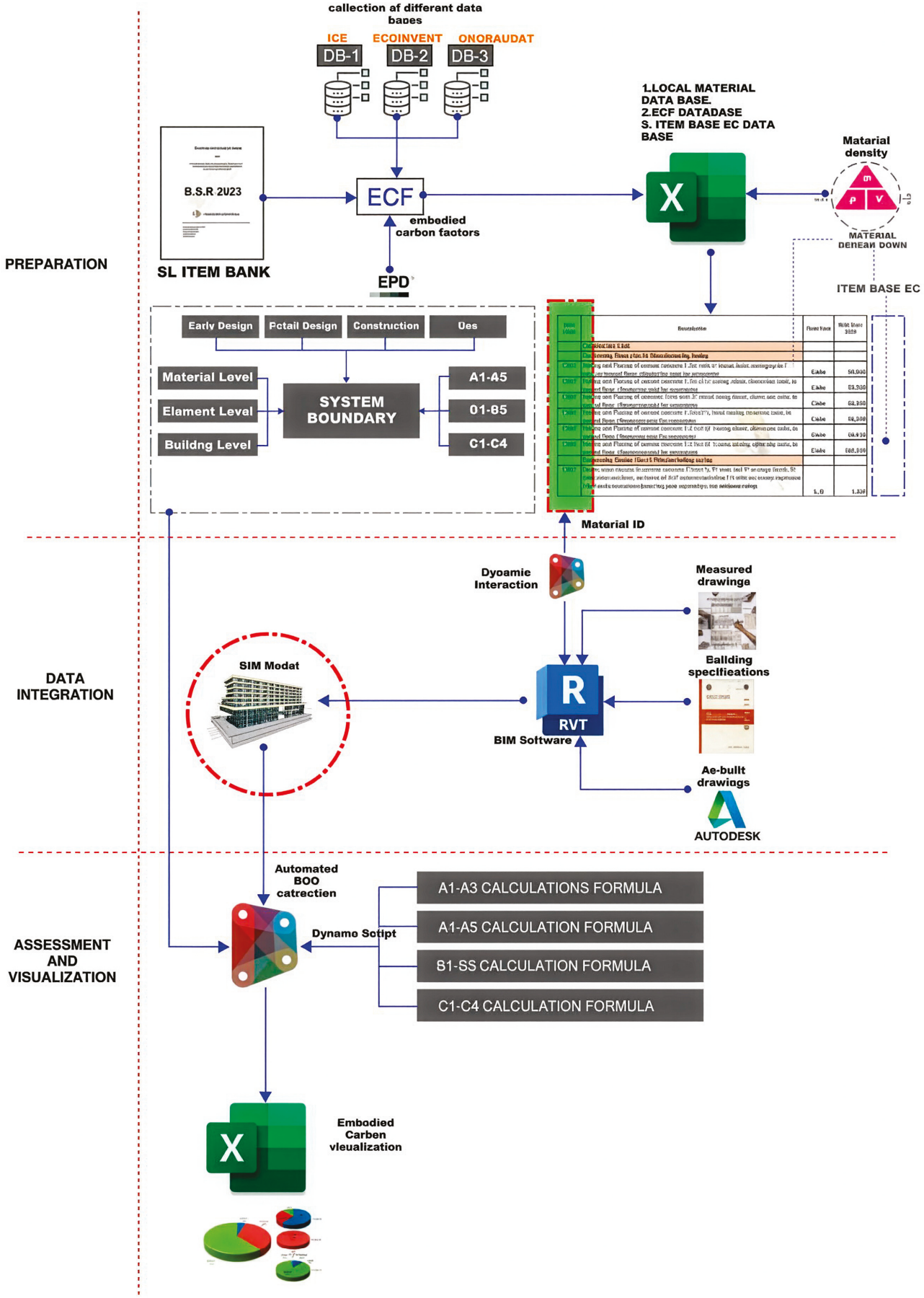


Figure 19. BIM-integrated EC assessment framework.

https://doi.org/10.3390/buildings16040814

The framework comprises six interconnected modules:

- **Module 1: Preparation and Goal Definition:** This foundational phase establishes clear assessment parameters.
- **Module 2: Data Infrastructure Development:** Establishing reliable EC calculation foundations through BSR enhancement and ECF compilation.
- **Module 3: BIM Model Development:** Creating information-rich digital representations enabling automated quantity extraction.
- **Module 4: Automated Data Integration via Dynamo:** Employing visual programming to link BIM model data with EC calculation logic.
- **Module 5: Calculation and Analysis:** Executing systematic EC quantification across multiple dimensions.
- **Module 6: Visualisation and Communication:** Translating numerical results into actionable insights through multiple presentation modes.

4.1. Key Steps and Elements of Framework

The initial discussion focuses on the development of the framework and its alignment with the research objectives. The first research objective (OBJ-01) involves laying the foundation by identifying existing frameworks. The literature review provides detailed discussions on findings related to OBJ-01, identifying conventional approaches, Industry Foundation Classes (IFC)-based approaches, plug-in-based approaches, and parametric modelling-based approaches. Notably, these approaches are predominantly used in developed countries, with limited application in developing countries. The subsequent step involves identifying key parameters in EC assessment frameworks to enhance precision in understanding critical variables. OBJ-2 aligns with this aspect, and in Section 3.2, BIM Model Geometry, Material Information, LCA Data, Transportation Data, Building Use and End-of-Life Considerations, Data Interoperability, Data Accuracy and Precision, and Energy Performance Data are identified as key parameters.

The content analysis identifies BIM tools, LCA tools, System boundaries and life-cycle stages, functional units, scope, and LCA databases as key variables for exploration in the framework's development. To establish correlations between variables and understand dependencies, the next step is crucial. This helps understand how changes in one aspect may affect others, aiding in predicting outcomes or behaviours. Findings reveal positive correlations between BIM software and LCA tools, as well as between BIM software and Country, as outlined in Section 3.7. Other variables showed independence with no correlation.

Consequently, a proposed framework is formulated, and its verification is conducted by BIM-LCA experts, in alignment with OBJ-03 of the research. Objectives 4 (OBJ-04) and 5 (OBJ-05), which focus on identifying the main challenges and barriers and providing guidelines for implementing sustainable construction practices in Sri Lanka for stakeholders, policymakers, and practitioners, are concluded based on outcomes from expert interviews and previous findings.

Broad stakeholder participation is ideal; however, such engagement is appropriate only after subject-matter experts have technically validated the conceptual structure, as this research represents the first stage of a multi-stage national framework development process. Methodological rigour requires prioritising expert depth rather than stakeholder breadth. The domain of BIM–LCA integration in Sri Lanka is still emergent, and the number of professionals with both theoretical and practical competence remains small. Therefore, the expert panel employed in this study served the intended purpose of validating the framework's logic, data pathways, and computational feasibility before expanding the validation process to architects, quantity surveyors, contractors, and engineers in subsequent phases.

https://doi.org/10.3390/buildings16040814

4.1.1. Preparation

This segment explores the developed framework based on the research findings. In the findings section, cradle-to-gate and cradle-to-grave system boundaries are prevalent, with an emphasis on addressing all boundaries despite data scarcity. A1–A3 life cycle stages dominate, aligning with Smith and Durham [114], while challenges in extending beyond cradle-to-gate are noted by Finkbeiner et al. [115]. The proposed framework targets a Cradle-to-Grave Approach, acknowledging the importance of EC despite existing data limitations. The findings indicate that the predominantly adopted functional unit is square meters. The proposed framework suggests unit conversions, recognising that the LCA scope of evaluation varies across material, component, and building levels. However, research data on the vast popularity of material-level calculations may be due to the availability of LCA databases for these calculations. The proposed framework introduces scripting to select different units and perform the necessary calculations.

As found in OBJ-01, ECF plays a key role in EC calculations and is included in LCA databases. The proposed framework extracts ECF from three main databases identified in OBJ-03: ICE, ecoinvent, and ÖKOBAUDAT. Using multiple databases reduces data collection effort and provides high-quality inputs for LCA, addressing the challenges highlighted by Chen, Matthews, and Griffin [116]. Although they highlight that different databases may give different results and insights. However, this study argues that, in cases where no country-specific databases exist, this method is suitable for developing countries such as Sri Lanka.

Additionally, the study introduces EPDs for extracting the missing ECFs within the framework. EPDs are often advocated for reporting construction material ECF due to their consistent and reliable environmental information, which aligns with EN 15804 and EN 15978 criteria [86]. The future is expected to witness increased accessibility to project- and country-specific EC data based on EPDs, as anticipated by Eleftheriadis, Duffour, and Mumovic [110].

One of the unique aspects of this framework is the development of a BSR into a comprehensive material database enriched with ECFs. The BSR, provided by the Sri Lankan government, serves as a valuable resource for information related to materials. Gomes et al. [117] contributed to country-specific data efforts. A similar approach is proposed with the BSR to populate the data. Figure 20 outlines the part extraction of the BSR document, and the item code F083-related material breakdown is illustrated in Figure 21. It consists of all material data, such as paving blocks and quarry dust, as well as machinery, transportation, and electricity-related data, all highlighted in different colours.

The final framework was amended to include information on material density, as stressed by the experts during the interviews. To calculate density, divide mass by volume. In BSR calculations, materials are typically quantified by volume, while ECFs are given in mass units (Kg/t). Thus, converting material volume to mass is necessary for EC calculations. In the Sri Lankan context, however, it is essential to clarify that consulting external resources for density values is only a temporary workaround and not an intended operational step for practitioners. The automation capabilities of the proposed BIM–BSR–Dynamo framework remain intact because density information is required only once during the creation of a material property library, after which the Dynamo scripts automatically perform all subsequent volume-to-mass conversions.

The expert interviews, therefore, highlight the need for a centralised Sri Lanka-specific density database as part of the wider data infrastructure development phase, rather than a limitation of the automation workflow itself. Once this database is established, either through government-led updates to the BSR or through industry-driven compilation, practitioners will no longer be required to manually search for densities, enabling full

https://doi.org/10.3390/buildings16040814

end-to-end automation of material transformations within the proposed framework. Some density-related information is provided in BSR, but it may not cover all materials. In such cases, online sources can be used to find relevant information.

	Cut pile carpeting		
F082	Supplying and laying 1/8 gauged, Wide Open Cut pile carpeting (USA or equivalent) with 5mm thick with Mac Form under layer , firmly bonded to the existing floor. Carpet having primary & Secondary backings, namely woven polypropylene & Classic back polypropylene, respectively. And having the minimum pile weight of 30 Oz per sq. yard. & loop density of 5320 Oz/Cu.yard. (Upto 150 Sq.ft only)	**Sq.ft**	**504**
	Interlocking paving		
F083	Supplying and Laying 80mm thick "Uni" type Coloured interlocking paving blocks (AMTRAD/SMS or equivalent) having Compressive Strength of 40N/mm2, layed on plain improved sub surface. Rate inclusive for Quarry dust bedding (Upto 150 Sq.ft only)	**Sq.ft**	**835**
F084	Supplying and Laying 80mm thick "Uni" type Natural cement colour interlocking paving blocks (AMTRAD/SMS or equivalent) having Compressive Strength of 40N/mm2, layed on plain improved sub surface. Rate inclusive for Quarry dust bedding. (Upto 150 Sq.ft only)	**Sq.ft**	**721**
	Paving tile Slabs		
F085	Supplying and Laying 300 x300 x50mm thick **Non Reinforced**, Natural cement colour, Concrete paving Slab, layed on plain improved sub surface. Rate inclusive for Quarry dust bedding. (Upto 150 Sq.ft only)	**Sq.ft**	**617**
F086	Supplying and Laying 300 x300 x50mm thick **Reinforced**, Natural cement colour, Concrete paving Slab, layed on plain improved sub surface. Rate inclusive for Quarry dust bedding. (Upto 150 Sq.ft only)	**Sq.ft**	**824**

Figure 20. Sample of a BSR Item description [20].

	Item Name	Unit
1	Supplying and paving(222 x111mm) 80mm thk Gr 40(40N/mm^2) unicolor inter locking concret block(Rate to include transporting & daving on 50 mm height Quarry dust layer)	Sqr
	Unicolor inter locking bliock(Gr 30)(222x111mm)	Nos
	Quarry dust	Cube
	Skilled Labourer	Day
	Unskilled Labourer	Day
	Transport Truck or tractor with trailor for interlock	Allow
	Loading & unloading	Allow
	Compacting by using plate compactor with transport (before and After laying)	Allow
	Water with bowser	Allow
	Handling tools	Allow
	Concrete cutting machine, concrete cutting wheel and electricity	Allow

Figure 21. BSR item F083 Rate Breakdown [20].

Similarly, experts emphasise the importance of considering Energy Source Emission Factors (ESEF) in EC assessments, as these vary by energy source [118]. Renewable sources, such as solar or wind energy, exhibit lower emission factors, while fossil fuel-based sources have higher factors due to the combustion of carbon-rich fuels [119]. This is crucial, particularly in the construction, in-use, and end-of-life stages, where the Ecoinvent database is widely utilised for comprehensive emission factor data [40], which is part of the proposed framework and aligns with the expert view.

4.1.2. Data Integration

Moving into the next section of the framework, according to the findings in OBJ-03, Section 3.3, Revit emerges as the predominant BIM authoring tool globally, particularly in Asia. This tool is crucial in generating BIM models, which serve as the cornerstone for EC calculations. OBJ-01 findings underscore that BIM models can be produced for both new and existing constructions. For new constructions, models require building specifications, often referenced from the Institute For Construction Training and Development

https://doi.org/10.3390/buildings16040814

(ICTAD) building specification in the Sri Lankan context. Existing constructions necessitate measured drawings, which may be in CAD files or manual paper drawings and can be imported into the BIM model or created from scratch.

According to the statistical findings, the BIM tool is closely connected to LCA tools. Findings in Section 3.7 reveal a positive correlation between these variables, with an R^2 value of 0.15, indicating a connection between the two tools. However, 85% of the variation is attributed to unknown factors, suggesting that other requirements, such as economic factors and ease of use, influence tool selection for the framework. Based on

Based on the above facts, the chosen framework selects Revit as the BIM tool and Dynamo scripting as the optimal method for data integration in the Sri Lankan context.

To establish a connection between the Excel file and the Revit model, Dynamo scripts must be created. This particular framework proposed two dynamo scripts for the process. Automating the creation of material names in the Revit library is the first Dynamo script to automate a time-consuming manual procedure. It utilises RGB colour values and material names stored in an Excel sheet, translating and converting them into the Revit library [106]. An Excel spreadsheet is generated by extracting material names and unique Revit IDs from the Revit library for constructing a mapped detail of ECF. It maintains row order, retains materials without an EC value, and ensures accuracy through material IDs during data import [106].

By combining material information from the Excel file and elemental data from calculation scripts, this Dynamo script automatically integrates key parameters into the Revit template. It ensures category inclusion, checks for parameter duplicates, and prevents overlap [104].

A Dynamo script imports the material parameters of the 'all materials LCI/ECF database' into Revit. The script reads, sorts, and imports the Excel file into parameters, making the template ready for use. Dynamo script logic involves defining material categories, extracting data, sorting, and importing parameters. Output is finally displayed. By the end of this step, the BIM model will be completed with all required information and links to the external Excel file for the next step's calculations.

4.1.3. Assessment and Visualisation

The subsequent phase of the framework involves developing the calculation Dynamo script, encompassing all four stages from A1 to C4, as illustrated below in the following formulas. Specific coding is implemented in Dynamo across various stages of calculation, covering each phase of the life cycle from A1 to C4. Experts emphasise the computational power required to execute large-scale data processing within the Dynamo environment. They suggest shifting calculations to Excel as a more efficient solution. Similarly, Weng et al. [120] propose distributing the code over a cluster of workstations using message-passing software to alleviate the computational demands of Dynamo, although this approach is highly technical. However, more case studies have demonstrated success with Dynamo, making it a viable starting point for developing countries like Sri Lanka.

In the final stage of the framework, the Dynamo script reveals EC amounts. It identifies significant contributors for each element category, adhering to the calculation formulas outlined below [84].

- **EC_{A1–A3}** = Σ (Quantity × ECF_{raw material extraction to manufacturing})
- **EC_{A4–A5}** = Σ (Quantity × Distance × ECF_{transportation and construction})
- **EC_{B1–B5}** = Σ (Quantity × Operational life × ECF_{use stage})
- **EC_{C1–C4}** = Σ (Quantity × ECF_{end-of-life})

The script computes EC per building using a structured approach and visualises the results using Dynamo [121]. The Dynamo script thoroughly analyses EC, pinpointing top

https://doi.org/10.3390/buildings16040814

contributors and validating model accuracy. The collected data are sorted, grouped, and exported to an Excel sheet, allowing users to identify the major contributors per element type within a category.

4.2. BIM and EC Assessment in Sri Lanka

Based on insights from expert interviews, several challenges and barriers related to integrated BIM-LCA EC assessment were identified. The first challenge emphasised the complexity of integrating multiple data sources, acknowledging the variability in results from different sources, as noted by Chen, Matthews and Griffin [116]. Despite potential uncertainties, the primary goal remains taking practical actions to mitigate environmental impact. The second challenge highlighted the unavailability of country-specific datasets for Sri Lanka. Developing such datasets is acknowledged as a meticulous process that involves defining the scope, collecting data from local sources, adapting global databases, consulting experts, considering environmental regulations, maintaining transparent documentation, conducting sensitivity analyses, and providing periodic updates [122–124]. While developing a local dataset is time-consuming, the current reliance on available global data is necessary.

The third challenge highlighted computational issues with Dynamo, specifically the requirement for substantial computational power to handle large projects with extensive datasets. However, literature suggests that the significant acceleration in modelling and documentation processes outweighs this challenge, providing an overall advantage [125]. The fourth challenge raised concerns about the high cost of BIM software and a shortage of BIM experts in Sri Lanka. Despite this, projections indicate a 5% annual rate of substantial growth in the Sri Lankan construction market between 2024 and 2027, potentially changing the BIM landscape in the country [126]. The fifth challenge focused on obtaining industry consent, disseminating technical knowledge, and providing adequate training. This challenge is indirectly related to the fourth challenge, and there is an expectation that perceptions may shift in response to the changing landscape, as highlighted in the fourth point.

4.3. Implications

The practical application of the framework relies significantly on the BSR. For effective implementation, government policy decisions are crucial to populate the BSR document with relevant ECFs, mirroring its annual update. Alternatively, private sector initiatives may be necessary to maintain the BSR document. Concurrently, policy decisions should be enacted to improve the affordability of BIM software, promote BIM-related training, and emphasise sustainability applications. Once fully implemented, setting targets for EC in building approvals could be explored through policy initiatives. The framework should be further investigated in the context of small projects, with an emphasis on its practical implications. Identifying components that require further improvement and conducting periodic reviews can help enhance the framework's efficacy.

As emphasised in the literature, B1–B5 and C1–C4 calculations are project-specific and challenging due to the extensive information required. Dixit [127] underscores the customisation of B1–B5 calculations for maintenance scenarios over a building's anticipated lifespan, acknowledging variations for different building types. For C1–C4, the availability of fuel consumption data from both tools and transport is identified as a critical requirement [84]. Consequently, refining the assessment and visualisation aspects of the framework through actual case study applications becomes imperative.

As in many developing countries, Sri Lanka is in a transitional phase in which hybrid datasets must be used until a national embodied carbon database becomes available. The proposed framework has therefore been designed to support this shift by allowing future

https://doi.org/10.3390/buildings16040814

Sri Lanka-specific ECFs to be incorporated directly into the BIM–BSR workflow without requiring structural changes to the automation logic. Upon implementation, the framework holds advantages for all stakeholders in the Sri Lankan construction industry, including architects and engineers. Extracting information from the BSR database for calculations creates a standardised approach within the country, making it a promising initiative for advancing sustainable practices in the Sri Lankan context.

While this study does not yet demonstrate a complete pilot application, this is an intentional methodological boundary rather than a limitation of scope. The expert validation stage confirms that the framework is technically sound and practically feasible, establishing the necessary foundation for the future Phase of this research programme. The next phase should involve applying the framework to live and retrospective building projects, enabling comparisons among automated Dynamo outputs, BSR-based manual estimates, and industry benchmarks. This staged progression ensures accuracy, reliability, and generalisability of findings, particularly important in a national context where EC data structures are only now beginning to emerge.

While Revit and Dynamo were derived from the research workflow, the framework itself is not constrained to Autodesk products. The data-flow structure, mapping BIM quantities to BSR items and external ECFs, is compatible with any toolchain that supports IFC-based modelling, attribute extraction and external data linkage. As such, the framework can be replicated using open-source ecosystems. This ensures that the proposed approach remains adaptable to varied technological and economic contexts within developing countries.

Several emerging developments are expected to influence the future evolution of BIM-integrated embodied carbon assessment in Sri Lanka. First, national-level efforts to establish Sri Lankan-specific embodied carbon factors and product Environmental EPDs will significantly enhance the accuracy of the BIM–BSR workflow. Second, open-source BIM and LCA tools are gaining international traction and may provide lower-cost alternatives to commercial software ecosystems. Third, the increasing global adoption of cloud-based digital construction platforms and automated LCA APIs suggests that Sri Lanka may eventually transition from standalone tools to fully integrated digital pipelines. Finally, expanded stakeholder participation, including QSs, contractors, regulatory agencies, and material manufacturers, will be critical for maturing the national embodied carbon ecosystem and ensuring that the proposed framework evolves into a scalable industry standard.

5. Conclusions

In response to the growing global imperative to address environmental concerns, particularly in the construction industry, this research endeavours to bridge the gap between sustainable construction practices and the adoption of BIM with a focus on EC assessments. The investigation is contextualised within the framework of SL, a nation experiencing rapid urbanisation and construction growth.

Aligned with the United Nations' 2015 Sustainable Development Goals, the study recognises the potential of low-carbon materials and innovative technologies to advance the economy and the environment. In the construction industry, BIM emerges as one of the most critical technological innovations. The integration of BIM into sustainable construction practices remains underexplored, especially in developing countries like Sri Lanka.

The research questions and objectives are formulated to address the adaptation of BIM methodologies to diverse construction practices, the integration of key parameters for EC assessment, and the identification and addressing of barriers and challenges to implementing a comprehensive conceptual framework. The empirical findings from the SLR provide insights into the current landscape of BIM-integrated EC assessments. Notably,

https://doi.org/10.3390/buildings16040814

there is a growing interest, as evidenced by the increasing number of publications in recent years. The identified key variables include BIM tools, LCA tools, system boundaries, life cycle stages, functional units, scope, and LCA databases. Building upon the identified variables, the study proposes a robust conceptual framework tailored for the Sri Lankan construction sector. The framework encompasses three critical stages: preparation, data integration, and assessment and visualisation.

The dynamo scripting approach, particularly utilising Revit and Dynamo, is chosen for data integration, given Revit's global prominence as a BIM authoring tool. The framework also emphasises the importance of material density and the extraction of EPDs and data extraction from multiple databases. The framework undergoes validation through expert interviews, adding a qualitative layer to the research. While they validate the framework, experts identify challenges related to data source integration, the absence of country-specific datasets, computational demands, cost implications, and the need for industry-wide awareness and training. These challenges highlight the multifaceted nature of implementing sustainable construction practices, which require collaboration among stakeholders, policy interventions, and technological advancements. The implications of the research extend beyond academic discourse to practical applications. The framework's effectiveness hinges on the government's commitment to maintaining and updating the BSR document with relevant ECFs. Private-sector initiatives are also vital to sustaining this database. This study suggests potential policy initiatives, such as setting targets for EC in building approvals and enhancing the affordability of BIM software.

The framework's practical application should be the focus of future research. Continuous refinement and periodic reviews are essential to enhance its efficacy. Addressing project-specific challenges, particularly in stages B1–B5 and C1–C4, requires further investigation and customisation for different building types and maintenance scenarios. Overall, this research provides a comprehensive, tailored approach to integrating BIM with EC assessments in Sri Lanka. It serves as a foundation for sustainable construction practices, offering policymakers, practitioners, and industry stakeholders valuable insights. As the global construction landscape evolves, the adoption of such frameworks becomes imperative for a sustainable and environmentally conscious future for Sri Lanka.

A key boundary of this study is that it presents a validated conceptual framework without yet executing a full-scale pilot demonstration. This is intentional and appropriate for the current state of Sri Lanka's construction data ecosystem. As national EC factors, BSR enhancements, and BIM capacities continue to evolve, this framework provides the critical foundation for the next phase of research, which will involve detailed pilot case studies, empirical validation of EC outputs, and benchmarking against existing manual workflows. The following research phase should be planned to ensure the framework's operational performance is rigorously tested and refined.

A further limitation of this study is that the expert validation stage involved a small, highly specialised panel. This is methodologically appropriate for an early-stage conceptualisation study, but does not yet represent all stakeholder groups within the construction sector. Subsequent phases of future research should include broader multidisciplinary validation workshops and pilot testing across real building projects to incorporate perspectives from architects, QSs, structural engineers, contractors, and regulatory bodies. Establishing the conceptual foundation in this paper is an essential prerequisite for such large-scale validation.

Author Contributions: Writing—original draft, T.P.A.L.P.; writing—review and editing, supervision, and project administration, A.H. and A.N.; conceptualisation and Data collection, T.P.A.L.P.; Reviews and supervision, M.L., A.K.S. and A.P. All authors have read and agreed to the published version of the manuscript.

https://doi.org/10.3390/buildings16040814

Funding: This research received no external funding.

Data Availability Statement: The original contributions presented in this study are included in the article. Further inquiries can be directed to the corresponding author.

Conflicts of Interest: The authors declare no conflicts of interest.

Abbreviations

The following abbreviations are used in this manuscript:

BIM	Building Information Modelling
BoQ	Bills of Quantities
BSR	Building Schedule of Rates
EC	Embodied Carbon
ECFs	Embodied Carbon Factors
EPDs	Environmental Product Declarations
ESEFs	Energy Source Emission Factors
GHG	Green House Gas

Appendix A. Interview Guideline

Interview Guideline

purpose of the interview:

To verify and validate the proposed framework for BIM-integrated embodied carbon assessment in Sri Lanka. The interview is confidential, and the data will be used for research purposes only and kindly Request consent for recording the interview.

Medium of the interview:

MS team/Zoom, via online.

Maximum Duration:

15 minutes

Interview questions

A interview is devised with the primary aim of **validating the relevance of the framework**. Additionally, the survey aimed to identify any **potentially** overlooked **additional requirements**. The interview questionnaire included the following questions.

Demographic questions

Question 1: What is your expertise and current designation?

Question 2: How many years of experience do you have in BIM and Carbon assessment field?
Less than 1 year
1-5 years
6-10 years
More than 10 years

Framework Understanding:

Question 3: How would you describe the proposed framework in your words?

Question 4: Are there any aspects of the framework that are unclear or need further explanation?

Framework Application:

Question 5: How do you see this framework being applied in your current role or projects?"

Question 6: What challenges do you anticipate when implementing this framework?"

Comparison with Existing Methods:

Question 7: How does this framework compare to other methods or frameworks you are familiar with for BIM-integrated embodied carbon assessment?"

Question 8: What advantages or disadvantages do you see in our framework compared to others?" Considering the preparation, data integration, assessment, and visualization stages.

https://doi.org/10.3390/buildings16040814

Question 9: Which elements of the framework do you find most valuable?"

Question 10: Are there any elements you believe are unnecessary or redundant?"

Barriers to Adoption:

Question 11: What barriers, if any, do you foresee in adopting this framework in Sri Lanka?"

Question 12: What resources or support would be beneficial in overcoming these barriers?"

Question 13: Do you have any other comments, concerns, or suggestions about the framework?

Appendix B. Qualitative Data Analysis

No	Q3	Theme
Question	How would you describe the proposed framework in your words?	
IN1	"The framework enables evaluating life cycle carbon footprint of buildings integrating BIM".	Understandable
IN2	"There are several comparable frameworks available for the assessment of embodied carbon using external tools, and it is advisable to avoid relying on third-party tools in the long run."	Understandable
IN3	"Process is connecting preparation, integration, Assessment and visualization. There is not mention, how to calculate A4-A5. and C1-C4 in visualization. If you do A4-A5. and C1-C4 , you need to add energy source emission factors to another data base to existing preparation process"	Missing part Interpretation
IN4	"Its a good approach"	Understandable
IN5	"This is useful for the construction industry, especially now that the industry is moving towards more green building sustainability. Then you could easily Quantify the environmental impacts to the building".	Understandable

No	Q4	Theme
Question	Are there any aspects of the framework that are unclear or need further explanation?	
IN1	"Which and what types of databases used were not clear."	Database names
IN2	"piece of data that is missing is the density. you need to convert the material I'm units in 2 kilograms of materials in order to be able to estimate embodied carbon Curry. density information from a different source and probably maybe have a library for density of different materials in my opinion. probably you'll find out if there's a standard document we can use."	material density info
IN3	"There is not mention, how to calculate A4-A5. and C1-C4 in visualization. If you do A4-A5. and C1-C4 , you need to add energy source emission factors to another data base to existing preparation process. If you use this only for A1-A3 embodied carbon process, then its ok".	Energy source emission factors
IN4	"To elaborate, maybe could be the structure of your database like how you're matching the materials within your excel and database. The rivets files would be useful too. Why there's such an off framework for like the materials or embodiment carbon, and how your lining up with that database would be very useful."	Database names
IN5	"The type of Input or Output data the modal generates is not clear"	Input Output Data

https://doi.org/10.3390/buildings16040814

No	Q5	Theme
Question	How do you see this framework being applied in your current role or projects?"	
IN1	"The data integration and data pipelines aspects are of interest and can be generalized for multiple fields and applications"	Applicable
IN2	"This information is valuable for academic endeavors, especially when it is aligned with the specific particular country."	Applicable
IN3	"Not familiarize the BIM soft wares, and also it is high cost. It is difficult to find BIM experts"	Difficult
IN4	"The framework is applicable. Most of this framework people come up with some of them, but the challenges are compiling in a way that Is useful. Cause if you take lets say, an error to the user is different for the person who worked on the framework. The challenge will be that they don't know about the details of the framework, and so even march and materials like embodiment carbon coefficients become a problem. But if it can't be designed in a way that the user doesn't have to change so much of the framework, then it can be applicable. So, some good compilation will be good. Very useful."	Applicable
IN5	"This can be used for promoting the low carbon emission buildings in the industry. Any Research in that area can be benefited for the expiration."	Applicable

No	Q6	Theme
Question	What challenges do you anticipate when implementing this framework	
IN1	"Significant efforts will be required to integrate multiple data sources. Also, unavailability of Sri Lanka specific datasets/background data could be challenge"	Database Integration
IN2	"Lack of country specific databases, Finding density factors of the materials"	Country specific data
IN3	Not familiarize and not available the BIM soft wares, and also it is high cost. It is difficult to find BIM experts	BIM knowledge
IN4	"I think one challenge that you might face will be the computation within Dynamo, because I happened to work on something like this and the challenge that was when you're working on a huge building, maybe instructing so many quantities into Dynamo, it becomes very slow even if you have high computational resources. The computation in Excel is better than Dynamo. Otherwise, you might have to use other tools. For instance, I tried rhino's grasshopper, because it was faster than Dynamo, and the rivet can be connected to grasshopper as well".	Computation power
IN5	"You must get consent from the industry that they are willing to apply this. The owners must ask the designer to include the information and to keep all the parties involved. Technical knowledge need to be adverted and provide some training".	Stake Holders acceptance

https://doi.org/10.3390/buildings16040814

No	Q7	Theme
Question	How does this framework compare to other methods or frameworks you are familiar with for BIM-integrated embodied carbon assessment?"	
IN1	"In general, it is similar to carbon footprint assessment frameworks. Integration of EPDs and already existing construction materials data offers novelty".	EPD integration Novel
IN2	"other tools like one click LCA EC3 with Revit add-on it is good to have own, country specific data base for claculation purposes".	Country specific
IN3	"Not familiar with BIM-integrated embodied carbon assessment. But familiar with LCA carbon and embodied carbon assessment"	Good approach
IN4	"The advantage if this framework is that it will be very useful because if you take some of these other tools, the problem is that the database is not applicable to the region which you are looking at. And so, you might have a fair idea of what impacts are generated. So I think the accuracy of this one will be better".	Accuracy
IN5	"It is very thoughtful. It generates most of the information related to sustainability. The Conversion of dollar values and good for the environment".	Dollar value

No	Q8	Theme
Question	What advantages or disadvantages do you see in our framework compared to others?" Considering the preparation, data integration, assessment, and visualization stages.	
IN1	"Framework focuses and provides a comprehensive approach on evaluating cradle-to-gate emissions. The use phase and end-of-life models can also be incorporated to evaluate cradle-to-grave emissions".	cradle to grave
IN2	"Non dependency of another piece of commercial tools and fast track of the LCA calculations are advantages. But visual coding knowledge is required and subscription fees of the BIM software's will be a disadvantage for medium size companies".	Independent from commercial software
IN3	"There is no this kind of frame work in Sri Lanka contest. So if we can develop this kind of frame work, It is very good. Because we are doing manual caculations. And also it is very difficult to calculate other stages. Introdusing this kind of automated system is very good".	Avoid manual calculation
IN4	"For the data integration it looks good. I don't have many details about it, but combining the Excel database and then your quantities and rebase is a smart approach so that you don't have to extract it or include a third-party software with just the two and your database. Otherwise, if you were to transfer data you might lose some data so that's really good. What you could do to improve is to maybe consider doing your calculations in Excel so you could just use Dynamo for Data instruction. And for the visualization in Excel is very good".	Try calculation in Excel
IN5	"It's pretty similar to the other ones. Dis Advantage Is that people need training to use the tools and they should able to invest money".	Training & investment

References

1. Płoszaj-Mazurek, M.; Ryńska, E. Artificial Intelligence and Digital Tools for Assisting Low-Carbon Architectural Design: Merging the Use of Machine Learning, Large Language Models, and Building Information Modeling for Life Cycle Assessment Tool Development. *Energies* **2024**, *17*, 2997. [CrossRef]
2. Lima, M.S.S.; Duarte, S.; Exenberger, H.; Fröch, G.; Flora, M. Integrating BIM-LCA to Enhance Sustainability Assessments of Constructions. *Sustainability* **2024**, *16*, 1172. [CrossRef]
3. Lützkendorf, T.; Balouktsi, M. Embodied carbon emissions in buildings: Explanations, interpretations, recommendations. *Build. Cities* **2022**, *3*, 964–973. [CrossRef]
4. Rondinel-Oviedo, D.R.; Keena, N. Embodied Carbon: A call to the building industry. *IOP Conf. Ser. Earth Environ. Sci.* **2022**, *1122*, 012042. [CrossRef]
5. Abeydeera, L.H.U.W.; Mesthrige, J.W.; Samarasinghalage, T.I. Perception of Embodied Carbon Mitigation Strategies: The Case of Sri Lankan Construction Industry. *Sustainability* **2019**, *11*, 3030. [CrossRef]

https://doi.org/10.3390/buildings16040814

6. Perera, C.; Palliyaguru, R. Adapting the standard forms of contract to minimize the contractual effects of COVID-19 on construction projects. In *Proceedings of the 10th World Construction Symposium, Virtually, 24–26 June 2022*; Emerald Group Publishing: Bingley, UK, 2022; pp. 76–88. [CrossRef]
7. CHEC Port City Colombo (Pvt) Ltd. About Port City Colombo—Sri Lanka's Global Business Hub. Available online: https://www.portcitycolombo.lk/about-port-city-colombo/ (accessed on 3 November 2025).
8. Mendis, A.P.K.D.; Jayatunge, D.A.S.R.; Disaratna, V.; Perera, B.A.K.S. Implementation of government policies in the construction industry: The case of Sri Lanka. *A/Z ITU J. Fac. Arch.* **2022**, *19*, 151–167. [CrossRef]
9. Gunathilake, S.; Ramachandra, T.; Madushika, U. Carbon footprint analysis of construction activities in sri lanka: An input—output table. In Proceedings of the 14th International Research Conference—FARU 2021, Virtually, 3–4 December 2021.
10. Amarasinghe, I.A.; Soorige, D.; Geekiyanage, D. Comparative study on Life Cycle Assessment of buildings in developed countries and Sri Lanka. *Built Environ. Proj. Asset Manag.* **2021**, *11*, 304–329. [CrossRef]
11. Nadeeshani, M.; Ramachandra, T.; Gunatilake, S.; Zainudeen, N. Carbon Footprint of Green Roofing: A Case Study from Sri Lankan Construction Industry. *Sustainability* **2021**, *13*, 6745. [CrossRef]
12. Nawarathna, A.; Alwan, Z.; Gledson, B.; Fernando, N. Embodied carbon in commercial office buildings: Lessons learned from Sri Lanka. *J. Build. Eng.* **2021**, *42*, 102441. [CrossRef]
13. Kumanayake, R.; Luo, H.; Paulusz, N. Assessment of material related embodied carbon of an office building in Sri Lanka. *Energy Build.* **2018**, *166*, 250–257. [CrossRef]
14. Kumari, T.; Kulathunga, U.; Hewavitharana, T.; Madusanka, N. Embodied carbon reduction strategies for high-rise buildings in Sri Lanka. *Int. J. Constr. Manag.* **2022**, *22*, 2605–2613. [CrossRef]
15. Amahmoud, A.; El Attar, M.M.; Meleishy, A. The Evolution of Life Cycle Assessment Approach: A Review of Past and Future Prospects. *IOP Conf. Ser. Earth Environ. Sci.* **2022**, *992*, 012002. [CrossRef]
16. Xu, J.; Teng, Y.; Pan, W.; Zhang, Y. BIM-integrated LCA to automate embodied carbon assessment of prefabricated buildings. *J. Clean. Prod.* **2022**, *374*, 133894. [CrossRef]
17. Hussain, M.; Zheng, B.; Chi, H.L.; Hsu, S.C.; Chen, J.H. Automated and continuous BIM-based life cycle carbon assessment for infrastructure design projects. *Resour. Conserv. Recycl.* **2023**, *190*, 106848. [CrossRef]
18. Rosayuru, H.D.R.R.; Waidyasekara, K.G.A.S.; Wijewickrama, M.K.C.S. Sustainable BIM based integrated project delivery system for construction industry in Sri Lanka. *Int. J. Constr. Manag.* **2022**, *22*, 769–783. [CrossRef]
19. Kaushalya, K.W.A.H.H.; Thayaparan, M.; Weerasinghe, L.N.K.; Attfield, A. Rogers' diffusion of innovation theory to enhance BIM implementation in the construction industry of Sri Lanka. *Intell. Build. Int.* **2024**, *16*, 182–198. [CrossRef]
20. Building Schedule of Rates (BSR). *Building Schedule of Rates For Urgent Special Repairs, Renovations, Additions and Improvements, Minor Works and Maintenance to Government Buildings-2023*; Department of Buildings: Battaramulla, Sri Lanka, 2023.
21. Manoharan, K.; Dissanayake, P.; Pathirana, C.; Deegahawature, D.; Silva, R. Labour-related factors affecting construction productivity in Sri Lankan building projects: Perspectives of engineers and managers. *Front. Eng. Built Environ.* **2022**, *2*, 218–232. [CrossRef]
22. Manoharan, K.; Dissanayake, P.B.; Pathirana, C.; Deegahawature, D.; Silva, K.R.R. A curriculum guide model to the next normal in developing construction supervisory training programmes. *Built Environ. Proj. Asset Manag.* **2022**, *12*, 792–822. [CrossRef]
23. Weerakoon, T.G.; Wimalasena, S.; Zvirgzdins, J. Assessment of Implementation of Circular Economy Framework in the Sri Lankan Construction Sector. *Balt. J. Real Estate Econ. Constr. Manag.* **2023**, *11*, 133–152. [CrossRef]
24. Rabiser, R.; Grünbacher, P.; Dhungana, D. Requirements for product derivation support: Results from a systematic literature review and an expert survey. *Inf. Softw. Technol.* **2010**, *52*, 324–346. [CrossRef]
25. Tugwell, P.; Tovey, D. PRISMA 2020. *J. Clin. Epidemiol.* **2021**, *134*, A5–A6. [CrossRef]
26. Pomponi, F.; Moncaster, A. Embodied carbon mitigation and reduction in the built environment—What does the evidence say? *J. Environ. Manag.* **2016**, *181*, 687–700. [CrossRef]
27. Karimi, S.; Iordanova, I. Integration of BIM and GIS for Construction Automation, a Systematic Literature Review (SLR) Combining Bibliometric and Qualitative Analysis. *Arch. Comput. Methods Eng.* **2021**, *28*, 4573–4594. [CrossRef]
28. Dangelico, R.M. Green Product Innovation: Where we are and Where we are Going. *Bus. Strat. Environ.* **2016**, *25*, 560–576. [CrossRef]
29. Deng, F.; Smyth, H. Contingency-Based Approach to Firm Performance in Construction: Critical Review of Empirical Research. *J. Constr. Eng. Manag.* **2013**, *139*, 04013004. [CrossRef]
30. Li, L.; Gao, L.; Zhang, X.; Xu, H.; Jiang, L. Research on Building's Carbon Emission Calculation and Reduction Strategy Based on Life Cycle Assessment (LCA) and Building in Formation Modeling (BIM): A Case Study in Beijing, China. *Buildings* **2025**, *15*, 1403. [CrossRef]
31. Moher, D.; Liberati, A.; Tetzlaff, J.; Altman, D.G. Preferred reporting items for systematic reviews and meta-analyses: The PRISMA statement. *Int. J. Surg.* **2010**, *8*, 336–341. [CrossRef] [PubMed]

https://doi.org/10.3390/buildings16040814

32. Thelwall, M. Journal and disciplinary variations in academic open peer review anonymity, outcomes, and length. *J. Libr. Inf. Sci.* **2023**, *55*, 299–312. [CrossRef]
33. Diane, S.; Casey, E.A. An Examination of the Sufficiency of Small Qualitative Samples. 2018. Volume 500. Available online: https://digitalcommons.tacoma.uw.edu/socialwork_pub/500 (accessed on 12 January 2026).
34. Rosyidah, U.; Sudarmiatin, S.; Sumarsono, H. Digitalization and internationalization of SMEs: A Systematic Literature Review. *J. Enterp. Dev.* **2023**, *5*, 479–499. [CrossRef]
35. de Andrade, C.E.C.; Neto, E.G.L.; Holanda, F.S.R.; Santos, L.D.V.; Júnior, L.C.D.A.; Bandeira, A.A. An analysis of overlapping terms to define articles key words. *Int. J. Innov. Educ. Res.* **2020**, *8*, 275–287. [CrossRef]
36. Nellessen, T.; Ebner, B.; Pyrgidis, N.; Ledderose, S.; Kretschmer, A.; Marcon, J.; Teupser, D.; Mayr, D.; Faihs, V.; Stief, C.G.; et al. Characterization of Human Papilloma Virus in Prostate Cancer Patients Undergoing Radical Prostatectomy—A Prospective Study of 140 Patients. *Viruses* **2023**, *15*, 1264. [CrossRef]
37. Hegazy, M.; Yasufuku, K.; Abe, H. Evaluating and visualizing perceptual impressions of daylighting in immersive virtual environments. *J. Asian Arch. Build. Eng.* **2021**, *20*, 768–784. [CrossRef]
38. Soysa, R.N.K.; Kumara, A.S.; Jayasena, D.M.; Samaranayake, M.K.S.M. Exploring major reported themes in corporate sustainability disclosures integrating the sustainable development goals: An analysis of Sri Lankan listed rms. *Res. Sq.* **2022**. [CrossRef]
39. De Jong, R.; Bus, D. *VOSviewer: Putting Research into Context*; Research Software Community: Leiden, The Netherlands, 2023.
40. Chen, Z.; Lau, S.S.Y.; Zhang, Z.; Lau, S.S.Y.; Kee, T. A modular framework for estimating carbon emissions from building component replacements in LCA. *Energy Build.* **2025**, *349*, 116424. [CrossRef]
41. Soust-Verdaguer, B.; García-Martínez, A.; Rey-Álvarez, B.; de Diego, B.; de la Fuente, A.; Röck, M. Data infrastructure for whole-life carbon emissions baselines of buildings in Spain. *Energy Build.* **2025**, *347*, 116307. [CrossRef]
42. Xu, H.; Chen, J.; Kim, J.I. An integrated LCA–BIM framework for assessing carbon emissions in buildings in China's cold regions. *J. Clean. Prod.* **2025**, *522*, 146255. [CrossRef]
43. Wu, X.; Wang, J.; Zhang, R.; Bi, Q.; Pan, J. Application of Prefabricated Public Buildings in Rural Areas with Extreme Hot–Humid Climate: A Case Study of the Yongtai County Digital Industrial Park, Fuzhou, China. *Buildings* **2025**, *15*, 2767. [CrossRef]
44. Xu, Y.; Gong, X.; Tao, X.; Kwok, H.H.; Limsawasd, C.; Cheng, J.C. Automated openBIM-based discrete event simulation modeling for cradle-to-site embodied carbon assessment. *Autom. Constr.* **2025**, *175*, 106217. [CrossRef]
45. Borkowski, A.S.; Hajdukiewicz, U.; Herbich, J.; Kostana, K.; Kubala, A. Analysis of the Tools for Evaluating Embodied Energy Through Building Information Modeling Tools: A Case Study of a Single-Unit Shell Building. *Earth* **2025**, *6*, 25. [CrossRef]
46. Li, Y.; Zha, Y.; Li, M.; Qian, L. Evaluating the carbon footprint of a hospital from the dynamic life cycle perspective:A case study in Shanghai. *Build. Environ.* **2025**, *277*, 112950. [CrossRef]
47. Baskaran, D.; Chockkalingam, U.; Muthalvan, R.S. Assessment of Sustainable Hybrid Formwork Systems Using Life Cycle Assessment and the Wear-Out Coefficient—A Case Study. *Buildings* **2025**, *15*, 1630. [CrossRef]
48. Sistos-Sescosse, G.; Atuahene, B.T.; Ajulo, O.; Adams, I. Examining the decision criteria on BIM-LCA: A case study. *Constr. Econ. Build.* **2025**, *25*, 203–220. [CrossRef]
49. Xiang, L.; Li, G.; Li, H. A Common Data Environment Framework Applied to Structural Life Cycle Assessment: Coordinating Multiple Sources of Information. *Buildings* **2025**, *15*, 1315. [CrossRef]
50. Strelets, K.; Zaborova, D.; Kokaya, D.; Petrochenko, M.; Melekhin, E. Building Information Modeling (BIM)-Based Building Life Cycle Assessment (LCA) Using Industry Foundation Classes (IFC) File Format. *Sustainability* **2025**, *17*, 2848. [CrossRef]
51. Gu, X.; Chen, C.; Fang, Y.; Mahabir, R.; Fan, L. CECA: An intelligent large-language-model-enabled method for accounting embodied carbon in buildings. *Build. Environ.* **2025**, *272*, 112694. [CrossRef]
52. Rodríguez, J.F.F.; Picardo, A.; Aguilar-Planet, T.; Martín-Mariscal, A.; Peralta, E. Data Transfer Reliability from Building Information Modeling (BIM) to Life Cycle Assessment (LCA)—A Comparative Case Study of an Industrial Warehouse. *Sustainability* **2025**, *17*, 1685. [CrossRef]
53. Al-Zrigat, Z. BIM framework to minimize embodied energy in heritage buildings: Old downtown Amman case studies. *Facilities* **2025**, *43*, 149–171. [CrossRef]
54. Mohammed, A.; Elmasoudi, I.; Ghannam, M. Life cycle environmental impact assessment of steel structures using building information modeling. *Innov. Infrastruct. Solutions* **2025**, *10*, 36. [CrossRef]
55. Ferreira, M.T.H.A.; Costa, A.A.; Silvestre, J.D. Environmental optimization and benchmarking of walls through a BIM plugin. *Arch. Eng. Des. Manag.* **2025**, 1–30. [CrossRef]
56. Ding, Y.; Guo, Z.Z.; Zhou, S.X.; Wei, Y.Q.; She, A.M.; Dong, J.L. Research on carbon emissions during the construction process of prefabricated buildings based on BIM and LCA. *J. Asian Arch. Build. Eng.* **2025**, *24*, 1426–1438. [CrossRef]
57. Lv, R. A carbon footprint evaluation model for the entire life cycle of building materials—Case study. *Arch. Civ. Eng.* **2025**, *71*, 63–81. [CrossRef]

https://doi.org/10.3390/buildings16040814

58. Safari, K.; Ghandehariun, S. An integrative BIM-based life cycle assessment framework to address uncertainties: A mixed-methods study under real construction project context. *Int. J. Constr. Manag.* **2025**, *26*, 54–75. [CrossRef]
59. Samniang, W.; Panuwatwanich, K.; Tangtermsirikul, S.; Papong, S. Development and implementation of BIM-integrated LCA method for carbon emission assessment of concrete construction: Case of overpass project in Thailand. *Smart Sustain. Built Environ.* **2025**. [CrossRef]
60. Pandimani; Bilgates, P.; Raviteja, Y. A holistic design approach for sustainable building environment—A case study of an educational building. *Int. J. Constr. Manag.* **2025**, *25*, 1982–1997. [CrossRef]
61. Yardımcı, Y.; Demirel, B.B.C.; Yıldız, M.E. Climatic Influences on the Environmental Performances of Residential Buildings: A Comparative Case Study in Turkey. *Buildings* **2024**, *14*, 4015. [CrossRef]
62. Kathiravel, R.; Feng, H. Structural and embodied carbon performance optimization for low carbon buildings through BIM-based integrated design. *J. Build. Eng.* **2024**, *98*, 111008. [CrossRef]
63. Aragón, A.; Alberti, M. Limitations of machine-interpretability of digital EPDs used for a BIM-based sustainability assessment of construction assets. *J. Build. Eng.* **2024**, *96*, 110418. [CrossRef]
64. Parece, S.; Resende, R.; Rato, V. A BIM-based tool for embodied carbon assessment using a Construction Classification System. *Dev. Built Environ.* **2024**, *19*, 100467. [CrossRef]
65. Abdelaal, M.A.; Seif, S.M.; El-Tafesh, M.M.; Bahnas, N.; Elserafy, M.M.; Bakhoum, E.S. Sustainable assessment of concrete structures using BIM–LCA–AHP integrated approach. *Environ. Dev. Sustain.* **2024**, *26*, 25669–25688. [CrossRef]
66. Ali, A.A.M. Cradle-to-gate life cycle assessment of interior floor material alternatives in Egypt. *J. Umm Al-Qura Univ. Eng. Arch.* **2024**, *15*, 282–297. [CrossRef]
67. Manifold, J.; Renukappa, S.; Suresh, S.; Georgakis, P.; Perera, G.R. Dual Transition of Net Zero Carbon and Digital Transformation: Case Study of UK Transportation Sector. *Sustainability* **2024**, *16*, 7852. [CrossRef]
68. Gao, J.; Shen, Z.; Shao, Z.; Pan, X.; Tang, D.; Zhao, K.; Chen, Y.; Lv, H. Carbon Emission Analysis of RC Core Wall-Steel Frame Structures. *Appl. Sci.* **2024**, *14*, 7727. [CrossRef]
69. Atik, Ş.; Aparisi, T.D.; Raslan, R. Mind the gap: Facilitating early design stage building life cycle assessment through a co-production approach. *J. Clean. Prod.* **2024**, *464*, 142803. [CrossRef]
70. Ullah, H.; Zhang, H.; Ye, H.; Ali, I.; Cong, M. Research on Low-Carbon Design and Energy Efficiency by Harnessing Indigenous Resources through BIM-Ecotect Analysis in Hot Climates. *Sustainability* **2024**, *16*, 6057. [CrossRef]
71. Han, Y.; Wang, Y.; Zhao, L.; Li, T.; Yang, Z.; Wang, Z.; Wang, H. BIM-Based Analysis and Strategies to Reduce Carbon Emissions of Underground Construction in Public Buildings: A Case on Xi'an Shaanxi, China. *Buildings* **2024**, *14*, 2134. [CrossRef]
72. Yavan, F.; Maalek, R.; Toğan, V. Structural Optimization of Trusses in Building Information Modeling (BIM) Projects Using Visual Programming, Evolutionary Algorithms, and Life Cycle Assessment (LCA) Tools. *Buildings* **2024**, *14*, 1532. [CrossRef]
73. Eslami, H.; Yaghma, A.; Jayasinghe, L.B.; Waldmann, D. Comparative life cycle assessment of light frame timber and reinforced concrete masonry structural systems for single-family houses in Luxembourg. *Heliyon* **2024**, *10*, e26083. [CrossRef]
74. Kylili, A.; Georgali, P.Z.; Christou, P.; Fokaides, P. An integrated building information modeling (BIM)-based lifecycle-oriented framework for sustainable building design. *Constr. Innov.* **2024**, *24*, 492–514. [CrossRef]
75. Topraklı, A.Y. Enabling circularity in Turkish construction: A case of BIM-based material management utilizing material passports. *Smart Sustain. Built Environ.* **2024**. [CrossRef]
76. Danso, A.K.; Edwards, D.J.; Adjei, E.K.; Adjei-Kumi, T.; Owusu-Manu, D.-G.; Fianoo, S.I.; Thwala, W.D. Analysis of the underlying factors affecting BIM-LCA integration in the Ghanaian construction industry: A factor analysis approach. *Constr. Innov.* **2024**. [CrossRef]
77. Sugiyama, G.T.; Rodrigues, M.F.; Rodrigues, H. Environmental impacts and BIM: A Portuguese heritage case study. *Int. J. Build. Pathol. Adapt.* **2024**, *43*, 1863–1877. [CrossRef]
78. Ma, L.; Azari, R.; Elnimeiri, M. A Building Information Modeling-Based Life Cycle Assessment of the Embodied Carbon and Environmental Impacts of High-Rise Building Structures: A Case Study. *Sustainability* **2024**, *16*, 569. [CrossRef]
79. Forth, K.; Abualdenien, J.; Borrmann, A. Calculation of embodied GHG emissions in early building design stages using BIM and NLP-based semantic model healing. *Energy Build.* **2023**, *284*, 112837. [CrossRef]
80. Boje, C.; Menacho, Á.J.H.; Marvuglia, A.; Benetto, E.; Kubicki, S.; Schaubroeck, T.; Gutiérrez, T.N. A framework using BIM and digital twins in facilitating LCSA for buildings. *J. Build. Eng.* **2023**, *76*, 107232. [CrossRef]
81. Di Santo, N.; Henriquez, L.G.; Dotelli, G.; Imperadori, M. Holistic Approach for Assessing Buildings' Environmental Impact and User Comfort from Early Design: A Method Combining Life Cycle Assessment, BIM, and Active House Protocol. *Buildings* **2023**, *13*, 1315. [CrossRef]
82. Arvizu-Piña, V.A.; López, J.F.A.; González, A.A.G.; Alarcón, I.G.B. An open access online tool for LCA in building's early design stage in the Latin American context. A screening LCA case study for a bioclimatic building. *Energy Build.* **2023**, *295*, 113269. [CrossRef]

https://doi.org/10.3390/buildings16040814

83. Yevu, S.K.; Owusu, E.K.; Chan, A.P.C.; Oti-Sarpong, K.; Wuni, I.Y.; Tetteh, M.O. Systematic review on the integration of building information modelling and prefabrication construction for low-carbon building delivery. *Build. Res. Inf.* **2023**, *51*, 279–300. [CrossRef]
84. Hunt, J.; Osorio-Sandoval, C.A. Assessing Embodied Carbon in Structural Models: A Building Information Modelling-Based Approach. *Buildings* **2023**, *13*, 1679. [CrossRef]
85. Mowafy, N.; El Zayat, M.; Marzouk, M. Parametric BIM-based life cycle assessment framework for optimal sustainable design. *J. Build. Eng.* **2023**, *75*, 106898. [CrossRef]
86. Feng, H.; Kassem, M.; Greenwood, D.; Doukari, O. Whole building life cycle assessment at the design stage: A BIM-based framework using environmental product declaration. *Int. J. Build. Pathol. Adapt.* **2023**, *41*, 109–142. [CrossRef]
87. Serrano-Baena, M.M.; Ruiz-Díaz, C.; Boronat, P.G.; Mercader-Moyano, P. Optimising LCA in complex buildings with MLCAQ: A BIM-based methodology for automated multi-criteria materials selection. *Energy Build.* **2023**, *294*, 113219. [CrossRef]
88. Guignone, G.; Calmon, J.L.; Vieira, D.; Bravo, A. BIM and LCA integration methodologies: A critical analysis and proposed guidelines. *J. Build. Eng.* **2023**, *73*, 106780. [CrossRef]
89. Soust-Verdaguer, B.; Gutiérrez, J.A.; Llatas, C. Development of a Plug-In to Support Sustainability Assessment in the Decision-Making of a Building Envelope Refurbishment. *Buildings* **2023**, *13*, 1472. [CrossRef]
90. Klumbyte, E.; Georgali, P.-Z.; Spudys, P.; Giama, E.; Morkunaite, L.; Pupeikis, D.; Jurelionis, A.; Fokaides, P. Enhancing whole building life cycle assessment through building information modelling: Principles and best practices. *Energy Build.* **2023**, *296*, 113401. [CrossRef]
91. Deng, X.; Lu, K. Multi-level assessment for embodied carbon of buildings using multi-source industry foundation classes. *J. Build. Eng.* **2023**, *72*, 106705. [CrossRef]
92. Tavares, V.; Freire, F. Life cycle assessment of a prefabricated house for seven locations in different climates. *J. Build. Eng.* **2022**, *53*, 104504. [CrossRef]
93. Soust-Verdaguer, B.; Galeana, I.B.; Llatas, C.; Montes, M.; Hoxha, E.; Passer, A. How to conduct consistent environmental, economic, and social assessment during the building design process. A BIM-based Life Cycle Sustainability Assessment method. *J. Build. Eng.* **2022**, *45*, 103516. [CrossRef]
94. Onososen, A.; Musonda, I. Barriers to BIM-Based Life Cycle Sustainability Assessment for Buildings: An Interpretive Structural Modelling Approach. *Buildings* **2022**, *12*, 324. [CrossRef]
95. Viscuso, S.; Monticelli, C.; Ahmadnia, A.; Zanelli, A. Integration of life cycle assessment and life cycle costing within a BIM-based environment. *Front. Sustain.* **2022**, *3*, 1002257. [CrossRef]
96. Li, X.J.; Xie, W.J.; Xu, L.; Li, L.L.; Jim, C.; Wei, T.B. Holistic life-cycle accounting of carbon emissions of prefabricated buildings using LCA and BIM. *Energy Build.* **2022**, *266*, 112136. [CrossRef]
97. Alotaibi, B.S.; Khan, S.A.; Abuhussain, M.A.; Al-Tamimi, N.; Elnaklah, R.; Kamal, M.A. Life Cycle Assessment of Embodied Carbon and Strategies for Decarbonization of a High-Rise Residential Building. *Buildings* **2022**, *12*, 1203. [CrossRef]
98. Abdelaal, F.; Guo, B.H. Stakeholders' perspectives on BIM and LCA for green buildings. *J. Build. Eng.* **2022**, *48*, 103931. [CrossRef]
99. Morsi, D.M.; Ismaeel, W.S.; Ehab, A.; Othman, A.A. BIM-based life cycle assessment for different structural system scenarios of a residential building. *Ain Shams Eng. J.* **2022**, *13*, 101802. [CrossRef]
100. Sameer, H.; Bringezu, S. Building information modelling application of material, water, and climate footprint analysis. *Build. Res. Inf.* **2021**, *49*, 593–612. [CrossRef]
101. Alwan, Z.; Nawarathna, A.; Ayman, R.; Zhu, M.; ElGhazi, Y. Framework for parametric assessment of operational and embodied energy impacts utilising BIM. *J. Build. Eng.* **2021**, *42*, 102768. [CrossRef]
102. Sobhkhiz, S.; Taghaddos, H.; Rezvani, M.; Ramezanianpour, A.M. Utilization of semantic web technologies to improve BIM-LCA applications. *Autom. Constr.* **2021**, *130*, 103842. [CrossRef]
103. Hao, J.L.; Cheng, B.; Lu, W.; Xu, J.; Wang, J.; Bu, W.; Guo, Z. Carbon emission reduction in prefabrication construction during materialization stage: A BIM-based life-cycle assessment approach. *Sci. Total. Environ.* **2020**, *723*, 137870. [CrossRef] [PubMed]
104. van Eldik, M.A.; Vahdatikhaki, F.; dos Santos, J.M.O.; Visser, M.; Doree, A. BIM-based environmental impact assessment for infrastructure design projects. *Autom. Constr.* **2020**, *120*, 103379. [CrossRef]
105. Durão, V.; Costa, A.A.; Silvestre, J.D.; Mateus, R.; Santos, R.; de Brito, J. Current Opportunities and Challenges in the Incorporation of the LCA Method in BIM. *Open Constr. Build. Technol. J.* **2020**, *14*, 336–349. [CrossRef]
106. Hollberg, A.; Genova, G.; Habert, G. Evaluation of BIM-based LCA results for building design. *Autom. Constr.* **2020**, *109*, 102972. [CrossRef]
107. Santos, R.; Costa, A.A.; Silvestre, J.D.; Pyl, L. Integration of LCA and LCC analysis within a BIM-based environment. *Autom. Constr.* **2019**, *103*, 127–149. [CrossRef]
108. Nizam, R.S.; Zhang, C.; Tian, L. A BIM based tool for assessing embodied energy for buildings. *Energy Build.* **2018**, *170*, 1–14. [CrossRef]

https://doi.org/10.3390/buildings16040814

109. Bueno, C.; Fabricio, M.M. Comparative analysis between a complete LCA study and results from a BIM-LCA plug-in. *Autom. Constr.* **2018**, *90*, 188–200. [CrossRef]
110. Eleftheriadis, S.; Duffour, P.; Mumovic, D. BIM-embedded life cycle carbon assessment of RC buildings using optimised structural design alternatives. *Energy Build.* **2018**, *173*, 587–600. [CrossRef]
111. Najjar, M.; Figueiredo, K.; Palumbo, M.; Haddad, A. Integration of BIM and LCA: Evaluating the environmental impacts of building materials at an early stage of designing a typical office building. *J. Build. Eng.* **2017**, *14*, 115–126. [CrossRef]
112. Williams, B.; Lee, J. Experts, expertise and health and physical education teaching: A scoping review of conceptualisations. *Curric. J.* **2021**, *32*, 14–27. [CrossRef]
113. von Soest, C. Why Do We Speak to Experts? Reviving the Strength of the Expert Interview Method. *Perspect. Politics* **2023**, *21*, 277–287. [CrossRef]
114. Smith, S.H.; Durham, S.A. A cradle to gate LCA framework for emissions and energy reduction in concrete pavement mixture design. *Int. J. Sustain. Built Environ.* **2016**, *5*, 23–33. [CrossRef]
115. Finkbeiner, M.; Ackermann, R.; Bach, V.; Berger, M.; Brankatschk, G.; Chang, Y.-J.; Grinberg, M.; Lehmann, A.; Martínez-Blanco, J.; Minkov, N.; et al. Challenges in Life Cycle Assessment: An Overview of Current Gaps and Research Needs. In *LCA Compendium—The Complete World of Life Cycle Assessment*; Springer Science and Business Media LLC: Berlin/Heidelberg, Germany, 2014; pp. 207–258.
116. Chen, X.; Matthews, H.S.; Griffin, W.M. Uncertainty caused by life cycle impact assessment methods: Case studies in process-based LCI databases. *Resour. Conserv. Recycl.* **2021**, *172*, 105678. [CrossRef]
117. Gomes, R.; Silvestre, J.D.; de Brito, J.; Lasvaux, S. Environmental datasets for cement and steel rebars to be used as generic for a national context. *J. Clean. Prod.* **2021**, *316*, 128003. [CrossRef]
118. Zhao, Y.; Ma, L.; Li, Z.; Ni, W. A Calculation and Decomposition Method Embedding Sectoral Energy Structure for Embodied Carbon: A Case Study of China's 28 Sectors. *Sustainability* **2022**, *14*, 2593. [CrossRef]
119. Ghezelbash, A.; Khaligh, V.; Fahimifard, S.H.; Liu, J.J. A Comparative Perspective of the Effects of CO_2 and Non-CO_2 Greenhouse Gas Emissions on Global Solar, Wind, and Geothermal Energy Investment. *Energies* **2023**, *16*, 3025. [CrossRef]
120. Weng, Y.; Mohamed, N.A.N.; Lee, B.J.S.; Gan, N.J.H.; Li, M.; Tan, M.J.; Li, H.; Qian, S. Extracting BIM Information for Lattice Toolpath Planning in Digital Concrete Printing with Developed Dynamo Script: A Case Study. *J. Comput. Civ. Eng.* **2021**, *35*, 05021001. [CrossRef]
121. Abouhamad, M.; Abu-Hamd, M. Life Cycle Assessment Framework for Embodied Environmental Impacts of Building Construction Systems. *Sustainability* **2021**, *13*, 461. [CrossRef]
122. de Saxcé, M.; Perwuelz, A.; Rabenasolo, B. Development of Data Base for Simplified Life Cycle Assessment (LCA) of Textiles. In Proceedings of the Congrès International sur lrqanalyse de Cycle de Vie, Lille, France, 3–4 November 2011.
123. Vigon, B.; Sonnemann, G.; Asselin, A.; Schrijvers, D.; Ciroth, A.; Chen, S.S.; Braga, T.; Poolsawad, N.; Mungkalasiri, J.; Boureima, F.; et al. Review of LCA datasets in three emerging economies: A summary of learnings. *Int. J. Life Cycle Assess.* **2017**, *22*, 1658–1665. [CrossRef]
124. Ciroth, A.; Di Noi, C.; Burhan, S.S.; Srocka, M. LCA database creation: Current challenges and the way forward. *Indones. J. Life Cycle Assess. Sustain.* **2019**, *3*, 41–51.
125. Yurosheva, T.A.; Kalinichenko, A.V.; Makiev, V.G. Algorithm for designing load-bearing structures of a multi-storey building using the visual programming environment DYNAMO STUDIO. *Her. Dagestan State Tech. Univ. Tech. Sci.* **2023**, *49*, 126–133. [CrossRef]
126. Sri Lanka Construction Market Size, Trends, and Forecasts by Sector—Commercial, Industrial, Infrastructure, Energy and Utilities, Institutional and Residential Market Analysis, 2024–2028. Available online: https://www.marketresearch.com/GlobalData-v3648/Sri-Lanka-Construction-Size-Trends-37639317/ (accessed on 3 November 2025).
127. Dixit, M.K. Life cycle recurrent embodied energy calculation of buildings: A review. *J. Clean. Prod.* **2019**, *209*, 731–754. [CrossRef]

Disclaimer/Publisher's Note: The statements, opinions and data contained in all publications are solely those of the individual author(s) and contributor(s) and not of MDPI and/or the editor(s). MDPI and/or the editor(s) disclaim responsibility for any injury to people or property resulting from any ideas, methods, instructions or products referred to in the content.

https://doi.org/10.3390/buildings16040814

MDPI AG
Grosspeteranlage 5
4052 Basel
Switzerland
Tel.: +41 61 683 77 34

Buildings Editorial Office
E-mail: buildings@mdpi.com
www.mdpi.com/journal/buildings



Disclaimer/Publisher's Note: The title and front matter of this reprint are at the discretion of the Guest Editors. The publisher is not responsible for their content or any associated concerns. The statements, opinions and data contained in all individual articles are solely those of the individual Editors and contributors and not of MDPI. MDPI disclaims responsibility for any injury to people or property resulting from any ideas, methods, instructions or products referred to in the content.





Academic Open
Access Publishing

mdpi.com

ISBN 978-3-7258-7209-1